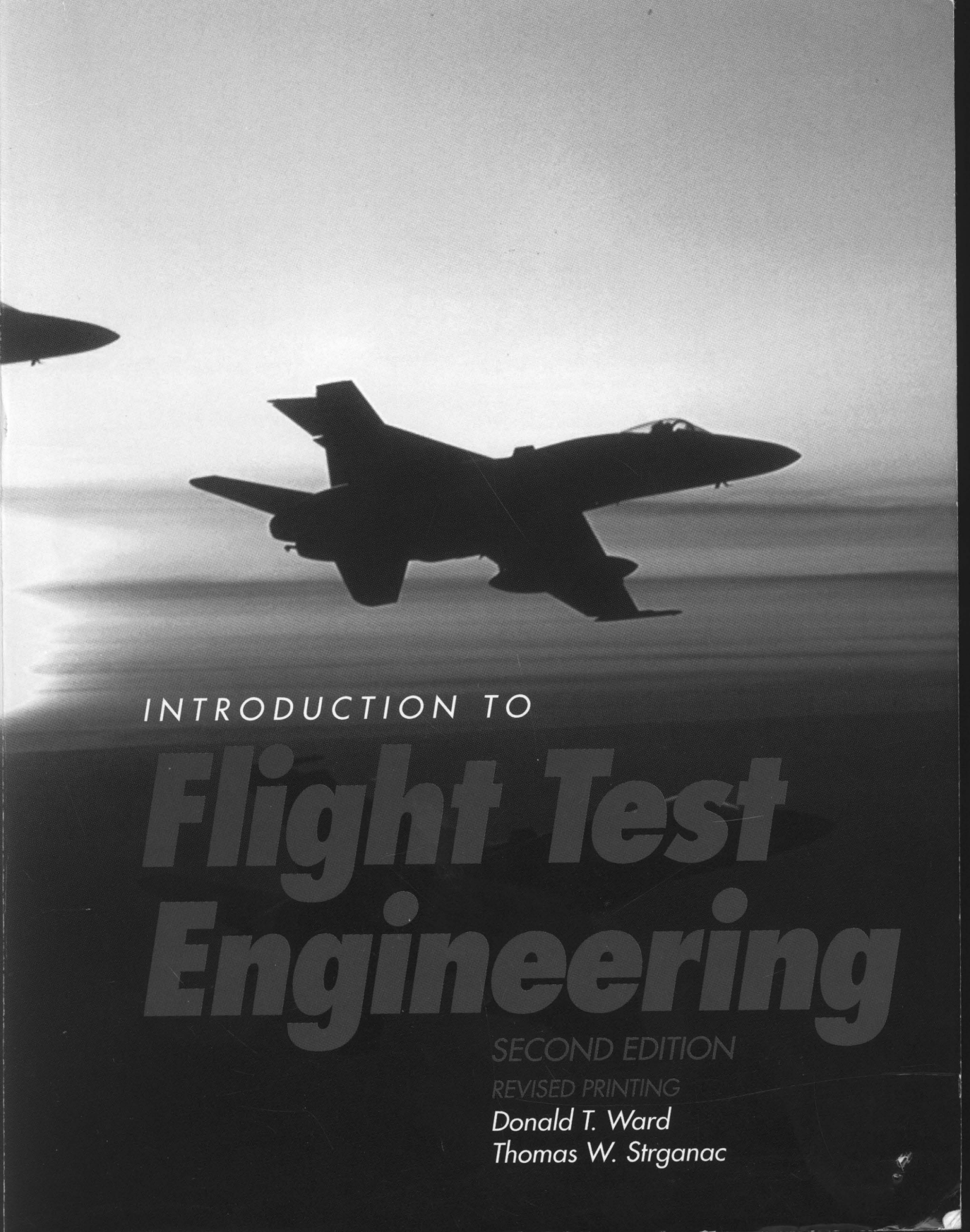

INTRODUCTION TO

Flight Test Engineering

SECOND EDITION

REVISED PRINTING

Donald T. Ward
Thomas W. Strganac

INTRODUCTION TO FLIGHT TEST ENGINEERING

Second Edition
Revised Printing

Donald T. Ward
and
Thomas W. Strganac
Texas A&M

KENDALL/HUNT PUBLISHING COMPANY
4050 Westmark Drive Dubuque, Iowa 52002

Revised Printing

ISBN 0-7872-7500-X

Printed in the United States of America
10 9 8 7 6 5 4 3 2

PREFACE

The purpose of this book is to consolidate the fundamental principles used in classical performance and flying qualities flight testing of manned aircraft. It is intended for use as an introductory text for undergraduate students or as a self-teaching reference for an engineer newly engaged in flight tests. Worked examples are included in each chapter.

The first half of the book covers performance measurements. Chapter 1 is devoted to an overview of why flight tests are conducted and what the most important constraints are. Chapter 2 reviews the standard atmosphere and applies basic aerodynamic equations to the basic measurement system found in virtually every airplane, the pitot-static system. Techniques used to calibrate this system are described and illustrated. Chapter 3 reviews basic point performance equations and applies them to explain how to measure climb, descent, and turn performance. Both steady state and energy approximation expressions are used to lead into discussion of the sawtooth climb, the check climb, the level unaccelerated turn, and the level acceleration flight test methods. Chapter 4 briefly introduces propulsion systems, both for propeller-driven and jet-powered airplanes and summarizes useful relationships for determining range and endurance for such airplanes. Speed power flight tests commonly used to collect cruise performance data are introduced to close out this chapter. Chapter 5 rounds out the performance section of the book by outlining the equations used to estimate takeoff and landing performance and then describing measurements that must be taken to document appropriate measures of merit during these critical phases of flight.

The second half of the book deals with aircraft stability and control, concentrating on measurements that must be made to ascertain flying qualities. Chapter 6 covers the foundations of longitudinal static stability, concluding with a discussion of the flight test techniques often used to obtain such data. Chapter 7 does the same thing for maneuvering stability. Chapter 8 summarizes both the theoretical differences in the equations of motion and the flight test methods used to measure static lateral-directional stability. Chapter 9 is a concise summary of dynamic stability and control for both symmetric (longitudinal) motions and asymmetric (lateral-directional) ones. The importance of qualitative pilot ratings in describing aircraft flying qualities and their usefulness as a communications tool between the test pilot and the test engineer are stressed. The chapter concludes with a discussion of typical flight test techniques, including several practical ways of interpreting dynamic response data. Chapter 10 introduces post-stall flight tests, intending to interest the beginning flight test student in more advanced topics.

Gratitude is due to many people. First and foremost, for their unflagging support, I thank my family, especially my wife, Joyce. It is due to her patience with my early and late hours that the manuscript is finally finished. She also encouraged me throughout my twenty-seven years in the flight test profession, even though she undoubtedly often wondered why I was so obsessed. I thank her and dedicate this effort to her. All the students who have been exposed to my attempts to teach this subject at the United States Air Force Test Pilot School, at Texas A&M, at the University of Kansas, and at the United States Air Force Academy have contributed in no small way to this effort. Finally, thanks are due to all of the colleagues who reviewed these pages. Dr. Richard Howard of the Naval Postgraduate School deserves special mention for his contributions both as a PhD student who understood the practicality of the subject and as a peer who made insightful suggestions. The faculty of the Aerospace Engineering Department at Texas A&M University were wholly supportive, especially Dr. Walter Haisler, Dr. John Junkins, and Dr. Tom Pollock. I hope this subject will provide as much pleasure and challenge to the reader as the writing of this book has brought to me.

Donald T. Ward
March 1993

Preface to the Second Edition

The second edition of **Introduction to Flight Test Engineering** has been expanded to include a new chapter (Chapter 10) outlining the background and techniques used to prepare for aeroelastic flight tests, a subject usually ignored in such an introductory volume. This addition is the major change in this edition. Of course, the other material has been slightly rearranged to accommodate this insertion and known errors in these other chapters have been corrected. Dr. Thomas W. Strganac, joins me in providing this new material. This new addition to the text is based largely on the teaching experience of both authors, notably on their short course, taught since 1991, titled "Hazardous Flight Tests". This course, sponsored by the Continuing Education Division of the University of Kansas, has provided much of the new material. We are very appreciative of the assistance provided by Mrs. Jan Roskam and her staff in this endeavor.

Donald T. Ward
July 1998

Of course, both of us are indebted to even more individuals than were mentioned in the original preface for their help in producing this text. I am indebted to those individuals who provided the many invaluable experiences afforded me during my 15 years as an engineer with NASA and 9 years on the faculty at Texas A&M University. The development and presentation of the "Hazardous Flight Test" short course with my co-author has been an extremely rewarding experience and collaboration. I dedicate my efforts as an engineer, researcher, and professor to my family. Sincere appreciation is given to my wife, Kathy, who has selflessly supported my pursuit of my professional interests. To my son, Christopher, who has begun to build his educational foundation in his desired profession (Paleontology) at the University of Texas, and to my daughter, Kasey, who continues to follow her love of life and horses, I hope the two of you will pursue your dreams with devotion.

Thomas W. Strganac
July 1998

TABLE OF CONTENTS

Chapter.Section _____ Page Number

Chapter.Section _____ *Page Number*

Chapter.Section — Page Number

Chapter.Section _____ *Page Number*

Chapter.Section _____ Page Number

Chapter.Section _____ *Page Number*

Chapter.Section _____ Page Number

CHAPTER 10 (Continued)

Chapter.Section _____ *Page Number*

CHAPTER 11 (Continued)

LIST OF FIGURES

CHAPTER 1

None

CHAPTER 2

CHAPTER 3

LIST OF FIGURES (continued)

Chapter.Figure Number *Page Number*

CHAPTER 4

CHAPTER 5

Chapter.Figure Number _____ Page Number

CHAPTER 6

CHAPTER 7

CHAPTER 8

LIST OF FIGURES (continued)

Chapter.Figure Number _____ *Page Number*

CHAPTER 9

CHAPTER 10

Chapter.Figure Number _____ *Page Number*

CHAPTER 10 (Continued)

CHAPTER 11

Chapter.Figure Number _____ *Page Number*

CHAPTER 11

LIST OF TABLES

LIST OF TABLES (continued)

Chapter.Table Number _____ *Page Number*

CHAPTER 9 (continued)

CHAPTER 10

CHAPTER 11

Chapter 1

PLANNING, DISCIPLINE, AND SAFETY

Flight testing piloted and unmanned aerospace vehicles is an interdisciplinary process fundamental to the development of new systems and to the advancement of aeronautical knowledge. Engineers from all branches of the engineering sciences are needed to successfully put a new system through a thorough and complete flight test program. Aerospace engineers often lead such efforts because of their special familiarity with aerodynamics and the effects of vehicle configuration upon performance and stability and control. Electrical engineers are indispensable in developing appropriate instrumentation, in evaluating feedback control loops, and in evaluating electronic subsystems. Mechanical engineers provide special expertise in designing mechanical, hydraulic and pneumatic subsystems. Computer specialists are essential to a reasonable integration of the on-board computers and their seemingly unlimited capacity to control and display information for the crew or the ground operators. Flight testing is a complex process. It requires many different technical skills, as well as good judgment in managing the process. Therefore, the right place to start a discussion of flight test methods is with a brief philosophy of cost effective flight testing.

1.1 WHY FLIGHT TEST?

Flight test organizations have a reputation for costing too much and taking too much time, the cardinal sins for a program manager. If the test engineer finds a flaw in the design, the usual reply to the recommended fix is: *"We cannot afford such a drastic change!"* or *"Why did you not find the problem in the preliminary tests?"* The flight test team is also the first to hear from the disgruntled user: *"You gave me another piece of junk! Why did you let them send it to the field?"* The implications of these comments (and they are not altogether rhetorical) is that the flight test engineer must do his job well and he must communicate effectively with those who control the purse strings if the product is to be useful. Exactly what is the purpose of flight testing? The introduction to the AGARD Flight Test Manual[1] lists three fundamental reasons for flight testing of piloted aircraft:

- *To determine the actual characteristics of the machine (as contrasted to the computed or predicted characteristics)*
- *To provide developmental information*
- *To obtain research information*

There is no reason to suggest that the testing of unmanned vehicles has purposes different than these basic ones. It is still true that "the proof of the pudding lies in the eating," and it is also still true that aerospace engineering is not an exact science. Some form of measurement must verify all of our theoretical and computed results. Consequently, flight testing is needed and is likely to be an integral part of the development of most if not all aerospace technology for the foreseeable future.

1.2 TYPES OF FLIGHT TESTS

Flight tests can be classified in many ways. Perhaps the most common classification is that associated with the stage of development of the project. The Department of

Defense (DOD) also classifies flight testing as to purpose. We will briefly discuss each of these classifications to introduce the terminology of flight test.

1.2.1 Stage of Development

A better new system depends on new technology. In the aerospace world, new technology inevitably means basic research and much of this research must be empirical. Computational techniques are stretched to the limit to provide design information on unusual configurations. Wind tunnel tests are almost always needed to verify innovative ideas. This tool, given to the aerospace engineer by the Wright Brothers, is invaluable in examining a large number of detailed changes when computational methods are not sufficiently advanced to produce believable results. But even the wind tunnel has its limitations. Stability derivatives obtained from wind tunnel tests should be verified at full scale Reynolds numbers and Mach numbers. Dynamic derivatives calculated from wind tunnel data often do not match the same parameters extracted from flight data. Ultimately, full scale flight tests are required to provide the credibility designers need to create the latest technological advances.

Subsystem technology also must be proved in the environment of flight to be credible. Radar, navigational systems, flight management systems, integrated displays, flight control systems, electro-optical target designator systems, defensive avionics systems, and communications systems are but a few of the subsystems that are sensitive to flight environments and therefore are frequently flown as breadboard and/or advanced developmental models on testbed aircraft before they are installed as part of the vehicle they were designed to enhance and support. Again, flight test is essential to the orderly development of such subsystems.

As the cost of operating new aircraft and missiles goes up, the domain and respectability of simulation grows. Commercial airline operations now do almost all of their training in new systems on sophisticated simulators and the military services are following suit. Once again, though, credible simulation demands a credible data base to guarantee the fidelity of the mathematical model. If the data base is accurate, simulators are welcomed. If not, they are ignored. All too often, simulator manufacturers have found, to their chagrin, that computed or wind tunnel estimates of the coefficients of the equations of motion were not the same as those experienced in flight. Flight tests usually pointed the way to changes that satisfied the users' demands. But all too often these flight tests were repetitions of tests done earlier and were therefore wasteful of precious time and money. As a result, many programs now include flight test data as a requirement to verify simulation models.

Prototypes of airplanes, helicopters, and missiles have always provided flight test answers that are believable. Historically, military systems have heavily leaned on prototyping to insure that performance and handling qualities goals were met. Since the early 1970's, the YF-22 and YF-23, the YF-16 and YF-17, the YA-9 and YA-10, and the AGM-109 and AGM-85 developments were all head-to-head flight test competitions between competing prototypes. All three are examples of the "fly-before-you-buy" concept of the DOD. Most major manufacturers of general aviation aircraft fly prototypes to check their design assumptions before committing to production. Examples of such general aviation prototypes include the Mooney M301, the Beech Starship, and the Piper Malibu. As can be inferred from these examples, prototype testing does not always lead to production. Often it leads to further development or even cancellation of a marginal design.

For all aircraft, military or civilian, the real development of a design is done on aircraft specifically built for certification (for civilian designs) or full-scale development (for military) purposes. These aircraft are one step removed from their prototype cousins, but in some cases are later modified to the production configuration. All too often, especially for complex designs, such modifications are too expensive or too extensive to be practical and these developmental aircraft become museum pieces. These aircraft usually carry a considerable amount of instrumentation specified by the flight test team to provide the data and measurements the designers need. These full scale development programs are the best opportunity for the flight test team to contribute to the improvement of the design. Because the aircraft are specifically set aside for the certification or development process, and because of the instrumentation available, shortcomings can be discovered during this phase of flight testing. Furthermore, they can be more easily corrected during this relatively early stage of design evolution. But the burden of getting everything right with only one chance to make the correction falls to the flight test team during this period. If discrepancies are missed here, the operator is justified in questioning the professionalism of the flight testers involved.

On more complex systems, there is usually a further period of refinement after the production configuration is frozen. Changes required at this point are much more costly to introduce into the production line and consequently flight tests are usually the only credible way to validate their usefulness. This follow-on developmental testing (after a production decision) is particularly appropriate if the total aerospace system is heavily dependent upon a rapidly changing technology. The current generation of military aircraft that take advantage of digital electronics in everything from cockpit displays to flight controls is a classic example. More often than not such improvements are introduced into the production line after some number of systems have been built. Follow-on development gives rise to different models of the same aircraft or missile, often with very different capabilities even though the external configuration of the machines may be quite similar.

1.2.2 Developmental Versus Operational Testing

Within the DOD, there has been a strong push for more user-oriented flight testing since a Blue Ribbon Defense Panel commissioned by then President Nixon recommended stronger emphasis on operational suitability testing in its report issued in July 1970. The net result was establishment of an independent operational test and evaluation (OT& E) agency within each of the services and a stronger integration of the eventual users of military systems into the development process. To quote one who was directly involved in the process, "the entire flight test portion of the acquisition cycle became a complex integration of tasks shared by the contractor, developing command, and using command."[2]

Developmental Test and Evaluation (DT&E) is defined[3] as:

> *...test and evaluation conducted to assist the engineering design and development process and verify the attainment of technical performance specifications and objectives.*

The flight test activity necessary to produce a system that meets its design goals clearly fits this definition. But it is not always clear just where DT&E ends and OT&E be-

gins, especially when the two are carried out concurrently as is the case during the initial stages of OT&E. Operational Test and Evaluation is defined[3] as:

> *...test and evaluation conducted to establish a system's operational effectiveness and operational suitability, identify needed modifications, and provide information on tactics, doctrine, organization, and personnel requirements.*

The key words here are operational suitability. They have led to testing under more realistic operational conditions than was formerly done: simulated enemy defenses for survivability, user maintenance rather than contractor support, and actual or simulated malfunctions. Flight testing for airborne systems fits naturally into this expanded requirement. Operational testing is meant to provide credible information for decision makers prior to commitment to production of expensive weapons systems.

1.3 FACTORS TO BE CONSIDERED IN TEST PLANNING

Testing airborne vehicles is a complex and interrelated process. To do this job effectively requires careful and detailed planning. One of the best measures of efficiency for a flight test team includes both time and dollar cost of the test program. Ultimately, the test manager will be graded on these two factors as well as the completeness and the accuracy of the information collected. The most significant cost for any program often occurs when safety considerations are ignored. Therefore, safety should be one of the dominant concerns throughout the planning and conduct of any series of flight tests.

1.3.1 Safety

Flight testing always carries some element of risk. One cannot fly without the possibility of having an accident. Nonetheless, a strong consciousness of risks taken and a concerted effort to reduce the probability of failures along with anticipation of the consequences of malfunctions must be a part of the planning process. Naturally, safety in the tests begins with the design. But the test team also has the obligation to review and question every aspect of the testing for unseen dangers. Loss of a multi-million aircraft or spacecraft during the flight test development program can "cancel" a development. What do you suppose might have happened to the NASA budget if a space shuttle orbiter had been lost on an early test flight? No one knows, of course, but at the very least the loss would have had grave consequences, not to mention the dollar cost of replacing it. Now, let's look at some of the ways that careful test planning can minimize risks.

In the early stages of test planning, listen to all interested parties. Though this conferring with others will take time, it is usually time well-spent. Specifically ask experts in each subdiscipline to surface any potential safety hazards just as religiously as they do needs for data. Then, ask safety specialists to analyze each hazard as to severity and consequences. Strive for continuity in the group which does this early planning; preferably, each member would stay on the test team and be accountable for his or her inputs throughout the test program. Make sure that this overall plan is put in writing and reviewed by each person; this step will often discourage second-guessing and is the test manager's best protection. Do not skimp on early test planning.

After the overall test plan has been hammered out, detailed planning for each test and each flight must continue. The engineer should maintain a careful matrix of required data and insure that the test crews understand exactly what is required on each flight. **Never**

go beyond what has been planned on a particular flight. This cardinal rule prevents surprises and dictates that considerable thought be given to test cards. These cards should be complete, but readily understood. It is the responsibility of the flight test engineer in charge to be sure that these reminders are in good order. Test cards should include more data requirements than can be collected on the mission that is planned; never let your flight test crew run short of things to do. There also should be alternative data requirements specified in case instrumentation malfunction or weather limitations prevent collecting the primary data.

Safety in test flying has not always been paramount, but at today's prices (in dollar cost for hardware and in opportunity cost for highly visible programs) no one can afford to treat risks lightly. Planning and attitude toward safety are all important.

1.3.2 Cost

The cost of flight testing is staggering. It is therefore up to responsible engineers to consider the cost of each test to be done, to look for ways to reduce that cost, and to question the value of the data to be collected. *Why am I doing this test?* is always a good first question. Some of the items that drive the cost of a test are: ground support needed; required (not desired) instrumentation; and the flying time required.

Ground and airborne support should be kept as simple as possible, consistent with the risks inherent in the tests, the complexity of the test, and the required information. It may be as simple as a mechanic to service the airplane and as complex as linked telemetry ranges to cover the complete flight profile. Question everything: *Is telemetry necessary? Do we need continuous radio communication? How much redundancy in measurements is enough? How many samples of data do we really need? Can we combine tests? Are chase aircraft really needed? Is real-time data reduction essential or nice to have? Is there a source of support available at better rates? What kind of flexibility is there in the range schedule?* Each of these questions leads to options and alternatives; all the good test planners keep their options open.

Instrumentation is one of the most difficult (and often most costly) technical area for flight testers. Skimping on instrumentation can lead to poor data or even no data. You may have to repeat the test--late, of course--if you accept inadequate instrumentation. At the other extreme, complexity in the instrumentation package can buy more downtime than the program can stand.

Finally, every bit of time spent in the air must be used productively. The utilization of flying time can be improved by combining tests; for example, collect data on the environmental control subsystem while flying low altitude performance tests. The time from takeoff to data altitude is often of low value. Aerial refueling, for airplanes equipped to refuel in-flight, can multiply productivity of test time. Real-time data reduction, though it requires complex instrumentation and extensive ground support, can significantly speed up some tests and preclude repeating flights. Choose the time of day (or night) that not only suits your test requirements, but that gives you the most efficiency in data collection. Allow time for the maintenance crews to properly prepare the aircraft and the instrumentation; overscheduling of flights can be counterproductive. Productive flying time is time when you collect useful data during flight testing; use it completely and wisely.

1.3.3 Schedule

Meeting a schedule is a fact of life for flight test, as it is in all other facets of engineering. For the company building civilian aircraft, missing a certification date often means lost sales and a poor marketing image. For the military customer, schedule slips can force a complete alteration in force structure--and, in the worst case, a return to Congress for approval of changes. Usually, the military contractor suffers contractual penalties when delays occur. Quite literally, time is money; plan wisely to meet the schedule.

If you are using government-owned ranges or even ground support facilities that do not belong to your organization, a schedule slip can put you off the schedule. Provision for rescheduling tests must be addressed in the original master test plan. Be sure you know what kind of scheduling flexibility is available and then conduct your test so as to never exercise that flexibility.

A major factor in meeting the test schedule is how many test vehicles are allocated to the flight test program. This factor can be particularly troublesome if the vehicles are expendable, as in tactical missiles or other unmanned vehicles. Reducing the number of prototypes or developmental aircraft is a favorite way of cutting the cost of a flight test program. It is up to the test manager to be sure his ability to meet the schedule is not removed along with the "excess" cost.

1.4 SUMMARY

Flight testing is one of the most exciting and at the same time, challenging, of all engineering problems. Early and meticulous planning is mandatory to keep safety, cost, and schedule considerations in balance. Discipline is essential throughout the process to stick to the plan and to make judicious revisions to it. Good flight testers are team workers, recognizing that collective judgment sometimes outweighs the advantage of quick decisions by a single individual. Ultimately, flight test provides both objective and subjective measurements that prove or disprove the designer's dream.

REFERENCES

1 Perkins, C. D., Dommasch, D. O., and Durbin, E. J. (Editors), **AGARD Flight Test Manual**, Pergamon Press, New York, 1959.

2 Van Pelt, L. G., "Flight Test Concept Evolution," AIAA Paper 81-2375, AIAA/SETP/SFTE/SAE/ITEA/IEEE 1st Flight Testing Conference, Nov. 11-13, 1981, Las Vegas, Nevada.

3 DODD 5000.3, "Test and Evaluation," Department of Defense, Dec. 26, 1975.

Chapter 2

PITOT-STATIC SYSTEM CALIBRATION

The nature of the atmosphere, more than any other set of conditions, determines the performance and handling qualities of an aircraft. Capriciously, it seems at times, the atmosphere's variables change continuously so that no two flight tests produce the same results unless the data are meticulously reduced to standard conditions. The performance and flying qualities of different vehicles can be rationally compared only on this basis. Thus, the flight test engineer spends an enormous amount of time and care ensuring that his measurements are corrected for non-standard atmospheric conditions. The subjects of this chapter are the characteristics of the standard atmosphere and the airspeed and altitude indicating systems on an airplane. The altimeter and airspeed indicator can be corrected for certain errors inherent in pressure-based measurement systems and those corrections are the subject of this chapter.

2.1 THEORETICAL FOUNDATIONS

2.1.1 Standard Atmosphere

Model atmospheres have been in existence for decades though in the United States the space program has dictated changes in and experimental verification of new atmospheric models time and again[1,2,3]. Internationally, the International Commission of Air Navigation (ICAN) Standard Atmosphere[4] was commonly used for many years. In 1952 the slight differences in the ICAN and NACA standard atmospheres were reconciled and the International Civil Aviation Organization (ICAO) Standard Atmosphere[5] became the international standard for member nations. In 1953 a committee was formed to extend the standard atmosphere and by 1956 the ICAO atmosphere had been extended to 300 kilometers. Further extensions were proposed in 1962 and again in 1975 as a result of the collection of more experimental data. In 1975 the International Organization for Standardization adopted a standard atmosphere which is virtually identical to the ICAO standard atmosphere up to 50 km, but also includes data up to 80 km. All of these standard atmospheres are quite similar, but the latter one is perhaps the most up-to-date. Many tabulations of these standard atmospheres have been published and we will not add to the size of this book by adding yet another such tabulation. Instead, the student is encouraged as a homework exercise to write a computer program that calculates the properties of the standard atmosphere.

Before briefly reviewing the theory of the standard atmosphere it is essential to define certain terms and restate the assumptions used. There are a variety of altitude definitions used in the literature and there is considerable ambiguity in usage. In this book the following definitions will be used consistently. However, the careful student must confirm the meaning of various terms in other sources. **Geometric altitude**, h_g, is the tapeline vertical distance from mean sea level to the point in question. Sometimes this altitude is also called **true altitude**. **Pressure altitude**, h_p, is the geometric altitude in a standard atmosphere at which a given pressure is found[6]. A properly calibrated altimeter, set to 29.92 inches of mercury (in. Hg), indicates pressure altitude. The altimeter must be set to this value by the flight test crew during all tests so that data can be referenced to this standard pressure. **Density altitude**, h_ρ , is the geometric altitude in a standard atmosphere at which a given density occurs. Unlike pressure, density is measured indirectly;

that is, it is calculated from measurements of pressure and temperature. Density altitude is of utmost concern in predicting available thrust or power from the propulsion system. **Absolute altitude**, h_a, is the distance measured from the center of the earth to the point in question. This altitude is of prime concern in orbital mechanics because the local gravitational acceleration, g, is a function of altitude.

$$g = g_0\left(\frac{R_E}{h_a}\right)^2 = g_0\left(\frac{R_E}{R_E + h_g}\right)^2 \tag{2.1}$$

where R_E is the radius of the earth.

Finally, **geopotential altitude**, h, is a fictitious altitude obtained from geometric altitude by assuming g is a constant from mean sea level up to any altitude.

$$dh = \frac{g}{g_0}dh_g, \text{ or integrating to get: } h = \left(\frac{R_E}{R_E + h_g}\right)h_g \tag{2.2}$$

For practical atmospheric flight the assumption that g is a constant introduces very little error. Below 200,000 feet the error in assuming that $h = h_g$ is less than 1%[7]; thus, for airplanes operating in the atmosphere, the assumption that h and h_g are equal is justified.

The standard atmosphere now widely accepted is based on the following assumptions meant to approximate atmospheric conditions at 40° North Latitude.

- Air is a perfect gas obeying the equation of state: $p = \rho RT$ (2.3)
  where $R = 1716.55$ ft^2/sec^2°R; T is the absolute temperature in °R.
  This assumption is valid up to a height of about 55 miles, where dissociation effects begin to play a major role.
- Temperature varies with altitude according to: $T = T_i + k_i(h - h_i)$ (2.4)
  where k_i is the lapse rate for the altitude band $h - h_i$; k_i, T_i, and h_i are given in Table 2.1 for altitudes up to 90 km (approximately 295,000 ft).

TABLE 2.1 Constants for the Standard Atmosphere

Index i	Lapse Rate k_i (°R/ft)	Base Temperature T_i (°R)	Base Geopotential Altitude h_i (ft)
0	-0.00356616	518.67	0.000
1	0.00000000	389.97	36,089.239
2	0.00054864	389.97	65,616.798
3	0.00153619	411.57	104,986.878
4	0.00000000	487.17	154,199.475
5	-0.00109728	487.17	170,603.675
6	-0.00219456	454.17	200,131.234
7	0.00000000	325.17	259,186.352

- Standard sea level conditions are:
  $p_0 = 2116.22$ psf = 760 mm Hg = 29.921 in Hg = 1.013250×10^5 N/m^2
  $T_0 = 518.67$ °R = 288.15 °K
- The gravitational constant is: $g_0 = 32.17405$ ft/sec^2 = 9.80665 m/sec^2
- Relative humidity is taken to be zero (dry air).

The standard atmosphere, based on the above assumptions, is built upon eqns. (2.3), (2.4), and the hydrostatic equation which results from summing the pressure forces and the gravitational forces acting on a unit element of air as shown in Fig. 2.1. This summation gives: $p - (p + dp) - \rho g_0 dh = 0$. Assuming that g_0 is a constant over the altitude interval of interest allows us to integrate the resulting hydrostatic equation. This assumption also makes the altitude in eqn. (2.5) geopotential altitude.

$$dp = -\rho g_0 dh \tag{2.5}$$

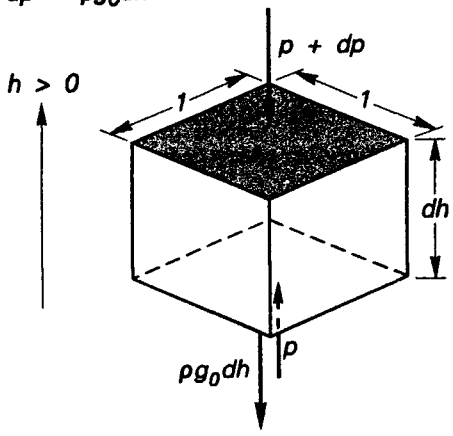

Fig. 2.1 Pressure Forces Acting on a Unit Element of Air

Combining eqns. (2.3) and (2.5): $\frac{dp}{p} = -g_0 \frac{dh}{RT}$

Recalling that $\frac{dT}{dh} = k_i$ and, if $k_i \neq 0$, $\frac{dp}{p} = -g_0 \frac{g_0 dT}{k_i RT}$

On the other hand, if $k_i \neq 0$ (the isothermal case), $\frac{dp}{p} = -\frac{g_0 dh}{RT}$

Integrating each of these expressions is straightforward; first, with $k_i \neq 0$,

$$ln\frac{p}{p_i} = -\frac{g_0}{k_i R} ln\frac{T}{T_i}$$

then, with $k_i = 0$, $ln\frac{p}{p_i} = -\frac{g_0}{k_i RT_i}(h - h_i)$.

Substituting eqn. (2.4) into the first of these expressions yields:

$$\frac{p}{p_i} = \left(1 + \frac{k_i}{T_i}(h - h_i)\right)^{-\frac{g_0}{k_i R}}, \; k_i \neq 0 \tag{2.6a}$$

The second expression becomes:

$$\frac{p}{p_i} = e^{-\frac{g_0}{T_i R}(h - h_i)}, \; k_i = 0 \tag{2.6b}$$

Utilizing the equation of state, eqn. (2.3), density can be similarly expressed as a function of geopotential altitude.

$$\frac{\rho}{\rho_i} = \left(1 + \frac{k_i}{T_i}(h - h_i)\right)^{-\frac{g_0}{k_i R} - 1}, \quad k_i \neq 0 \tag{2.7a}$$

$$\frac{\rho}{\rho_i} = e^{-\frac{g_0}{T_i R}(h - h_i) - 1}, \quad k_i = 0 \tag{2.7b}$$

Equations 2.6 and 2.7 apply to any region in the standard atmosphere, where, as noted before, we assume a constant temperature lapse rate. In the troposphere, $i = 0$ and standard sea level conditions are the relevant initial conditions. In the stratosphere, the index $i = 1$ and $k_1 = 0$, $T_1 = 389.97$ °R. Similarly, constants corresponding to $i = 2,3,...,7$ represent the standard atmosphere in higher regions. That is, a standard temperature variation, based on experimental evidence, along with eqns. (2.6) and (2.7), plus the equation of state, completely define a standard atmosphere.

Standard atmospheres are frequently tabulated in non-dimensional form for pressure, density, and temperature. These non-dimensional variables are defined by simply dividing each property by its counterpart at standard, sea level conditions.

$$\delta = \frac{p}{p_0} \qquad \sigma = \frac{\rho}{\rho_0} \qquad \theta = \frac{T}{T_0} \qquad \delta = \sigma\theta \tag{2.8}$$

□

The last expression is simply the equation of state written in non-dimensional terms.

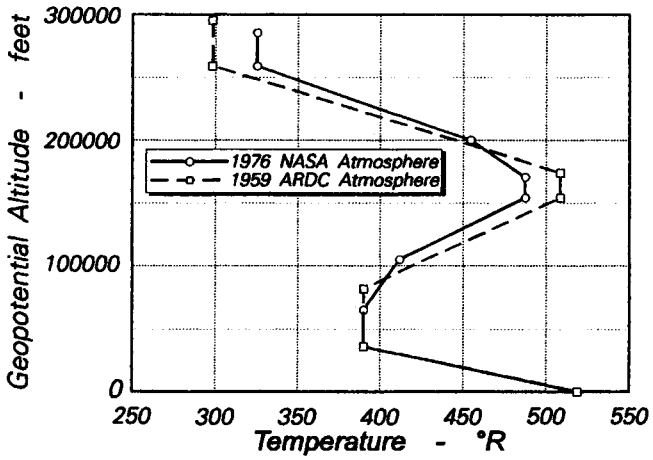

Fig. 2.2 Temperature Variations for Two Standard Atmospheres

Figure 2.2 compares the temperature variation in the standard atmosphere we will use (1976 NASA Standard Atmosphere) with an earlier standard atmosphere.

Example 2.1: Calculate δ, σ, and θ for standard day geopotential altitudes of 10,000 feet and 40,000 feet.

At $h = 10{,}000$ feet, use eqn. (2.4) to directly calculate the temperature ratio.

$$\theta_{10K} = \frac{T}{T_0} = 1 + \frac{k_0(10000 - 0)}{T_0} = 1 + \frac{(-0.00356616)(10000)}{518.67} \qquad \boxed{\theta_{10K} = 0.9312}$$

Equation (2.6a) gives δ_{10K}

$$\delta_{10K} = \frac{p}{p_0} = \theta_{10K}^{-\frac{g_0}{k_0 R}} = \theta_{10K}^{-\frac{32.17405}{(-0.00356616)(1716.55)}} = \theta_{10K}^{5.2559}$$

$$\boxed{\delta_{10K} = 0.6877}$$

Equation (2.7a) gives σ_{10K}

$$\sigma_{10K} = \frac{\rho}{\rho_0} = \theta_{10K}^{-\frac{g_0}{k_0}-1} = \theta_{10K}^{4.2559}$$

$$\boxed{\sigma_{10K} = 0.7385}$$

For h = 40,000 ft, use eqn. (2.4) again with $k_1 = 0$

$$\boxed{\theta_{40K} = 0.7519}$$

$$\theta_{40K} = \theta_{tropopause} = \frac{389.97}{518.67}$$

$$\delta_{tropopause} = \theta_{40K}^{5.2559} = (0.7519)^{5.2559}$$

$$\frac{p_{40K}}{p_{tropopause}} = 0.22336$$

$$\frac{p_{40K}}{p_{tropopause}} = e^{-\frac{g_0}{RT_1}(h-h_1)} = e^{-\frac{32.17405}{(1716.55)(389.97)}(40000-36089.239)} = 0.82864$$

$$\delta_{40K} = \frac{p_{40K}}{p_{tropopause}} \frac{p_{tropopause}}{p_0} = (0.82864)(0.22336)$$

$$\boxed{\delta_{40K} = 0.1851}$$

$$\frac{p_{tropopause}}{p_0} = \theta_{40K}^{-\frac{g_0}{k_0 R}-1} = \theta_{40K}^{4.2559} = 0.29707 \text{ and using } \frac{p_{40K}}{p_{tropopause}} = 0.82864 \text{ again}$$

$$\sigma_{40K} = \frac{\rho_{tropopause}}{\rho_0} \frac{p_{tropopause}}{p_0} = (0.29707)(0.82864)$$

$$\boxed{\sigma_{40K} = 0.2462}$$

2.1.2 Airspeed Theory

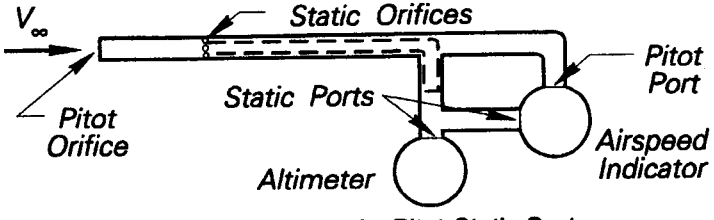

Fig. 2.3 Schematic Diagram of a Pitot-Static System

Having specified a standard medium in which airplanes typically operate, we now must develop airspeed measuring equations. Both altitude and airspeed measuring systems are typically pressure sensing systems as Fig. 2.3 suggests. However, an airspeed indicator (ASI) measures differential pressure while an altimeter measures absolute pressure. Both use the same static pressure source, but an ASI measures the pressure difference between impact pressure (sensed at the total head orifice) and static pressure. Writing Euler's equation for steady, streamline flow:

$$\frac{dp}{\rho} + VdV = 0$$

Integrating gives either the incompressible or the compressible Bernoulli equation:

$$p + \frac{\rho V^2}{2} = \text{constant (incompressible), or } \int \frac{dp}{\rho} + \frac{\rho V^2}{2} = \text{constant (compressible)}$$

For an isentropic process, $\left(\frac{p}{\rho}\right)^{\gamma} = \left(\frac{p_T}{\rho_T}\right)^{\gamma} = \text{constant}$. A convenient form of the compressible Bernoulli equation results after solving for ρ and integrating:

$$\frac{\gamma p}{\rho(\gamma - 1)} + \frac{V^2}{2} = \text{constant} \tag{2.9}$$

If eqn. (2.9) is applied to the flow into the total head orifice of the ASI where $V_\infty = 0$ and to the streamline flow past the static orifices in the pitot-static system,

$$\frac{\gamma p}{\rho(\gamma - 1)} + \frac{V^2}{2} = \frac{\gamma p_T}{\rho_T(\gamma - 1)}$$

The differential pressure sensed by a conventional pitot-static system, q_c, is not simply the dynamic pressure, though it has a similar form as we shall see in eqn. (2.14):

$$q_c = p_T - p = p\left(\frac{p_T}{p} - 1\right)$$

Isentropically, $\frac{p_T}{p} = \left(1 + \frac{\gamma - 1}{2} M^2\right)^{\frac{\gamma}{\gamma - 1}}$, so

$$\frac{q_c}{p} = \left(1 + \frac{\gamma - 1}{2} M^2\right)^{\frac{\gamma}{\gamma - 1}} - 1 = \left(1 + \frac{\gamma - 1}{2} \frac{V^2}{\gamma RT}\right)^{\frac{\gamma}{\gamma - 1}} - 1 \tag{2.10}$$

Solving for V and multiplying both sides by $\sqrt{\sigma}$:

$$V\sqrt{\sigma} = \sqrt{\frac{2\gamma p}{(\gamma - 1)\rho_0}\left(\left(\frac{q_c}{p} + 1\right)^{\frac{\gamma}{\gamma - 1}} - 1\right)} \tag{2.11}$$

Careful examination of eqns. (2.10) or (2.11) reveals that calibrating a differential pressure gage (which the ASI is) in velocity units is not as easy as it first appears. Pressure and/or density are different at each pressure altitude and, even with V as the measure of velocity, that means a new scale would be needed for each pressure altitude. Such scaling is obviously impractical and in 1925 the U. S. Army and Navy agreed upon a scale based on standard day sea level conditions[6]. Virtually all airspeed indicators in the United States are based on this **calibrated airspeed** which is defined by:

$$V_{cal} = V\sqrt{\sigma}\big|_{\rho = \rho_0} \tag{2.12}$$

where $\sqrt{\sigma}$ is evaluated at standard day sea level pressure (but not necessarily standard day sea level temperature).

$$V_{cal} = \sqrt{\frac{2\gamma p_0}{(\gamma-1)\rho_0}\left(\left(\frac{q_c}{p_0}+1\right)^{\frac{\gamma}{\gamma-1}}-1\right)} \tag{2.13}$$

For incompressible flow, the difference between total and static pressure is **dynamic pressure**, q, which is a measure of the kinetic energy of a unit volume of air. It is not identical to q_c; the two parameters are equal only for incompressible flow. For incompressible flow, $V\sqrt{\sigma} = \sqrt{\frac{2q}{\rho_0}}$, if $V < 200$ mph and $h_p < 15000$ ft.

$$q = p_T - p = \frac{\rho V^2}{2} \tag{2.14}$$

Equivalent airspeed is the name given to $V\sqrt{\sigma}$ and is a direct measure of the kinetic energy of a volume (V) of moving fluid.

$$V\sqrt{\sigma} = V_e \tag{2.15}$$

$$\text{Kinetic energy} = \frac{mV^2}{2} = \frac{\rho V V^2}{2} = \frac{\rho_0 V V_e^{\,2}}{2}$$

Equivalent airspeed appears in all force and moment equations and therefore commonly correlates directly to structural loads on the airframe. Relating the ASI reading and V_e clearly requires a correction.

$$\frac{V_e}{V_{cal}} = \sqrt{\frac{p\left(\frac{q_c}{p}+1\right)^{\frac{\gamma-1}{\gamma}}-1}{p_0\left(\frac{q_c}{p_0}+1\right)^{\frac{\gamma-1}{\gamma}}-1}}$$

This ratio has been tabulated[8] for ease of use or, more commonly, the difference between V_{cal} and V_e is plotted as a function of pressure altitude and calibrated airspeed (Fig. 2.4). This correction term has been erroneously called a "compressibility" correction; though as the preceding development shows, it is merely the result of a choice of airspeed indicator calibration constants and has nothing to do with compressibility itself.

$$\Delta V_c = V_e - V_{cal} \tag{2.16}$$

One final type of airspeed, **indicated airspeed**, must be defined for flight test data reduction. It is simply the dial reading from the specific differential pressure gage used. Each such gage used in experimental work should be calibrated periodically with a known differential pressure source against eqn. (2.13). A record of the deviations must be maintained for each ASI by serial number if precise data reduction is to be done. Altimeters should also be calibrated periodically in a similar manner.

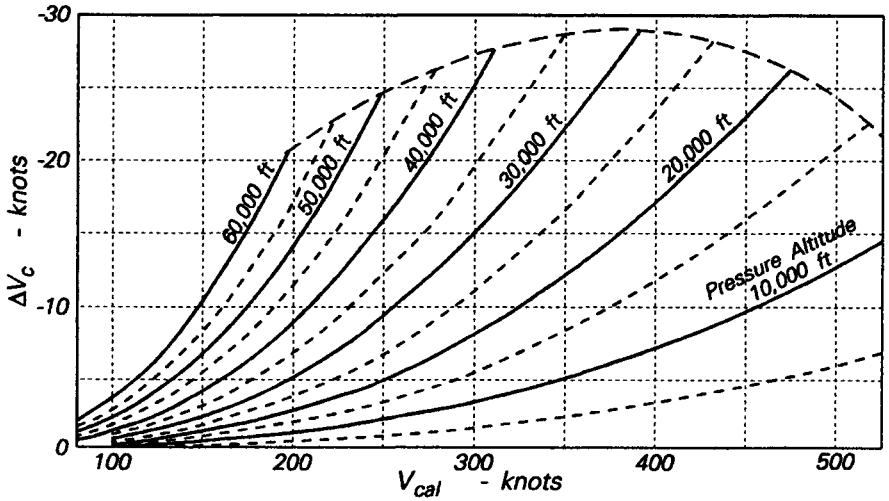

Fig. 2.4 Correction Factor (ΔV_C)

Example 2.2: A high altitude remotely piloted vehicle (RPV) is flying at a pressure altitude of 40,000 feet where the temperature is -47°F. If the RPV's airspeed indicator is perfect, and it registers a calibrated airspeed of 200 KCAS, what is the true airspeed?
At 200 KCAS and $h_p = 40{,}000$ feet, Fig. 2.4 gives: $\Delta V_c = -9$ kts $= V_e - V_{cal}$
$V_e = V_{cal} + \Delta V_c = 200 - 9 = 191$ KEAS
To obtain TAS, $V_e = V\sqrt{\sigma}$ and $h_p = 40{,}000$ feet implies p in a standard atmosphere; ρ can be calculated from eqn. (2.3), knowing both p and T_0. Using the results from Example 2.1 for $\delta = 0.1851$ and then calculating ρ from the given data, $\theta = 0.7956$, $\sigma = \frac{\delta}{\theta} = 0.1473$. So, $V = \frac{191}{\sqrt{0.1473}} = 396 knots$.

So far, our discussion has assumed no error in measurement of p_T and p, but there are a number of measurement uncertainties that must be considered.

2.1.3 Pitot-Static Measurement Errors

The pitot-static system suffers from all of the following errors:

- instrument error
- pressure lag error
- position error

Each of these errors will be defined and their relative importance will be discussed in this section.

2.1.3.1 **Instrument Error**. Instrument error is simply the deviation of the instrument indications from a known differential pressure standard. It results from imperfections in the gage itself and is typically measured in a calibration laboratory with the instrument disconnected from other parts of the pitot-static system. A concise description of laboratory calibration procedures is given by Gracey[10]. Several factors contribute to instrument error: scale error, manufacturing deviations, magnetic fields, temperature fluctuations, coulomb and viscous friction, and the inertia of moving parts.

Several points must be kept in mind when calibrating airspeed indicators in the laboratory for instrument error. These differential pressure gages may be calibrated statically and dynamically. Typically, the static calibration is sufficient for most flight test measure-

ments. Data should be taken in both directions so that hysteresis can be determined. If hysteresis loops are significant, the instrument should not be used for data collection. An instrument vibrator may reduce the effects of hysteresis, but care in design of the vibrator is essential to avoid electronic interference with data acquisition or with communications. Laboratory calibration data must be checked carefully for repeatability, and if it is not up to standard, the instrument should not be used for data collection. Wear will obviously change the calibration of an indicator over time. Consequently, a high rate of change in the calibration is an indication of wear reaching an unacceptable level.

Instrument corrections are usually given as the differences between instrument corrected values and gage readings. Notice that we now begin using $_{ic}$ as a subscript to imply readings that have been corrected using laboratory calibration data for a specific instrument. Also, an $_{i}$ subscript alone refers to the actual gage reading at a given condition. The corrections determined by such a ground calibration for each gage are:

$$\Delta V_{ic} = V_{ic} - V_i \tag{2.17}$$

$$\Delta h_{ic} = h_{ic} - h_i \tag{2.18}$$

These corrections can be either positive or negative depending on the particular instrument. A typical altimeter correction curve is given in Fig. 2.5.

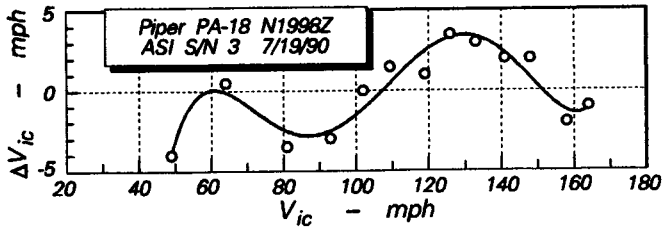

Fig. 2.5 Instrument Error Calibration Curve

2.1.3.2 **Pressure Lag Error**. Any pressure sensing system, like the conventional aircraft pitot-static sensing system, is subject to errors due to time delay in transmitting the pressure from the point of measurement to the sensor. In an airplane, this error is typically significant only when rates of change of pressure are high, such as in a rapid climb or descent. For a given rate of change of pressure, the lag error depends primarily on the length and diameter of the pressure tubing and the volume of the instruments. Obviously, a leak in the pressure lines will also affect the lag error. In all cases the lag error is proportional to the pressure drop through the system lines from the pressure orifice to the pressure indicator.

The flow rate of the air in the system sets the lag error because of two types of time-dependent phenomena. First, acoustic lag occurs because the pressure changes are transmitted through the lines at the speed of sound. Since the speed of sound at low altitudes is typically on the order of 1000 fps, tubing lengths must be quite long before acoustic lag is significant. For most systems and flight envelopes, acoustic lag can be safely ignored. Second, and more important for practical flight test considerations, the air flowing in the lines produces a pressure drop. Following Gracey[10], the lag constant due to pressure drop with laminar flow in the tubing is:

$\lambda = p\frac{\Delta p}{\Delta t}$ or, for laminar flow in the tubing: $\lambda = \frac{128mLC}{pd^4p}$ (2.19)

where L = length of tubing,
μ = viscosity of air,
d = internal diameter of tubing,
p = nominal pressure, and
C = volume of instrument chamber.

Once λ is known for a given system and a specified flight condition, the pressure drop Δp can be estimated for a given rate of climb or descent, which we will specify as $\frac{\Delta p}{\Delta t}$. Remember, eqn. (2.19) is valid only for laminar flow in the pressure lines and the limiting pressure drop for straight tubing is approximately:

$$\frac{\Delta p}{L} = \frac{p_0}{p}\left(\frac{\mu}{\mu_0}\right)^2\left(\frac{0.0065}{d^3}\right) \quad (2.20)$$

When lag error must be known with greater precision or when the laminar flow assumption is not warranted, the lag can be determined experimentally with procedures described by Huston[11].

Because the static portion of the system typically has line lengths considerably greater than those for the pitot portion, the pressure lag errors in the airspeed indicating system are not "balanced." The lag in the static measurements will be considerably less than the lag in the pitot pressures. This imbalance is a dynamic imbalance since it depends on differing flow rates in each set of lines. It may be necessary to measure these errors experimentally as Wildhack[12] has suggested, but a more pragmatic approach suggested by Hamlin[6] is to merely add volume to the pitot lines. In a pressure chamber the volume (or length of tubing) needed can be determined readily by changing the pressure at a rate commensurate with those encountered in representative maneuvers. Balancing the system in this fashion may cause significant errors for maneuvers other than those simulated by the balancing procedure. Reducing lag error is essentially a pitot-static system design problem. The basic goal should be to keep line lengths as short as possible. Both acoustic lag and pressure drop lags depend directly on line length. Pressure drop, the dominant lag error in most installations, can also be minimized by increasing tube diameter or reducing instrument volume. Bends and connections in the pressure lines should also be kept to a minimum. Electronic pressure transducers now in use are small enough both to help reduce line length (when mounted close to their sensing orifices) and to keep the instrument volume low.

2.1.3.3 **Position Error**. Position error in pitot-static systems comes from two sources: 1) location of the static source in the pressure field of the aircraft and 2) the shape of the total pressure head or the flow direction relative to it.

Of these two errors, the first is of most concern in flight test measurements, simply because careful attention to design of the total pressure head will reduce the total pressure position error to a negligible value. Obviously, the total pressure pickup cannot be located behind a propeller, in the wing wake, in the boundary layer, or in or behind a region of supersonic flow without inducing errors. (The effect of a shock wave produced by a properly shaped total pressure probe can be accounted for through the Rayleigh for-

mula.[13]) Once a suitable location for the total pressure sensor is selected, the shape of the sensor surface and the flow direction determine the pitot head position error. The shape must be suited to the application, but adequate design information is available, with Gracey's work a standard[10]. Probes designed with care sense no significant total pressure error at flow inclinations of up to approximately 20°. For this reason, total pressure error is usually ignored in pitot-static calibrations.

It is not generally possible, however, to eliminate static pressure position errors because the pressure field depends on Mach number, Reynolds number, angle of attack, and sideslip angle. With such an array of variables to be considered, rarely can a location for the static source be found so that the sensed pressure will be freestream static pressure throughout the flight envelope. The effects of flow inclination (α and β) can be minimized by manifolding two or more orifices on opposite sides of the aircraft or, on boom installations, by drilling static ports circumferentially. Figure 2.6 illustrates how locations can be chosen to minimize static pressure error for a subsonic airplane. Figure 2.7 likewise illustrates guidelines for choosing static pressure locations for a pitot-static boom mounted on the nose of a supersonic airplane.

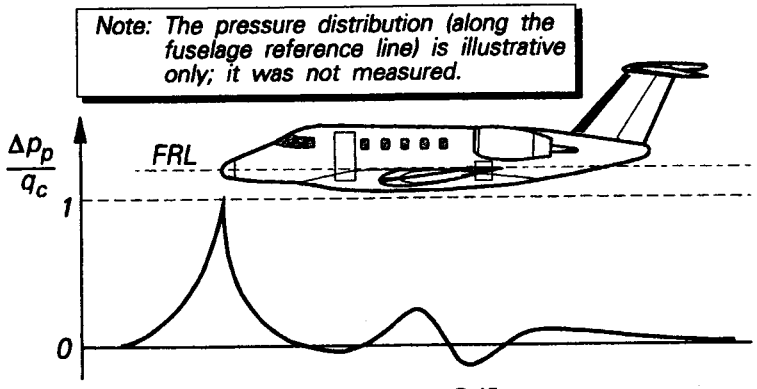

Fig. 2.6 Locations for Static Pressure Orifices

Static position error can now be defined quantitatively.

$$\Delta p_p = p_s - p_\infty \tag{2.21}$$

where the $_s$ subscript indicates sensed pressure

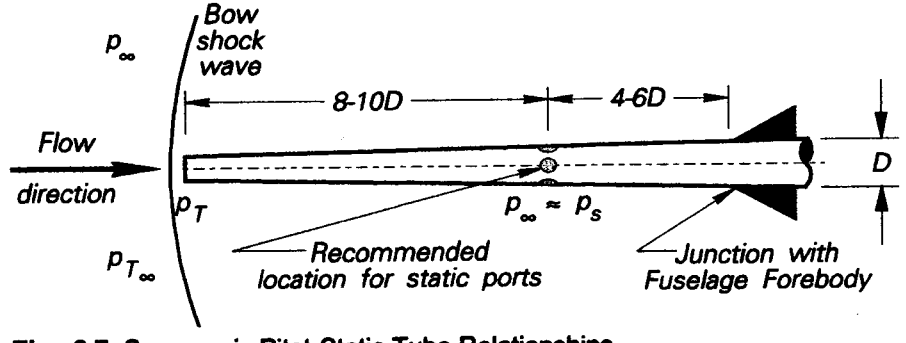

Fig. 2.7 Supersonic Pitot-Static Tube Relationships

Altitude and airspeed static position error corrections are both functions of Δp_p and are defined by (The subscript $_{ic}$ denotes measurements corrected for instrument error):

$$\Delta h_{pc} = h_{cal} - h_{ic} \tag{2.22}$$

$$\Delta V_{pc} = V_{cal} - V_{ic} \tag{2.23}$$

Of course, both these corrections come from readings of pressure gages, each with different scales. Both the altimeter and the airspeed indicator sense the same physical quantity, p_s, and therefore Δh_{pc} and ΔV_{pc} are not independent variables. Our task in the remainder of this section is to find an expression relating Δh_{pc} and ΔV_{pc}.

Starting with eqn. (2.5) in approximate incremental form, we first express the dependence of Δh_{pc} on Δp_p. (We also introduce yet another subscript $_{std}$ for standard day conditions.) Let $dp \rightarrow \Delta p_p$; that is, the Δp of interest is error in sensed static pressure and, correspondingly, $dh \rightarrow -\Delta h_{pc}$, the altimeter's static pressure error correction. Then, eqn. (2.5) becomes:

$$\Delta p_p = \rho_{std} g_0 \Delta h_{pc} \quad \text{or} \quad \Delta h_{pc} = \frac{\Delta p_p}{\rho_{std} g_0} \tag{2.24}$$

$$\text{Then, } \frac{\Delta p_p}{\rho_{std} g_0} = \rho_{std} g_0 = \rho_0 \sigma_{std} g_0 = 0.0764749 \sigma_{std} \tag{2.25}$$

$$\text{But } \sigma_{std} = \frac{\rho_{std}}{\rho_0} = \frac{\rho_{std}}{\rho_i}\frac{\rho_i}{\rho_0} = \frac{\rho_i}{\rho_0}\left(1 + \frac{k_i}{T_i}(h - h_i)\right)^{-\frac{g_0}{k_i R} - 1}, \quad k_i \neq 0, \text{ or}$$

$$\sigma_{std} = \frac{\rho_i}{\rho_0} e^{-\frac{g_0}{T_i R}(h - h_i)}, \; k_i = 0$$

For $i = 0$, we substitute: $-\frac{g_0}{k_0 R} = 5.25592$, $T_0 = 518.67$ °R, $k_0 = -0.00356616$ °R/ft

$$\sigma_{std} = \left(1 - \frac{6.87559}{1000000000} h\right)^{4.2559} \tag{2.26}$$

$$\text{For } i = 1, \; \sigma_{std} = \frac{\rho_{tropopause}}{\rho_0}\frac{\rho_{std}}{\rho_{tropopause}} = \sigma_{tropopause} e^{-\frac{g_0}{T_i R}(h - h_i)} \tag{2.27}$$

$$= 0.2979725 e^{-(0.000048063797)(h - 36089.239)}$$

Fortunately, these equations for σ_{std} can be, and usually are, plotted and/or programmed for table lookup.

Approximate relationships between Δp_p and airspeed indications can also be obtained in a straightforward manner. Assuming no error in sensed total pressure, measured dynamic pressure is:

$$q_{c_{ic}} = p_T - p_s.$$

The dynamic pressure without static pressure error is just:

$q_c = p_T - p_\infty$

Static pressure error is, therefore, just the difference between q_c and $q_{c_{ic}}$.

$\Delta p_p = p_s - p_\infty = q_c - q_{c_{ic}}$

Rearranging eqn. (2.10)

$$\frac{q_c}{p} = \left(1 + \frac{(\gamma - 1)V^2}{2\gamma RT}\right)^{\frac{\gamma}{\gamma - 1}} - 1$$

This pressure ratio can be applied to any set of temperature and velocity measurements so long as the process is approximately isentropic. Specializing this expression to calibrated airspeed, which implies substituting p_0 for p and T_0 for T;

$$\frac{q_c}{p_0} = \left(1 + \frac{(\gamma - 1)V_{cal}^2}{2a_0^2}\right)^{\frac{\gamma}{\gamma - 1}} - 1 = \left(1 + \frac{(\gamma - 1)(V_{ic} + \Delta V_{pc})^2}{2a_0^2}\right)^{\frac{\gamma}{\gamma - 1}} - 1 \qquad (2.28)$$

and, for instrument corrected airspeed V_{ic}, $q_{c_{ic}}$ replaces q_c

$$\frac{q_{c_{ic}}}{p} = \left(1 + \frac{(\gamma - 1)V_{ic}^2}{2a_0^2}\right)^{\frac{\gamma}{\gamma - 1}} - 1$$

Now, we can obtain an approximate expression relating Δp_p and ΔV_{pc} in the same way Herrington[9] does by using only the expression above and the definition $q_{c_{ic}} = p_T - p_s$. If p_T is measured with negligible error, then $dq_{c_{ic}} = -dp_s$. Differentiating and replacing $dq_{c_{ic}}$ with $-dp_s$ gives eqn. (2.29):

$$\frac{dp_s}{dV_{ic}} = -\frac{\gamma p_0 V_{ic}}{a_0^2}\left(1 + \frac{(\gamma - 1)V_{ic}^2}{a_0^2}\right)^{\frac{1}{\gamma - 1}} \qquad (2.29)$$

Approximating the differentials with finite differences: $\Delta p_p \approx dp_s$ and $\Delta V_{pc} \approx -dV_{ic}$,

$$\frac{\Delta p_p}{\Delta V_{pc}} \approx \frac{\gamma p_0 V_{ic}}{a_0^2}\left(1 + \frac{(\gamma - 1)V_{ic}^2}{a_0^2}\right)^{\frac{1}{\gamma - 1}} \qquad (2.30)$$

We have developed this approximation based on eqn. (2.10), which is a valid expression for an isentropic process; that is, no shock waves can exist. Equation (2.30) is valid only if $V_{ic} < a_0$. However, a similar approach, starting with the Rayleigh supersonic

pitot formula, gives an approximation when the pitot tube does have an attached normal shock wave.

$$\frac{q_c}{p} = \left(\frac{(\gamma+1)V^2}{2a^2}\right)^{\frac{\gamma}{\gamma-1}} + \left(\frac{(\gamma+1)V^2}{1-\gamma+2\gamma\frac{V^2}{a^2}}\right)^{\frac{1}{\gamma-1}} - 1$$

Factoring out $1-\gamma$ from the $\left(\frac{(\gamma+1)V^2}{1-\gamma+2\gamma\frac{V^2}{a^2}}\right)^{\frac{1}{\gamma-1}}$ term, and rearranging gives

$$\frac{q_c}{p} = \left(\frac{(\gamma+1)V^2}{2a^2}\right)^{\frac{\gamma}{\gamma-1}} + \left(\frac{\gamma+1}{\gamma-1}\right)^{\frac{1}{\gamma-1}} + \left(\frac{2\gamma V^2}{(\gamma-1)a^2}\right)^{\frac{1}{\gamma-1}} - 1 \qquad (2.31)$$

Substituting $\gamma = 1.4$ for air:

$$\frac{q_c}{p} = (1.2^{3.5})(6^{2.5})\left(\frac{V}{a}\right)^7\left(7\frac{V^2}{a^2}-1\right)^{2.5} - 1 = 166.92158\left(\frac{V}{a}\right)^7\left(7\frac{V^2}{a^2}-1\right)^{2.5} - 1$$

If we now replace V with V_{ic}, p with p_0, and a with a_0, we can solve for the instrument corrected dynamic pressure read on the ASI by using the following equations:

$$\frac{q_{cic}}{p_0} = 166.92158\left(\frac{V_{ic}}{a_0}\right)^7\left(7\frac{V_{ic}{}^2}{a_0{}^2}-1\right)^{2.5} - 1$$

Still assuming no measurement error in p_T, and taking the derivative with respect to V_{ic},

$$\frac{dq_{c_{ic}}}{dV_{ic}} = (7)(166.92158)\left(\frac{V_{ic}}{a_0}\right)^6 \frac{\left(2\frac{V_{ic}^2}{a_0^2}-1\right)}{\left(7\frac{V_{ic}^2}{a_0^2}-1\right)^{3.5}} = -\frac{dp_s}{dV_{ic}}$$

Using our finite difference approximations again, $\Delta p_p \approx dp_s$ and $\Delta V_{pc} \approx -dV_{ic}$,

$$\frac{\Delta p_p}{\Delta V_{pc}} \approx 52.85333\left(\frac{V_{ic}}{a_0}\right)^6 \frac{\left(2\frac{V_{ic}^2}{a_0^2}-1\right)}{\left(7\frac{V_{ic}^2}{a_0^2}-1\right)^{3.5}} \qquad (2.32)$$

where $\frac{\Delta p_p}{\Delta V_{pc}}$ is in inches of Hg/knot. (Changing the constant to 2214.795 in eqn. (2.32) gives $\frac{\Delta p_p}{\Delta V_{pc}}$ in psf/fps.)

The approximate expressions in eqns. (2.30) and (2.32) for $\frac{\Delta p_p}{\Delta V_{pc}}$ are valid only for fairly small errors in pressure measurement; Herrington[9] says that ΔV_{pc} must be less than 10 knots, which is usually quite adequate for well-designed pitot-static systems.

Since both Δh_{pc} and ΔV_{pc} are functions of the error in measuring static pressure, they must be related. Having determined one, we should be able to calculate the other. Dividing eqns. (2.30) or (2.32) by eqn. (2.25), for $\frac{V_{ic}}{a_0} < 1$ or $\frac{V_{ic}}{a_0} > 1$, respectively, and then using the appropriate form of σ_{std} from either eqn. (2.26) or (2.27),

$$\frac{\Delta h_{pc}}{\Delta V_{pc}} \approx 58.566\left(\frac{V_{ic}}{\sigma_{std} a_0}\right)\left(1+0.2\frac{V_{ic}^2}{a_0^2}\right)\frac{V_{ic}}{a_0} \quad for \quad \frac{V_{ic}}{a_0}<1 \tag{2.33}$$

where $\frac{\Delta h_{pc}}{\Delta V_{pc}}$ is in feet/knot.

Similarly, for $\frac{V_{ic}}{a_0} > 1$,

$$\frac{\Delta h_{pc}}{\Delta V_{pc}} \approx 48{,}880\left(\frac{V_{ic}}{a_0}\right)^6 \frac{\left(2\frac{V_{ic}^2}{a_0^2}-1\right)}{\left(7\frac{V_{ic}^2}{a_0^2}-1\right)^{3.5}} \tag{2.34}$$

Equations (2.33) and (2.34) are plotted in Fig. 2.8 and are valid approximations if $\Delta h_{pc} < 1{,}000$ feet and $\Delta V_{pc} < 10$ knots. For larger position error corrections, Herrington has developed and plotted more exact equations[9], good for $\Delta V_{pc} < 50$ knots. If increased range is needed for this correction, the interested reader should consult Herrington's handbook.

Example 2.3: An airplane is flying at 303 KIAS at an indicated pressure altitude of 29,750 feet. The outside air temperature is -25°F for these test conditions. The instrument corrections include $\Delta V_{ic} = -3$ knots, $\Delta h_{pc} = 250$ feet, and $\Delta h_{ic} = 75$ feet. Calculate $\frac{\Delta h_{pc}}{\Delta V_{pc}}$, ΔV_{pc}, V_e, V_∞, and M_∞.

First, we will use our definitions to relate indicated and true airspeed

$V_\infty = V_{ic} + \Delta V_{pc} + \Delta V_c$, but $V_{ic} = V_i + \Delta V_{ic} = 303 - 3 = 300$ knots

Also, using $a_0 = \sqrt{(1.4)(1716.55)(518.67)} = 1116.4$ feet/sec $= 661.489$ knots, from eqn. (2.33),

$$\frac{\Delta h_{pc}}{\Delta V_{pc}} = \left(\frac{(58.566)(300)}{\sigma_{std}\,661.489}\right)\left(1 + 0.2\frac{300^2}{661.489^2}\right)^{2.5}$$

To obtain σ_{std}, we need p from the pressure altitude, which is:

$h = h_i + \Delta h_{ic} + \Delta h_{pc} = 29{,}750 + 75 + 250 = 30{,}075$ feet

Equation (2.6a) gives $\frac{p}{p_0} = 0.29595$ and $p = 626.29$ psf. Then,

$$\sigma = \frac{626.29}{(1716.55)(434.67)(0.0023769)} = 0.35314, \text{ so}$$

$$\boxed{\frac{\Delta h_{pc}}{\Delta V_{pc}} = 83.19 \ \frac{ft}{kt}}$$

$$\Delta V_{pc} = \frac{250\ ft}{83.189\ ft/kt} =$$

$$\boxed{\Delta V_{pc} = 3.01 knots}$$

From Fig. 2.4, $\Delta V_c = -15$ kts $= V_e - V_{cal}$, so $V_e = V_{cal} - 15$ kts $= 300 - 15$

$$\boxed{V_e = 285 knots}$$

$$V_\infty = \frac{V_e}{\sqrt{\sigma}} = \frac{285}{\sqrt{0.35314}}$$

$$\boxed{V_\infty = 479.59 knots = 809.98 fps}$$

$$M_\infty = \frac{V_\infty}{\sqrt{\gamma RT}} = \frac{809.98}{\sqrt{(1.4)(1716.55)(434.67)}}$$

$$\boxed{M_\infty = 0.79}$$

2.2 POSITION ERROR CALIBRATION METHODS

From the preceding discussion of pitot-static system errors it should be obvious that any pitot-static system calibration must be primarily concerned with determining the static position error. Gracey[10] classifies position error calibration methods under four headings:

- Freestream static pressure methods in which Δp_p is obtained from measurement of p_s and p_∞.
- True airspeed methods in which Δp_p is derived from values of V_∞ calculated from ground speed measurements or from anemometer readings.
- A temperature method in which Δp_p is determined from measured temperature and a pressure-temperature survey.
- Mach number methods in which Δp_p is obtained from Mach number.

Of these four types of calibration methods the first two are the ones most often used. They are especially well-suited for low speed and low altitude, although the first category of methods includes several techniques useful at high altitudes and airspeeds. Instrumentation needs can be kept to a minimum with these two approaches. For brevity, we will describe in detail only three calibration procedures, two that are freestream static pressure methods and one that is a true airspeed method. We will also restrict our detailed descriptions to subsonic methods. For the reader whose needs go beyond this introductory material, Gracey lists fourteen methods of calibration and summarizes relative accuracies (when data are available) and limitations.

After describing the three selected techniques, the discussion will focus on the sensitivity of the position error correction to three major effects: gross weight changes, altitude variations, and Mach number deviations.

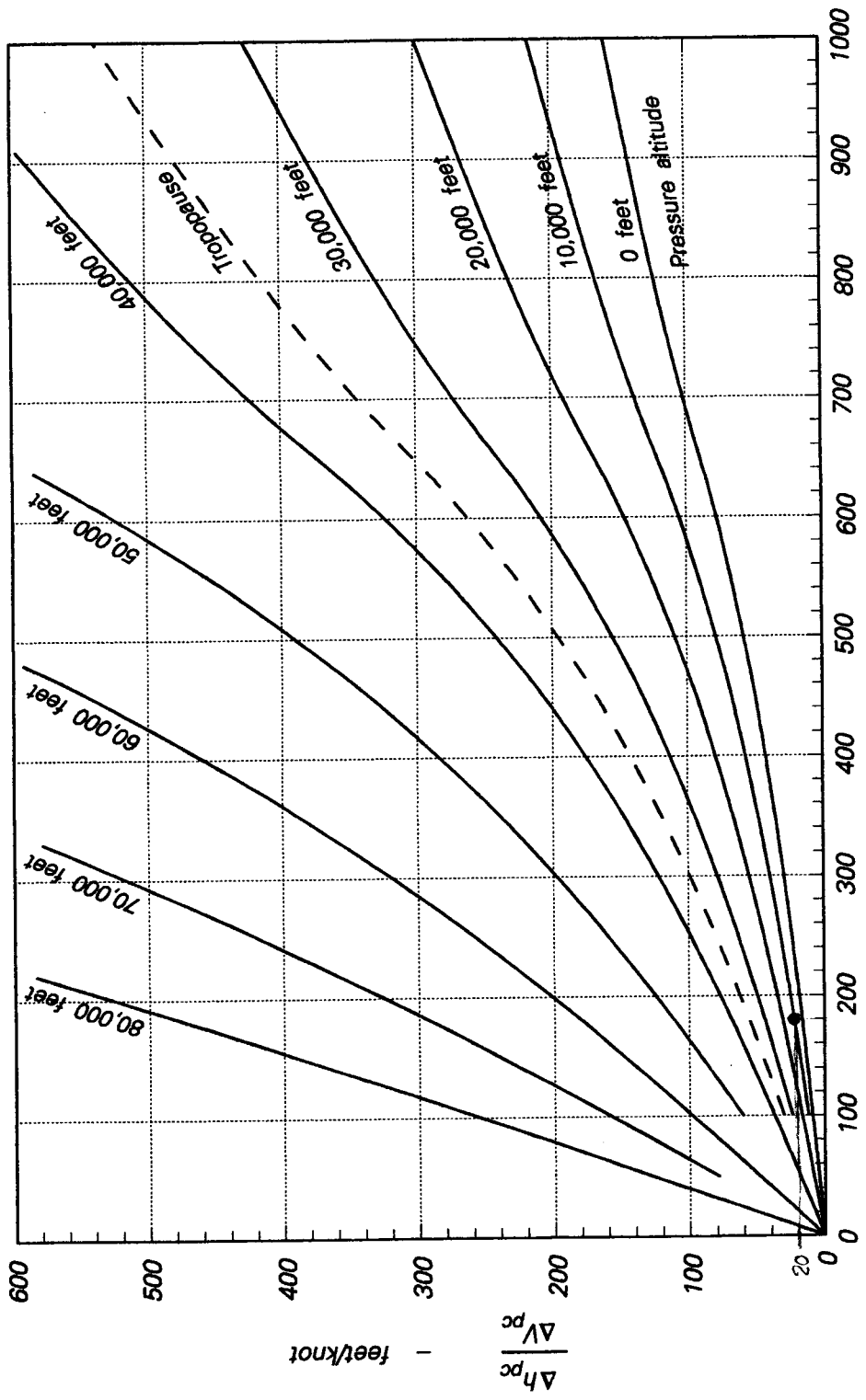

Fig. 2.8 Ratio of Altimeter to Airspeed Indicator Position Error Correction

2.2.1 Freestream Static Pressure Methods

These methods depend on accurate experimental determination of the difference between measured static pressure and the actual freestream static pressure at each of the flight conditions. There are at least four ways to determine this differential pressure. First, Δp_p can be obtained from a reference pressure source moving with the aircraft but located outside the pressure field of the vehicle. The test aircraft may carry this reference pressure sensor along (trailing cone or trailing bomb) or the calibrated reference sensor may be carried in another airplane (pacer aircraft) flying formation with the test vehicle. Second, the reference value of p_∞ may be obtained by interpolating the pressure gradient optically (tower flyby) for low altitude calibrations or with tracking radar for medium and high altitudes. Third, p_∞ may be calculated by measuring p and T at the ground and assuming a temperature gradient up to the altitude where temperature is measured. Fourth, p_∞ at a given altitude can be obtained from measuring indicated pressure and temperature and noting the changes in height from an altitude where Δp_p is known. Ordinarily, for these freestream static methods where pressure differences are measured by aircraft instruments, the altimeter position error, Δh_{pc}, is the measured correction because h_{cal} is relatively easy to determine and the altimeter provides better resolution than the ASI. For example, at sea level and 150 knots, a ΔV_{pc} of 2 knots corresponds approximately to a Δh_{pc} of about 38 feet and to a Δh_{pc} of approximately 116 feet at 500 knots . Let us now single out the tower flyby technique and the pacer aircraft technique and discuss in detail the data collection and data reduction procedures for each of them. We will also suggest some of the advantages and limitations of each approach.

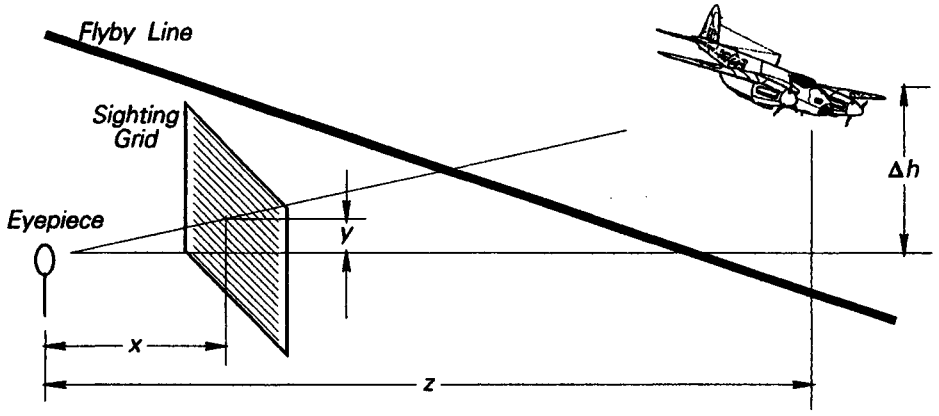

Fig. 2.9 Tower Flyby Geometry

2.2.1.1 **Tower Flyby Method**. In this technique, the calibrated altitude of the vehicle is determined by triangulation relative to a surveyed point on the ground (Fig. 2.9). The airplane is flown down the tower flyby line at an altitude approximately level with the eyepiece in the tower. The altitude and the airspeed both must be completely stabilized as the airplane passes directly abeam the tower. The height of the airplane in the sighting grid (y) and the pressure altitude in the tower should be recorded for each pass. Then the calibrated altitude of the airplane's altimeter can be calculated by adding the pressure altitude of the tower to Δh, where $\Delta h = z \frac{y}{x}$.

Figure 2.10 illustrates how calibrated altitudes from the two ground blocks are used to obtain h_c at each test point. The data reduction for tower flyby information proceeds along the following lines. Determine the calibrated altitude of the test airplane's altimeter at each test point during the flight. The so-called "ground block" method, which assumes a constant change of calibrated altitude with time of day, is the most commonly used means of obtaining hc for each test point. The flight test crew must obtain a preflight and postflight reading of the aircraft altimeter (set at 29.92 in Hg, of course) at a point of known elevation on the ramp. Then, $h_{cal_{ramp}} = h_{i_{ramp}} + \Delta h_{ic}$.

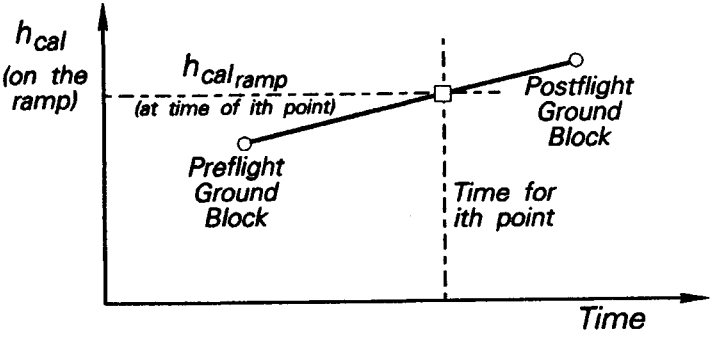

Fig. 2.10 Use of Ground Block Calibrated Altitudes

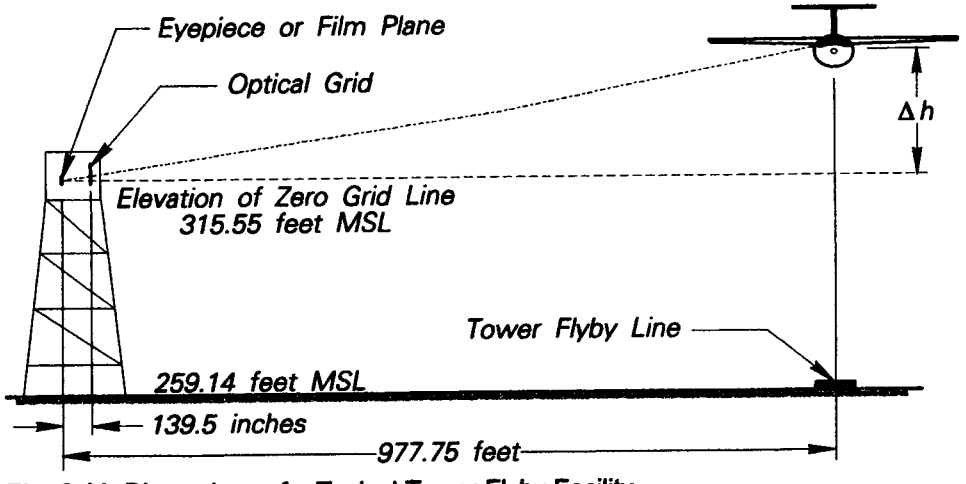

Fig. 2.11 Dimensions of a Typical Tower Flyby Facility

Using this interpolated value for the calibrated altitude on the ramp, calculate the calibrated altitude at the eyepiece in the flyby tower. Figure 2.11 is a sketch illustrating a typical tower flyby course. The eyepiece in the tower is 315.55 feet above mean sea level, the optical grid is 139.5 inches from the eyepiece and grid lines are 1 inch apart. The bottom grid line is at the same level as the eyepiece. The flyby line is 977.75 feet in front of the tower eyepiece. In using this method you must also take into account the height above the ground of the altimeter for the particular airplane you are testing.

$$h_{cal_{eyepiece}} = h_{cal_{ramp}} + \Delta h_{cal_{eyepiece}} - \Delta h_{cal_{altimeter}}$$

The calibrated altitude of the test aircraft is then obtained from

$$h_{cal} = h_{cal_{eyepiece}} + \frac{T_\infty}{T_{std}}\Delta h \tag{2.35}$$

where $\frac{T_\infty}{T_{std}}$ is the correction for nonstandard temperature conditions.

Next, we must find the test day pressure-related parameters with instrument corrections. For this introductory course, we will consider only h_{ic}, V_{ic}, and $q_{c_{ic}}$, leaving M_{ic} to more detailed descriptions.

$h_{ic_t} = h_i + \Delta h_{ic}$ and $V_{ic_t} = V_i + \Delta V_{ic}$. As we saw in Section 2.1.3.3,

$$q_{c_{ic}} = \left(1 + 0.2\frac{V_{ic}^2}{a_0^2}\right)^{3.5} - 1$$

Finally, we standardize Δh_{pc} and ΔV_{ic} to a reference altitude approximately equal to standard day elevation at the test site. The tower eyepiece elevation in Fig. 2.11 is approximately 315 feet; therefore, we will correct each test day measurement to standard day at this elevation. No lag correction is necessary for steady state test data, so:

$$\Delta h_{pc_t} = h_{cal_t} - h_{ic_t}$$

To correct to standard day conditions at 315 feet, considering only small altitude and angle of attack changes:

$$\Delta h_{pc_{315}} = \Delta h_{pc_t}\frac{\theta_{315}}{\theta_t}$$

where $\theta = 1 - 0.00000687559h_{cal}$

$$\text{So, } \Delta h_{pc_{315}} = \Delta h_{pc_t}\frac{0.9978343}{\theta_t} \tag{2.36}$$

To correct V_{ic_t} to $V_{ic_{315}}$, assume that each test point was flown at 315 feet and the test day Mach number. Then, we observe that

$$\frac{q_{c_{ic_{std}}}}{p_{s_{std}}} = \frac{q_{c_{ic_t}}}{p_{s_t}} = \frac{q_{c_{ic_{std}}}}{p_0\delta_{315}}.$$

For subsonic airspeeds, we solve this expression for $V_{ic_{315}}$:

$$V_{ic_{315}} = a_0\sqrt{5\left(\left(\frac{q_{c_{ic_{std}}}}{p_0\delta_{315}} + 1\right)^{0.2857142} - 1\right)} \tag{2.37}$$

$\Delta V_{pc_{315}}$ can then be obtained from eqn. 2.33 or from Fig. 2.8, knowing $\Delta h_{pc_{315}}$.

This data reduction scheme has been simplified considerably by assuming small differences in altitude measurements and test day calibrated altitudes, small correction terms, and subsonic flight conditions. For other conditions ($M_{ic} > 1$, for example), different equations must be used. Do not apply these data reduction equations to data for which

Δh_{pc} > 1000 feet or ΔV_{pc} > 10 knots. Consult Herrington[9] and/or other flight test handbooks for complete details that are beyond the scope of this book.

The tower flyby method requires very little instrumentation and is quite a straightforward, though tedious, procedure. Photographic or theodolite equipment are often used to record the aircraft elevation at each measurement point, but it is not essential and hand-recorded optical data are also usable. Gracey[10] concluded from tests at NASA's Langley Research Center that Δp_p can be measured within ± 1% of q_c, even for very low speeds ($M = 0.15$ and 90 knots). The method is least accurate for such low speed points because angle of attack effects dominate. For higher speeds ($M = 0.3$ and 190 knots), accuracy within ± 0.2% of q_c was found. Obviously, altitude effects cannot be investigated using the tower flyby method and the speed range is somewhat limited because the technique is a low altitude procedure. The lowest test speeds must offer a safe margin above stall speed and the highest test speed is limited to the maximum level flight speed of the vehicle at low altitude.

2.2.1.2 **Pacer Aircraft Technique**. There are at least two variations of the pacer method, one in which the reference source is in an airplane flying formation with the test aircraft and one in which the test aircraft flies at various speeds past the reference airplane. The reference carrier simply maintains a constant speed and altitude. The latter method, though less demanding for the reference airplane, is not as accurate as the formation method because of the practical difficulties in determining small differences in the height of the two aircraft and in obtaining simultaneous readings. Lag errors are also more likely to affect data from the latter technique.

When the calibration tests are flown in formation, the test aircraft may be either the lead or the wing man. The important points are that the two aircraft are flown at the same level, that their speeds are perfectly matched, and that they are far enough apart so that neither of the pitot-static systems are affected by the pressure field of the other. The last requirement means that at least half a wing span in spacing is required between the two aircraft. However, the precise formation flying required to guarantee matched altitudes and airspeeds for each point suggests that the lateral spacing should be little more than this half a wing span. Level, in the case of dissimilar aircraft, means that the two altimeters being used should be at the same height.

Data reduction for the pacer aircraft (formation) method is relatively simple. First, find h_{cal} and V_{cal} for the pacer's reference altimeter using its indicated readings, the laboratory corrections for its instruments, and the known static position error corrections.

$$h_{cal_{pacer}} = h_{i_{pacer}} + \Delta h_{ic_{pacer}} + \Delta h_{pc_{pacer}}$$

$$V_{cal_{pacer}} = V_{i_{pacer}} + \Delta V_{ic_{pacer}} + \Delta V_{pc_{pacer}}$$

It is assumed, of course, that the pacer aircraft system has a full and accurate set of calibrations.

Next, obtain h_{ic_t} and V_{ic_t} for the test aircraft just as was described for the tower flyby technique in Section 2.2.1.1. Then, calculate Δh_{pc} and ΔV_{pc} for the test aircraft under the assumption that both aircraft were at the exactly the same test day calibrated altitude and airspeed at each test point.

$$\Delta h_{pc_t} = h_{cal_{pacer}} - h_{i_{test}} - \Delta h_{ic_{test}}$$

Correct Δh_{pc_t} to the nominal altitude for the test point just as we did the tower flyby data with eqn. (2.36).

$$\Delta V_{pc_t} = V_{cal_{pacer}} - V_{i_{test}} - \Delta V_{ic_{test}}$$

This approach gives ΔV_{pc} independent of the approximate conversion equations developed previously (eqns. 2.33 and 2.34) and offers a crude method of checking the total pressure error if any exists. (Caution: The measurement errors in the pacer method may be large enough to imply erroneously that the total pressure error is significant. Use this comparison only as an indication that further tests may be required. Remember you are obtaining the correction by differencing two large numbers.)

The pacer aircraft method, particularly when the two aircraft are closely matched and can be flown in formation, is a very accurate calibration method. Gracey[10] reports an accuracy in $\frac{\Delta p_p}{\Delta q_c}$ of ±0.7% at M = 0.5 and ±0.2% at M = 1.0 for this method. Also, altitude effects can be fully investigated within the envelope of the two vehicles and supersonic calibrations are feasible. Low speeds and, for some aircraft, transonic speeds may cause some difficulty in stabilizing in formation because of the handling qualities of the specific aircraft. Finally, the pacer aircraft method lends itself to collecting static position error corrections rapidly, though the cost of operating a pacer aircraft may not be warranted.

2.2.2 True Airspeed Methods

Static position errors can also be calculated by measuring true airspeed and determining V_{cal} from the measurements. The speed-course technique is that uses this approach. Obviously, the wind must be recorded at the time and altitude of the test; wind effects can be minimized by flying reciprocal headings if the wind is constant. Tests should be conducted when the wind speed is as near zero as possible to reduce such uncertainties. Calibrations are often carried out near sunrise or sunset for this reason.

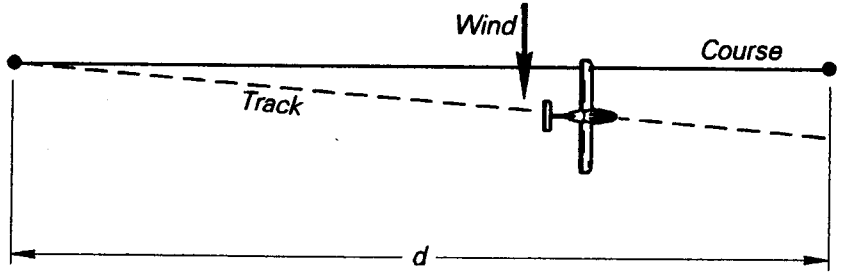

Fig. 2.12 Speed Course Geometry

Figure 2.12 is a sketch depicting the ground track of a speed course calibration test. Notice that the aircraft is aligned with a heading parallel to the desired course; no drift correction is used. The data needed from each pass are h_i, V_i, T_i, and time between the two points. If no other instrumentation is available, observers can note the time the airplane passes over each of the known points. However, radar or optical trackers will reduce the likelihood of human error in recording time accurately. The test should be planned so the timing interval is large compared to the error in marking the start and stop times. The

most important parameter to be held constant is indicated airspeed and, if turbulence or poor pilot technique causes a variation of over ±1 knot, the data point is suspect. Accurate ambient temperature at the test altitude is also necessary. This temperature becomes particularly important whenever medium altitude calibrations are attempted.

To reduce speed course data we must first find the average true airspeed.

$$V_{avg} = \frac{1}{2}\left(\frac{d}{t_1} + \frac{d}{t_2}\right)$$

where d is the course length; t_1 and t_2 are the times required to traverse the course in reciprocal directions.

Next, find the freestream temperature at the test altitude. If precise weather data collection equipment is available, one might obtain this information from the meteorologist. If the indicated temperature from the airplane is used, it must be corrected for the gage laboratory correction and the temperature recovery factor. Since the temperature gage reads the total temperature except for the kinetic term which requires a recovery factor because the flow is not perfectly adiabatic,

$$\frac{T_T}{T_\infty} = 1 + K(\gamma - 1)\frac{V_\infty^2}{2\gamma RT} \approx \frac{T_{ic}}{T_\infty}$$

where K is the temperature recovery factor.

Usually K is essentially constant throughout the flight envelope and for a good flight test measurement system it will be in the range of 0.95 to 1.0. However, with sloppy design or careless installation of the temperature probe, K may range as low as 0.7 and may be a function of airspeed. To summarize, ambient temperature is calculated from:

$$T_\infty = (t_i + \Delta T_{ic} + 459.67) - K(\gamma - 1)\frac{V_\infty^2}{2gR}$$

where t_i is in °F.

Next, find the test day instrument corrected altitude and airspeed. Notice that these values are based on the average indicated gage readings during the run. If large variations in either of these readings occur, the data will be unusable.

$$h_{ic_t} = h_{i_{avg}} + \Delta h_{ic} \quad \text{and} \quad V_{ic_t} = V_{i_{avg}} + \Delta V_{ic}$$

Then, obtain V_{cal} from the average true airspeed and the ambient temperature. Calculate the density ratio, using the perfect gas law and the measured temperature from the second step above, and substitute in the expression for equivalent airspeed.

$$V_e = V\sqrt{\sigma} = V_{cal} + \Delta V_c$$

Figure 2.4 offers a convenient means of graphically iterating on this expression to obtain V_{cal}. Then, calculate ΔV_{pc_t} and Δh_{pc_t} from $\Delta V_{pc_t} = V_{cal} - V_{ic_t}$ and Fig. 2.8. Finally, standardize Δh_{pc_t} and ΔV_{pc_t} to nominal altitude conditions exactly as was done for the tower flyby test data.

The speed course method is one of the least accurate techniques for obtaining the static position error correction. Gracey, taking a different approach to the reduction of the data than shown above, says that it is valid for a very limited airspeed range (speeds safely above the stall speed up to approximately 130 knots at sea level or about $M = 0.2$) and offers no estimate of the accuracy or precision[10]. On the other hand, the technique requires almost no instrumentation, apart from observers, a stopwatch or two, and an accurately known distance between two points on the ground. This simplicity does offer a simple way to calibrate the pitot-static system but questions about accuracy will linger if the flight test team does not take meticulous care in flying and recording the data.

2.2.3 Factors Affecting Position Error Measurements

It can be shown by dimensional analysis that the static pressure anywhere in the pressure field surrounding a body moving through the air is a function of at least five variables, two dealing with the flow direction and three non-dimensional parameters: angle of attack (α), sideslip angle (β), Mach number (M), Reynolds number (Re), and Prandtl number (Pn). If we neglect heat transfer effects, Pn is of no consequence; and if the static source is outside the boundary layer, Re effects will be negligible. Finally, we will assume that sideslip can be minimized for those maneuvers for which we insist that pitot-static system measurements be reliable. Then,

$$\frac{p_s}{p_\infty} = f(M, \alpha)$$

where $f(x, y)$ is an unspecified function of two variables, with $x = M$ and $y = \alpha$.

For vehicles operating in the linear angle of attack range, C_L varies directly with α. Therefore, with a slightly altered functional relationship, we may write $\frac{p_s}{p_\infty} = f(M, C_L)$.

But $$C_L = \frac{2L}{\rho V^2 S} = \frac{2nW}{\left(p/RT\right)V^2 S} = \frac{2nW}{\left(S\gamma p_0 V^2 / \gamma RT\right)} = \frac{2nW}{\delta M^2 \gamma p_0 S}.$$

So, the functional expression becomes:

$$\frac{p_s}{p_\infty} = f\left(M, \frac{nW}{\delta}\right) \tag{2.38}$$

This simple expression clearly shows that there are three major variables affecting the sensed static pressure, p_s, from the pitot-static system. The three variables are Mach number, the weight supported by the lifting surfaces, and the altitude. To return to our standard usage, the pressure difference is the prime variable of interest, so the functional relationship of eqn. (2.38) can also be written as:

$$\frac{\Delta p_p}{q_{c_{ic}}} = f\left(M_{ic}, \frac{nW}{\delta_{ic}}\right) \tag{2.39}$$

If M_{ic} is less than about 0.3, the flow field is essentially unaffected by compressibility effects. [Some references even suggest using a much higher limit for Mach number[13].]

Then the pressure coefficient of eqn. (2.39) is a function of lift coefficient only. It is also true that for $M < 0.3$, altitude effects are generally negligible. Then eqn. (2.39) becomes

$$\frac{\Delta p_p}{q_{c_{ic}}} = f\left(\frac{nW}{V_{ic}^2}\right) \tag{2.40}$$

At constant V_{ic}, this equation suggests that Δp_p is a function of angle of attack only (which must change to accommodate changes in either load factor or weight while maintaining level flight). For aircraft where the weight change as fuel is used or payload is changed is a large fraction of the total weight, there is a family of curves for ΔV_{pc}. Figure 2.13a illustrates such a family of curves. On the other hand, if angle of attack changes are small for the flight envelope, these curves collapse to a single curve as shown in Fig. 2.13b.

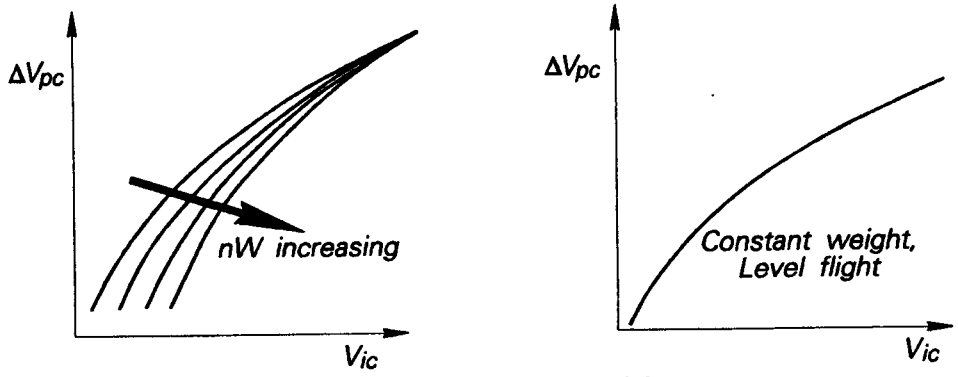

Fig. 2.13 Velocity Position Error Corrections for M < 0.3

However, Δh_{pc} is a function of altitude even if there are no angle of attack effects. The pressure difference is a function of altitude because the geometric altitude takes on a different value for every pressure level in the atmosphere. Figure 2.14 depicts the changes in Δh_{pc} as a function of V_{ic} and altitude.

In the transonic flight regime, especially near $M_\infty = 1$, it is very difficult to accurately measure static position errors. Certainly the complete functional, eqn. (2.39), is necessary. In fact, at high speeds the importance of changes in angle of attack diminishes because angle of attack changes little is small in any case. Mach number then becomes the dominant term. Figure 2.15 illustrates a complete variation of pressure coefficient with both low speed effects and the discontinuities in slope that occur in the transonic region. These discontinuities are the result of shock waves forming ahead of the static orifice. Figure 2.15 emphasizes the point that in this region the pressure coefficient is primarily a function of Mach number. Mach number is different for each V_{ic}, so ΔV_{pc} is a function of altitude in this region. Figure 2.16 illustrates this variation. Plotted versus V_{ic}, Δh_{pc} results in a family of curves displaced both vertically and horizontally for different altitudes, though if plotted versus M_{ic}, the horizontal displacement is removed.

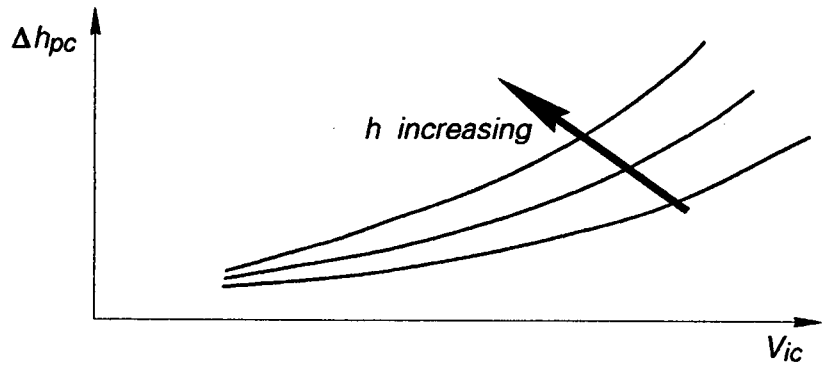

Fig. 2.14 Altitude Position Error Corrections for $M < 0.3$

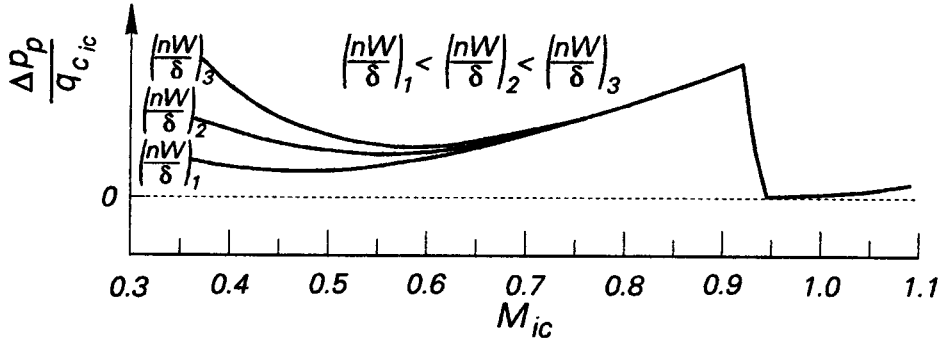

Fig. 2.15 Pressure Coefficient Versus Mach Number

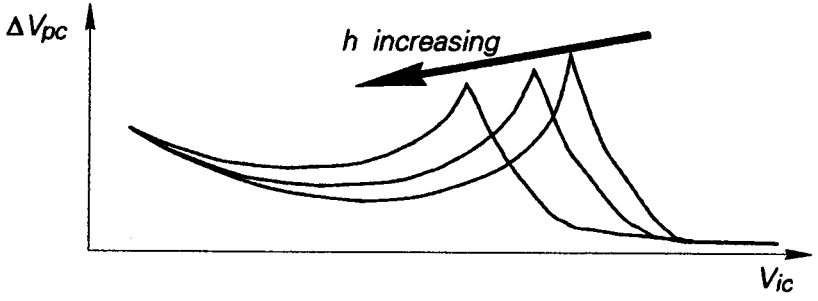

Fig. 2.16 Airspeed Position Error Correction for Transonic Flight Conditions

2.3 SUMMARY

In this chapter the subject of pitot-static system calibrations has been introduced. Starting with the mathematical model that produced the standard atmosphere, the theoretical basis for these calibrations was laid. Experience has shown that only the static position error correction is important for many flight test purposes, so three different methods of obtaining this information were discussed in detail.

Since such tests are rather tedious both to conduct and to reduce the data, no attempt is made in this introductory course to discuss all the available methods of calibration. The reader who needs or desires detailed information on other methods of calculation will find a wealth of material in the list of references. While the engineer who is responsible for such calibrations is often accused of "measuring with a micrometer what is later to be cut with a hacksaw," careful pitot static calibrations are the foundation for accurate performance and stability and control flight test data. The calibration process cannot be shorted without paying the price later.

REFERENCES

1 Diehl, W. S., "Standard Atmosphere -- Tables and Data," NACA Technical Report 218, 1925.

2 "Standard Atmosphere --Tables and Data for Altitudes to 65,800 Feet," NACA Report 1235, 1955.

3 "U. S. Standard Atmosphere, 1962," U. S. Government Printing Office, Washington, 1962.

4 Minzner, R. A., Champion, K. S. W., and Pond, H. L., "The ARDC Model Atmosphere," AF CRC-TR-59-267, 1959.

5 "U. S. Standard Atmosphere Supplements, 1966," U. S. Government Printing Office, Washington, 1966.

6 Hamlin, B., **Flight Testing Conventional and Jet-Propelled Airplanes**, The Macmillan Company, New York, 1946.

7 Anderson, J. D., Jr., **Introduction to Flight**, McGraw-Hill Book Company, New York, 1978.

8 Schoolfield, W. C., "A Simple Method of Applying the Compressibility Correction in the Determination of True Airspeed," **Journal of the Aeronautical Sciences**, Vol. 9, Oct. 1942, pp. 457-464.

9 Herrington, R. M., Shoemaker, P. E., Bartlett, E. P., and Dunlap, E. W., "Flight Test Engineering Handbook," AFFTC TR-6273 (AD 636392), Air Force Flight Test Center, Edwards AFB, California, May 1951 (Revised June 1964 and January 1966).

10 Gracey, W., "Measurement of Aircraft Speed and Altitude," NACA Reference Publication 1046, May 1980.

11 Huston, W. B., "Accuracy of Airspeed Measurements and Flight Calibration Procedures," NACA Report 919, 1948.

12 Wildhack, W. A., "Pressure Drop in Tubing in Aircraft Instrument Installations," NACA TN 593, 1937.

13 "Performance," FTC-TIH-70-1001, Air Force Flight Test Center, Edwards AFB, California, 1970.

14 Kline, R. E., Crews, A. H., and Knight, W. J., "F-5A Category II Performance Test," FTC-TR-65-15, Air Force Flight Test Center, Edwards AFB, California, July 1965.

Chapter 3

CLIMB, DESCENT, AND TURN PERFORMANCE TESTS

Every airplane on every flight; takes off, climbs, turns, descends, and lands. Thus, immediately after the pitot-static system is calibrated the test team can begin collecting performance data for these phases of flight. Since takeoff and landing performance is a more difficult measurement task, climb, descent, and turn performance will be tackled first.

The climb performance of a vehicle is of utmost importance to the operator and is directly related to lift, drag, and thrust capabilities of the aircraft. Generally, measurements are made to determine either a speed or Mach number profile that will optimize a single performance parameter like minimum time to altitude, minimum fuel to altitude, minimum time to a total energy level, or such like. The actual altitude and velocity measurements can be manipulated to describe the maneuver capability of the airplane or to evaluate the tactical capability of the vehicle relative to an adversary.

Turning performance is an important measure of merit for some classes of aircraft (like fighters or acrobatic craft) and is hardly ever used for others (like general aviation or commercial jets). It is more important for airplanes with an intended aggressive maneuvering combat role than for any other group of airplanes. The measurements can be made in a number of ways and with relatively simple sensors (like a stopwatch and the normal cockpit instruments). Therefore, it is useful, at least in a learning environment, to measure turn rates and radii even on airplanes for which turn performance is not used for certification or to qualify contractual guarantees.

This chapter is concerned then with performance measurements that are relatively straightforward: climbs, descents, and turns. All of them are strongly related to the excess thrust or power available from the engine-airframe combination. However, these performance categories are extremely important in assessing the utility of a design.

3.1 THEORETICAL FOUNDATIONS

Table 3.1 FAR 23.65 Climb Requirements (All Engines Operating)

Power Setting	Configuration	Speed	Minimum Steady Climb Rate	Minimum Angle
Max Continuous	Max Wt < 6000 lbs Flaps TO, Gear UP, Cowl flaps COOL	Most Favorable	> 300 fpm at sea level	1:12 Landplane 1:15 Seaplane
Takeoff	Max Wt < 6000 lbs Flaps TO, Gear UP, Cowl flaps COOL	Most Favorable	>300 fpm or > $11.5V_{s_1}$	No Requirement

Note: If V_{s_0} < 61 knots, no climb requirement is specified. If V_{s_0} < 61 knots, use the requirement for a maximum weight > 6000 lbs. V_{s_0} is the power off stall speed, landing configuration. The power off stall speed, clean (cruise) configuration is V_{s_1}.

The climb performance required of a given aircraft may be spelled out in one of several documents. Tables 3.1 and 3.2 summarize the climb requirements stated in FAR 23.65 for small multiengine airplanes. For military airplanes, these requirements most often come from the contractual specifications provided by the procurement agency. For commercial aircraft, the buyer (an airline, for example) may have specific climb perform-

ance requirements, but such unique requirements are not likely to be less stringent than those of the applicable Federal Aviation Regulations (FAR).

Table 3.2 FAR 23.67 Climb Requirements (Critical Engine Inoperative, Propeller in Minimum Drag Position)

Weight/Performance	Minimum Rate of Climb in fpm at 5000 feet	Power Setting/Configuration
Max Wt > 6000 lbs	R/C = $0.027V_{S_0}{}^2$ (V_{S_0} in knots)	Maximum Continuous (or less)
Max Wt < 6000 lbs V_{S_0} > 61 knots	R/C = $0.027V_{S_0}{}^2$ (V_{S_0} in knots)	Gear UP, Flaps OPTIMUM, Cowl Flaps as per FAR 23.1041-23.1047
Max Wt < 6000 lbs V_{S_0} < 61 knots	No minimum specified, actual rate must be determined	

Military requirements are similar to those listed in these tables although they are often more specific and more detailed. In any case, these examples suggest that the flight test team must verify or determine the optimum climb speed schedule as one of its first tasks for measuring the climb performance of the vehicle. Then, and only then, can either the minimum rate of climb or the minimum angle of climb be determined for a required configuration. However the requirement is stated, determination of climb (or descent) and turning performance is based on the familiar lift-weight and thrust-drag force balances, which we will now review briefly.

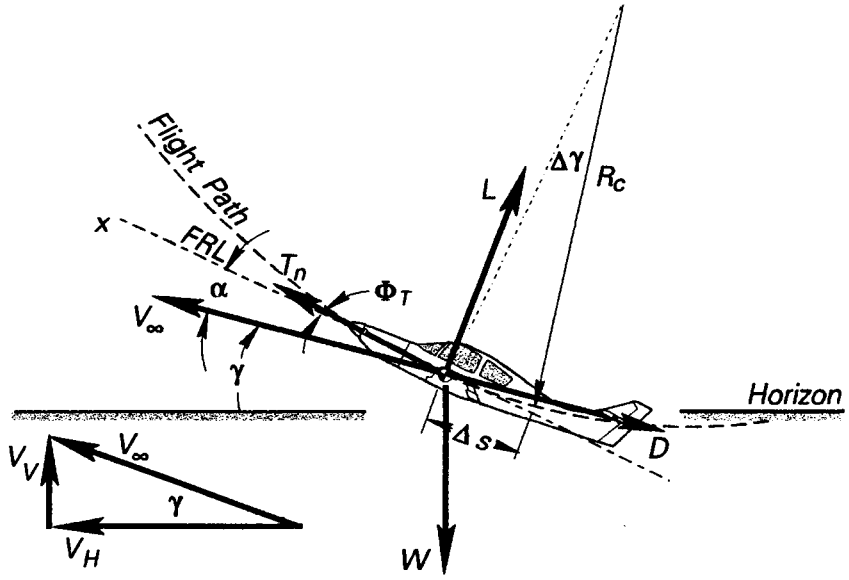

Fig. 3.1 Forces Acting on an Airplane in a Climb

3.1.1 Governing Equations

A free-body diagram of the basic forces acting on an airplane in a climb is sketched in Fig. 3.1. The forces perpendicular and parallel, respectively, to the flight path are:

$$L + T_n \sin(\alpha + \Phi_T) - W\cos\gamma = \frac{W}{g}\frac{V_\infty^2}{R_c} \tag{3.1}$$

$$T_n \cos(\alpha + \Phi_T) - D - W\sin\gamma = \frac{W}{g}\frac{dV_\infty}{dt} \tag{3.2}$$

where R_c = radius of curvature of the flight path.

The instantaneous velocity (or true airspeed) of the airplane's center of gravity is related to the time rate of change of the flight path angle γ, which is obtained by:

$$\lim_{\Delta t \to 0}\left(\frac{\Delta s}{\Delta t}\right) = \lim_{\Delta t \to 0}\left(\frac{R_c \Delta\gamma}{\Delta t}\right) = \frac{R_c d\gamma}{dt} = V_\infty$$

Or, we can write: $\dot{\gamma} = \dfrac{V_\infty}{R_c}$

Thus, eqn. 3.1 can be rewritten as

$$L - W\cos\gamma + T_n \sin(\alpha + \Phi_T) = \frac{W}{g} V_\infty \dot{\gamma} \tag{3.3}$$

If flight path curvature is slight ($R_c \to \infty$) and $\alpha + \Phi_T \approx 0$, eqns. 3.1 and 3.3 yield:

$$L = W\cos\gamma \tag{3.4}$$

Eqn. 3.2 becomes: $T_n - D - \dfrac{W}{g}\dfrac{dV_\infty}{dt} = W\sin\gamma$

The angle of climb is then obtained from

$$\sin\gamma = \frac{T_n - D}{W} - \frac{1}{g}\frac{dV_\infty}{dt} \tag{3.5}$$

Recalling that rate of climb is $\dfrac{dh}{dt} = V_\infty \sin\gamma$, we substitute to obtain:

$$\frac{dh}{dt} = \frac{(T_n - D)V_\infty}{W} - \frac{V_\infty}{g}\frac{dV_\infty}{dt} \tag{3.6}$$

3.1.1.1 **Steady State Approximation**. Equations 3.4, 3.5, and 3.6 are the governing equations for climb (or descent) performance. To further simplify the equation, it is often assumed that there is no acceleration along the flight path. Then, $\dfrac{dV_\infty}{dt} = 0$ and

$$\sin\gamma = \frac{T_n - D}{W} \tag{3.7}$$

$$\frac{dh}{dt} = \frac{(T_n - D)V_\infty}{W} \tag{3.8}$$

Equations 3.7 and 3.8 are very common approximations for low performance aircraft. If indicated airspeed is held constant and climb rate is low, the rate of change of true airspeed with altitude (and time) is small and this approximation is adequate. Or, if true airspeed is changing rapidly during the climb, rate of climb can be rewritten as

$$\frac{dh}{dt} = \frac{(T_n - D)V_\infty}{W} - \frac{V_\infty}{g}\frac{dV_\infty}{dh}\frac{dh}{dt}$$

$$\left(\frac{dh}{dt}\right)\left(1 + \frac{V_\infty}{g}\frac{dV_\infty}{dh}\right) = \frac{(T_n - D)V_\infty}{W}$$

$$\left(\frac{dh}{dt}\right) = \frac{(T_n - D)V_\infty}{W(1 + AF)} \qquad (3.9)$$

where AF = acceleration factor = $\dfrac{V_\infty}{g}\dfrac{dV_\infty}{dh}$

3.1.1.2 **Accelerated Climb Equations**. More generally, the performance equations can be constructed by assuming only that the angle $\alpha + \Phi_T$ is small and allowing both γ and V_∞ to be functions of time. Then the climb performance equations can be expressed concisely as a set of first-order nonlinear differential equations.

$$\dot{x} = \begin{pmatrix} \dot{\gamma} \\ \dot{V}_\infty \\ \dot{h} \end{pmatrix} = \begin{pmatrix} L + \dfrac{T_n(\alpha + \Phi_t)}{W} - \cos\gamma \\ g\dfrac{T_n - D}{W} - \sin\gamma \\ V_\infty \sin\gamma \end{pmatrix}$$

These equations can be extended to include other time-dependent variables such as

$$\dot{R} = V_\infty \cos\gamma \quad \text{or} \quad \dot{W} = \dot{w}_f$$

where R = horizontal distance covered or ground range and $\dot{w}_f$ = fuel flow rate

This set of first order differential equations suggests the use of state variables, which opens the door for use of more powerful mathematical tools (like the calculus of variations) to optimize performance parameters. But our purposes are served in this chapter by simply using this formulation to lead into a discussion of Rutowski's energy approximation[1].

3.1.2 The Energy Approximation

If the airplane comprises a dynamical system having a total energy made up of the sum of its kinetic energy and its potential energy, a slightly different, yet equivalent, set of climb performance equations can be written. Then, total energy is given by

$$E = \frac{1}{2}mV_\infty^2 + mgh$$

To more easily compare aircraft of different masses, it is customary divide by mg and rewrite total energy in terms of specific energy $\dfrac{E}{W}$ with units of distance or altitude:

$$h_e = h + \frac{V_\infty^2}{2g} \tag{3.10}$$

where h_e = specific energy or energy height

The time rate of change of specific energy, or specific excess power P_S, is

$$P_S = \dot{h}_e = \dot{h} + \dot{V}_\infty \frac{V_\infty}{g} \tag{3.11}$$

Recalling the V_∞ equation from the state variable set in Section 3.1.1.2,

$$\dot{V}_\infty = g\left(\frac{T_n - D}{W} - \sin\gamma\right)$$

Multiplying by V_∞, we get: $V_\infty \dot{V}_\infty = V_\infty g\left(\frac{T_n - D}{W} - \sin\gamma\right)$

But, $\dot{h} = V_\infty \sin\gamma$, so

$$\frac{(T_n - D)V_\infty}{W} = \dot{h} + \dot{V}_\infty \frac{V_\infty}{g} = P_S \tag{3.12}$$

Equation 3.12 merely confirms our earlier assertion that the energy approach to obtain specific excess power is equivalent to the force balance state equation relating V_∞ to T, D, W, and γ. Several books[2,3] elaborate on the utility of the energy approach, but it suffices for our purposes to simply point out that the energy definitions allow computation of climb performance from thrust and drag measurements under accelerated flight conditions, not just constant true airspeed maneuvers. This simple result merely scratches the surface in demonstrating the uses of the energy approximation. Rutowski's approach leads naturally to performance optimization of not only climb and descent performance, but also of maneuvering flight. As an example of such maneuvers, consider a level turn.

3.1.3 Forces in a Level, Unaccelerated Turn

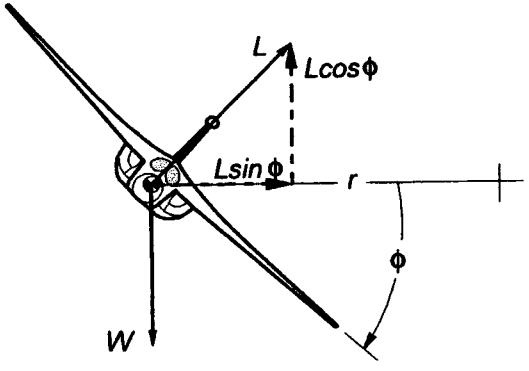

Fig. 3.2 **Forces in a Level Turn**

Consider first the idealized force and moment diagram (Fig. 3.2). It can be inferred from the diagram that the forces are in equilibrium (as long as you accept the notion of

"centrifugal" forces being produced by a constant acceleration). This idealization really describes a constant airspeed, constant altitude, and constant bank angle turn -- often simply called a stabilized turn or a level, unaccelerated turn. As we will see from the simple force equilibrium, the load factor in such a turn is constant also.

The force equations are almost trivial, but they do show the important variables we need to measure.

$L\cos\phi - W = 0$ or $L\cos\phi = W$, so

$$\boxed{n = \frac{L}{W} = \frac{1}{\cos\phi}} \tag{3.13}$$

In this expression we have used the definition of load factor n to show why a constant bank angle in a steady, level turn implies that n is a constant. Quite obviously, bank angle is a parameter we are likely to want to measure and that can be done by recording the load factor if the test airplane is equipped with an accelerometer (g-meter) or with an accurate vertical gyro. We will also see later that other parameters can be obtained from such simple relationships and that even simpler instrumentation will suffice.

Another equation springs from the horizontal force "balance" -- equating the component of lift acting in a horizontal direction to the "centrifugal force":

$$L\sin\phi = m\left(\frac{V^2}{r}\right) \tag{3.14}$$

where r is the radius of the turn (as suggested in Fig. 3.2)

V is the true airspeed (constant)

Using eqn. 3.13 with lift written in coefficient form and solving for turn radius:

$$\boxed{r = \frac{2\left(W/S\right)}{\rho C_L \sin\phi}} \tag{3.15}$$

Equation 3.15 shows clearly that the turn radius: (1) varies directly with wing loading (W/S), (2) inversely with altitude (that is, increasing altitude increases r), and (3) inversely with lift coefficient. Minimum turn radius will occur, therefore, at low gross weights, low altitude, and at maximum lift coefficient.

Other expressions that are useful in flight test are related to the previously developed expressions. For example, we can take eqn. 3.14 again and rearrange it to express load factor in terms of the other parameters. Knowing that $n = \frac{1}{\cos\phi}$ and using basic trigonometric definitions, we notice that $\sin\phi = \frac{\sqrt{n^2 - 1}}{n}$. Making this substitution and solving for r gives:

$$\boxed{r = \frac{gV^2}{\sqrt{n^2 - 1}}} \tag{3.16}$$

Similarly, starting with the same expressions and recognizing that the turn rate is simply the angular velocity associated with the level turn and is therefore defined by V/r, we can easily repeat the algebra and obtain an expression for the turn rate:

$$\omega = \frac{V}{r} = \frac{g\sqrt{n^2 - 1}}{V} \tag{3.17}$$

As suggested earlier, eqns. 3.16 and 3.17 demonstrate that calculating the important turn performance parameters like radius of turn and rate of turn, requires only a stop watch to time a specified heading change (usually 360°) and the pitot-static measurements that give true airspeed. An accelerometer could also be used, but it is not absolutely necessary.

Having now developed some simple (but quite effective) equations to calculate turning performance, let us now turn our attention to the kinds of turning performance that are of interest in our introduction to flight tests.

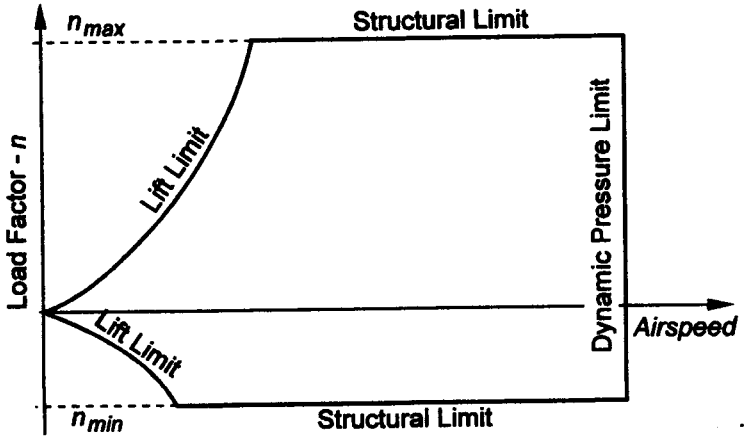

Fig. 3.3 *V-n* Diagram

3.1.3.1 **Types of Turning Performance**. The equations in the preceding section need to be related to operational considerations and modified to provide better indications of the actual capability of a given aircraft. The unaccelerated level turn is closely related to sustained turning performance, but instantaneous turning is often of even greater interest for combat maneuvering and is more closely related to specific excess power (especially when the aircraft is limited by thrust). The *V-n* diagram (Fig. 3.3) contains many of the elements important to both sustained and instantaneous turn performance. However, as we show later, there are more informative ways to present turning performance results.

Sustained turn performance is usually described in terms of energy state; it is a measure of the excess power of the airframe-engine combination, especially at load factors greater than one. The *V-n* diagram limits clearly affect and constrain the sustained turn performance since they describe the aerodynamic and the structural limits for the airframe. The stall characteristics of the airfoil, the planform, and other configurational features of the airplane prescribe lift limits. The maneuvering loads that the airframe can withstand typically set the upper and lower structural limits. In today's modern fighters,

these limits are usually expressed in g's and for these load limits are usually +9g and -3g, accelerations which are now approaching the physiological limits of the human pilot. Said another way, the turning performance of modern fighter airplanes is often not an airframe limit; instead, the pilot is may be unable to tolerate the achievable accelerations. G-Loss-of-Consciousness (G-LOC) is an example of such a physiological limit.

On the other hand, **instantaneous turning performance** ignores any change in airspeed that may occur during the maneuver. It is not necessarily a steady state maneuver. It is important in combat when the aircraft has weapons that can be employed with the nose pointing (perhaps only momentarily) at the adversary. It is particularly important in either getting off a first shot or in defeating an enemy's tracking solution. Instantaneous turning performance is important any time it is advisable to sacrifice energy to gain or regain tactical advantage. Again, the limits shown on the *V-n* diagram are useful in showing important characteristics of the turn performance, but there are more meaningful plots. The point where maximum lift coefficient and maximum load factor coincide is the maneuver point . The true airspeed associated with that point is called the corner velocity; at this speed the airplane can turn with the smallest radius and the highest turn rate.

3.1.3.2 **Limitations on Turning Performance**. Though we have alluded to turning performance limitations already, we have not clearly spelled out the types of limitations that are associated with the airframe and its powerplant. They can be classified and discussed under three general headings for any airplane.

3.1.3.2.1 *Thrust-Limited (or Power-Limited) Turning Performance*. To turn at constant altitude the airplane's lifting surfaces must produce lift over and above that required to maintain level flight with the wings level (Fig. 3.2). However, if additional lift must be generated, that lift inevitably produces additional induced drag. This additional drag must be balanced with additional thrust to maintain constant airspeed as assumed at the outset of this discussion. Of course, in many aircraft this additional drag grows to a point that available thrust from the powerplant cannot overcome the additional drag and the aircraft will decelerate in the turn. The airframe and powerplant are thrust-limited in the turn.

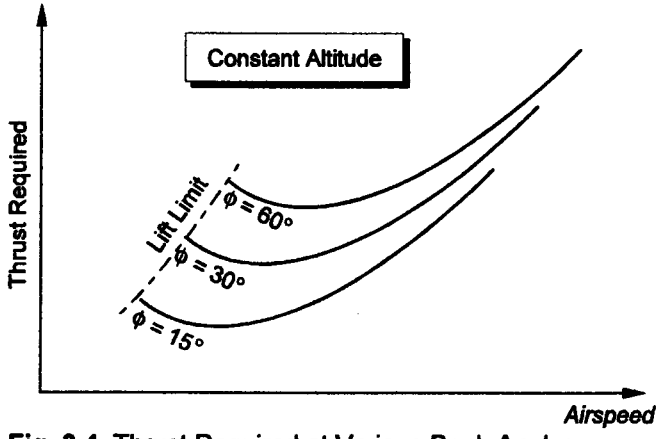

Fig. 3.4 Thrust Required at Various Bank Angles

Naturally, as bank angle increases, the thrust required increases rapidly (Fig. 3.4). Of course, there are many fighter aircraft today with very high thrust-to-weight ratios. Rarely do they encounter thrust limitations during turns, which suggests we must consider the

limits on the left side of Fig. 3.4 that are based on the maximum lift the wings of the aircraft can develop.

If you are conducting turning performance tests in a propeller-driven airplane, it will be necessary to consider how changes in induced drag change the power required curves rather than thrust required curves as shown in Fig. 3.4. However, power required is simply $\frac{DV}{550}$.

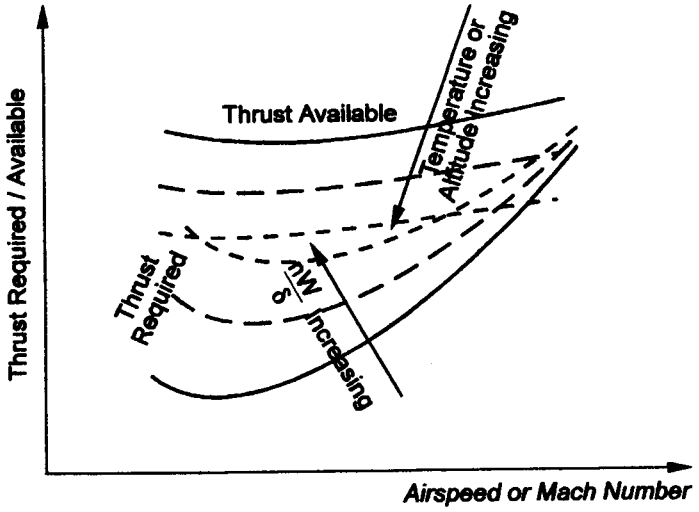

Fig. 3.5 Parameters That Affect Thrust-Limited Turning Performance

The thrust-limited turn is usually the primary focus of turn performance. This type of performance is closely tied to the energy concepts discussed earlier. In fact the same test technique (the level acceleration) provides data for turning performance and is used to determine optimum climb performance. This fact has led us to discuss turning performance in the same chapter as climb tests. Since P_s is relevant to both types of performance, we can readily see that thrust-limited turning performance is affected by exactly the same factors that affect climb performance (Fig. 3.5); anything that affects excess thrust changes turning performance. Corrections to turning performance are based on similar considerations:

(1) Temperature effects on thrust
(2) Pressure altitude effects on thrust
(3) Weight effects on induced drag
(4) Pressure altitude effects on drag

3.1.3.2.2 *Lift-Limited Turning Performance.* The dashed line in Fig. 3.4 indicates the maximum lift coefficient the wing can generate; that is, the lift limit is indicated by this line, simply because the wing will stall if it is exceeded. Stall speed in a turn is directly proportional to the load factor and the stall speed in level flight; that is, $V_{s\phi} = nV_s$, where $V_{s\phi}$ is the stall speed in an unaccelerated turn at a constant bank angle. This result suggests that the dashed line in Fig. 3.4 increases as $\frac{1}{\cos\phi}$.

This lift boundary for turning performance is a part of the envelope that is of particular interest in fighter and trainer aircraft. Sometimes specially designed tests are laid out to explore the lift boundary. However, the interest then is primarily one of controllability. For example, what levels of buffet are to be expected? Will they adversely affect the ability of the pilot to operationally maneuver and track an adversary for weapons delivery? Is there a strong likelihood that the airplane will go out of control with little or no warning? Though the lift limit does bound the performance as suggested in Figs. 3.3 and 3.4, these considerations are properly discussed under handling qualities testing. For that reason we will not dwell on them in this section.

3.1.3.2.3 *Load-Limited (Structural) Turning Performance.* The loads that the airframe is designed to carry are statically tested on the ground and monitored during early envelope clearance flights. These load limits are normally expressed in load factor (both positive and negative) as suggested in Fig. 3.3. These limits are typically specified in the contract and/or by the certification agency. Federal Aviation Regulations in the United States spell out limits of +4.4/-2.2 g for utility category aircraft certified under FAR Part 23. These load limits are seldom achieved in flight and there is always a margin of safety applied by the designer to allow for unexpected turbulence in the atmosphere or inadvertent overstressing of the aircraft.

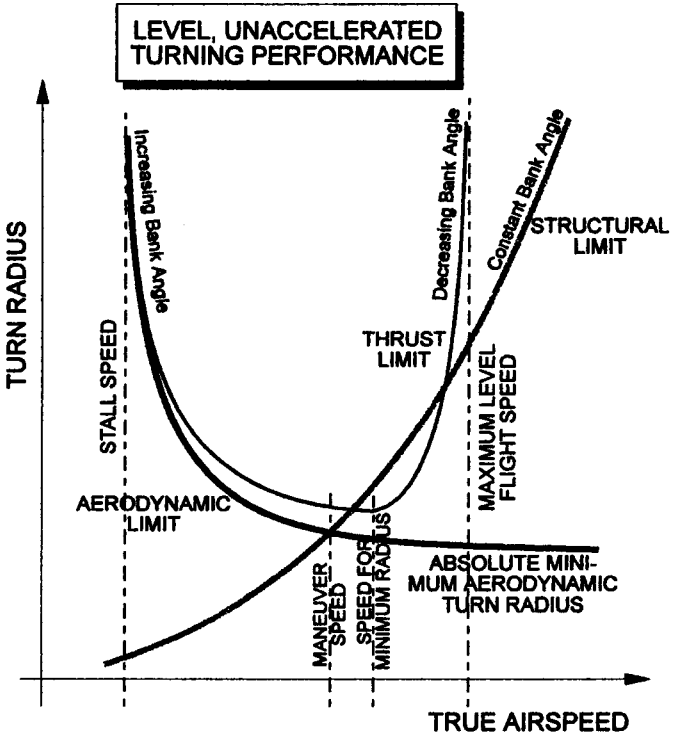

Fig. 3.6 Summary of Turning Performance Limitations

Figure 3.6 is yet another way to show and summarize possible limitations on turning performance. At speeds less than the maneuver speed shown in this sketch, even aircraft that are not thrust-limited cannot reach the limit load factor. They are aerodynamically (lift)

limited. At higher speeds the vehicle may be limited by either the strength of the structure or by the available excess thrust. For example, most general aviation airplanes are thrust-limited throughout much of their envelope.

3.1.4 Experimental Versus Analytical Performance Methods

Performance measurements have little meaning unless the data are reduced to some common basis of comparison. This common basis is the standard atmosphere. Hence, performance reduction refers to the data reduction schemes by which test data taken under nonstandard day conditions are converted to standard day results. As Lush[4] puts it, "...reduction methods are necessary to rationalize the test results so that they may be used for valid prediction and comparison."

As the title of this section suggests, there are two broad categories of performance data reduction. Experimental methods are so named because they require no advance knowledge of the components of the dynamical system. For an airplane, for example, no knowledge of the power plant characteristics would be required under this method. Analytical methods do require a priori sources to complete the analysis and are somewhat more widely used. Analytical methods are further broken down into differential methods and performance analyses. Differential methods are based on the notion, that for small corrections, linearization is appropriate. These methods depend on a generalized characterization of airframe drag and engine behavior. The differential technique is not useful, for example, when compressibility effects are significant. Performance analyses rely on advance information of engine behavior and are generally used when experimental methods are inconvenient or simply impractical.

One of the most perplexing problems in performance reduction is the number and type of variables to be considered, some of which are controllable while others are not. Engine parameters are, for example, usually quite controllable over the range of interest but outside air temperature is not. Tests are ordinarily planned to cover a suitable range of the controllable variables, while those variables that cannot be controlled are "standardized". Choice of a standard weight, like 95% of the takeoff weight, is typical of the latter case.

3.1.4.1 **Experimental Methods**. Dimensional analysis is a tool that allows us to reduce the number of variables by grouping them. Furthermore, if uncontrolled variables can be associated with controlled variables, experimental methods may be used to deduce standard day performance from nonstandard day test data. One of the simplest illustrations of this technique is in reducing performance data for turbojet airplanes. We will briefly introduce the subject for now and illustrate it in greater detail in Chapter 4. The success of dimensional analysis rests upon the assumption that all pertinent variables can be conceptually identified, though the mathematical form of the relationships may remain unknown. We could assume, for instance, that the climb rate of a turbojet-powered airplane depends explicitly on true airspeed, engine compressor speed, aircraft weight, outside air temperature, and pressure. If such a function exists, it can be represented by: $f_1(V_\infty, N, W, T_\infty, p_\infty) = 0$. (Notice that $_\infty$ has been used with T_∞ to differentiate it from T for thrust, as used previously. We will stick to that convention for the rest of the book.) If Buckingham's Pi Theorem is applied (we will return to this theorem later), the variables

can be reduced to three: $f_2\left(\frac{V_\infty}{\sqrt{T_\infty}}, \frac{ND}{\sqrt{T_\infty}}, \frac{W}{p_\infty D^2}\right)$. In the first expression there are five independent variables and two of them, W and T_∞, are not easy to control or adjust during flight tests. Dimensional analysis reduces the number of independent variables by two. This reduction of the number of independent variables by two is generally the level of simplification realized by application of dimensional analysis.

Pragmatically, reducing the number of independent variables by only two often makes it difficult to use experimental methods. Usually, there are still too many variables affecting the performance reduction. However, if one is able to assume that only a few of the variables affect performance strongly, experimental methods can be used. A good example of such a simplification is the level flight performance of a jet aircraft (discussed in detail in Chapter 4). If the constant test altitude is reasonably close to standard conditions, it is usually acceptable to omit viscosity, for example, as an independent variable in determining the level speed of the airplane.

3.1.4.2 **Analytical Methods**. Of the two "analytical" methods, the differential method is the easiest to use when the background data are available. This type of performance data reduction is with conventional reciprocating engine powered aircraft. The database for reciprocating engines is rather extensive and most of this class of airplanes do not approach any compressibility effects, making the differential method both convenient and accurate to use. The a priori knowledge necessary to use this method does not have to be extremely precise because the differential corrections for nonstandard conditions are usually relatively small. Turboprop-powered aircraft are generally analyzed using this approach, though the jet thrust introduces more variables and reduces the precision of the corrections. The second analytical method, performance analysis, is based on determination of drag and/or power curves (both required and available) over the altitude and airspeed envelope of the airplane. Again, one needs a priori information on the output of the propulsion system and propeller efficiencies, along with the effects of changes in temperature and forward speed on these parameters.

Choosing the appropriate performance reduction method is a difficult task. The most important considerations involved are the amount of data required (number and character of variables to be measured), the size of the flight envelope (altitude, Mach number, airspeed, load factors) to be covered, and the availability and nature of generalized data on the airplane and its power plant. In virtually every instance, the choice is a compromise and it is often a combination of the various methods. Now, let us turn our attention from these general considerations to the specifics of climb performance reduction.

3.2 CLIMB PERFORMANCE TEST METHODS

Climb performance tests fall into two broad categories: those designed to determine an optimum speed or Mach number schedule or those designed to measure the actual performance of the vehicle. For the first category of tests, the optimization may be carried out with any of the following purposes:

- minimum time to altitude
- minimum time to energy level
- minimum fuel to altitude
- minimum fuel to energy level
- maximum climb angle

The second category of climb tests are sometimes called "check" climbs or "performance" climbs since they are meant to verify that a chosen profile meets the specified optimization objectives. This validation should also ensure that cooling considerations, lack of forward visibility, poor handling qualities, or some other operational consideration does not dictate deviation from the optimized climb schedule. Both types of these tests will be introduced in this section, along with some of the techniques used. The reduction of climb data from such tests to standard day conditions will also be described briefly.

3.2.1 Climb Schedule Determination

Optimization of a climb schedule is based on the airplane's lift, drag, and thrust relationships (reviewed in Section 3.1) over an appropriate speed range. The measurement may be either direct or, more often, indirect. The two most common techniques, the sawtooth or partial climb test and the level acceleration test, will be discussed in this introductory text. Of these two test methods, the sawtooth climb is easier to understand and requires only the most rudimentary instrumentation. However, it is only useful for low climb rates. The level acceleration test provides more data for the same investment of flying time (data that are useful for more than just determining a climb schedule, too) and is applicable to high performance aircraft with high climb rates. It does require some means of automatically recording altitude and airspeed as a continuous function of time. We consider sawtooth climbs first.

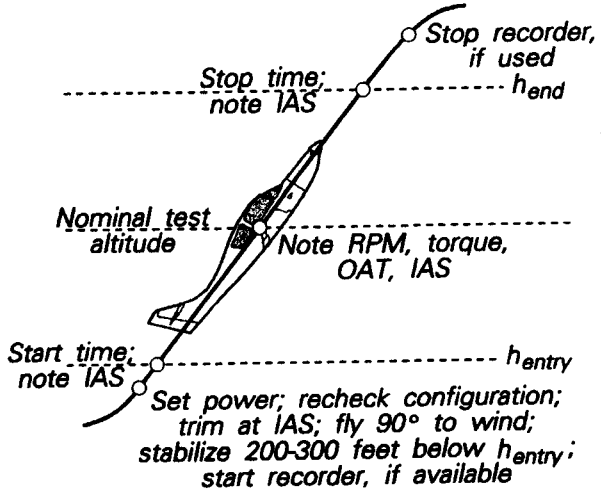

Fig. 3.7 Sawtooth Climb Procedure

3.2.1.1 **Sawtooth Climb Method**. The sawtooth climb, so named because of the shape of the altitude trace it produces, is used to determine the airspeed for maximum rate of climb at a nominal pressure altitude under test day conditions. A series of timed climbs is made over an altitude band bracketing the nominal pressure altitude chosen. Figure 3.7 illustrates the data collection. Increments of altitude used for each airspeed point should be chosen so that timing can be carried out precisely; if a stopwatch is manually started and stopped as suggested in Fig. 3.7, the altitude increments should be chosen so that the elapsed time is at least 1 minute. Indicated airspeed or Mach number must be main-

tained very precisely (±1 knot is desirable) to obtain valid results without excessive scatter. The landing gear, flaps, cowl flaps (in other words, the configuration) as well as the desired power setting must be set before commencing the data run. Trim should only be adjusted between runs. The pilot should be briefed to make data runs so that the heading is approximately 90° to the wind for the test altitude and he should attempt to conduct each climb in approximately the same air mass. Enough different constant airspeeds should be flown to define the shape of the rate of climb curve. Typical time to climb data are shown in Fig. 3.8 (open circles). For each nominal altitude, a minimum and a maximum speed point (using the same configuration and power setting) should be flown first to anchor the ends of the curve. A running plot of the observed time to climb through the altitude band, as shown by the open circles in Fig. 3.8, often gives clues as to which of the data points should be repeated to better define the maximum rate of climb speed.

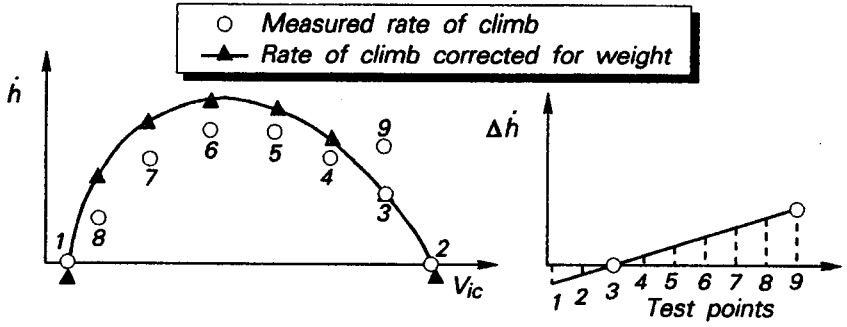

Fig. 3.8 Weight Correction of Sawtooth Climb Data

Dommasch[6] suggests that no corrections are necessary for nonstandard weight or for power changes due to nonstandard atmospheric conditions if sawtooth climb data are used solely to determine the maximum rate of climb speed schedule. It is current practice to correct for both these conditions[3,5] and those due to wind gradients. Both these references provide detailed discussion of the data reduction techniques, but for our introductory purposes we will describe only the simplest two of the possible ways to correct for changes in gross weight. Ways to minimize the effects of wind shear will also be briefly discussed.

The simplest way to correct sawtooth climb data for differences in gross weight during a set of climbs is illustrated in Fig. 3.8. It amounts to prorating the change in rate of climb over the time interval and requires that a second climb be repeated at a selected airspeed. This repeated point should be flown near the end of the series to provide a comparison with a point flown at a heavier weight earlier in the series. Points 3 and 9 in Fig. 3.8 illustrate this repetition. It is assumed that rate of climb varies linearly with time due to the change in gross weight. The solid triangles in Fig. 3.8 illustrate how the measured times to climb (or rates of climb) might change with this form of correction. Alternatively, if the weight of the airplane is known for each data point, the rate of climb may be corrected by a simple ratio of weights.

$$h_{corrected} \approx \frac{W_t}{W_{avg}} h_i$$

Both of these approximations produce roughly the same results and both of them ignore an induced drag correction term. However, they are easy to use and provide results that are little different from more elaborate schemes.

Nonstandard temperature conditions may also require corrections to the power output of the propulsion system. If so, the effects of atmospheric variations on engine performance must be known in advance and outside air temperature measurements become necessary. The Empire Test Pilots' School (ETPS) Handbook[7] gives a detailed account of British practice in making such corrections for reciprocating engine aircraft. Since these types of corrections depend entirely on the engine data available and are totally unique to each installation, we will discuss them no further.

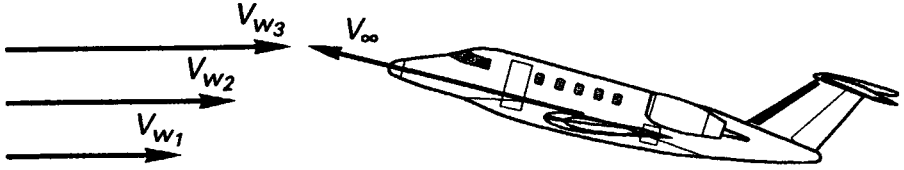

Fig. 3.9 Effect of Vertical Wind Shear on Sensed Rate of Climb

Finally, sawtooth climb data may be affected by both changes in wind speed and direction. Shifts in wind direction are usually of little consequence since the altitude band traversed is usually small and directional variations affect only the measured pressures. They can usually be ignored. Vertical speed gradients cannot, however, be ignored. Referring to Fig. 3.9, at constant true airspeed the pitot-static system senses an increasing wind speed as a deceleration. The effect in the rate of climb equation is the same as an acceleration factor (eqn. 3.9).

$$\frac{dh}{dt} = \frac{(T_n - D)V_\infty}{W\left(1 + \frac{V_\infty}{g}\frac{dV_\infty}{dh}\right)} \quad or \quad \frac{dh}{dt} \approx \frac{(T_n - D)V_\infty}{W\left(1 - \frac{V_\infty}{g}\frac{\Delta V_\infty}{\Delta h}\right)}$$

where $\Delta V_\infty = V_{w_{i+1}} - V_{w_i}$

If the vertical wind gradient $\frac{\Delta V_\infty}{\Delta h}$ is positive, rate of climb increases and, if the vertical wind gradient is negative, rate of climb decreases. But this knowledge is not easy to use. Determining wind gradients is very difficult and since they constantly change, correcting for them mathematically is impossible. The best way to handle wind effects on sawtooth climb data is by flying data runs close to perpendicular to the wind direction. One other possible technique is to repeat each data point (each V_{ic}) on reciprocal headings. Unfortunately, this approach also doubles test time required to complete determination of the climb schedule. In short, it is difficult to correct sawtooth climb data for vertical wind shears; shears problem should be avoided with good flight planning if possible.

Example 3.1: The following data were collected in flight on a twin-engine STOL transport during a series of sawtooth climb tests. The nominal (midpoint) test pressure altitude was 8,750 feet. Assume that the first six points were flown at constant weight and that the last six points were flown at a different (lighter) constant weight. Between the two sets of sawtooth points, a maximum speed of 120 KIAS was obtained at the climb power setting used. Plot the two curves thus obtained and find the average curve between the two

sets of faired data. Based on this average curve, what is the best rate of climb speed (KIAS) for this airplane at 8750 feet pressure altitude?

V_i (KIAS)	Δt (sec)	Δh (feet)	Rate of Climb (ft/sec)
71	57.0	900	15.79
79	55.0	900	16.36
88	59.5	900	15.13
96	65.5	900	13.74
109	139.0	900	6.47
106	100.0	900	9.00
95	63.0	900	14.23
85	51.0	900	17.65
76	48.5	900	18.56
70	52.0	900	17.31

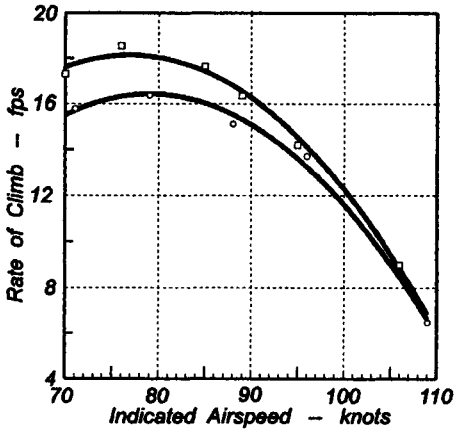

The plot on the right above shows the resulting sawtooth curves with the peak rate of climb occurring at approximately 77 KIAS. Thus, these sawtooth tests suggest that, for maximum rate of climb, an indicated airspeed of 77 KIAS should be maintained as the airplane passes through 8,750 feet.

3.2.1.2 **Level Acceleration Method**. Equation 3.6 shows that by maintaining a constant altitude and recording the change in true airspeed with time one can measure indirectly the excess power available from any airframe-powerplant combination. Furthermore, this measurement is easy enough to make even in high performance airplanes with a suitable means of recording airspeed variation with time. Motion picture film, video, magnetic tape, or telemetered signals can provide such time histories readily. Furthermore, acceleration data can also be used to define the maneuvering capability of the design, especially if the purchaser is interested in the energy maneuverability. Finally, the acceleration performance itself is sometimes used as a measure of merit in the contractual specifications.

The level acceleration technique is a simple concept. The airplane is merely accelerated, with a fixed power setting and configuration, from near its minimum level flight speed to its maximum level flight speed. The piloting task is simply to maintain constant pressure altitude. Of course, there are complications. First, the pilot does not usually have a pressure altitude indicator and altitude measurements must be corrected for pitot-static errors. Since the pilot must keep these corrections as small as possible, knowledge of static pressure error as a function of indicated airspeed is used to plan data runs. Because the altimeter has hysteresis error, reversals in altimeter readings should be avoided. Therefore, an acceleration or deceleration run should be planned to hold a slight climb or descent (100-200 fpm maximum), whichever minimizes the altitude error after the static pressure error correction is applied. The flight test team must take care to obtain ground block readings with the altimeter set at 29.92 (remember all test data taken at a pressure altitude must be taken with this altimeter setting). Typically, the airplane is trimmed at some midpoint speed for the range of speeds to be covered and the trim setting is not changed. The pilot must exercise care in passing through this point to transition from back pressure to forward pressure smoothly and not allow an altimeter reversal. If the airplane is capable of a wide speed range, it is possible to piece together several different acceleration runs. If such a procedure is used, the test team may have to account for small

changes in drag due changes in trim. A particularly sensitive part of the acceleration run occurs at speeds near Mach 1 when the pitot-static system is affected by shock waves. Ordinarily it is best to simply maintain the same rate of change of attitude (by using either visual references or guidance system commands derived from the airplane's inertial reference system) until the pitot-static system settles down in supersonic flight.

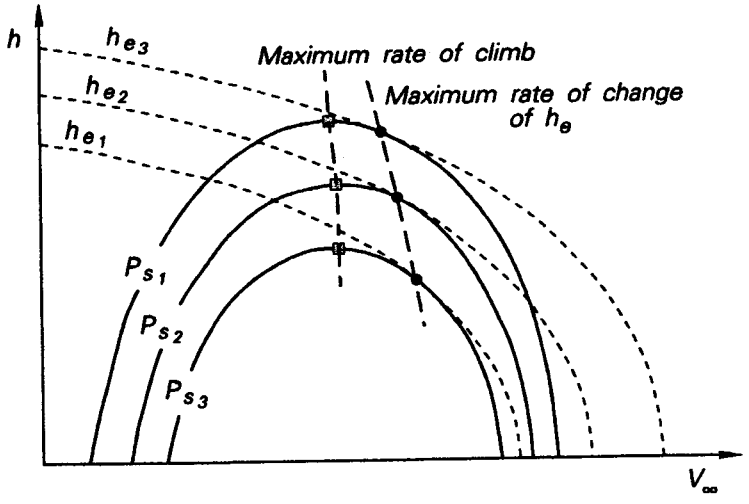

Fig. 3.10 Uses of P_S Contours

Level acceleration data can be used to optimize climb schedules in any one of the several ways suggested at the beginning of this section (Fig. 3.10 Illustrates). For the purposes of these introductory notes, we will only discuss the reduction of level acceleration data for either the maximum rate of climb schedule or the minimum time to an energy level. For either of these purposes, specific excess power P_S is the preferred measure of merit. As Fig. 3.10 shows, the maximum rate of climb can be estimated from constant altitude (horizontal) tangent lines to the various P_S contours and the maximum change in energy level can be estimated from contours of constant total energy level (the parabolic tangents in Fig. 3.10). Obviously, the two climb schedules are different, even for a subsonic airplane as is depicted in the sketch. This abbreviated discussion merely hints at the usefulness of specific excess power contour maps in terms of altitude and velocity parameters.

With regard to standard day corrections, P_S data from level accelerations can be treated as rates of climb. To be complete, the data reduction process should include corrections for nonstandard temperature effect on the thrust output of the propulsion system, both inertia and induced drag weight corrections, and wind gradient corrections. In most cases not all of these corrections will be significant and the test team must choose the ones to be made. In this section we will discuss the weight correction only, leaving the nonstandard temperature correction discussion to the check climb section. The wind gradient correction is identical that of the sawtooth climb technique. The only means of taking such gradients into account is through careful flight planning and execution.

In considering the weight correction for sawtooth climbs, no mathematically rigorous analysis was used. Another approach is to express test day thrust as a function of the other variables and then see how weight affects them. As a part of this analysis, it will be convenient to refer all calculations to a standard weight for ease of comparison. The general expression for P_s on a given test day is

$$P_{s_t} = \frac{\left(T_{n_t} - D_t\right)V_{\infty_t}}{W_t}$$

Rearranging to express test day thrust as:

$$T_{n_t} = \frac{W_t}{V_{\infty_t}} P_{s_t} + D_t$$

The effects of weight on the acceleration due to thrust are given by differentiating with respect to weight.

$$\frac{dT_{n_t}}{dW_t} = \frac{W_t}{V_{\infty_t}} \frac{dP_{s_t}}{dW_t} + \frac{P_{s_t}}{V_{\infty_t}} + \frac{dD_t}{dW_t} = 0$$

Typically, thrust is affected little by changes in weight at constant power setting (usually military or maximum) as the airplane accelerates in level flight. Angle of attack also has little effect on thrust available for acceleration, so

$$\frac{dP_{s_t}}{dW_t} = -\frac{P_{s_t}}{V_{\infty_t}} - \frac{V_{\infty_t}}{W_t} \frac{dD_t}{dW_t} = 0 \tag{3.18}$$

Defining the weight difference at any instant in the maneuver as $\Delta W = W_{std} - W_t$ and expressing all differentials in eqn. 3.18 as differences

$$\Delta P_s \approx -\left(\frac{P_s \Delta W}{W_t} + \frac{\Delta D_i V_{\infty_t}}{W_t}\right) \tag{3.19}$$

Equation 3.19 assumes that the only change in drag is because the weight is not the nominal weight, which leads to changes in induced drag. This simplified differential correction method yields two primary correction terms, the first due to inertia of the vehicle and the second due to induced drag changes between test weight and standard weight. The induced drag term can be further expanded by writing D_i as:

$$D_i = C_1 (nW)^2 \frac{\cos^2 \gamma}{b^2 e M^2 \delta}, \qquad \text{where } C_1 = \frac{2}{k \pi p_0}$$

Then ΔD_i becomes

$$\Delta D_i = C_1 \left(\frac{\cos^2 \gamma}{b^2 e M^2}\right)\left(\left(\frac{(nW)^2}{\delta}\right)_{std} - \left(\frac{(nW)^2}{\delta}\right)_t\right) = \left(\frac{2\cos^2 \gamma}{k p_\infty b^2 e M^2}\right)\left(n_{std}^2 W_{std}^2 \frac{\delta_t}{\delta_{std}} - n_t^2 W_t^2\right)$$

where k is the ratio of specific heats (typically, 1.4) and γ is the flight path angle.

The P_s correction for nonstandard weights then follows:

$$\Delta P_{s_{wt}} = -P_{s_t}\frac{\Delta W}{W_t} + \left(\frac{2\cos^2\gamma}{kp_\infty b^2 eM^2}\right)\left(n_t^2 W_t^2 - n_{std}^2 W_{std}^2 \frac{\delta_t}{\delta_{std}}\right)\frac{V_{\infty_t}}{W_t} \tag{3.20}$$

Since $n_{std} = n_t = 1$ and $\cos\gamma = 1$ for the level accelerations, eqn. 3.20 can be written as

$$\Delta P_{s_{wt}} = -P_{s_t}\frac{\Delta W}{W_t} + \left(\frac{2V_{\infty_t}}{kp_\infty b^2 eM^2 W_t}\right)\left(W_t^2 - W_{std}^2 \frac{\delta_t}{\delta_{std}}\right) \tag{3.21}$$

With regard to standard day corrections, P_s data from level accelerations can be treated as rates of climb. To be complete, the data reduction process should include corrections for nonstandard temperature effect on the thrust output of the propulsion system, both inertia and induced drag weight corrections, and wind gradient corrections. Usually, not all these corrections will be significant and the test team must choose the ones to be made. In this section we will discuss the weight correction only, leaving the nonstandard temperature correction to the check climb section. The wind gradient correction is identical as discussed under the sawtooth climb technique and the only satisfactory means of taking such gradients into account is careful flight planning and execution. Typical level acceleration data reductions include the following:

1. Correct the indicated gage readings for instrument corrections for each individual gage and each data point to be reduced; that is, for every V_i, h_i, and T_{∞_i}, calculate the corresponding V_{ic}, h_{ic}, and $T_{\infty_{ic}}$. Then, apply the appropriate position error corrections to obtain calibrated values of each parameter.

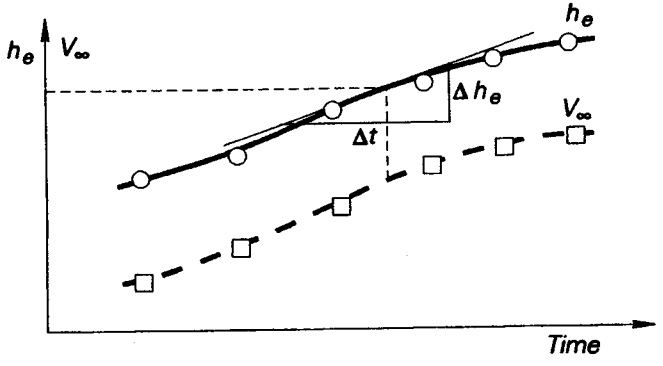

Fig. 3.11 Determining P_s Graphically

2. Calculate the test day true airspeed from calibrated airspeeds for each data point. Plot these points versus time as shown in Fig. 3.11 or arrange them in a time history array for step 5 in this process.
3. Calculate test day P_s from $P_s = \dot{h}_e = \dot{h} + \frac{V_\infty \dot{V}_\infty}{g}$ and plot these points on the same graph with the true airspeed time history as suggested in Fig. 3.11. Alternatively, arrange the h_e points in a time history array similar to the true airspeed array so that energy height can be numerically differentiated.

4. Estimate P_s for test day conditions by numerically differentiating the energy height time history to obtain an approximate rate of change of h_e for each instant of time and the corresponding true airspeed. Again, this process is easiest to visualize as a graphical process, though the actual work can be carried out by manipulating the appropriate data arrays in a computer relatively easily.
5. Correct P_{s_t} to standard day and standard weight conditions as suggested previously for rate of climb data.

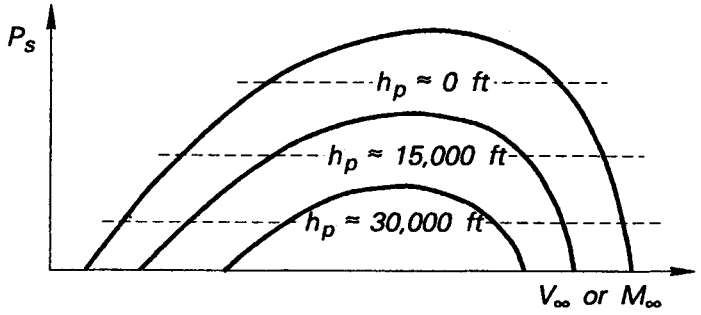

Fig. 3.12 Specific Excess Power versus Airspeed

6. Plot P_s versus V_∞ (or M_∞) for several altitudes. Notice that the resulting curves, as sketched in Fig. 3.12, are very similar in appearance to sawtooth climb curves for low performance airplanes. However, the shape of P_s curves for supersonic airplanes is quite different.
7. Crossplot P_s as a function of pressure altitude and velocity by taking lines of constant P_s across the constant altitude curves of Fig. 3.12. The resulting crossplot of constant P_s curves as a function of altitude and true airspeed, sketched previously in Fig. 3.5, is perhaps the most common way to depict level acceleration data. Recall that this format allows the determination of both the maximum rate of climb schedule and the minimum time to energy height climb schedule.

This procedure is by no means the only way to get P_s contours from level acceleration data; for example, you may choose to plot both test day true altitude and test day true airspeed versus time and numerically differentiate both quantities. Using these estimates for $\frac{dh}{dt}$ and $\frac{dV_\infty}{dt}$ in eqn. 3.11 gives P_s for the test day also. Whichever of the measured quantities is numerically differentiated, the test engineer should be careful to smooth the data and remove fluctuations with a half-cycle less than 20 to 30 seconds. Potential to kinetic energy exchanges simply do not occur more rapidly than this rate and higher frequency disturbances are usually noise in the data.

Level accelerations return a considerable amount of useful data in a relatively short amount of test time. It is a very efficient flight test technique. Optimized climb schedules for both subsonic and supersonic airplanes can be extracted using this approach. The acceleration characteristics of a given airframe-powerplant combination are direct measurements. Finally, the maneuvering capability of the machine can be derived from level accelerations conducted at different load factors. This introductory text will not go into this latter technique; interested students may refer to references 1,3, and 5 for details of this

extension of the level acceleration method. Data collected from level accelerations in high performance airplanes are usually more consistent and repeatable than data collected with the sawtooth climbs, both because of the use of the acceleration term and because vertical wind shear has little effect on level flight data. However, data handling is slightly more complex than it is for sawtooth climbs. Data must be recorded automatically and synchronized with time; so slightly more sophisticated instrumentation is required. Data reduction itself is rather more tedious and begs for automated processing. Neither of these objections is particularly troublesome with modern instrumentation and computer capabilities.

Example 3.2: Level acceleration data for a fictitious small jet trainer are tabulated below. These data were collected at a pressure altitude of 20,000 feet and they have been partially reduced (that is, standard day true airspeed and pressure altitude have already been calculated from the test measurements). Calculate and plot the P_s curve for this airplane at 20,000 feet. Based on this curve, what is the true airspeed for best rate of climb?

First, we estimate $\dot{h}$ and $\dot{V}$ from $\frac{\Delta h}{\Delta t} \approx \dot{h}$ and $\frac{\Delta V}{\Delta t} \approx \dot{V}$. For example, the first two lines in the table give: $\dot{h} = \frac{19970.7 - 19970.0}{0.2} = 3.5$ fps and $\dot{V} = \frac{86.8 - 86.1.0}{0.2} = 3.5\ \text{fps}^2$

Time (sec)	TAS (fps)	Altitude (feet)	$\dot{h}$ (fps)	$\dot{V}$ (fps^2)	P_s (fps)
0.40	86.8	19970.7	3.50	3.50	12.904
0.80	88.2	19973.0	7.00	3.50	16.557
1.20	90.1	19978.0	20.00	2.50	26.982
1.60	91.5	19985.0	15.00	4.50	27.735
2.00	93.3	19991.0	15.00	4.50	27.986
2.40	95.6	19996.0	10.00	6.50	29.182
2.80	98.2	20000.0	10.00	6.50	29.708
3.20	100.9	20003.7	13.50	5.50	30.654
3.60	103.9	20007.0	10.00	7.00	32.453
4.00	107.6	20009.6	4.50	10.00	37.632
4.40	111.6	20011.7	5.50	10.50	41.578
4.80	115.6	20014.9	4.50	11.00	43.646
5.20	120.4	20016.7	3.00	12.50	49.291
5.60	126.4	20012.9	-15.00	16.00	47.062
6.00	132.5	20007.1	-13.00	14.50	46.061
6.40	137.6	20002.8	-11.00	12.50	41.974
6.80	142.1	19998.0	-10.00	10.00	33.855
7.20	144.7	19997.0	5.00	4.50	25.175
7.60	146.1	19999.1	0.50	4.50	20.871
8.00	147.4	19999.2	-2.00	3.50	13.997

Then, eqn. 3.11 gives:

$$P_s = \dot{h} + \frac{V}{g}\dot{V} = 3.5 + \frac{(86.1 + 86.8)(3.5)}{(2)(32.17405)}$$

$P_s = 12.904$ fps

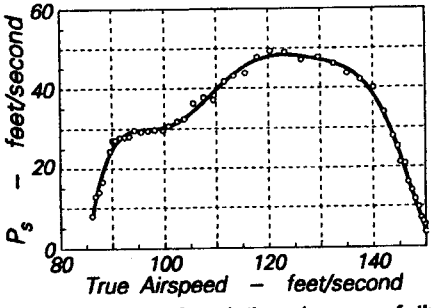

We could have found the slopes of the curves with elaborate numerical schemes, but this straight-line average is adequate with closely spaced data points. The plot above, with a spline fit, shows an approximate maximum maximum climb airspeed of 123 fps.

$V_{max\ rng} = 123$ fps

3.2.2 Performance Climbs

Once a climb schedule for a given purpose is determined, it must be validated by actually flying the schedule and measuring performance. Time to climb, climb angle, fuel used during the climb, and distance traveled during the climb are measured along the optimized path to prove that contractual specifications or certification requirements have been met by the design. These easily measured quantities are not all that the test team must evaluate in performance climbs, however. Operational factors, even though they may be qualitative rather than quantitative, are also important. Pilot visibility and general

handling qualities fall in this category. Subsystems operation may also be affected by the climb schedule. Engine cooling, critical altitudes for supercharging, and other powerplant characteristics are typical of the subsystem operational characteristics that must be examined during the performance climb. All in all, performance climbs are the validity check of not just the climb speed schedule established by the flight test team, but a verification that the entire vehicle and all its subsystems perform as expected in a climb.

Project Name

Pilot _____ FTE _____

Runway Temperature _____ Pressure Altitude _____ Wind _____

TAXI AND TAKEOFF		*Fuel Allowance* _____		
Data Point	Time	Fuel Reading	Counter Number	Remarks
Engine Start				
Brake Release				
Start Climb Profile				

CHECK CLIMB				
h_i	V_i	Time	Event Number	Remarks
2000	175			
4000	175			
6000	175			
—	—			

Fig. 3.13 Example Performance Climb Data Card

3.2.2.1 **Performance Climb Procedures**. Figure 3.13 illustrates a typical data card for a performance climb and emphasizes some of the data collection requirements. Generally, the piloting task during a performance climb demands considerable concentration on the part of the pilot. Therefore, it is best to have an automatic data recording device (video camera, photopanel, magnetic tape, or telemetry) if the airplane is occupied by only the pilot. With a second crewmember and a relatively low performance configuration, data can be hand recorded. Ordinarily, it is best to treat hand-recorded data as backup to be used only in case of instrumentation failure.

One of the keys to a successful performance climb is the entry to the maneuver. The desired power, configuration, and altitude (or rate of change of altitude) should be established and stabilized before data collection starts. The climb schedule itself must be religiously followed; if, for example, indicated airspeed is used as the primary cue for the pilot, it should be maintained as close to the desired as possible. A sensitive instrument (airspeed or Mach meter) must be used to see these small changes in the controlling variable quickly. (Even a ± 0.5 knot variation calls for control actions on the part of the pilot).

As with sawtooth climb tests and level accelerations, plan ahead to minimize the effects of wind gradients. Since a significant change in altitude is involved, you should fly 90° to the average wind.

Each airplane and each configuration will dictate different control techniques, but the pilot must be positive and make smooth changes at all times. Where there are abrupt changes in the profile, either due to mechanical constraints in the propulsion system, limits on the airframe, or an unusual climb profile, the pilot must anticipate the required changes

and the flight test engineer must expect to correct the data for variations from the optimum. At high altitude and/or low airspeed (low dynamic pressure), deviations from the profile must also be expected.

3.2.2.2 **Performance Climb Data Reduction**. The data reduction procedures for sawtooth climbs and level accelerations are subsets of the corrections required for the complete performance climb. To round out the discussion of climb corrections, it is convenient to restate the kinds of corrections that may be required. Three types of corrections are usually of interest:

- Correction for nonstandard atmospheric conditions
- Acceleration errors
- Weight corrections

Of these three classes of corrections, nonstandard weight corrections and induced drag corrections have already been discussed. Therefore, only the first two types of corrections need explanation to complete performance reduction methods for climb performance.

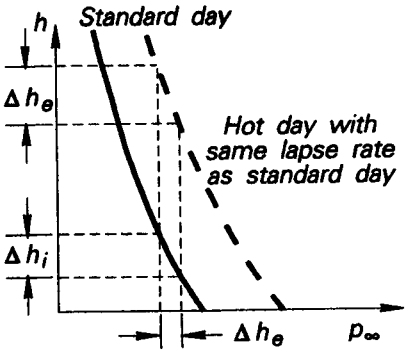

Fig. 3.14 Tapeline Altitude Correction for Rate of Climb

The correction for nonstandard atmospheric conditions takes into account the effects that test day temperatures at the measured pressure (geopotential) altitudes have on altitude measurements, airspeed measurements, and available thrust from the powerplant. Figure 3.14 shows that as test day altitude increments (as measured by an altimeter set at 29.92 in. Hg.) are not the same as actual or tapeline altitude changes if temperature does not follow the assumed standard temperature profile. This temperature deviation may be due to either a nonstandard lapse rate or to a warmer (or cooler) surface temperature with a standard rate of decay of temperature. The latter condition is sketched in Fig. 3.14 and is the first correction normally made to rate of climb data. Indicated ambient pressure change Δp_∞ reflects a potential energy change of Δh_i, not the actual potential energy change Δh_e. To correct for this shortcoming in the measurement system, the hydrostatic equation (eqn. 2.5) can be written for each altitude increment.

$$\Delta h_i = \frac{\Delta p_\infty}{\rho_{std} g_0} \qquad \text{and} \qquad \Delta h_e = \frac{\Delta p_\infty}{\rho_t g_0}$$

Then, dividing Δh_i by Δh_e

$$\frac{\Delta h_i}{\Delta h_a} = \frac{\rho_t}{\rho_{std}} = \frac{p_t / RT_{\infty_t}}{p_{std} / RT_{\infty_{std}}} = \frac{T_{\infty_{std}}}{T_{\infty_t}}$$

$$\frac{\Delta h_i}{\Delta t} = \frac{\Delta h_a}{\Delta t} = \frac{T_{\infty_{std}}}{T_{\infty_t}}$$

Finally, this so-called tapeline altitude correction (good for small deviations only, of course) can be expressed as the limit of the altitude increment divided by the corresponding time increment. By convention this correction is labeled with the subscript $_2$ to indicate that it is the tapeline altitude correction.

$$\left(\frac{dh}{dt}\right)_2 = \frac{dh}{dt}\frac{T_{\infty_{std}}}{T_{\infty_t}} \tag{3.22}$$

Example 3.3: During a check climb on a new jet trainer an indicated rate of climb of 1100 fpm was recorded at 9000 feet pressure altitude. The outside air temperature was 32° F at that test altitude. Calculate the tapeline altitude correction for this measured rate of climb under these conditions.

To make the correction, we must have absolute temperatures at the test altitude on the test day and on a standard day.

$T_{\infty_t} = 459.69 + 32 = 491.69°R$ and $T_{\infty_{std}} = 486.61°R$ from standard atmosphere tables.

Then, eqn. 3.22 gives:

$$\left(\frac{dh}{dt}\right)_2 = \frac{dh}{dt}\frac{T_{\infty_{std}}}{T_{\infty_t}} = 1100\frac{486.61}{491.69}$$

$$\boxed{\left(\frac{dh}{dt}\right)_2 = 1008.635 \text{ fpm}}$$

The next correction made is for changes in thrust output of the powerplant due to nonstandard temperature variation. Thrust horsepower available can be written as

$THP_A = T_n V_\infty$ and $THP_R = DV_\infty$

(Note: Net thrust is denoted by T_n in the following development. Do not confuse this symbol with any temperature. In the literature conflict is sometimes avoided by denoting thrust with F_n.) If $_{std}$ and $_t$ continue to denote standard day or test day conditions, respectively, the ratios between standard day power and test day power are:

$$\frac{THP_{A_{std}}}{THP_{A_t}} = \frac{T_{n_{std}} V_{\infty_{std}}}{T_{n_t} V_{\infty_t}} = \frac{T_{n_{std}}}{T_{n_t}}\sqrt{\frac{T_{\infty_{std}}}{T_{\infty_t}}}$$

$$\frac{THP_{R_{std}}}{THP_{R_t}} = \frac{D_{std} V_{\infty_{std}}}{D_t V_{\infty_t}} = \sqrt{\frac{T_{\infty_{std}}}{T_{\infty_t}}}, \text{ since } M_t = M_{std} \text{ implies that } D_{std} = D_t$$

The square root of the temperature ratio is obviously an important correction parameter for thrust output on a nonstandard day. The key to this simple relationship is that Mach number for test day conditions is the same as for standard day conditions. Defining a new corrected rate of climb as:

$$\left(\frac{dh}{dt}\right)_3 = \frac{THP_{A_{std}} - THP_{R_{std}}}{W} \tag{3.23}$$

Let the increment of net thrust be: $\Delta T_n = T_{n_{std}} - T_{n_t}$ or $\frac{T_{n_{std}}}{T_{n_t}} = 1 + \frac{\Delta T_n}{T_{n_t}}$

Substituting into eqn. 3.23:

$$\left(\frac{dh}{dt}\right)_3 = \left(\frac{T_{n_{std}}}{T_{n_t}} THP_{A_t} - THP_{R_t}\right)\frac{1}{W}\sqrt{\frac{T_{\infty_{std}}}{T_{\infty_t}}} = \left(THP_{A_t} - THP_{R_t} + \frac{\Delta T_n}{T_{n_t}} THP_{A_t}\right)\frac{1}{W}\sqrt{\frac{T_{\infty_t}}{T_{\infty_{std}}}}$$

If we make the tapeline altitude correction first and assume that it fully reflects test day power available and power required,

$\left(\frac{dh}{dt}\right)_2 = \frac{THP_{A_t} - THP_{R_t}}{W}$, which directly substitutes into the correction above,

$$\left(\frac{dh}{dt}\right)_3 = \sqrt{\frac{T_{\infty_{std}}}{T_{\infty_t}}}\left(\left(\frac{dh}{dt}\right)_2 + \frac{THP_{A_t}\Delta T_n}{W T_{n_t}}\right) \tag{3.24}$$

The climb correction expressed in eqn. 3.24 now includes both the tapeline altitude correction and an allowance for the difference in engine thrust available and required on the test day rather than on a standard day. Notice, however, that to make this differential power correction we need to measure the difference between test day net thrust and standard day net thrust. It is very difficult to make such a measurement for most airplanes; usually, we must rely on engine manufacturer's data rather than direct measurement. Since this thrust differential is so hard to measure directly, $\left(\frac{dh}{dt}\right)_3$ is often one of the most controversial rate of climb corrections.

Example 3.4: For the climb of Example 3.3, 100% of rated rpm of its nonafterburning engine was used. The calibrated test engine was instrumented with pressure taps and net thrust was calculated as 4627 lbs while climbing at a true airspeed of 375 fps. The engine manufacturer has tested the engine and shown that on a standard day at 9000 feet the engine should develop 4800 lbs of thrust. The initial weight of the airplane was 12780 lbs and 2100 lbs of fuel have been burned. Calculate the rate of climb correction for variation in thrust horsepower due to nonstandard temperature for this test point.

Again, $T_{\infty_{std}}$ and T_{∞_t} are needed. Using the values previously calculated, eqn. 3.24 gives:

$\left(\frac{dh}{dt}\right)_3 = \sqrt{\frac{486.61}{491.69}}\left(1088.635\ fpm + \frac{(4800 - 4627)(4627)(375\ fps)(60)}{(12780 - 2100)(4627)}\right)$. Notice that units must be consistent between the two additive terms inside the ( ).

$$\boxed{\left(\frac{dh}{dt}\right)_3 = 1445.6\ fpm}$$

The third and last correction in this series of rate of climb corrections takes into account the effect of nonstandard temperature lapse rates on measured true airspeeds. Figure 3.15 (following page) illustrates the rationale for this correction, remembering that, even for constant indicated airspeeds, true airspeeds for each indicated pressure altitude

will be affected by nonstandard temperature. This apparent acceleration will occur whether the climb is made at constant airspeed or at constant Mach number.

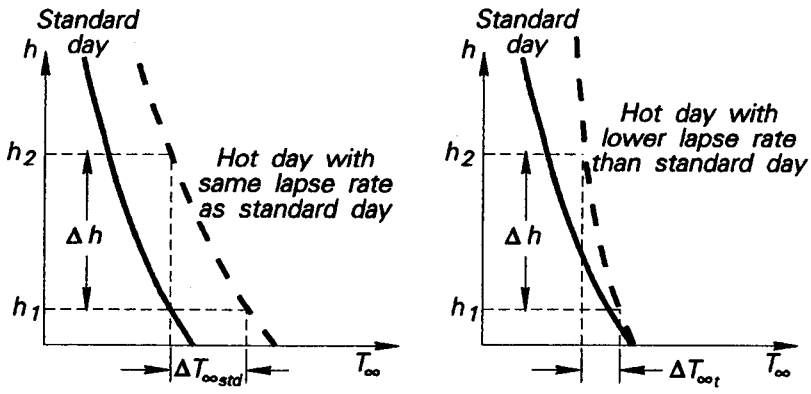

Fig. 3.15 Apparent Acceleration Correction

The apparent acceleration correction due to nonstandard temperature lapse rate can be made using the acceleration factor introduced earlier. Applying eqn. 3.9 to obtain the accelerated rate of climb for both standard day and test day conditions

$$\left(\frac{dh}{dt}\right)_{std} = \frac{\left(T_{n_{std}} - D_{std}\right)V_{\infty_{std}}}{W\left(1 + \frac{V_{\infty_{std}}}{g}\frac{dV_{\infty_{std}}}{dh_{std}}\right)} \quad \text{and} \quad \left(\frac{dh}{dt}\right)_{t} = \frac{\left(T_{n_t} - D_t\right)V_{\infty_t}}{W\left(1 + \frac{V_{\infty_t}}{g}\frac{dV_{\infty_t}}{dh_t}\right)}$$

After dividing to obtain the ratio between these two rates of climb, apply the binomial theorem to each of the terms containing the acceleration factor and retain only first order terms since only small changes (differential corrections) will be considered. The result is

$$\frac{dh_{std}/dt}{dh_t/dt} = \left(1 - \frac{V_{\infty_{std}}}{g}\frac{\Delta V_{\infty_{std}}}{\Delta h_{std}}\right)\left(1 + \frac{V_{\infty_t}}{g}\frac{\Delta V_{\infty_t}}{\Delta h_t}\right) \approx \left(1 + \frac{V_{\infty_t}}{g}\frac{\Delta V_{\infty_t}}{\Delta h_t} - \frac{V_{\infty_{std}}}{g}\frac{\Delta V_{\infty_{std}}}{\Delta h_{std}} + H.O.T.\right)$$

If it is also assumed that $V_{\infty_{std}} \approx V_{\infty_t}$ and that $\Delta h_{std} \approx \Delta h_t$.

$$\left(\frac{dh}{dt}\right)_{std} = \left(\frac{dh}{dt}\right)_{t}\left(1 - \frac{V_{\infty_{std}}}{g\Delta h}\left(\Delta V_{\infty_{std}} - \Delta V_{\infty_t}\right)\right)$$

Reverting to serial numbering of the rate corrections

$$\left(\frac{dh}{dt}\right)_{4} = \left(\frac{dh}{dt}\right)_{3}\left(1 - \frac{V_{\infty_{std}}}{g\Delta h}\left(\Delta V_{\infty_{std}} - \Delta V_{\infty_t}\right)\right) \tag{3.25}$$

Note that in eqn. 3.25 Δh and ΔV_∞ are small increments in altitude and true airspeed over which the measured climb rate is measured. These differences must be small for our approximations to be valid; so climb rate must be measured over a small altitude change and the corresponding airspeeds must also be small.

Example 3.5: Continuing our performance climb corrections as introduced in Examples 3.3 and 3.4, the airplane's rate of climb is measured between 8500 feet and 9500 feet to obtain the measured rate of climb. At each of these altitudes, the outside air temperature was 32.7°F and 31.3°F, respectively, and a constant Mach number was maintained for this segment of the climb. For the same pressure altitude band, calculate the apparent acceleration correction to the rate of climb previously corrected with tape-line altitude corrections and for power available due to nonstandard test day conditions.

First, calculate ΔV_∞ for the Δh in question. The temperatures at each altitude are: $T_{\infty_{t_1}} = 459.69 + 32.7 = 492.39°R$ and $T_{\infty_{t_2}} = 459.69 + 31.3 = 490.99°R$. Also, the constant M_∞ (identical at both test and standard day conditions) comes from standard day conditions:

$$M_\infty = \frac{375}{\sqrt{(1.4)(1716.55)(486.61)}} = 0.3469.$$

For the test day lapse rate, the ΔV between the two measurement altitudes is:

$$\Delta V_{\infty_t} = M_\infty \sqrt{\gamma R}\left(\sqrt{T_{\infty_{t_2}}} - \sqrt{T_{\infty_{t_1}}}\right) = -5.3679 \text{ fps}$$

For a standard lapse rate: $\Delta V_{\infty_t} = M_\infty \sqrt{\gamma R}\left(\sqrt{T_{\infty_{std_2}}} - \sqrt{T_{\infty_{std_1}}}\right) = -13.578 \text{ fps}$

Substituting into eqn. 3.25,

$$\left(\frac{dh}{dt}\right)_4 = 1445.6\left(1 - \frac{375}{(32.17405)(1000)}\right)(-13.7578 + 5.3679) \qquad \boxed{\left(\frac{dh}{dt}\right)_4 = 1587.0 \text{ fpm}}$$

Example 3.5 clearly illustrates how a nonstandard test day temperature lapse rate affects the correction of test day climb corrections to standard day conditions. The need for rate of climb corrections is obvious from the size the cumulative correction, $\left(\frac{dh}{dt}\right)_4$.

3.2.2.3 **Summary of Rate of Climb Corrections**. Collecting all rate of climb corrections (including those developed earlier), the complete correction is:

$$\left(\frac{dh}{dt}\right)_{std} = \sqrt{\frac{T_{\infty_{std}}}{T_{\infty_t}}}\left(\left(\frac{dh}{dt}\right)_t + THP_{A_t}\frac{\Delta T_{n_t}}{WT_{n_t}}\right)$$

$$+\left(\frac{-V_{\infty_t}\Delta V_w}{g\Delta h}\right)\sqrt{\frac{T_{\infty_{std}}}{T_{\infty_t}}}\left(\left(\frac{dh}{dt}\right)_t + THP_{A_t}\frac{\Delta T_{n_t}}{WT_{n_t}}\right)$$

$$+\left(\frac{-V_{\infty_t}}{g\Delta h}\left(\Delta V_{\infty_{std}} - \Delta V_{\infty_t}\right)\right)\left(\frac{-V_{\infty_t}\Delta V_w}{g\Delta h}\right)\sqrt{\frac{T_{\infty_{std}}}{T_{\infty_t}}}\left(\left(\frac{dh}{dt}\right)_t + THP_{A_t}\frac{\Delta T_{n_t}}{WT_{n_t}}\right) \qquad (3.26)$$

3.2.3 Turn Performance Flight Test Techniques

Turning performance is usually determined in one of two ways: (1) directly from level turning flight at constant power settings or (2) from level acceleration tests. The instrumentation required is typically quite minimal for the first kind of tests and the results are presented in several different ways. Cockpit instruments are often used to simply set the bank angle, the load factor, and the airspeed. Timing may be done with a stopwatch and the results are adequate. Thrust-limited turning performance can often be determined in this way quite satisfactorily.

3.2.3.1 **Level, Unaccelerated Turn Technique**. The simplest approach to measuring thrust-limited turning performance is to simply fly turns at constant altitude, constant power setting, and selected constant airspeeds. Typically, the powerplant is operating at a power setting at or near military or maximum power (since we are discussing thrust-limited turns). Obviously, in such a stabilized level turn the bank angle and the load factor are also constant. The instrumentation required is simply a stopwatch to time the total heading change. Frequently, a stabilized turn of 360° is used for convenience in this timing, though the turn could be through any heading change desired. To avoid significant timing errors due to human reaction times, it is usually best to turn for at least a minute, preferably two minutes. Turns should be made in both directions to check for any secondary effects on the turn performance. Care must be exercised by the pilot to guarantee that altitude and speed variations are kept small, usually less than ±50 feet and ±1 to 2 knots throughout the maneuver. It is far more important to maintain a constant airspeed throughout the timing period than it is to make the turn at exactly the aim airspeed. Depending on the resolution of the cockpit sensors available, the pilot may use either the attitude indicator (or some more precise bank angle indicator) or the accelerometer to maintain constant load factor. At high load factors with the bank angle increasing beyond 60° for level flight, greater care must be exercised to stay within acceptable tolerances. If the turn continues beyond 360° and the pilot has maintained the altitude precisely, he may encounter the jet wash of the test airplane. Such an event can upset the stabilized turn, but usually is nothing more than a nuisance. The reliability of cockpit heading indications should be checked; if they are reliable in turns at all load factors, the heading indicator can provide starting and stopping points that are useful. Hand recorded data are usually quite adequate, but if other instrumentation (rate gyros, stable platforms, event markers, and the like) is available, it should be used and backed up with hand-recorded data. As with all tests, care must be taken to observe all aircraft structural and aerodynamic limits. At speeds near the predicted maneuvering speed (corner velocity) the pilot is responsible for insuring that the maximum allowable load factor is not exceeded. Another caution in this part of the performance envelope: remember to relax the load factor before rolling out of the maneuver; typically, the load factor limit in a rolling maneuver is considerably lower than in a pure pitching maneuver with zero roll rate.

3.2.3.2 **Level Acceleration Technique**. This technique for level acceleration data is identical to that described in section 3.2.1.2. The only change is in how the data are used to describe the performance of the airplane. It is important to carry the level acceleration out to maximum airspeed so that the point for zero excess thrust is established. The usefulness of the data to characterize turning performance depends on the thrust limitations. Said another way, P_S (again as discussed in section 3.2.1.2) is just as useful as a measure of merit for thrust-limited turning performance as it is for climb performance. Figure 3.16 (next page) illustrates one of the plots commonly produced from level acceleration data to depict the turn performance capability of a fighter aircraft. These plots, sometimes called "doghouse" plots because of their characteristic shape, often include both the turn performance measures like rate and radius of turn and P_S contours.

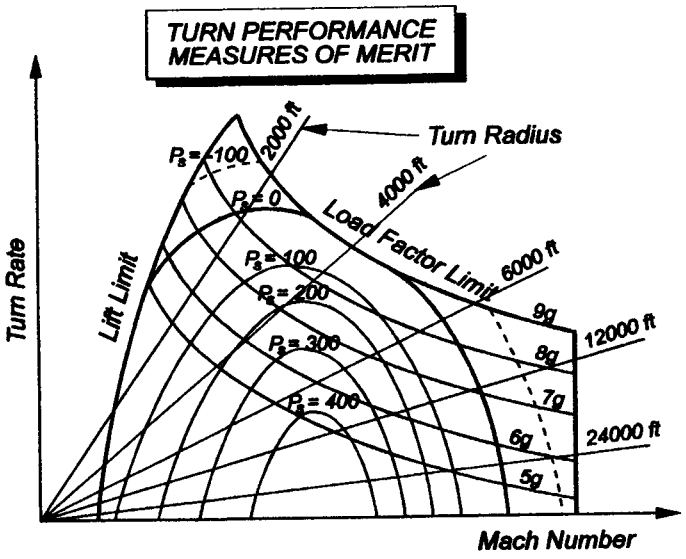

Fig. 3.16 Turning Performance Measures of Merit

By overlaying the P_s contours, whether the turn rates and radii are for sustained or instantaneous turns can be determined. If the turn rate and Mach number are such that P_s is negative, the indicated turning performance is an instantaneous turning capability. The aerodynamic and structural limits also are clearly indicated in the "doghouse" plot.

3.3 SUMMARY

This chapter has introduced the most common flight test methods used to optimize climb schedules, to validate climb schedules, and to measure turn performance. The methods are straightforward, though somewhat time-consuming, with the level acceleration technique holding a definite advantage over sawtooth climbs and level, unaccelerated turns in efficiency of data collection. Like most flight tests, climb tests are relatively easy to describe in theory, but they demand careful attention to detail in data reduction to achieve the accuracies needed for certification or specification compliance purposes. Turn performance flight tests are related to climb and descent performance largely because they are usually limited by available excess thrust. This fact allows test data to be collected in level accelerations for use in characterizing both optimized climb paths and instantaneous and sustained turning performance. Stabilized level turns with little or no instrumentation other than what is available in the cockpit also provide considerable insight into the capability of the airplane and certainly provide opportunity for a simple introduction to the measurement of this important aspect of aircraft performance.

REFERENCES

1 Rutowski, E. S., "Energy Approach to the General Aircraft Performance Problem," **Journal of the Aeronautical Sciences**, Vol. 21, Mar. 1954, pp. 187-195.

2 Nicolai, L. M., **Fundamentals of Aircraft Design**, METS, Inc., San Jose, California, 1975.

3 "Performance," Volume I, FTC-TIH-70-1001 (Revised December 1976), USAF Test Pilot School, Edwards AFB, California, 1976.

4 Lush, K. J., "A Survey of Performance Reduction Methods," Chapter 3, Vol. I, **AGARD Flight Test Manual**, Pergamon Press, New York, 1959.

5 "Fixed Wing Performance, Theory and Flight Test Techniques," USNTPS-FTM_No. 104, Naval Air Test Center, Patuxent River, Maryland, Jul. 1977.

6 Dommasch, D. O., "Data Reduction and Performance Test Methods for Reciprocating Engine Aircraft," Chapter 6, Vol. 1, **AGARD Flight Test Manual**, Pergamon Press, New York, 1959.

7 "Performance, Book B-2," Empire Test Pilots' School, Royal Aircraft Establishment, Farnborough , England, 1966.

8 Bryson, A. E., Jr., Desai, M. N., and Hoffman, W. C., "Energy-State Approximation in Performance Optimization of Supersonic Aircraft," **Journal of Aircraft**, Vol. 6, Nov. 1969, pp. 481-488.

9 Lan, C. E. and Roskam, J., **Airplane Aerodynamics and Performance**, Roskam Aviation and Engineering Corporation, Ottawa, Kansas, 1980.

10 McNamar, L. F. and Gordon, H. C., "T-38A Category II Performance Test," TDR No. 63-27, Air Force Flight Test Center, Edwards AFB, California, Nov. 1963.

11 Payne, J. H., "Flight Test Handbook," JP Aviation, USAF Academy, Colorado, 1990.

12 "Performance Flight Test Techniques," Volume III, FTC-TIH-70-1001 (Revised August 1975), USAF Test Pilot School, Edwards AFB, California, 1975.

13 Roberts, S. C., "Light Aircraft Performance for Test Pilots and Flight Engineers," Flight Research, Inc., Mojave, California, 1980.

Chapter 4

CRUISE PERFORMANCE TESTS

The cruise performance of any vehicle is one of the most important matters to be determined by flight test. Estimates of cruise performance are made from the very beginning of the conceptual design. Range and endurance under specified mission profiles are contractual requirements that must be validated for any aerospace vehicle. Hence, the topic is one of prime concern to the flight test team.

The elemental aerodynamic variable in determining cruise performance is the drag produced by the airframe-engine combination for the particular configuration or configurations and the specified mission profile. Unfortunately, there is no direct way to measure drag in flight. Test engineers therefore usually rely on approximate mathematical models for drag to start cruise performance analyses. Figure 4.1 is a block diagram representing types of drag and suggesting possible ways to simplify the mathematical model.

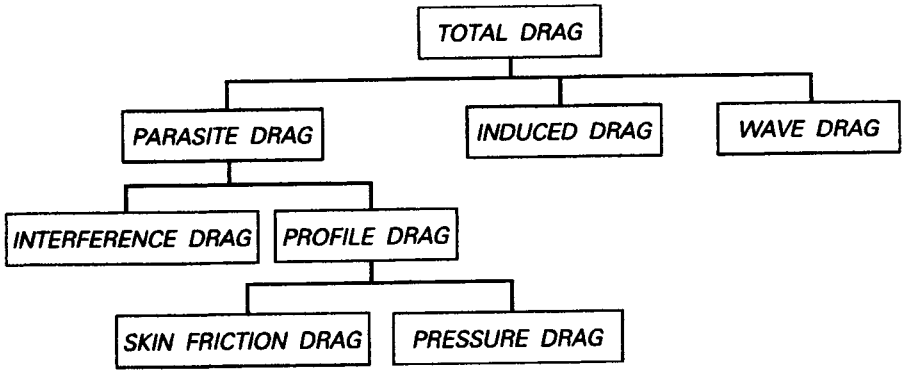

Fig. 4.1 Types of Drag

One of the simplest mathematical models for low speed airplanes is the subsonic drag polar given in eqn. 4.1.

$$C_D = C_{D_p} + \frac{C_L^2}{\pi e AR} \tag{4.1}$$

where C_D is the total drag coefficient and C_{D_p} is the effective parasite drag coefficient

Equation 4.1 is valid only for airplanes in which compressibility drag rise is not a factor; in this book the parabolic drag polar is assumed to be a good approximation for airplanes powered by reciprocating engines.

4.1 THEORETICAL FOUNDATIONS

Cruise performance is determined by both the available thrust (or power) from the powerplant and the thrust (or power) required by the airframe. Thus, it is necessary to correct the outputs from different propulsion systems to standard day conditions, much like the corrections required in climb performance data reduction. However, because of the fundamental differences between propeller-driven and jet-propelled airplanes, it will be convenient to discuss the performance reductions under separate sections. Different performance reduction methods are used for the two types of powerplants. Propeller-

driven aircraft will be considered first since they tend to be lower performers and the data reduction procedures are simpler (though perhaps more tedious). Typically, propeller-driven airplanes are analyzed using an analytical performance reduction method that draws upon the extensive data bank supplied by reciprocating engine manufacturers. Turboprop-powered aircraft usually are also analyzed with an analytical method, although a mixture of the analytical approach with differential techniques from the experimental performance method is often necessary to account for missing information on the powerplant. Turbojet and turbofan powered airplanes typically are analyzed with an experimental performance reduction method.

4.1.1 Propeller-Driven Aircraft

The analytical performance reduction method by which propeller-driven aircraft performance is usually analyzed relies heavily upon data collected by the engine manufacturer, usually brake horsepower data taken at sea level. For any airplane, $THP_r = \frac{DV_\infty}{550}$, with V_∞ in fps and D in pounds. With the usual definitions of dynamic pressure q, aspect ratio AR, Oswald's efficiency factor e, and assuming a parabolic drag polar with $L = W$:

$$THP_r = \frac{\rho_\infty V_\infty^2 C_{D_P} S V_\infty}{1100} + \frac{\rho_\infty V_\infty^2 C_L^2 S V_\infty}{1100 \pi e AR} = \frac{\rho_\infty V_\infty^3 C_{D_P} S}{1100} + \frac{W^2}{275 \rho_\infty S V_\infty \pi e AR}$$

Inflight measurement of thrust, especially from a reciprocating engine-propeller combination, is both uncertain and requires expensive instrumentation. Consequently, it is common practice to fall back on measured brake horsepower data from the engine manufacturer. But the propeller efficiency must be included in the horsepower relationship.

$$\eta_p BHP_r = THP_r$$

$$\text{So, } BHP_r = \frac{\rho_\infty V_\infty^3 C_{D_P} S}{1100 \eta_p} + \frac{W^2}{275 \rho_\infty S V_\infty \pi e AR \eta_p}$$

$$\text{Setting } A = \frac{C_{D_P} S}{1100 \eta_p} \quad \text{and} \quad B = \frac{1}{275 \pi e b^2 \eta_p}, \text{ and multiplying by } V_\infty,$$

$$BHP_r V_\infty = \rho_\infty A V_\infty^4 + \frac{B W^2}{\rho_\infty} \tag{4.2}$$

This relationship, with weight and density identified as dependent variables, clearly shows the dependence of power required upon airplane weight and altitude, the two variables that must be standardized if performance data are to be comparable between different tests. However, the power requirements can be further generalized to allow all test data for a given configuration to fall on a single power required curve. In other words, this further generalization of the power equation will allow direct comparison of test data and easy interpolation of the generalized curve to points within the envelope where test data were not collected to verify the mathematical model. Such an approach allows minimum flight test data collection to validate the mathematical model. Choose a standard weight

W_{std} for the configuration and use ρ_0 to define a generalized velocity parameter *VIW* and a generalized power parameter *PIW*.

$$VIW = \sqrt{\frac{2W_{std}}{\rho_0 C_L S}} \quad and \quad PIW = \frac{DVIW}{550} = \frac{1}{550}\sqrt{\frac{2W_{std}^3 C_D^2}{\rho_0 C_L^2 S}} \tag{4.3}$$

$$\text{since } L = W_{std} = \frac{1}{2}\rho_\infty V_\infty^2 S C_L \quad and \quad D = \frac{W_{std} C_D}{C_L}$$

At a given altitude and C_L: $V_\infty = \sqrt{\frac{2W}{\rho_\infty C_L S}}$ *and* $THP_r = \frac{1}{550}\sqrt{\frac{2W^3 C_D^2}{\rho_0 C_L^2 S}}$

If each term in eqns. 4.3 is multiplied by "one" in the appropriate form,

$$VIW = V_\infty \frac{\sqrt{\frac{2W_{std}}{\rho_0 C_L S}}}{\sqrt{\frac{2W}{\rho_\infty C_L S}}} = V_\infty \sqrt{\frac{\sigma W_{std}}{W}} \tag{4.4}$$

$$PIW = \frac{THP_r}{550} \frac{550\sqrt{\frac{2W_{std}^3 C_D^2}{\rho_0 C_L^2 S}}}{\sqrt{\frac{2W^3 C_D^2}{\rho_\infty C_L^2 S}}} = THP_r \sqrt{\sigma\left(\frac{W_{std}}{W}\right)^3} \tag{4.5}$$

Using eqn. 4.2, THP_r can be written as $THP_r = \eta_p\left(\rho_0 \sigma A V_\infty^3 + \frac{BW^2}{\rho_0 \sigma V_\infty}\right)$

Multiplying both sides by $\sqrt{\sigma\left(\frac{W_{std}}{W}\right)^3}$:

$$PIW = THP_r\sqrt{\sigma\left(\frac{W_{std}}{W}\right)^3} = \eta_p\left(\rho_0 \sigma A V_\infty^3 + \frac{BW^2}{\rho_0 \sigma V_\infty}\right)\sqrt{\sigma\left(\frac{W_{std}}{W}\right)^3}$$

Since ρ_0 and W_{std} are constants and η_p is approximately constant, we readily obtain

$$PIW/VIW = A_1 VIW^4 + B_1 \tag{4.6}$$

$$\text{where } A_1 = \frac{\rho_0 C_{D_p} S}{1100} \quad and \quad B_1 = \frac{W_{std}^2}{275\rho_0 \pi e b^2}$$

A generalized power curve (Fig. 4.2) is a reasonable approximation for a parabolic drag curve and constant propeller efficiency except at either the high or the low speed ends. At low speed (high α) nonlinearities due to separated flow appear. At low C_L, compressibility effects are important and the curve often splits into multiple branches. So, eqn. 4.6 is a simplified, but useful, mathematical model of the cruise performance for a low

speed, propeller-driven aircraft. The slope and intercept of this generalized curve readily give estimates of Oswald's efficiency factor and of the minimum drag coefficient.

$$e = \frac{W_{std}^2}{275 B_1 \rho_0 \pi b^2} \tag{4.7}$$

and $$C_{D_p} = \frac{1100 A_1}{\rho_0 S} \tag{4.8}$$

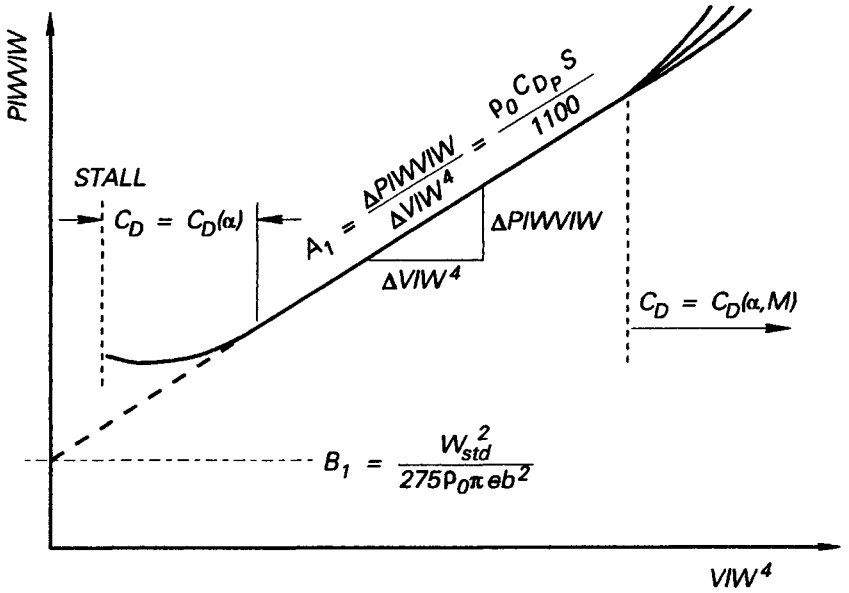

Fig. 4.2 Generalized Power Curve

Table 4.1 Cruise Data for a Propeller-Driven Airplane

TAS (kts)	TAS (fps)	BHP_r	THP_r	W_t (lbs)	VIW (fps)	PIW	VIW^4 ($\times 10^{-9}$)	PIW(VIW)
55	92.828	512	424.960	5512	80.64	334.86	0.0423	27002.57
60	101.267	442	366.860	5430	88.63	295.65	0.0617	26203.83
65	109.706	383	317.890	5376	96.50	260.06	0.0867	25094.84
70	118.144	343	284.690	5322	104.45	236.45	0.1190	24696.38
75	126.583	318	263.940	5288	112.27	221.34	0.1588	24848.28
80	135.022	286	237.380	5236	120.34	202.04	0.2097	24313.51
90	151.900	248	205.840	5198	135.88	177.12	0.3409	24066.47
100	168.778	225	186.750	5165	151.46	162.23	0.5262	24571.56
110	185.656	221	183.430	5111	167.48	161.88	0.7868	27112.15
120	202.533	225	186.750	5079	183.28	166.37	1.1285	30492.86
130	219.411	235	195.050	5021	199.70	176.78	1.5904	35303.81
140	236.289	252	209.160	4948	216.64	193.78	2.2028	41981.70
160	270.044	302	250.660	4875	249.44	237.47	3.8712	59233.66
180	303.800	375	311.250	4805	282.65	301.34	6.3829	85174.16
200	337.556	458	380.140	4722	316.81	377.78	10.0740	119683.50

Example 4.1: Table 4.1 shows data for a general aviation airplane with a propeller efficiency of 0.83. Data were collected at 6000 feet pressure altitude with an outside air temperature of 40°F. The airplane's "stan-

dard" weight is 5000 lbs. Wing area is 175 ft^2 and aspect ratio is 5.5. Calculate C_{D_p} and e by plotting a generalized power required curve and measuring the slope and the intercept of that curve.

First, density is calculated from $\rho = \frac{p}{RT}$, with $T = 40 + 459.69 = 499.69°R$; that is,

$\rho = \frac{1696}{(1716.55)(499.69)} = 0.0019773$ slugs/ft^3. Then, $\sigma_t = \frac{0.0019773}{0.0023769} = 0.83188$. With $V_\infty = 55$ knots = 92.828 fps, $VIW = 98.828\sqrt{\frac{(0.83188)(5000)}{5512}} = 80.638$ fps. Also, $PIW = THP_r\sqrt{\sigma\left(\frac{W_{std}}{W_t}\right)^3} = \eta_p BHP_r\sqrt{\sigma\left(\frac{W_{std}}{W_t}\right)^3}$ or $PIW = (0.83)(512)\sqrt{0.83188\left(\frac{5000}{5512}\right)^3} = 335$ hp. Finally, carrying out the multiplications for $(PIW)(VIW)$ and VIW^4 gives the last two columns in Table 4.1. The plot below shows the resulting generalized power curve. A linear curve was fitted to the last 8 data points in Table 4.1. The resulting straight line had a slope of 0.0000100502 and a PIW-VIW intercept of 19573.9. Utilizing eqns. 4.7 and 4.8, we estimate the required parameters:

$$e = \frac{5000^2}{(275)(962.5)(0.0023769)(19573.9)} \qquad \boxed{e = 0.646}$$

$$C_{D_p} = \frac{(0.0000100502)(1100)}{(0.0023769)(175)} \qquad \boxed{C_{D_p} = 0.0266}$$

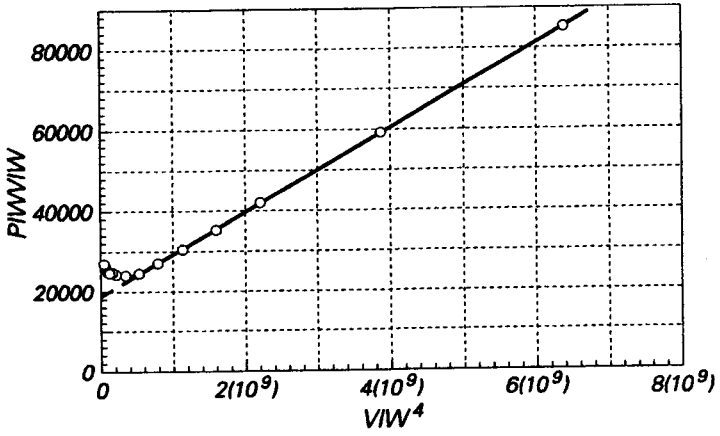

4.1.1.1 **Propeller Efficiency**. Propeller efficiency is not easily measured in flight, although Bull and Bridges[1] have used specially designed instruments and a maximum likelihood mathematical modeling technique to measure it. Their approach shows considerable promise, but the method is not yet widely used. More commonly, propeller efficiency is estimated by either an analytical technique[2] or a semi-empirical method[3]. Each of these methods is relatively simple, provided the appropriate inputs are known. To use them, one must know altitude, true airspeed, brake or shaft horsepower, and number of propeller blades, all readily obtainable configuration constants. In addition, variables like advance ratio, activity factor, solidity ratio, and integrated design lift coefficient that are peculiar to propeller performance must be derived. Advance ratio J is defined as the forward speed of the propeller divided by the rotational speed:

$J = \frac{V_\infty}{nD}$, where n is propeller rotational rate in revolutions/second

Activity factor AF is a measure of the power absorbed by the propeller and is defined as

$$AF = \frac{100000}{16} \int_{x_h}^{1.0} \frac{c}{D} x^3 dx \tag{4.9}$$

where $x = \frac{r}{R}$, $D = 2R$, and $c = c(x)$ (Fig. 4.3.)

The non-dimensional hub radius, usually taken to be about 0.15, is x_h. The solidity ratio SR is simply the ratio of total blade area to the disk area swept by the rotating blades.

$SR = SR = \frac{Bc}{pR}$ where B is the total number of blades.

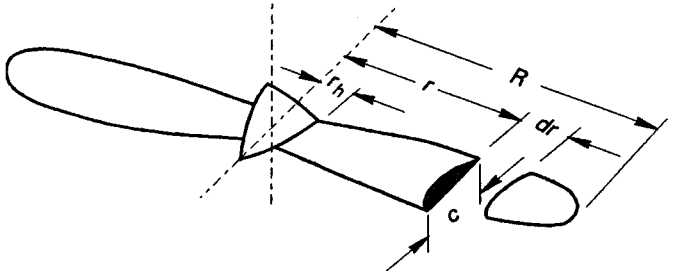

Fig. 4.3 Geometric Variables for a Propeller

The integrated design lift coefficient is defined as

$$C_{L_i} = 4 \int_{x_h}^{1.0} c_{\ell_d} x^3 dx \tag{4.10}$$

where c_{ℓ_d} is the individual blade section design lift coefficient and is a function of x.

Optimizing the propeller for cruise performance generally means that C_{L_i} will be small (on the order of 0.35), while optimizing the propeller for high thrust at lower forward speeds (climb speeds, for example) will result in an integrated design lift coefficient of about 0.60.

It is convenient (for the same reasons that we use nondimensional coefficients like C_L, C_D, and C_m) for engineers to describe propeller performance using nondimensional coefficients. Three terms typically characterize an aircraft powerplant's output: power, thrust, and torque. The three important propulsive coefficients include:

- Power coefficient $C_P = 550 \frac{BHP}{\rho_\infty n^3 D^5}$
- Thrust coefficient $C_T = \frac{T_n}{\rho_\infty n^2 D^4}$
- Torque coefficient $C_Q = \frac{Q}{\rho_\infty n^2 D^4}$

Having indicated how propeller efficiency can be estimated, consider next how we estimate the power available from the engine.

4.1.1.2 **Power Available**. Earlier, it was pointed out that for propeller-driven aircraft it is common to use engine manufacturer's data to estimate the power output available from the engine. Certainly this approach is a widely accepted practice for reciprocating engines. However, it is possible to directly measure the output power to the propeller shaft. A torque meter can be installed on many engines for this purpose. Production torque meters, which generally do not provide the accuracies needed for flight test, are routinely installed on airplanes powered by turboprop powerplants. To find *BHP*, you only need the torque meter reading, the rotational rate of the propeller shaft, and a calibration constant for the torque meter (usually found during ground tests using a dynamometer).

$$BHP = \frac{2pnQ}{550} \quad \text{or} \quad BHP = K_{n_{ic}} Q_{ic}$$

Flight test quality torque meters are hard to install, require frequent calibration, and are expensive. Smaller engines cannot accommodate commercially available torque meters and many project budgets cannot afford their cost. So, engine characteristic curves, obtained from ground test stands, provide estimates of available engine power.

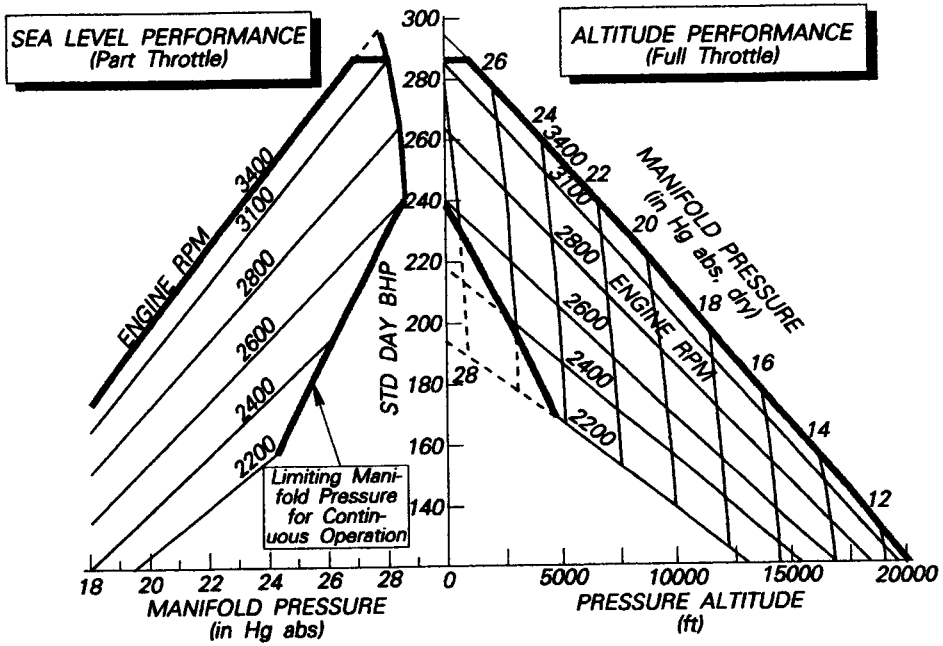

Fig. 4.4 Engine Power Chart for Normally Aspirated Engines

Since the manufacturer's data sheets (similar to Figs. 4.4 and 4.5) are usually based on ground tests, the flight test analyst must estimate engine output data for a given test condition from charts like those shown. Remember that measurements are usually taken at or near sea level for such charts. The altitude estimates are usually calculated by the powerplant engineers. For reciprocating engines these data are usually quite accurate

and their ready availability makes them attractive for use. Also, they are usually based on standard day conditions; corrections must be made for nonstandard conditions. The flight test engineer must carefully study the engine data sheets for his powerplant to be sure that all nonstandard conditions have been considered. Once again, a few terms must be defined to make this process easier.

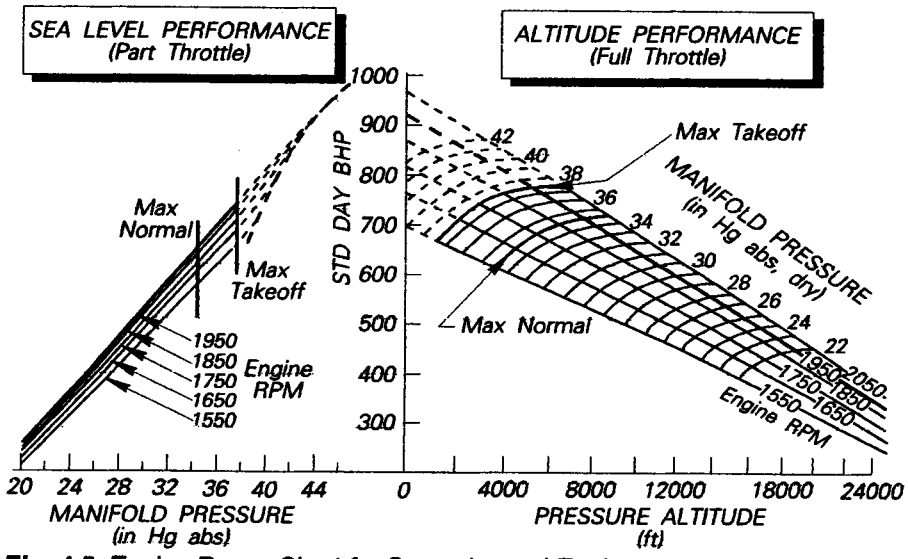

Fig. 4.5 Engine Power Chart for Supercharged Engines

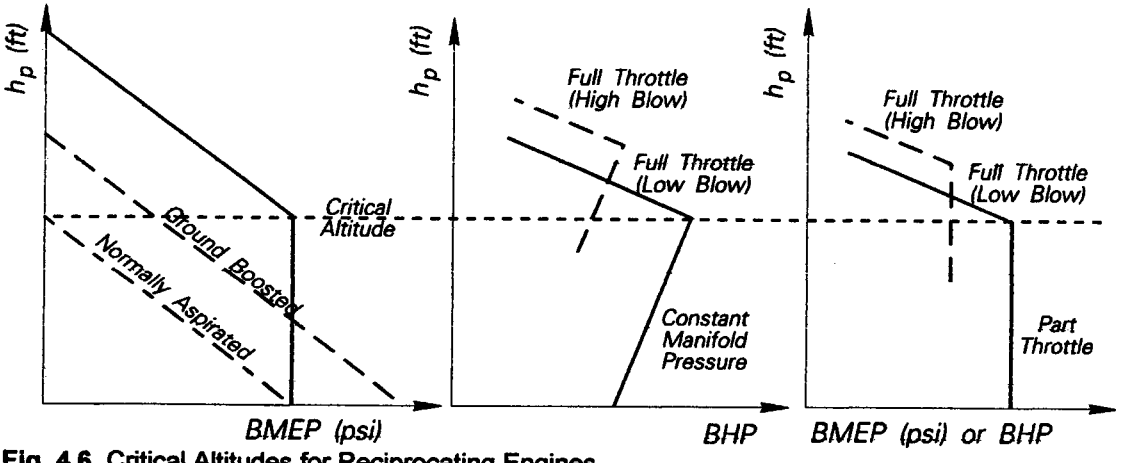

Fig. 4.6 Critical Altitudes for Reciprocating Engines

For a reciprocating engine the **critical altitude** is the altitude at which the throttle must be fully opened to develop rated power at rated RPM (Fig. 4.6). The British give this altitude a more descriptive name, **full-throttle height**, because critical altitude is the altitude at which the throttle must be fully open to produce the specified horsepower. Critical altitude is the altitude at which the power begins to decrease regardless of the position of the throttle. Whenever an engine reaches a structural limit because of cylinder pressures or if the manufacturer seeks longer life, or for any other practical operational reason, rated

power may be produced at part throttle up to the critical altitude. Such "de-rating" is, in fact, more common than having not having any operating limits. Figure 4.6 illustrates this idea for the case when the power output of the engine is limited by the pressure allowed in the cylinders. Turbosuperchargers are the most common form of supercharging in modern reciprocating engines and engine limits may be set by BMEP, BHP, turbine RPM, or turbine temperatures. Of course, multi-stage supercharging results in more than one critical altitude (again, see Fig. 4.6).

A reciprocating engine that takes in ambient air and does not compress it prior to the combustion process is **normally aspirated**. If a geared compressor is attached to the crankshaft accessory drive, the pressure of the air used in the combustion process may be raised to produce more power. Such engines are called **ground-boosted** engines. Both normally aspirated and ground-boosted engines may have sea level as a critical altitude.

Fuel-air mixture setting also strongly affects available brake horsepower. Figure 4.7 illustrates how deviation from the desired fuel-air ratio affects reciprocating engine performance. Obviously, the mixture must be set carefully during cruise performance tests.

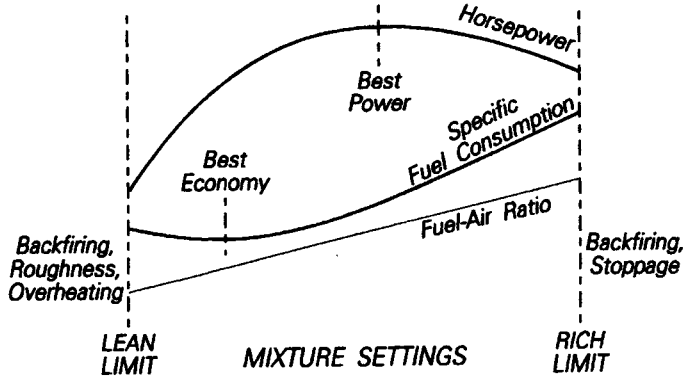

Fig. 4.7 Effect of Mixture Setting

4.1.1.3 **Corrections to BHP Available**. For part throttle operation with no mechanical limitations, corrections to power available (primarily those dealing with temperature) from a reciprocating engine are usually given on engine charts (Fig. 4.8).

To estimate actual test day horsepower from manifold pressure, engine rpm, altitude, and inlet temperature on such typical charts, the following procedure is recommended. The outlined procedure helps explain how and why flight tests are necessary to verify installed engine characteristics from manufacturer's data. Keep in mind that these charts are usually based on test data taken near sea level; altitude performance is calculated from that information. A typical estimate of test day power available is obtained by:

1. Locate point A on the full throttle altitude curve for a given dry manifold pressure-full throttle rpm curve.
2. Find the corresponding point B on the sea level performance curve for the manifold pressure and rpm used in step 1.
3. Project the horsepower for point B to the ordinate on the altitude performance scale (point C) and connect points A and C with a straight line.

4. At the test day pressure altitude and standard day temperature (nomogram at the bottom of the altitude performance chart in Fig. 4.8) project upward to the straight line found in step 3 to locate point D.
5. Modify the horsepower at point D using the following expression to estimate actual (nonstandard) power output available under test conditions.

$$BHP_{std} = BHP_t \sqrt{\frac{T_{std}}{T_t}} \quad or \quad MAP_{std} = MAP_t \sqrt{\frac{T_{std}}{T_t}}$$

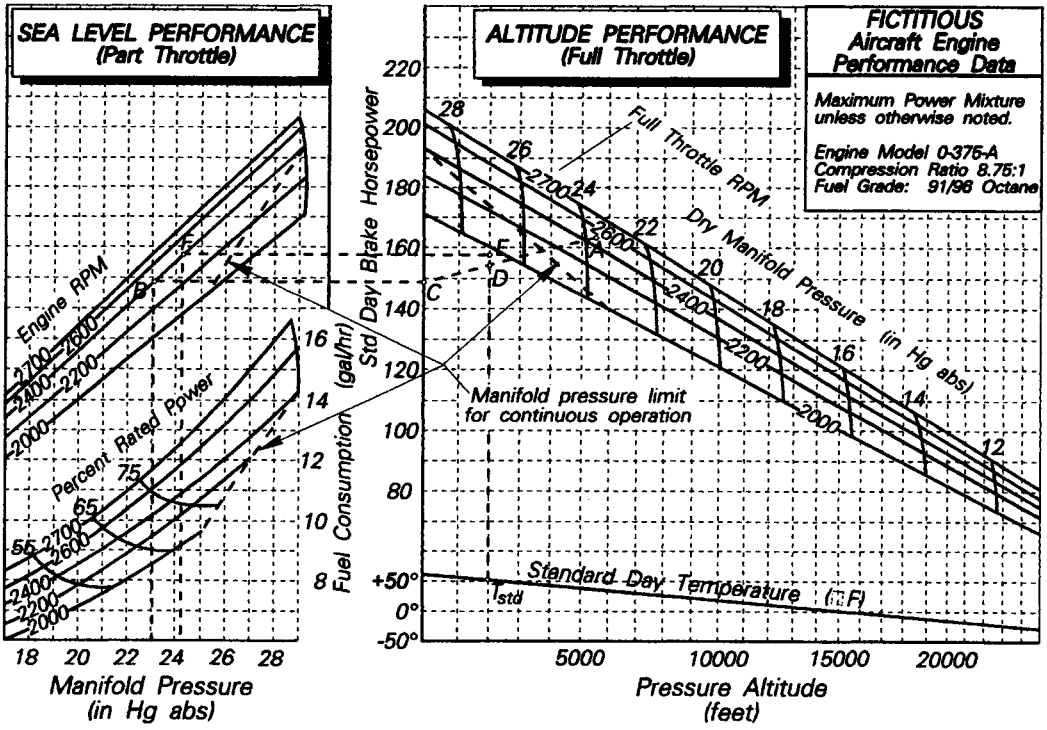

Fig. 4.8 Engine Operating Charts

Full throttle operations often involve other limits or constraints that require corrections including:

- Nonstandard intake temperature (carburetor or supercharger inlet)
- Nonstandard exhaust back pressure
- Nonstandard BHP
- Nonstandard turbine RPM

For a given engine and installation, consult the manufacturer's data base for such limits that apply to the specific configuration under test. Any limit that may differ because test atmospheric conditions are not standard day conditions is a subject for careful study.

Having introduced the performance reduction methods most commonly used for propeller-driven aircraft, attention must now be given to jet-powered airplanes for which experimental methods are more appropriate.

4.1.2 Jet-Powered Aircraft

Experimental performance reduction methods are quite commonly applied to jet-powered aircraft because their lift-drag relationship is complicated by their dependence on Mach number. Wave drag, shown in dashed lines in Fig. 4.1, must be included for these higher performing airplanes. The simple parabolic drag polar is usually not an adequate model, except for a few specific flight conditions. Performance measurements for jet airplanes, therefore, are somewhat more complicated by the number of variables that must be considered. Dimensional analysis, based on Buckingham's Pi theorem, is frequently used to reduce the number of parameters that must be covered in the test program. Even so, performance analysis is usually specialized to take into account instrumentation available, time and money available, and/or accuracy demanded by the tests to be conducted. The latter consideration leads to different sets of nondimensional variables for different purposes. The objective of this introductory text is to introduce the fundamentals with a typical set of variables used for cruise performance and give the student a foundation for when he is called upon to apply the principles to a particular problem.

4.1.2.1 **Buckingham's Pi Theorem**. Buckingham's Pi Theorem can be stated as:

> If a physical problem is characterized by n variables having p fundamental units, then the functional relationship between the variables can be expressed in $n - p$ dimensionless numbers.

For the typical flight mechanics problem (like the turbojet performance problem), the fundamental units are mass, length, and time, abbreviated m, L, and t. Then, assuming that there only n variable that significantly affect performance, Buckingham's Pi Theorem asserts that the total number of parameters that must be measured to characterize the performance is reduced from n to $n - 3$, if one measures performance in appropriate dimensionless variables rather than the n physical variables. For flight test purposes, this reduction in the total number of variables is extremely important to make the testing more cost-efficient and less time-consuming. The steps in this process include:

- Select p variables from the physical variables. These variables should include all the fundamental units so the following algebra can be completed.
- Form $n - p$ dimensionless equations by combining each of the variables from step 1 in turn with each of the others.

This procedure will be illustrated with an example in the next paragraph. But, it must be emphasized that the process is totally dependent on the original assumptions made; that is, if one or more of the significant physical variables is omitted from the set p in step 1, its effect will be left out of the answers.

Consider now the output of a jet engine. The important measurements might be taken as net thrust T_n, weight flow rate of air $\dot{w}_a$, weight flow rate of fuel $\dot{w}_f$, and characteristic temperatures T_j. (T_j might be turbine inlet temperature, exhaust gas temperature, or a host of other temperatures depending on the specific engine under consideration.) These measurements may be functions of true airspeed V_∞, ambient temperature T_∞, ambient static pressure p_∞, a physical dimension of the engine like the diameter of the compressor rotor D, a characteristic rpm N of the rotating parts like the compressor rotor, air viscosity μ, and various engine component efficiencies like inlet efficiency η_i, compressor efficiency

η_c, burner efficiency η_b, turbine efficiency η_t, and nozzle efficiency η_n. The list of variables might be simplified by assuming that each of the component efficiencies is also a function of V_∞, T_∞, p_∞, N, and D. Further, viscosity can be eliminated as an independent variable if it can be described adequately as a function of p_∞ and T_∞. Notice that this assumption is tantamount to saying that Reynolds number effects are not important. If Reynolds number effects do significantly affect the engine performance, the model will not account for them.

Example 4.2: Applying Buckingham's Pi Theorem to the functional relationships described above, that is, $T_n = T_n(V_\infty, T_\infty, p_\infty, N, D)$. Select the variables T_n, N, and D and operate on the dimensions of V_∞, T_∞, and p_∞ to group T_n, N, and D as dimensionless constants π_1, π_2, π_3.

First, we select $\pi_1 = T_n{}^a N^b D^c V_\infty$ and apply Buckingham's Theorem:

$$L^0 m^0 t^0 = \left(\frac{mL}{t^2}\right)^a \left(\frac{1}{t}\right)^b \left(\frac{L}{1}\right)^c \left(\frac{L}{t}\right).$$

Solving for equal exponents on both sides of this equation

L:	0	=	$a + c + 1$	a	=	0
m:	0	=	a	b	=	-1
t:	0	=	$-2a - b - 1$	c	=	-1

Therefore, $\pi_1 = \dfrac{V_\infty}{ND}$ (4.11)

Similarly, the other two nondimensional groupings can be found by solving the dimensional equations for T_n, N, and D with temperature first and then with pressure. Consider next, $\pi_2 = T_n{}^a N^b D^c T_\infty$, which gives:

$$L^0 m^0 t^0 = \left(\frac{mL}{t^2}\right)^a \left(\frac{1}{t}\right)^b \left(\frac{L}{1}\right)^c \left(\frac{L}{t}\right)^2.$$

L:	0	=	$a + c + 2$	a	=	0
m:	0	=	a	b	=	-2
t:	0	=	$-2a - b - 2$	c	=	-2

So, $\pi_2 = \dfrac{T_\infty}{(ND)^2}$ (4.12)

Finally, $\pi_3 = T_n^a N^b D^c p$, which gives $L^0 m^0 t^0 = \left(\frac{mL}{t^2}\right)^a \left(\frac{1}{t}\right)^b \left(\frac{L}{1}\right)^c \left(\frac{m}{Lt^2}\right)$.

L:	0	=	$a + c - 1$	a	=	-1
m:	0	=	$a + 1$	b	=	0
t:	0	=	$-2a - b - 2$	c	=	2

So, $\pi_3 = \dfrac{p_\infty D^2}{T_n}$. (4.13)

Continuing to specialize the example to jet engine performance, any of the functional relationships suggested by eqns. 4.11, 4.12, or 4.13 can be written in reciprocal form. For example,

$$\pi_3 = f_1(\pi_1, \pi_2) \text{ implies } \pi_3 = \frac{p_\infty D^2}{T_n} = f_1\left(\left(\frac{V_\infty}{nD}\right)\left(\frac{T_\infty}{(ND)^2}\right)\right) \text{ or } \frac{T_n}{p_\infty D^2} = f_2\left(\left(\frac{V_\infty}{nD}\right)\left(\frac{ND}{\sqrt{T_\infty}}\right)\right)$$

Noting that ND has units of length over time, and that $\sqrt{T_\infty}$ is proportional to sonic velocity and has the same units, the nondimensional groups can be altered to the following form without affecting the results of the dimensional analysis.

$$\frac{T_n}{p_\infty D^2} = f_3\left(\left(\frac{V_\infty}{\sqrt{T_\infty}}\right)\left(\frac{ND}{\sqrt{T_\infty}}\right)\right) = f_4\left(M_\infty, \left(\frac{ND}{\sqrt{T_\infty}}\right)\right)$$

If the engine has fixed geometry so that the characteristic length D is not a variable, the functional relation can be further simplified. While reordering the constants for engine geometry in the functional relationship, it is also convenient to reference the net thrust and temperature to standard day sea level conditions, rather than to ambient conditions alone. Making these adjustments in the constants results in

$$\frac{T_n}{\delta} = f_5\left(M_\infty, \frac{N}{\sqrt{\theta}}\right) \tag{4.14}$$

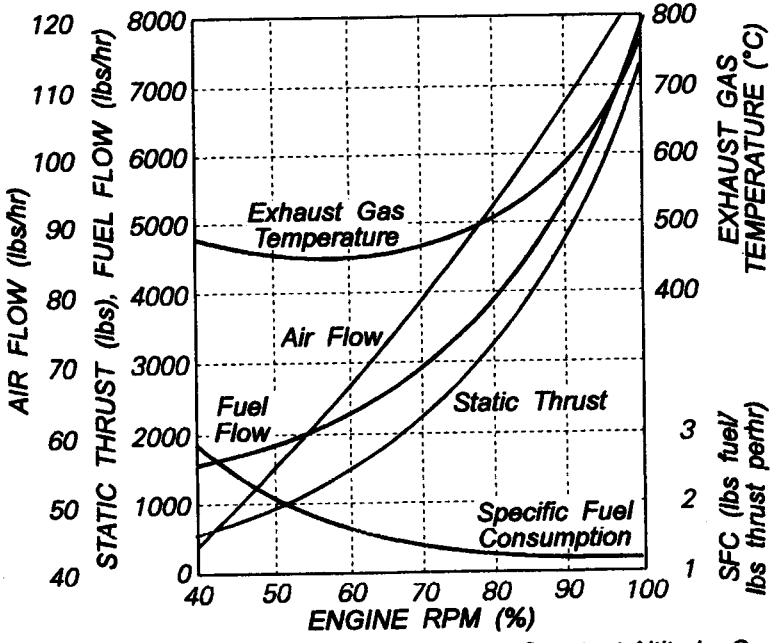

Fig. 4.9 Dimensional Engine Performance: Constant Altitude, Constant TAS

You may still question the usefulness of nondimensional parameters. Figures 4.9 and 4.10 depict representative sets of variables that describe jet engine performance. Figure 4.9 illustrates engine performance for a single altitude and a single true airspeed. (Static thrust, rather than net thrust, is shown; but that fact is not important to understanding the utility of nondimensionalization.) Figure 4.10 shows what happens when just one of these parameters is charted for just two altitudes and three throttle settings. Six curves result for net thrust alone. Obviously, merely presenting the data becomes a cumbersome task. Collecting flight test data at each of the needed altitudes and at a complete set of engine rpm settings is simply not feasible. And, even if such a data collection effort were completed, the resulting data base would be quite unwieldy.

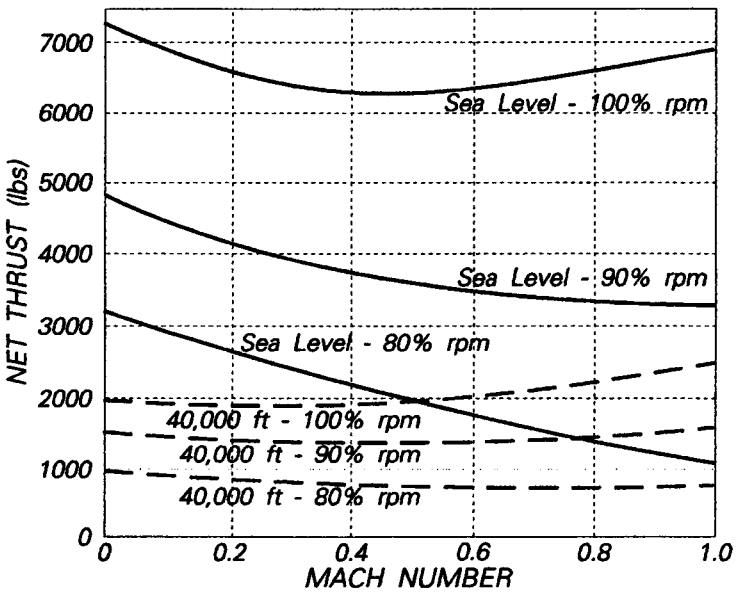

Fig. 4.10 Net Thrust Versus Altitude and Engine RPM

Nondimensional parameters are used to generalize data from several different altitudes, throttle settings, and atmospheric conditions into a single curve ideally. The principle is exactly the same as that used in generalizing the power curve for propeller-driven airplanes in section 4.1.1. Of course, no generalization is perfect; single curves rarely result. Instead, fairly closely related families of curves usually result. Figure 4.11 illustrates how Mach number effects (and other parameters that were ignored in the original assumptions) generate a family of generalized net thrust curves for $\frac{T_n}{\delta}$ versus $\frac{N}{\sqrt{\theta}}$.

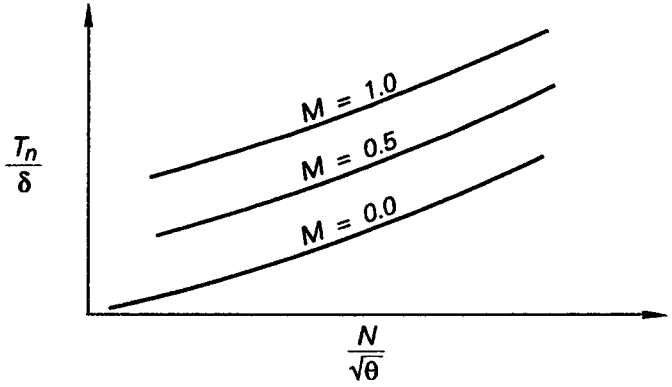

Fig. 4.11 Generalized Net Thrust

Part of the reason that these plots do not generalize perfectly lies in the assumptions used to develop the nondimensional relationships. Reynolds number effects were ignored by ignoring viscosity. But, if the component efficiencies depend strongly on Reynolds number, the generalization we seek does not occur. A family of curves results, rather than a single curve, just as Fig. 4.12 illustrates. Figures 4.12 and 4.13 suggest that mass flow

rates and fuel flow rates do not generalize as well as thrust. Other variables (and Reynolds number is clearly one of them) could be included in the nondimensionalization procedure. However, this simplified model serves our purpose of introducing the Buckingham Pi Theorem and its usefulness in flight test planning.

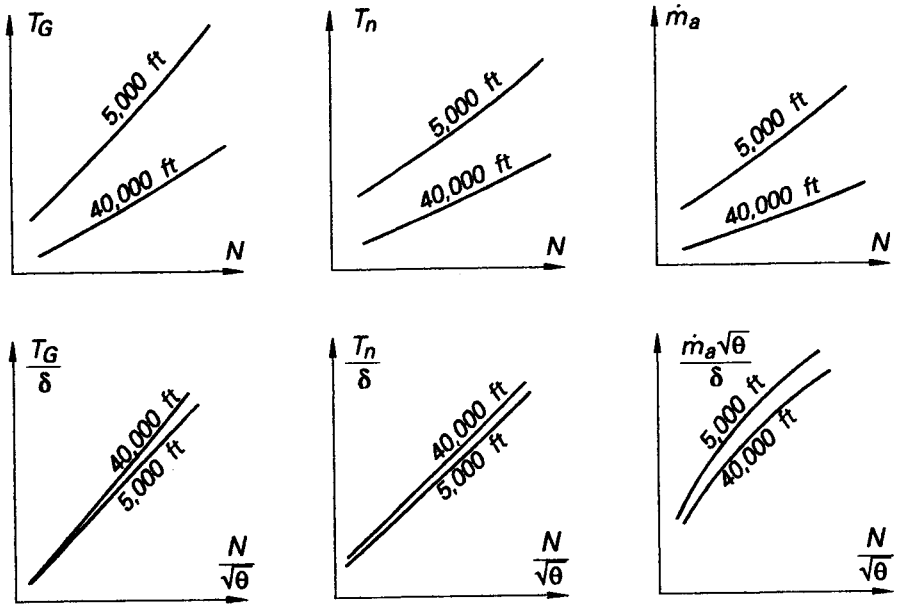

Fig. 4.12 Generalized Thrust and Mass Flow Rate

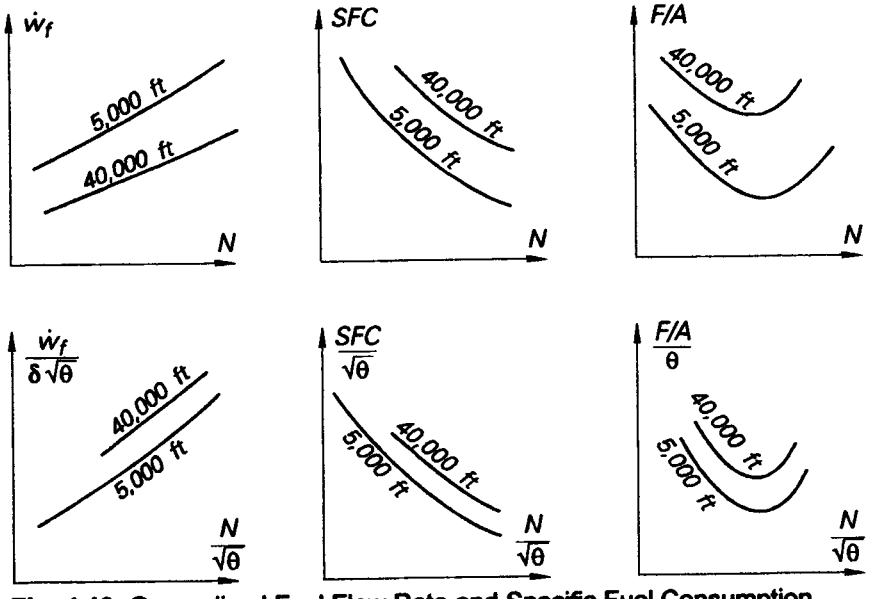

Fig. 4.13 Generalized Fuel Flow Rate and Specific Fuel Consumption

Developments similar to the one illustrated in Example 4.2 result in nondimensional groups as shown in Table 4.2. Nondimensional parameters corresponding to each of the

performance measures of merit can be obtained with the Buckingham Pi approach; they fully describe engine performance. And, equally important to the flight test engineer, they allow test day performance data to be corrected to standard conditions easily.

Table 4.2 Nondimensional Jet Engine Performance Parameters

Dimensional Parameter	Dimensions	Nondimensional Groups
Net Thrust	$\frac{mL}{t^2}$	$\frac{T_n}{\delta} = f\left(\frac{N}{\sqrt{\theta}}, M_\infty\right)$
Fuel Flow	$\frac{mL}{t^3}$	$\frac{\dot{w}_f}{\delta\sqrt{\theta}} = f\left(\frac{N}{\sqrt{\theta}}, M_\infty\right)$
Air Flow	$\frac{m}{t}$	$\frac{\dot{m}_a}{\delta} = f\left(\frac{N}{\sqrt{\theta}}, M_\infty\right)$
Temperature	$\frac{L^2}{t^2}$	$\frac{T_j}{\theta} = f\left(\frac{N}{\sqrt{\theta}}, M_\infty\right)$
SFC	none	$\frac{\dot{w}_f}{T_n} = f\left(\frac{N}{\sqrt{\theta}}, M_\infty\right)$

Dommasch[5] lists and derives a more complete set of nondimensional parameters. It is quite clear that grouping sets of physical variables systematically, as the Buckingham Pi theorem allows us to do, is extremely helpful in planning flight tests for cruise performance. These techniques are most useful for jet airplanes, though many of the concepts can also be applied to propeller-driven aircraft.

4.1.2.2 **Combining Engine and Airframe Parameters**. To utilize the power of dimensional analysis and to reduce the size of the test matrix for an experimental performance reduction, we now need to express airframe parameters as well as engine parameters in nondimensional terms. This nondimensionalization is straightforward if you simply arrange the aerodynamic forces in functional form. Lift can be written

$$L = \frac{2W}{\rho_\infty V_\infty^2 S} = \frac{2WRT_\infty}{p_\infty V_\infty^2 S} = \frac{2W}{\gamma p_\infty M_\infty^2 S} = \frac{2W/\delta}{\gamma p_0 M_\infty^2 S} \quad \text{or} \quad C_L = F_1\left(M_\infty, \frac{W}{\delta}\right) \tag{4.15}$$

Similarly, $C_D = F_2\left(M_\infty, \frac{W}{\delta}\right)$ (4.16)

In steady, unaccelerated flight net thrust is equal to drag and eqns. 4.16 and 4.14 can be equated: $f_5\left(M_\infty, \frac{W}{\delta}\right) = F_2\left(M_\infty, \frac{W}{\delta}\right)$. Though the form of the functional relationship is unknown, this expression can be used to "solve" for any one of the three variables in terms of the other two. Choosing Mach number as the independent variable,

$$M_\infty = F_3\left(\frac{W}{\delta}, \frac{N}{\sqrt{\theta}}\right) \tag{4.17}$$

the task has been simplified to controlling two variables $\left(M_\infty \text{ and } \frac{N}{\sqrt{\theta}}\right)$ and holding $\frac{W}{\delta}$ constant by adjusting altitude. Thus, dimensional analysis makes experimental performance data reduction tractable for jet-powered airplanes. We have also avoided measuring thrust directly. Instead, performance is obtained indirectly from more easily measured variables like engine RPM, Mach number, weight, atmospheric pressure, and atmospheric temperature. These measured variables can be readily evaluated. One difficulty in this indirect approach is that engine RPM may not be a constant measure of engine thrust over the entire life of the engine. Mechanical wear will take its toll. There is also variation from engine to engine in the relationship between RPM and thrust. If these differences are relatively small, the performance of a fixed geometry turbojet engine can be validated experimentally using the nondimensional parameters shown in Fig. 4.14.

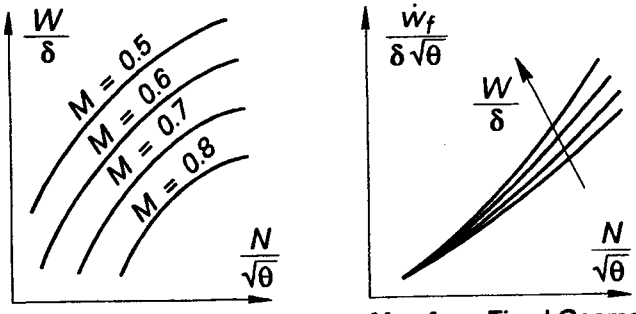

Fig. 4.14 Typical Performance Map for a Fixed Geometry Engine

For variable geometry engines the functional relationship of eqn. 4.17 must include at least one more parameter. Therefore, it is usually best to map variable geometry engine performance in terms of one of the nondimensional thrust parameters. The same suggestion holds for dual rotor engines because the additional performance variable complicates the performance relationships in the same way. In any case, the use of nondimensional variables simplifies the task of experimentally measuring the performance of the jet-powered airplane. Without this simplification, validating the performance would be an even more tedious process.

4.1.3 Endurance

The total time that an airplane can loiter on a specified amount of fuel is simply a function of how much fuel is carried and how fast is it consumed. The most obvious difference in the endurance equation between propeller-driven airplanes and jet-powered airplanes is in how fuel consumption is expressed.

4.1.3.1 **Propeller-Driven Aircraft**. Fuel flow rate is the basic parameter of interest for endurance. Typically, during cruise tests, the entire weight change is due to fuel consumed. Consequently, $\dot{w}_f = -\frac{dW}{dt}$. For a propeller-driven airplane, specific fuel con-

sumption is expressed as pounds of fuel burned per horsepower produced at the propeller shaft: $c = \frac{\dot{w}_f}{BHP_r} = SFC$. Rearranging this relationship and integrating

$$E = \int_0^E dt = -\int_{W_0}^{W_E} \frac{dW}{\dot{w}_f} = \int_{W_E}^{W_0} \frac{DW}{cBHP_r}$$

where W_0 = aircraft weight at start of cruise segment
W_E = aircraft weight at end of cruise segment
E = endurance for a given fuel load, $W_E - W_0$

(Note: E is often defined simply as the maximum time the airplane can fly with a full fuel load. In this book, that time is denoted by E_{max}.)

But $BHP_r = \frac{\Delta V_\infty}{\eta_p}$, so

$$E = \int_{W_E}^{W_0} \frac{\eta_P dW}{cDV_\infty} = \int_{W_E}^{W_0} \frac{\eta_P W dW}{cWDV_\infty} = \int_{W_E}^{W_0} \frac{\eta_P}{c} \frac{L}{D} \frac{dW}{WV_\infty}$$

True airspeed can also be written as $V_\infty = \sqrt{\frac{2W}{\rho_\infty S C_L}}$ for level flight. Then

$$E = \int_{W_E}^{W_0} \frac{\eta_P}{c} \sqrt{\frac{\rho_\infty S}{2}} \frac{C_L^{1.5}}{C_D} \frac{dW}{W^{1.5}} \tag{4.18}$$

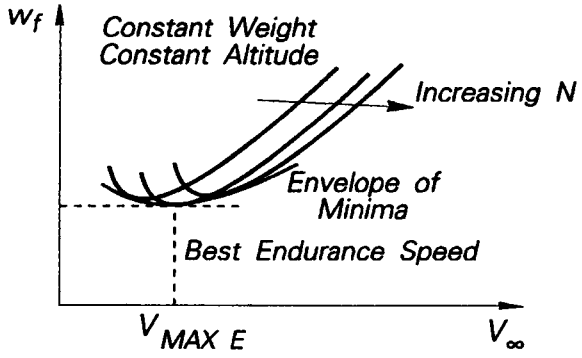

Fig. 4.15 Envelope of Fuel Flow Curves

The quantities to be measured include primarily fuel flow rate and weight of the airplane (eqn. 4.18). The aerodynamic term $\frac{C_L^{1.5}}{C_D}$ guarantees that maximum endurance will occur at a specific airspeed. Speed for maximum endurance can be obtained by plotting a family of constant altitude and constant weight fuel flow curves for increasing propeller RPM (see Fig. 4.15). For small changes in weight, changes in $\frac{\eta_P}{c}$ are often negligible. If so and if the drag curve is parabolic, the true airspeed for maximum endurance can be es-

timated from the commonly used Breguet approximation: $V_{E_{max}} = V_{(C_L^{1.5}/C_D)_{max}}$. Recall that, under these simplifying assumptions, $3C_{D_p} = C_{D_i}{}^3$.

Propeller-driven aircraft endurance is readily measured by recording fuel flow rates accurately. Altitude has a small effect, but care must be taken to ensure that the mixture settings are consistent between comparable data runs. Weight flow rate of the fuel should be measured, since the specific gravity of aviation gasoline varies significantly with temperature, an uncontrollable variable. Configuration, including power settings, must be set up painstakingly to avoid excessive scatter in cruise data.

4.1.3.2 **Jet-Powered Aircraft**. Measuring endurance for a jet airplane is very similar to measuring it for propeller-driven airplanes. Endurance is still defined from measurement of weight fuel flow rates; hence, the integral equation for endurance is unchanged. However, specific fuel consumption for the jet engine is expressed in different units and is called thrust specific fuel consumption to highlight that difference.

$$TSFC = c_t = \frac{\dot{W}_f}{T_n}$$

where c_t is in pounds of fuel per unit time per pound of thrust

The endurance equation can then be written

$$E = \int_{W_E}^{W_0} \frac{dW}{\dot{W}_f} = \int_{W_E}^{W_0} \frac{dW}{c_t T_n} = \int_{W_E}^{W_0} \frac{1}{c_t}\frac{L}{D}\frac{dW}{W} = \int_{W_E}^{W_0} \frac{1}{c_t}\frac{C_L}{C_D}\frac{dW}{W} \tag{4.19}$$

Notice that airframe aerodynamics again appear through the *L/D* ratio. For simplifying assumptions similar those used earlier (constant c_t, parabolic drag polar), maximum endurance (E_{max}) occurs at the velocity for maximum *L/D* where $C_{D_p} = C_{D_i}$.

4.1.4 Range

Analogous to the definition of endurance, range is the distance an aircraft can fly on a given amount of fuel. Range, too, is affected by how the specific fuel consumption is expressed for the type of powerplant. The distance term in the definition for range performance can be either air distance or the distance covered over the ground. In the first case, the range is called air range and no wind effects are considered.

4.1.4.1 **Propeller-Driven Aircraft**. The integral expression for range in calm air (which is valid for general drag polars and for variations in η_p and *c*) comes from the definition of true airspeed for steady, straight cruising flight. Using this definition and the relationships described in section 4.1.3 to relate fuel flow rate, specific fuel consumption, thrust horsepower, and aerodynamic forces,

$$R = \int_0^t V_\infty dt = -\int_{W_0}^{W_E} V_\infty \frac{dW}{\dot{W}_f} = \int_{W_E}^{W_0} V_\infty \frac{\eta_P}{cTHP_r}\frac{W}{W}dW = \int_{W_E}^{W_0} V_\infty \frac{\eta_P}{cDV_\infty}\frac{L}{W}dW = \int_{W_E}^{W_0} \frac{\eta_P}{c}\frac{C_L}{C_D}\frac{dW}{W} \tag{4.20}$$

where R = range for a given fuel load, $W_E - W_0$

To maximize range, the integrand or at least $\frac{\eta_P}{c}\frac{C_L}{C_D}$ must be maximized. If η_P is constant and the drag curve fits the usual polar form, R_{max} occurs with $C_{D_p} = C_{D_i}$.

4.1.4.2. **Jet-Powered Aircraft**. The form of the range expression for jet-powered airplanes is affected in much the same way as endurance is by the definition of specific fuel consumption.

$$R = \int_0^t V_\infty dt = -\int_{W_0}^{W_E} V_\infty \frac{dW}{\dot{w}_f} = \int_{W_E}^{W_0} V_\infty \frac{1}{c_t T_n}\frac{W}{W} dW = \int_{W_E}^{W_0} V_\infty \frac{1}{c_t}\frac{L}{D}\frac{dW}{W}, \text{ but } V_\infty = \sqrt{\frac{2W}{\rho_\infty S C_L}}$$

$$R = \int_{W_E}^{W_0} \frac{\sqrt{\frac{2}{\rho_\infty S}}}{c_t}\frac{\sqrt{C_L}}{C_D}\frac{dW}{\sqrt{W}} \tag{4.21}$$

Maximizing the integrand of eqn. 4.21 must include consideration of both an altitude effect and an aerodynamic term, even with c_t constant. The density term in the denominator indicates why jet-powered vehicles fly at high altitude for their best range performance. An upper limit on the altitude for best range is not apparent because it depends on how component efficiencies of the engine are affected by altitude. When these efficiencies become small, c_t will dominate the integrand. If the usual simplifying assumptions are made, the aerodynamic term is maximized when $C_{D_p} = 3C_{D_i}$.

4.2 CRUISE PERFORMANCE TEST METHODS

Cruise performance tests determine the related performance parameters, endurance and range. Endurance is time the airplane can spend in the air for a given fuel load and range is the total distance (usually measured in air miles) that can be flown on a given fuel load. For both propeller-driven and jet-powered airplanes, both fuel consumption and drag dictate what cruise performance can be achieved. The speed-power test, with its several variants, is the most common flight test technique for measuring both range and endurance. Occasionally, it may be necessary to fly a demonstration profile to verify the actual performance, but more often data from speed-power tests is used to calculate range performance.

Data for cruise performance measurements are usually collected using the speed-power test method. Essentially, such tests require flying cruise leg segments for a range of airspeeds that cover both the speed for maximum endurance and maximum range. Either pressure altitude or the nondimensional parameter $\frac{W}{\delta}$ is held constant for each data point. The appropriate engine parameters like RPM, manifold pressure, and/or mixture setting, are stabilized prior to starting the data run. The engine parameters, atmospheric conditions, and fuel flow rate are recorded. Each of these variables must be measured accurately to obtain useful results. Apart from the sensors for the engine variables and temperature, instrumentation requirements for this test are minimal. All data are steady state data and can be recorded by hand. Timing can be done with a stopwatch.

4.2.1 Speed-Power Test Method for Propeller-Driven Airplanes

For propeller-driven airplanes, cruise data are usually taken at constant pressure altitude. The speed-power points should be designed to cover the operating envelope of the airplane with concentration on those areas where limitations of the powerplant will affect performance. Full throttle constraints must be checked for a number of altitudes if cylinder pressures limit throttle opening at lower altitudes. Maximum speed should be checked for a number of altitudes. The data to be measured, either directly or indirectly, include *BHP* at full throttle, V_∞, THP_r as a function of V_∞, maximum manifold pressure as a function of altitude, and fuel flow rates throughout the envelope. Reduction to standard day conditions is best done by using generalized power required versus velocity unless the polar form of the drag curve cannot be assumed. Range and endurance data are also obtainable and operational handling (cooling procedures, mixture setting procedures, and such like) information for the engine come from these tests.

4.2.2 Speed-Power Test Method for Jet-Powered Airplanes

For jet-powered airplanes the speed-power test, holding $\frac{W}{\delta}$ constant, is used to collect cruise data. Tests must be designed to measure fuel flow rates, drag characteristics, and range and endurance for all weights, speeds, and power settings. Covering this complete envelope demands that the data collection be carefully planned and that maximum use of nondimensional groups be made. Otherwise, the experimental performance reduction method simply will not be feasible.

Preflight preparation for constant $\frac{W}{\delta}$ speed-power tests includes preparation of either charts or tabulated data. The test team member who prepares these test cards must include the effects of altitude position error, instrument error, instantaneous weight of the airplane, and airspeed calibration errors. The following procedure may be used to obtain a chart that can be used in flight to and maintain constant $\frac{W}{\delta}$ for each data run.

(1) Calculate pressure ratios for a range of altitudes at least 2000 feet on either side of this altitude. A range of altitudes is necessary because the weight of the airplane will be changing as fuel is consumed during the test.

(2) Select the standard reference weight. Ordinarily, this weight should be the average weight for the test segment. Alternatively, this $\left(\frac{W}{\delta}\right)_{ref}$ itself may be specified (as in Example 4.3). Calculate the reference value of $\frac{W}{\delta}$.

(3) Using this reference $\frac{W}{\delta}$ and eqn. 4.22, calculate the corresponding weights for each of the altitudes above and below the nominal altitude selected in step 1. This constant $\frac{W}{\delta}$ line is the lower curve in Fig. 4.16.

$$W_i = \left(\frac{W}{\delta}\right)_{ref} \delta_i, \quad i = 1,2,3,...n \tag{4.22}$$

(4) Next, construct a line relating cockpit fuel readings to changes in airplane weight. The scale on the right side of Fig. 4.16 illustrates this step for the case where fuel quantity is available as total fuel used. This straight line may cross the constant $\frac{W}{\delta}$ line and it may have the scales inverted if fuel is displayed to the test crew as fuel remaining rather than fuel used. Thus, for any fuel reading, the test pilot or flight test engineer can read across from the fuel quantity scale and down to find the calibrated altitude to fly.

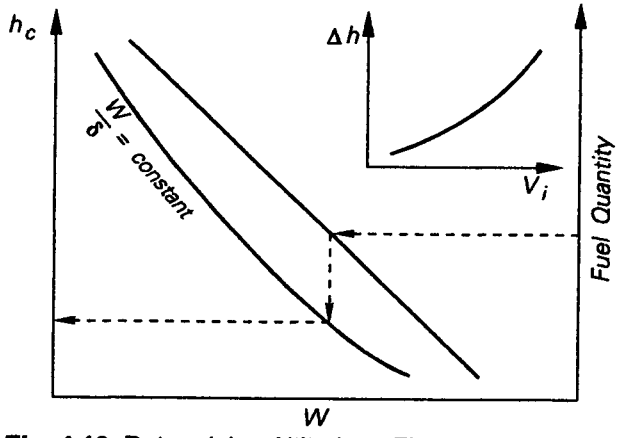

Fig. 4.16 Determining Altitude to Fly

(5) Finally, to make this chart useful in flight, Δh_{ic} and Δh_{pc} corrections for the subject airplane must be included. The inset in the upper right corner of Fig. 4.16 illustrates this correction. Notice that $\Delta h = \Delta h_{ic} + \Delta h_{pc}$; it is a lumped correction for the altimeter for each indicated airspeed. This correction must be applied to obtain the aim h_i for the test crew to fly during any constant $\frac{W}{\delta}$ cruise performance data run.

Example 4.3: The cruise performance of a small business jet is tested at a nominal pressure altitude of 25,000 feet at a reference $\frac{W}{\delta}$ of 55,000 pounds. The weight of the airplane with full fuel is 24500 pounds. The altimeter correction charts for the pilot's altimeter are shown below as functions of indicated airspeed. Construct a chart similar to Fig. 4.16 to be used to fly a set of constant $\frac{W}{\delta}$ cruise performance tests over an indicated airspeed range of 250 to 350 knots. The fuel used out of an available 10000 pounds is estimated to be 3800 pounds at the start of the cruise segment tests; the fuel flow rate should average approximately 1000 lb/hr during the cruise points. Assume constant fuel temperature and that each point will require approximately 6 minutes of flying time to stabilize and to collect the required data.

First, we must obtain δ for altitudes between 23000 and 25000 feet to give the test crew flexibility in flying the point. (That is, we must allow for the likelihood that the aircraft will not arrive at the test conditions with exactly the nominal weight; fuel consumption will vary with air traffic control delays, management of the flight profile, and atmospheric conditions--none of which can be fully controlled by the test crew.) These values to maintain constant $\frac{W}{\delta}$ = 55,000 pounds are tabulated in the table on the following page.

h_c	δ_i	W_i
27000	0.3398	18689
26000	0.3552	19536
25000	0.3711	20410
24000	0.3876	21318
23000	0.4047	22258

With these values we can plot a curve of h_c versus W (Fig. 4.18). On the right side of this plot we append a scale that corresponds the fuel used for each aircraft weight. (One could also use fuel remaining, though such a scale is rather uncommon.) With either form of fuel reading, a straight line of fuel used or fuel remaining versus weight is drawn.

To be useful in flight, h_c must be converted to h_i. One approach is to add a small Δh_{pc} and Δh_{ic}, as suggested in the inset in Fig. 4.16. Δh is a sum of two corrections; $h_c = h_i + \Delta h_{pc} + \Delta h_{ic} = h_i + \Delta h$ or $\Delta h = \Delta h_{pc} + \Delta h_{ic}$. The sample corrections illustrated below in Fig. 4.17 lead to a usable Δh inset.

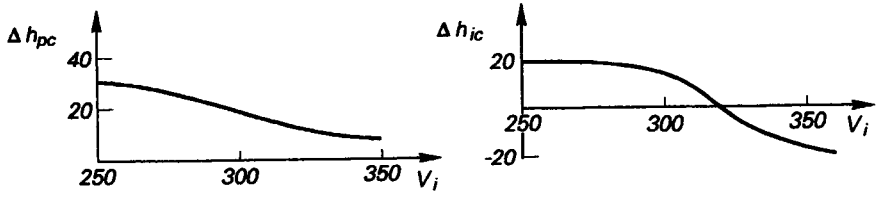

Fig. 4.17 Pitot-Static and Instrument Corrections for Example 4.3

The final results are shown in Fig. 4.18.

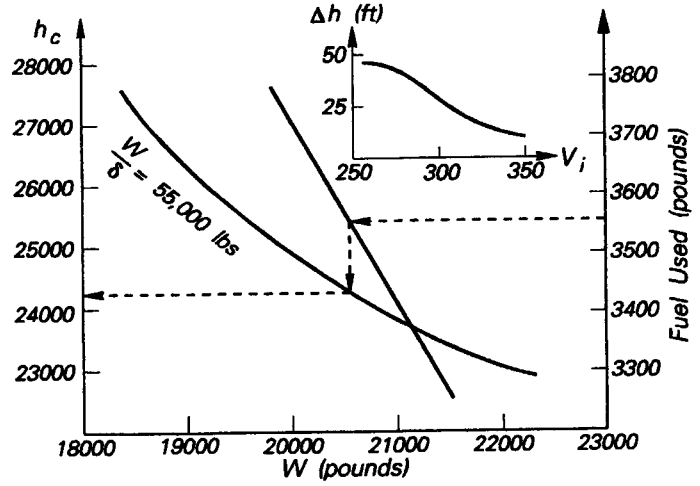

Fig. 4.18 Speed-Power Flight Test Card Corrections for Example 4.3

There are several tips that will speed up inflight collection of speed-power data and reduce data scatter. First, jet airplanes generally decelerate quicker than they accelerate, especially if the configuration has speed brakes. Therefore, it is usually best to climb to just above the desired altitude for the first data point, which should be at the maximum speed for that set of altitude runs. Use excess potential energy to accelerate to the desired speed. Subsequent data points can then be flown at decreasing speeds. Make sure that each point is completely stabilized or else repeat the point. Altitude should not vary

more than ±20 feet and airspeed must not vary more than ±1 knot. Do not start timing until all engine variables have reached equilibrium and fly at least 3 minutes in the stabilized condition. Stabilizing at low airspeeds (especially at high altitudes) may be very difficult. For these conditions it is useful to simply hold airspeed constant and smoothly adjust power to control rate of climb or descent. Any rate of descent or climb should be stabilized at 50 fpm or less. A longer data run, perhaps 5 minutes, should be used at these low speed points. The BHP_r can be corrected for the small variations in potential energy with

$$BHP_r = BHP_i + \frac{Wh}{33000\eta_P} \tag{4.23}$$

Figures 4.19 through 4.21 illustrate how speed-power data for a jet airplane can be reduced to range and endurance information. The nondimensional specific endurance parameter $\frac{\dot{w}_f}{\delta\sqrt{\theta}}$ and $\frac{W}{\delta}$ are plotted versus Mach number and altitude (Fig. 4.19).

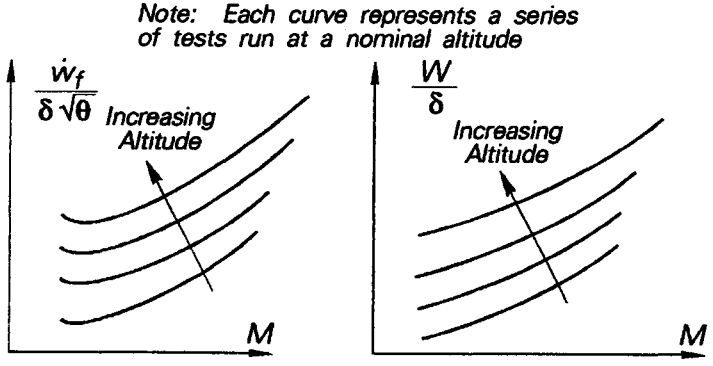

Fig. 4.19 Specific Endurance and $\frac{W}{\delta}$ versus Mach Number

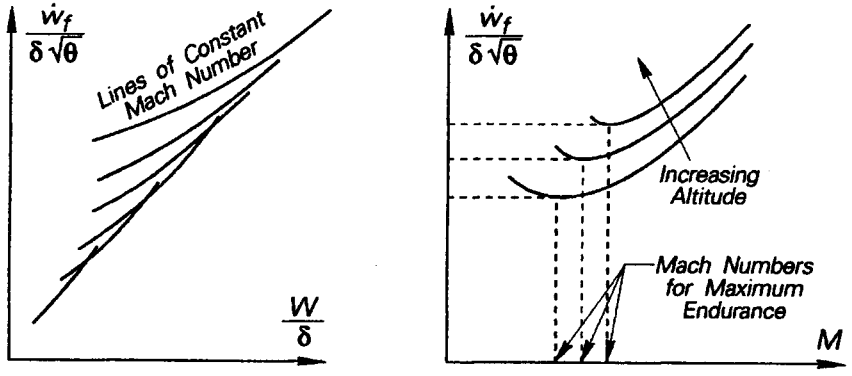

Fig. 4.20 Specific Endurance Crossplots

Since both families of curves are functions of M_∞, they can be transposed to a crossplot of $\frac{\dot{w}_f}{\delta\sqrt{\theta}}$ versus $\frac{W}{\delta}$ by picking off values of specific endurance and $\frac{W}{\delta}$ for any desired altitude and M_∞. The resulting curves are sketched in Fig. 4.20. The asymptote to these

curves gives $\frac{\dot{w}_f}{\delta\sqrt{\theta}}$ achievable at a given $\frac{W}{\delta}$ for any selected M_∞. Obviously, the length of time that the jet airplane can fly on a given amount of fuel increases significantly as either weight (and fuel load) or altitude, that is, $\frac{1}{\delta}$, increases.

Applying this technique again to $\frac{\dot{w}_f}{\delta\sqrt{\theta}}$ plotted versus Mach number with the family of curves now spread over $\frac{W}{\delta}$ illustrates how maximum endurance and the appropriate Mach number to fly to attain this maximum endurance can be graphically determined from such nondimensional parameters. The final result is sketched in Fig. 4.21.

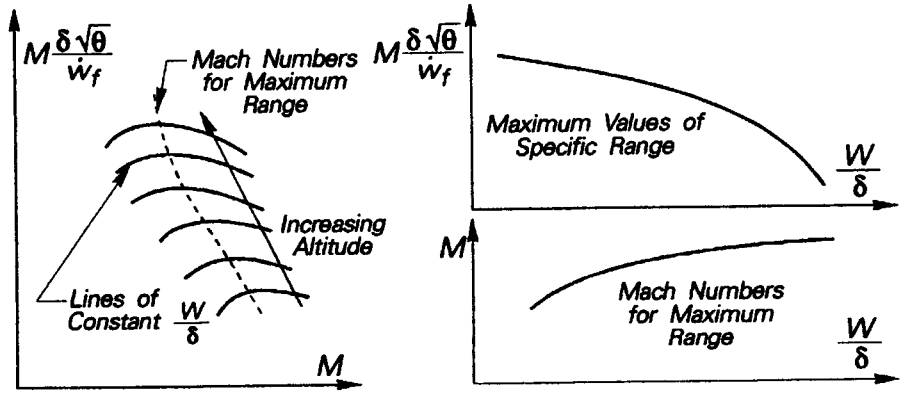

Fig. 4.21 Specific Range Crossplots

A similar graphical approach for the specific range parameter $M\frac{\delta\sqrt{\theta}}{\dot{w}_f}$ typically results in a family of constant $\frac{W}{\delta}$ curves (Fig. 4.21). The dashed line connects the peak values of specific range for each $\frac{W}{\delta}$ and allows construction of the other two curves, which graphically depict the correct Mach number to fly in order to obtain maximum specific range for any $\frac{W}{\delta}$ and the maximum specific range available for the weight and altitude.

4.3 SUMMARY

This chapter has introduced the theory underpinning the speed-power flight test method, which is used to measure the level flight cruise performance of both propeller-driven and jet-powered airplanes. Methods for performance reduction for these two types of airplanes were discussed and it was shown how analytical methods apply to propeller-driven vehicles. Dimensional analysis was used to develop the experimental method for jet-propelled aircraft. The utility of nondimensional variables was illustrated and connected to range and endurance, the primary physical variables of interest.

REFERENCES

1 Bull, G. and Bridges, P. D., "A Method for Flight-Test Determination of Propulsive Efficiency and Drag," **Journal of Aircraft**, Vol. 22, Mar. 1985, pp. 200-207.

2 Cooper, J. D., "The 'Linearized Inflow' Propeller Strip Analysis," WADC TR 56-615 (AD 118078), Wright Air Development Center, Wright-Patterson AFB, Ohio, February 1957.

3 Lan, C. E., and Roskam, J., **Airplane Aerodynamics and Performance**, Roskam Aviation and Engineering Corporation, Ottawa, Kansas, 1980.

4 Kuethe, A. M. and Chow, C. Y., **Foundations of Aerodynamics: Bases of Aerodynamic Design**, John Wiley & Sons, New York, 1976.

5 Dommasch, D. O., "Performance of Turbojet Engines," Chapter 4, Volume 1, **AGARD Flight Test Manual**, Pergamon Press, New York, 1959.

6 "Performance Flight Test Techniques," Volume III, FTC-TIH-70-1001 (Revised August 1975), USAF Test Pilot School, Edwards AFB, California, 1975.

7 "Fixed Wing Performance, Theory and Flight Test Techniques", USNTPS-FTM-No. 104, Naval Air Test Center, Patuxent River, Maryland, July 1977.

8 "Performance, Book B", Empire Test Pilots' School, Royal Aircraft Establishment, Farnborough, England, 1966.

9 Lush, K. J. and Moakes, J. K., "Performance Reduction Methods for Turbo-Propeller Aircraft," Chapter 5, Volume 1, **AGARD Flight Test Manual**, Pergamon Press, New York, 1959.

Chapter 5

TAKEOFF AND LANDING FLIGHT TESTS

Since every successful flight begins with a takeoff and ends with a landing, it seems redundant to say that the performance and handling qualities of an airplane during these phases of flight are very important. Redundant it may be, but the statement is quite true. Since takeoff and landing performance involves accelerations and decelerations, we also must concern ourselves with measurement of dynamic conditions, both in flight and on the ground. Thus, we usually break up takeoff and landing measurements into a ground phase and an air phase. Another fact that makes takeoff and landing (TO&L) flight tests difficult is that few (if any) maneuvers are more difficult to perform consistently. Pilot technique can easily mask some of the most important trends in such data. This human variability makes it virtually impossible to exactly compare different sets of such data and puts the onus on flight test personnel to standardize procedures and techniques as much as possible. Even so, elementary statistical tools are needed to correlate individual measurements and to compare the data to requirements. Average values of distances for number of takeoffs and/or landings are typically used to decide whether or not goals have been met. The large number of variables that affect TO&L performance further complicates these tests. Moreover, many of them are completely uncontrollable. For example, runway surface condition can only be changed with full fidelity by waiting for or by going to natural weather conditions (ice, snow, slush, rain, etc.) to occur. But it is clearly impractical to delay a flight test program for months waiting for Mother Nature to supply all these conditions. So, we usually the runway with foam or other substances to simulate reduced friction. Finally, not only are TO&L tests difficult to perform repeatably, they are some of the most dangerous tests conducted in certifying an airplane. They require the flight test crew to establish flight envelope limits (and thus to occasionally exceed them!) while on or very close to the ground with the airplane in its least controllable configuration. And that is where most accidents occur! So, while takeoff and landing tests are very important and can be crucial to a developmental effort, they are also one of the most demanding of all test demonstrations. They deserve your utmost in care and attention to detail.

5.1 THEORETICAL FOUNDATIONS

5.1.1 Definitions and Terminology

The TO&L vocabulary is rather extensive and at times very confusing, especially since the various requirements documents use different terms to mean "almost" the same thing. First, you intuitively know what a takeoff and a landing are, but we need to set some limits even for these terms.

5.1.1.1 Takeoff and Landing. Dekker and Lean[1] define **takeoff** and **landing** as:

> **Takeoff** is the process by which an airplane is brought from standstill to a safe flight condition.

Landing is the process by which an airplane is safely brought from a safe flight condition to a standstill.

For takeoff, this "safe flight condition" is clarified further to mean the point in the climb where the airplane first reaches a specified obstacle clearance height above the point of departure from the ground (liftoff) at an instantaneous true airspeed which is usually labeled V_2 or V_{CL}. For landing the height at which the landing starts is a specified level above the runway, again usually chosen to simulate obstacle clearance. In some instances, the type of maneuver flown, especially how the transition is made from ground roll to climb path (or vice versa for the landing), is extremely important. We will discuss this transition shortly, but first we need to define the two basic phases of takeoffs and landings: the ground phase and the air phase (Fig. 5.1).

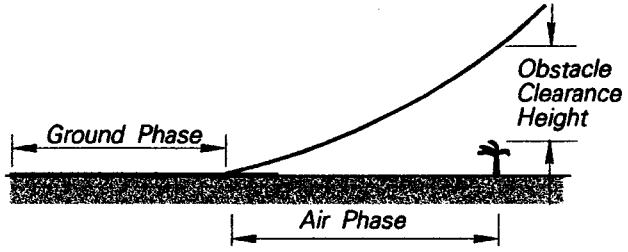

Fig. 5.1 Takeoff and Landing Phases

5.1.1.2 **Ground Phase**. As suggested above, the ground phase of the takeoff maneuver begins at brake release and ends when the airplane lifts off the takeoff surface (provided, of course, a minimum margin of speed above stall speed and/or above the minimum control speeds has been reached). It is also customary to include a short allowance in the ground run estimate for the distance traveled while the airplane is rotated to the takeoff attitude, with times of 3 to 4 seconds now quite common[2,5]. While no attempt is usually made to measure this distance separate from the total ground run distance, we will discuss it separately as part of the design and analysis process since its estimation is important to predicting takeoff distances accurately. Test measurements must be made to ascertain ground run distance, lift off airspeed, and velocity and/or acceleration profiles during the ground phase. Usually, measurement of ground run distance, s_G, is the primary consideration. This parameter is frequently a certification measure of merit and is estimated[2] during the design process. The standard day takeoff distances need to be determined within ±5%. The accuracy of such measurements is affected by so many uncontrollable factors that it should be treated as a random variable. Dekker and Lean point out that for a nominal scatter of 4% in the measured ground roll, a probability calculation gives a high (95%) confidence level of being within 5% of the true distance if at least 5 measurements are made for a given configuration[1]. Six test runs make ±2.5% accuracy attainable for 4% scatter; so, good practice calls for planning at least 6 takeoffs for each configuration. Of course, additional runs reduce the precision required for each measurement to still achieve the overall 5% accuracy.

As a minimum, the ground speed at which the airplane lifts off, surface headwind, ambient temperature, and ambient pressure must also be measured during the ground phase -- as well as s_G. Determining the exact point at which the airplane lifts off has always been troublesome. Event markers, triggered by extension of the landing gear struts,

are perhaps the most accurate means of defining the lift off location. Such devices can fire a marker onto the runway itself or they can trigger a flash of light that can be recorded photographically as part of the data. Such a trigger can also be used to photograph or videotape the airspeed indicator at lift off. Alternatively, a continuous record of the airspeed readings can be made with event trigger used to note the point of lift off. This latter approach can, after a rather tedious data reduction, provide a measured velocity profile. Another approach is to record an analog signal that is proportional to the indicated airspeed reading (a differential pressure, of course) and then convert this pressure signal to standard day true airspeed in the data reduction scheme. Of course, this analog signal is usually sampled at appropriate intervals to reduce the data reduction workload.

An entirely different approach to takeoff measurements has become popular since modeling of aircraft performance has become so important for high fidelity simulations. In this approach the complete takeoff profile is recorded. Depending on the available instrumentation, the acceleration throughout the takeoff is the primary measurement. Very accurate acceleration profiles can be obtained with modern accelerometers. High accuracy inertial navigation systems (INS) have been used for this purpose[3]. Then, the accelerations are integrated once to obtain the velocity profile and integrated again to obtain positional information. A variation on this technique is to measure the position coordinates by a very accurate means (laser tracker, video tracker, or other optical device) and then to differentiate the position measurements to obtain velocity and acceleration profiles. This approach requires continuous coverage of the entire takeoff maneuver, dictating the use of multiple cameras and merging of data files from these cameras. Either of these two techniques that give a complete time history of the maneuver gives direct or indirect measurement of the air distance (Fig. 5.2) as well as the ground distance.

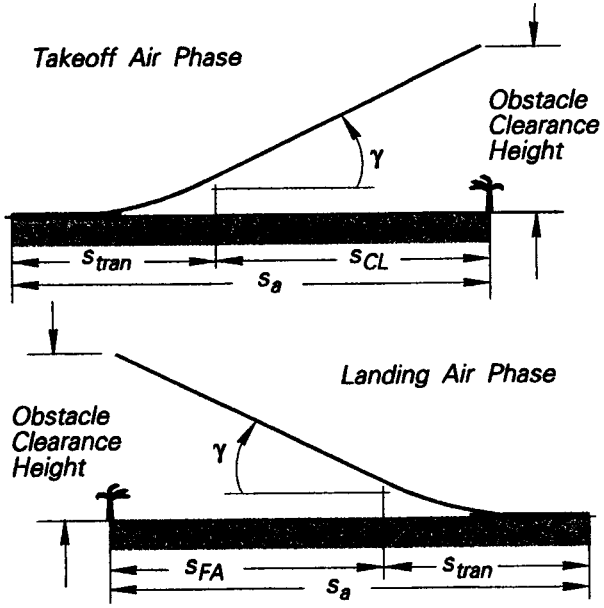

Fig. 5.2 Takeoff and Landing Air Phases

5.1.1.3 **Air Phase**. The air phase of these maneuvers poses an even more complicated measurement problem than the ground phase. As suggested in Fig. 5.1, for takeoff the **air phase** begins at liftoff and ends when the airplane first reaches obstacle clearance height at V_{CL}. For landing the **air phase** begins at the obstacle clearance height with either a constant rate of descent or a constant approach angle established and ends when the airplane first touches the runway.

In both takeoffs and in landings, the air distance can be further broken down into a transition segment and into steady climb or descent segments. Figure 5.2 schematically illustrates typical air phases and how they can be broken down. For takeoffs, the transition is merely the accelerating trajectory between liftoff and the initial climb speed. It is sometimes called the takeoff flare. For high performance aircraft or for a low obstacle clearance height (FAR part 25 specifies 35 feet as the obstacle clearance height, for example.), a steady initial climb speed is not attained until after obstacle clearance height is achieved. In that case, only the transition trajectory is included in the air distance. For landings, the transition includes the approach path from obstacle clearance height down through some landing flare to touchdown. The flare maneuvers, shown as acceleration and deceleration segments in Fig. 5.2, are often approximated with some simple curve like a circular arc. In any event, air distance is difficult to predict and difficult to measure directly. It is the phase of TO&L trajectories most affected by piloting technique.

5.1.1.4 **Available Runway**. We now turn to the essential definitions.

> The **runway available (RA)** is the actual runway length less a prescribed allowances (usually 200 feet) for lineup distance.

5.1.1.5 **Critical Field Length and Balanced Field Length**. These two terms, often confused and misunderstood, are closely related. The former is more often applied to military aircraft and the latter is usually associated with commercial aviation requirements.

> **Critical field length (CFL)** is the total length of runway required to accelerate on all engines to critical engine failure speed (V_{CEF}), experience an engine failure, and then either continue the takeoff with remaining engines or stop[4].

CFL is calculated as part of preflight planning for multiengine aircraft (not single engine aircraft, of course) and must be less than runway available for a safe takeoff.

> **Balanced field length (BFL)** is the sum of the distance required to accelerate to V_{CEF} and the distance required to either continue the takeoff over 35 feet with one engine inoperative or to brake to a stop[2].

Thus, BFL satisfies both a takeoff requirement and the civil accelerate-stop requirements. FAR Part 25 also stipulates a field length that the greater of either the accelerate-and-go distance or 115% of the all-engines-operating distance to a height of 35 feet. Fig. 5.3 illustrates the components of a BFL computation. This definition of BFL leads to the conclusion that V_{CEF} must be determined so that $s_{DEC} + s_{STOP} = s_{LO_{SE}} + s_{a_{SE}}$.

5.1.1.6 **Critical Engine Failure Speed**. As already suggested in the definitions of CFL and BFL:

Critical Engine Failure Speed (V_{CEF}) is the speed to which a multiengine airplane can be accelerated, lose an engine, and then either continue the takeoff with the remaining engines, or stop.

Both possibilities require the same total runway distance.

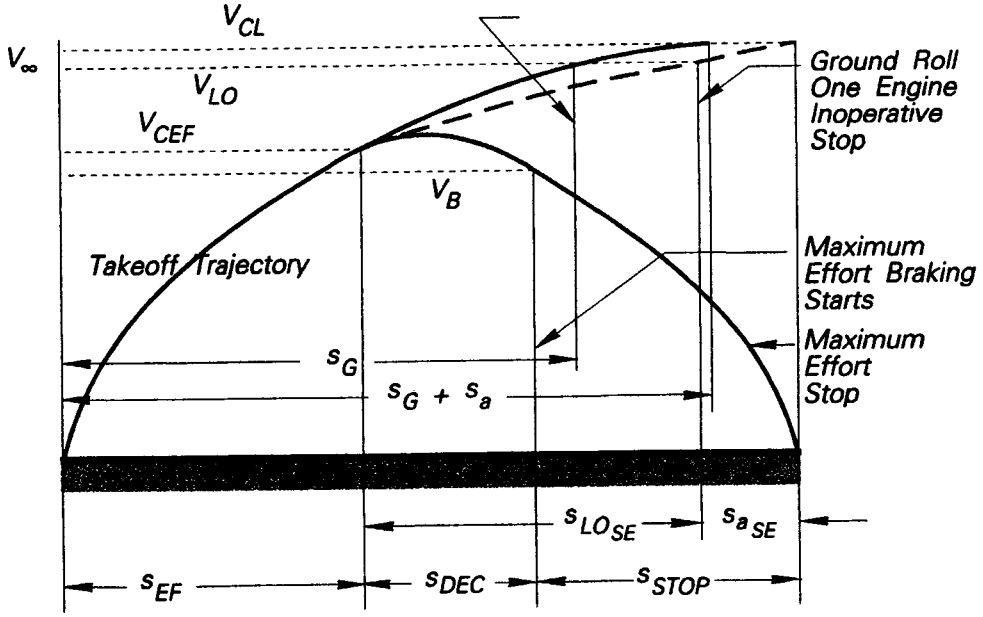

Fig. 5.3 Balanced Field Length Components

Figure 5.4 illustrates critical engine failure speed trajectories for multiengine airplanes. (Note: V_{CEF} is also called V_1 in some documents[1,4] and critical speed, V_{CRIT}, in others[2].) Strictly speaking, V_{CEF} does not apply to single engine airplanes, but the principle applies, as we notice in the definition of refusal speed.

5.1.1.7 **Refusal Speed and Refusal Distance**.

Refusal speed (V_{REF}) is the maximum speed that an aircraft can obtain under normal acceleration conditions and then stop in the available runway.

Clearly, V_{REF} and V_{CEF} are quite similar; $V_{CEF} = V_{REF}$ for multiengine airplanes. In other words, V_{REF} applies to both single engine and to multiengine aircraft. In this regard multiengine airplanes have an advantage over single engine craft; they can takeoff if an engine fails above V_{REF}. But neither type can stop in the available runway if a takeoff is aborted above V_{REF}. For this reason, during flight tests to determine V_{REF}, the pilot's reaction time to recognize an engine failure must be included (simulated) in the test. Usually, 2-3 seconds delay is sufficient.

Refusal distance is the takeoff ground run required to attain V_{REF}.

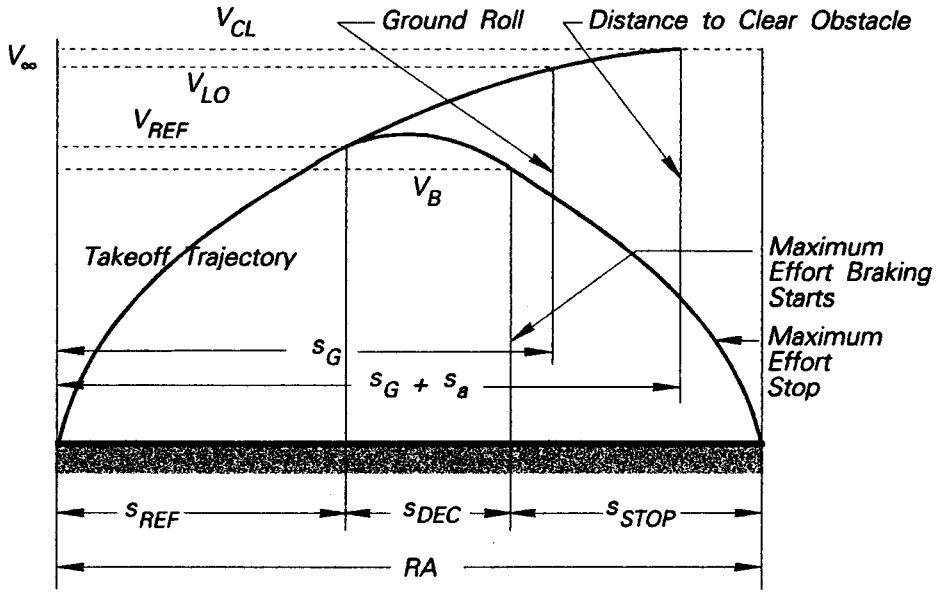

Fig. 5.4 Velocity Profiles for RA = CFL

5.1.1.8 **Ground and Air Minimum Control Speeds**. Controllability of a multiengine airplane after the loss of an outboard engine is a major concern, especially during takeoff when the necessity to establish a safe rate of climb dictates that the engines be operated at high thrust or power levels. Rudder authority and the magnitude of the yawing moment due to asymmetric thrust that the rudder must counteract are major factors in the decision of whether or not to continue a takeoff after the loss of an engine.

> The minimum speed at which a multiengine airplane, while on the ground, can lose an outboard engine and maintain directional control is the **ground minimum control speed**, V_{mcg}.

For V_{CEF} to have meaning, it must be less than V_{mcg}.

> The **air minimum control speed**, V_{mca}, is the minimum airspeed (out of ground effect) at which the critical engine can fail and directional control can be maintained using full rudder deflection and not more than 5° of bank.

When determining V_{mca}, the pilot must be able to regain directional control and maintain straight, steady flight at the same airspeed without reducing power and without retrimming. Moreover, the control forces and heading divergence must be within specified limits. These tests should be conducted at the most aft center of gravity loading and at maximum gross weight for the configuration. To be useful, $V_{mca} > V_s$, where V_s is the stall speed for the takeoff configuration.

5.1.1.9 **Safe Single Engine Speeds**. During takeoffs or landings with one engine inoperative, a multiengine airplane must be operated with some margin of safety. Some literature calls this speed the takeoff safety speed, V_{TOS}, but the most common terminology in the United States is safe single engine speed, V_{SSE}.

Safe single engine speed (V_{SSE}) is the airspeed below which a multiengine aircraft must not be operated after leaving ground effect with one engine inoperative.

V_{SSE} must exceed both V_s and V_{mca} by a safe margin. While V_{SSE} is most important during takeoff, prudence dictates that the airspeed not be reduced below V_{SSE} during a single engine landing until the landing is assured.

With this terminology firmly established, we now turn our attention to basic physics.

5.1.2 Performance Equations

Because of the large number of factors that affect TO&L performance, it is practically impossible to model it perfectly. Major influences include:

- Gross weight
- Thrust available
- Ambient temperature
- Pressure altitude
- Wind direction and velocity
- Slope of the runway
- Coefficient of friction

To make any rational analysis of performance measurements, we will have to make several simplifying assumptions.

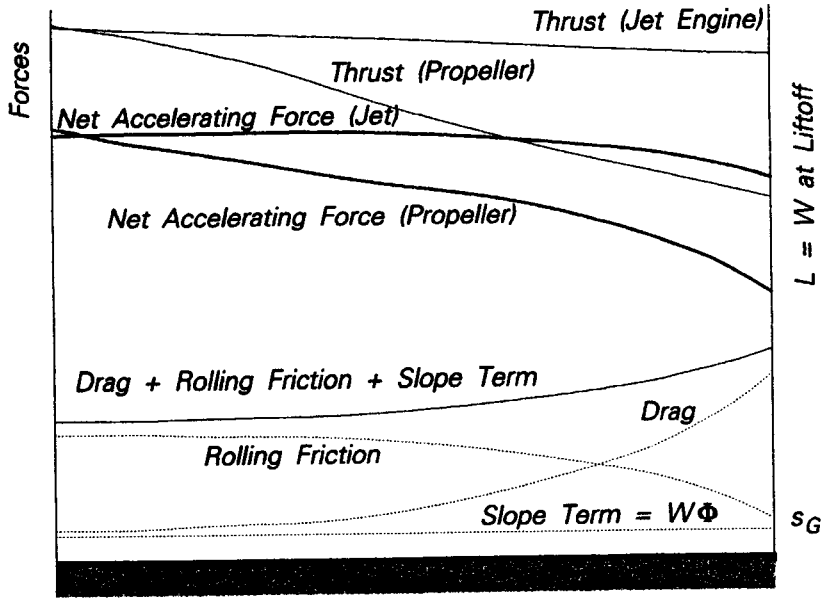

Fig. 5.5 Forces During Ground Run

5.1.2.1 **Ground Run Equations**. First, let us consider the distance while the airplane is strictly rolling on the ground during either a takeoff or a landing. The takeoff or landing

flares are not a part of this analysis; the distance covered during rotation during takeoff will be approximated separately. Hence, we will call this distance s_{G_1} for the takeoff, differentiating it from s_G (the total ground run distance to liftoff). The forces acting on an airplane during this first portion of the ground run of a takeoff or the last portion of a landing are sketched in Fig. 5.5. The contributing aerodynamic forces are defined in the usual sense: L and D, as shown, are conventional, as are T and W. The frictional force F_f is rather difficult to ascertain, but it is usually defined in terms of a friction coefficient μ and the net normal force. That is, $F_f = L - W$. Lan and Roskam[2] give typical values for μ as shown in Table 5.1. Of course, the slope of the runway also produces a small component of W ($W \sin \Phi \approx W\Phi$) acting parallel to the takeoff surface, along with a small reduction in normal force. This latter component is usually neglected, since Φ is typically a very small angle (usually less than 3°). The runway gradient, or slope, is positive if the takeoff is uphill. So the net force accelerating the airplane parallel to the surface of the runway is

$$F = ma = T - D - \mu(W - L) - W\Phi \tag{5.1}$$

TABLE 5.1 Values for Runway Surface Friction Coefficients

Type of Surface	Range for μ
Concrete	0.02-0.030
Hard turf or short grass	0.05
Long grass	0.10
Soft ground	0.10-0.30

We also want to consider wind effects: let $\pm V_w$ = wind speed. Here, "+" implies a tail wind and "-" a head wind. So, at any point in the takeoff ground roll the ground speed is

$$\frac{ds_G}{dt} = V \pm V_w \tag{5.2}$$

Of course, the acceleration is $a = \frac{dV}{dt}$, which we rearrange to $dt = \frac{dV}{a}$, and

$$ds_G = (V \pm V_w)\frac{dV}{a} \tag{5.3}$$

Integrating eqn. 5.3 yields an exact expression for takeoff ground run distance, provided we know a, V, and V_w throughout the takeoff roll and we can accurately determine the true airspeed at liftoff.

$$s_G = \int \frac{(V \pm V_w)dV}{a} \tag{5.4}$$

Of course, we can not generally express each of these parameters analytically, but they can be measured by several means. If we solve the basic force equation (eqn. 5.1) for the acceleration and substitute it into eqn. 5.4,

$$s_G = \int \frac{W(V \pm V_w)dV}{g[T - D - \mu(W - L) - W\Phi]} \tag{5.5}$$

Equation 5.5 is the basic equation for ground roll distance for either takeoffs or landings; it will be used in modified form for both purposes. We will use a second set of subscripts ("$_L$") to denote landing conditions. Notice that in eqn. 5.5 we have adhered the our sign convention that $\Phi > 0$ for uphill takeoffs. Remember that the acceleration during the ground roll after landing is negative and that the thrust term can be either positive or negative, depending on whether or not the test vehicle has thrust reversing or not. Though we have not included it, another similar term must be added if the airplane uses a deceleration device, like a drag parachute or a speed brake, to reduce the ground roll. We choose to lump this added drag with the aerodynamic drag. Even more important, the braking friction coefficient (μ_b) is quite different than it was for takeoff because the brakes are applied at some point during this segment of the landing. Typically, rolling friction coefficients vary considerably. Notice that μ_b is a strong function of runway surface conditions (wet or icy surfaces) and whether or not the tires are skidding or not (Fig. 5.6). Modern aircraft often have antiskid brake units to avoid tire slippage during heavy braking. It is usually not feasible to test for these stopping distances under actual runway surface conditions like those shown in Fig. 5.6. It becomes the flight test engineer's job to identify and plan for simulating such conditions. Often this task is one of the more difficult ones faced by the flight test engineer. The approach that is now most common is to develop a mathematical model and then carry out a limited number of tests to validate this model. Naturally, one of the more difficult facets of this kind of testing is measuring actual braking coefficients for other than dry runway surfaces. Sometimes, aerodynamic braking is so important that during the early stages of the rollout the recommended procedure is to maintain a high pitch attitude, applying brakes only after the nose is lowered.

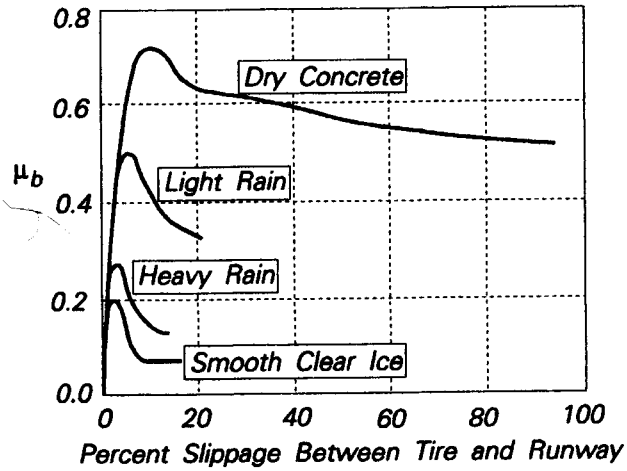

Fig. 5.6 Coefficients of Friction during Landing Ground Run

Figure 5.7 illustrates this procedure and also shows how useful a drag chute is for some designs. While the landing ground roll distance equation is of the same form as the takeoff equation, the values of the terms may be significantly different; there are terms present that are not in the takeoff equation. These differences are indicated by the changed symbols and the apparent reversed order of integration (which accounts for the deceleration) in the following expression:

$$s_{G_L} = \int_{V_{TD}}^{0} \frac{W_L(V \pm V_w)dV}{g\left[T_L - D_L - \mu_b(W_L - L_L) - W_L\Phi\right]} \tag{5.6}$$

The T_L, μ_b, and the D_L in this equation are the landing roll expressions for the corresponding quantities in eqn. 5.5; the subscripts are merely used to remind you that these parameters are considerably different from those in the takeoff roll expression.

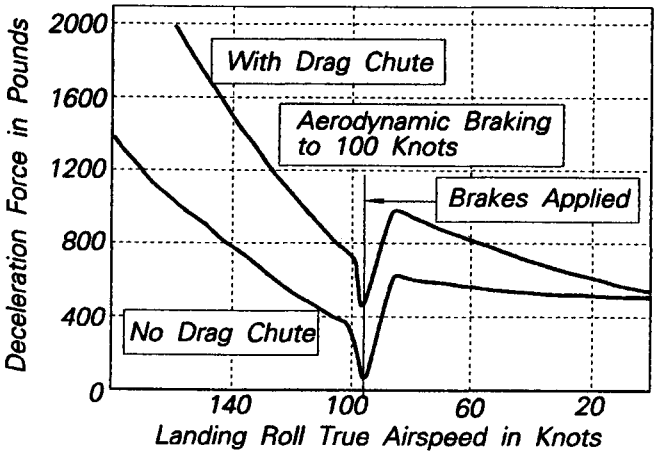

Fig. 5.7 Effect of Aerodynamic Braking and/or Drag Chute

Example 5.1: An airplane with a wing area of 230 square feet weighs 9900 pounds and the speed brakes are opened for landing. In this configuration it has a drag equation: $C_D = 0.144 + 0.055C_L^2$. The speed brakes remain extended down to approximately 75 ktas. Idle thrust of the engine at sea level, standard day conditions is constant at 700 pounds with the airspeed at or below final approach speed. Touchdown on the main wheels occurs at 100 knots. If the average rolling coefficient of friction on dry concrete is 0.03 and the average braking coefficient of friction is 0.5, estimate the total landing distance from touchdown to a complete stop. Assume no wind. The nose wheel is lowered (instantaneously) to the runway at 75 knots, but the test pilot maintains a constant angle of attack after touchdown until he lowers the nose, giving $C_L \approx 1.25$ during this phase of the landing. As soon as the nose wheel is on the runway, the wheel brakes are applied and braking begins. With the airplane in this three-point attitude, $C_L \approx 0.1$.

V (ktas)	V (fps)	Lift ($C_L \approx 1.25$)	ΔD	Integrand	Σ	$\Sigma\Delta s_L$(feet)
100	138.889	9745.88	1792.75	-47.36	–	–
95	160.444	8795.65	1617.96	-51.91	-49.36	419.1
90	152.000	7894.16	1452.13	-57.58	-104.37	881.42
85	143.556	7041.40	1295.26	-64.86	-165.59	1398.4
80	135.111	6237.36	1147.36	-74.61	-235.33	1987.2
75	126.667	5482.06	1008.42	-88.39	-316.83	2675.4

This problem breaks down into two parts: (1) from main wheel touchdown until the nose wheel is on the runway and braking begins and (2) from nose wheel touchdown until the airplane comes to rest. The first phase is dominated by aerodynamic braking. Wheel brakes provide most of the deceleration during the second part of the rollout. Equation 5.5 applies to the first phase and eqn. 5.6 to the second. At main wheel touchdown $L \approx W$. As the airplane brakes aerodynamically, eqn. 5.5 shows that the friction term becomes a more important part of the retarding force. But the principal deceleration still comes from aerodynamic drag. The aerodynamic drag decreases as V decreases, even though C_L is held constant. Tabulat-

ing these lift and drag changes at discrete speeds during the landing roll, in the table above we numerically approximate the integration of eqn. 5.5. The table summarizes the results of this numerical integration and estimates the ground roll prior to commencement of braking at 2675 feet.

The second phase of the ground roll is calculated using the same procedure, except that the terms in eqn. 5.6 are changed to the appropriate values for C_L and to μ_b (0.1 and 0.5, respectively) for this phase of the rollout. This calculation is illustrated below and shows that the ground roll distance after the nose wheel is lowered is only 554 feet. Deceleration distances (after the brakes are applied) are tabulated on page 101.

V (ktas)	V (fps)	Lift ($C_L \approx 0$)	ΔL	Integrand	Σ	$\Sigma \Delta s_L$(feet)
75	126.667	438.56	633.94	-8.36	–	–
70	118.222	382.04	552.24.	-7.89	-8.12	68.6
65	109.778	329.41	476.16	-7.41	-15.77	133.2
60	101.333	280.68	405.72	-.6.91	-22.92	193.6
55	92.889	235.85	340.92	-6.39	-29.57	249.7
50	84.444	194.92	281.75	-5.86	-35.70	301.4
45	76.000	157.88	228.22	-5.32	-41.28	348.6
40	67.556	124.75	180.32	-4.76	-46.32	391.2
35	59.111	95.51	138.06	-4.19	-50.80	429.0
30	50.667	70.17	101.43	-3.61	-54.70	461.9
20	33.778	31.19	45.08	-2.43	-60.74	512.9
10	16.889	7.80	11.27	-0.61	-65.31	551.5
0	0.000	0.00	0.00	0.00	-65.62	554.1

So, our approximation for the total landing roll is the sum of the two increments: $\boxed{s_{G_L} = 3230 \text{ feet}}$

5.1.2.2 **Rotation Distance**. As was pointed out earlier, most takeoff distance predictions for modern high performance aircraft should include an allowance for the distance covered during the takeoff flare or the rotation down from touchdown attitude to the attitude where all wheels are on the ground and brakes are applied. We will call this distance either s_{G_2} (for takeoff) or s_{L_2} (for landing). Typically, the estimate is made by simply assuming a reasonable average time to complete the pitch rotation. The time chosen will be different for each airplane considered, but 3 to 4 seconds is a reasonable approximation for many types. The distance is assumed to be traversed at a constant speed, either V_{LOF} or V_{TD} (again, for liftoff or landing, respectively).

$$s_{G_2} = t_r V_{LOF} \quad \text{or} \quad s_{L_2} = t_r V_{TD} \tag{5.7}$$

where t_r is the approximate average time used to carry out the takeoff or landing flare, respectively

5.1.2.3 **Transition Distance**. Part of the air distance estimate is based on rather arbitrary assumptions. After liftoff the aircraft must transition from an essentially level acceleration along the runway surface to either a constant airspeed climb or a constant angle climb. For certification and for design purposes, the latter is usually taken to attain clearance height above any obstacles in the flight path near the ground. Later, another transition to a constant airspeed or a constant Mach number climb path is may when well clear of any ground-based obstacles. During the landing approach flare maneuver is used to transition from the ideal constant glide path angle descent to touchdown. We will concern ourselves in this paragraph with how far the airplane travels in a horizontal direction while making these transitions. To simplify the estimate (and this distance is highly approximate), we will assume that this transition path is a circular arc. To maintain

a circular path, the velocity will be constant and the acceleration is $\frac{V^2}{R_C}$, where R_C is the radius of the circular transition path. Clearly, to fly through such a circular path requires an acceleration toward the center of the circular arc. The force producing this acceleration comes from additional lift generated by the lifting surfaces and this added lift can be measured as an increment in load factor given by:

$$\Delta n = \frac{V^2}{gR_C} = \frac{\Delta C_L \rho V^2 S}{2W} \tag{5.8}$$

The velocity in eqn. 5.8 (and in eqn 5.9 below) can be either V_{LOF} or V_{TD} depending on whether we are dealing with a takeoff rotation or a landing flare. In either case we can rearrange eqn. 5.8 to calculate R_C.

$$R_C = \frac{V^2}{g\Delta n} = \frac{2W}{g\,\Delta C_L \rho V^2 S} \tag{5.9}$$

Another variation uses the R_C found from the total lift coefficient during transition ($C_{L_{tran}}$).

$$L = \frac{WV^2 C_{L_{tran}}}{V_s^2 C_{L_{max}}} = W + \frac{WV^2}{gR_C}$$ where V_s is the stall speed for the appropriate configuration and $C_{L_{max}}$ is the corresponding maximum lift coefficient (Fig. 5.8). Then

$$R_C = \frac{V^2}{g\left(\frac{V^2 C_{L_{tran}}}{V_s^2 C_{L_{max}}} - 1\right)} \tag{5.10}$$

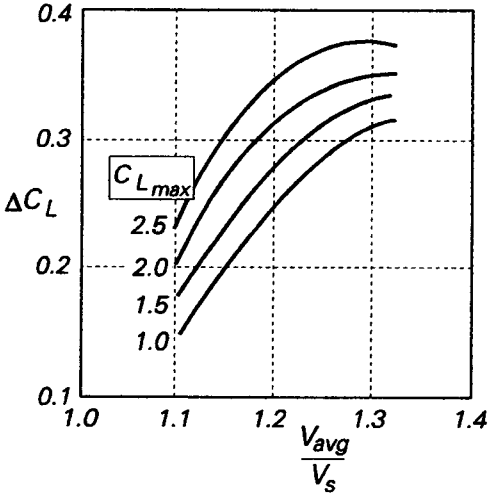

Fig. 5.8 Empirical Values of ΔC_L used in Equation 5.9

Of course, the estimate improves if the velocity in the calculation of R_C is improved. One approach is to use an average speed during the takeoff transition or the landing flare

in the equations above. This mean speed is essentially the average of V_{LO} and the speed during the initial climb for a takeoff transition or of V_{TD} and the final approach speed for a landing flare. Lan and Roskam[2] point out that Williams used this approach, including the effects of ΔC_L's in the maneuvers. Figure 5.8 is an adaptation of their data.

Knowing the radius of the circular arc, the transition distance (Fig. 5.9) is a simple matter of trigonometry. The horizontal distance covered during either transition is:

$$s_{tran} = R_c|\sin\theta_{CL}| \tag{5.11}$$

The absolute value accounts for negative flight path angles during a landing approach.

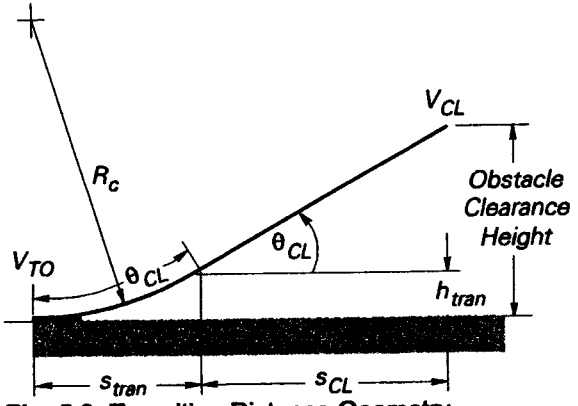

Fig. 5.9 Transition Distance Geometry

5.1.2.4 **Climbout Distance**. The last part of the air distance phase of the takeoff or landing performance estimation is the distance covered during the initial climb before the standard obstacle distance is cleared or during the final approach after the obstacle is cleared but before the landing flare begins. Naturally, in some cases this part of the air distance may be zero. If the altitude at the end of the takeoff transition is greater than the obstacle clearance height or if the landing flare begins above the obstacle clearance height, then this distance has no meaning and is not included in the air distance. Therefore, we must also find the height at the end of the takeoff transition (or the height at the beginning of the landing flare), h_{tran} (Fig. 5.9). The geometry is again quite simple:

$$h_{tran} = R_c\left(1 - |\cos\theta_{CL}|\right) = \frac{s_{tran}}{|\sin\theta_{CL}|}\left(1 - |\cos\theta_{CL}|\right) \tag{5.12}$$

If h_{tran} > obstacle clearance height, then we are through with estimating the required distances. If h_{tran} < obstacle clearance height, we again refer to the geometry sketch (Fig. 5.9) and observe that for an obstacle clearance height of 50 feet:

$$s_{CL} = \frac{50 - h_{tran}}{|\tan\theta_{CL}|} \tag{5.13}$$

Example 5.2: Consider the airplane of Example 5.1. It has a stall speed of 92 knots and it lifts off at $1.2V_s$. Estimate the transition distance and the climbout distance to the climb path. Assume that the transition

path is a circular arc and $\frac{C_{L_{tran}}}{C_{L_{max}}} = 0.8$ during transition to the climb path. Also, assume that $V = V_{LOF}$ and that this speed is constant during this part of the takeoff. Of course, $C_{l_{max}}$ occurs at V_s. The thrust during this transition phase is constant at 7000 pounds.

Then, $C_{L_{max}} \frac{2W}{\rho S V_s^2} = \frac{2(9000)}{0.00023769(92 \times 1.688889)^2(230)} = 1.5$. With this value of $C_{L_{max}}$ and also using $V = V_{LOF} = 1.2V_s$ during the transition, we obtain, either from eqn. 5.9 or from Fig. 5.9, $\Delta C_L = 0.2757$. Calculating R_c from the other form of eqn 5.9:

$$R_c = \frac{2W}{\rho \Delta C_L S g} = \frac{2(9000)}{0.00023769(0.2757)(230)(32.17405)} = 4079 \text{ feet.}$$

As the note on Fig. 5.8 emphasizes, this value of the flight path radius is based on an assumption that the piloting technique is aggressive; the rotation is called a "maximum effort" rotation. Equation 5.9, on the other hand does not require this assumption; if we calculate R_c without a maximum effort rotation,

$$R_c = \frac{1.2(92 \times 1.688889)^2}{\left[1.2C_D = 0.12 + 0.04C_L^2(0.8) - 1\right] - 32.17405} = 7109 \text{ feet.}$$

Notice that there is a wide range in the results (a change of about 75%) depending on whether or not the "maximum effort" assumption is used. This oversimplified calculation underscores just how sensitive takeoff and landing performance estimates are to piloting technique.

Climb angle is set by the excess thrust available during the transition period; that is, $\sin\theta_{CL} = \frac{T_n - D}{W}$, with each of the variables evaluated during the transition phase. In the takeoff configuration the speed brakes are retracted and the flaps are at their takeoff setting. So, $C_D = 0.12 + 0.04C_L^2$. Since the maximum usable $C_L = 1.5 \times 0.8$, $C_D = 0.12 + 0.04(1.44)^2 = 0.1776$. Thus, the average drag during transition is about 1688 pounds. With these intermediate estimates available, $\sin\theta_{CL} = \frac{7000 - 1688}{9900}$. This expression gives, $\theta_{CL} = 34.5°$. Now, we can finally estimate the transition distance, using a "maximum effort" flare to minimize R_c; that is, $s_{tran} = R_c = \sin\theta_{CL}$.

$$\boxed{s_{tran} = 2310 \text{ feet}}$$

$h_{tran} = R_c(1 - \cos\theta_{CL}) = (4079 \text{ ft})(1 - \cos 34.5°) = 717 \text{ feet.}$ Since $h_{tran} > 50$ feet,

$$\boxed{s_{CL} = 0 \text{ feet}}$$

Airplanes with high thrust-to-weight ratios often reach or exceed obstacle clearance height before completing the takeoff flare. Lower performance airplanes will require calculation of s_{CL} using eqn. 5.13.

5.1.2.5 **Summary of Equations**. Having developed the component expressions making up total takeoff or landing distance, we simply sum the component parts to complete our estimate and our discussion of the takeoff and landing performance analysis.

$$s_{TO} = s_G + s_{G_2} + s_{tran} + s_{CL} \tag{5.14}$$

$$s_{LND} = s_L + s_{G_2} + s_{L_{tran}} + s_{FA} \tag{5.15}$$

5.1.3 Parametric Analysis of Takeoff Performance

Shevell[3] advocates a different approach to takeoff performance that is simple and allows straightforward comparison of competing designs. With judicious assumptions, he generalizes takeoff performance for most commercial airliners so that takeoff and field lengths can be estimated from a few charts. The underlying premise of this parametric approach is that "...takeoff performance is basically an acceleration to the required speed plus a climb segment to a 35-ft height (civil turbine-powered transports) or a 50-ft height (piston-powered, general aviation, or military aircraft)." Required runway length is defined

as the distance from the start of the takeoff point to the point where these obstacle heights are reached.

5.1.3.1 **Key Parametric Assumptions**. In laying out this parametric approach, Shevell makes the following basic assumptions:

- Even though acceleration is not constant (as we have seen in preceding sections, it depends on thrust and drag and both are functions of speed), the effective average excess thrust (T - D) occurs at $\overline{V} = \frac{V_{LOF}}{\sqrt{2}}$.
- Drag is small compared to thrust during the takeoff run.

5.1.3.2 **Basic Parametric Equation**. Considering only the first assumption above and denoting the acceleration at $\overline{V}$ as $\overline{a}$, we can approximate ground run distance simply:

$$s_G \approx \frac{V_{LOF}^2}{\overline{a}} \tag{5.16}$$

FAR Part 25.107[4] mandates that the minimum takeoff speed ($V_{2_{min}}$) cannot be less than $1.2V_s$ for two-engine and three-engine turboprop and reciprocating engine-powered airplanes and for all large turbojet transports that do not have provisions for significantly reducing the one-engine inoperative power-on stall speed. So, we choose this nominal value and let $V_{LOF} = 1.2V_s = 1.2\sqrt{\frac{2W}{\rho S C_{L_{max}}}}$. Then eqn. 5.16 becomes:

$$s_G \approx 1.44 \frac{W^2}{\rho S C_{L_{max}} (T_n - D) V} \tag{5.17}$$

The constant in eqn 5.17 depends solely on $\frac{V_{LOF}}{V_s}$. Under certain constraints, this value can be reduced to 1.15. Then, the constant in eqn 5.17 becomes 1.3225 in stead of 1.44. In general, the distance for accelerating a body is directly proportional to the square of the speed and inversely proportional to the average acceleration. But V itself depends directly on wing loading W/S, inversely on $C_{L_{max}}$, and inversely on ρ. Acceleration, under the restriction of the second assumption on the previous page, is directly proportional to T/W. Lumping all these terms together and expressing s_G in functional form to allow for different constants and to correct for nonstandard density conditions:

$$s_G = f\left(\frac{W^2}{\sigma S C_{L_{max}} \overline{T}_V}\right) \tag{5.18}$$

Equation 5.18 is a generalized takeoff performance approximation similar to the generalized performance curves introduced for turbojet-powered aircraft in Chapter 4. Shevell asserts, moreover, "...that if we plot takeoff distance for each airplane against the parameter $s_G = f\left(\frac{W^2}{\sigma S C_{L_{max}} \overline{T}_V}\right)$, the points will form a single curve." The scatter is small for

similar airplanes and a single fairing gives a good approximation to the takeoff distance. Since the ground run is usually greater than the air distance plus the transition distance (by as much as 4 to 1), the total distance to the obstacle clearance height can also be approximated by an expression like eqn. 5.18. Figure 5.10 (adapted from Shevell's data) approximates required runway lengths under FAR Part 25. It was obtained by plotting a large number of takeoffs for different turbojet and turbofan-powered commercial transports and fairing a single curve through the points. This curve applies only to takeoff field lengths with all engines operating. FAR Part 25.113 requires a field length of 115% of the measured obstacle clearance distance; the faired curve includes this safety margin.

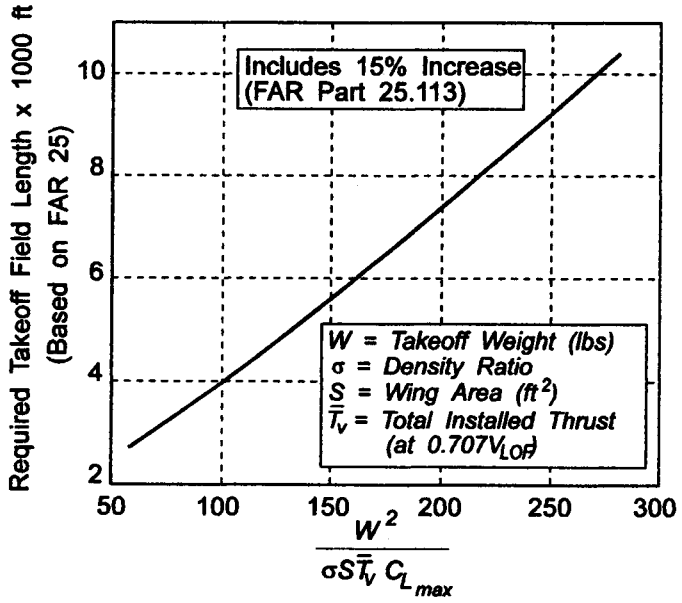

Fig. 5.10 Distance to 35-Foot Obstacle Height for Large Jet Transports (All Engines Operating)

Similarly, Fig. 5.11 is a chart constructed from measured takeoff field lengths, again based on FAR Part 25 requirements, for the same aircraft as Fig. 5.10 but with one engine inoperative. Again, the required 115% margin for uncertainty required by the certification regulation is applied in this chart.

For large commercial transports powered by reciprocating engines the takeoff field lengths required can be approximated from similar parametric charts. However, the acceleration is directly proportional to average installed horsepower, rather than average installed thrust (notice that both terms are installed values, not thrust or power available from engine manufacturer's charts). Then, eqn. 5.18 is modified to:

$$s_G = f\left(\frac{W^2}{\sigma S C_{L_{max}} \bar{P}_V}\right) \tag{5.19}$$

Also, the obstacle height in the regulations is 50 feet for propeller-driven airplanes, rather than the 35 feet used for commercial jet transports. The required field length, under

the assumptions listed at the beginning of this section, collapses to a single curve. Figure 5.12 illustrates such a curve for a DC-6.

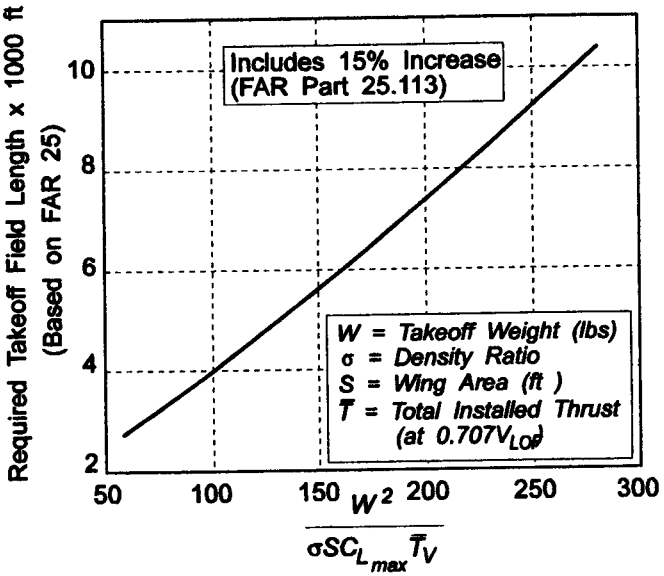

Fig. 5.11 Distance to 35-Foot Obstacle Height for Large Jet Transports (One Engine Inoperative)

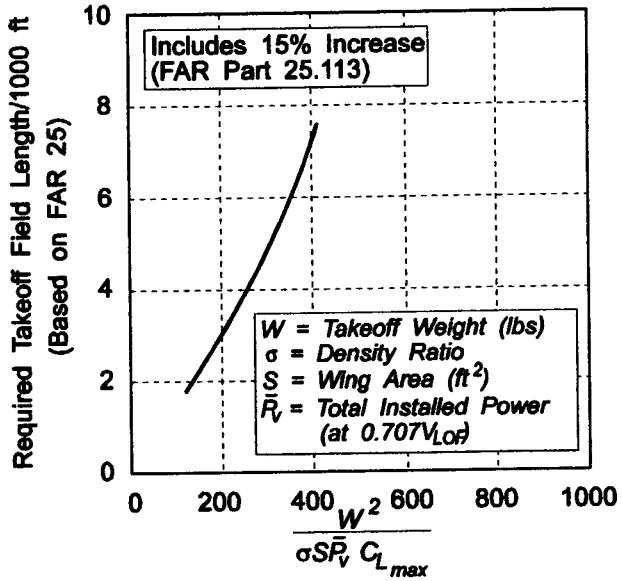

Fig. 5.12 Distance to 50-Foot Obstacle Height for Four-Engine Propeller Transports (One Engine Inoperative)

Turboprop takeoff performance may be estimated from charts like Fig. 5.12 if total installed power is known or from curves like Figs. 5.10 and 5.11 if the total installed thrust is

known. In every case the form of the expressions is the same; only the experimental measurements (which change the slope and curvature of the generalized curve) differ. Typically, this approximation is more difficult to apply to such hybrid powerplants.

Finally, Shevell strongly underscores the value of such a parametric estimation process. He says, "...the parametric method can be used to check the reasonableness of detailed calculations of takeoff (performance)." This basic awareness is essential to a flight test engineer engaged in planning a series of takeoff and landing tests. From such reasonable approximations come those elusive qualities called "intuition" and "engineering judgment". They are acquired skills, not innate intelligence!

5.2 FLIGHT TEST METHODS

The nature of takeoff and landing measurements leaves much to be judgment of the individual flight test team; there is no well-defined "standard" for making these measurements as there is for pitot-static calibrations, climb performance, or cruise performance. This statement does not imply that the requirements documents for military full scale developments or for certification under FARs are imprecise or vague. Rather, these documents are often so specific that the test team must tailor a takeoff and landing test to the individual test program. Consequently, this section is more general and can offer only guidelines. Fortunately, the theory and "analytical" equations presented in section 5.1 are quite pragmatic; so, tailoring to the specific requirements of a given flight test program is usually straightforward.

5.2.1 Requirements for Takeoff and Landing Flight Tests

Takeoff and landing tests are made to provide data for the operator during these critical phases of flight. Apart from special tests conducted with a specific research goal in mind (for example, changes in stability derivatives in ground effect), both military and civil requirements are heavily slanted toward collecting information that goes into the Airplane Flight Manual (AFM). These flight tests are a combination of performance and handling qualities assessments. As such, they involve measurement of performance parameters of interest. But they also usually involve some degree of subjective evaluation as to how the airplane's stability and controllability affect the pilot's ability to precisely maneuver the airplane during these terminal phases of flight. Partly because of the dual nature of such evaluations, certification requirements and military specifications spell out a very complicated matrix of test conditions. This matrix includes not only normal operating conditions, but also a large number of abnormal or emergency procedures in order to "demonstrate" that each standard is met. Ordinarily, this phrasing means that a flight test demonstration is required. Specifically, Part 23.21 states:

(a) Each requirement of this subpart must be met at each appropriate combination of weight and center of gravity within the range of loading conditions for which certification is requested. This must be shown –

(1) By tests upon an airplane of the type for which certification is requested, or by calculations based on, and equal in accuracy to, the results of testing; and

(2) By systematic investigation of each probable combination of weight and center of gravity inferred from combinations investigated.

(b) The following general tolerances are allowed during flight testing. However, greater tolerances may be allowed in particular tests:

Item	*Tolerance*
Weight	*+5%, -10%*
Critical items affected by weight	*+5%, -1%*
Center of gravity	*+7% of total travel*

While each of the subparts of FAR Part 23 listed below is applicable for takeoff and landing demonstrations and should be carefully studied by the test team, those subparts marked with an asterisk pertain directly to these flight tests. Most of the other compliance requirements can be extracted from tests that these subsections dictate. Since this book introduces the subject and does not attempt to comprehensively cover all aspects, the discussion is limited to these most important subparts.

Part 23.33 Propeller speed and pitch limits
Part 23.49 Stalling Speed
Part 23.51 Takeoff*
Part 23.75 Landing*
Part 23.143 Controllability and maneuverability: general
Part 23.145 Longitudinal control
Part 23.147 Directional and lateral control
Part 23.149 Minimum control speed
Part 23.177 Directional and lateral stability
Part 23.179 Instrumented stick force maneuvers
Part 23.181 Dynamic longitudinal stability
Part 23.201 Wings level stall
Part 23.207 Stall warning
Part 23.231 Ground and water handling characteristics: Longitudinal stability and control*
Part 23.233 Ground and water handling characteristics: Directional stability and control*
Part 23.153 Control during landings*
Part 23.155 Elevator control force in maneuvers
Part 23.157 Rate of roll
Part 23.161 Trim
Part 23.171 Stability: general
Part 23.173 Static longitudinal stability
Part 23.175 Demonstration of longitudinal stability
Part 23.235 Ground and water handling characteristics: Taxiing conditions
Part 23.239 Ground and water handling characteristics: Spray conditions
Part 23.251 Vibration and buffeting

5.2.1.1 **Use of Mathematical Models and Simulation**. One of the more significant recent trends in evaluating takeoff and landing performance is a shift from overall measurements (which are rather imprecise mainly due to variations in piloting technique) to measurement of segments of these maneuvers and use of modeling or mathematical simulation to tie segments together. The primary objective of most TO&L measurements is to determine and demonstrate for the user of the airplane how to achieve reasonable takeoff and landing distances and safe speeds for everyday operations. Flight tests are typically used to verify individual portions of the mathematical model rather than attempting to measure the performance on complete maneuvers. These "patched" maneuvers (or maneuver segments) can be compared and standardized more easily than can measurements from complete takeoffs or landings. Both military and civilian flight test engineers are permitted to use either approach. Of course, complete takeoffs and landings, with careful attention to consistent piloting techniques, are still demonstrated. But the modeling approach allows thoughtful choice of valid maneuvers and better control of test variables.

In practice the test team should plan to collect data on almost every takeoff and/or landing until a rather complete data base is established for normal procedures. Even though repeatability in technique is emphasized, there will be wide variation in results. But, individual segments where nearly identical rotation rates and usable airspeeds are matched can be collected from several different runs and statistically evaluated for consistency before the complete maneuvers are flown for validation of the modeled takeoff or landing. Such mathematical simulations are particularly useful in establishing takeoff acceleration profiles and in predicting landing rollout under slippery runway conditions. The segmented approach allows the test engineer to use portions a of a maneuver to establish performance, even though the entire maneuver may have flaws in it that make the overall distances and velocities invalid. From this perspective, segmented testing is more efficient; it allows almost every maneuver flown to contribute to the data base and thereby adds statistical relevance.

However, complete maneuvers must also be done as final validation of the takeoff or landing model. As one FAA document[6] puts it: ",,,actual takeoffs using the AFM (recommended technique) should be conducted to verify that the actual distance to the 50-foot height does not exceed the calculated takeoff distance to the 50-foot height." Complete takeoffs and landings, with attention to consistent piloting techniques, must still be demonstrated: but not many of them.

5.2.1.2 **Position and Velocity Measurement Techniques**. The instrumentation used to measure distances and velocities varies widely in precision, in complexity, and in versatility. The most useful measurement tools allow simultaneous capture of both horizontal and vertical position and velocity during either the takeoff or the landing.

Probably the most widely used equipment for measuring ground roll distances is some form of tracking device -- laser, radar, optical, or video. In each case the flight test engineer is responsible for choosing the type of tracker and for guaranteeing (1) that its precision is adequate to satisfy the certifying agency, (2) that any special transponders or illuminating devices operate reliably, and (3) that the data reduction effort required to convert the spatial measurements into meaningful engineering units is compatible with program budget and schedules. With regard to (2), the test engineer should be alert for any "undesirable side effects" result from the transponder or illuminator. A laser tracker often needs a reflective surface painted on the airplane and the laser beam is intended to point at this surface only. The flight test engineer will have to satisfy safety review authorities that a misdirected laser beam cannot harm (even temporarily) the pilot and/or the airplane and its systems. A radar tracker may also need a radar reflector or a transponder to return accurate spatial information; the test engineer must be sure that such an electronic device does not interfere with other aircraft or test instrumentation subsystems. Optical devices need clearly discernible levels of contrast so that data reduction does not become overly tedious. The same statement is also true of video imaging systems, which do lend themselves to at least partially automated data reduction[7].

At least for the ground roll portions of takeoff and landing trajectories, distances can also be measured by integrating accelerations and then velocities from inertial navigation systems (INS) if the airplane is so equipped. Cheney and Pham[8] describe how such an approach [along with instrument landing system (ILS) and radio altimeter measurements] was used to validate and certify Category III autoland performance for the MD-80 and the MD-87 commercial airliners. This indirect form of distance measurement is accurate pro-

vided (1) the INS is not strongly affected by acceleration errors during takeoff and (2) the events in question (liftoff, touchdown, and passage through obstacle clearance height can be precisely defined on the data records. This latter point means that the test planner must thoroughly evaluate techniques to define these events. Sometimes the flight test engineer may have to design additional equipment or improvise procedures to define the events critical to his measurement data. Landing gear microswitches and photoelectric beams are two such specialized devices that have been used for this purpose. Often the preparation for a full-blown set of takeoff and landing tests must include qualification and proof testing of these kinds of specialized instrumentation before useful data can be collected. The wise flight test planner includes time in his schedule for such proof tests.

These secondary measurements are crucial since the flight test engineer must correct his data for nonstandard conditions. The growing use of segmented, mathematical simulations to reduce test time and cost underscores the necessity for these data in making appropriate corrections to measurements. All of these atmospheric variables affect propulsive thrust and/or directly affect ground speed as measured by tracking equipment. Takeoff and landing measures of merit are drastically affected if this atmospheric information is missing; however, it is often necessary to use expensive instrumented runways (available at all major test facilities). As always, the cost of having such instrumentation is often prohibitive to small or underfunded development efforts.

Of course, spatial measurements (tracking data, whether radar-derived, optical, or otherwise), made repeatedly and rapidly against an accurate time base, are a satisfactory way to estimate velocities only if atmospheric conditions are recorded at the same time. Consequently, most major test ranges have runways that are heavily instrumented with atmospheric sensors. As a minimum, TO&L flight test data used for certification or proof of performance, require the following atmospheric instruments[6]:

(1) an altimeter or a sensitive barometer set to 29.92 inches of mercury to measure altitude;
(2) one or more anemometers that measure wind velocity and direction at the takeoff or landing surface (It is also useful is some means of measuring wind velocity and direction up through the obstacle height is available.);
(3) an accurate thermometer to provide free air temperature, again at the takeoff or landing surface; and
(4) when appropriate (as when tests are conducted in high temperature, high humidity conditions), relative humidity at the takeoff or landing surface.

5.2.2 Typical Part 23 Test Groups

5.2.2.1 **Takeoff Tests**. In laying out a series of takeoff tests, most of the data is collected during other tests; after all, every successful flight must begin with a takeoff and end with a landing. However, every test plan should include a matrix of test conditions that covers specific TO&L test maneuvers. The test engineer can then simply cross off the appropriate data as it is collected, analyzed, and validated. For a typical light twin to be certified under FAR Part 23, the takeoff test matrix groups that must be expanded into detailed test cards for individual flights might look like those in Table 5.2 on the following page.

Table 5.2 Takeoff Conditions for a Light Twin Certification

Test Description	Conditions	Primary Purpose	References
Determination of V_r	Normal takeoff	Select techniques	Part 23.51, AC-23-xx
Demonstrate takeoff performance[2], including ground roll, flare distance, distance to clear obstacle, speed at obstacle height	At nominal weights[3], cg locations[4], flap settings, and atmospheric variables[5]	Proof of compliance, data for AFM	Part 23.51, AC-23-xx
Demonstrate minimum control speeds[7]	Specified weights[3], cg locations[4], sideslip conditions, and bank angles	Proof of compliance, data for AFM	Part 23.51, AC-23-xx
Demonstrate required roll responsiveness in the takeoff configuration[8]	At nominal weights[3], cg locations[4], and atmospheric variables[5]	Proof of compliance, data for AFM	Part 23.51, AC-23-xx Part 23.157

Notes: 1. Stall speeds must be determined before this matrix is begun.
2. Emphasis is on achieving a speed so that all maneuvers can be performed safely in the event of a power failure in reasonably turbulent conditions.
3. Takeoff distance tests are conducted at maximum weight and at a range of cg locations.
4. Takeoff distance demonstrations are performed at the most critical cg location (usually the most forward cg).
5. Humidity is measured and accounted for (Part 23.45) and wind velocity and direction is measured adjacent to the takeoff surface. Wind velocities should be as low as possible, not to exceed $1.2V_{s_1}$ or 10 knots.
6. The airplane is presumed to have the desired maneuvering capability at the obstacle clearance height if the speed attained at this point is the higher of $1.1V_{mc}$, $1.3V_{s_1}$, or some speed > $1.3V_{s_1}$ down to V_x + 4 knots (for multiengine airplanes). Since V_{mc} has no meaning for single airplanes, the first speed requirement at the obstacle height does not apply.
7. Minimum control speed tests, obviously apply only to multiengine airplanes and are not takeoff tests in the strictest sense. The test team must determine the "critical" engine and must investigate all flap settings recommended for use. Dynamic or static V_{mc}, whichever is greater, will be included in the AFM.
8. Demonstrations should be accomplished by rolling the airplane in both directions.

5.2.2.2 **Landing Tests**. Landing tests are also outlined to help organnize the test matrix during the test planning phase. The primary difference between them and takeoff tests lies in the demonstration of adequate longitudinal control authority for the landing flare maneuver. Table 5.3 summarizes a typical grouping of such tests, again for a small twin-engine airplane. Again, the detailed test planning involves laying out detailed test cards that cover all items in this matrix. The test planner must also anticipate considerable variation in the landing data, since the performance during this maneuver is quite uncertain due to a number of factors including: (1) atmospheric turbulence is common for landing, (2) pilot technique varies widely for making a "good" landing, and (3) ground effect changes the handling qualities for each airplane and pilot combination. For all these reasons, it is imperative to measure a statistically significant number of landings carried out by a representative sample of pilots to obtain quality landing data.

Table 5.3 Landing Tests for a Light Twin Certification

Test Description	Conditions	Primary Purpose	References
Determination of Approach and landing speeds[1]	Landing at all proposed flap settings, cg locations[4], and power	Select techniques	Part 23.75, AC-23-xx
Demonstrate landing performance[2], including ground roll, flare distance, distance to clear obstacle, speed at obstacle height	At nominal weights[3], cg locations[4], flap settings, and atmospheric variables[5]	Proof of compliance, data for AFM	Part 23.75, AC-23-xx
Demonstrate longitudinal control during landing[6]	Specified weights[3], cg locations[4]	Proof of compliance, data for AFM	Part 23.153, AC-23-xx
Demonstrate required roll responsiveness in the landing configuration[7]	At nominal weights[3], cg locations[4], and atmospheric variables[5]	Proof of compliance, data for AFM	Part 23.157, AC-23-xx

Notes:
1. Stall speeds must be determined before this matrix is begun.
2. Emphasis is on achieving a steady speed at the obstacle height with the power set so the airplane passes through this reference point in stabilized conditions. A smooth flare to touchdown should be made. Normal pilot reaction times should be used for power reduction, brake application, and actuating other deceleration devices. At least six landings on the same wheels, tires, and brakes should be demonstrated to ensure serviceability.
3. Landing distance tests are conducted at maximum allowable landing weight and at a range of lesser weights expected in normal service.
4. Landing tests are performed at the "critical" (usually the most forward) cg location and the most aft cg location certified, as well as a range of other cg locations expected in normal service.
5. Humidity is measured and accounted for (Part 23.45) and wind velocity and direction is measured adjacent to the takeoff surface. Wind velocities should be as low as possible, not to exceed $1.2V_{s_1}$ or 10 knots.
6. The primary purpose of this demonstration is to ensure that airplanes over 6000 pounds gross weight have sufficient flare capability to overcome any excessive sink rate that may develop at a speed 5 knots lower than recommended normal approach speed and to ensure that control forces are not excessive. If the airplane is to be certified at approach speeds < $1.3V_{s_1}$, compliance with Part 23.153 must be demonstrated at the selected approach speed.
7. Demonstrations should be accomplished by rolling in both directions.

5.3 SUMMARY

This chapter introduces methods of estimating takeoff and landing distances and speeds critical to attainment of this performance. We review both piecewise estimation techniques and parametric computations. Test methods for these flight tests are neither as clearly defined nor as precise as for some performance measurements; pilot technique plays an important role. Although it is usually easy to gather large amounts of takeoff and landing data, it is difficult to obtain repeatable data for complete maneuvers. It is common practice to select consistent segments of each of several similar maneuvers and use them to verify mathematical models of takeoff and landing for a given configuration. This approach is a good example of how simulation augments experimental measurements and makes flight testing more efficient. Finally, general test groups for a simple airplane are suggested that outline detailed test matrices for certification compliance demonstrations.

REFERENCES

1 Dekker, F. E. D. and Lean, D., "Takeoff and Landing Performance: Chapter 8, Volume 1," **AGARD Flight Test Manual**, Pergamon Press, New York, 1959.

2 Lan, C. E. and Roskam, J., **Airplane Aerodynamics and Performance**, Roskam Aviation and Engineering Corporation; Ottawa, Kansas, 1980.

3 Shevell, R. S., **Fundamentals of Flight**, Prentice Hall, Englewood Cliffs, New Jersey, 1983.

4 Federal Aviation Regulation, FAR 25, Federal Aviation Administration, Government Printing Office, Washington, Mar. 30, 1967.

5 Federal Aviation Regulation, FAR 23, Federal Aviation Administration, Government Printing Office, Washington, Mar. 30, 1967.

6 Flight Test Guide for Certification of Small Airplanes, Advisory Circular 23-xx, Federal Aviation Administration, Government Printing Office, Washington, Nov. 14, 1983.

7 Dorsett, K., Robson, R., Pollard, S., and Albright, R., and Ward, D. T., "Takeoff and Landing Measurements with a Video Imaging Technique," Unpublished report, Texas A&M University, 1988.

8 Cheney, H. K. and Pham, C. T., "A New Method to Confirm Category II Autoland Performance," AIAA Paper 88-2126, Aug. 1988.

Chapter 6

LONGITUDINAL STABILITY TESTS

Longitudinal stability is usually the first subject introduced when one begins a study of the stability and controllability of airplanes. For relatively mild maneuvers and perturbations, this subject is a convenient introductory topic since only one moment equation is involved and the complications of coupled motions can be avoided. The development of flight test methods has generally followed the same pattern. It is also convenient to start the discussion with the fundamental definitions and assumptions for static stability before going on to the dynamics of the problem.

To evaluate the relative merit of any airplane's flying qualities, it is essential that all parties accept a yardstick. For years the flight test community struggled with standards (and on occasion still does!), but in time both the civil regulatory bodies and the military produced requirements documents that spell out what is expected in any class of aircraft. Van Pelt[1] gives some of this history to go with his examples[2,3] of such requirements. The student should recognize that these requirements change frequently and may be modified by specific contractual documents. Each flight test team must carefully examine the specifications that are applicable to the design being evaluated before they design the test matrix needed to adequately explore its flying qualities.

6.1 THEORETICAL FOUNDATIONS

To lay the groundwork for longitudinal stability test methods, we first briefly review the meaning of static and dynamic stability and the basic equations that govern such motions. To evaluate airplane stability rationally, the test team must be keenly aware that flying qualities are important primarily as they affect the pilot. Therefore, in this book how the pilot reacts to an engineering modification will be a most important consideration.

6.1.1 Definitions

To understand longitudinal stability, the concept of equilibrium must be clearly understood. The most basic definition of equilibrium for any body simply requires constant linear momentum and constant angular momentum. Thus, a rigid body of constant mass must either be at rest or in unaccelerated motion to be in an equilibrium state. For an airplane, both the forces and the moments about the center of gravity must be balanced.

> An airplane is in equilibrium or is trimmed when the sum of the external forces is zero and the sum of the moments about the center of gravity is zero.

That is, the equilibrium state for an airplane is one of unaccelerated linear translation.

Aircraft static longitudinal stability is typically defined in terms of its initial tendency to return to equilibrium after a disturbance. Dynamic longitudinal stability, on the other hand, considers behavior about the pitch axis as a function of time after a perturbation. Disturbances can take many forms, but the one most often of interest is an angle of attack change. (Many older texts use C_L rather than α as the independent variable; however, as Etkin[4] points out, there are cogent reasons for using C_{m_α} as the measure of static

longitudinal stability.) Perturbations in true airspeed often are also important to flying qualities investigations but they are studied less often than are disturbances in α.

> An airplane is said to be **statically stable** in pitch if a disturbance in angle of attack produces an initial pitching moment that tends to restore the airplane to its trim angle of attack.

This definition is primarily of use to an engineer; the pilot senses static longitudinal stability in an entirely different way. He senses static longitudinal stability through the forces he must apply to move the elevator and the displacement of the control stick or column available to him in the cockpit. He perceives positive static stability as an aft stick movement or a pull force on the stick as airspeed is reduced from the trim airspeed. Similarly, a push force or a forward movement of the stick is expected as speed increases (α is reduced) from the trim condition. Both the control movement and the control forces indicate to the pilot whether or not the airplane is statically stable. The fact that there are two ways to sense static longitudinal stability indicates that there are two different types of stability of concern to the flight test team. Each is important for different reasons.

First, **stick-fixed stability** is a measure of the free response of the airplane being tested. The stick or control wheel is held stationary by the pilot so that the control surfaces will not move with changes in the aerodynamic forces on the surfaces.

> **Stick-fixed static longitudinal stability** is positive when the pilot's longitudinal controller must be deflected aft for α greater than α_{trim}.

The converse, of course, must be true for $\alpha < \alpha_{trim}$. For conventional tail-aft airplanes, this definition means that the elevator must move trailing edge up (TEU) when the speed is reduced below the trim speed and trailing edge down (TED) when the speed is increased above the trim speed. Stick-fixed static longitudinal stability is fundamentally important for all other kinds of stability. It applies to airplanes with both reversible and irreversible flight control systems.

When the elevator is allowed to float freely (zero stick force applied by the pilot), a different form, as a different level, of static longitudinal stability can be evaluated. The pilot's force that must be applied to trim the airplane is a key issue and becomes a primary measure of this form of stability.

> **Stick-free static longitudinal stability** is positive when the force applied to the pilot's longitudinal controller is an aft (pull) force for α greater than α_{trim}.

With these basic concepts reviewed, we now turn our attention to quantifying them . But to do so, we must first establish sign conventions for our analysis.

6.1.1.1 **Sign Conventions**. Figure 6.1 shows the sign conventions commonly used in the literature and in this book. The positive coordinate directions x, y, z and the right-hand rule define positive force, angular velocity, and moment vectors as illustrated. The most common (though by no means universal) sign conventions for control surface deflections are shown. While most stability and control textbooks use the "standard" convention (Fig. 6a) for control surface deflections, we will use the flight convention shown in Fig. 6b. In former convention the observer is assumed to be sighting along the positive

z axis and using the right hand rule to define positive angular deflections of the rudder; that is, left rudder deflection is positive. Positive elevator deflection is obtained by sighting along the positive y direction and again applying the right hand rule. This approach gives a positive deflection of the elevator surface when it is moved trailing edge down (TED). Aileron movement is defined to positive when the right aileron is moved trailing edge up (TEU). Similarly, if a "rolling tail" is used for lateral control, TEU for the right half of the stabilizer is considered positive. On the other hand, the flight test community typically uses a less positive moment about the respective axis.

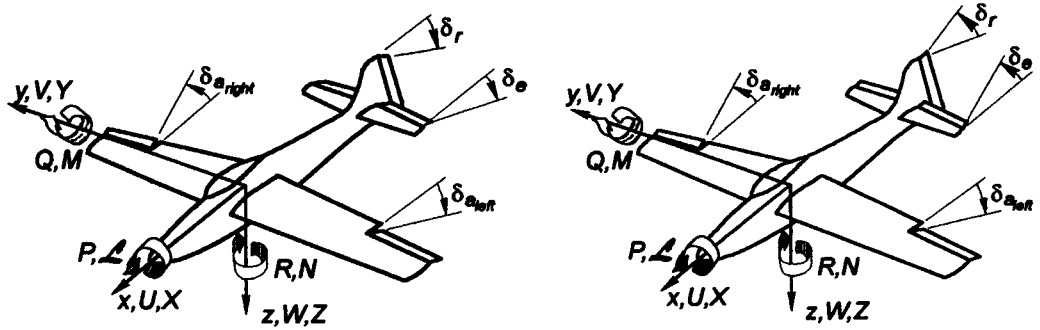

(a) "Standard" Convention (b) Flight Test Convention

Fig. 6.1 Sign Conventions

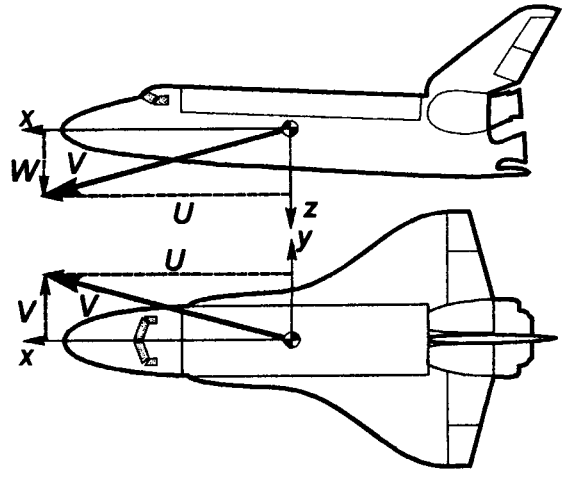

Fig. 6.2 Definitions of α and β

6.1.1.2 **Angle of Attack and Sideslip**. To analyze the longitudinal handling qualities of an airplane with respect to disturbances in angle of attack (α), α must be precisely defined. Figure 6.2 defines α and β (sideslip angle) which will be used to evaluate lateral-directional handling qualities. Looking at longitudinal stability first, we note that α is defined by vector components of true airspeed lying entirely in the vehicle's plane of symmetry.

$$\alpha \equiv \tan^{-1}\frac{W}{U} \tag{6.1}$$

Similarly, even though this definition will not be used in this chapter,

$$\boxed{\beta \equiv \sin^{-1}\frac{V}{V_\infty}} \tag{6.2}$$

Of course,

$$\boxed{V_\infty = \sqrt{U^2 + V^2 + W^2}}$$

6.1.1.3 **Inertial Orientation**. Euler attitude angles are often used to specify the orientation of the body-fixed stability axes relative to an inertial coordinate system located at the center of the earth. These inertial angles must be measured in a specified order to fit the usual aircraft conventions: 1) a yaw rotation (Ψ) about the inertial Z axis; 2) a pitch rotation (Θ) about the position of the y body axis after the first rotation; and 3) a roll rotation (Φ) about the position of the x body axis after the first two rotations. These inertial attitude angles are shown in Fig. 6.3.

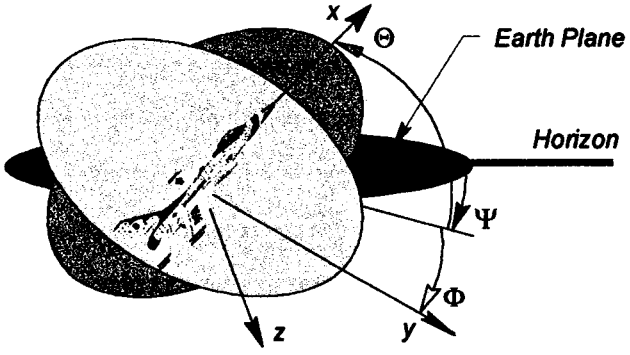

Fig. 6.3 Definitions of Euler Angles

It is important to realize that the Euler attitude angles, Ψ, Θ, and Φ are not vectors, nor can they be thought of as vector components since the order of rotation spells out the final position. However, the angular velocity of the aircraft is a vector and can be expressed in either inertial components $\begin{bmatrix}\dot{\Phi} & \dot{\Theta} & \dot{\Psi}\end{bmatrix}^T$ or body axis components $\begin{bmatrix}p & q & r\end{bmatrix}^T$.

6.1.1.4 **Angular Velocity Transformations**. Figure 6.4 shows the projections of $\dot{\Psi}$ on each of the body axis coordinate directions. First, Ψ is a rotation about the positive z-axis. If there is no pitch or roll rotation, $r_1 = \dot{\Psi}$. If the aircraft is then pitched nose up, as shown in Fig. 6.4b, $r_2 = \dot{\Psi}\cos\Theta$. If the airplane is banked through an angle Φ, $r = \dot{\Psi}\cos\Theta\cos\Phi$. Similarly, after three rotations, $p = -\dot{\Psi}\sin\Theta$ and $q = \dot{\Psi}\cos\Theta\sin\Phi$. Next, resolving $\dot{\Theta}$. in the same way, $q = \dot{\Theta}.\cos\Phi$ and $r = -\dot{\Theta}.\sin\Phi$. Resolving the roll rate ($\dot{\Phi}$) into body axis components, $p = \dot{\Phi}$. Collecting the individual vector components, and writing the resulting linear equations in matrix form:

$$\omega = \begin{pmatrix}p\\q\\r\end{pmatrix} = \begin{pmatrix}1 & 0 & -\sin\Theta\\ 0 & \cos\Phi & \cos\Theta\sin\Phi\\ 0 & -\sin\Phi & \cos\Theta\cos\Phi\end{pmatrix}\begin{pmatrix}\dot{\Phi}\\\dot{\Theta}\\\dot{\Psi}\end{pmatrix} \tag{6.3}$$

Inverting the matrix to solve for the Euler angular velocities:

$$\omega = \begin{pmatrix} \dot{\Phi} \\ \dot{\Theta} \\ \dot{\Psi} \end{pmatrix} = \begin{pmatrix} 1 & \sin\Theta\tan\Phi & \tan\Theta\cos\Phi \\ 0 & \cos\Phi & -\sin\Theta \\ 0 & \sec\Theta\sin\Phi & \sec\Theta\cos\Phi \end{pmatrix} \begin{pmatrix} p \\ q \\ r \end{pmatrix} \tag{6.4}$$

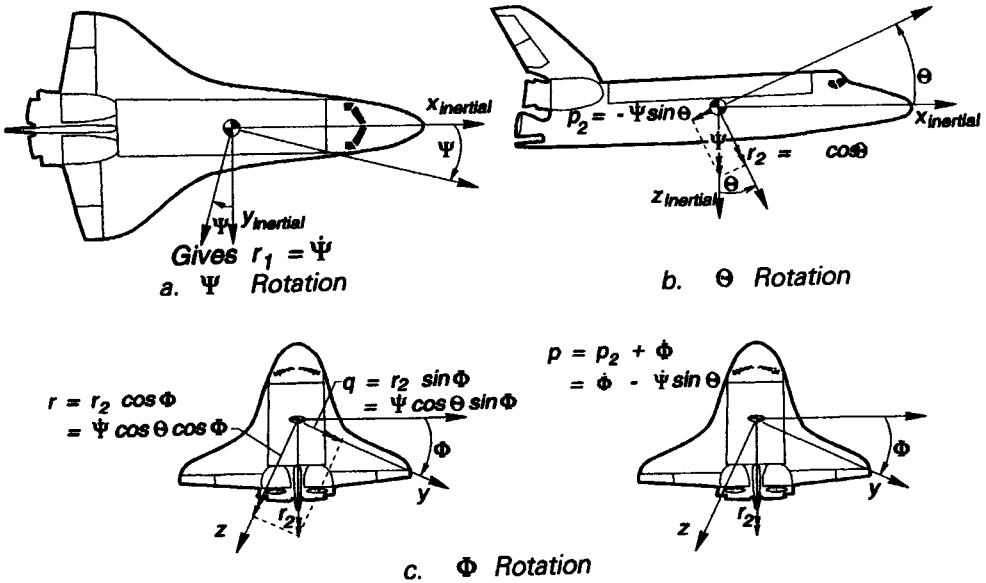

Fig. 6.4 Body Axis and Inertial Angular Velocity Components

6.1.2 Straight Flight Paths

Logically, the next terms to be defined are those used to specify static longitudinal stability quantitatively. From a flight test point of view, the discussion always starts with an engineering concept and proceeds to the pragmatism of how a pilot recognizes and determines the degree of static longitudinal stability for the airplane under consideration.

6.1.2.1 **Neutral Point Concepts**. The stick-fixed and stick-free neutral points are terms used to relate center of gravity (cg) location to the degree of stability of the configuration. Quantitative equations for both neutral points will be developed later, but to fix the concept, consider the following definition.

> **The stick-fixed neutral point** is that cg position for which the pitching moment is independent of α with the longitudinal control surfaces held stationary.

Again, much of the flight test literature[1,5,6] defines neutral point using C_L as the independent variable. As suggested earlier, neutral points defined in this way and associated with zero values of $\frac{dC_m}{dC_L}$ are not always directly related to stability with respect to angle of attack disturbances. Both C_m and C_L are functions of Mach number, Reynolds number, thrust coefficient, and dynamic pressure. Even with the longitudinal control surface and

the cg position held fixed, both the derivatives of interest depend on the parameters listed in addition to α. Consequently, setting $\frac{dC_m}{dC_L} = 0$ to obtain the neutral point is only valid if the other variations are unimportant for disturbances in angle of attack. For low speed airplanes, however, this assumption is valid. To sum up, the neutral point is that cg position for which $C_{m_\alpha} = 0$.

The floating characteristics of the longitudinal control surfaces also affect the stick-free neutral point definition. (Of course, "stick-free" conditions may be ignored for irreversible control systems since the control surfaces do not float with aerodynamic loads.)

> The stick-free neutral point, when appropriate, is the cg position for which C_m is independent of α with the longitudinal control surfaces unrestrained.

Comparing these definitions to the aerodynamic center, the neutral point is conceptually identical to the aerodynamic center of the entire airplane. Recall that the total pitching moment coefficient for the airplane can be written as:

$$C_m = C_{m_0} + C_{m_\alpha}\alpha$$

where C_{m_0} pitching moment coefficient about the cg when lift is 0. C_{m_0} can also be written as:

$$C_{m_0} = C_{m_{0_{wb}}} + V_H C_{L_{\alpha t}}(i_t + \varepsilon_0)$$

where $C_{m_{0wb}}$ pitching moment coefficient for the wing-body combination (no horizontal tail) at zero wing-body lift

V_H horizontal tail volume coefficient, $\frac{S_t \ell_t}{S\bar{c}}$

$C_{L_{\alpha t}}$ tail lift curve slope $\frac{\partial C_L}{\partial \alpha_t}$ evaluated at trim conditions

i_t tail-setting or incidence angle

ε_0 downwash angle when wing-body lift is 0

Etkin has shown that

$$C_m = C_{m0_{wb}} + C_{L_{\alpha_{wb}}}\alpha_{wb}\left(\left(\frac{x_{cg}}{\bar{c}} - \frac{x_{ac_{wb}}}{\bar{c}}\right) - V_H \frac{C_{L_{\alpha t}}}{C_{L_{\alpha_{wb}}}}\left(1 - \frac{\partial \varepsilon}{\partial \alpha}\right)\right) + C_{L_{\alpha t}}(i_t + \varepsilon_0)$$

where x_{cg} cg position

$\bar{c}$ mean aerodynamic chord

$x_{ac_{wb}}$ aerodynamic center or neutral point of the wing-body alone

Differentiating with respect to α (while also assuming $\alpha \approx \alpha_{wb}$)

$$C_{m_\alpha} = C_{L_{\alpha_{wb}}}\left(\left(\frac{x_{cg}}{\bar{c}} - \frac{x_{ac_{wb}}}{\bar{c}}\right) - V_H \frac{C_{L_{\alpha t}}}{C_{L_{\alpha_{wb}}}}\left(1 - \frac{\partial \varepsilon}{\partial \alpha}\right)\right)$$

Setting $C_{m_\alpha} = 0$ and solving for x_{cg} gives the stick-fixed neutral point::

$$\frac{x_{np}}{\bar{c}} = \frac{x_{ac_{wb}}}{\bar{c}} + V_{H_n}\frac{C_{L_{\alpha_t}}}{C_{L_{\alpha_{wb}}}}\left(1 - \frac{\partial\varepsilon}{\partial\alpha}\right) \tag{6.5}$$

where V_{H_n} = value of V_H for the cg located at x_{np}. The difference $\frac{x_{np}}{\bar{c}} - \frac{x_{cg}}{\bar{c}}$ is called the ***stick-fixed static margin*** and it is a measure of the static stability with respect to angle of attack disturbances.

$$C_{m_\alpha} = C_{L_\alpha}\left(\frac{x_{cg}}{\bar{c}} - \frac{x_{np}}{\bar{c}}\right) = C_{L_\alpha}(-Static\,Margin) \tag{6.6}$$

6.1.2.2 **Elevator Trim Angle**. The point was made earlier that pilots sense static longitudinal stability of an airplane through the control movements and forces, mainly the forces. The pilot's feel for the neutral point also comes from elevator movement per unit change in angle of attack. Said another way, the change in elevator angle required to trim the airplane is the pilot's index to stick-fixed static margin. Consider how longitudinal control surface deflections affect the pitching moment curves, as sketched in Fig. 6.5. For each elevator setting, equilibrium conditions can be maintained at only one angle of attack. For example, with $\delta_e = 0$, the trim angle of attack occurs at point A. Increments of lift and pitching moment are usually assumed to vary linearly with small changes in α; the C_m-α curves depicted are not strictly straight lines, which is common behavior. The pertinent relationships include: $\Delta C_L = C_{L_{\delta_e}}\delta_e$, with $C_{L_{\delta_e}} > 0$ for the sign convention specified in Fig. 6.1 and $\Delta C_m = C_{m_{\delta_e}}\delta_e$, with $C_{m_{\delta_e}} < 0$, using the same sign conventions. Then, we assume linearity in both $C_L = C_{L_\alpha}\alpha + C_{L_{\delta_e}}\delta_e$ and $C_m = C_{m_0} + C_{m_\alpha}\alpha + C_{m_{\delta_e}}\delta_e$. Setting $C_m = 0$ in this last expression gives the elevator angle for trim,

$$\delta_{e_{trim}} = -\frac{C_{m_0} + C_{m_\alpha}\alpha_{trim}}{C_{m_{\delta_e}}} \tag{6.7}$$

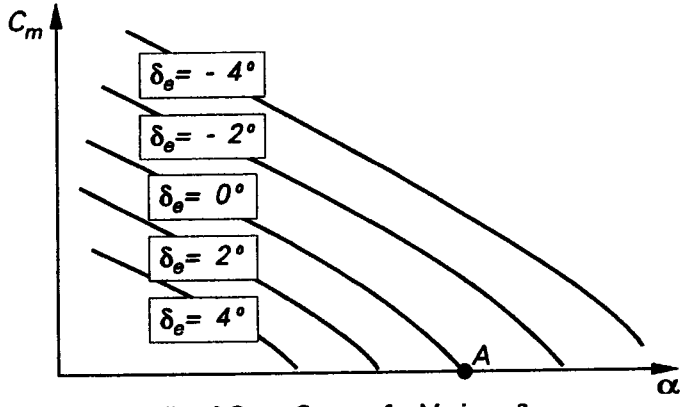

Fig. 6.5 Family of C_m-α Curves for Various δ_e

The trim lift coefficient is:

$$C_{L_{trim}} = C_{L_\alpha}\alpha_{trim} + C_{L_{\delta_e}}\delta_{e_{trim}}$$

Eliminating α_{trim} from eqn. 6.7:

$$\delta_{e_{trim}} = \frac{C_{m_0} C_{L_\alpha} + C_{m_\alpha} C_{L_{trim}}}{C_{m_\alpha} C_{L_{\delta_e}} - C_{L_\alpha} C_{m_{\delta_e}}} \tag{6.8}$$

In equation 6.8 we have assumed that δ_e is measured with respect to a trail position; that is, $\delta_e = 0$ when $\alpha = \alpha_{trim}$. The above expressions are valid approximations for conventional tail-aft airplanes. However, for tailless aircraft or other unconventional configurations, the equations must be developed assuming that C_{m_0} also varies with δ_e.

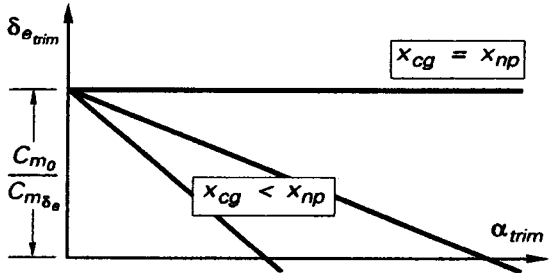

Fig. 6.6 Dependence of $\delta_{e_{trim}}$ on cg Position

Equation 6.8 ideally assumes a straight line variation of $\delta_{e_{trim}}$ with angle of attack (Fig. 6.6). This relationship between $\delta_{e_{trim}}$ and cg location (or static margin) suggests a way to determine the stick-fixed neutral point from flight test data. Since the slopes of these curves are clearly functions of cg location, we differentiate equation 6.8 with respect to $C_{L_{trim}}$.

$$\boxed{\frac{\partial \delta_{e_{trim}}}{\partial C_{L_{trim}}} = -\frac{C_{m_\alpha}}{C_{L_\alpha} C_{m_{\delta_e}} - C_{m_\alpha} C_{L_{\delta_e}}}} \tag{6.9}$$

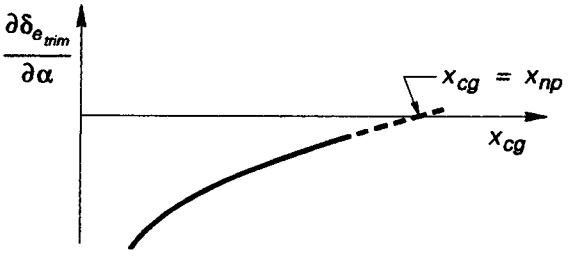

Fig. 6.7 Trim-Slope Criterion for Determining the Stick-Fixed Neutral Point

Figure 6.7 illustrates the use of eqn. 6.9 and depicts the so-called "trim-slope" criterion. Notice that the derivative was taken with respect to $C_{L_{trim}}$, not α. This change of independent variable means that this equation is strictly true only if Mach number effects and speed effects are negligible. Etkin[4] emphasizes this fact and lays out the rationale quite clearly. Nonetheless, this criterion is a common approach for estimating the stick-fixed neutral point for low speed airplanes and serves well to introduce flight test measurement of the neutral point.

6.1.2.3 **Elevator-Free Considerations**. In section 6.1.2.1 the concept of a stick-free neutral point was introduced. We must now detail the description of static longitudinal stability theory. Even with a perfectly rigid body assumed for the airframe, a manual control system will result in some freedom of movement for the control surfaces. Cable stretch and pilot inputs alone dictate at least some movement. An irreversible control system closely approximates the stick-fixed assumption. But a manual control system demands that the flight test engineer understand the effects of aerodynamic hinge moments on the longitudinal stability of the airplane. Generally, configurations are less stable when the control surfaces are free to rotate under the influence of these hinge moments. The hinge moments are the result of the force distribution on the control surface. Since friction is always present in a control system, the actual stability perceived by the pilot lies someplace between the two extremes of the stick-fixed and the stick-free analyses.

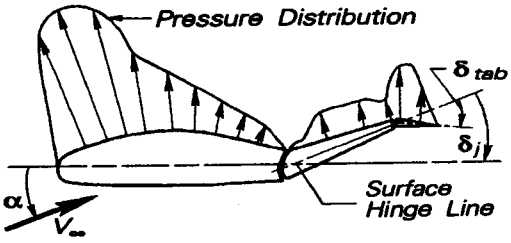

Fig. 6.8 Control Surface Floating Angle

Consider the force distribution illustrated in Fig. 6.8. The surface hinge moment can be written as a linearized function of the local angle of attack at the surface (α_j), the control surface deflection angle (δ_j), the tab setting (δ_{tab}), and a term describing the mass balance of the surface. (The subscript j is generic; it can indicate any control surface attached to the trailing edge of a lifting panel -- elevator, aileron, or rudder.)

$$C_{h_j} = C_{h_0} + C_{h_{\alpha_j}} \alpha_j + C_{h_{\delta_j}} \delta_j + C_{h_{\delta_{tab}}} \delta_{tab} + \frac{W_j x_j}{\bar{q} S \bar{c}} \tag{6.10}$$

where W_j weight of the jth surface ($_j$ can stand for $_e$, $_a$, or $_r$, depending on which control surface is being considered)

x_j cg position of the jth surface relative to the hinge line (If the surface is perfectly mass balanced, $x_j = 0$.)

$\bar{q}$ freestream dynamic pressure (to distinguish it from pitch rate)

C_{h_0} hinge moment coefficient at $\alpha_j = \delta_j = 0$

$C_{h_{\alpha_j}}$ rate of change of hinge moment coefficient with local angle of attack, evaluated at trim conditions $\left(\frac{\partial C_h}{\partial \alpha_j}\right)_{trim}$

$C_{h_{\delta_j}}$ rate of change of hinge moment coefficient with surface deflection, evaluated at trim conditions $\left(\frac{\partial C_h}{\partial \delta_j}\right)_{trim}$

$C_{h_{\delta_{tab}}}$ rate of change of hinge moment coefficient with trim tab deflection, evaluated at trim conditions $\left(\frac{\partial C_h}{\partial \delta_{tab}}\right)_{trim}$

The leading term in equation 6.10, C_{h_0}, depends upon several geometric factors like airfoil shape, nose bluntness, and gap seal effectiveness. Oversimplifying for the sake of clarity, we will assume a symmetrical airfoil, a surface with perfect mass balance, and a fixed trim tab. Then, with the surface floating freely so $C_h = 0$, equation 6.10 gives:

$C_{h_{\alpha_j}}\alpha_j + C_{h_{\delta_j}}\delta_j = 0$ or,

$$\delta_{j_{free}} = -\frac{C_{h_{\alpha_j}}\alpha_j}{C_{h_{\delta_j}}} \tag{6.11}$$

Both $C_{h_{\alpha_j}}$ and $C_{h_{\delta_j}}$ are usually negative, although $C_{h_{\alpha_j}}$ may be positive when a large horn balance is designed into the surface or when the hinge line is set far back from the surface's leading edge. Taking the usual case with both $C_{h_{\alpha_j}}$ and $C_{h_{\delta_j}}$ negative, a positive local angle of attack at the surface produces:

$$C_{L_j} = C_{L_{\alpha_j}}\alpha_j + a_j\delta_{j_{free}} = C_{L_{\alpha_j}}\alpha_j\left(1 - \frac{C_{h_{\alpha_j}}a_j}{C_{h_{\delta_j}}C_{L_{\alpha_j}}}\right)$$

$$\text{where } a_j = \left(\frac{\partial C_{L_j}}{\partial \delta_j}\right)_{trim} \text{ and } C_{L_{\delta_j}} = a_j\frac{S_t}{S}$$

If we now focus on the longitudinal axis and define the free elevator factor as:

$$F \equiv 1 - \frac{C_{h_{\alpha_e}}a_e}{C_{h_{\delta_e}}C_{L_{\alpha_t}}}, \text{ where } a_e = \left(\frac{\partial C_{L_t}}{\partial \delta_e}\right)_{trim} \text{ and } C_{L_{\delta_e}} = a_e\frac{S_t}{S}$$

Then the coefficient of lift developed by the horizontal tail is:

$$C_{L_t} = F\,C_{L_{\alpha_t}}\alpha_t \tag{6.12}$$

If $F < 1$, a freely floating surface is less effective than a fixed one. Of course, if $F > 1$ (as would be the case if $C_{h_{\alpha_j}}$ were positive), then the surface produces more lift when free than when fixed. Denoting stability coefficients with primes when the elevator is free to float under the influence of the hinge moment, the aircraft lift coefficient is:

$C_L' = C_{L_\alpha}'\alpha'$

$$\text{where } C_{L_\alpha} = C_{L_{\alpha_{wb}}}\left(1 + F\frac{C_{L_{\alpha_t}}}{C_{L_{\alpha_{wb}}}}\frac{S_t}{S}\left(1 - \frac{\partial\varepsilon}{\partial\alpha}\right)\right) \text{ and } \alpha' = \alpha_{wb} - F\frac{S_t}{S}(\varepsilon_0 + i_t)$$

The aircraft pitching moment coefficient with the elevator free is:

$C_m' = C_{m_0}' + C_{m_\alpha}'\alpha'$

$$\text{where } C_{m_0}' = C_{m_{0_{wb}}} + F\,C_{L_{\alpha_t}}V_{H_n}'(\varepsilon_0 + i_t) \text{ and } C_{m_\alpha}' = C_{L_\alpha}'\left(\frac{x_{cg}}{\bar{c}} - \frac{x_{np}'}{\bar{c}}\right)$$

Solving eqn. 6.5 for the stick-free neutral point,

$$\frac{x'_{np}}{\bar{c}} = \frac{x_{ac_{wb}}}{\bar{c}} + V'_H \frac{C_{L_{\alpha_t}}}{C'_{L\alpha}} \frac{S_t}{S}\left(1 - \frac{\partial\varepsilon}{\partial\alpha}\right) \text{ or } \frac{x'_{np}}{\bar{c}} = \frac{x_{ac_{wb}}}{\bar{c}} + V'_{Hn} \frac{C_{L_{\alpha_t}}}{C_{L_{\alpha_{wb}}}} \frac{S_t}{S}\left(1 - \frac{\partial\varepsilon}{\partial\alpha}\right) \quad (6.13)$$

where V_{H_n}' = tail volume coefficient when the cg is at the stick-free neutral point.

V_H' = tail volume coefficient when the cg is at the wing-body aerodynamic center.

If the variation of tail volume coefficient with cg position can be neglected,

$$\frac{x_{np}}{\bar{c}} - \frac{x'_{np}}{\bar{c}} = (1 - F)V_{Hn} \frac{C_{L_{\alpha_t}}}{C_{L_{\alpha_{wb}}}} \frac{S_t}{S}\left(1 - \frac{\partial\varepsilon}{\partial\alpha}\right) \quad (6.14)$$

Etkin[4] gives exact expressions for the difference between the two types of neutral points, but this approximate expression will suffice for our purposes.

Analogous to the trim-slope criterion outlined in section 6.1.2.2, the trim tab angle required to produce various free floating angles gives an estimate of stick-free neutral point. If δ_{tab} is not zero, equation 6.11 becomes:

$$\delta_{e_{free}} = -\frac{C_{h_{\alpha_t}} \alpha_t + C_{h_{\delta_{tab}}} \delta_{tab}}{C_{h_{\delta_e}}}$$

Solving for the tab angle necessary to trim and using eqn. 6.7,

$$\delta_{tab_{trim}} = \frac{C_{h_{\delta_e}}}{C_{h_{\delta_{tab}}} C_{m_{\delta_e}}}\left(C_{m_0} + C_{m_\alpha}\alpha - C_{m_{\delta_e}} \frac{C_{h_{\alpha_t}}}{C_{h_{\delta_e}}}\alpha_t\right) \quad (6.15)$$

Substituting $\varepsilon = \varepsilon_0 + \left(\frac{\partial\theta}{\partial\alpha}\right)_{wb}$ in the expression for α_t,

$$\alpha_t = \alpha\left(1 - \frac{\partial\varepsilon}{\partial\alpha}\right) - (\varepsilon_0 + i_t)\left(1 - \frac{C_{L_{\alpha_t}}}{C_{L_\alpha}} \frac{S_t}{S}\left(1 - \frac{\partial\varepsilon}{\partial\alpha}\right)\right) \quad (6.16)$$

Using this expression to eliminate α_t from eqn. 6.15,

$$\delta_{tab_{trim}} = \frac{C_{h_{\delta_e}}}{C_{h_{\delta_{tab}}}}\left(\left(\frac{C_{m_\alpha}}{C_{m_{\delta_e}}} - \frac{C_{h_{\alpha_t}}}{C_{h_{\delta_e}}}\left(1 - \frac{\partial\varepsilon}{\partial\alpha}\right)\right)\alpha + \frac{C_{m_0}}{C_{m_{\delta_e}}} + (\varepsilon_0 + i_t)\left(1 - \frac{C_{L_{\alpha_t}}}{C_{L_\alpha}} \frac{S_t}{S}\left(1 - \frac{\partial\varepsilon}{\partial\alpha}\right)\right)\right)$$

Differentiating with respect to α:

Substituting expressions for C_{m_α}, $C_{m_{\delta_e}}$, and F and rearranging:

$$\frac{\partial\delta_{tab_{trim}}}{\partial\alpha} = \frac{C_{h_{\delta_e}}}{C_{h_{\delta_{tab}}}} C_{L_\alpha}\left(\frac{x_{cg}}{\bar{c}} - \frac{x'_{np}}{\bar{c}}\right) \quad (6.17)$$

Equation 6.17 is exact only when $V_H = V_{H_n}'$. Notice that the negative of the parenthetical term is exactly like the stick-fixed static margin defined earlier, except that now it

should be called the **stick-free static margin**. Obviously, eqn. 6.17 indicates that the slope of the elevator trim tab required to trim longitudinally with changing angle of attack is a measure of stick-free static longitudinal stability. Recalling the difference between V_H and V_{H_n}', and using the approximate difference between the stick-fixed and the stick-free neutral points (eqn. 6.14), eqn. 6.17 quantifies a "tab-slope" criterion for obtaining the location of the stick-free neutral point from measured variations of trim tab versus angle of attack. Figure 6.9 illustrates this approach.

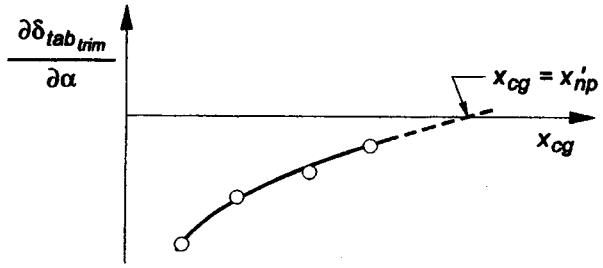

Fig. 6.9 Tab-Slope Criterion for Stick-Free Neutral Point

6.1.3 Other Concepts of Static Stability

Currently, military specifications[2] do not directly use neutral points in spelling out requirements for piloted airplanes. The authors of such standards apparently feel that these concepts are no longer appropriate for high performance aircraft that often operate with relaxed static stability and very complex automatic control systems. Whether one agrees with this approach or not, it is important that the flight test engineer be prepared to work in this environment by understanding the terminology.

6.1.3.1 **Speed Stability**. The basic stability criterion set down by the military specification is that of ***speed stability***. Paragraph 3.2.1 of the primary document[2] states:

> ...there shall be no tendency for airspeed to diverge aperiodically when the airplane is disturbed from trim with the cockpit controls fixed and with them free. This requirement will be considered satisfied if the variations of pitch control force and pitch control positions are smooth and the local gradients stable...

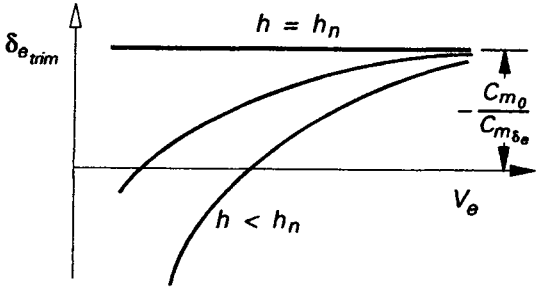

Fig. 6.10 Stick-Fixed Speed Stability

The specification goes on to say that the speed stability criterion must be met in level flight at constant altitude with no change in throttle setting or trim movements over a range of ±50 knots or ±15% about the trimmed equivalent airspeed. Figure 6.10 illustrates a

stable airplane with respect to stick-fixed speed stability; the elevator trim position to maintain equilibrium meets the requirement.

Etkin[4] has succinctly related speed stability to the neutral point for those cases where compressibility, aeroelasticity, and propulsive effects are negligible. Figure 6.10 also summarizes this concept. Since $\delta_{e_{trim}}$ is a unique function of C_L with these restrictions and since $C_{L_{trim}} = \frac{2W}{\rho_0 V_e^2 S}$, the trim elevator angle is a unique function of V_{EAS} also. As speed increases, $\delta_{e_{trim}}$ increases monotonically for a stable airplane. If $x_{cg} = x_{np}$, the required trim setting is the same for all equivalent airspeeds. Hence, the airplane is neutrally stable, both in the speed sense and under the neutral point concept. However, the speed stability concept is more general in that the trim setting can also be considered a function of propulsive effects, Mach number, and dynamic pressure, as well as angle of attack. Equation 6.8 can be rearranged to give

$$\delta_{e_{trim}} = -\frac{C_{m_0} C_{L_\alpha} + C_{m_\alpha} C_{L_{trim}}}{C_{L_\alpha} C_{m_{\delta_e}} - C_{m_\alpha} C_{L_{\delta_e}}}$$

Since each of these stability coefficients varies with Mach number, for example, then $\delta_{e_{trim}}$ also varies with Mach number. A sketch of typical variations with Mach number is shown in Fig. 6.11.

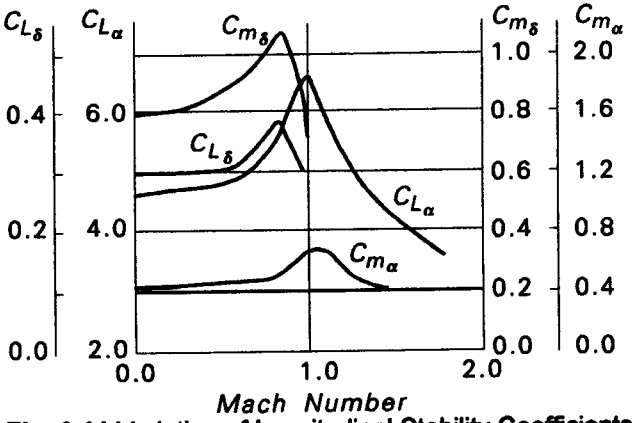

Fig. 6.11 Variation of Longitudinal Stability Coefficients with Mach Number

In transonic flight Mach number dependence demands modification of the concept of longitudinal speed stability as a measure of static longitudinal stability. MIL-F-8785C relaxes the requirement for an airplane that has a trim curve like that shown in Fig. 6.12. This airplane is not speed stable in the transonic region. Physically, the airplane may start out in equilibrium at point A. If the speed is perturbed to point B by a gust or some other disturbance, $\frac{\partial \delta_{e_{trim}}}{\partial M}$ will be negative even though speed is increasing. Thus, the ordinary C_{m_α} criterion for static longitudinal stability has no meaning in this case.

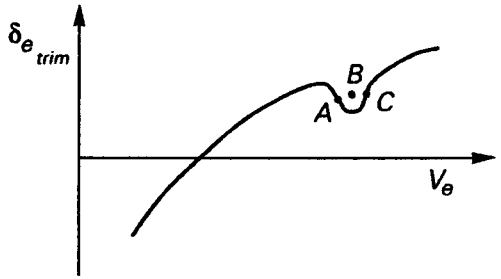

Fig. 6.12 Transonic Effects on Static Longitudinal Stability

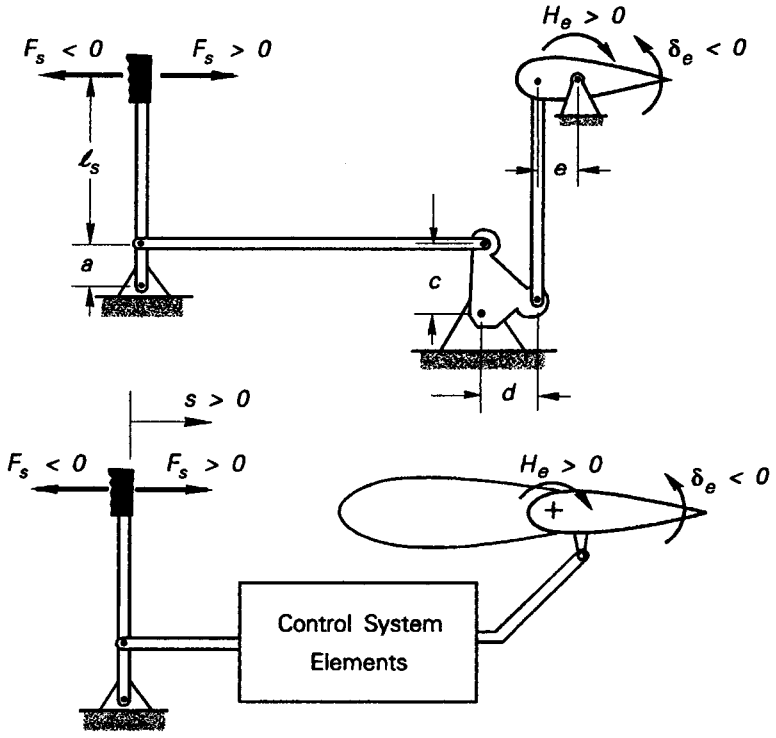

Fig. 6.13 Control System Schematic

6.1.3.2 **Force Gradient for Speed Stability**. Even though most of the airplanes covered by MIL-F-8785C have irreversible flight control systems, the document is more concerned with force the pilot must apply than in the elevator travel itself. At least one proposed revision[7] recommends omitting the constraint on a stable surface displacement. Once again, the pilot's perception of stability is the most important issue. Consider the control system schematic sketched in Fig. 6.13, noting that a positive stick force is a pull force (in the aft direction). A positive stick force results in a negative elevator deflection, though it produces a positive pitching moment. The gearing ratio (or gain) is a constant relating stick force and hinge moment: $F_s = GH_e$. Applying the principle of virtual work,

$$F_s \Delta s + H_e \Delta \delta_e = 0$$

Then, $G = -\dfrac{\Delta\delta_e}{\Delta s}$

Writing the stick force in terms of hinge moment coefficient,

$F_s = GC_{h_e} S_e c_e \bar{q}$

Assuming that V_H = constant and that $C_{h_0} = 0$; $C_{h_e} = C_{h_{\alpha_e}}\alpha_t + C_{h_{\delta_e}}\delta_{e_{trim}} + C_{h_{\delta_{tab}}}\delta_{tab}$. If we can also expect $C_{L_{\delta_e}}$ to be small, eqn. 6.8 reduces to:

$$\delta_{e_{trim}} = -\frac{C_{m_0}}{C_{m_{\delta_e}}} - \frac{C_{m_\alpha} C_{L_{trim}}}{C_{L_\alpha} C_{m_{\delta_e}}}$$

Substituting $\delta_{e_{trim}}$ into the hinge moment coefficient expression and eliminating α_t with equation 6.16,

$$C_{h_e} = -\frac{C_{h_{\delta_e}}}{C_{m_{\delta_e}}}\left(\frac{x_{cg}}{\bar{c}} - \frac{x'_{np}}{\bar{c}}\right)C_{L_{trim}} + C_{h_{\delta_{tab}}}\delta_{tab} - C_{h_{\delta_e}}\frac{C_{m_0}}{C_{m_{\delta_e}}} - C_{h_{\alpha_t}}(\varepsilon_0 + i_t)\left(1 - \frac{C_{L_{\alpha_t}}}{C_{L_\alpha}}\frac{S_t}{S}\left(1 - \frac{\partial\varepsilon}{\partial\alpha}\right)\right)$$

For level flight cruising conditions $\left(L = W \text{ and } C_{L_{trim}} = \dfrac{W}{\bar{q}S}\right)$, F_s becomes:

$$F_s = A + B\bar{q} \tag{6.18}$$

where $$A = -GS_e c_e \frac{C_{h_{\delta_e}}}{C_{m_{\delta_e}}}\left(\frac{x_{cg}}{\bar{c}} - \frac{x'_{np}}{\bar{c}}\right)$$

$$B = GS_e c_e C_{h_e} C_{h_{\delta_e}}\left(\frac{C_{h_{\delta_{tab}}}\delta_{tab}}{C_{h_{\delta_e}}} - \frac{C_{m_0}}{C_{m_{\delta_e}}} - C_{h_{\alpha_t}}(\varepsilon_0 + i_t)\left(1 - \frac{C_{L_{\alpha_t}}}{C_{L_\alpha}}\frac{S_t}{S}\left(1 - \frac{\partial\varepsilon}{\partial\alpha}\right)\right)\right)$$

Equation 6.18 leads to the following conclusions:

- Stick force is directly proportional to the product of the elevator area and the elevator chord, that is, the size of the elevator.
- Stick force is directly proportional to the gearing ratio.
- Retrimming (altering $\delta_{e_{tab}}$) changes the shape of the parabola as indicated by the dashed lines in Fig. 6.14. Positive $\delta_{e_{tab}}$ reduces the force to be held by the pilot at a given speed.
- The weight affects stick force through the wing loading term $\dfrac{W}{S}$ and an increase in wing loading has the same effect as a forward shift in cg.
- Altitude affects only the second term through $\bar{q}$. For a given true airspeed, increasing altitude reduces F_s. Naturally, the second term in the stick force expression varies directly with the square of the true airspeed.
- Shifting the cg location only affects the constant term (A) of equation 6.18. Moving the cg forward translates the curve upward and moving it aft translates the curve downward. Figure 6.14 also illustrates this translation.

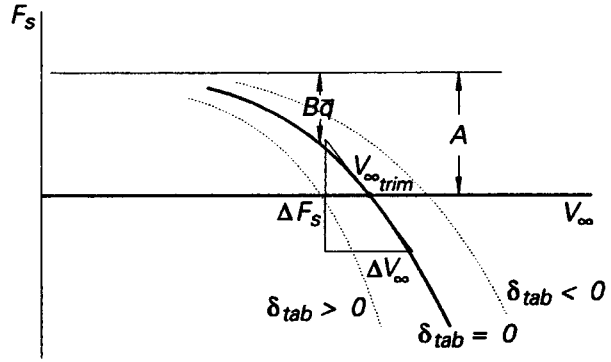

a. Effect of Tab Deflection on Stick Force Gradient

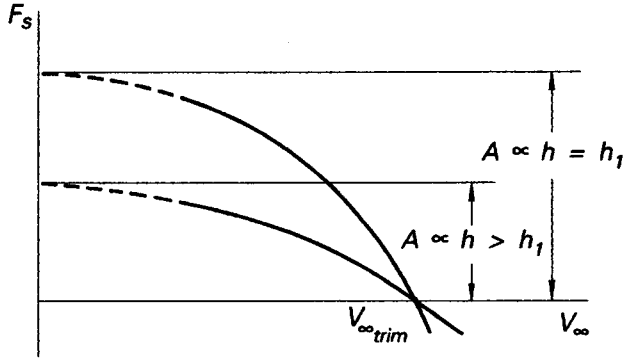

b. Effect of cg Location on Stick Force Gradient

Fig. 6.14 Stick Force Variation with Speed

The slope of the stick force curve is a very important handling qualities parameter. The pilot judges loss of longitudinal stability by the rate of change of stick force with airspeed change. Hoh[7] clearly spells out the recommended maximum allowable size of any unstable gradients in the transonic regime. Equation 6.18 leads to an expression for the stick force gradient. Taking the derivative with respect to V_∞, $\frac{\partial F_s}{\partial V_\infty} = B\rho V_\infty$ or

$$\frac{\partial F_s}{\partial V_\infty} = \rho V_\infty G S_e c_e C_{h_e} C_{h_{\delta_e}} \left(\frac{C_{h_{\delta_{tab}}} \delta_{tab}}{C_{h_{\delta_e}}} - \frac{C_{m_0}}{C_{m_{\delta_e}}} - C_{h_{\alpha_t}} (\varepsilon_0 + i_t) \left(1 - \frac{C_{L_{\alpha_t}}}{C_{L_\alpha}} \frac{S_t}{S} \left(1 - \frac{\partial \varepsilon}{\partial \alpha} \right) \right) \right)$$

At the trim point (where $F_s = 0$), the stick force gradient is:

$$\frac{\partial F_s}{\partial V_\infty} = 2GS_e c_e \frac{C_{h_{\delta_e}}}{C_{m_{\delta_e}}} \frac{W}{S} \left(\frac{x_{cg}}{\bar{c}} - \frac{x'_{np}}{\bar{c}} \right) = 2GS_e c_e \frac{C_{h_{\delta_e}}}{C_{m_{\delta_e}}} \frac{W}{S} (-SM_{free}) \qquad (6.19)$$

6.1.3.3 **Flight-Path Stability**. Paragraph 3.2.1.3 of MIL-F-8785C describes yet another type of longitudinal stability related to "backside-of-the-power-curve" operations:

Flight-path stability is defined in terms of the change in flight-path angle when the airspeed is altered by use of pitch control only (throttle not reset by the pilot).

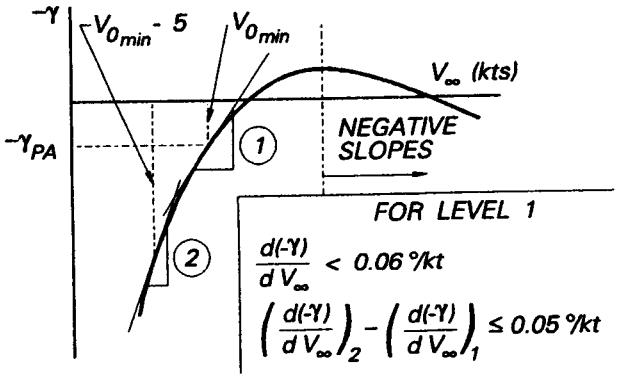

Fig. 6.15 Local Slope Definitions for Flight-Path Stability

This type of stability is especially important for precise control of airspeed, as is essential for carrier approaches or other short-field landings. If the elevator alone is used to control airspeed, it can be shown[7] that a closed (pilot-in-the-loop) loop instability can occur at speeds below the minimum drag speed. The requirement is quantified in terms of the local slopes for each level of handling qualities. For level 1, the local slopes must be either negative or less positive than 0.06 °/knot. Figure 6.15 illustrates the allowable local slopes. Compensation for poor flight-path stability can be made if a secondary flight path controller, like power or direct lift control, is incorporated into the design. Short takeoff and landing (STOL) aircraft often utilize this means of compensating for poor flight-path stability since their landing approaches are frequently made at speeds well below the minimum drag speed. Naturally, the secondary flight path controller itself must have satisfactory response characteristics if it is to have acceptable closed loop handling qualities.

6.2 LONGITUDINAL STATIC STABILITY TEST METHODS

The commonly used flight test techniques to obtain longitudinal stability data are relatively simple and straightforward, although very careful trimming and flying must be done. To obtain reliable quantified data, it is practically imperative that the instrumentation include some form of automatic recording and the sensors used are almost always some kind of electronic device. The net effect of both these factors is that stability and control data are harder to obtain than are performance data. The so-called stabilized method and the slow acceleration-deceleration method are the techniques most often used to gather information about the speed stability or neutral points. These methods will be discussed first, followed by a brief discussion of the way that flight path stability tests are conducted. However, before the data procedures are detailed, it is necessary to examine two factors that govern the quality of the data collected whatever the method used.

6.2.1 Stability and Control Flight Test Measurements

Stability and control testing is an exacting process. As suggested previously, virtually all interesting parameters must be measured indirectly and the control surfaces and con-

trol tabs are the most common measurements used to back out the desired information. Forces are often measured directly and they are variables of primary interest, but even so, the data must be further manipulated to obtain engineering terms of interest like neutral points and force gradients. For these reasons, data must be taken with as much precision as possible and it is particularly important that the flight test engineer understand the uncertainties introduced by the mechanical parts of the control system.

6.2.1.1 **Trim**. The first of these uncertainties is introduced because most longitudinal static stability measurements are taken about an equilibrium condition. The requirement quoted in section 6.1.3.1 measures static stability from such a trim condition. Trimming to an absolute equilibrium condition is not trivial, but flight test engineers must insist that the flight crew establish an accurate trim condition. A good rule of thumb is to require the pilot to release all controls for a minimum of ten seconds after he has established the trim airspeed and altitude. If the airplane deviates at all within that period of time, trim should be reset and the check repeated. This process should be repeated until no deviation from the desired conditions can be detected during the specified time interval.

To adequately cover the flight envelope, it will be necessary to set up separate trim conditions at convenient airspeed intervals as illustrated in Fig. 6.16. The exact increments of airspeed to be used will depend upon the data to be collected and the regime of flight. Smaller increments between trim conditions should always be used where surface deflection gradients and/or stick force gradients are expected to change rapidly. The transonic region is certainly such a region for those airplanes designed to operate there.

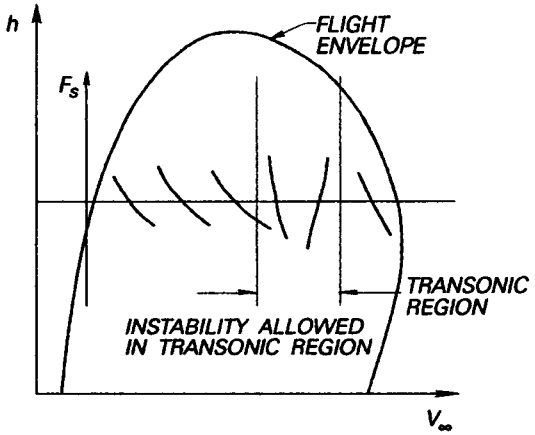

Fig. 6.16 Trim Conditions for a Specified Altitude

6.2.1.2 **Friction and Breakout Forces**. The second uncertainty affecting the precision of stability and control measurements is the mechanical friction of the mechanisms through which the pilot controls the machine. For the pilot to have a feel for the neutral positions of the controls, there is usually an initial force to be overcome in moving the control out of the neutral position. While this kind of force serves a useful purpose in defining the neutral position for the pilot, the control stick will also require some force to overcome the initial resistance to motion at any point in the control throw. This type of force is lumped under the term "breakout force."

Breakout force is defined as that stick force which must be applied to the control system before the control surface begins to move.

It is customary to call the remaining frictional forces simply friction.

Friction is that stick force required to overcome sliding, rolling, or any other form of dynamic frictional forces in the control linkages.

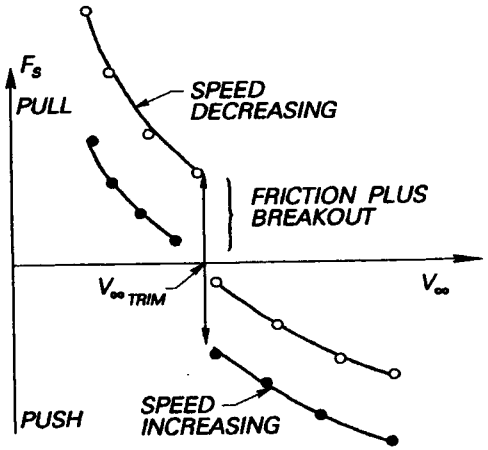

Fig. 6.17 Control System Friction Band

Figure 6.17 illustrates how friction and breakout forces appear if measured carefully at various airspeeds near an equilibrium condition. Though friction and breakout have been defined in terms of forces, they both also affect the movement of the pilot's controller. Because of friction and breakout there is no guarantee that resetting the pilot's controller to exactly the same position will set the control surface to the same setting. If either the stick force or the control surface gradients are very small, friction and breakout can introduce large percentage uncertainties into longitudinal stability data. The flight test team must plan and execute the tests in a manner that minimizes these uncertainties to the maximum extent possible. The separation of the two curves resembles the hysteresis loop common in almost any physical system when precise measurements are made. The circles indicate data taken when the pilot was moving the controller aft and the squares represent stick movement in the opposite direction. If care had not been taken to keep the controller moving in the same direction at all times, the data points would be scattered between the two curves.

6.2.2 Stabilized Method

One flight test method for obtaining longitudinal static stability is to fly a series of stabilized airspeeds above and below the trim airspeed and measure the appropriate control parameters. As in all the techniques, the trim conditions must be established carefully and care must exercised to insure that the stick force, control surface, and control tab measurements are made with the surfaces on one side or the other of the friction band for any points to be joined as a continuous curve. The stabilized method is based on use of the

longitudinal control to vary airspeed at constant power setting and most of all at constant trim setting. Once the trim conditions are established and recorded, the longitudinal control alone is used to slow down or speed up to predetermined airspeed points. Altitude is obviously not constant, but should be controlled within a specified band, usually no more than ±1000 feet from the trim condition. For military requirements, this variation of airspeed about the trim condition should be set to cover a range of ±15% or ±50 KEAS, whichever is less. A good rule of thumb is to plan for at least three points (preferably more) at speeds equally spaced above and below the trim airspeed. As the speed is stabilized at each of these airspeeds, care must be exercised to have the stick on one or the other sides of the hysteresis loop sketched in Fig. 6.17. Generally, it is easiest for the pilot to accomplish this rather delicate task by attempting to keep the control stick moving forward as speed is increased and aft as the speed is decreased.

Example 6.1: A light twin general aviation airplane was tested for static longitudinal stability at two cg locations. The stabilized technique was used, resulting in the data give in the table below.

Stabilized Static Longitudinal Stability Data

x_{cg} = 2.3 feet aft of datum		x_{cg} = 2.75 feet aft of datum	
C_L	δ_e	C_L	δ_e
0.25	*-0.5*	*0.7*	*0.36*
0.61	*-2.3*	*0.6*	*0.64*
0.81	*-3.4*	*0.5*	*1.07*
1.03	*-4.5*	*0.4*	*1.34*

$\bar{c} = 11.0$ *feet* $V_H = 0.42$

Find the stick-fixed static margin when the cg is 1.98 feet aft of the datum and the elevator angle required for trim with $C_L = 0.63$. Calculate $C_{L_{\delta_e}}$ for the horizontal if $C_{m_0} = 0.04$. What is the position of the stick-fixed neutral point?

Plotting the data given in the table above:

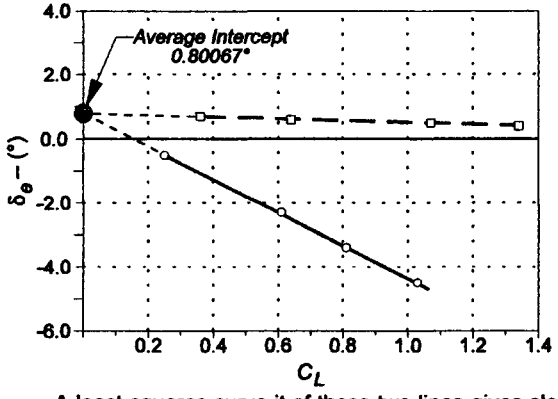

A least squares curve it of these two lines gives slopes of -5.14889 and -0.29423. Notice that the intercepts of these two lines will never be identical, simply because no measurements are perfect. A simple average is usually a reasonable approximation. Clearly, it would be preferable to have measurements at more than two cg locations. The desirability of having multiple measurements is illustrated in the plot below of these two straight lines. This plot, using the slopes of the two lines versus x_{cg} (utilizing our assumed linear relationship), illustrates how the neutral point is obtained. Notice that these fictitious data indicate the airplane was flown very near a neutrally stable condition, which is very unlikely! Instead, the flight test engineer usually must extrapolate more than is shown here to find the neutral point. The need for this extrapolation makes it imperative that data be collected for several cg locations, rather than just two.

A straight line is obtained by connecting these two slopes on a plot of elevator angle with change in C_L (could also be elevator angle change with angle of attack) as shown above. Solving this expression when $\frac{\partial \delta_e}{\partial C_L} = 0$ gives us the neutral point location:

$$\frac{x_{np}}{\bar{c}} = 0.2525 \quad or \quad x_{np} = 2.777 \text{ feet aft of datum}$$

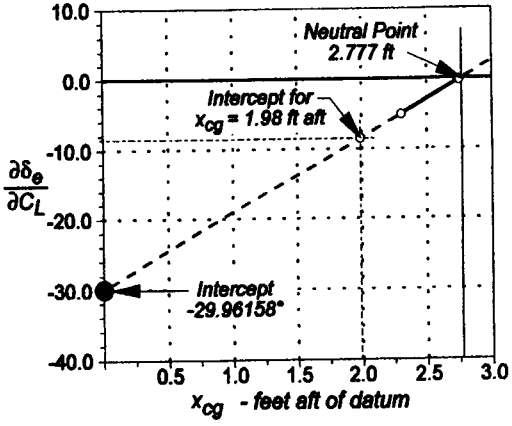

For the third cg location, we calculate $\frac{\partial \delta_e}{\partial C_L} = -8.60109$ from our straight line average of the intercepts for the tabulated data on the previous page. The average intercept of the two plotted lines is 0.80067, giving $\delta_e = -8.60109 C_L + 0.80067$ for the given x_{cg}. With $C_L = 0.63$:

$$\delta_e = -7.80^\circ \text{ and } S.M. = 0.0725$$

The stick-fixed static margin is calculated using $\frac{x_{np}}{\bar{c}} - \frac{x_{cg}}{\bar{c}} = 0.24679 - 0.180$. Recognizing that the intercept in the above calculation should be a reasonable approximation for $-\frac{C_{m_0}}{C_{m_{\delta_e}}}$, we get

$$C_{m_{\delta_e}} \approx -\frac{0.04}{0.80067}$$

$$C_{m_{\delta_e}} \approx -0.0499$$

6.2.3 Slow Acceleration/Deceleration Method

This test method is perhaps the one most commonly used to collect static longitudinal stability data because it is very efficient. A large amount of data can be collected in a short time and it is particularly useful for large airspeed envelopes. It is not quite as accurate as the stabilized method, since absolute equilibrium is never attained. Generally though, if the acceleration/deceleration rates are limited to no more than 2 knots/second, the data is entirely adequate for most purposes. An automatic recording scheme is absolutely necessary, preferably one from which the data can be acquired and formatted directly into data files for further reduction on a computer.

As is the case for all stability and control flight tests, the first step in performing a slow acceleration/deceleration is to trim carefully. The importance of this step cannot be overemphasized; the airplane must be trimmed precisely at this equilibrium condition because this point is the only one where a true equilibrium is attained in this method. The pilot or

test engineer should activate the data recording system to automatically record the trim conditions.

Figure 6.18 shows how data from a slow acceleration/deceleration should look after reduction and plotting. Leave the data recorder running and mark the point where a smooth acceleration or deceleration is begun. Apply smooth control inputs throughout the acceleration/deceleration. Power (or thrust) for level flight should be noted during the trim shot. Use as small a change as possible from this trim power setting to accomplish the acceleration or deceleration. About 5% change in power usually avoids large changes in pitching moment with power. The longitudinal trim should not be changed throughout the maneuver. Continue the acceleration or deceleration to the appropriate end of the airspeed range and then reverse the sense of the rate of change of the longitudinal control force. It is important that this reversal occur only at the extremes of the airspeed range; otherwise, the hysteresis effects pointed out in paragraph 6.2.1.2 will inject considerable uncertainty in the data. Continue the acceleration or deceleration to the other end of the airspeed range and again reverse the force rate of change. The maneuver should be completed by coming back to the original trim condition and again recording the trim shot. The advantages of using an automated data formatting and reduction scheme should be obvious from the number of data points shown for this one maneuver.

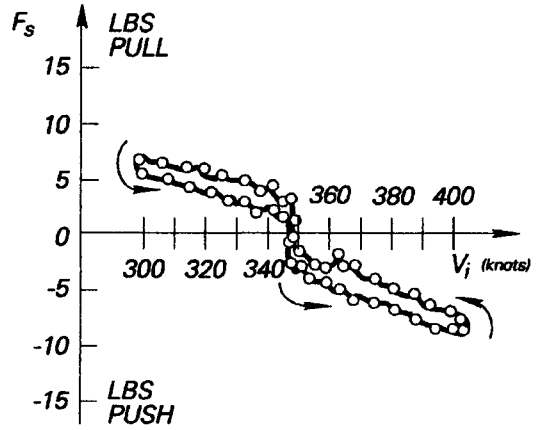

Fig. 6.18 Slow Acceleration/ Deceleration Data

6.2.4 Power Acceleration/Deceleration Method

This technique is identical to the slow acceleration/deceleration method except that larger power changes (up to maximum power or back to idle) are used to accelerate and decelerate and altitude is maintained approximately constant. This procedure can only be used with configurations for which the change in pitching moment with power setting is negligible. An automatic recording device is again essential. Like the previous method, equilibrium is attained only at the initial trim condition and the rate of acceleration or deceleration is constantly changing.

As usual, start with a careful trim shot. Smoothly set the throttle, allowing the recorder to run continuously. Mark the minimum speed and the top of the speed range. Reset the throttle and reverse the direction of the force change and continue the maneuver to the

opposite end of the speed range. It may be desirable to shut off the recording device while making these changes outside the data range and then restarting the recorder before the data band. The same care must be taken to avoid reversing control forces, as mentioned before. Upon reaching the other end of the speed range, reset the power and reverse the rate of change of stick force until reaching the equilibrium point. Constant pressure altitude should be maintained as nearly as possible by flying a slight climb or descent appropriate for the position error correction of the test airplane.

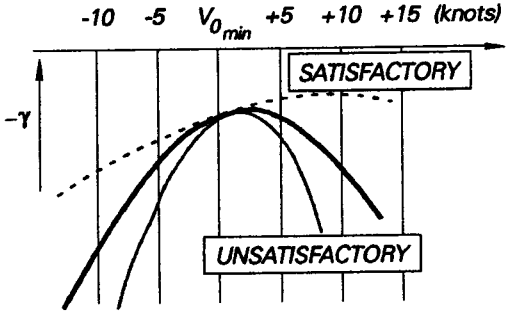

Fig. 6.19 Flight-Path Stability Limits

6.2.5 Flight-Path Stability Method

The technique to measure flight-path stability (applicable to power approach configurations) is a specialization of the stabilized method. Figure 6.19 is a sketch of allowable limits. After setting gear and flaps, the airplane is trimmed in a normal glide path for a power-on approach at $V_{0_{min}}$, the normal final approach speed. The airspeeds for this condition over a range of weights are calculated by the flight test engineer during preflight planning along with anticipated rates of descent for a 3° glide path. Trimming must be precise, even though the configuration and airspeed combination make trimming difficult. The trim condition should be set up at a predetermined nominal altitude. Once the configuration and the rate of descent are selected for the test weight, the pilot climbs approximately 2000 feet above the nominal altitude and starts the maneuver by setting the power to give the desired rate of descent with a tolerance of no more than ±100 fpm. Altitude, airspeed, and rate of descent are recorded as soon as they stabilize. The nose of the aircraft is then raised to smoothly reduce the airspeed about 5 knots. Altitude, airspeed, and rate of descent are again recorded with airspeed is stabilized 5 knots below $V_{0_{min}}$. Airspeed control within 1/2 knot is essential for good data. This procedure is repeated for $V_{0_{min}}$ - 10, $V_{0_{min}}$ + 5, and for $V_{0_{min}}$ again. At least four points are required to define the slope at $V_{0_{min}}$ and $V_{0_{min}}$ - 5 knots for MIL-F-8785C. These data must be obtained as quickly as possible to minimize altitude loss; more than 4000 feet of change in altitude leads to inaccurate thrust corrections. Repeating $V_{0_{min}}$ as the last point provides a reference for correcting even hand-recorded data.

Example 6.2: The data in the table below were collected on a standard day to measure the flight path stability of a jet trainer. Does the airplane meet the level 1 criteria of MIL-F-8785C? Carefully plot the curve and show the slopes used to make this determination. $V_{0_{min}}$ = 146 knots (TAS) for the test weight.

Flight Path Stability Example Data

Calibrated Airspeed (knots)	Rate of Descent (fpm)	Pressure Altitude (feet)
130	1000	11,000
126	980	10,700
124	900	10,400
120	800	10,200
136	750	9,550
130	800	9,100

Flight Path Stability Calculated Performance

Calibrated Airspeed (knots)	Pressure Altitude (feet)	Density Ratio	True Airspeed (knots)	Corrected Rate of Descent (fpm)	Flight Path Angle (degrees)
130	11,000	0.7155	153.68	1000.0	-3.6816
126	10,700	0.7224	148.25	1001.2	-3.8610
124	10,400	0.7292	145.21	963.2	-3.7531
120	10,200	0.7338	140.08	884.2	-3.5713
136	9,550	0.7490	157.15	902.6	-3.2494
130	9,100	0.7596	149.16	1000.0	-3.7934

The first step is to find the density ratio for each of the pressure altitudes at which data were hand recorded. using eqn. 2.7a, we can calculate density ratios for each of the pressure altitudes listed above in the data table. Then, the equivalent airspeed could be calculated using the expression that generated Fig. 2.4 (see page 13). In fact Fig. 2.4 shows clearly that $V_e \approx V_{cal}$ (or, at least, $\Delta V_{cal} < 1.0$) for the altitudes where the data were taken. Using this approximation, the true airspeed becomes $V_\infty = \frac{V_e}{\sqrt{\sigma}} \approx \frac{V_{cal}}{\sqrt{\sigma}}$. Having this true airspeed estimate allows calculation of the flightpath angle from the indicated vertical velocity: $\sin\gamma = \frac{V_V}{V_\infty}$, where both velocities must be in the same units of course. Moreover, the vertical velocities recorded from the vertical velocity indicator must be corrected for changes in engine thrust over the 1900 feet of altitude spanned in the descents. That is, $V_{v_{corrected}} \approx V_{v\,ind} + \frac{(11{,}000 - h_{ind})200}{1900}$. Then, the definition of flight path angle (given above) is used to calculate the flight path angle for each of the test points. Notice that each of these angles is negative, which is consistent with the descent that is typical for both a normal landing approach and the way the data were taken. The results of the calculations described above are summarized in the table on the previous page.

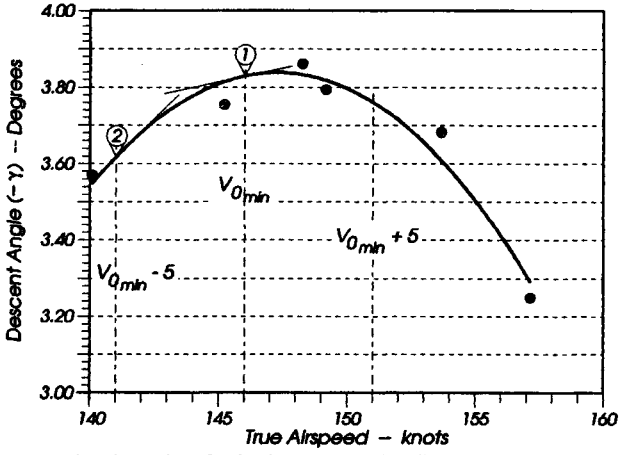

Finally, plotting the calculated flight path angles versus true airspeed and fitting a second-order curve to the data, we obtain the plot above.

As was discussed in section 6.1.3.2, the slope at point 1 must be less than 0.06 °/knot and the difference between the slopes at points 1 and 2 must be less than or equal to 0.05 °/knot to satisfy Level 1 handling qualities for flight path stability. Taking the second-order polynomial least squares curve fit shown above as a reasonable fairing for the very few measurements taken, the equation for γ is:

$\gamma = -0.00562286V^2 + 1.65626V - 118.127$

Taking the derivative with respect to V to get the required slopes, $\frac{d\gamma}{dV} = -0.01124572V + 1.65626$, the slope at the recommended true airspeed for final approach (146 knots) is: *0.014385* °/knot, which meets the first part of the requirement. The slope at $V_{0_{min}} - 5$ knots (141 knots) is: *0.076135* °/knot. Subtracting we find the necessary difference in slopes is *0.05623* °/knot, which does not meet the requirement.

6.3 SUMMARY

This chapter introduced stability and control flight test techniques used to evaluate the static longitudinal stability of an airplane. The theoretical concepts of stick-fixed and stick-free neutral points were reviewed and this background will be built upon in succeeding chapters. The importance of the pilot's perception of engineering measurements was emphasized throughout. How elevator control surface deflections and trim tab deflections can be utilized as a measure of stick-fixed and stick-free static longitudinal stability was explained in some detail. Speed stability, defined in MIL-F-8785C, was related to the neutral point concept for airplanes not affected by compressibility or Mach number effects. Flight-path stability was introduced as a specialized, but important type of stability, to be measured. The importance of trim techniques, friction and breakout forces, and piloting precision for stability and control measurements was emphasized. Finally, the stabilized, the slow acceleration/deceleration, and the power acceleration/deceleration methods were introduced. With this basic introduction to stability flight testing, the student should be ready to proceed to more difficult tasks.

REFERENCES

1 Perkins, C. D., "Introduction," Chapter 1, Volume II, **AGARD Flight Test Manual**, Pergamon Press, New York, 1959.

2 "Military Specification, Flying Qualities of Piloted Airplanes", MIL-F-8785C, November 1980.

3 "Federal Air Regulations, Volume III, Part 23, Airworthiness Standards: Normal, Utility, and Acrobatic Category Airplanes, Federal Aviation Administration, Washington, 1969.

4 Etkin, B., **Dynamics of Flight-Stability and Control**, (2nd Edition), John Wiley & Sons, New York, 1982.

5 "Stability and Control Flight Test Theory," Vol. I, Chapter 3, AFFTC-TIH-77-1, USAF Test Pilot School, Edwards AFB, California, Revised February 1977.

6 "Fixed Wing Stability and Control: Theory and Flight Test Techniques," USNTPS-FTM-No. 103, Naval Air Test Center, Patuxent River, Maryland, January 1975 (Revised November 1981).

7 Hoh, R. H., et al, "Proposed MIL Standard and Handbook -- Flying Qualities of Air Vehicles," Vol. II: Proposed MIL Handbook, AFWAL-TR-82-3081, Air Force Wright Aeronautical Laboratories, Wright-Patterson AFB, Ohio, November 1982.

Chapter 7

LONGITUDINAL MANEUVERABILITY TESTS

In Chapter 6 we discussed longitudinal static stability strictly in terms of unaccelerated, equilibrium conditions. Now we need to consider how to test an airplane under conditions in which the flight path is curved by either banking the wings or performing a wings-level pull-up or pushover. In either of these cases the vehicle's center of gravity will be accelerated by the force imbalance. Obviously, static longitudinal maneuvering tests are related to turning performance tests, but the purposes are entirely different and the techniques are quite different. The concepts of stick-fixed and stick-free maneuver points, which are very much kin to stick-fixed and stick-free neutral points, are reviewed and flight test techniques for determining maneuvering characteristics are discussed.

7.1 THEORETICAL FOUNDATIONS

Longitudinal maneuvering stability is concerned with disturbances in angle of attack and load factor, but not speed. In other words, the subject matter in this chapter will concentrate on load factor as the parameter of primary interest and ignore speed changes in contrast to Chapter 6 where load factor was always one. Parallel to the development of stick-fixed neutral point concepts with respect to elevator deflection, stick-fixed maneuvering stability concepts will be based on elevator angle deflections. Similarly, the stick-free maneuver point will be studied through the changes in stick force experienced by the pilot. These ideas lead to the following figures of merit:

- Elevator angle per g (stick-fixed maneuvering)..... $\frac{\Delta\delta_e}{g}$
- Stick force per g (stick-free maneuvering)..... $\frac{\Delta F_s}{g}$

To begin our study of accelerated flight, let us consider one of the simplest cases, a wings-level pull-up.

$$\Delta C_m = C_{m\alpha}\Delta\alpha + C_{m\delta_e}\Delta\delta_e + \frac{\partial C_m}{\partial q}\Delta q \tag{7.1}$$

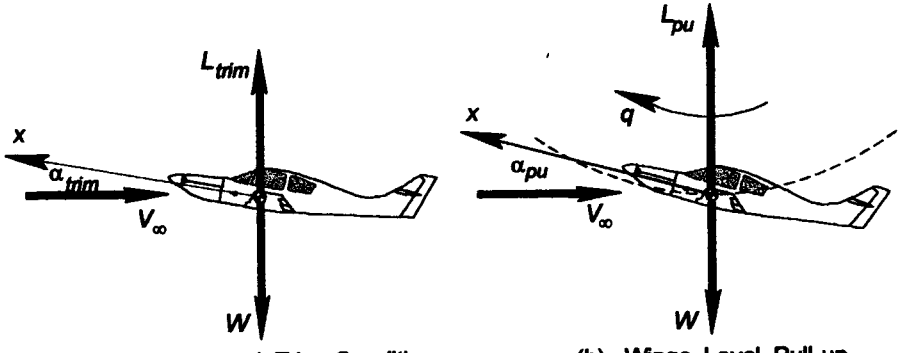

(a) Straight and Level Trim Condition ($L = W$)

(b) Wings Level Pull-up ($L = nW$)

Fig. 7.1 Differences Between Level, Unaccelerated Flight and a Wings-Level Pull-up

7.1.1 Steady, Wings-Level Pull-up

Consider an airplane that has been trimmed for level flight at a given true airspeed. Assume that it is climbed and then dived without altering the power setting (changing both the altitude and airspeed) and then a pull-up is initiated using the elevator alone. Instantaneously, the airplane will pass through the level flight trimmed (equilibrium) condition during the maneuver and if care is taken this condition can be attained at the original altitude. As suggested in Fig. 7.1, both angle of attack and load factor will be greater in the accelerated maneuver than in level flight. Lift coefficient will increase and there will be a positive pitch rate generated. These changes in angle of attack and in pitch rate cause a change in pitching moment coefficient compared to the original level flight equilibrium. Hinge moments for the control surface are also affected; that is, both C_m and C_{h_e} are functions of α, δ_e, and q. Notice that q is pitch rate, not dynamic pressure. To avoid confusion, dynamic pressure is denoted by $\bar{q}$ in this book.

Considering pitch rate an instantaneous source of centrifugal acceleration (that is, at any instant of time, the flight path can be approximated by a circular arc) and using Newton's second law relates pitch rate to normal load factor and true airspeed as follows:

$$q = \frac{(n-1)g}{V_\infty} \tag{7-2}$$

This pitch rate contributes to the total pitching moment experienced by the airplane by effectively increasing the angle of attack at the horizontal tail or the canard. (For simplicity, we will consider only conventional tail-aft configurations in this introductory course.) Figure 7.2 illustrates how the angle of attack at the horizontal tail is affected by the airplane's pitch rate.

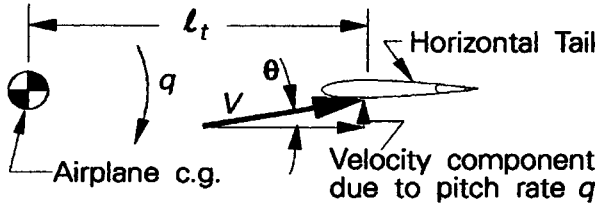

Fig. 7.2 Effective Increase in Horizontal Tail Angle of Attack Due to Pitch Rate

7.1.1.1 **Elevator Angle per G**. Following Etkin's approach[1] with minor modifications, we can derive the first of our measures of merit. The pitching moment increment due to the pitch rate in curvilinear flight depends on changes in angle of attack, elevator position, and pitch rate. If the total pitching moment coefficient can be considered a linear combination of contributions due to each of these variables suggested in eqn. 7.1. The increment of C_m due to the pitch rate during a wings-level pull-up that has negligible angular acceleration (this restriction implies a nearly circular path) can be written as:

$$\Delta C_m = C_{m_\alpha}\Delta\alpha + \frac{\partial C_m}{\partial q}\Delta q + C_{m_{\delta_e}}\Delta\delta_e$$

With our assumption of a near circular path, the pitching moment increment due to rotation is 0, just as it is in straight and level flight equilibrium condition. Then,

$$\Delta\delta_e = \frac{C_{m_\alpha}\Delta\alpha + \frac{\partial C_m}{\partial q}\Delta q}{C_{m_{\delta_e}}} \tag{7.3}$$

The increment in angle of attack due to pitch rate can be related to the increment in lift coefficient necessary to sustain the maneuver.

$$\Delta C_L = \frac{\Delta L}{\bar{q}S} = \frac{(n-1)W}{\bar{q}S} = (n-1)C_{L_{trim}}$$

where C_{Ltrim} ≡ the lift coefficient in straight and level flight at the given speed and altitude.

The change in angle of attack is then given by:

$$\Delta\alpha = \frac{\Delta C_L - C_{L\delta_e}\Delta\delta_e}{C_{L_\alpha}}$$

Substituting this expression for $\Delta\alpha$ and eqn. 7.1 for q,

$$\Delta\delta_e = -\frac{\frac{C_{m_\alpha}\left(\Delta C_L - C_{L_{\delta_e}}\Delta\delta_e\right)}{C_{L_\alpha}} + \frac{\partial C_m}{\partial q}q}{C_{m_{\delta_e}}} = -\frac{\frac{C_{m_\alpha}\left[(n-1)C_{L_{trim}} - C_{L_{\delta_e}}\Delta\delta_e\right]}{C_{L_\alpha}} + \frac{\partial C_m}{\partial q}\frac{(n-1)g}{V_\infty}}{C_{m_{\delta_e}}}$$

which simplifies to:

$$\frac{\Delta\delta_e}{n-1} = -\frac{C_{m_\alpha}C_{L_{trim}} + \frac{\partial C_m}{\partial q}\frac{(n-1)g}{V_\infty}}{C_{L_\alpha}C_{m_{\delta_e}} - C_{m_\alpha}C_{L_{\delta_e}}}$$

Using $C_{m_\alpha} = C_{L_\alpha}\left(\frac{x_{cg}}{\bar{c}} - \frac{x_{np}}{\bar{c}}\right)$ with $C_{m_q} = \frac{\partial C_m}{\partial\left(\frac{q\bar{c}}{2V_\infty}\right)} = \frac{\partial C_m}{\partial q}\frac{2V_\infty}{\bar{c}}$, while recalling that $C_{L_{trim}} = \frac{W}{\bar{q}S}$, and defining the relative mass parameter as $\mu = \frac{2m}{\rho_\infty S\bar{c}}$, the expression for elevator angle per g becomes:

$$\boxed{\frac{\Delta\delta_e}{n-1} = -\frac{C_{L_\alpha}C_{L_{trim}}\left(\frac{x_{cg}}{\bar{c}} - \frac{x_{np}}{\bar{c}}\right) + \frac{C_{m_q}}{2\mu}}{C_{L_\alpha}C_{m_{\delta_e}} - C_{m_\alpha}C_{L_{\delta_e}}}} \tag{7.4}$$

7.1.1.2 **Stick-Fixed Maneuver Point**. Paralleling our previous definition of stick-fixed neutral point, we now define the ***stick-fixed maneuver point*** as the airplane center of

gravity position for which elevator angle per g vanishes. Mathematically, we set eqn. 7.4 to *0* and define x_{mp} as the stick-fixed maneuver point:

$$0 = C_{L_\alpha} C_{L_{trim}} \left(\frac{x_{mp}}{\bar{c}} - \frac{x_{np}}{\bar{c}} \right) + \frac{C_{m_q}}{2\mu}$$

which is solved for $\frac{x_{mp}}{\bar{c}}$ to give: $$\frac{x_{mp}}{\bar{c}} = \frac{x_{np}}{\bar{c}} - \frac{C_{m_q}}{2\mu} \left(\frac{1}{C_{L_\alpha} C_{L_{trim}}} \right) \tag{7.5}$$

Of course, $\frac{\Delta\delta_e}{n-1}$ can be rewritten with this expression for stick-fixed maneuver point:

$$\frac{\Delta\delta_e}{n-1} = -\frac{C_{L_\alpha} C_{L_{trim}} \left(\frac{x_{cg}}{\bar{c}} - \frac{x_{mp}}{\bar{c}} \right)}{C_{L_\alpha} C_{m_{\delta_e}} - C_{m_\alpha} C_{L_{\delta_e}}} \tag{7.6}$$

The quantity in parentheses suggests another margin analogous to the stability margin in Chapter 6 (page 121). The **stick-fixed maneuver margin** is a measure of aircraft maneuverability and is defined as:

$$\boxed{MM \equiv \frac{x_{mp}}{\bar{c}} - \frac{x_{cg}}{\bar{c}}} \tag{7.7}$$

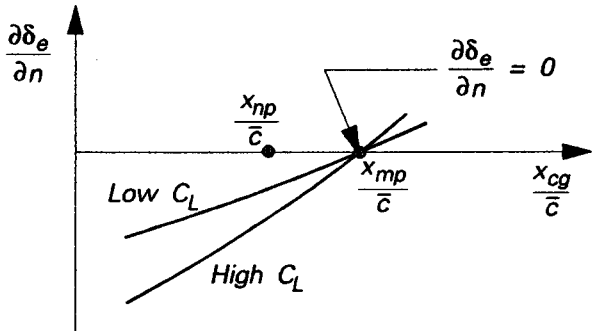

Fig. 7.3 Stick-Fixed Neutral and Maneuver Points

Typically, the stick-fixed maneuver point is about $0.06\bar{c}$ behind the stick-fixed neutral point for a conventional tail-aft airplane[1]. Considering the definition of the relative mass parameter,

$$\mu = \frac{2m}{\rho_\infty S \bar{c}} = \frac{2\left(W/S\right)}{\rho_\infty g \bar{c}} \tag{7.8}$$

it is clear that as either altitude or wing loading increases, μ increases. Equations 7.5 and 7.8 imply that either of these changes causes the maneuver point to move closer to the neutral point. Taken as a whole, a large airplane with a large tail and long tail moment arm, having a low wing loading, and flying at sea level will lead to the greatest difference between the stick-fixed neutral point and the stick-fixed maneuver point. Said another

way, large transport airplanes tend to be more sluggish than fighter airplanes and they are hardest to maneuver at sea level. Figure 7.3 illustrates the relative positions of the two stick-fixed points. Notice also that the elevator angle required to maintain a constant load factor increment in the pull-up does not reverse sign until the cg moves aft of the maneuver point, that is, the airplane can be maneuvered even though it is statically unstable. Of course, this statement does not take into account the dynamics involved and should not be construed to suggest that one should always design for this condition. It does, however, suggest one of the reasons that relaxed static stability has become an attractive alternative for high performance airplanes.

7.1.1.3 **Stick Force per G**. In Chapter 6 we learned that stick force is proportional to the elevator hinge moment. It is natural to infer that the increment of stick force necessary to maintain an increment in load factor in a wings-level pull-up is also proportional to the increment in hinge moment.

$$\Delta F_s = G\bar{q}S_e\bar{c}_e C_{h_e}$$

Still considering conventional tail-aft tail configurations only, the contribution of pitch rate to local angle of attack at the horizontal tail is illustrated in Fig. 7.2. The angle θ is defined by the ratio of the velocity component due to rotation to the velocity component due to translation.

$$\tan\theta = \frac{q\ell_t \cos\alpha_w}{V_\infty} \text{ or, for small changes in angle of attack}$$

$$\theta \approx \frac{q\ell_t}{V_\infty} \text{ in radians} \qquad (7.9)$$

Then the total increment in angle of attack at the horizontal tail is due to both the increment in wing angle of attack required to provide the necessary additional lift and the increment in angle of attack due to pitch rotation at the tail.

$$\Delta\alpha_t = \Delta\alpha_w\left(1 - \frac{\partial\varepsilon}{\partial\alpha}\right) + \theta$$

$$\text{But } \Delta\alpha_w = \frac{\Delta C_L}{C_{L_\alpha}},\ \Delta C_L = \frac{(n-1)W}{\bar{q}S},\ \text{and } q = \frac{(n-1)g}{V_\infty}$$

$$\text{Then } \Delta\alpha_t = (n-1)\left(\frac{\Delta C_L}{C_{L_\alpha}}\left(1 - \frac{\partial\varepsilon}{\partial\alpha}\right) + \frac{g\ell_t}{V_\infty^2}\right)$$

By assuming that $\Delta\alpha_w = \frac{\Delta C_L}{C_{L_\alpha}}$, we neglect any contribution to C_L due to elevator deflection. This assumption is equivalent to taking $C_{L_{\delta_e}} = 0$ for this maneuver. Recalling eqn. 7.4 with this assumption incorporated,

$$\frac{\Delta\delta_e}{n-1} = \frac{C_{L_{trim}}\left(\frac{x_{cg}}{\bar{c}} - \frac{x_{mp}}{\bar{c}}\right)}{C_{m_{\delta_e}}} \text{ and the incremental change in elevator hinge moment is:}$$

$$\Delta C_{h_e} = C_{h_{\alpha_t}} \Delta\alpha_t + C_{h_{\delta_e}} \Delta\,\delta_e$$

It follows that the change in hinge moment per g is obtained by using the definition of $C_{L_{trim}}$ and the facts that

$$\frac{g}{V_\infty^2} = \frac{C_{L_{trim}} \rho_\infty S}{2m} \text{ and } C_{m_{\delta_e}} = -a_e V_H \text{ to get}$$

$$\frac{\Delta C_{h_e}}{n-1} = \frac{\Delta C_{h_{\alpha_t}} C_{L_{trim}} \left(1 - \frac{\partial\varepsilon}{\partial\alpha}\right)}{C_{L_\alpha}} + \frac{C_{h_{\alpha_t}}}{V_\infty^2} - \frac{C_{h_{\delta_e}} C_{L_{trim}} \left(\frac{x_{cg}}{\bar{c}} - \frac{x_{mp}}{\bar{c}}\right)}{C_{m_{\delta_e}}}$$

or

$$\frac{\Delta C_{h_e}}{n-1} = \frac{C_{h_{\alpha_t}} C_{L_{trim}}}{a_e V_H} \left(\frac{C_{h_{\alpha_t}} a_e V_H}{C_{h_{\delta_e}} C_{L_\alpha}} \left(1 - \frac{\partial\varepsilon}{\partial\alpha} + \frac{C_{L_\alpha} \ell_t}{\mu\bar{c}}\right) + \frac{x_{cg}}{\bar{c}} - \frac{x_{mp}}{\bar{c}} \right) \tag{7.10}$$

Turning our attention to stick-free conditions, we compared the stick-fixed and stick-free neutral points in eqn. 6.14

$$\frac{x_{np}}{\bar{c}} - \frac{x'_{np}}{\bar{c}} = (1-F) V_{H_n} \frac{C_{L_{\alpha_t}}}{C_{L_\alpha}} \left(1 - \frac{\partial\varepsilon}{\partial\alpha}\right)$$

where $V_{H_n} \approx V_{H'_n}$ and the free elevator factor is defined as $F \equiv 1 - \dfrac{C_{h_{\alpha_t}} a_e}{C_{L_{\alpha_t}} C_{L_{\delta_e}}}$

Then, $\dfrac{x_{np}}{\bar{c}} - \dfrac{x'_{np}}{\bar{c}} = V_H \dfrac{C_{L_{\alpha_t}}}{C_{L_\alpha}} \left(1 - \dfrac{\partial\varepsilon}{\partial\alpha}\right) \dfrac{C_{h_{\alpha_t}} a_e}{C_{L_{\alpha_t}} C_{L_{\delta_e}}}$

which, when substituted into eqn. 7.10, leads to:

$$\frac{\Delta C_{h_e}}{n-1} = \frac{C_{h_{\delta_e}} C_{L_{trim}}}{a_e V_H} \left(\frac{x_{np}}{\bar{c}} - \frac{x'_{np}}{\bar{c}} + \frac{C_{h_{\alpha_t}} a_e V_H}{C_{h_{\delta_e}} C_{L_\alpha}} \left(\frac{a_e \ell_t}{\mu\bar{c}}\right) + \frac{x_{cg}}{\bar{c}} - \frac{x_{mp}}{\bar{c}} \right) \tag{7.11}$$

Next, we consider the tail contribution to the damping in pitch in order to eliminate the x_{mp} term from eqn. 7.11. This increment in pitching moment is by far the most important contribution to the damping in pitch, usually at least 90% of the total C_{m_q}[1]. This increment in pitching moment is given by:

$$\Delta C_m = -V_H \Delta C_{L_t} = -\frac{V_H C_{L_{\alpha_t}} q \ell_t}{V_\infty} \text{ which implies that } \left(\frac{\partial C_m}{\partial q}\right)_t = -\frac{V_H C_{L_{\alpha_t}} \ell_t}{V_\infty} \text{ and}$$

$$C_{m_{q_t}} = \left(\frac{2V_\infty}{\bar{c}}\right)\left(\frac{\partial C_m}{\partial q}\right)_t = -\frac{2V_H C_{L_{\alpha_t}} \ell_t}{\bar{c}}$$

Since the tail contribution is such a large part of C_{m_q}, we will simply allow for the wing and body contributions to this damping derivative through K, where K is on the order of 1.1, and write the damping in pitch for the complete airplane configuration as

$$C_{m_q} = -\frac{K 2 V_H C_{L_{\alpha_t}} \ell_t}{\bar{c}} \tag{7.12}$$

Substituting eqn. 7.12 into eqn. 7.5 and solving: $\frac{x_{mp}}{\bar{c}} = \frac{x_{np}}{\bar{c}} + \frac{K 2 V_H C_{L_{\alpha_t}} \ell_t}{\mu \bar{c}}$ (7.13)

Returning to equation 7.10, substituting for x_{mp}, and using $\frac{C_{h_{\alpha_t}}}{C_{h_{\delta_e}}} = \frac{C_{L_{\alpha_t}}}{a_e (F-1)}$,

$$\frac{\Delta C_{h_e}}{n-1} = \frac{C_{h_{\delta_e}} C_{L_{trim}}}{a_e V_H} \left(\frac{x_{cg}}{\bar{c}} - \frac{x'_{np}}{\bar{c}} + (K + F - 1) \left(\frac{a_e \ell_t V_H}{\mu \bar{c}} \right) \right) \tag{7.14}$$

The increment in stick force that the pilot must apply to generate the wings-level pull-up we have been analyzing is related to the required change in hinge moment through the gearing ratio G.

$$\Delta F_s = \Delta C_{h_e} G \bar{q} S_e c_e$$

Rearranging eqn. 7.12 and substituting ΔC_{h_e} into the expression for stick force

$$\frac{\Delta F_s}{n-1} = G \bar{q} S_e c_e \left(\frac{C_{h_{\delta_e}} C_{L_{trim}}}{a_e V_H} \right) \left(\frac{x_{cg}}{\bar{c}} - \frac{x'_{np}}{\bar{c}} + (K + F - 1) \left(\frac{a_e \ell_t V_H}{\mu \bar{c}} \right) \right) \tag{7.15}$$

This expression is one form of a stick force per g expression. However, we can simplify the form somewhat by developing the concept of a maneuver point to include a stick-free case analogous to the neutral point definitions.

7.1.1.4 **Stick-Free Maneuver Point**. The ***stick-free maneuver point*** is defined as the airplane center of gravity position for which the stick force per g vanishes. In pilot terms, it is that cg position at which zero stick force is required to pull up at any normal acceleration. Using the definition of $C_{L_{trim}}$ again, eqn. 7.15 reduces to

$$\frac{\Delta F_s}{n-1} = G S_e c_e \left(\frac{W C_{h_{\delta_e}}}{a_e S V_H} \right) \left(\frac{x_{cg}}{\bar{c}} - \frac{x'_{np}}{\bar{c}} + (K + F - 1) \left(\frac{a_e \ell_t V_H}{\mu \bar{c}} \right) \right)$$

Then, the stick-free maneuver point x'_{mp} comes from

$$\frac{x'_{mp}}{\bar{c}} = \frac{x'_{np}}{\bar{c}} + (K + F - 1) \left(\frac{a_e \ell_t V_H}{\mu \bar{c}} \right) \tag{7.16}$$

Equation 7.16 lets us write stick force per g in terms of the stick-free maneuver point:

$$\frac{\Delta F_s}{n-1} = G(W/S)S_e c_e \left(\frac{C_{h_{\delta_e}}}{a_e V_H}\right)\left(\frac{x_{cg}}{\bar{c}} - \frac{x'_{mp}}{\bar{c}}\right) \tag{7.17}$$

Recognizing that $\frac{\Delta F_s}{n-1}$ is an approximate form of stick force per g (strictly speaking, stick force per g is the gradient $\frac{\partial F_s}{\partial n}$); thus, in the limit:

$$\frac{\partial F_s}{\partial n} = G(W/S)S_e c_e \left(\frac{C_{h_{\delta_e}}}{a_e V_H}\right)\left(\frac{x_{cg}}{\bar{c}} - \frac{x'_{mp}}{\bar{c}}\right) \tag{7.18}$$

As we did with the stick-fixed maneuver point, let us close this section with a summary of the physical meaning of these results. First, the preceding analysis is based entirely on a steady state load factor being maintained throughout a wings-level pull-up. The equations shed no light on transient conditions between the initiation of the pull-up and the time that the steady state trajectory is reached. Furthermore, if the stick force per g or the elevator angle per g is measured in turning flight, the equations must be altered as we will see in the next section. Having reminded you of these limitations, we note:

- Stick force per g varies linearly with cg position and is negative for $x_{cg} > x_{mp}'$. It must be emphasized that this statement has nothing to do with stick travel per g, only stick force per g. Stick travel per g is related to stick-fixed conditions.
- Stick force per g varies directly with wing loading and directly as the "volume" ($S\bar{c}$) of the airplane. High wing loading airplanes like the F-15 require more force to move the controls and almost always use an irreversible control system to help the pilot. Large transport or cargo airplanes with large control surfaces also require a mechanical advantage of some type to fly with acceptable pilot forces while maneuvering.
- In the absence of Mach number and Reynolds number effects, stick force per g is independent of speed. This result shows up in that eqn. 7.18 contains no speed or speed dependent term other than $C_{h\delta_e}$. Of course, this derivative, like most other stability derivatives, is strongly dependent upon Mach number.
- The relative mass parameter affects the relative distance between the stick-free neutral and maneuver points in just the same ways (altitude, size, and wing loading) as it did the difference between the stick-fixed neutral and maneuver points (see section 7.1.2).

7.1.2 Turns

As noted above, the theory developed so far does not properly account for the pitch rate contribution to either elevator angle per g or stick force per g in turning flight. Collecting maneuvering stability data in a turn can be a much less time-consuming process than collecting data with a series of wings-level pull-ups. Since time, especially flight test time, is money, the well-informed flight test engineer must understand the differences in maneuvering flight test measurements taken with both test methods. There are two types of turns ordinarily used to collect maneuvering stability information: (1) a steady level turn

and (2) a windup turn. A steady level turn implies a constant load factor, constant altitude, and constant true airspeed. A windup turn is a dynamic maneuver in which a constant load factor is maintained as airspeed is allowed to decrease until some limiting condition is reached.

Consider the forces acting during a constant altitude, constant airspeed turn as sketched in Fig. 7.4. Dividing the vertical component of lift by its horizontal component:

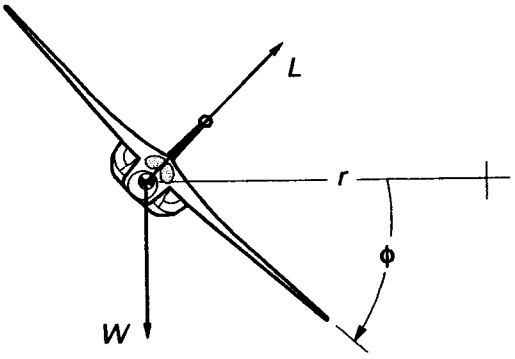

Fig. 7.4. Load Factor in a Turn

$$\frac{L\cos\Phi}{L\sin\Phi}=\frac{gr}{V_\infty^2} \text{ or } \frac{V_\infty}{r}=\frac{g\tan\Phi}{V_\infty}=\Omega$$

where Ω is the angular velocity about the local vertical axis. The components of Ω can be resolved as shown in Fig. 7.4. Notice that in a steady level turn, there is a component of Ω about the *y* body-axis and a component about the *z* body axis. We are interested in the pitch rate *q*, which is the component about the *y*-axis.

$$q=\Omega\sin\Phi=\frac{g\sin^2\Phi}{V_\infty\cos\Phi}=\frac{g\left(1-\cos^2\Phi\right)}{V_\infty\cos\Phi}=\frac{g}{V_\infty}\left(\frac{1}{\cos\Phi}-\cos\Phi\right)=\frac{g}{V_\infty}\left(n-\frac{1}{n}\right)$$

Taking equilibrium (trim) as a steady level turn at n_0

$$q-q_0=\frac{g}{V_\infty}\left(n-\frac{1}{n}\right)-\frac{g}{V_\infty}\left(n_0-\frac{1}{n_0}\right)$$

Simplifying, $q=\frac{g}{V_\infty}(n-n_0)(1+nn_0)$. Recalling eqn. 7.3 and modifying it slightly to fit level turn dynamics, $\Delta\delta_e=-\dfrac{C_{m_\alpha}\Delta\alpha+\dfrac{\partial C_m}{\partial q}q}{C_{m_{\delta_e}}}$, and also modifying the expression for the incremental angle of attack in a similar fashion for the change in load factor to go with the pitch rate in the turn, $\Delta\alpha=\dfrac{(n-n_0)C_{L_{trim}}-C_{L_{\delta_e}}\Delta\delta_e}{C_{L_\alpha}}$

We can now express the increment of elevator deflection required to maintain the pitch rate in the level turn.

$$\Delta\delta_e = -\frac{\frac{C_{m_\alpha}}{C_{L_\alpha}}\left((n-n_0)C_{L_{trim}} - C_{L_{\delta_e}}\Delta\delta_e\right)\Delta\alpha + \frac{\partial C_m}{\partial q}\frac{g}{V_\infty}(n-n_0)(1+nn_0)}{C_{m_{\delta_e}}}$$

Collecting terms that do not have the factor $(n - n_0)$ on the left side and those that do on the right side and solving for $\frac{\Delta\delta_e}{n-n_0}$

$$\frac{\Delta\delta_e}{n-n_0} = \frac{C_{m_\alpha}C_{L_{trim}} + C_{L_\alpha}C_{m_{\delta_e}}\frac{\bar{c}g}{2V_\infty^2}(1+nn_0)}{C_{m_\alpha}C_{L_{\delta_e}} - C_{L_\alpha}C_{m_{\delta_e}}}$$

If we take the limit as $n \to n_0$, $\frac{\Delta\delta_e}{n-n_0} \to \frac{\partial\delta_e}{\partial n}$. Using the definitions of the relative mass parameter and $C_{L_{trim}}$,

$$\frac{\partial\delta_e}{\partial n} = \frac{C_{m_\alpha}C_{L_{trim}} + C_{L_\alpha}C_{m_q}\frac{cg\rho_\infty SC_{L_{trim}}}{4W}\left(1+\frac{1}{n^2}\right)}{C_{m_\alpha}C_{L_{\delta_e}} - C_{L_\alpha}C_{m_{\delta_e}}}$$

Then, using $C_{m_\alpha} = C_{L_\alpha}\left(\frac{x_{cg}}{\bar{c}} - \frac{x_{np}}{\bar{c}}\right)$ to simplify the expression slightly,

$$\frac{\partial\delta_e}{\partial n} = \frac{C_{L_\alpha}C_{L_{trim}}\left(\frac{x_{cg}}{\bar{c}} - \frac{x_{np}}{\bar{c}} + \frac{C_{m_q}\left(1+\frac{1}{n^2}\right)}{2\mu}\right)}{C_{m_\alpha}C_{L_{\delta_e}} - C_{L_\alpha}C_{m_{\delta_e}}} \qquad (7.19)$$

Setting eqn. 7.19 to zero to solve for the stick-fixed maneuver point gives

$$\frac{x_{mp}}{\bar{c}} = \left(\frac{x_{np}}{\bar{c}} - \frac{C_{m_q}\left(1+\frac{1}{n^2}\right)}{2\mu}\right) \qquad (7.20)$$

Equation 7.20 clearly shows that the difference between measuring the maneuver points in a turn and in a wings-level pull-up is a factor of $1+\frac{1}{n^2}$. This difference shows up in each of the maneuver points with no change in the rest of the form for the rest of the equations. Obviously, as n gets large, each pair of measurements is approximately equal. Johnson[3] has provided a comparison of data for the two types of maneuvers as sketched in Fig. 7.5 (next page). Notice that as n gets larger, the slopes of the two curves become nearly identical, precisely what the theory predicted.

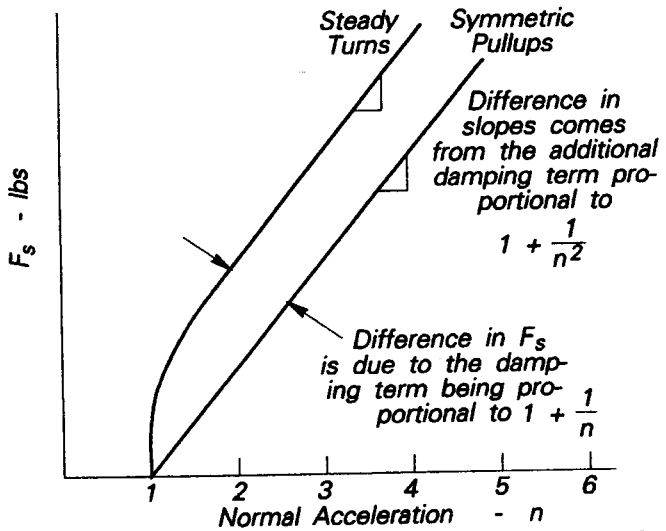

Fig. 7.5 Variation of Control Forces in Different Test Maneuvers

7.2 LONGITUDINAL MANEUVERABILITY TEST METHODS

It is the flight test engineer's responsibility to prepare a matrix of test conditions (airspeeds, airplane configurations, power settings, altitudes, and the like) the test team will use to collect maneuvering flight data. Typically, this matrix will be decided well in advance of the actual flights, perhaps even in the master plan agreed upon before the first flight. One of his primary concerns will be how to reduce the size of the matrix and still adequately define the handling characteristics of the vehicle. Obviously, the contractual specifications and the FAR requirements that must be demonstrated will guide this planning process. A brief discussion of the techniques used in flying each maneuver will also be of assistance in test planning.

In each of the test methods, as in all stability and control testing, careful trimming of the airplane to specified speed and altitude is absolutely essential to obtaining good data. The pilot should be held to very close tolerances on trim conditions if precise measurements of angular position and control forces are to be made.

7.2.1 Symmetric Pull-up Method

The objective in this maneuver is to establish a steady load factor as early in the maneuver as possible and maintain it as the airplane pitches through the horizontal. The data recorded includes indicated airspeed, normal acceleration, elevator position, and applied stick force. Automatic recording is almost essential because the pilot must try to achieve the nominal test conditions (airspeed, altitude, and constant acceleration) with the longitudinal reference axis as nearly horizontal as possible. Figure 7.6 illustrates good and bad data runs for a wings-level pull-up.

This test method is very time-consuming and the piloting technique requires practice, skill at estimating speed decay, and aggressive maneuvering to arrive at the required test conditions without delay. After trimming the airplane in level flight at the desired conditions

and recording these trim conditions on the data record, a climb is made to start the maneuver 200 to 500 feet above the test altitude at some airspeed slower than the trim airspeed. Power is set and a dive angle selected that will accelerate the airplane back to the trim airspeed just before reaching the trim altitude. Ideally the pull-up would be initiated and the normal acceleration established so that the aim load factor, airspeed, and altitude all occur just as the airplane is pitching through level flight. As Fig. 7.6 shows, it is ideal to have the g onset be smooth and rapid with no overshoot and for the load factor to remain constant until the control input is released. A common error is sketched in the right part of Fig. 7.6 where the load factor has been allowed to decrease as the airspeed decayed. Getting an ideal data trace may take several practice runs to iterate and find the right starting airspeed, altitude, and dive angle combination. It is also very helpful to have a real-time data display with at least normal acceleration and indicated airspeed so that data points which need to be repeated can be identified before trim conditions are changed. In judging quality of a data point, the following conditions are important:

- Load factor must be constant (zero slope) at the instant data are read.
- Stick forces must be constant.
- Trim must be set carefully and recorded to insure that equilibrium stick forces are measured precisely.

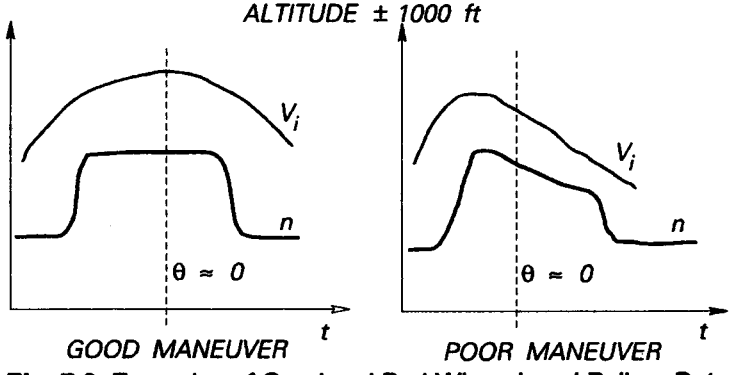

Fig. 7.6 Examples of Good and Bad Wings-Level Pull-up Data

In sum, the wings-level pull-up is an accurate, though not very time-efficient, method for collecting longitudinal maneuvering stability information. Now, let us consider alternative test methods.

7.2.2 Steady Turn

7.2.2.1 **Stabilized Load Factor**. Trimming carefully and recording the equilibrium data are just as important for this turning maneuver as for the wings-level pull-up. After trim conditions are recorded, a climb is made up to about 2000 feet above the test altitude and then the airplane is banked to a fixed angle while maintaining the selected load factor and airspeed precisely. Speed is maintained by carefully adjusting pitch attitude and climbing or descending as necessary. Both airspeed and load factor must be maintained precisely. (Typical limits for acceptable variations during the maneuver are ±1 knot and ±0.1g for bank angles up to 30° and ±2 knots and ±0.1g up to about 60°.) The need for such precision demands that the pilot have sensitive accelerometers and sensitive air-

speed indicators in the cockpit for continuous references. All data should be collected within a maximum altitude band of ±2000 feet from the trim altitude.

When a bank angle of 60° is reached, the usual technique is to maintain a constant bank angle while attempting to step up through the load factor range in 0.5g increments. As for the lower bank angles, airspeed is maintained constant by adjusting the pitch attitude. To stabilize at each of these increments of load factor becomes increasingly more difficult as load factor increases because the load factor goes up exponentially with bank angle. Consequently, this technique is largely applicable for configurations where the limit load factor is not much greater than 2. Transport/cargo airplanes and other airplanes in the power approach configuration allow the use of the stabilized g steady turn.

7.2.2.2 **Slowly Varying Load Factor**. This variation of the steady turn is most appropriate for highly maneuverable airplanes with limit load factors greater than 4 and permits a more economical data collection at the high load factors. It is often combined with the stabilized g method.

After the usual careful trim shot is recorded at the nominal test altitude, the working data band is again chosen. Typically, a band of ±2000 feet is used for this method as well. The airplane is slowly rolled into a continuously increasing bank while the load factor is simultaneously increased. The rate of onset of g is held at 0.1g/second or less and indicated airspeed is maintained as closely as possible (±1 knot is desired). Care must be exercised to avoid reversing the stick forces during this dynamic maneuver; otherwise, the friction and breakout force deadband will make it very difficult to interpret the data. It will usually be necessary to "piece together" the data since it is rare to obtain the complete range of load factors without descending outside the ±2000 feet allowed for data collection. Using the stabilized g method up to about 60° bank angle and then switching to the slowly varying g method is the most common way to collect maneuvering flight test data for fighter and trainer airplanes.

7.2.3 Windup Turn

This method is sometimes called the constant g method since the primary goal of the pilot is to maintain a constant load factor. In this case the trim conditions are chosen close to the maximum speed for the test. Since the maneuver is certainly a dynamic flight condition, you do not have to insist on trimming exactly on aim airspeed. However, the trim state should be recorded before taking data and there must be no compromise that the equilibrium was stable for at least 10 seconds with hands off.

After the trim condition has been established and recorded the airplane is placed in a turn at some constant load factor and the data recorder is started. Pitch attitude is adjusted to climb or dive the airplane and maintain a 2 to 5 knots/second rate of airspeed decay. Typically, a slight climb will be required to maintain this airspeed decay rate at small bank angles and a descent will be needed as the bank angle increases. Data should only be collected within the ±2000 feet specified for all maneuvering flight tests. Maintaining the load factor constant (not necessarily exactly at the selected nominal load factor) during the maneuver is absolutely essential to acquire repeatable maneuvering flight data. Frequently, it will be necessary to discontinue taking data because the altitude tolerance from the trim altitude has been exceeded. The pilot should note the airspeed departing the altitude band and the next segment of data should be started at an airspeed

slightly above this airspeed once the airplane has been climbed back into the allowable altitude band. This procedure will allow the engineer to reduce the data with a check on the continuity of the data. Airspeed records should also be marked where at the onset of buffet and when the constant load factor can no longer be maintained (often called the "g-break"). Windup turns can then be repeated at the same trim conditions for increasing increments of load factor. Typically, 0.5g increments are used at higher altitudes and about 1g increments are used at low altitudes. The exact values of load factor are not important; it is important that a constant load factor be maintained throughout any given windup turn and that the entire range of allowable range of load factors is covered. As in all flight testing, care must be taken to avoid exceeding established limits, especially when the flight envelope is being explored for the first time. Maneuvering flight tests, especially windup turns, are particularly susceptible to inadvertently overstressing the vehicle. Figures 7.7 and 7.8 show windup turn data[2]; these plots illustrate typical ways to present data.

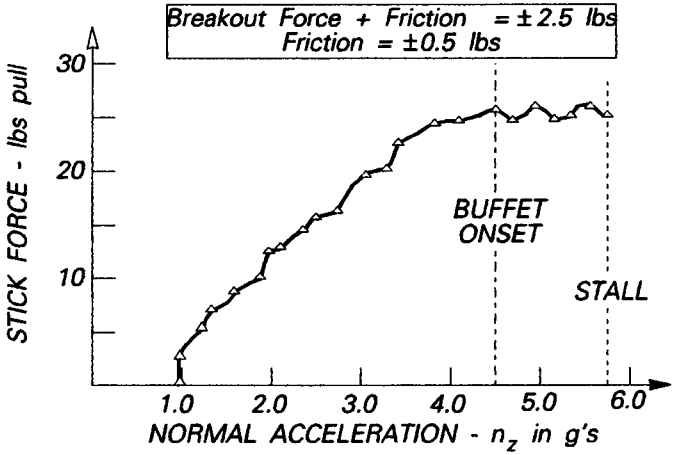

Fig. 7.7 Stick Force per G from a Windup Turn

7.2.4 Concluding Remarks

7.2.4.1 **Instrumentation Required**. From these brief descriptions of longitudinal maneuvering test methods, the necessity for automatic recording of the pertinent parameters is obvious. The minimum instrumentation required, as suggested by Johnson[3] but with details and emphasis added, includes the following:

- Normal acceleration must be measured as close to the airplane center of gravity as is feasible, displayed for the pilot, and recorded automatically. As already noted, the pilot's display of load factor must allow him to fly to a resolution of approximately 0.1g if he is to be expected to produce acceptable maneuvering flight test data. A magnetic tape recorder, telemetry, or some other means of continuous automatic data collection is a must for obtaining accurate samples of continuously varying data like these.
- Airspeed indications must be displayed on a sensitive indicator for the pilot, especially for those methods that require constant airspeed. Automatic recording is also essential to alleviate the pilot's workload and to insure precision.

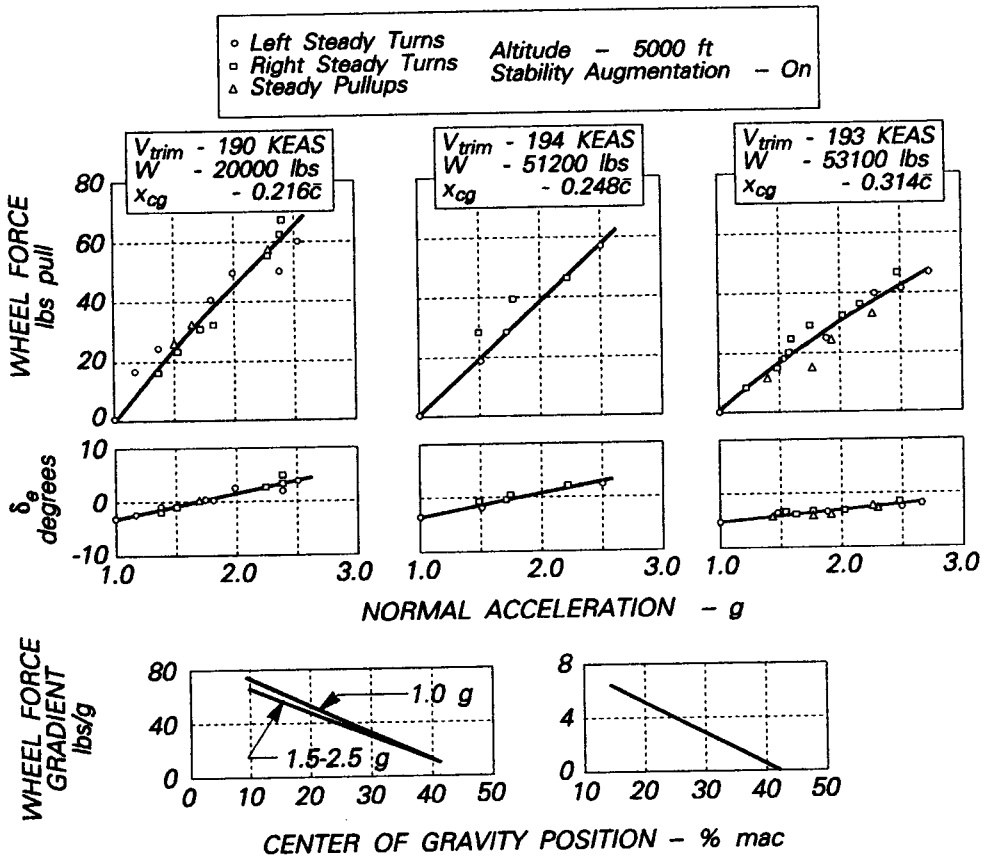

Fig. 7.8 Longitudinal Maneuvering Flight Test Data

- Altitude can be recorded from a standard altimeter, set to 29.92 inches of Hg to provide pressure altitude. It is not absolutely necessary to record altitude information on the recorder, though it often is.
- The forces typically applied by the pilot must be recorded, but no display is required for the pilot. It is very desirable to have a near real-time display for the flight test engineer to examine so the pilot can be advised when it is necessary to refly a maneuver prior to retrimming the airplane at a new flight condition. Such a quick-look capability usually pays for itself in test time saved in short order.
- Positions of control surfaces, of the pilot's controller (stick, wheel, or hand), and of longitudinal trimming devices should also be recorded and displayed on strip charts or other near real-time displays. It is possible to omit the last two of these position measurements, but they are highly desirable and are well used to help interpret the data.
- Angle of attack should be recorded continuously during longitudinal maneuvering. Again, pilot display of angle of attack is not absolutely essential but it is very convenient for the pilot and helps the engineer reduce the data and compare it to other sources of information like wind tunnel tests.

- Accurate tracking of center of gravity movement for the airplane is imperative for this type of test. Often, this tracking can be done by hand-recording the fuel counter readings or even fuel gage readings, on a cruder scale. (Production fuel gages are notoriously inaccurate and should only be used as a last resort.)
- The recording device should have some means of recording time elapsed and synchronizing all of the data channels to the same time base. For digital systems, the flight test engineer must be very careful in comparing continuously varying data that has been sampled at different times. Even small time differences can introduce artificial phase shifts between important variables. This synchronization of the data is particularly important for control surfaces moving at near their maximum rates. Of course, this factor is more important for the dynamic data to be discussed in Chapter 9, but it can also be important in determining stick force per g variation when the inputs are made rapidly.

Example 7.1: The following maneuvering flight data were collected in a Bell P-63 at 5000 feet on a standard day and a nominal gross weight of 7780 pounds. The aircraft was in its normal cruise configuration (gear and flaps up, cowl flaps closed). Estimate the stick force gradients from each set of data (considering each direction of turn as a separate set of data). Use these estimates to find the predict the average stick-free maneuver point for these conditions.

$\frac{x_{cg}}{\bar{c}} = 0.231$

Left Windup Turn		*Right Windup Turn*	
F_s	n	F_s	n
2.5	1.3	6.15	1.95
10.0	2.8	17.5	4.25
16.0	4.1	26.0	5.6
23.5	5.4		

$\frac{x_{cg}}{\bar{c}} = 0.262$

Left Windup Turn		*Right Windup Turn*	
F_s	n	F_s	n
2.0	1.4	2.5	1.4
3.5	2.25	13.0	4.3
10.0	4.0	17.5	5.5
14.0	5.2	20.5	6.3

$\frac{x_{cg}}{\bar{c}} = 0.274$

Left Windup Turn		*Right Windup Turn*	
F_s	n	F_s	n
3.1	2.2	3.0	1.8
3.6	3.7	3.2	3.5
8.0	4.5	9.5	5.3
10.3	6.0	13.0	6.6

$\frac{x_{cg}}{\bar{c}} = 0.304$

Left Windup Turn		*Right Windup Turn*	
F_s	n	F_s	n
1.6	1.95	3.0	3.7
2.0	3.0	5.6	5.7
3.0	4.7		
3.6	6.8		

We will estimate the stick-free maneuver point graphically, assuming that all curves are linear (which allows us to use a linear least-squares curve fit to each set of data). Plotting the points shown in the tables above and fitting each set of points with a straight line gives the charts on the next page. Clearly, there is enough data scatter that not all the straight lines have the same intercept (as they theoretically would if the measurements were perfect and if our simplifying assumptions were all absolutely correct). Nonetheless, we can easily extract the slopes of each curve for the given center of gravity locations. Tabulating these slopes and plotting them against cg location, the following table and charts result.

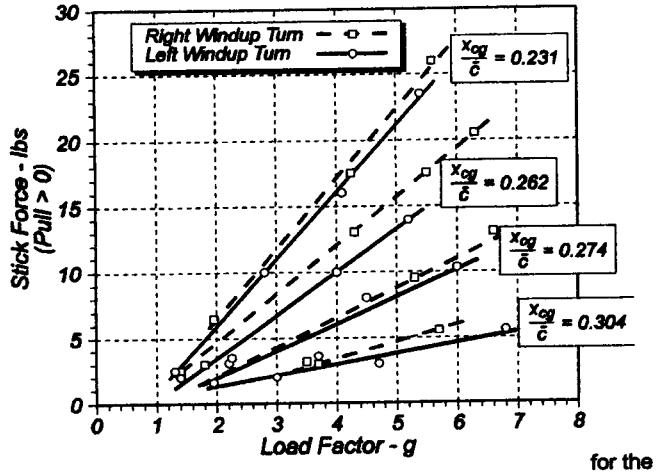

$\frac{x_{cg}}{\bar{c}}$	Slope for Left Turn	Slope for Right Turn
0.231	5.070	5.283
0.262	3.269	3.669
0.274	2.048	2.226
0.304	0.825	1.300

As the chart on the lower left shows, the intercepts on the abscissa give estimates of the stick-free maneuver point for each set of turns. The least squares straight-line curve fits give:

$$\frac{\Delta F_s}{\Delta n} = -59.343\frac{x_{cg}}{\bar{c}} + 18.692$$

for the left turn and

$$\frac{\Delta F_s}{\Delta n} = -56.343\frac{x_{cg}}{\bar{c}} + 18.205$$

for the right turn. Solving these two equations for the two estimates and averaging, we get:

$$\frac{x'_{mp}}{\bar{c}} = \frac{1}{2}\left(\frac{18.692}{59.343} + \frac{18.205}{56.343}\right) \text{ or}$$

$$\frac{x'_{mp}}{\bar{c}} \approx \frac{0.315 + 0.323}{2}$$

$$\boxed{\frac{x'_{mp}}{\bar{c}} \approx 0.319}$$

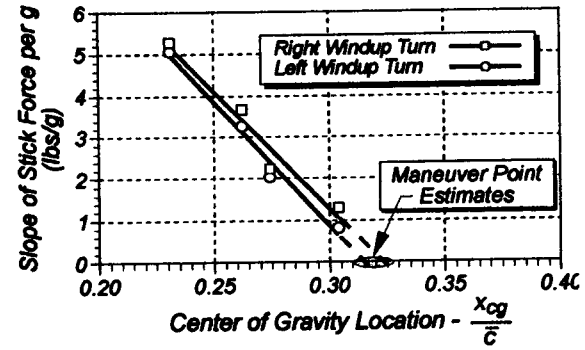

Of course, the problem could have been solved by ignoring the difference between the left and right turn data. However, by considering the data as it is naturally grouped the test team is encouraged to explore reasons for the differences in the data. Often this kind of approach will lead to better understanding of the underlying physics of the experiment.

7.2.4.2 **Estimation of Stability Derivatives**. Johnson[3] also suggests that maneuvering flight data can provide good estimates of $C_{L_{\delta_e}}$, $C_{h_{\delta_e}}$, and $C_{h_{\alpha_t}}$. First, plot the pertinent gradients versus the center of gravity in feet, as sketched in Fig. 7.9 (page 158). Elevator effectiveness can then be approximated using the inverse slope of the rate of change of elevator angle with lift coefficient versus cg position.

$$C_{L_{\delta_e}} = \frac{\partial x_{cg}}{\partial\left(\frac{\partial \delta_e}{\partial C_N}\right)} \frac{S\bar{q}}{S_t \bar{q}_t \ell_t} \tag{7.21}$$

where C_N is the airplane's normal force coefficient defined as $C_N \equiv \frac{n_z W}{\bar{q} S}$

The elevator hinge moment parameter due to elevator deflection comes from

$$C_{h_{\delta_e}} = \frac{\left(\frac{\partial\left(F_s/g\right)}{\partial x_{cg}}\right)\tau C_{L_{\alpha_t}} S_t \ell_t}{G b_e c_e^2 W} \tag{7.22}$$

where τ is the ratio of elevator lift effectiveness to stabilizer lift effectiveness and G is the elevator gearing in radians/ft.

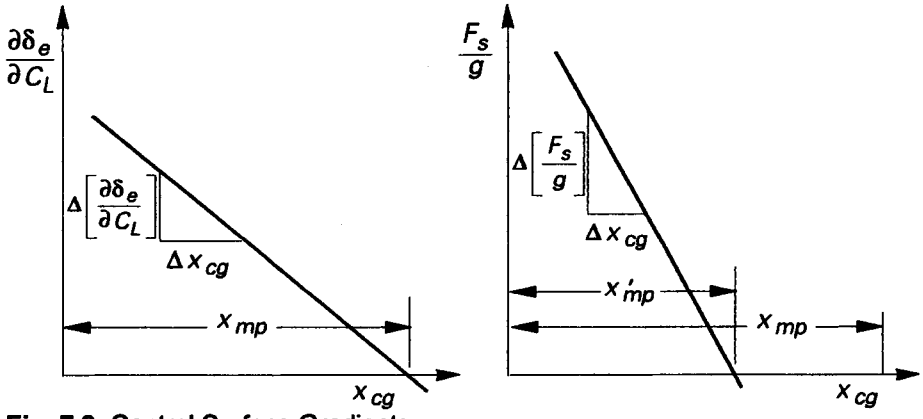

Fig. 7.9 Control Surface Gradients

If τ is set equal to 1 and the elevator dimensions are replaced by the corresponding stabilizer dimensions, eqn. 7.22 applies to an all-moving horizontal tail. Also, both eqns. 7.21 and 7.22 apply without modification to data collected in either steady turns or in wings-level pull-ups. Finally, $C_{h_{\alpha_t}}$ can be calculated from

$$C_{h_{\alpha_t}} = \frac{\left(x_{mp} - x'_{mp}\right) C_{h_{\delta_e}} \bar{q}}{C_{L_{\delta_e}} \bar{q}_t S_t \ell_t \left(\frac{1 - \frac{\partial \varepsilon}{\partial \alpha}}{C_{L_\alpha} S}\right) + \frac{180}{\pi S}\left(1 + \frac{1}{n}\right)} \tag{7.23}$$

if the data were collected in a steady turn. If instead the data were collected in wings-level pull-ups, the term $1 + \frac{1}{n}$ is left out of the denominator.

7.3 SUMMARY

This chapter reviewed the basic principles governing maneuvering flight stability and described concisely how to collect flight test data to measure the necessary stick forces, control surface deflections, pilot input forces, and normal load factor that typically are used as measures of merit for this kind of stability. The feel of the airplane (and therefore the pilot's opinion of it) depend rather strongly on these maneuverability measurements. We will have more to say about the pilot's subjective opinion in Chapter 9 when dynamic stability measurements are introduced. Typical flight test measurements for maneuverability may be made either using wings-level pull-ups or in a turn. In either case the dynamical system is not truly in static equilibrium, but a pseudo-equilibrium (constant non-zero acceleration is assumed to simplify the techniques. Corrections between the two basic types of trajectories (wings-level pull-ups or turns) are necessary if data taken using the two different maneuvers are to be compared; these corrections are particularly important for maneuvering load factors just slightly in excess of one.

REFERENCES

1 Etkin, B., **Dynamics of Flight - Stability and Control**, (2nd Edition), John Wiley & Sons, New York, 1982.

2 "Fixed Wing Stability and Control: Theory and Flight Test Techniques," USNTPS-FTM-No. 103, Naval Air Test Center, Patuxent River, Maryland, January 1975 (Revised November 1981).

3 Johnson, H. I., "Flight Testing Aircraft for Longitudinal Maneuvering Characteristics," Chapter 4, Volume II, **AGARD Flight Test Manual**, Pergamon Press, New York, 1959.

4 "Stability and Control Flight Test Theory," Vol. I, Chapter 4, AFFTC-TIH-77-1, USAF Test Pilot School, Edwards AFB, California, Revised February 1977.

5 "Stability and Control Flight Test Techniques," Vol. II, Chapter 5, AFFTC-TIH-77-1, USAF Test Pilot School, Edwards AFB, California, Revised February 1977.

Chapter 8

STATIC LATERAL-DIRECTIONAL STABILITY TESTS

The concept of static stability for the lateral-directional modes of motion cannot be as simply presented as it can for the longitudinal modes. First, there are two moment equations and one force equation involved and the moment equations are coupled kinematically through the product of inertia I_{xz}, as well as aerodynamically. Second, the lateral mode (roll) has no inherent static stability; no aerodynamic restoring moment is generated directly by rolling. Rather, a secondary moment is generated through the directional axis due to sideslip and dihedral effect becomes the dominant factor. Third, the controls used to produce moments about either of the axes also produce moments about the other. Aileron deflections produce yawing moments and the rudder produces a significant rolling moment. In spite of these three facts, it is still instructive to measure the static directional stability and the dihedral effect through steady state tests and to quantify the control authorities about the *x* and *z* axes with steady state maneuvers. These steady state test methods are the subject of this chapter, but the reader will do well to keep in mind that lateral-directional dynamics (see Chapter 9) are very important because of the strong coupling between these two axes.

8.1 THEORETICAL FOUNDATIONS

For this introduction to static lateral-directional flight test methods it is sufficient to ignore the side force equation and concentrate on the two moment equations. Using the notation of Etkin[1] and simplifying the equations slightly:

$$C_{\mathcal{L}} = C_{\mathcal{L}_\beta}\beta + C_{\mathcal{L}_p}p + C_{\mathcal{L}_r}r + C_{\mathcal{L}_{\delta_a}}\delta_a + C_{\mathcal{L}_{\delta_r}}\delta_r \tag{8.1}$$

$$C_n = C_{n_\beta}\beta + C_{n_p}p + C_{n_r}r + C_{n_{\delta_a}}\delta_a + C_{n_{\delta_r}}\delta_r \tag{8.2}$$

Of course, for static conditions, $p = r = 0$, and these equations simplify to:

$$C_{\mathcal{L}} = C_{\mathcal{L}_\beta}\beta + C_{\mathcal{L}_{\delta_a}}\delta_a + C_{\mathcal{L}_{\delta_r}}\delta_r \tag{8.3}$$

$$C_n = C_{n_\beta}\beta + C_{n_{\delta_a}}\delta_a + C_{n_{\delta_r}}\delta_r \tag{8.4}$$

Equations 8.3 and 8.4 emphasize that the dominant aerodynamic terms for static conditions are $C_{\mathcal{L}_\beta}$ and C_{n_β}, with stationary controls. For static directional stability ("weathercock" stability), $C_{n_\beta} > 0$; and for the airplane to have "wing leveling" tendencies, $C_{\mathcal{L}_\beta} < 0$.

8.1.1 Directional Stability and Control

As indicated above directional stability depends primarily on the value of C_{n_β} and the major contributor to this derivative is the vertical tail. The fuselage and nacelles produce a significant effect, though secondary to the vertical tail in most conventional designs. Directional control is exercised primarily through the rudder, though the ailerons contribute a significant yawing moment about the *z* axis also. This coupling of the controls are another important reason that lateral stability and directional stability must be considered as interrelated problems. These two axes cannot be separated for any meaningful stability and control analyses.

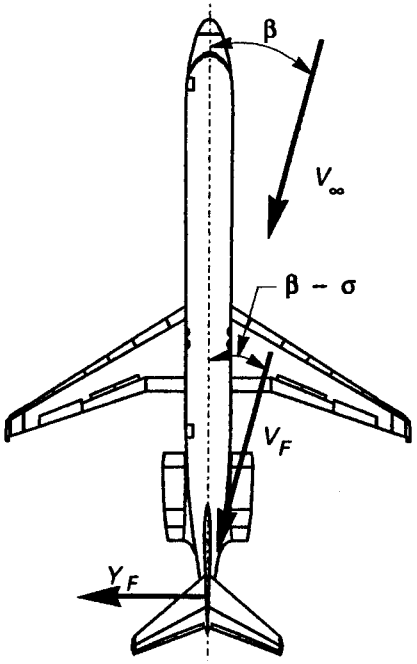

Fig. 8.1 Yawing Moment Produced by Sideslip

8.1.1.1 **Weathercock Stability**. ***Weathercock stability*** refers to the tendency of a vehicle to turn into the relative wind when sideslip is encountered. To have directional stability, the sideslip must produce an aerodynamic yawing moment that tends to restore the airplane to a zero sideslip condition (Fig. 8.1). The relevant stability derivative, which must be positive with the usual sign conventions for positive sideslip and yawing moment, is C_{n_β}, represented by the slope of the curve in Fig. 8.2. Although C_{n_β} is similar to C_{m_α} in that both are the dominant terms for static stability, the wing configuration and the center of gravity position have relatively minor effects on C_{n_β}. For a more complete discussion of the contributions of the vertical tail, the fuselage and nacelles, and the wing, see Etkin[1], Roskam[2], or the notes from one of the Test Pilot Schools[3,4,5].

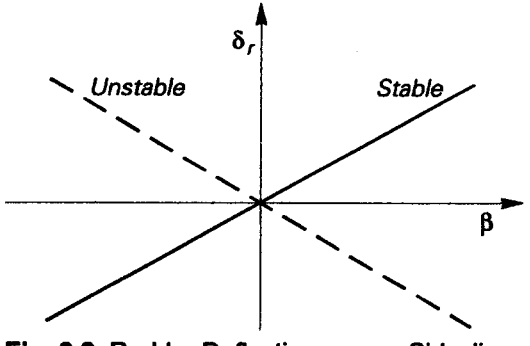

Fig. 8.2 Rudder Deflection versus Sideslip

8.1.1.2 **Directional Control**. Aircraft and missiles are, for the most part, symmetric vehicles. If a symmetric vehicle has positive directional stability, it will tend to fly at zero sideslip. Rarely are such machines intentionally flown with the sideslip angle other than zero for long periods of time. However, when engine failure occurs or when some other asymmetric flow field occurs (like slipstream rotation from a propeller or simply turning flight), sideslip must be controlled. In conventional airplanes the rudder is used for this purpose. The stability derivative that characterizes this control authority is called "rudder power" and is represented by $C_{n_{\delta_r}}$. Rudder deflections are necessary to maintain constant sideslip whenever asymmetric power is applied, to hold steady sideslips, and to coordinate turns when aileron deflections produce unwanted sideslip. This derivative is one of those that has different algebraic signs, depending on what scheme is used for denoting positive angular deflections. The most common method, the one used in most NASA publications, is not always convenient in flight test. Left rudder, under this convention, leads to a negative yawing moment. Hence, $C_{n_{\delta_r}}$ is negative. The other approach[3], preferred in flight test, makes $C_{n_{\delta_r}}$ positive since positive control deflections are defined as those which produce a positive moment about the axis in question. The reader is cautioned to take careful note of the method used to assign positive signs to the control deflections in any literature studied.

Steady sideslips lead to a simple method for measuring rudder power. During any steady sideslip the rudder deflection itself is proportional to the ratio of the weathercock stability C_{n_β} to $C_{n_{\delta_r}}$, as can be readily deduced from eqn. 8.3 by solving for δ_r and then taking the partial derivative with respect to β. The result is

$$\frac{\partial \delta_r}{\partial \beta} = -\frac{C_{n_{\beta\ fixed}}}{C_{n_{\delta_r}}} \tag{8.5}$$

where the "*fixed*" subscript simply emphasizes that the rudder is not free to float.

Recalling that the signs for C_{n_β} and $C_{n_{\delta_r}}$ are both positive using the "flight test convention" eqn. 8.5 and Fig. 8.2 illustrate that the slope of the rudder deflection versus sideslip curve must be positive under this convention for static directional stability to exist.

Example 8.1: A small business jet with a conventional (reversible) control system has the following lateral-directional control derivatives: $C_{\mathcal{L}_{\delta_a}}$ = - .065/rad; $C_{n_{\delta_a}}$ = 0.00005/rad; $C_{\mathcal{L}_{\delta_r}}$ = -0.00001/rad; $C_{n_{\delta_r}}$ = 0.005/rad.

Sideslip (°)	Aileron (°)	Rudder (°)
-4.50	3.12	34.98
-4.02	2.78	31.21
-2.03	1.41	15.82
0.01	0.04	-0.02
2.04	-1.40	-15.48
3.99	-2.77	-31.22
4.51	-3.11	-35.02

For a series of steady, straight sideslips at 30,000 feet and a Mach number of 0.55, the following set of aileron and rudder deflections were measured. Assuming $C_{\mathcal{L}_{\delta_a}}$ and $C_{n_{\delta_r}}$ are much larger than $C_{\mathcal{L}_{\delta_r}}$ and $C_{n_{\delta_a}}$, calculate approximate values of the stick-fixed directional stability and the dihedral effect at these flight conditions.

From the data given, approximate slopes are:

$\frac{\partial \delta_r}{\partial \beta}$ = - 7.8 /rad and $\frac{\partial \delta_a}{\partial \beta}$ = 0.69 /rad.

Using equation 8.5 and its counterpart for dihedral effect:

$$C_{\mathcal{L}_\beta} = -0.045 \text{ / rad}$$

$$C_{n_\beta} = 0.039 \text{ / rad}$$

8.1.1.3 **Effect of a Freely Floating Rudder.** The rudder hinge moment coefficient is approximated by specializing eqn. 6.10 (for a symmetric airfoil and no tab deflection).

$$C_h = C_{h_{\alpha_F}} \alpha_F + C_{h_{\delta_r}} \delta_r \tag{8.6}$$

The rudder float angle is obtained by setting C_h to zero and solving eqn. 8.6 for $\delta_{r_{free}}$.

$$\delta_{r_{free}} = -\frac{C_{h_{\alpha_F}} \alpha_F}{C_{h_{\delta_r}}} \tag{8.7}$$

Defining a_r like a_e in section 6.1.2.3; that is, $a_r = \left(\frac{\partial C_Y}{\partial \delta_r}\right)_{trim}$ and $C_{Y_{\delta_r}} = a_r \frac{S_V}{S}$. The vertical tail side force coefficient is given by

$$C_{Y_F} = C_{Y_{\alpha_F}} (-\beta + \sigma) + a_r \delta_r ; \tag{8.8}$$

so, eqn. 8.7 and the definition $\varphi_F \quad -\dagger +$ can be used to eliminate δ_r for rudder free conditions (again using a prime to denote a floating surface).

$$C'_{Y_F} = C_{L_{\alpha_F}} \alpha_F - a_r \frac{C_{h_{\alpha_F}}}{C_{h_{\delta_r}}} \alpha_F = C_{L_{\alpha_F}} \alpha_F \left(1 - \frac{a_r C_{h_{\alpha_F}}}{C_{L_{\alpha_F}} C_{h_{\delta_r}}}\right) \tag{8.9}$$

8.1.1.4 **Yawing Moment Due to Lateral Control.** The yawing moment due to aileron (for conventional airplanes) is often called a ***cross-coupling*** derivative because it produces a moment about an axis other than the one for which it is primarily intended. Aileron deflection is used to produce rolling moment, but inevitably it also produces yawing moment as a secondary effect. Lateral control devices generally cause a rolling moment by creating an unbalanced lift about the plane of symmetry. For conventional ailerons the half of the wing with the higher lift will also have higher induced drag, producing a yawing couple about the z axis. Of course, deflecting a surface like an aileron also produces a change in profile drag. For conventional ailerons at subsonic flight conditions, induced drag usually dominates and the yawing moment produced by deflecting ailerons is opposite to the desired direction of roll. The effect is then called adverse yaw; $C_{n_{\delta_a}}$ is negative for this case. If profile drag predominates, as it usually does at supersonic speeds for a conventional aileron surface, $C_{n_{\delta_a}}$ is positive. The effect is then called proverse or complementary yaw. It is desirable for $C_{n_{\delta_a}}$ to be zero or even slightly positive; designers may go to considerable lengths to achieve this goal.

8.1.2 Lateral Stability and Control

The rolling moment equation is the one aircraft moment equation for which there is no natural stability. That is, an angular displacement in bank angle produces no tendency to return to an equilibrium bank angle. This state of affairs is in contrast to the tendency to return to a static equilibrium angle of attack when displaced in pitch about the y axis or to the equilibrium sideslip angle (usually zero) when displaced about the z axis. The natural tendency about the x axis is to return to a zero roll rate, but not to an equilibrium bank angle. It is, however, desirable to return to wings level flight after a small bank disturbance

for most purposes: this characteristic is the only sense in which we can speak of lateral "stability." The dominant term in eqn. 8.2 is C_{ℓ_β}, which produces this effect.

8.1.2.1 **Dihedral Effect**. Dihedral effect or C_{ℓ_β} is affected most by the geometric dihedral and/or by the sweep angle of the wing. Both Etkin[1] and Roskam[2] (and many other texts) give excellent discussions of the physical mechanisms that cause this "wings-leveling" phenomenon. Wing-body aerodynamic interference also increases or decreases dihedral effect, depending on the vertical placement of the lifting surfaces on the fuselage. A high wing produces an increment of rolling moment that returns the airplane to wings level when sideslip occurs and a low wing gives the opposite effect. Finally, the vertical tail also contributes an increment in C_{ℓ_β} that depends primarily on the size of the vertical tail and the vertical tail moment arm. This moment arm changes with angle of attack and, for large angles of attack, can reverse the sign of this increment. Secondary factors that may affect C_{ℓ_β} include aspect ratio, taper ratio, external tanks, and wing flaps. Again, Roskam's discussion of the individual contributions to C_{ℓ_β} and his illustrations of typical variations with Mach number will be valuable to the interested student.

8.1.2.2 **Lateral Control Power**. The most common lateral control devices are ailerons, although spoilers and differential horizontal tail deflection are also common. Differential elevons, seen frequently on tailless designs, are similar in principle to ailerons. Ailerons, the most representative of lateral control surfaces, produce a roll command different to either the rudder or the elevator. In fact all forms of lateral control mentioned result in a rate of roll (rate command) instead of an angular displacement. Lateral control power, $C_{\ell_{\delta_a}}$, is negative using either the sign convention suggested by Etkin[1] or the flight test approach. That is, a positive aileron deflection (right aileron up) produces a positive rolling moment because of the decreased lift produced over the right wing and the increased lift produced over the left wing. The exact value of the lateral control power (or aileron effectiveness as used by some texts) is difficult to estimate accurately and wind tunnel testing is usually in order. An expression[3] relating aileron control power to airfoil section (after aileron deflection), ratio of the area of the control surface to the area of the wing, and the location of the wing center of pressure along the span is given by

$$C_{\ell_{\delta_a}} = \frac{C_{L_{\alpha_a}} S_a y}{Sb} \tag{8.10}$$

where $C_{L_{\alpha_a}}$ is the lift curve slope with the ailerons deflected and y is the distance from the airplane x axis to the wing center of pressure, again with ailerons deflected.

8.1.2.3 **Rolling Moment Due to Directional Control**. Another of the cross-coupling derivatives is $C_{\ell_{\delta_r}}$, the rolling moment coefficient produced by deflection of the rudder. Simply stated, this derivative is the non-dimensional rolling moment resulting from the side force generated by the rudder multiplied by the non-dimensional moment arm measured from the reference body axis up to the center of side force on the vertical tail. Because it is measured from the reference x axis (trim condition), this length is a function of the perturbed angle of attack.

$$C_{\mathcal{L}_{\delta_r}} = \frac{C_{Y_{\delta_r}} z_V}{b} \tag{8.11}$$

Because of this dependence on z_v, $C_{\mathcal{L}_{\delta_r}}$ decreases with increasing C_L.

8.1.3 Lateral-Directional Matrix Equations

The static lateral-directional equations (8.3 and 8.4 plus the side force equation) can be expressed more compactly in matrix form. The aerodynamics are clearly coupled, unlike the static longitudinal case. Of the four control derivatives in equation 8.12, only the side force derivatives, $C_{Y_{\delta_a}}$ and $C_{Y_{\delta_r}}$, are negligible for most airplanes.

$$\begin{pmatrix} C_Y \\ C_{\mathcal{L}} \\ C_n \end{pmatrix} = \begin{pmatrix} C_{Y_\beta} & C_{Y_{\delta_a}} & C_{Y_{\delta_r}} & C_L \\ C_{\mathcal{L}_\beta} & C_{\mathcal{L}_{\delta_a}} & C_{\mathcal{L}_{\delta_r}} & 0 \\ C_{n_\beta} & C_{n_{\delta_a}} & C_{n_{\delta_r}} & 0 \end{pmatrix} \begin{pmatrix} \beta \\ \delta_a \\ \delta_r \\ \Phi \end{pmatrix} \tag{8.12}$$

Another complicating factor, from the stability and control test engineer's perspective, is that the lateral control (δ_a) is of a different type than the directional control (δ_r). The rudder, like the elevator, is a control that commands displacement; that is, the rudder is used to command an angular position. On the other hand, the ailerons are used to command an angular rate; they are rate controls. This difference means that different sensors are needed to measure the effectiveness of each type of control. In fact, measurement of the primary usefulness of the lateral control cannot be measured by static means. A dynamic test method (described in Chapter 9) must be used.

These facts mean that static lateral-directional flight tests are slightly more difficult to conduct than longitudinal ones. There are at least twice as many parameters to be recorded simultaneously for these tests as was the case for static longitudinal measurements. Automated data collection, therefore, becomes more desirable.

8.2 STEADY STATE FLIGHT TEST METHODS

Requirements for lateral-directional static stability handling qualities vary considerably from civil to military specifications, as do longitudinal requirements. Of course, the prudent flight test engineer should be less concerned with the requirement and more interested in insuring that the design being tested is safe to fly and easily controlled by the typical pilot who will fly the machine. The requirements are merely guides which try to insure that minimum standards are met. Any design is a compromise pitting these good handling qualities against the pragmatic and very real need to produce a cost-effective airplane. This compromise is evaluated in every flight test, but lateral-directional requirements are particularly subjective.

FAR requirements[9,10] illustrate this subjectivity:

(1) The static directional stability, as shown by the tendency to recover from a skid with the rudder free, must be positive for any landing gear and flap position appropriate to the takeoff, climb, cruise, and approach configurations. This must be shown with symmetrical power up to a maximum continuous power, and at speeds from $1.2V_{S_1}$ up to the maximum allowable speed for the condition being

investigated. The angle of skid for these tests must be appropriate to the type of airplane. At larger skid angles up to that at which full rudder is used or a control force limit in Part 23.143 is reached, whichever occurs first, and at speeds from $1.2V_{S_1}$ to V_A, the rudder pedal force must not reverse.

(2) The static lateral stability, as shown by the tendency to raise the low wing in a slip, must be positive for any landing gear and flap positions. This must be shown with symmetrical power up to 75% of the maximum continuous power at speeds above $1.2V_{S_1}$, up to the maximum allowable speed for the configuration being investigated. The static lateral stability may not be negative at $1.2V_{S_1}$. The angle of slip for these tests must be appropriate to the type of airplane, but in no case may the slip angle be less than that obtainable with 10° of bank.

(3) In straight, steady slips at $1.2V_{S_1}$ for any landing gear and flap positions, and for any symmetrical power conditions up to 50% maximum continuous power, the aileron and rudder control movements and forces must increase steadily (but not necessarily in constant proportion) as the angle of slip is increased up to the maximum appropriate to the type of airplane. At larger slip angles up the angle at which the full rudder or aileron is used or a control force limit contained in Part 23.143 is obtained, the rudder pedal force may not reverse. Enough bank must accompany slipping to hold constant heading. Rapid entry into, or recovery from, a maximum slip may not result in uncontrollable flight characteristics.

FAR Part 23.177a

Static lateral stability must be positive; meaning that dihedral effect C_{l_β} must be negative. There must be a wing-leveling tendency when sideslip is generated. Observe also that these requirements cover virtually the entire flight envelope, including the speed range just above stall up to maximum allowable speed and reasonable configurations. It should strike you that demonstrating compliance with these requirements can take an enormous amount of flight test time! You should also be impressed with how nonspecific the adjectives are and how much room that leaves for interpretation by individual FAA inspectors.

The requirements for transport category airplanes is rather similar:

(a) The static directional stability (as shown by the tendency to recover from a skid with the rudder free) must be positive for any landing gear and flap position and symmetrical power condition, at speeds from V_{S_1} up to V_{FE}, V_{LE}, or V_{FC}/V_{MC} (as appropriate).

(b) The static lateral stability (as shown by the tendency to raise the low wing in a sideslip with the aileron controls free and for any landing gear and flap position and symmetrical power condition) must be positive at V_{FE}, V_{LE}, or V_{FC}/V_{MC} (as appropriate).

(c) In straight, steady sideslips (unaccelerated forward slips) the aileron and rudder control movements and forces must be substantially proportional to the angle of sideslip, and the factor of proportionality must lie between limits found necessary for safe operation throughout the range of sideslip angles appropriate to the operation of the airplane. At greater angles, up to the angle at which full rudder control is used or a pedal force of 180 pounds is obtained, the rudder pedal forces may not reverse and increased rudder deflection must produce increased

angles of sideslip. Unless the airplane has a yaw indicator, there must be enough bank accompanying sideslipping to clearly indicate any departure from unyawed flight. FAR Part 25. 177

The military specification[11] that spells out static lateral-directional requirements is a bit more specific. Like the FAR, rudder deflection or force must produce sideslip opposite to the direction of applied directional control to meet the military specification. In addition the rudder forces and rudder deflections must remain linear for ±10° and ±15° sideslip, respectively. The military document also limits maximum allowable rudder pedal force to 250 pounds for maximum rudder deflection at any point in the envelope. Furthermore, in a steady sideslip, aileron deflection in the same direction as sideslip must accompany the rudder requirements. The wing-leveling tendencies due to dihedral effect shall not be so strong that more than 75% of roll control power nor more than 10 or 20 pounds (depending on the whether the lateral controller is a stick or a wheel) of force are required in normal use. These examples illustrate the quantified requirements incorporated into the military handling qualities requirements, though they are not all the considerations for such lateral-directional tests. The responsible flight test engineer will carefully study and analyze all applicable requirements documents for complete details during the test planning phase.

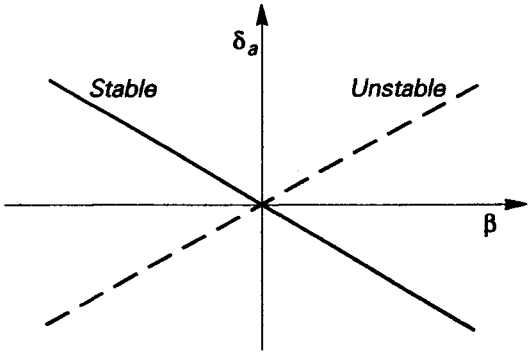

Fig. 8.3 Aileron Deflection versus Sideslip

From this discussion of typical static-lateral directional requirements and from the theoretical considerations discussed in section 8.1, it is clear that the measures of merit used in such flight tests are closely tied to control forces and surface deflections. Van der Maas[7] refers to this approach to measuring stability as ***control position*** stability. Qualitatively, Figs. 8.2 and 8.3 indicate the relationship between control surface deflections and sideslip that are expected for a subsonic airplane with acceptable controls-fixed lateral-directional characteristics. Similar sketches could be drawn for aileron and rudder forces as a function of sideslip with the controls-free (vehicles utilizing reversible flight control systems). Of course, controls-free stability considerations have no meaning for a fully powered (irreversible) control system like the ones on most high performance fighters.

8.2.1 Test Methods to Determine Dominant Stability Coefficients

The basic test method is the steady, straight sideslip -- a classical, proven way to determine static directional stability and dihedral effect from a single maneuver. It depends, though, on prior knowledge of the control derivatives like $C_{\mathcal{L}_{\delta_a}}$ and $C_{n_{\delta_r}}$. Like any other

stability and control testing, the method also demands appropriate instrumentation, careful attention to trim, and precise control of airspeed and altitude. Because data are collected point by stabilized point in the steady, straight sideslip technique, it takes a lot of flying time to completely explore the flight envelope for all configurations of a given airplane. Consequently, ***slowly varying*** methods are also used to speed up the process. Both methods will be discussed in the following paragraphs.

8.2.1.1 **Steady, Straight Sideslips**. The classical steady, state test method is commonly used to obtain measures of $C_{\ell_{\delta_a}}$ and $C_{n_{\delta_r}}$ for all classes of airplanes. The standard data collection technique is fairly efficient for most airplanes and flight conditions and therefore needs modification. Simplicity is its strength.

Setting up for this maneuver is essentially the same as for other stability tests. After leveling off at the nominal test altitude the test pilot must trim the airplane with the usual care for stability and control data. To check the trim prior to taking data, he should release the controls and the airplane's airspeed and altitude should not change for at least 10 seconds. The control surface positions and forces at these trim conditions should be recorded just before starting the maneuver. Sideslip limits for the flight conditions must be meticulously observed; they should be reviewed in the preflight briefing and, if the instrumentation and ground support include real time read outs, this parameter should be monitored as a flight safety item. Exceeding sideslip limits has caused loss of control and even structural damage in the past. Though steady, straight sideslips are not normally considered hazardous tests, normal prudence should be exercised.

In this test maneuver data are collected at constant, stabilized headings. The pilot should choose a reference point on the distant visual horizon and use it to fly a stabilized heading for each individual point (sideslip angle). Rudder and aileron are applied, essentially simultaneously, to set up a stabilized sideslip. This ***cross-controlled*** condition is an unnatural piloting technique; the rudder is normally used to maintain zero sideslip in all maneuvers. Using rudder and aileron in opposite directions, particularly at large sideslip angles, gives the pilot a sensation of "sliding sideways in the seat" due to the lateral forces that are applied. These unusual sensations and unnatural control applications mean that the pilot must concentrate carefully on setting up the conditions and maintaining them. Crosschecking the point chosen on the visual horizon along with the cockpit instruments for constant heading and bank angle should allow the pilot to determine when he has achieved a steady, stabilized sideslip. When equilibrium conditions have been attained, the data system should be turned on to record altitude, airspeed, sideslip angle, bank angle, control surface deflections (aileron, rudder, and elevator), and control forces for all three axes. From such data, plots like Figs. 8.2 and 8.3 can be constructed and, assuming the control power derivatives are known, $C_{\ell_{\delta_a}}$ and $C_{n_{\delta_r}}$ can be calculated from slopes $\frac{\partial \delta_a}{\partial \beta}$ and $\frac{\partial \delta_r}{\partial \beta}$ of the curves.

8.2.1.2 **Slowly Varying Sideslips**. As was indicated earlier, the pure steady, straight sideslip method can be time-consuming and is often modified to make the data collection more efficient. The time saving is largely achieved by changing the sideslip conditions continuously rather than stabilizing at each rudder/aileron position. Trimming is done the same as for the stabilized method and the pilot must still pick out a point on the distant horizon and maintain a constant path toward it. But, at this point the technique changes.

Rudder and opposite aileron are blended in slowly and in concert so that a constant track is maintained. To acquire the data, automatic recording of some form must be used and the data are collected continuously. The slowly varying method obviously saves time if ϯ does not change too rapidly (no more than about 1 °/second is a good rule of thumb) and if the test pilot can maintain the proper integrated rate of change of rudder and aileron to give constant track. Such a dynamic maneuver is harder to fly than the stabilized one and, when conditions are not carefully maintained, the point must be flown again. Naturally, such repetitions eliminate the advantage of the method. But, the potential for saving significant amounts of flight test time favors the slowly varying technique and it is probably the most common way to collect static lateral-directional data.

8.2.1.3 **Steady Turns with Rudder Fixed**. This flight test technique, though no longer widely used since parameter estimation techniques have become popular, offers the advantage of simplicity and relatively uncomplicated instrumentation requirements. For our purposes, it is a useful way to teach the fundamentals of such measurements.

As always, the airplane must be carefully trimmed at the desired altitude and airspeed conditions. The pilot then holds the rudder at the trim position and banks the airplane using the lateral control alone. This bank should be entered slowly since a steady sideslip and bank angle is sought and too abrupt an aileron (or lateral control) input may induce a Dutch roll oscillation that hinders data collection. Once equilibrium has been attained, δ_a, δ_r, F_a, F_r, ϕ, β, and r are recorded, preferably with some form of automatic recording instrumentation. Sensors for measuring each of these quantities must be provided. The procedure is repeated at several increments in bank angle and the same parameters are recorded at each test point. Care must be taken not to exceed sideslip limits and it may become increasingly difficult to maintain airspeed and remain within 1000 feet of the nominal test altitude at larger bank angles. The elevator should be used to control airspeed but care must be taken to not introduce spurious lateral control movements while making corrections with the elevator. Measurements should be made during turns in either direction.

Data from these tests are plotted to obtain trim curves of δ_a and F_a versus bank angle and plots of β and ϕ as functions of nondimensional yaw rate $\frac{rb}{2V}$. These plots can be used to calculate the damping derivative C_{n_r}, though we will pursue this data reduction.

8.2.1.4 **Steady Turns with Ailerons Fixed**. This test method is essentially identical to the one discussed in the preceding section, except that the turns are commanded by rudder alone and information is measured to calculate $C_{\mathcal{L}_r}$ rather than C_{n_r}. Again, we will not pursue this damping cross derivative further in this introductory text.

8.2.1.5 **Use of Steady Sideslip Data**. The basic steady sideslip flight test technique is a very useful one. Obviously, it provides a quick, but accurate assessment of the static lateral-directional stability of the airplane. In addition steady sideslip data can be used to measure the rudder control power derivative $C_{n_{\delta_r}}$ and the aileron control power derivative $C_{\mathcal{L}_{\delta_a}}$, as we will illustrate more completely in the next section. To obtain additional information, like these control derivatives, the flight test planner must often add equipment or devise means of applying known external moments. But, the usefulness of such a simple test is remarkable.

8.2.2 Test Methods to Determine Control Effectiveness

Measuring the effectiveness of the controls is one of the more important purposes of static lateral-directional flight tests. Since the rolling and yawing moment equations are so tightly coupled, these tests are also some of the more difficult to conduct with certainty. There are methods that utilize movement of the vertical position of the cg to measure aileron effectiveness but they are not very accurate and, consequently are not in general use[8]. We will ignore them, too. However, steady, straight sideslips at differing longitudinal c.g. locations can produce rudder control effectiveness data that are usable. A second approach that will be discussed for measuring $C_{n_{\delta_r}}$ involves the use of a parachute at a known location on the wing. If the parachute's drag coefficient is also known, the resulting drag force can be calculated. The rudder necessary to overcome this known yawing moment is a direct measure of its effectiveness. Similarly, an asymmetric moment can be applied about the roll axis by positioning a weight at a known spanwise location and measuring the aileron deflection necessary to counteract it in equilibrium flight. This latter method is straightforward and is quite accurate since it can involve no change in drag other than the induced drag due to deflection of the aileron. Obviously, all these tests still take into account the coupling between lateral and directional modes.

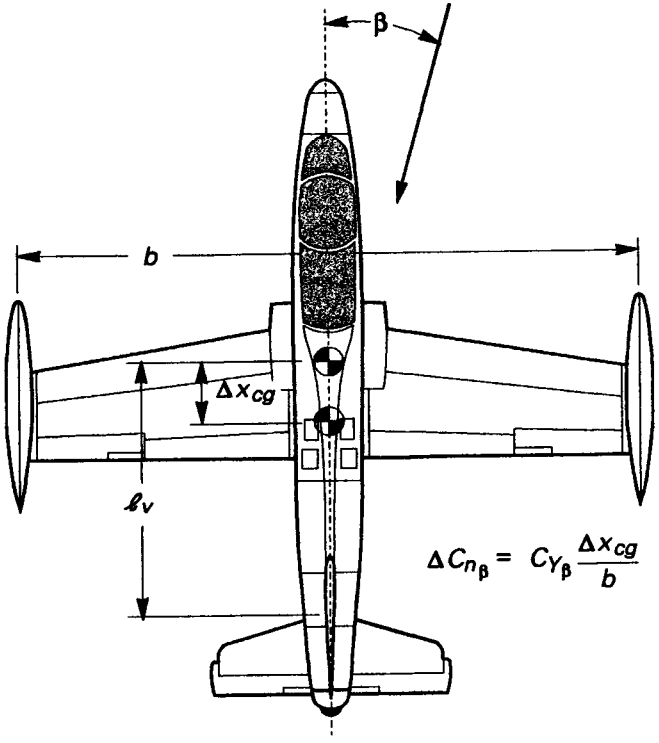

Fig. 8.4 Effect of cg Shift on C_{n_β}

8.2.2.1 **Steady, Straight Sideslips at Different C.G. Locations**. In eqns. 8.12 we can usually ignore the effect of aileron (or other lateral controls) on the side force. If the rudder side force term can be neglected and ϕ is small, the equations reduce to:

$$\begin{pmatrix} C_Y \\ C_{\mathcal{L}} \\ C_n \end{pmatrix} = \begin{pmatrix} C_{Y_\beta} & 0 & 0 & C_L \\ C_{\mathcal{L}_\beta} & C_{\mathcal{L}_{\delta_a}} & C_{\mathcal{L}_{\delta_r}} & 0 \\ C_{n_\beta} & C_{n_{\delta_a}} & C_{n_{\delta_r}} & 0 \end{pmatrix} \begin{pmatrix} \beta \\ \delta_a \\ \delta_r \\ \Phi \end{pmatrix} \tag{8.13}$$

If we now fly a series of steady, straight sideslips covering a range of β, equations 8.13 can be written and solved for each of the flight conditions. If we move the c.g. location between two such series of steady, straight sideslips, the only aerodynamic coefficients that change significantly are C_{n_β} and $C_{n_{\delta_r}}$. As long as the tail moment arm is large compared to the shift in c.g. location, $C_{n_{\delta_r}}$ is also essentially independent of c.g. position. The change in C_{n_β} can be calculated from (using the geometry of Fig. 8.4, page 172):

$$C_{n_{\beta_2}} = C_{n_{\beta_1}} + C_{Y_\beta} \frac{\Delta x_{cg}}{b} \tag{8.14}$$

Using equations 8.13 and the slopes $\frac{\partial \phi}{\partial \beta}$ and $\frac{\partial \delta_r}{\partial \beta}$ from the series of steady, straight sideslips, C_{Y_β} can be calculated:

$$C_{Y_\beta} = -C_L \frac{\partial \phi}{\partial \beta} \tag{8.15}$$

The slopes $\frac{\partial \phi}{\partial \beta}$ and $\frac{\partial \delta_r}{\partial \beta}$ are usually independent of cg location, but it is good practice to check this assumption by taking sideslip data at several cg positions. Eliminating the side force equation, any two sideslip conditions can be evaluated using

$$C_{n_{\beta_2}} = C_{n_{\delta_a}} \left(\frac{\partial \delta_a}{\partial \beta}\right)_2 + C_{n_{\delta_r}} \left(\frac{\partial \delta_r}{\partial \beta}\right)_2 = 0 \quad \text{and} \quad C_{n_{\beta_1}} = C_{n_{\delta_a}} \left(\frac{\partial \delta_a}{\partial \beta}\right)_1 + C_{n_{\delta_r}} \left(\frac{\partial \delta_r}{\partial \beta}\right)_1 = 0$$

Defining $\Delta C_{n_\beta} = C_{n_{\beta_2}} - C_{n_{\beta_1}}$ and observing that the aileron slope change with sideslip is usually quite small,

$$\Delta C_{n_\beta} + C_{n_{\delta_r}} \left(\left(\frac{\partial \delta_r}{\partial \beta}\right)_2 - \left(\frac{\partial \delta_r}{\partial \beta}\right)_1 \right) \approx 0 \tag{8.16}$$

If the moment arm for the vertical tail (distance the center of pressure of the vertical tail is above the c.g. for an aft tail airplane) is established, $C_{Y_{\delta_r}}$ can be estimated from the value of $C_{n_{\delta_r}}$ calculated from eqn. 8.16:

$$C_{Y_{\delta_r}} = -C_{n_{\delta_r}} \frac{b}{\ell_V} \tag{8.17}$$

The data reduction for this test is very straightforward, though the flying can be tedious because it is not always easy to alter the longitudinal c.g. location in flight. Rudder deflection and bank angle are plotted as functions of sideslip angle as they are for all sideslip tests. At $\beta = 0$ the slopes of these curves are obtained and C_L is calculated for

the test conditions and the test weight. The slopes $\frac{\partial \delta_r}{\partial \beta}$ and $\frac{\partial \phi}{\partial \beta}$ are plotted for each cg location. Then, C_{Y_β}, $C_{n_{\delta_r}}$ and $C_{Y_{\delta_r}}$ are computed from eqns. 8.15, 8.16, and 8.17.

This test method is rather cumbersome and is only moderately accurate. A large number of sideslip points are required to credibly establish the small differences that determine the slopes of the measured variables. These differences come from two relatively large numbers so the information is highly uncertain. The technique is not often used because of the test time needed to acquire the data.

8.2.2.2 **Yawing Moment Produced by a Wing Parachute**. The second method of directly measuring rudder effectiveness is also cumbersome to use. It is, of course, imperative that the parachute can be deployed in flight and jettisoned after the data are taken. Safety concerns can become hazards if care is not taken to ensure that parachute deployment and jettison is completely reliable. Uncertainty added to the process because few parachutes are completely stable after deployment.

Typical installations for a wing parachute are sketched in Fig. 8.5 on the next page. Figure 8.5b shows one possible way to provide some stability for the parachute, especially when the wing tip vortex excites the oscillations. The more simplistic (and less practical hardware configuration) is illustrated in Fig. 8.5a. The simpler installation gives the incremental yawing moment created by the parachute as:

$$\Delta N = T\ell \tag{8.18}$$

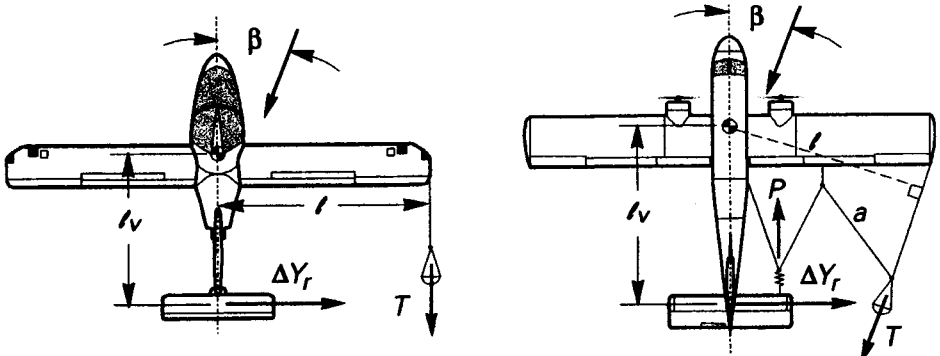

(a) *Direct Measurement of Parachute Force*

(b) *Indirect Measurement of Parachute Force*

Fig. 8.5 Wing Parachute Installations

The measurements can be made and the results expressed in terms of x_{cg}, a, and the force P rather than direct measurements like T and ℓ. If this arrangement is used, Van der Maas suggests taking data at several different tether cable lengths.

The condition for equilibrium at zero sideslip (eqns. 8.13) is simply $\Delta C_n = C_{n_{\delta_r}} \Delta \delta_r$, where ΔC_n is the incremental yawing moment coefficient.

A known ΔC_n is provided by the parachute since it can be calculated from the parachute's drag coefficient and the moment arm in Fig. 8.5a. Of course, the parachute force can be measured directly (further complicating the instrumentation scheme) with either a

force gage in parachute riser or in the tether cable as suggested in Fig. 8.5a. But by definition ΔC_n is also

$$\Delta C_n = \frac{\Delta N}{\bar{q} S b}$$

and a direct calculation of rudder effectiveness is then possible. The rudder side force coefficient follows from eqn. 8.17 with the required rudder control effectiveness given by:

$$C_{n_{\delta_r}} \approx \frac{\Delta C_n}{\Delta \delta_r}$$

The piloting technique for these tests is that described for the steady, straight sideslip method. Care must be taken to avoid oscillations and, if the Dutch roll oscillation is not well damped for the airplane, it may be difficult to stabilize the parachute. Safety procedures should be carefully rehearsed in advance. Clearly, this test is one of the those which might benefit enormously from flight simulation of the planned profiles and careful evaluation of possible emergency procedures on an engineering flight simulation.

8.2.2.3 **Measurements with Weights at Known Spanwise Locations**. A technique similar to the one described above can be used to measure lateral control effectiveness. Like most other static lateral-directional tests, this one also involves flying a series of steady, straight sideslips. An unbalanced rolling moment is generated by positioning a weight at a known spanwise location. If the airplane can carry fuel in tanks that provide an adjustable and precisely known lateral imbalance, there is no need to install special stores or to add weights than can alter the flutter characteristics of the vehicle. How to achieve the known lateral imbalance and still guarantee adequate handling qualities during landing and takeoff is a practical issue of significance to the test planner. Aileron and rudder deflections (and the corresponding control forces) required to balance the known asymmetric rolling moment are measured over a range of sideslips.

At zero sideslip the equilibrium condition suggested by eqns. 8.13 reduces to:

$$\Delta C_{\mathcal{L}} = C_{\mathcal{L}_{\delta_a}} \Delta \delta_a ,$$

giving an expression that allows direct calculation of the aileron control effectiveness from measurement of $\Delta C_{\mathcal{L}}$ and $\Delta \delta_{a_r}$:

$$C_{\mathcal{L}_{\delta_a}} \approx \frac{\Delta C_{\mathcal{L}}}{\Delta \delta_a} \qquad (8.19)$$

At the same time the aileron deflection produces an increment in yawing moment that must be counteracted by the rudder.

$$C_{n_{\delta_a}} \Delta \delta_a + C_{n_{\delta_r}} \Delta \delta_r = 0$$

From this equilibrium expression it follows that

$$C_{n_{\delta_a}} \approx -C_{n_{\delta_r}} \frac{\Delta \delta_r}{\Delta \delta_a} \qquad (8.20)$$

Pilot procedures for this test are no different from those described for other steady, straight sideslip tests. Most of the care to be exercised is associated with fuel transfer or stores jettisoning to attain the desired lateral imbalance. At least two different measurable

lateral cg positions must be tested. Three or more such cg locations are necessary to check for nonlinearities in the estimated data.

Data reduction for this test is similar to previous ones. First, measured δ_a values are plotted against β. The slope of this curve at $\beta = 0°$ is needed, but measurements at other sideslips allow fairing of the δ_a - β curves and give a better estimate of the slope at zero sideslip. Then, with the rolling moment known, eqns. 8.19 and 8.20 allow direct calculation of the two aileron control derivatives $C_{n_{\delta_a}}$ and $C_{n_{\delta_r}}$.

8.2.3 Estimation of Stability Derivatives from Steady Lateral-Directional Tests

Having detailed tests that provide flight test estimates of the control effectiveness derivatives, let us briefly summarize how these static lateral-directional test measurements are used to confirm wind tunnel data and analytical estimates of these same derivatives.

First, the control effectiveness derivatives $C_{n_{\delta_a}}$, $C_{n_{\delta_r}}$, $C_{Y_{\delta_a}}$, and $C_{y_{\delta_r}}$ are determined from one or more of the control effectiveness tests described in section 8.2.2. With these values in hand the dominant lateral-directional stability derivatives, C_{ℓ_β} and C_{n_β} (along with the less important C_{Y_β}) are determined from plots of control surface deflections and forces measured at each of the sideslip angles. The resulting functional relationships, hopefully all linear for conventional airplanes, are experimentally determined in steady, straight sideslip tests or the slowly varying sideslip variation of the test. Next, the yaw rate derivatives, C_{ℓ_r} and C_{n_r}, are calculated from data recorded in steady turns initiated with aileron or rudder alone. In this fashion, nine of the most important lateral-directional parameters can be estimated with reasonable accuracy from essentially static tests.

8.3 SUMMARY

Static lateral-directional flight tests are slightly more complicated both in measurement techniques and in data reduction requirements than are their longitudinal counterparts. Coupling between the two relevant moment equations accounts for this complication. However, if control effectiveness derivatives are known or can be measured accurately with specially designed tests, simple steady, straight sideslip tests can reliably determine the dominant lateral-directional derivatives C_{ℓ_β} and C_{n_β}. While they are not as often conducted nowadays (since parameter estimation identification algorithms have become so widely used), steady turns using aileron or rudder alone also make it possible to straightforwardly estimate C_{ℓ_r} and C_{n_r}. All in all, these kinds of flight tests provide a wealth of information for a moderate amount of effort and rather minimal data reduction schemes. Their most serious drawback is that they do require more data collection time than some of the more modern techniques like parameter estimation. Of course, such techniques also need sophisticated instrumentation and they consume large amounts of digital computer time to extract the same stability coefficients.

REFERENCES

1 Etkin, B., **Dynamics of Flight: Stability and Control** (2nd Edition), John Wiley & Sons, New York, 1982.

2 Roskam, J., **Airplane Flight Dynamics and Automatic Controls, Part I**, Roskam Aviation and Engineering Corporation, Lawrence, Kansas, 1979.

3 "Stability and Control Flight Test Theory," Vol. I, Chapter 5, AFFTC-TIH-77-1, USAF Test Pilot School, Edwards AFB, California, Revised February 1977.

4 "Stability and Control Flight Test Techniques," Vol. II, Chapter 7, AFFTC-TIH-77-1, USAF Test Pilot School, Edwards AFB, California, Revised February 1977.

5 "Fixed Wing Stability and Control: Theory and Flight Test Techniques," USNTPS-FTM-No. 103, Naval Air Test Center, Patuxent River, Maryland, January 1975 (Revised November 1981).

6 Perkins, C. D., "Introduction," Chapter 1, Volume II, **AGARD Flight Test Manual**, Pergamon Press, New York, 1959.

7 Van der Maas, H. J., "Lateral and Directional Control and the Measurement of Aerodynamic Coefficients in Steady Asymmetric Flight and Flight on Asymmetric Power," Chapter 5, Volume II, **AGARD Flight Test Manual**, Pergamon Press, New York, 1959.

8 Hunter, P. A., "Flight Techniques Used to Determine Adequacy of Lateral Control," Chapter 6, Volume II, **AGARD Flight Test Manual**, Pergamon Press, New York, 1959.

9 "Airworthiness Standards: Normal, Utility, and Acrobatic Category Airplanes", FAR Part 23, Federal Aviation Administration, Washington, 1969.

10 "Airworthiness Standards: Large Commercial Transport Category Airplanes", FAR Part 25, Federal Aviation Administration, Washington, 1969.

11 "Military Specification, Flying Qualities of Piloted Airplanes", MIL-F-8785C, November 1980.

Chapter 9

DYNAMIC STABILITY TESTS

Flight testing to determine the dynamic stability of an airplane is even more complicated than the tests outlined in the previous three chapters for static stability tests. Although is it usually still possible to decouple the equations of motion for the longitudinal and the lateral-directional cases, the analysis is considerably more complicated. Dynamic stability, as the name implies, is concerned with the long-term effects of disturbances on the vehicle. It requires that we study the time-related behavior of the response of the dynamic system, not just its initial tendency after a disturbance from equilibrium. Anderson[1] has captured the essence of dynamic stability:

> A body is dynamically stable if, out of its own accord, it eventually returns to and remains at its equilibrium position over a period of time.

Static stability measurements are necessarily made with all forces and moments in equilibrium. Conversely, dynamic stability measurements, while they are usually initiated after carefully trimming the vehicle, must be made with the forces and moments not in equilibrium. Furthermore, measurement of these dynamic quantities must include some form of time correlation in order to have meaning.

Of course, dynamic stability is closely related to static stability. While an airplane can be statically stable without being dynamically stable, it cannot be dynamically stable without being statically stable. Moreover, dynamic stability testing is concerned with the ability that the vehicle affords the pilot (or controller) to change from one equilibrium condition to another. The speed and precision with which these changes can be made is determined by the characteristic modes of motion of the vehicle.

Dynamic stability is not the only concern of the flight test team engaged in this facet of flight testing. The handling qualities (sometimes called controllability) of a manned airplane are also of prime importance and many of the requirements that drive dynamic stability spring from the handling qualities as well. Again, both static and dynamic stability, along with the characteristics of the control system, the kind of airplane, and the task to be accomplished, determine the handling qualities of the airplane. Controllability has been defined in terms of what the pilot is tasked to do:

> **Controllability** may be defined as the capability of the airplane to perform, at the pilot's wish, any maneuvering required in total mission accomplishment[2].

However, controllability means something quite different to the controls engineer and the term handling qualities is to be preferred because of this ambiguity. From this discussion it should be clear that the handling qualities of any manned aircraft depend heavily on subjective assessments. Certainly most handling qualities requirements are based on pilot opinion[3].

Before the test team can measure the characteristics of such dynamic motions, it is essential that they have a thorough understanding of these and other terms, the modes of motion, and how to quantitatively define them. Let us turn now to laying the theoretical foundation for the measurement of these dynamic properties.

9.1 THEORETICAL FOUNDATIONS

To properly understand the dynamics of aerospace vehicles requires a brief return to the six degree-of-freedom equations of motion that have been developed in many textbooks[4,5,6] and to the definitions used to quantify the modes of motion. First, we need to fix the definition of certain terms used in dynamic flight analysis.

9.1.1 Definition of Terms and Assumptions

As stated in the introductory paragraphs, dynamic stability requires that the motion of a body ultimately return to its equilibrium position. There are at least two ways in which physical systems return to (or diverge from) equilibrium as shown in Fig. 9.1. The exponential decay (or divergence) is associated with a linear factor in the governing characteristic equation, while the damped (or divergent) oscillation is associated with a quadratic term in the characteristic equation. Of course it is also possible for oscillatory motion to be undamped and this condition implies neutral dynamic stability. Fortunately, all linear systems can be represented mathematically represented by a combination of either linear terms or quadratic terms in the characteristic equation; that is, the time-dependent solutions are linear combinations of either exponential decays or divergences and damped, neutrally damped, or divergent oscillations.

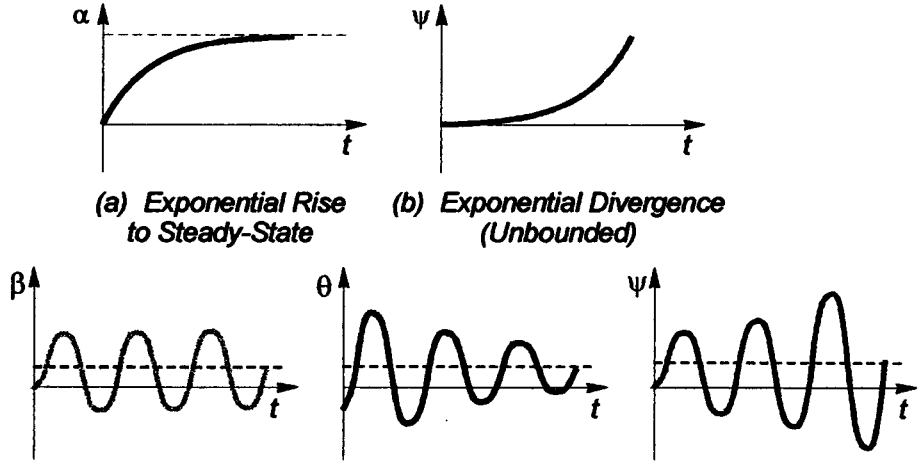

(a) Exponential Rise to Steady-State *(b) Exponential Divergence (Unbounded)*

(c) Undamped Sinusoid (Neutral Dynamic Stability) *(d) Damped Oscillation (Dynamically Stable)* *(e) Divergent Oscillation (Dynamically Unstable)*

Fig. 9.1 Possible Responses of Linear Dynamic Systems

Since any linear dynamic system can be represented by a combination of no more than second order factors, it is instructive to review the definitions used to describe the dynamic behavior of an airplane. Figure 9.2 depicts a spring-mass-damper system that we will use in making these definitions.

Mathematically the solution to the second order spring-mass-damper system is identical to solution of the airplane's longitudinal equations of motion. Only the constants change. The equation describing the spring-mass-damper system with no external forcing function is:

$m\ddot{x} + c\dot{x} + kx = 0$ and the characteristic equation is: $\lambda^2 + \frac{c}{m}\lambda + \frac{k}{m} = 0$ (9.1)

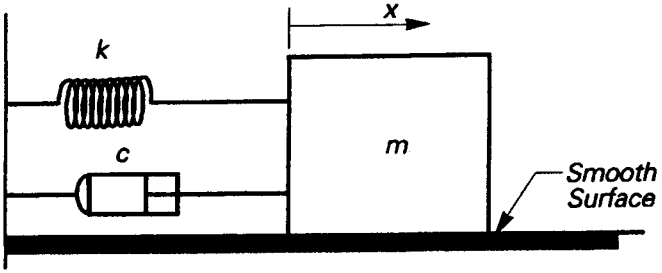

Fig. 9.2 Spring-Mass-Damper Analog

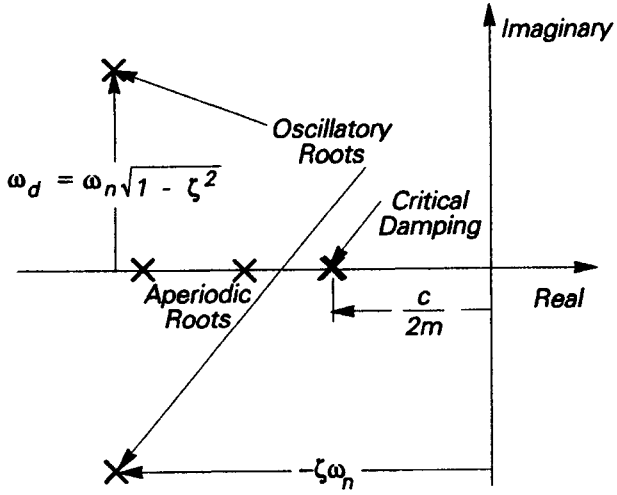

Fig. 9.3 Characteristic Roots in the Complex Plane

For the airplane's longitudinal analog of this motion one needs only to define the aerodynamic "spring" that corresponds to k and the damping terms that correspond to c. Typically, the stability derivative C_{m_α} adequately describes the aerodynamic "spring" and the pitch damping C_{m_q} relates to the damping coefficient c in the analogous aerodynamic system. The aircraft moment of inertia is the analog to the mass m in the simpler mechanical system.

To introduce additional definitions of interest in an airplane's dynamic behavior, let us now consider the roots of eqn. 9.1 and how they are affected by changes in $\frac{c}{m}$ and $\frac{k}{m}$. These roots are:

$$\lambda_{1,2} = -\frac{c}{2m} \pm \sqrt{\left(\frac{c}{2m}\right)^2 - \frac{k}{m}} \tag{9.2}$$

If $\left(\frac{c}{2m}\right)^2 > \frac{k}{m}$, the roots lie along the real axis in the complex plane (Fig. 9.3). This situation results in an exponential decay if a root is negative or an exponential divergence

if the root is positive. The time-domain behavior of such a root is illustrated in Fig. 9.1a. Other terms used to describe this type of dynamic behavior are **aperiodic** motion or deadbeat subsidence (for a negative root). A system that has a decaying exponential mode of motion is often referred to as **overdamped**. If the damping is reduced or if the spring constant is increased until $\left(\frac{c}{2m}\right)^2 = \frac{k}{m}$, the system is said to be **critically damped**. Critical damping is indicated on Fig. 9.3 by the point on the real axis where both real roots coincide: $\lambda_{1,2} = -\frac{c}{2m}$ at point *C*. The motion is still aperiodic at this point, but it is on a boundary. Any increase in $\frac{k}{m}$ or decrease in $\frac{c}{m}$ will produce a complex conjugate solution to the characteristic equation because $\left(\frac{c}{2m}\right)^2 - \frac{k}{m} < 0$. Physically, an oscillation will result. The characteristic equation can also be written in terms used to define oscillatory behavior and compared to eqn. 9.2,

$$\lambda_{1,2}^2 + 2\zeta\omega_n + \omega_n^2 = 0$$

which has the solution

$$\lambda_{1,2} = -\zeta\omega_n \pm \omega_n\sqrt{1-\zeta^2} \tag{9.3}$$

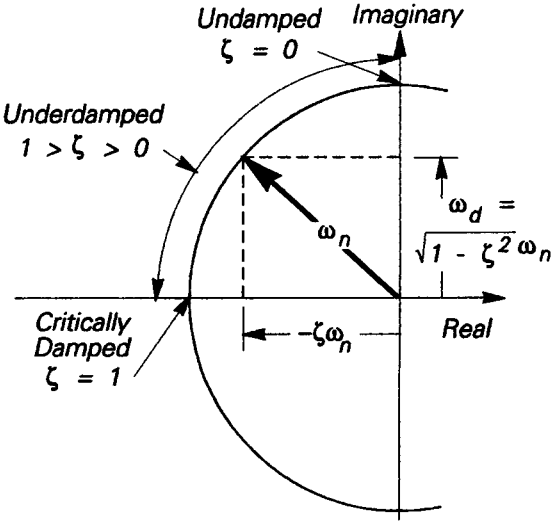

Fig. 9.4 Motion Parameters on the Complex Plane

The **damping ratio** ζ, which compares the actual damping to critical damping (Fig. 9.4), is a measure of how rapidly an oscillation decays or of how rapidly an exponential decay or divergence occurs. For critical damping, $\zeta = 1$. The system is said to be **underdamped** if $0 < \zeta < 1$ and undamped (or neutrally damped) if $\zeta = 0$. The **undamped natural frequency** ω_n is a measure of how often the peak amplitudes occur. The

damped frequency of the oscillation (which, strictly speaking, is not a frequency) is simply $\omega_d = \omega_n\sqrt{1-\zeta^2}$. (The time response is not purely periodic unless $\zeta = 0$. Consequently, ω is sometimes called a conditional frequency[7], indicating that it has the units and many of the properties of a frequency.) The **period** of the oscillation is $T = \frac{2\pi}{\omega_d}$. Each of these parameters is used to quantify the characteristics of oscillatory roots. The angle θ is measured from negative real axis to a line drawn from the origin in the complex plane to the characteristic root (or eigenvalue) in question. Therefore, this angle defines a vertical line of constant damping ratio. Clearly, a number of parameters associated with the modes of motion can be represented on the complex plane.

The transient response of the dynamic system to inputs also must be characterized in terms of "quickness" parameters and there are terms used that indicate both the speed with which the system responds and whether or not it reaches the ultimate value commanded by the input without exceeding or "overshooting" that value. The **steady state** (or new equilibrium) response of the system to an input is that value which the output will eventually reach. Typical steady state output responses to a step input are shown in Fig. 9.5. Generally, second order systems will show some oscillatory behavior as suggested by Fig. 9.5a. The **damping factor** $\zeta\omega$ is the real component of the characteristic root that controls the rate of rise or the rate of decay of the system response after an input. It appears as the constant in the exponential term of the time-domain solution of the system equations. As sketched in Fig. 9.5a, this constant defines the shape of the envelope bounding the peak amplitudes of the oscillation typical of second order dynamic system. The **time-to-half-amplitude** (or **time-to-double-amplitude** in the case of an oscillatory divergence) is the time required for the amplitude of the motion variable under consideration to change by a factor of two. The **time-to-peak-amplitude** t_p is the time required to reach the maximum amplitude of the output.

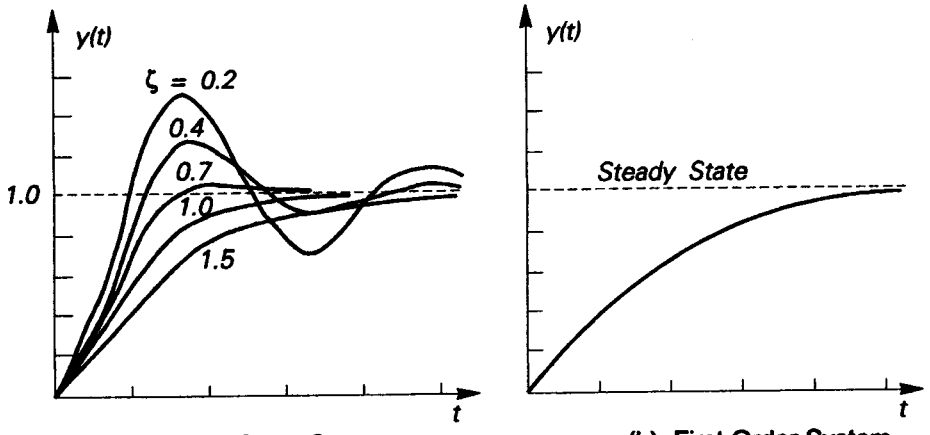

(a) Second Order System (b) First Order System

Fig. 9.5 Responses to a Step Input

Maximum overshoot (or peak overshoot) is the largest deviation of the output response to a step input during the transient motion and this amplitude is a strong indicator of the relative stability of the system. It indicates how precisely the system can move from

one equilibrium state to another. It follows that the **percentage maximum overshoot** is given by:

$$Percent\ Maximum\ Overshoot = \frac{maximum\ overshoot}{steady state} \times 100\%.$$

Settling time t_s is another parameter used to measure the transient behavior of a stable linear system. It is defined as the time required for the response to a step input to decrease and stay within a specified percentage of its steady state value. **Rise time** t_r is defined as the time required for the output to increase from 10% of its steady state value to 90% of its steady state value when the system is excited by step response. (An alternative approach sometimes used is to give the rise time the value of the reciprocal of the slope of the step response at the instant when the output is at 50% of its final value.) **Delay time** t_d is the time required for the output response to a step input to reach 50% of its final value.

All of these time measures of merit are related to the **time constant** τ. This characteristic is defined as the time to reach 63.2 per cent of the steady state value for this first order response (as shown in Fig. 9.5b) or for the envelope of the oscillatory peaks to reach the same value. This latter fact means we can still use our definition of the time constant for a second order response; it is still the real part of the root (and that is the only part for a first order system) that sets the rate of convergence or divergence. An instability or divergence implies a positive root. Note, though, that the damping factor as shown on the complex plane is a negative number for stable systems. Since ω is always positive, the damping ratio ζ is described as being negative when a positive real eigenvalue exists. Heuristically, this "negative" damping is an appealing way to describe a diverging system. (Again, strictly speaking, damping cannot be negative; but the terminology is widely accepted and understood.)

9.1.2 Equations of Motion

There are two approaches commonly used in the United States to approximately model the linear dynamic motions of an aircraft:. Both are based on Bryan's approach to linearizing the equations by assuming that the aerodynamic forces and moments can be adequately represented with a first order Taylor series expansion. (Etkin[4] correctly points out that this approach is mathematically flawed, specifically for cases where the aerodynamic forces and moments change abruptly or when the control surfaces are rapidly displaced, the first order approximation is inadequate. However, the transfer function approximation that Etkin suggests to replace Bryan's method has not been widely accepted and it depends on convergence of an infinite series that is not always mathematically well-behaved.) We will restrict our comments to the two formulations that use Bryan's approach, simply because it fits our purposes in this introductory text better than any other approach for two reasons: (1) the flight test engineer is more likely to be provided data based on Bryan's approach from wind tunnel and computational estimates and (2) the bulk of the experimental measurements he must make can be readily verified with this relatively simple linear model. These reasons are clearly pragmatic, rather than scientifically satisfying. Nonetheless, they are appropriate for introducing the flight test engineer to dynamic stability tests.

The first formulation utilizes dimensional equations that virtually every textbook on the subject of aircraft stability and control[4, 5, 6, 17] develop, often in excruciating detail. Table 9.1 below summarizes the results, using dimensional stability parameters.

Table 9.1 Linearized, Small Perturbation Equations Using Dimensional Parameters

Longitudinal Equations

$$\begin{aligned} su + W_0 q + g\theta\cos\Theta_0 &= X_u + X_w w + X_{\dot{w}}\, sw + X_q q + X_{\delta_e}\delta_e \\ sw + U_0 q + g\theta\sin\Theta_0 &= Z_u u + Z_w w + Z_{\dot{w}}\, ww + Z_q q + Z_{\delta_e}\delta_e \\ sq &= M_u u + M_w w + M_{\dot{w}}\, sw + M_q q + M_{\delta_e}\delta_e \end{aligned} \qquad (9.4)$$

Lateral-Directional Equations

$$\begin{aligned} sv + U_0 r - W_0 p - g\phi\cos\Theta_0 &= Y_v v + Y_{\dot{v}}\, sv + Y_p p + Y_r r + Y_{\delta_a}\delta_a + Y_{\delta_r}\delta_r \\ sp - \frac{I_{xz}}{I_x} sr &= \mathcal{L}_v v + \mathcal{L}_{\dot{v}} sv + \mathcal{L}_p p + \mathcal{L}_r r + \mathcal{L}_{\delta_a}\delta_a + \mathcal{L}_{\delta_r}\delta_r \\ sr - \frac{I_{xz}}{I_x} sp &= N_v v + N_{\dot{v}} sv + N_p p + N_r r + N_{\delta_a}\delta_a + N_{\delta_r}\delta_r \end{aligned} \qquad (9.5)$$

In Table 9.1 lower case letters (except for s, which is the Laplace operator) represent perturbed quantities; for example, $U = U_0 + u$, where the upper case symbols with the 0 subscript are the equilibrium (or trim) values for the parameter in question. It is assumed in the equations presented that $P_0 = Q_0 = R_0 = V_0 = 0$ and that all control surfaces are initially in the trail position ($\delta_{e_0} = \delta_{a_0} = \delta_{r_0} = 0°$) in the trim condition. There is by no means consensus about the use of these symbols; Etkin uses ξ, η, and ζ to denote the perturbation control surface variables, while Nelson uses $\Delta\delta_e$, $\Delta\delta_a$, and $\Delta\delta_r$ to identify the same deflections. McRuer[6] and his co-authors point out that the terminology most commonly used ("dimensional stability derivatives") is more properly "dimensional stability parameters" and the common usage is to include either mass or moment of inertia terms the definitions: that is, $X_u \equiv \frac{1}{m}\frac{\partial X}{\partial u}$ is the form used for force derivative parameters and $M_q \equiv \frac{1}{I_y}\frac{\partial M}{\partial q}$ is the form used for moment derivative parameters. Nelson[17] calls these parameters "derivatives divided by mass (or inertia)". Each of these parameters is evaluated at trim conditions in the Bryan linearization and is therefore a constant in eqns. 9.4 and 9.5. It is important to note that this nondimensional formulation is concerned with direct measurements, while a second approach that still uses Bryan's linearization is concerned with force and moment coefficients and nondimensional velocities. Most of the aerodynamic stability derivative data that comes from wind tunnel measurements is presented in this nondimensional form. Table 9.2 lists a common set of equations using this approach. Typically, when the analysis is concerned with the data base itself, the flight test engineer will use nondimensional forms. However, when he turns to calculation of transfer functions, actual time histories, or carrying out complicated time domain simulations that are best illuminated with physical engineering units, the flight test engineer usually prefers the dimensional form for the data. In any event, the flight test engineer must be able to readily recognize and convert between the two forms of data.

Table 9.2 Linearized, Small Perturbation Equations Using Nondimensional Coefficients

Longitudinal Equations

$$(2\mu D - 2C_{L_0}\tan\Theta_0 - C_{X_u})\hat{u} - C_{X_\varphi}\alpha + C_{L_0}\Theta_0 - C_{X_{\delta_e}}\delta_e = 0$$
$$(2C_{L_0} - C_{Z_u})\hat{u} + (2\mu D - C_{Z_{\dot\alpha}} D - C_{Z_\alpha})\alpha - (2\mu + C_{Z_q})\hat{q} + C_{L_0}\tan\Theta_0\theta - C_{Z_{\delta_e}}\delta_e = 0 \quad (9.6)$$
$$- C_{m_u}\hat{u} - (C_{m_{\dot\alpha}} D - C_{m_\alpha})\alpha + (i_B D - C_{m_q})\hat{q} + C_{m_{\delta_e}}\delta_e = 0$$
$$\hat{q} - D\theta = 0$$

Lateral-Directional Equations

$$2\mu D - C_{Y_\beta})\beta - C_{Y_p}\hat{p} + (2\mu D - C_{Y_r})\hat{r} - C_{L_0}\phi - C_{Y_{\delta_a}}\delta_a - C_{Y_{\delta_r}}\delta_r = 0$$
$$- C_{\mathcal{L}_\beta}\beta + (i_A D - C_{\mathcal{L}_p})\hat{p} - (i_E D + C_{\mathcal{L}_r})\hat{r} - C_{\mathcal{L}_{\delta_a}}\delta_a - C_{\mathcal{L}_{\delta_r}}\delta_r = 0$$
$$- C_{n_\beta}\beta - (i_E D + C_{n_p})\hat{p} + (i_C D - C_{n_r})\hat{r} - C_{n_{\delta_a}}\delta_a - C_{n_{\delta_r}}\delta_r = 0 \quad (9.7)$$
$$\hat{p} + \hat{r}\tan\Theta_0 - D\phi = 0$$
$$\hat{r}\sec\Theta_0 - D\psi = 0$$

Small angle approximations are used to simplify these linearized equations. There are several different forms for these equations, as Etkin points out clearly. The chief differences lie in the definition of the normalizing unit of time (t^* defined below), the choice of the characteristic length (in fact, ℓ is defined differently for the longitudinal and for the lateral-directional equations), and the definitions used for the nondimensional stability coefficients themselves. Summarizing, the following definitions apply in Table 9.2:

$$\alpha \approx \frac{w}{U_0};\quad \beta \approx \frac{v}{U_0};\quad \ell = \frac{\bar{c}}{2} \text{ or } \frac{b}{2};\quad t^* = \frac{\ell}{U_0};\quad \mu \equiv \frac{m}{\rho S \ell};\quad \hat{u} = \frac{u}{U_0};\quad \hat{q} = \frac{q\bar{c}}{2U_0};\quad i_B = \frac{I_y}{\rho S \ell^3}$$
$$\hat{p} = \frac{p\bar{c}}{2U_0};\quad \hat{r} = \frac{r\bar{c}}{2U_0};\quad i_A = \frac{I_x}{\rho S \ell^3};\quad i_C = \frac{I_z}{\rho S \ell^3};\quad i_E = \frac{I_{xz}}{\rho S \ell^3};\quad \hat{t} = \frac{t}{t^*}$$

Derivatives with respect to $\hat{t}$ are indicated by D.

9.1.2.1 **Longitudinal Modes of Motion**. For a stable vehicle, the longitudinal motion characteristic equation results in two different oscillations; the eigenvalues are two complex conjugate pairs. One pair, usually called the **phugoid**, describes a low frequency interchange of potential energy and kinetic energy, which is very lightly damped with a period of 30 seconds or longer. It typically takes place with negligible change in φ. A second oscillation, the **short period**, occurs at V_∞. Its period is usually an order of magnitude less than that of the phugoid; hence, its name. Fortunately, this oscillation is well-damped throughout most of the flight envelope.

9.1.2.2 **Lateral-Directional Modes of Motion**. Solving the quartic lateral-directional characteristic equation typically produces two real roots and a single pair of complex roots for a stable conventional airplane. The real roots correspond to the **roll mode** and to the **spiral mode**. Typically, the roll mode has a time constant that is much shorter than the spiral mode. The oscillation described by the complex pair is called the **Dutch roll** mode of motion and it is moderately damped within the flight envelope for a conventional vehicle.

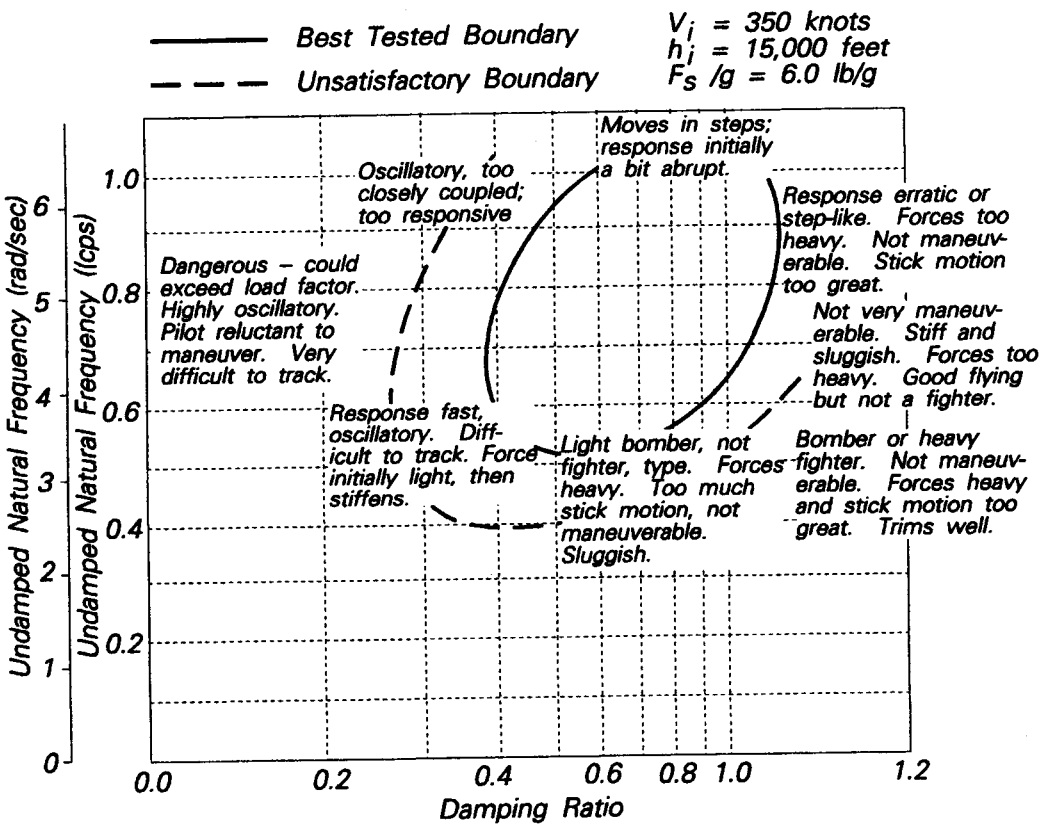

Fig. 9.6. Use of Pilot Opinion Ratings[10]

9.1.3 Handling Qualities

The parameters defined above are excellent tools for engineers and designers; in fact, these individuals must have a solid grasp of such dynamic measures of merit. Unfortunately, few operational pilots are engineers. And it is the pilot alone who has the ultimate responsibility for controlling the airplane. The ease with which the pilot (whether he or she is in the machine or on the ground) can fly the vehicle to accomplish the tasks which it was designed has a very strong influence on the usefulness of the machine. How easy an airplane is to fly for a given operational task comes under the subjective heading of **handling qualities**. For the design engineer and for the flight test team it then becomes necessary to communicate with the pilot and assess the handling qualities of a design before it can be developed to have, not just "good" performance, but also "good" handling qualities. Since "goodness" is a subjective measure, there is a need to relate the engineering parameters defined previously and the pilots' opinions regarding the airplane. The most useful guidelines that have evolved over the years are the military's handling qualities specifications[7,18] for manned aircraft and their substantiating documents[8]. These specifications spell out the ranges of parameters that historically have given acceptable handling qualities. Nonetheless, these documents are historical and often there is no information on how a new design innovation might affect handling qualities.

For that reason the test pilot and the flight test team must be familiar with pilot rating schemes and how they should be used in the evaluation of handling qualities.

Pilot opinion surveys, utilizing pilot rating scales like the Cooper-Harper scale, have been used extensively to quantify this subjective information[8]. Figure 9.6, adapted from Cooper and Harper[10], illustrates the general principle. A large number of pilots were asked to fly a specific airplane performing a well-defined task and ζ and ω_n were altered over a wide range of values. From this statistical base and the opinions recorded, an acceptable and an unacceptable range of values of ζ and ω_n were inferred. This rather simplistic illustration does not tell the whole story, however.

9.1.3.1 **Closed Loop Response versus Open Loop Response**. The damping ratio and the undamped natural frequency discussed above are properties determined solely by the airplane and its flight control system, that is, they are open loop parameters. The pilot's inputs close the loop, since he or she acts as an observer (or sensor) and a controller (control law and actuator). The open loop part of the system is shown in the dashed rectangle in Fig. 9.7, which depicts the closed loop system as well. The component block labeled pilot command is itself a very complex transfer function. A given pilot, performing a particular task at a specific time will have one set of dynamic response characteristics. Change any of these conditions and the human response is likely to change. This human variability (or, in the best light, adaptability) dictates that flying qualities experiments be carried out under carefully controlled conditions. It also means that the real test of an airplane's handling qualities is in providing satisfactory closed loop response with a large number of pilots.

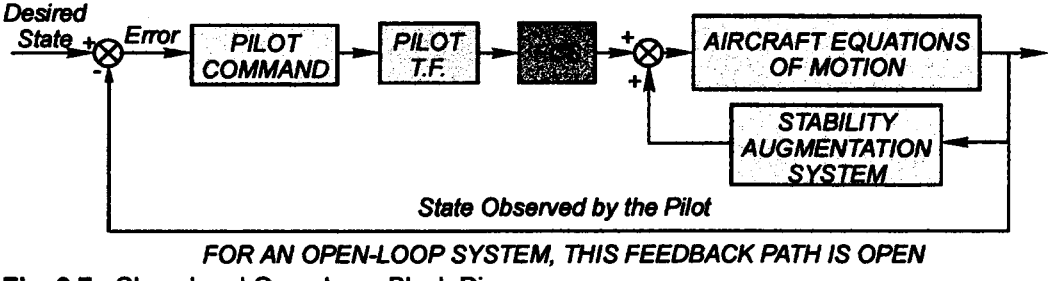

Fig. 9.7. Closed and Open Loop Block Diagram

9.1.3.2 **Pilot Rating Scales**. In the mid-1950s the Society of Experimental Test Pilots (SETP) organized a session of technical papers at an annual meeting of the Institute of Aeronautical Sciences, one of the predecessor organizations for the present American Institute of Aeronautics and Astronautics (AIAA). One of the papers[11] presented was titled "Understanding and Interpreting Pilot Opinion." In 1984 Robert P. Harper, Jr., was invited to give the Wright Brothers Lecture[11] at the 25th AIAA Aircraft Systems Design, Operations, and Test Meeting in San Diego. Much of this work was carried out in variable stability airplanes and in ground simulators but perhaps the most significant result was the widely used 10-point Cooper-Harper rating scale (Fig. 9.8). This rating scheme is based on a series of binary decisions in response to the following questions:

- Is the configuration controllable or uncontrollable?
- Is the airplane acceptable or unacceptable?

- Is the airplane satisfactory?

Except for a "no" answer to the first question, each of the responses leads to a possibility of three different levels of controllability, acceptability, or satisfaction. If the pilot will lose control of the vehicle during some portion of the mission, then it receives a rating of 10 (the worst qualitative assessment). Now, let's turn our attention to defining the terms that govern these dichotomous decisions.

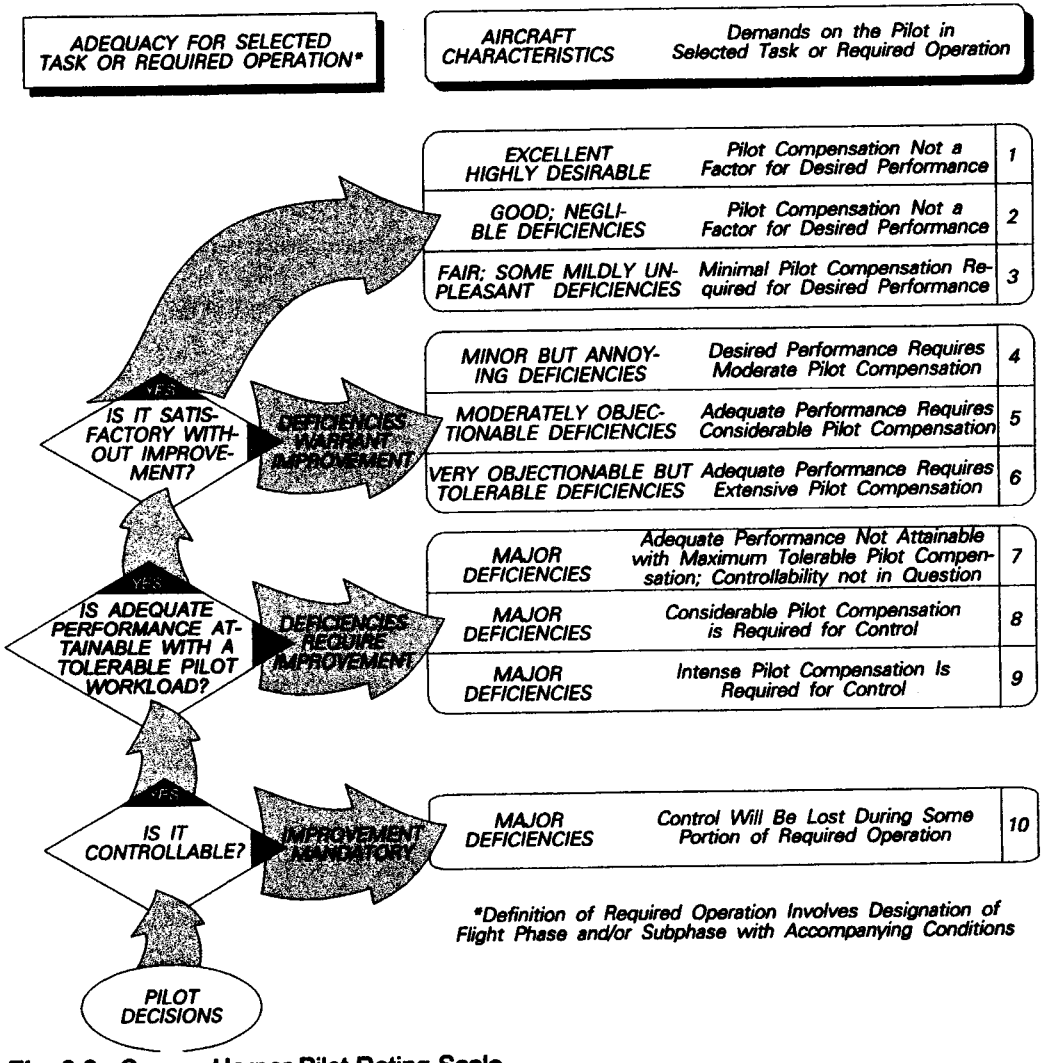

Fig. 9.8. Cooper-Harper Pilot Rating Scale

Controllability is the ability to command a desired response which is dictated by the intended use. In answering the first question, how much attention the pilot must pay to achieve the desired control is not considered. The airplane is **controllable** if he can command the desired response even if he has concentrate all his attention on flying the machine to the exclusion of all other matters. However, it is not controllable in the context of the mission if he cannot maintain control of the airplane with the effort and attention

available over and above his other mission duties. Hence, the airplane can be uncontrollable for a given mission, even though it does not crash. Cooper-Harper pilot ratings always assess controllability for an intended mission. Therefore, the mission and its individual tasks must be clearly and completely defined before pilot ratings have meaning.

Acceptable suggests that the vehicle can accomplish the mission. Acceptable does not say how well the required tasks can be performed. It may require an inordinate amount of the pilot's attention to achieve the required level of performance, but it can be done. If the effort, the concentration, and the workload necessary to complete the mission are too high, the pilot may reject the airplane and declare it unacceptable.

Satisfactory implies "adequate for the purpose." In pilot ratings, satisfactory does not necessarily imply perfection (almost no machine is perfect!). It is good enough that he is not asking that it be fixed; it can meet all the requirements of the assigned mission.

To infuse as much objectivity as possible into the pilot rating process, definition of the mission is perhaps the single most important factor. Not only must the mission be defined, it must be understood alike by both the evaluation pilot and by the test engineer. What the pilot is required to accomplish with the vehicle and the circumstances under which he must perform the mission are two essential elements in this definition. The circumstances may be part of the system being evaluated (like the cockpit displays, the configuration of the airplane, or the weapon controls, for example) or they may come from external influences (like whether turbulence is present or absent, the pilot's level of fatigue, or his proficiency in the task). Since virtually all engineering tests must simulate to some degree, this lack of total realism must be clearly understood by both the test engineer conducting the test and the evaluation subject. It would, for example, be quite impractical to evaluate a close air support airplane in an environment including all the ground-to-air defenses that were found in Central Europe in the 1980s.

It is absolutely wrong to presume that any numerical pilot rating totally describes any subject's qualitative assessment. The data collection phase during pilot rating experiments must also include these narrative comments. The rating itself is merely a summary of all his subjective feelings with regard to the defined task. Any evaluation pilot should be required and encouraged to make qualitative comments over and above the numerical rating. A good flight test engineer will thoughtfully prepare for the debriefing session, seeking to ask questions that will bring out the subtleties that the numerical ratings frequently gloss over. This debriefing session, where these extra comments are most likely to be elicited, should occur immediately after each evaluation. This need for immediacy suggests strongly that a voice recorder is needed during the flight for complex mission profiles. Communication, as is true throughout such an experimental process, is of the utmost importance.

Perhaps the most important single element in the subjective rating process is trust between the evaluation pilot and the engineer conducting the experiment. The pilot must be encouraged to believe that the engineer is vitally interested in the qualitative data, and the engineer must be just as assured that the pilot wants to give him accurate, meaningful data. Even when the pilots' comments oppose the engineer's judgement of how the airplane ought to behave based on his knowledge of its characteristics, both parties must strive to communicate and understand each other.

Let us now return to the linearized longitudinal equations of motions succinctly summarized in Table 9.1.

9.1.4 Longitudinal Dynamics

If we define the state vector for the nondimensional equations as $\boldsymbol{x} = [u \quad \alpha \quad \hat{q} \quad \theta]^T$, then the dynamic system can be expressed in conventional state space form.

$$\begin{aligned}
2\mu D\hat{u} &= (2C_{L_{trim}}\tan\Theta_{trim} + C_{X_u})\hat{u} + C_{X_\alpha}\alpha - C_{L_{trim}}\theta + C_{X_{\delta_e}}\delta_e \\
(2\mu - C_{Z_{\dot\alpha}})D\alpha &= (2C_{L_0} + C_{Z_u})\hat{u} + C_{Z_\alpha}\alpha + (2\mu + C_{Z_q})\hat{q} + C_{Z_{\delta_e}}\delta_e \\
i_B D\hat{q} - C_{m_{\dot\alpha}}D\alpha &= C_{m_u}\hat{u} + C_{m_\alpha}\alpha + C_{m_q}\hat{q} + C_{m_{\delta_e}}\delta_e \\
D\theta &= \hat{q}
\end{aligned} \tag{9.8}$$

Equations 9.8 are easily manipulated into matrix form:

$$\boldsymbol{C_1\dot{x} = A_1 x + B_1 u} \tag{9.9}$$

where,

$$\boldsymbol{C_1} = \begin{pmatrix} 2\mu & 0 & 0 & 0 \\ 0 & 2\mu - C_{Z_{\dot\alpha}} & 0 & 0 \\ 0 & -C_{m_{\dot\alpha}} & i_B & 0 \\ 0 & 0 & 0 & 1 \end{pmatrix}; \quad \boldsymbol{A_1} = \begin{pmatrix} 2C_{L_{trim}}\tan\theta_{trim} + C_{X_u} & C_{X_\alpha} & 0 & -C_{L_{trim}} \\ 0 & C_{Z_\alpha} & 2\mu + C_{Z_q} & 0 \\ 0 & C_{m_\alpha} & C_{m_q} & 0 \\ 0 & 0 & 1 & 0 \end{pmatrix}$$

$$\boldsymbol{B_1} = \begin{pmatrix} C_{X_{\delta_e}} \\ C_{Z_{\delta_e}} \\ C_{m_{\delta_e}} \\ 0 \end{pmatrix}; \text{ and, of course, } \boldsymbol{x} = \begin{pmatrix} \hat{u} \\ \alpha \\ \hat{q} \\ \theta \end{pmatrix}$$

In this simplified longitudinal case, where we have assumed that the elevator is the control (that is, power is not changed and there are no other moveable longitudinal controls), $\boldsymbol{u}$ is a scalar -- not a vector; that is, $\boldsymbol{u} = \delta_e$. If $\boldsymbol{C_1}^{-1}$ exists, eqns. 9.9 can be put into "standard" form by taking $\boldsymbol{C_1}^{-1}\boldsymbol{A_1} = \boldsymbol{A}$ and $\boldsymbol{C_1}^{-1}\boldsymbol{B_1} = \boldsymbol{B}$. Then $\dot{\boldsymbol{x}} = \boldsymbol{Ax} + \boldsymbol{Bu}$. $\boldsymbol{A}$ is called the plant matrix and $\boldsymbol{B}$ is called the control matrix.

Operating on eqns. 9.9 with the Laplace operator, they are transformed into algebraic equations which can be solved straightforwardly. If we take Laplace transforms with the usual assumption of zero initial conditions,

$$\begin{aligned}
(2\mu s - 2C_{L_{trim}}\tan\Theta_{trim} - C_{X_u})\,\hat{u}(s) - C_{X_\alpha}\alpha(s) - C_{L_{trim}}\theta(s) &= C_{X_{\delta_e}}\delta_e(s) \\
(2C_{L_0} - C_{Z_u})\hat{u}(s) + [(2\mu - C_{Z_{\dot\alpha}})s - C_{Z_\alpha}]\alpha(s) - (2\mu + C_{Z_q})\,\hat{q}(s) &= C_{Z_{\delta_e}}\delta_e(s) \\
-C_{m_u}\hat{u}(s) - (C_{m_{\dot\alpha}}s + C_{m_\alpha})\alpha(s) + (i_B s - C_{m_q}(s))\,\hat{q}(s) &= C_{m_{\delta_e}}\delta_e(s) \\
s\theta - \hat{q}(s) &= 0
\end{aligned} \tag{9.10}$$

Of course, the free response is obtained by solving the equations with the forcing functions ($\boldsymbol{Bu}$) set to zero. Since the system is linear, the forced response can be obtained separately and added to the solution for the free response. The free response can be readily obtained using Cramer's rule or any similar method for solving linear algebraic equations. Symbolically solving for α due to an elevator input, Cramer's rule gives:

$$\frac{\alpha(s)}{\delta_e(s)} = \frac{det\, N_\alpha^{\delta_e}(s)}{det\, \Delta(s)}$$

where $$N_\alpha^{\delta_e}(s) = \begin{pmatrix} 2C_{L_{trim}} \tan\theta_{trim} + C_{X_u} & C_{X_{\delta_e}} & 0 & -C_{L_{trim}} \\ 0 & C_{Z_{\delta_e}} & 2\mu + C_{Z_q} & 0 \\ 0 & C_{m_{\delta_e}} & C_{m_q} & 0 \\ 0 & 0 & 1 & 0 \end{pmatrix}$$

$$\Delta(s) = \begin{pmatrix} 2C_{L_{trim}} \tan\theta_{trim} + C_{X_u} & C_{X_\alpha} & 0 & -C_{L_{trim}} \\ 0 & C_{Z_\alpha} & 2\mu + C_{Z_q} & 0 \\ 0 & C_{m_\alpha} & C_{m_q} & 0 \\ 0 & 0 & 1 & 0 \end{pmatrix}$$

The denominator determinant in the above equation is simply the determinant of the pseudo-plant matrix A_1, which when set to 0, is the characteristic equation of the dynamic system and its roots are called the eigenvalues. For our simplified longitudinal equations the characteristic equation is a quartic and, for most conventional airplanes, it can be factored into two quadratic terms. These two quadratics describe two oscillations of widely differing frequency; both are illustrated in Fig. 9.9. The lower frequency one is called the phugoid and the higher frequency one is the short period mode of motion.

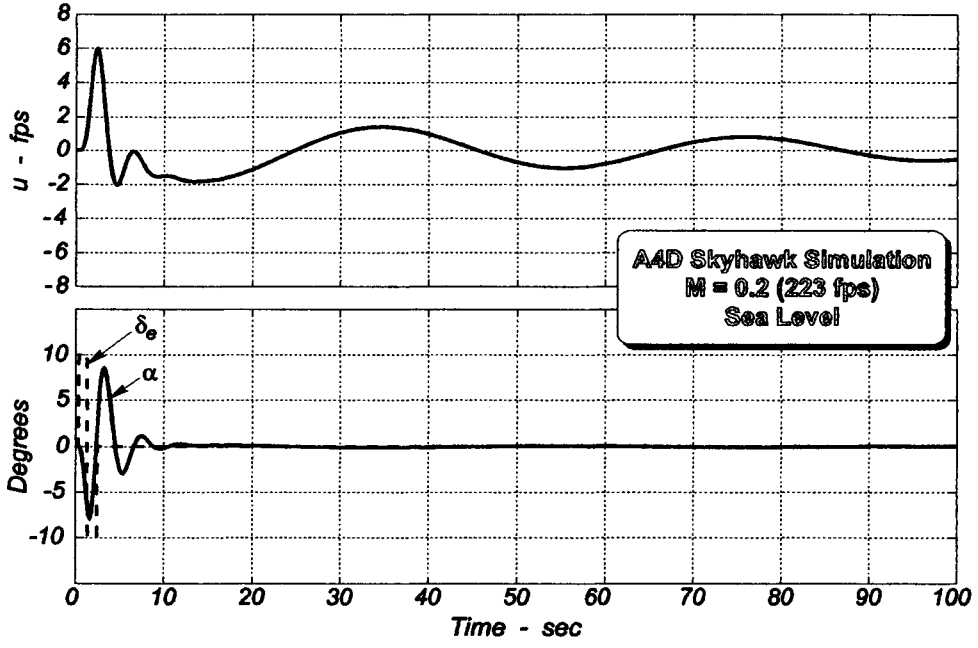

Fig. 9.9 Computed Time Histories after an Elevator Input

Typical periods for the phugoid are on the order of 30 seconds to a minute and a half, while those for the short period are usually an order of magnitude less. The phugoid is also very lightly damped or even slightly divergent. The pilot's inputs are made often enough that he usually can control a divergent phugoid and not even be aware of a long period instability. Such handling qualities often occur when the airplane is configured for

landing (the power approach (PA) configuration in handling qualities requirements[3].) The short period oscillation is consequently of greater importance because the pilot must control it immediately if it is not well-damped. If his reactions are too slow or are phased improperly, his commands may even drive the closed loop system unstable. Of course, the dynamics of the control system itself may hamper or even preclude the pilot from making appropriate corrections. Such short period motion occurs essentially at constant true airspeed. This fact leads us to an approximation (section 9.1.4.2) for the short period that can be useful in planning flight tests.

9.1.4.1 **Dimensional Form of the Equations**. The linearized longitudinal equations of motions have also been written utilizing dimensional derivatives. McRuer, Ashkenas, and Graham[6] developed these equations with assumptions that essentially parallel the previous development. Taking stability axes that align the *x*-axis with the relative wind in the trim condition, $W_{trim} = 0$. $X_{\dot{w}} = X_q = 0$ have also proven to be satisfactory assumptions. Then, eqns. 9.4 can be rewritten in matrix form:

$$\boldsymbol{C_2\dot{x} = A_2x + B_2u} \tag{9.11}$$

where $\boldsymbol{C_2} = \begin{pmatrix} 1 & 0 & 0 & 0 \\ 0 & 1 - Z_{\dot{w}} & 0 & 0 \\ 0 & -M_{\dot{w}} & 1 & 0 \\ 0 & 0 & 0 & 1 \end{pmatrix}$; $\boldsymbol{A_2} = \begin{pmatrix} X_u & X_w & 0 & -g\cos\theta_{trim} \\ Z_u & Z_w & U_{trim} + Z_q & 0 \\ M_u & M_w & M_q & 0 \\ 0 & 0 & 1 & 0 \end{pmatrix}$

and $\boldsymbol{B_2} = \begin{pmatrix} X_{\delta_e} \\ Z_{\delta_e} \\ M_{\delta_e} \\ 0 \end{pmatrix}$; and, $\boldsymbol{x} = \begin{pmatrix} u \\ \alpha \\ q \\ \theta \end{pmatrix}$

9.1.4.2 **Short Period Approximation**. Considering eqns. 9.6 with $\hat{u} = 0$ (no perturbation in true airspeed), four equations in three unknowns result. Since $\hat{q}$ is simply related to the pitch attitude by taking the derivative with respect to time and since the *x* force equation represents a balance of momentum change in the direction of *u*, it is logical to select the *z* force equation and the pitching moment equation to approximate the two unknowns of interest, α and θ. Sticking to the Laplace operator form and the non-dimensional stability coefficients and assuming that $C_{Z_{\dot{\alpha}}}$ and C_{Z_q} are negligible, eqns. 9.6 reduce to:

$$(2\mu s - C_{Z_\alpha})\alpha - (2\mu s + C_{L_{trim}}\tan\Theta_{trim})\theta = C_{Z_{\delta_e}}\delta_e \tag{9.12}$$

$$-(C_{m_{\dot{\alpha}}}s + C_{m_\alpha})\alpha + (i_B s - C_{m_q})s\theta = C_{m_{\delta_e}}\delta_e$$

For these simplified equations the characteristic determinant yields a cubic in *s* that factors readily into a trivial $s = 0$ factor and a quadratic factor if we assume that $\Theta_{trim} = 0$

$$a_2s^2 + a_1s + a_0 = 0 \tag{9.13}$$

where $a_2 = 2\mu i_B$

$$a_1 = -2\mu(C_{m_{\dot{\alpha}}} + C_{m_q}) - C_{Z_\alpha}i_B$$

$$a_0 = C_{m_\alpha}C_{Z_q} - 2\mu C_{m_\alpha}$$

Dividing eqn. 9.13 by a_2 and comparing this result with the standard form for dynamic response given in eqn. 9.3:

$$\omega_{n_{sp}} \approx \sqrt{\frac{C_{m_q}C_{z_\alpha} - 2\mu C_{m_\alpha}}{2\mu i_B}} \quad \text{and} \quad \zeta_{sp} \approx \frac{-2\mu(C_{m_{\dot\alpha}} + C_{m_q}) - C_{z_\alpha} i_B}{2\omega_{n_{sp}}} \tag{9.14}$$

These approximations are too complicated to provide ready insight into the important derivatives that affect the short period mode's undamped natural frequency and damping ratio. In the expression above for $\omega_{n_{sp}}$, the product $C_{m_q}C_{z_\alpha}$ is often quite small relative to the C_{m_α} term. Thus, C_{m_α} is clearly the dominant derivative in estimating $\omega_{n_{sp}}$, though physical configuration and flight conditions also play a part through μ and i_B. Similarly, in the first term for ζ_{sp}, $C_{m_{\dot\alpha}}$ may be small (though , more often, it is simply ignored) in comparison to C_{m_q}. Omitting $C_{m_{\dot\alpha}}$ from the expression alters the form of the result not at all and often the value of the damping term very little. The damping ratio depends primarily on the stability derivative C_{m_q}. Of course, the moment of inertia about the *y* axis again is important, as are the flight conditions. Taking these assumptions into account, eqns. 9.14 simplify to:

$$\omega_{n_{sp}} \approx \sqrt{\frac{-C_{m_\alpha}}{i_B}} \quad \text{and} \quad \zeta_{sp} \approx \frac{-2\mu C_{m_q} - C_{z_\alpha} i_B}{2\omega_{n_{sp}}} \tag{9.15}$$

With dimensional derivatives these approximations take the form:

$$\omega_{n_{sp}} \approx \sqrt{-M_\alpha} \quad \text{and} \quad \zeta_{sp} \approx \frac{-M_q - Z_w}{2\omega_{n_{sp}}} \tag{9.16}$$

Care must be exercised in applying these approximations. The primary reason for introducing them is to clarify which stability derivatives most influence each of the dynamic figures of merit. Do <u>not</u> use eqns. 9.15 or 9.16 when precise values for $\omega_{n_{sp}}$ and ζ_{sp} are needed. Too many assumptions are involved.

9.1.4.3 **<u>Phugoid Approximation</u>**. As Fig. 9.9 suggests, the phugoid oscillation occurs at essentially constant angle of attack (remember α is the perturbation in angle of attack from the trim condition). Thus, the equations of motion can be reduced from 4 to 2 with a line of reasoning similar to that used for the short period approximation. In this case the moment equation is the logical candidate for elimination since the rotational motion has little effect on the exchange of kinetic and potential energy that the phugoid represents. If we neglect C_{z_q}, again take $\Theta_{trim} = 0$, and also utilize the fact that $\alpha \approx 0$ during most of the phugoid oscillation, the *x* and *z* force equations reduce to:

$$\begin{aligned}(2\mu s - C_{x_u})\hat{u} + C_{L_{trim}}\theta - C_{x_{\delta_e}}\delta_e &= 0\\ (2C_{L_{trim}} - C_{z_u})\,\hat{u} - 2\mu s\theta - C_{z_{\delta_e}}\delta_e &= 0\end{aligned} \tag{9.17}$$

Naturally, the resulting characteristic equation for these approximate equations is slightly simpler than for the full set. Noticing that the lift is little different from the weight so long as we do not perturb the vehicle too far from the equilibrium (trim) conditions, a quadratic equation like (9.13) again results with these coefficients:

$$a_2 = 4\mu^2$$

$$a_1 = -2\mu C_{X_u}$$

$$a_0 = 2C_{L_{trim}}^2 - C_{L_{trim}} C_{Z_u}$$

$$\omega_{n_p} \approx \frac{\sqrt{C_{L_{trim}}(2C_{L_{trim}} - C_{Z_u})}}{2\mu} \quad \text{and} \quad \zeta_p \approx -\frac{C_{X_u}}{2\sqrt{C_{L_{trim}}(2C_{L_{trim}} - C_{Z_u})}} \tag{9.18}$$

However, except for the transonic flight regime, C_{Z_u} is usually small compared to $2C_{L_{trim}}$; consequently

$$\omega_{n_p} \approx \frac{C_{L_{trim}}}{\mu\sqrt{2}} \quad \text{and} \quad \zeta_p \approx -\frac{C_{X_u}}{2\sqrt{2}C_{L_{trim}}} \tag{9.19}$$

To interpret eqns. 9.19 physically, we must recall that ω_{n_p} is expressed in nondimensional time units; that is, radians/airsec, where as noted in Table 9.2, $t^* = \frac{\ell}{u_0}$. So to put ω_{n_p} into physical time units, we must divide eqn. 9.17a by this parameter. Carrying out this division and noting that $C_{L_{trim}} = \frac{2W}{\rho u_{trim}^2 S}$ and that $\mu = \frac{W}{\rho g S \ell}$,

$$\omega_{n_p} \approx \frac{2W}{\rho u_{trim}^2 S} \frac{\rho g S \ell}{\sqrt{2}W} \frac{u_{trim}}{\ell} \approx \frac{\sqrt{2}g}{u_{trim}} \tag{9.20}$$

In trimmed level flight, still ignoring transonic effects, $C_{X_u} = -2C_{D_0}$. Thus,

$$\zeta_p \approx \frac{C_{D_0}}{\sqrt{2}C_{L_{trim}}} \approx \frac{D_0}{\sqrt{2}L_{trim}} \tag{9.21}$$

The phugoid damping ratio can also be approximated with dimensional derivatives:

$$\zeta_p \approx -\frac{X_u}{2\omega_{n_p}} \tag{9.22}$$

Equations 9.20 through 9.22 must be used carefully, but they show that the phugoid natural frequency is inversely proportional to true airspeed. This approximation suggests that the phugoid time constant $\tau_p = 0.138u_0$. It also indicates ω_{n_p} and τ_p are roughly independent of altitude and gross weight of the airplane. Blakelock[12] shows that both these frequency parameters do depend on variations in density, evidently because of the effects of terms neglected in this analysis. For equilibrium flight eqn. 9.21 implies that ζ_p is directly proportional to total vehicle drag. As trim airspeed increases at constant altitude, phugoid damping ratio increases as the square of the airspeed. Similarly, if true airspeed is held constant, ζ_p decreases in direct proportion to the change in density with altitude. While these approximate equations do not give accurate answers, they do offer insight into the most important stability derivatives affecting the phugoid.

Example 9.1: Several examples of typical aircraft dimensional stability derivative data are given by McRuer, Ashkenas, and Graham[6]. The data in Table 9.3 summarize such stability derivatives for an attack airplane flying at low subsonic speeds. Solving the characteristic equation that results from equations 9.11 with the data in Table 9.3 we get: $\omega_{n_{sp}} = 1.5611$ *rad/sec* and $\zeta_{sp} = 0.3588$. Using approximations like eqns. 9.20 and 9.22: $\omega_{n_{sp}} \approx 1.5082$ and $\zeta_{sp} \approx 0.2609$

Table 9.3 Longitudinal Data for a Subsonic Fighter ($M = 0.2$, h = sea level)

X_u	-0.0813 *(sec^{-1})*	M_u	-0.0029 *(ft-sec)$^{-1}$*
X_w	-0.0312 *(sec^{-1})*	M_w	-0.0102 *(ft-sec)$^{-1}$*
X_{δ_h}	0.00432 *(ft/sec^2/rad)*	$M_{\dot{w}}$	-0.000646 *(ft^{-1})*
Z_u	-0.026 *(sec^{-1})*	M_q	-0.48 *(sec^{-2})*
Z_w	-0.307 *(sec^{-1})*	M_{δ_e}	-2.21 *(sec^{-2})*
$Z_{\dot{w}}$	-0.001681	M_{δ_h}	0.000152 *(sec^{-2})*
Z_{δ_e}	-7.07 *(ft/sec^2/rad)*		

Note: This airplane has both a trimmable horizontal tail and an elevator (denoted by subscripts δ_h and δ_e, respectively, above). Elevator deflection does not affect the X force equation.

The approximate undamped natural frequency differs from that calculated from the full characteristic equation by approximately 3.4% while the estimated damping ratio is about 17% higher. A similar calculation for the phugoid mode yields considerably less satisfactory results, with the approximation giving an error of approximately 34% in ω_{n_p} and over 200% in ζ_p. These approximations are useful for quick estimates of the short period but the phugoid estimates are extremely crude.

Table 9.4 Stability Derivatives Significantly Affecting Longitudinal Oscillations[12]

Aerodynamic Parameter	Motion Parameter Affected Most	Effect on Motion Parameter
C_{m_q}	Short period damping ratio, ζ_{sp}	ζ_{sp} increases with increasing C_{m_q}
C_{m_α}	Short period undamped natural frequency, $\omega_{n_{sp}}$	$\omega_{n_{sp}}$ increases with increasing C_{m_α}
C_{x_u} or D_0	Phugoid damping ratio, ζ_p	ζ_p increases with increasing C_{x_u} or D_0
C_{Z_u} or $\left(\frac{1}{V_\infty}\right)$	Phugoid undamped natural frequency, ω_{n_p}	ω_{n_p} increases with increasing C_{Z_u} or $\left(\frac{1}{V_\infty}\right)$

9.1.4.4 **Sensitivity to Longitudinal Stability Derivatives**. Blakelock[12] has also examined the sensitivity of the damping and natural frequency of the longitudinal modes of motion to variations in C_{x_u}, C_{x_α}, C_{z_u}, $C_{x_{\dot{\alpha}}}$, C_{m_α}, $C_{m_{\dot{\alpha}}}$, and C_{m_q}. Table 9.4 summarizes his findings for a four engine jet transport.

9.1.4.5 **Summary of Linear Longitudinal Dynamics**. The linearized longitudinal equations of motion used to analyze airplane pitch dynamics illustrate the complexity of dynamic flight tests. Approximate equations of motion, obtained to help the flight test engineer anticipate trends in dynamic figures of merit, must be used with good judgment. They give insight to help you plan dynamic flight tests more efficiently and to help you spot trends in data collected that indicate undesirable longitudinal dynamic characteristics.

9.1.5 Lateral-Directional Dynamics

The linearized lateral-directional equations (see Tables 9.1 and 9.2) are separated from the longitudinal ones by assuming that the product of inertia I_{xz} is negligible and that there are no other aerodynamic or control surface coupling terms are of significance. With these decoupled equations we can study the asymmetric dynamic response of an airplane or a missile. If we choose the state vector to be $\boldsymbol{x} = [\beta \quad \hat{p} \quad \hat{r} \quad \phi]^T$, we can put eqns. 9.7 in matrix form:

$$\begin{aligned} 2\mu D\beta &= C_{y_\beta}\beta + C_{y_p}\hat{p} - (2\mu - C_{y_r})\hat{r} + C_{L_{trim}}\phi + C_{y_{\delta_a}}\delta_a + C_{y_{\delta_r}}\delta_r \\ i_A D\hat{p} - i_E D\hat{r} &= C_{\mathcal{L}_\beta}\beta + C_{\mathcal{L}_p}\hat{p} + C_{\mathcal{L}_r}\hat{r} + C_{\mathcal{L}_{\delta_a}}\delta_a + C_{\mathcal{L}_{\delta_r}}\delta_r \\ -i_E D\hat{p} + i_C D\hat{r} &= C_{n_\beta}\beta + C_{n_p}\hat{p} + C_{n_r}\hat{r} + C_{n_{\delta_a}}\delta_a + C_{n_{\delta_r}}\delta_r \\ D\phi &= \hat{p} \end{aligned} \tag{9.23}$$

These equations can also be put into the matrix form of eqn. 9.9

$$\boldsymbol{C_3} = \begin{pmatrix} 2\mu & 0 & 0 & 0 \\ 0 & i_A & -i_E & 0 \\ 0 & -i_E & i_C & 0 \\ 0 & 0 & 0 & 1 \end{pmatrix}; \quad \boldsymbol{A_3} = \begin{pmatrix} C_{Y_\beta} & C_{Y_p} & C_{Y_r} - 2\mu & C_{L_{trim}} \\ C_{\mathcal{L}_\beta} & C_{\mathcal{L}_p} & C_{\mathcal{L}_r} & 0 \\ C_{n_\beta} & C_{n_p} & C_{n_r} & 0 \\ 0 & 0 & 0 & 1 \end{pmatrix}$$

$$\boldsymbol{B_3} = \begin{pmatrix} C_{y_{\delta_a}} & C_{y_{\delta_r}} \\ C_{\mathcal{L}_{\delta_a}} & C_{\mathcal{L}_{\delta_r}} \\ C_{n_{\delta_a}} & C_{n_{\delta_r}} \\ 0 & 0 \end{pmatrix}; \text{ and, of course, } \boldsymbol{x} = \begin{pmatrix} \beta \\ \hat{p} \\ \hat{r} \\ \phi \end{pmatrix}$$

Again, if $\boldsymbol{C_3^{-1}}$ exists, this control equation can be put into "standard" form by premultiplying the plant and the control matrices by $\boldsymbol{C_3^{-1}}$: $\boldsymbol{C_3^{-1}A_3 = A}$ and $\boldsymbol{C_3^{-1}B_3 = B}$.

9.1.5.1 **Dimensional Form of the Equations**. The linearized lateral-directional equations of motions can also be written to utilize dimensional derivatives. Again, see McRuer, Ashkenas, and Graham[6] for the full development and the complete set of assumptions.

$$\boldsymbol{C_4\dot{x} = A_4 x + B_4 u} \tag{9.24}$$

where $\boldsymbol{C_4} = \begin{pmatrix} 1 & 0 & 0 & 0 \\ 0 & I_x & -I_{xz} & 0 \\ 0 & -I_{xz} & I_z & 0 \\ 0 & 0 & 0 & 1 \end{pmatrix}$; $\boldsymbol{A_4} = \begin{pmatrix} Y_v & Y_p & Y_r - V_\infty & -g\cos\theta_{trim} \\ \mathcal{L}_v & \mathcal{L}_p & \mathcal{L}_r & 0 \\ N_v & N_p & N_r & 0 \\ 0 & 0 & 0 & 1 \end{pmatrix}$

$$\boldsymbol{B_4} = \begin{pmatrix} Y_{\delta_a} & Y_{\delta_r} \\ \mathcal{L}_{\delta_a} & \mathcal{L}_{\delta_r} \\ N_{\delta_a} & N_{\delta_a} \\ 0 & 0 \end{pmatrix} \text{ and } \boldsymbol{x} = \begin{pmatrix} v \\ \hat{p} \\ \hat{r} \\ \phi \end{pmatrix}$$

For either set of lateral-directional equations the control vector includes at least two elements. For conventional aircraft, $u^T = [\ \delta_a\ \delta_r\ ]$. The plant matrix sets the free response of the dynamic system: its eigenvalues describe transient behavior. These characteristic roots typically include two aperiodic and one oscillatory mode of motion (two linear factors and one quadratic factor). These three modes of motion make up the asymmetric dynamics for a conventional airplane. In Figure 9.10 all three of the modes are superimposed after an aileron input excites them. It is almost impossible to pick out to the roll mode. The oscillatory Dutch roll mode appears to dominate.

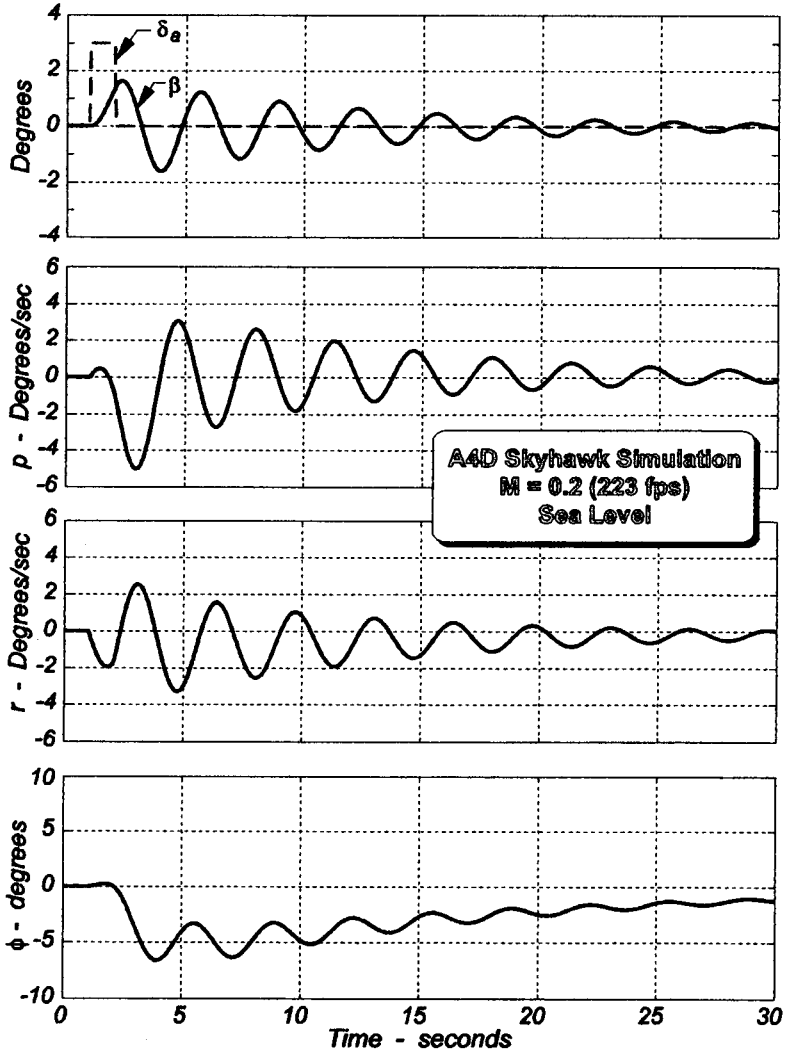

Fig. 9.10 Lateral-Directional Dynamic Response

9.1.5.2 **Roll Mode**. The roll mode, as the name implies, describes the response of the airplane to a lateral or roll command. For a conventional airplane, the control surface input would be the aileron. The expected response is a decaying exponential in roll rate with a small time constant, usually on the order of 1 or 2 seconds. MIL-F-8785 requires that this time constant be less than 3 seconds[3]. This mode is illustrated later in Fig. 9.17.

9.1.5.3 **Roll Mode Approximation**. Etkin[4], Blakelock[12], and Roskam[5] all retain only the rolling moment equation to give an approximate expression that will show which of the stability derivatives most directly influences the roll mode time constant. The rolling moment alone is assumed to contain all needed information. Moreover, the β and $\hat{r}$ terms are neglected.

$$I_x \dot{\hat{p}} - \mathcal{L}_p \hat{p} = 0 \tag{9.24}$$

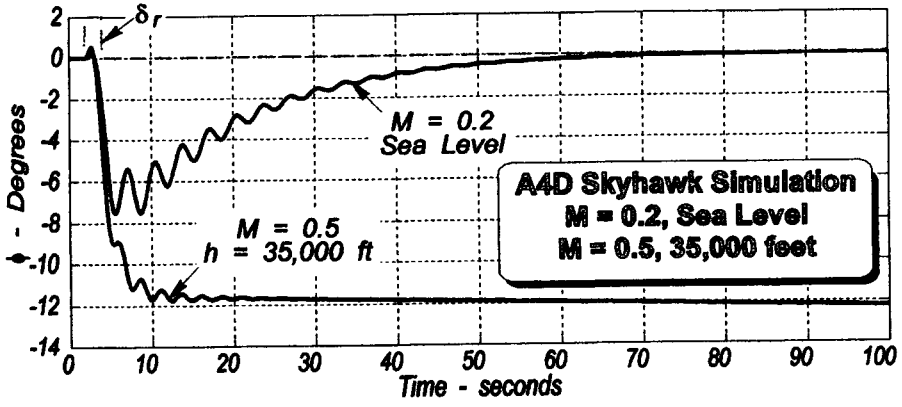

Fig. 9.11 Stable and Unstable Spiral Modes of Motion

9.1.5.4 **Spiral Mode**. The second first order response from the lateral-directional equations of motion has a much longer time constant, typically about 10 times that of the roll mode. This spiral mode relates time to the airplane's tendency to roll and descend if no control action is taken. Bank angle is the most logical dynamic flight test measurement used to describe the spiral mode. Like the phugoid mode discussed under the longitudinal response, the spiral mode can be controlled easily by the pilot under normal circumstances even if the bank angle is divergent. The time-to-double-amplitude must, however, be long enough so that the pilot does not have to devote an excessive amount of his attention to this correction. Figure 9.11 illustrates both a divergent and a convergent spiral mode, from simulations for the A-4 Skyhawk aircraft model given by McRuer, Ashkenas, and Graham[6]. The spiral mode is typical of many aircraft in that at high altitude and relatively high angle of attack the spiral often becomes divergent. Also, notice that the time constant for the divergence is quite long, suggesting that this instability will likely be a minor nuisance to the pilot. Both military and civilian requirements documents for this mode of motion allow some instability of the relative ease with which such divergences can be controlled by the pilot.

9.1.5.5 **Spiral Mode Approximation**. Roskam[5] suggests an approximate expression for the spiral mode, generated using the same general approach as above. However, as we will see shortly, this approximation is often quite inaccurate. The highly coupled nature of lateral and directional modes of motion is largely responsible for making such estimates unacceptably crude. Part of the difficulty lies in deciding which of the four equations best represents this mode of motion. We note that β changes little in a spiral, suggesting that elimination of the side force equation may work; further, in the spiral transient, the roll rates are usually quite low. So, following Roskam, we will try taking $p = 0$ while ignoring

the side force equation. Simplifying eqns. 9.7 with these approximations, extracting the simplified characteristic equation, and solving for λ_S yields:

$$\lambda_S = \frac{C_{\mathcal{L}_\beta} C_{n_r} - C_{n_\beta} C_{\mathcal{L}_r}}{\frac{I_z C_{\mathcal{L}_\beta}}{S\bar{q}b} + \frac{I_{xz} C_{n_\beta}}{S\bar{q}b}} \tag{9.26}$$

For conventional airplanes and stability axes, $I_{xz}C_{n_\beta} << I_z C_{\mathcal{L}_\beta}$ because of the relative sizes of I_z and I_{xz}. Then, eqn. 9.26 simplifies further

$$\lambda_S \approx \frac{C_{\mathcal{L}_\beta} C_{n_r} - C_{n_\beta} C_{\mathcal{L}_r}}{\frac{I_z C_{\mathcal{L}_\beta}}{S\bar{q}b}} \tag{9.27}$$

The inaccuracy of this approximation is highlighted by using Blakelock's example of a jet transport and calculating the spiral mode eigenvalue and its associated time constant from the full set of equations. The results are: $\lambda_S = 0.004$/sec and $T_S = 250$ sec. By way of comparison, eqn. 9.27 gives: $\lambda_S \approx 0.099$/sec and $T_S \approx 10.1$ sec. Rather obviously, the approximation leaves much to be desired. About all we can say is that it did show the spiral to be unstable; but this approximation does a very poor job of predicting the time response character of the mode. Roskam points out that the asymmetric aerodynamic forces depend on β, $\dot{\phi}$, and $\dot{\psi}$, rather than on β, ϕ, and ψ. The damping terms associated with $\dot{\phi}$ and $\dot{\psi}$ are often of the same magnitude as those due to β. Consequently, they cannot be neglected safely. However, the approximation exercise was not wholly futile, for we can pick out the significant stability derivatives from eqn. 9.27. The numerator term on the right, coupled with the knowledge that dihedral effect is negative for a conventional airplane, leads to the following condition for a stable spiral mode.

$$C_{\mathcal{L}_\beta} C_{n_r} > C_{n_\beta} C_{\mathcal{L}_r} \tag{9.28}$$

Again, because the spiral mode has a relatively long time constant, it is not absolutely essential that it be stable. As Blakelock shows, many airplanes have divergent spiral modes at low speeds and convergent ones at high speed. It is often quite within the capability of the pilot to correct for spiral divergences. In fact the spiral mode and the Dutch roll mode are both strongly affected by dihedral effect; increasing dihedral (making $C_{\mathcal{L}_\beta}$ more negative) to drive the spiral mode more stable can reduce Dutch roll damping. Often a slight spiral instability is accepted to improve Dutch roll damping, a parameter that often has a much larger effect on lateral-directional handling qualities. So, except during the performance of certain tasks (instrument approaches, for example) requiring virtually all of the pilot's attention, the handling qualities as perceived by the pilot may be largely unaffected by an unstable spiral mode. Moreover, the spiral mode can be controlled fairly easily with stability augmentation; yaw dampers, even in their simplest forms, can be designed to improve spiral stability in a closed loop automatic control system.

9.1.5.6 **Dutch Roll Mode**. This lateral-directional oscillation is a tightly coupled rolling and yawing motions usually occurring at medium to high frequency and having moderate to light damping with no yaw damper installed. Typically, at cruise conditions the period of the oscillation is on the order of 3 seconds. The ratio of bank angle to sideslip an-

gle $\frac{\phi}{\beta}$ is a key parameter; it often indicates how pilots will react to such an oscillation. Usually, a low $\frac{\phi}{\beta}$ ratio (yaw dominates the Dutch roll) is more acceptable to pilots than an oscillation in which relatively large bank angle excursions take place. If the Dutch roll is lightly damped and/or the frequency is too high, it may be necessary to add a yaw damper or similar automatic flight control system component to augment the natural characteristics of the aircraft.

9.1.5.7 **Dutch Roll Approximation**. Roskam[5], Blakelock[12], and Nelson[19] approximate the Dutch roll oscillation by simplifying the equations of motion, though each uses a slightly different approach. They also arrive at similar conclusions. Blakelock suggests that examination of the rudder input transfer function $\frac{\beta(s)}{\delta_r(s)}$ shows that there is a pole-zero cancellation that effectively negates the roll subsidence factor in the lateral-directional characteristic equation. This cancellation implies that the rolling moment equation can be ignored for an approximation to the Dutch roll mode. It is assumed, therefore, that Dutch roll consists of only sideslip and yaw. Moreover, pure sideslip (that is, $\beta = -\psi$) and zero change in the V_∞ during the maneuver are postulated. Then $r = \dot{\Psi}$. Under these assumptions the side force equation does not contribute at all to the free yawing motion; that is, $-Y_\beta \beta = Y_{\delta_r}\delta_r$. Thus, Blakelock's approximation is based entirely on the yawing moment equation.

$$\left(N_\beta + s^2 - N_r s\right)\psi \approx 0 \text{ or } \left(s^2 - N_r s + N_\beta\right)\Psi \approx 0 \tag{9.29}$$

If we compare eqn. 9.29 to the standard form for a damped quadratic,

$$\omega_{n_{Dr}} \approx \sqrt{N_\beta} \tag{9.30}$$

This expression clearly shows the dependence of $\omega_{n_{Dr}}$ on N_β. Also, $N_\beta = \frac{C_{n_\beta}\bar{q}Sb}{I_z}$, which emphasizes the direct link of $\omega_{n_{Dr}}$ to altitude (through $\bar{q}$). Like the short period, $\omega_{n_{Dr}}$ is also directly proportional to V_∞. So, increasing airspeed increases $\omega_{n_{Dr}}$ and increasing altitude decreases $\omega_{n_{Dr}}$.

Alternatively, we could slightly improve our approximation by solving the reduced order set of equations (side force and yawing moment equations only) as both Roskam[5] and Nelson[19] do. This approach is useful for airplanes with low dihedral effect. The resulting characteristic equation is

$$s\left(s^2 - s\left(N_r + \frac{Y_\beta}{V_\infty}\right) + \left(\frac{Y_\beta N_r}{V_\infty} + N_\beta - \frac{N_\beta Y_r}{V_\infty}\right)\right) = 0$$

Now, the approximate expression for $\omega_{n_{Dr}}$ is slightly more complicated.

$$\omega_{n_{Dr}} \approx \sqrt{\frac{Y_\beta N_r + N_\beta V_\infty - N_\beta Y_r}{V_\infty}} \tag{9.31}$$

The middle term in eqn. 9.31 usually dominates the lateral-directional oscillation; so, this approximation is in effect adding small terms to the approximation of eqn. 9.30.
From the characteristic equation the damping ratio ζ_{Dr} is approximated by:

$$\zeta_{Dr} = -\frac{Y_\beta + V_\infty N_r}{2\omega_{n_{Dr}} V_\infty} \tag{9.32}$$

Damping ratio is dominated by the second term, which is set by the ratio $-\frac{N_r}{\sqrt{N_\beta}}$, and it is also related to $\bar{q}$, using similar reasoning as we did for $\omega_{n_{Dr}}$.

Example 9.2: Returning to the airplane considered earlier to illustrate longitudinal dynamics to provide additional insight into lateral-dynamics and our approximations. The data[6] are summarized in Table 9.5.

Table 9.5 Lateral-Directional Data for an Attack Airplane (M = 0.2, h = sea level)

Y_β	- 22.9 (ft/sec^2/rad)	$\mathcal{L}_{\delta_a}$	1.875 (sec^{-2})
Y_{δ_a}	- 0.606 (ft/sec^2/rad)	$\mathcal{L}_{\delta_r}$	0.1284 (sec^{-2})
Y_{δ_r}	- 0.00272 (ft/sec^2/rad)	N_β	2.8 (sec^{-2})
$\mathcal{L}_\beta$	- 3.21 (sec^{-2})	N_p	- 0.111 (sec^{-1})
$\mathcal{L}_p$	- 0.412 (sec^{-1})	N_r	- 0.296 (sec^{-1})
$\mathcal{L}_r$	- 0.0317 (sec^{-1})	N_{δ_a}	- 0.0242 (sec^{-2})
		N_{δ_r}	- 1.272 (sec^{-2})

Table 9.6 Effect of Altitude and Airspeed on the Roll Mode of an Attack Airplane

Flight Conditions		Time Constant (seconds)	
Altitude (feet)	Airspeed (fps)	Approximation (eqn. 9.25)	Full Equations (eqns. 9.7)
Sea Level	223	2.42	1.78
Sea Level	950	0.26	0.26
35,000	487	1.87	1.78
35,000	681	1.23	1.19

Substituting the derivatives from Table 9.5 into the approximate relations and comparing to the solution of the complete small perturbation lateral-directional equations gives an approximate $\omega_{n_{Dr}}$ that is about 8.5% smaller than comes from the complete equations: $\omega_{n_{Dr}}$ is 1.894 rad/sec from the complete set of equations, while the approximation gives 1.6823 rad/sec. The same comparison for ζ_{Dr} shows that Dutch roll damping ratio is overpredicted significantly; ζ_{Dr} is approximated as 0.1185, compared to 0.0502 for the complete equations result. This error is over 100%. For this example at least, this Dutch roll approximation gives a fairly reasonable estimate of Dutch roll frequency, but the damping ratio is unreliable. The approximation typically gives such results. Roskam applies a similar approximation to a small business jet and finds that the Dutch roll frequency is predicted quite well (1.62 rad/sec from the approximation compared to 1.618 rad/sec from the approximation). Again, the damping ratio is not predicted well (0.058 from the ap-

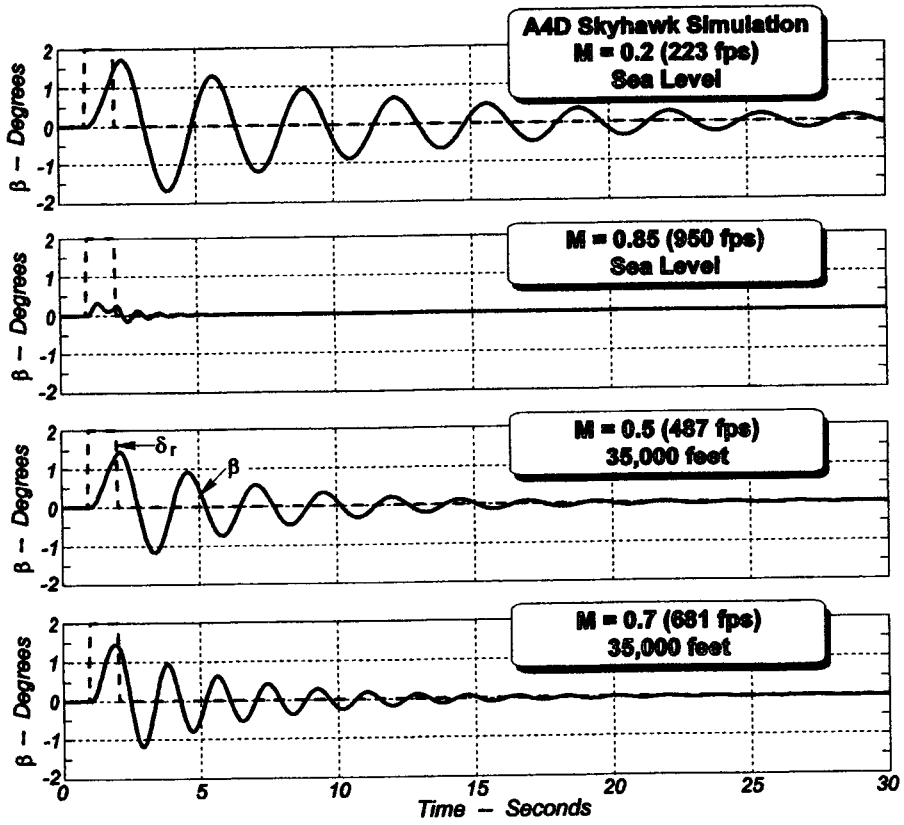

Fig. 9.12 Dutch Roll Transient Response (Full 6 DOF Response to Rudder)

Table 9.7 Effect of Altitude and Airspeed on the Dutch Roll Mode of an Attack Airplane

Flight Conditions		Damping Ratio		ω_n (rad/sec)	
Altitude (feet)	Airspeed (fps)	Approximations (eqns. 9.31/ 9.32)	Full Equations (eqns. 9.24)	Approximations (eqns. 9.31/ 9.32)	Full Equations (eqns. 9.24)
Sea Level	223	0.1185	0.0502	1.68	1.89
Sea Level	950	0.1180	0.1203	8.58	8.29
35,000	487	0.06980	0.0734	2.34	2.55
35,000	681	0.06580	0.0625	3.37	3.47

Table 9.6 summarizes the effects of airspeed and altitude on the roll mode and Table 9.7 illustrates the effect of these variables on the Dutch roll mode. Each tabulation shows the errors introduced in using our approximations. Clearly, the complete equations are preferable. These complete equations generated the time histories in Fig. 9.12, showing the character of the Dutch roll. The time histories show the strong damping that develops at high dynamic pressure; there is a stark contrast between the first two time histories in Fig. 9.12 that illustrate this effect. Also, the decrease in $\omega_{n_{Dr}}$ as altitude increases is clearly seen. Finally, notice the large increase in $\omega_{n_{Dr}}$ as airspeed increases at either altitude

9.1.5.8 **Sensitivity to Lateral-Directional Stability Derivatives**. Blakelock[12] also considers the sensitivity of the lateral-directional modes of motion to variations in the asymmetric derivatives. Table 9.8 summarizes and compares the effects of the most significant of these derivatives on this type of motion, just as we previously did for the longitudinal modes of motion. Notice that our example, using the mathematical model of a rather different airplane, leads to the same conclusions.

Table 9.8 Effects of Stability Derivatives on Asymmetric Modes of Motion[12]

Stability Derivative	Motion Parameter Affected Most	Effect on Motion Parameter
C_{n_r}	ζ_{Dr}	Increase $\lvert C_{n_r} \rvert$ to increase damping
C_{n_β}	$\omega_{n_{Dr}}$	Increase C_{n_β} to increase natural frequency
$C_{\mathcal{L}_p}$	Roll Subsidence	Increase $\lvert C_{\mathcal{L}_p} \rvert$ to increase roll mode time constant
$C_{\mathcal{L}_\beta}$	Spiral Divergence	Increase $\lvert C_{\mathcal{L}_\beta} \rvert$ to improve spiral stability

9.1.5.9 **Summary of Linear Lateral-Directional Dynamics**. The linearized lateral-directional equations of motion illustrate clearly just how complex asymmetric motions are. The approximate equations are even more inaccurate than they were for the symmetric motions. Though these approximations are useful for planning flight tests, they must be used with discretion.

9.2 DYNAMIC FLIGHT TEST METHODS

Flight tests designed to determine dynamic characteristics of airplanes are some of the most challenging. The flying precision required and the care in data reduction required are primarily responsible for this challenge. Moreover, the subjective character of closed loop handling qualities is tied very closely to open loop dynamic characteristics of the vehicle and its control system; so, cooperation and understanding between the pilot and the flight test engineer are absolutely essential to obtaining meaningful results from such tests. First, consider how open loop dynamics can best be excited.

9.2.1 Types of Control Inputs

An infinite number of inputs could be used; indeed, random excitations from atmospheric disturbances excite the dynamics when encountered. However, most linear dynamic theory is built around three ideal inputs -- step inputs, pulse inputs, and doublets (Fig. 9.13). Except for the phugoid and the spiral modes, dynamic motions are usually excited by rapid pilot inputs. No control system can provide an infinite rate of surface movement; ideal inputs cannot be achieved. Even if the control system could provide such rates, pilots cannot perfectly return the surface exactly to its trim position for stick-fixed inputs. Pilot inputs are not repeatable from test point to test point, much less from pilot to pilot. Some flight test programs now use automatic flight control system inputs to excite dynamic modes. Repeatability is improved when electromechanical inputs are programmed into the flight profile. The Shuttle Orbiter and the X-29 are two test programs

where such programmed inputs were used to advantage. Both the test pilot and the test engineers on the ground simply monitor the resulting motion.

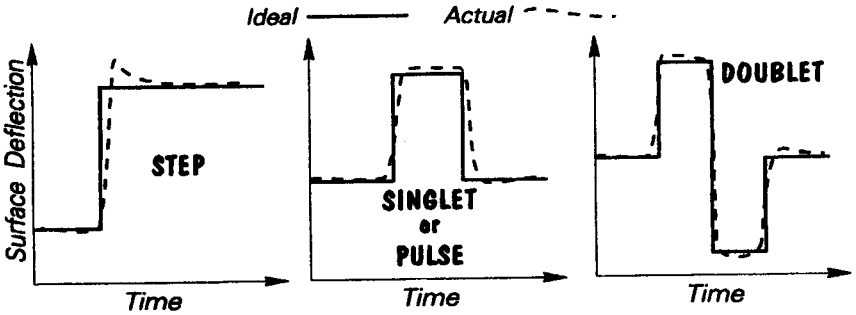

Fig. 9.13 Control Inputs for Dynamic Testing

9.2.1.1 **Step Input**. Ideally, a step input is a movement of the control surface to the desired position in zero time. The surface then remains in that new position, either because the pilot holds it there or because the surface has no tendency to float with aerodynamic forces (as in an irreversible control system). Of course, if the stick or rudder is freed and the trim mechanism moves the stick or rudder back to the original position, the input is no longer a step. The final level is not maintained. No real control system can provide an input in zero time; therefore, as Fig. 9.13 shows, there is a finite slope to the actual input. Naturally, a step input has the undesirable effect of setting the control surface to a new trim position, which causes the vehicle to take on a new equilibrium state. An elevator step input will cause an airplane to stabilize in a new attitude and at a new trim airspeed some time after the step input is made. In other words, any oscillation that is excited by a step input will not return to the original equilibrium state. Dealing with these two equilibrium states in response measurements can be tedious.

9.2.1.2 **Singlet**. As Fig. 9.13 also shows, a singlet (often called a pulse) is merely a step input, followed a short time later by a negative step input of the same size but opposite sense. The surface deflections occur instantaneously in an ideal singlet. Again, such infinite rates of movement of any physical mechanism are impossible.

9.2.1.3 **Doublet**. A doublet, merely a singlet followed immediately by a second pulse opposite in sense to the first one, is an even more common technique used to excite dynamic modes of motion. A doublet is ordinarily used when an oscillation exactly (or as close as possible) about the original equilibrium point is sought. For quick evaluation of dynamic characteristics without mathematical analysis, such a time history is easy to interpret. As can be seen from Fig. 9.13, the doublet is a periodic function if performed perfectly. This picture makes it easy to visualize the frequency content of this type of input excitation. As you might expect, the nature of the response depends on the frequency of this input. We will have more to say about this frequency dependence when we turn our attention to the longitudinal modes of motion. Let us consider first the phugoid, which has little dependence on the nature of the input; in fact, one does not even have to use the primary control surfaces to excite this oscillation.

9.2.2 Phugoid Test Methods

The first step in setting up for virtually any of the dynamic tests is to carefully trim the airplane at the desired test conditions. The engineer should insist that the desired equilibrium conditions are attained before any excitation is applied. Of course, there are some types of tests where the airplane cannot be trimmed completely. For example, the Shuttle Orbiter (or any other glider, for that matter) cannot be trimmed for constant airspeed and altitude. So, data must be collected in a dynamic environment. However, most of the elementary test methods described in this book start from true equilibrium conditions and the pilot must trim the airplane with care. A good rule of thumb is that, if airspeed and airspeed can be maintained within 0.5 KIAS and 20 feet for 10-15 seconds, trim is satisfactorily established. The pilot must make no control inputs during this time. The phugoid test is one of the tests for which such a careful trim point is essential.

A singlet of fairly long duration is used to excite the phugoid. Actually, the duration of the singlet is not critical; it is best to simply hold the initial step in long enough to reduce (or increase) the indicated airspeed by some set amount (approximately 5% of the trim indicated airspeed is a good starting estimate). Care should be taken to return the control surface as nearly as possible to the original trim position; otherwise, the oscillation will have a climb or dive superimposed on it and the analysis is a bit more difficult. Depending on which type of measurements are sought, the pilot may fix the stick after returning it to the neutral position (stick-fixed oscillations) or he may release it after returning it to the neutral position (stick-free oscillations). Both types of oscillations should be examined if the control system is reversible. Of course, the airplane's free response is sought, the pilot must make no longitudinal inputs after returning the stick to the neutral position. However, small lateral control inputs to keep the wings level are allowed while the oscillation is being recorded. But, bank angles as small as 5°-10° may affect the phugoid damping ratio (ζ_p) and its undamped natural frequency (ω_{n_p}). For some vehicles, it is more convenient to reduce the airspeed using speed brakes or even power than by elevator or horizontal tail inputs alone. Any method that will start the exchange between potential and kinetic energy is satisfactory.

As with all dynamic parameters, it is best to record the phugoid oscillation with some form of automatic recording device, though this oscillation is usually of low enough frequency that the pilot can time a period with a stop watch. Airspeed, altitude, or pitch attitude all give accurate phugoid oscillation parameters with their response character. If you lack instrumentation, a video tape or motion picture camera of the instrument panel will provide an accurate measurement of the phugoid parameters. One trick to obtain repeatable periods for the phugoid is to mark the time when the vertical velocity indicator passes through zero rate of climb or descent. Of course, the period of the oscillation is between the adjacent times for zero rate of climb when the indicator is moving in the same direction. You should not start timing to obtain this parameter until after the short period (if it is excited by the input) has damped out. Typically, a half cycle of the phugoid is quite adequate for the short period motion to be negligible; so timing for the phugoid should start no sooner that one phugoid half-cycle after the input excitation is removed.

Calculated phugoid time histories are shown in Fig. 9.14. We will defer discussing how to extract phugoid damping ratios and frequencies until we have reviewed meas-

urement of lateral-directional dynamic modes. Notice that the phugoid oscillation is lightly damped in all cases and that ω_{n_p} increases as altitude increases.

9.2.3 Short Period Test Methods

The pilot is quite sensitive to short period frequency and damping; these parameters have a strong influence on pilot ratings for virtually any precision flying task. The pilot senses dynamic parameters through both visual and tactile perceptions. He observes the pitch attitude variations, he feels the normal accelerations, and he visually records information from all available indicators (angle of attack indicator, accelerometer, or pitch rate indicator). All of these cues are integrated in the human brain to give frequency response information about the airplane's dynamic behavior. The stability and control manuals[2,9] from the test pilot schools have more complete discussions of how each of the dynamic parameters affects pilot opinion of an airplane. Perhaps the most complete document discussing this important aspect of airplane dynamics is Chalk's work[8]. This document is "required" reading for those regularly engaged in flying qualities tests.

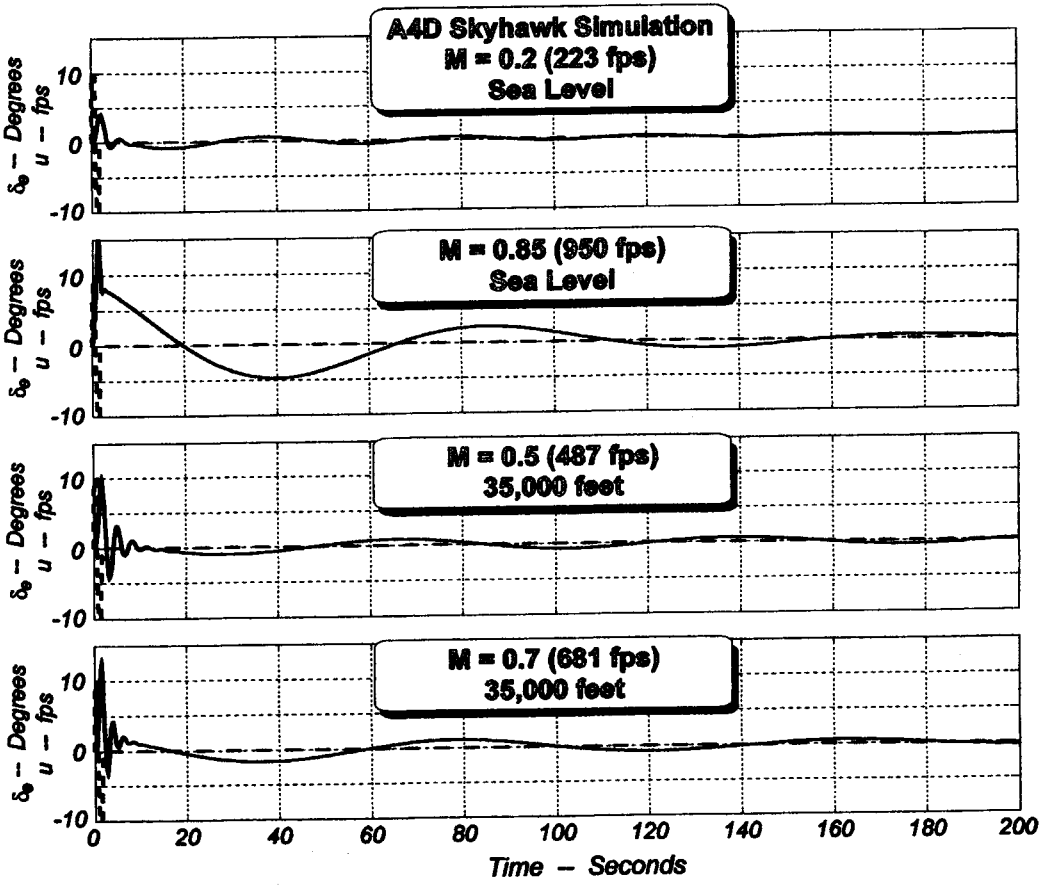

Fig. 9.14 Phugoid Oscillation

The most common input used to excite the short period is the doublet discussed previously (see Fig. 9.13). This type of input is usually quite good for exciting the short period while suppressing the phugoid, simply because the input begins and ends at the trim pitch attitude at very nearly the trim airspeed if performed correctly. Starting the doublet with a nose down pitch rate first is slightly more comfortable for most pilots, but satisfactory data can be obtained with the opposite initial pitch rate. This periodic input causes transient deviations in pitch rate, normal acceleration, angle of attack, and pitch attitude that are associated with the short period motion. A typical short period oscillation for a light twin is shown in Fig. 9.15.

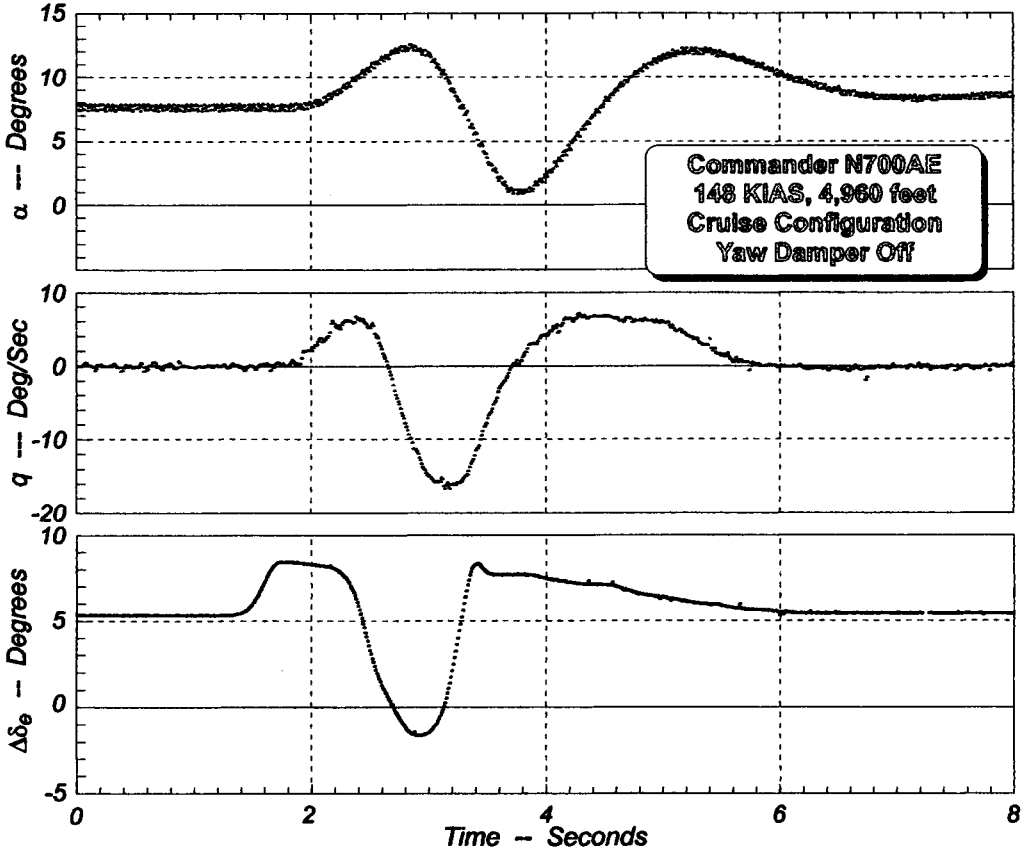

Fig. 9.15 Short Period Response to a Doublet for a Light Twin

The airplane response must be measured after the control inputs have ceased; but, unlike the phugoid measurements, the important part of the time history is immediately after the doublet is completed. For that reason it is important that control inputs be recorded simultaneously with the other dynamic parameters. It should also be obvious that recording devices are essential for obtaining quantitative measures like short period damping ratio, undamped natural frequency, and damped natural frequency (ζ_{sp}, $\omega_{n_{sp}}$, and $\omega_{d_{sp}}$, respectively). The pilot can obtain a rough estimate of ζ_{sp} by counting the number of peaks of the oscillation in pitch attitude until he can no longer discern an oscillation. If the damping ratio is $0.1 < \zeta_{sp} < 0.7$, as it is for most aircraft,

$$\zeta_{sp} \approx \frac{7 \text{ - number of peaks counted}}{10}$$

The singlet can also be used to excite the short period mode of motion. Unfortunately, especially for slow-responding airplanes like most commercial airliners and most bombers and tankers, this type of input also excites the phugoid and it is not easy to separate the two quadratic factors in analyzing the data. It is useful for quick-responding airplanes that also have enough pitch damping to cause the short period to subside before the phugoid oscillation develops.

Finally, a form of the step input can also be used to excite the short period when the airplane has a low frequency short period and/or heavy damping of this oscillation. It is especially appropriate for this type of airplane when a larger amplitude motion is needed for accurate data reduction. The disadvantages of this excitation method are that it requires more test time and maneuvering by the pilot. It will likely not be quite as repeatable as the simpler doublet form of excitation. This technique is sometimes called the "2g pull-up" method, though of course any normal acceleration level consistent with the airplane limitations and the pilot's skill could be used. After carefully trimming (as always), airspeed is traded for altitude and then the pilot pushes over to establish a shallow dive. The dive angle must be adjusted for each configuration and for different points in the operating envelope. This adjustment is often an iterative process and adds to the amount of test time that this excitation method requires. Trim altitude should be approached in a steep enough nose-down attitude so that the pilot can pull up sharply to the desired normal acceleration and establish a constant pitch rate. As the airplane approaches the initial trim attitude in this rotation, the pitch rate should be constant, normal acceleration should be constant at approximately the desired value, and the altitude should be very close to the initial trim altitude. At that point the longitudinal controller should be smartly neutralized and either fixed in the neutral trim position or freed at that position.

The use of the traditional second-order dynamic system measures of merit (like damping ratio and undamped natural frequency) alone has led to inexplicable discrepancies between pilot opinion ratings and these measures of merit. The military specifications[3,8] state requirements in terms of another parameter, $\frac{n}{\alpha}$. The ratio of maximum pitching acceleration to steady state normal acceleration during maneuvers is roughly equal to the ratio $\frac{\omega_{n_{sp}}^2}{n/\alpha}$. This parameter seems to indicate initial response better than ζ_{sp} and $\omega_{n_{sp}}$ alone. Obtaining this parameter for each test condition is often a simple task if analog recording devices are available or if digital systems have a high enough sample rate. If the normal acceleration and the angle of attack at any desired flight condition can be recorded, obtaining $\frac{n}{\alpha}$ is a simple division. One way to obtaining such data is a near-sinusoidal pumping of the longitudinal controller while recording normal acceleration and angle of attack. The frequency of the periodic input can be varied to cover the entire range of frequencies of interest. These data can also be used to determine the minimum transient stick force per g ratio. This ratio is usually obtained when the stick is pumped at

a frequency close to $\omega_{n_{sp}}$. Care must be taken by the test pilot in making such inputs to keep them small enough to avoid overstressing the airplane when the input frequencies are close enough to $\omega_{n_{sp}}$ that they might excite a resonance or lead to pilot-induced oscillations. Use very small amplitude inputs and build up to larger ones only if needed for data analysis when conducting such a test. Having completed our discussion of longitudinal dynamic test methods; we now turn to lateral-directional measurements.

9.2.4 Dutch Roll Test Methods

The only remaining oscillatory motion normally encountered in dynamic flight testing is the coupled lateral-directional oscillation. The other lateral-directional modes are typically aperiodic. For that reason we will defer discussion of the test methods associated with the spiral mode and the roll mode until after discussing the Dutch roll.

This oscillation can be quite uncomfortable to both crew and passengers and may seriously affect the utility of an airplane if it is objectionable. Swept-wing commercial airliners often need yaw dampers to augment the natural damping of the aircraft. Otherwise, passengers might even become ill from Dutch roll excited by atmospheric turbulence. Military ground attack aircraft may not allow precise tracking of targets at low altitudes if this oscillation is not damped artificially.

Dutch roll, like the short period, is most commonly excited by a doublet, though other forms of inputs can be used. The rudder pedals are usually the pilot controller used to input this doublet. If the pilot input is not quite symmetric, it is very easy to excite the roll mode and/or the spiral mode and make data analysis difficult. Also, the test team must keep the dynamic sideslip limitations of the airplane in mind when performing deliberate Dutch rolls. Finally, on vehicles operated at high dynamic pressures, deliberately inducing Dutch rolls can load the vertical surfaces highly. Several test aircraft have lost parts of the vertical tail or the rudder due to excessive aerodynamic loads during such dynamic overshoots. Appropriate care must be exercised; loads may be monitored in real time if the aircraft is highly instrumented and has telemetry capability.

An aileron singlet can also be used to excite the Dutch roll. Ordinarily, such a maneuver is started with the airplane at some steady bank angle. Aileron is applied as rapidly as possible (near a step input) to roll out of the turn. Opposite aileron is abruptly applied as the wings approach level flight. For some aircraft, like those with large mass and high inertias, this technique often provides more realistic amplitudes of Dutch roll oscillation than do rudder doublets. This input, like the rudder doublet, may end with the rudders fixed or free in the neutral position.

The Dutch roll can be also be excited by another form of the singlet, though this control input involves the use of two controls simultaneously. The controls are abruptly released from a steady, straight sideslip by simultaneously neutralizing both the rudder and the ailerons (and then either fixing or freeing both of these controls at the neutral point). This technique is applicable for some airplanes for which a single control input (either rudder doublet or aileron singlet) does not adequately excite the Dutch roll oscillation. Ordinarily, it is only needed if the Dutch roll is highly damped. Releasing the controls abruptly from a large sideslip can produce unexpected results, from dynamic overshoots of maximum allowable sideslip angle to structural overloads on the vertical tail. Such safety considerations dictate that the pilot should build up cautiously by starting with small values of β and then increasing β incrementally until an oscillation with satisfactory char-

acteristics is achieved. Do not attempt this form of excitation from maximum static sideslip angles without such a preliminary buildup.

Whatever the type of input, quantitatively analyzing Dutch roll measurements also requires recording devices to be on the airplane. Like all the other airplane oscillations, extremely high frequency data recording is not essential. Frequencies of interest in these motions are usually on the order of 10-25 Hz; so, digital recording is possible with relatively low cost instrumentation. Do not forget, however, that the sampling theorem states that discrete sampling rates must be at least twice that of the highest frequency of interest. Most flight test agencies target a sampling rate an order of magnitude greater than the highest motion frequency being studied.

A typical Dutch roll oscillation is depicted in Fig. 9.16. This particular test sequence was initiated by a rudder doublet. Notice that the aperiodic lateral-directional modes affect this oscillation. It is virtually impossible to excite the Dutch roll without exciting the other two modes of motion. To extract ζ_{Dr} and $\omega_{n_{Dr}}$ from such response time histories, we must first understand how to test for the spiral mode and the roll mode.

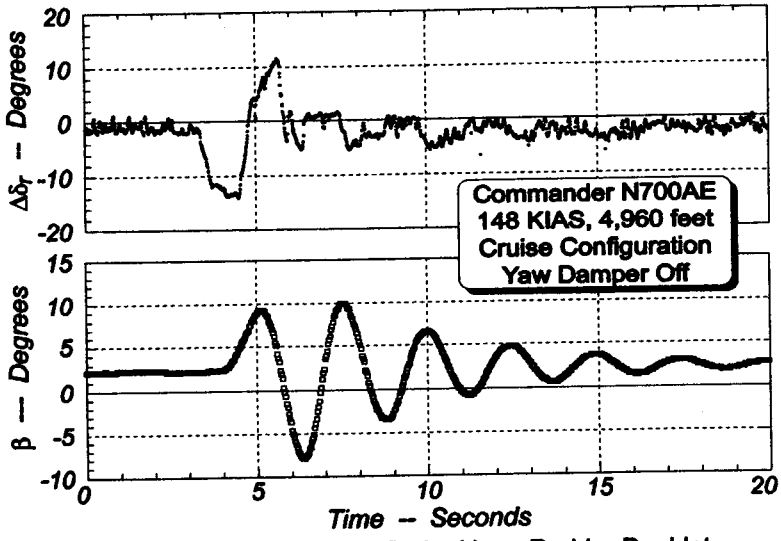

Fig. 9.16 Dutch Roll Oscillation Excited by a Rudder Doublet

9.2.5 Spiral Mode Test Methods

The first aperiodic mode to be considered is a slow divergence or convergence in heading when the airplane is displaced in roll from the wings level equilibrium state. Exciting this mode requires no control input. After trimming carefully at the desired test conditions, simply roll the aircraft to a bank angle of approximately 10° and stabilize in the ensuing turn. Then, either fix or free the ailerons and the rudder (the elevator may be used to maintain airspeed constant). If the airplane tends to roll out of the turn, the spiral mode is stable (convergent). The time-to-half-amplitude can be measured by timing how long it takes to roll from a 20° bank to a 10° bank. Conversely, if the airplane tends to roll further into the bank, the mode is unstable and the time-to-double-amplitude can be

obtained by noting how long it takes to proceed from the original 10° bank condition to 20° bank. When using this test method, care should be taken to avoid bank angles greater than 20°. If ϕ gets larger than this value, the linearizing assumptions used in the small perturbation equations are no longer valid. For multiengine airplanes, care must be taken to ensure that all engines are producing the same thrust; otherwise, the asymmetric moment produced by the engines will overpower the spiral mode behavior.

The spiral mode usually has such a long time constant that it has little effect on the handling qualities of a conventional airplane even if it is unstable. This point is illustrated in Table 9.9[8]. Notice that the minimum times-to-double-amplitude are significantly longer than the usual Dutch roll period, but if they are shorter than indicated, pilots object because the spiral mode will require attention during precise maneuvering tasks. Such additional pilot workload is particularly unwelcome during any precision maneuver that occurs over a long time period, like instrument approaches or takeoffs and landings.

Table 9.9 Typical Spiral Stability Requirements: Time-to-Double-Amplitude (seconds)

Class	Flight Phase Category	Level 1	Level 2	Level 3
I and IV	A	12	12	4
	B and C	20	12	4
II and III	All	20	12	4

--Adapted from Chalk[9]

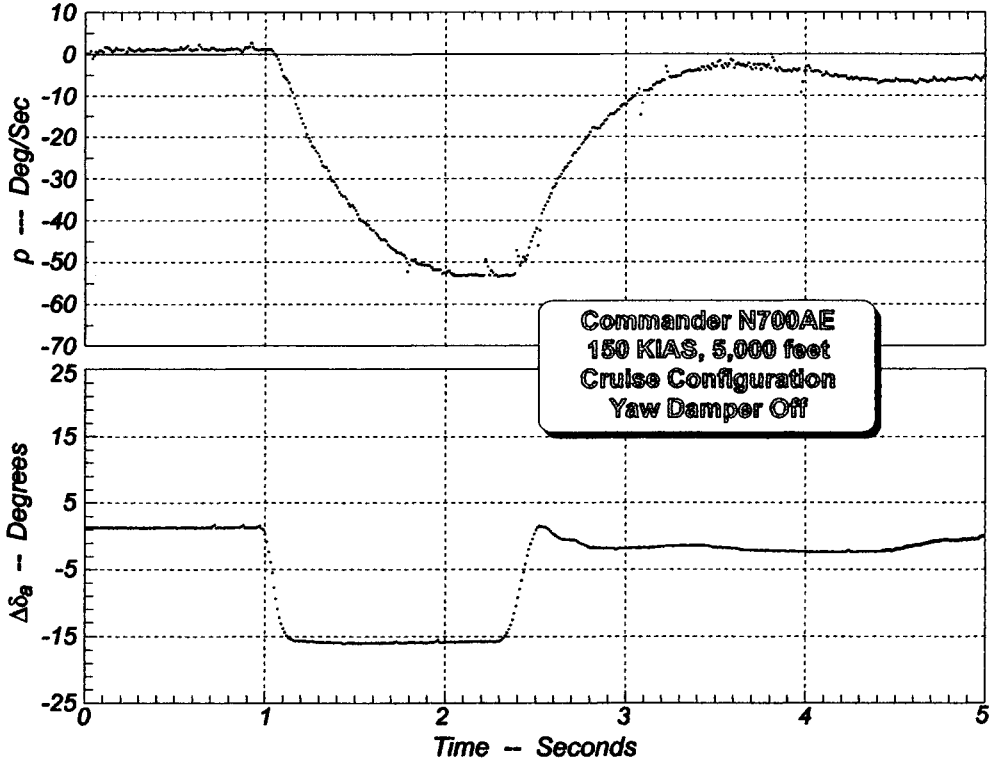

Fig. 9.17 Roll Mode Tests: 45°-45° Bank Change for a Light Twin

9.2.6 Roll Mode Test Methods

The roll mode is most often excited by a step or a singlet aileron input. Figure 9.17 illustrates the results of a roll mode test excited by a step input for a general aviation light twin. Procedurally, the most efficient way to collect roll rate measurements is to roll from a chosen bank angle to the same bank angle of the opposite sign; once stabilized at this opposite bank angle, roll back in the other direction with an identical step aileron input of the same magnitude. Temporary stops are often used to keep the aileron inputs to approximately the same size and to make them precise and repeatable. Of course, the usual necessity for trimming precisely at the desired flight conditions applies to this test also. The choice of the initial bank angle to use largely depends on the type of aircraft being tested. Typically, fighters, trainers, and other smaller airplanes are more maneuverable and 45° is used. This bank angle change was used for the light twin in the maneuver depicted in Fig. 9.17. For larger aircraft, 30° is more appropriate. Some requirements documents specify times to roll through 60° or 90°; if these data are also sought, be sure the pilot carries the roll slightly beyond the bank angle of opposite sign before stopping the roll. Otherwise, the times will be inaccurate. For timing such rolls, recording bank angle and surface position time histories is highly desirable, though stop watch timing of such rolls gives approximate information if instrumentation is meager. In any case, you must record such time histories to extract the dynamic information; the roll mode time constant is almost always too short to be observed manually. It is also useful to record variations in airspeed during roll mode testing, especially as you build up to maximum aileron deflections. It is permissible to use the longitudinal control (elevator) to help maintain airspeed during rapid rolls. Such roll tests should be carried out in both directions, since there are often factors that produce different roll dynamics in each direction.

9.2.7 Basic Data Reduction Methods

As promised earlier, we now turn our attention to data reduction techniques. In this introductory text we will confine our study to simple methods, techniques that would have been called "hand-calculations". Of course these basic tools could be implemented on a computer, but before you automate a process, you need to understand it. So, we will describe the data manipulations in graphical terms to make the material easy to understand. Most of the calculations can be readily automated; in fact, homework exercises used by the author in formal classes often ask students to write simple programs to obtain pertinent dynamic parameters from response data. Much of the material in this section is adapted from Appendices III and VB of Chalk's report[8].

Table 9.10 Applicability of Basic Graphical Techniques For Determining ζ and ω_n

Name of Method	Range of Applicable Damping Ratio
Transient Peak Ratio (TPR)	$-0.5 < \zeta < 0.5$
Modified TPR (MTPR)	$-0.5 < \zeta < 0.5$
Time-Ratio (TR)	$0.5 < \zeta < 1.2$
Maximum Slope (MS)	$0.5 < \zeta < 1.2$
Separated-Real-Roots (SRR)	$\zeta > 1.1$

Adapted from Chalk[8]

While it would be useful to apply more advanced tools like parameter estimation to response data collected in flight, these more advanced topics simply cannot be adequately covered in an introductory volume. The student should not take this omission to suggest that these more advanced topics are unimportant. In fact these tools are routinely used in every major flight test center. Iliff[13] has worked in this field throughout his career at the NASA Ames-Dryden Flight Research Facility. His 1987 Wright Brothers Lecture is a very good overview of this approach to both modeling dynamics and estimating stability derivatives. Ljung's textbook[14] gives an even broader view of parameter estimation methods. While these topics are important, we have chosen to limit the scope of this text to introductory material only. Even if you use parameter identification extensively, these simpler techniques should be helpful in evaluating your computerized results.

There are four basic data reduction techniques (plus variations) to be discussed and each of them is best suited for analysis of specific problems. All of them give ζ and ω_n for a second order system and, of course, our usual quartic characteristic equations readily break down to no higher than second order components. Table 9.10 summarizes the applicability of these four methods for extracting ζ and ω_n from measured oscillations. The choice of method is tied rather closely to the damping ratio of the mode of motion to be analyzed. The most important method to be discussed is the transient peak ratio (TPR) method. It is the most usable of the reduction schemes if - 0.5 < ζ < 0.5, the most common range for ζ_{ph}, ζ_{sp}, and ζ_{Dr}. The time-ratio (TR) method and the maximum slope (MS) method both fit a slightly higher range of ζ, 0.5 < ζ < 1.0, though both of them may be helpful for ζ up to 1.4. The separated-real-roots (SRR) is useful for the real roots common with the lateral-directional quartic. All of the methods presented assume that the time history being analyzed starts with zero slope at the initial time, t_0. It is also assumed that this timing starts with t_0 = 0. Of course, the assumption is made that any of the oscillations associated with aircraft dynamics can be isolated and analyzed as either a first or second order response. With these applicabilities and assumptions established, let us now turn to a detailed description of each method.

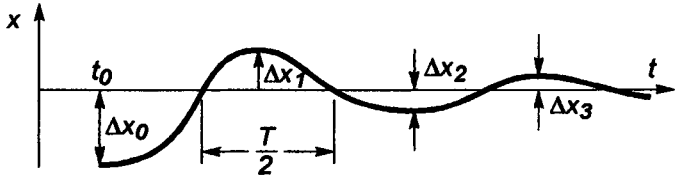

a. Transient Peak Ratio Measurements

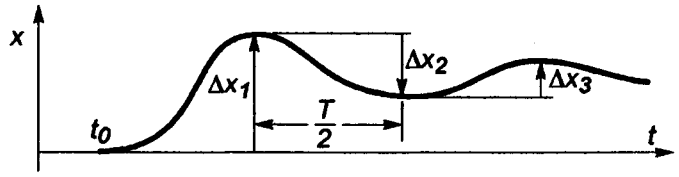

b. Modified Transient Peak Ratio Measurements

Fig. 9.18 Measurements for TPR and MTPR Methods

9.2.7.1 **Transient Peak Ratio Method**. Figure 9.18a shows the basic TPR method, while Fig. 9.18b illustrates a modification that does not require finding a steady state system response. First, we determine the transient peak ratio (TPR) from:

$$\frac{\Delta x_1}{\Delta x_0} = \frac{\Delta x_2}{\Delta x_1} = \frac{\Delta x_3}{\Delta x_2} = \cdots$$

or if the modified TPR method is used: $\frac{\Delta x_3}{\Delta x_2} = \frac{\Delta x_2}{\Delta x_1} = \cdots$. If the ratios are not identical (and they typically are not, for actual flight test measurements), an average of the measurements is often used. Whatever the procedure, once the TPR is selected, the damping ratio can be read from a chart like Fig. 9.19. Finally, ω_n comes from the measurements, since the damped period, T, is scaled as the time between the local maxima or minima or is the measured time between the steady state crossings (Fig. 9.18a). Then, ω_n is $\frac{2\pi}{T\sqrt{1 - \zeta^2}}$.

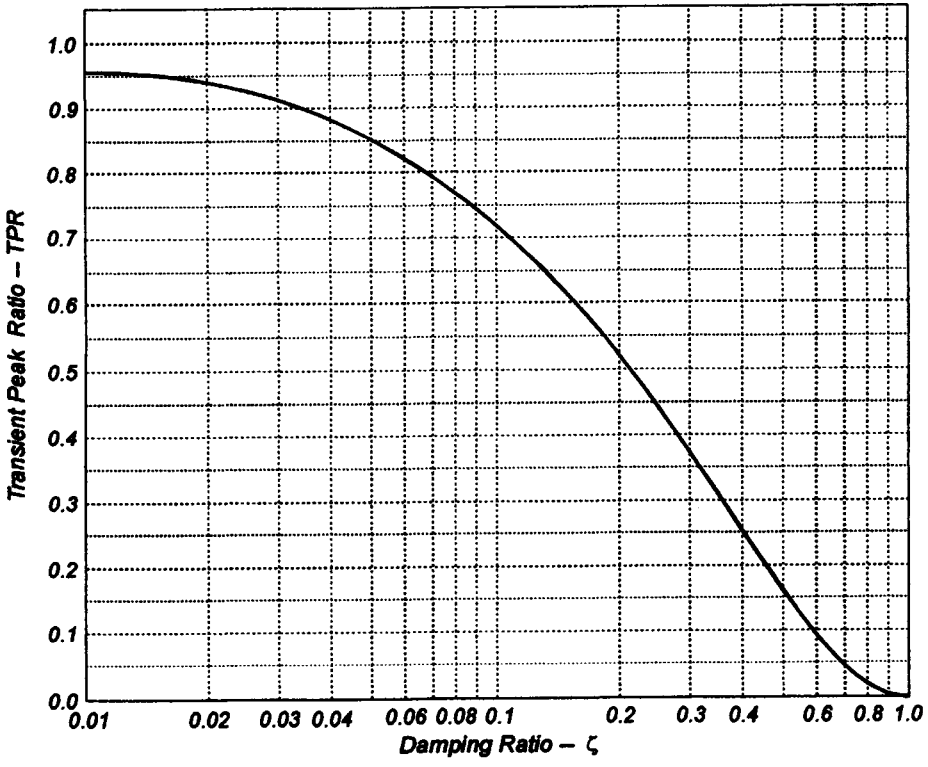

Fig. 9.19 Transient Peak Ratio Versus Damping Ratio

9.2.7.2. **Time-Ratio Method**. To use the time-ratio (TR) method, you must be able to ascertain steady state equilibrium after the excitation has subsided. This method, described by Dolbin[15], utilizes three specific values along the output response curve to calculate three estimates of ζ, at selected fractions of the change in the output variable. As shown in Fig. 9.20, these times are measured where x, the output response, is $0.736\Delta x$, $0.406\Delta x$, and $0.199\Delta x$ below the final steady state value, respectively, for Δt_1, Δt_2, and Δt_3. Then the ratios $\Delta t_2/\Delta t_1$, $\Delta t_3/\Delta t_1$, and $(\Delta t_3 - \Delta t_2)/(\Delta t_2 - \Delta t_1)$ are calculated and used to enter the chart shown in Fig. 9.21.

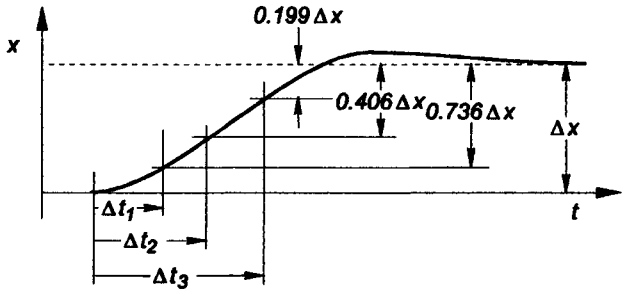

Fig. 9.20 Measurements for TR Method

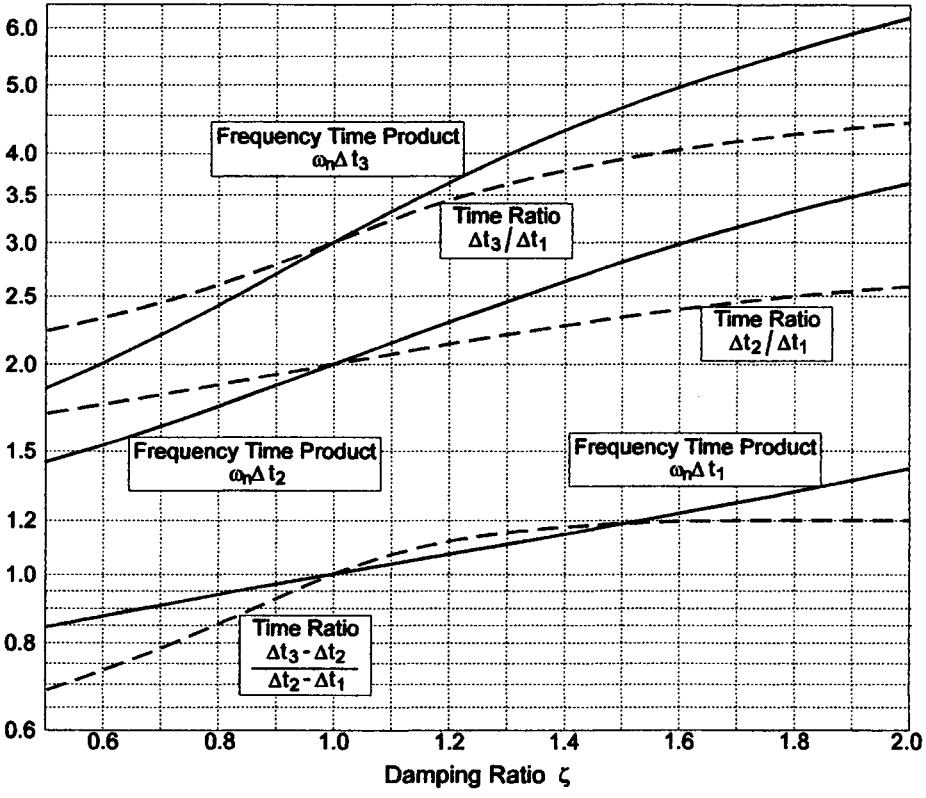

Fig. 9.21 Chart for Determining ζ and ω_n by TR Method

Figure 9.21 yields three estimates of ζ. We could simply average these three numbers, though it is a good idea to weight the ζ according to how much the oscillation measurements are distorted from a pure second order system. Generally, Δt_1 is the least accurate of the time measurements because it is quite sensitive to our choice of t_0. Moreover, the response is often affected significantly in this region by control system dynamics, which introduce higher order responses. On the other hand Δt_3 can also be in error due to uncertainty in choosing the final steady state value. These factors mean that you should use some engineering judgment in considering which damping ratio to choose. But, the TR method does provide you with three checks. Finally, the undamped natural

can also be determined straight from the chart in Fig. 9.21, just as the values for ζ were obtained. The only difference is that $\omega_n t_1$, $\omega_n t_2$, and $\omega_n t_3$ are read from the ordinate of the chart and then divided by the appropriate time to obtain three estimates of ω_n. Naturally, the remarks about use of engineering judgment in either averaging or choosing the best estimate of ω_n are still applicable.

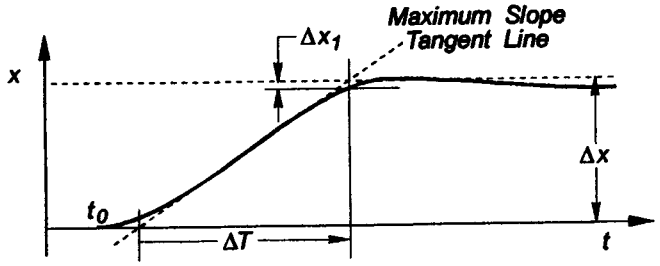

Fig. 9.22 Measurements for the Maximum Slope Method

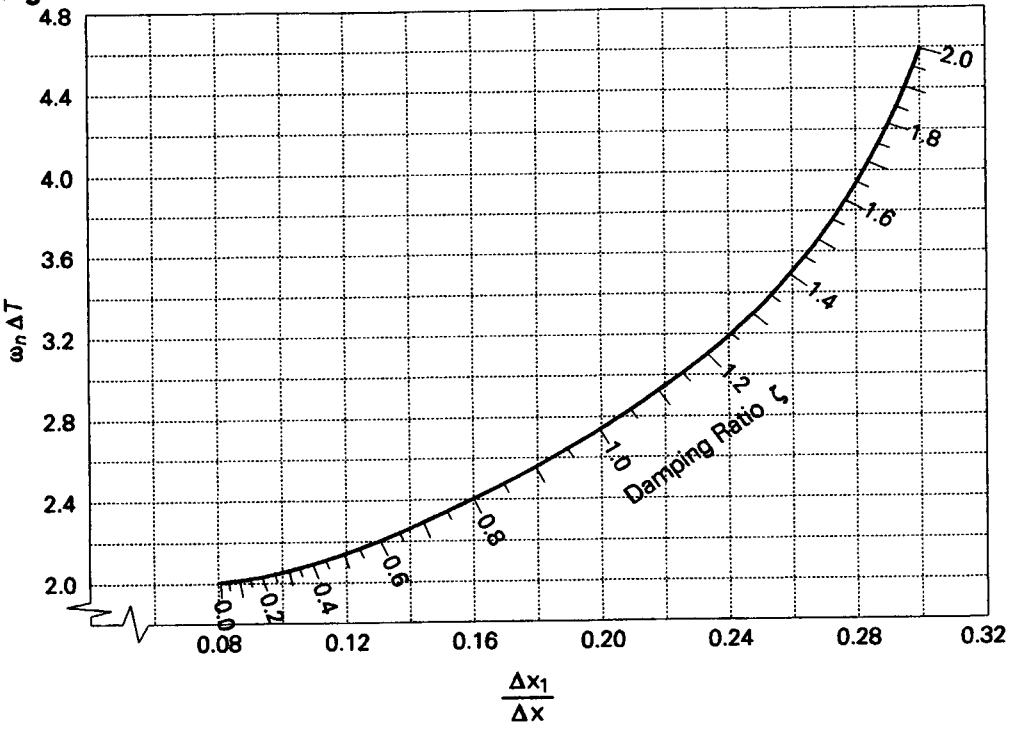

Fig. 9.23 Chart for Determining ζ and ω_n by the Maximum Slope Method

9.2.7.3 **Maximum Slope Method**. The maximum slope (MS) method was developed[16] to reduce the inaccuracies in the TR method that are associated with determining the steady state response. Figure 9.22 shows the basic parameters to be taken from the response time history for the MS calculation. In this approach, the peak amplitude of the response and the maximum slope of the tangent to the transient rise are used instead of intermediate times (as in the Time Ratio method). However, the MS technique has its own

inherent error source: the amplitude Δx_1 is usually very small and difficult to measure accurately. This error effects ζ mostly; ω_n is largely unaffected by this uncertainty. The ratio $\frac{\Delta x_1}{\Delta x}$ is then calculated and used to enter Fig. 9.23, where both ζ and $\omega_n \Delta T$ can be obtained graphically. Then, rather simplistically, $\omega_n = \frac{\omega_n \Delta T}{\Delta T}$.

9.2.7.4 **Separated-Real-Roots Method**. As Table 9.10 indicates, the separated-real-roots (SRR) technique was developed to evaluate responses composed of two unequal real roots. It is useful only if the damping ratio is large enough to ensure strongly convergent aperiodic modes of motion. Typically, the roll mode from the lateral-directional quartic is characterized by such behavior. Therefore, it is often analyzed using the SRR technique, especially if the spiral mode is also convergent. Figure 9.24 sketches out the parameters to be taken from the output response measurements. Once again, it is necessary to select the steady state output and the method is moderately sensitive to how accurately this value can be determined. Moreover, with this approach you must also plot $\Delta x(t)$ on semilog paper. After the faster root (t_2) has decayed, the semilog paper will be a straight line, whose slope determines the lower root (t_1). Then, $t_2 = t_1 \frac{\Delta x_0}{\Delta x_0'}$, where $\Delta x_0'$ is the intercept of the straight line on the semilog graph. Alternatively, t_2 can be determined from the slope of a semilog plot of $\Delta x(t)$ versus t.

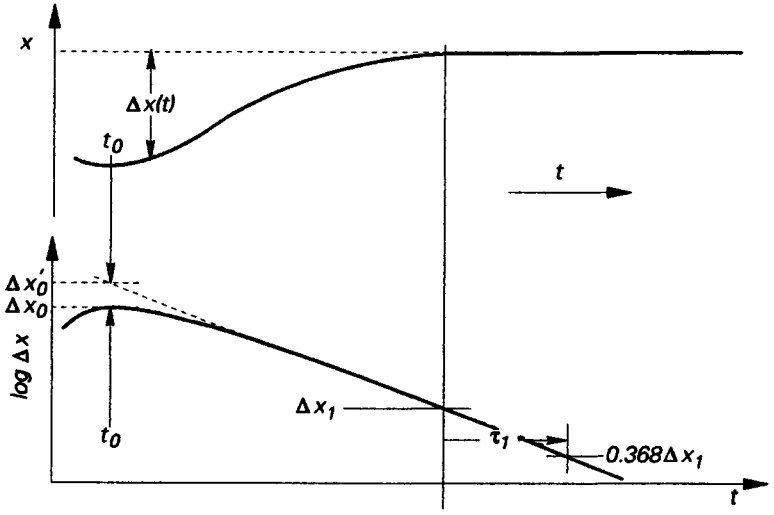

Fig. 9.24 Measurements for the Separated-Real-Roots Method

Whichever of these two graphical methods is used to obtain t_1 and t_2, the damping ratio and the undamped natural frequency come from:

$$\zeta = \frac{(t_1 + t_2)\omega_n}{2} \quad \text{and} \quad \omega_n = \sqrt{\frac{1}{t_1 t_2}}$$

To help reduce the sensitivity of the SRR procedure to errors in graphically estimating the steady state response, a modification (due to Dolbin[15]) may be helpful. The values of

$\Delta x(t)$ are simply measured in such a way that determining the steady state response level is unnecessary. They are measured at equal time increments as suggested in Fig. 9.25a. Then, each value of is $\Delta x(t)$ simply: $x(t + \Delta T) - x(t)$,

where $\Delta T = (t_1 - t_0) = (t_2 - t_1) = \cdots = (t_{n+1} - t_n)$

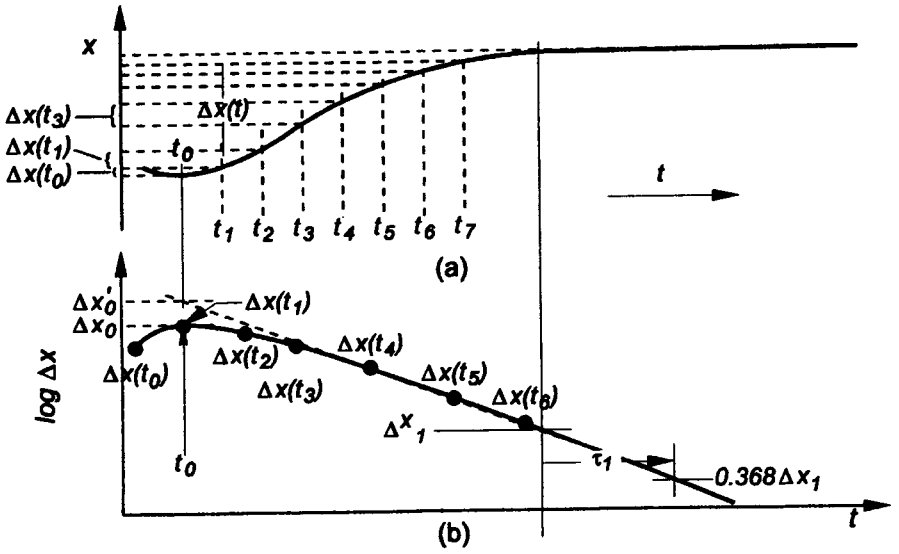

Fig. 9.25 Measurements for Dolbin's Modified Separated-Real-Roots Method

Plotting $\Delta x(t)$ on the semilog scale as suggested for the basic SRR method leads to the same result as before, except that no steady state value for the response had to be graphically determined. There is usually more scatter in the data points on the semilog plot with this modified approach, but the slope of the faired line is often more accurate. If you are using the unmodified SRR technique and assuming that $\zeta > 1$, but it is actually less than 1, you may not be able to find a part of the semilog plot that can be adequately fitted with a straight line. It will probably be obvious that some sort of error has occurred. With the modified method, this sort of faulty assumption is not as likely to be noticed. You can usually fit a straight line with reasonable scatter to these points. However, with the two real roots that you extract from these modified calculations, ζ and ω_n will be grossly in error. If you suspect that the damping ratio is only slightly greater than 1, check the results of the SRR method using the TR or the MS methods.

Example 9.3: The time histories on the next page were generated from a simulation of an F-89 Scorpion flying at 20,000 feet on a standard day at a Mach number of 0.638 (660 fps). The airplane weight was 30,500 pounds. Graphically estimate the short period damping ratio and the undamped natural frequency using the time-ratio method. Then, repeat the estimate using the maximum slope technique. The first plot shows the overall pitch rate response of the Scorpion for several seconds after a very small step elevator input (just over 1 degree change in elevator position). This small input is removed approximately 1 second after initiation. Clearly, the free response is heavily damped.

To graphically estimate the required damping ratio and undamped natural frequency, we must greatly expand the scales to have any hope of reasonable accuracy. We will choose the region where the response trace just drops into the negative range and analyze the overshoot characteristics. However, for the time ratio method we also must know the steady state value and we notice from the above chart that it

is just slightly above the zero grid line, at approximately 0.01 degrees/second. We could even take the statistical average of the readings at 10 seconds or beyond to get this value.

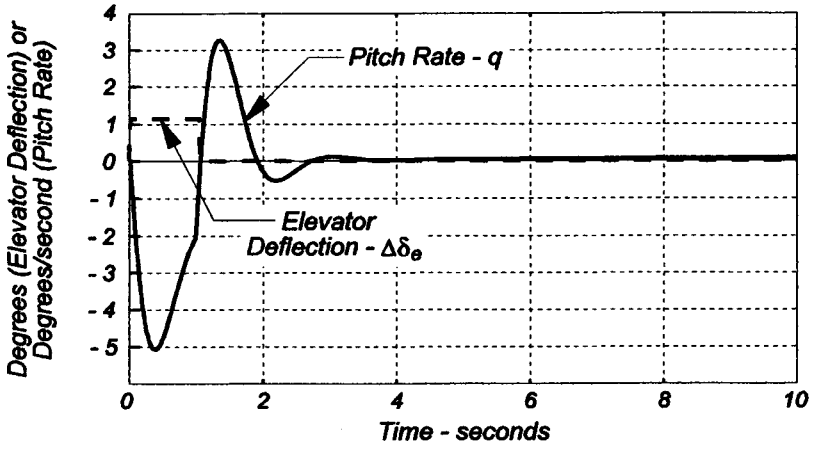

Next, we measure from this steady state value for pitch rate down to the minimum pitch rate (as shown in the figure below) to get a Δx of approximately 0.568 degrees/second.

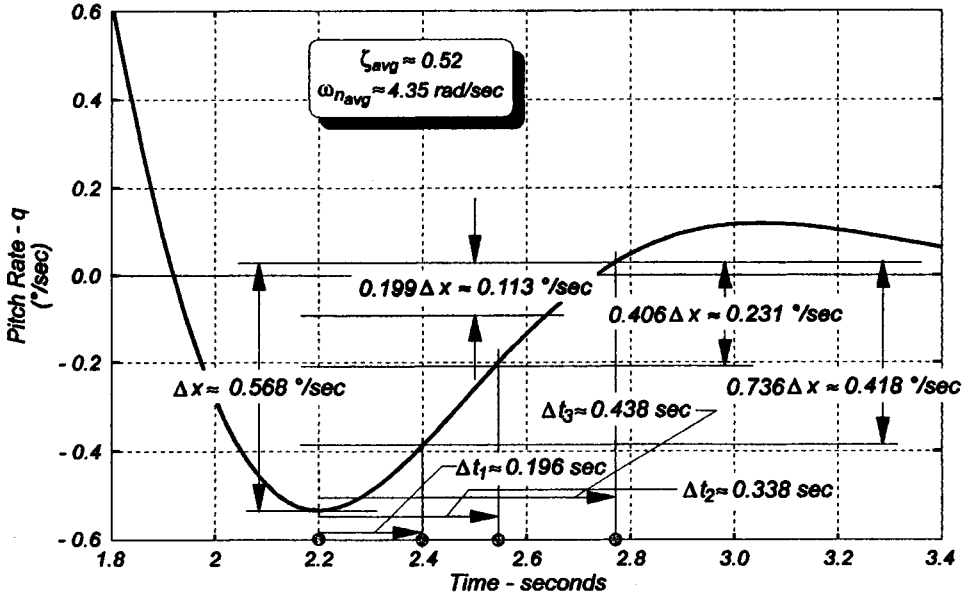

Next, draw the three horizontal lines in that correspond to the three levels of overshoot from the steady state value of q suggested in Fig. 9.20 (0.199 Δx, 0.406 Δx, and 0.736 Δx). Where these overshoot levels intersect the response curve, drop three vertical lines to the time axis and graphically measure the indicated time increments from the time when the minimum q was achieved (the peak overshoot time). For this example those values are shown on the chart above as: $\Delta t_1 \approx 0.196$ seconds, $\Delta t_2 \approx 0.338$ seconds, and $\Delta t_3 \approx 0.438$ seconds. Forming the ratios necessary to enter Fig. 9.21:

$\frac{\Delta t_2}{\Delta t_1} \approx 1.72$ which gives $\zeta \approx 0.50$ from Fig. 9.21; $\frac{\Delta t_3}{\Delta t_1} \approx 2.23$ which gives $\zeta \approx 0.51$ from Fig. 9.21; and

$\frac{\Delta t_3 - \Delta t_2}{\Delta t_2 - \Delta t_1} \approx 0.70$ which gives $\zeta \approx 0.55$ from Fig. 9.21. Averaging these values, $\boxed{\zeta_{avg} \approx 0.52}$

Reading from the other solid lines in Fig. 9.21 (the Frequency Time Product lines), we obtain the following values for $\omega_n \Delta t$ and then ω_n: $\omega_n \Delta t_1 \approx 0.865$, $\omega_n \Delta t_2 \approx 1.46$, and $\omega_n \Delta t_3 \approx 1.90$.

Dividing by the appropriate times and averaging again: $\omega_{n_{avg}} \approx 4.35$ rad / sec

Now we turn to estimating the same parameters using the maximum slope method. We still need the expanded scale drawing of the response curve, which is repeated below. For this procedure start by drawing a line tangent to the response curve at the point of maximum slope for the response. for this pitch rate response segment of the data, that line is tangent at approximately 2.5 seconds on our time scale. Next, draw two horizontal lines at the minimum q and at the maximum q for the segment of data we have chosen to analyze and extend them right and left, respectively, until they intersect the maximum tangent line. From these points of intersection drop vertical lines to the time axis and measure $\Delta T \approx 0.5$ seconds. Then, measure the approximate value of the second overshoot (the positive overshoot) above the steady state value of q. Graphically, $\Delta x_1 \approx 0.08$ °/sec. Then, forming the ratio needed to enter Fig. 9.23,

$$\frac{\Delta x_1}{\Delta x} \approx \frac{0.08}{0.65} \approx 0.123$$

$\zeta \approx 0.48$

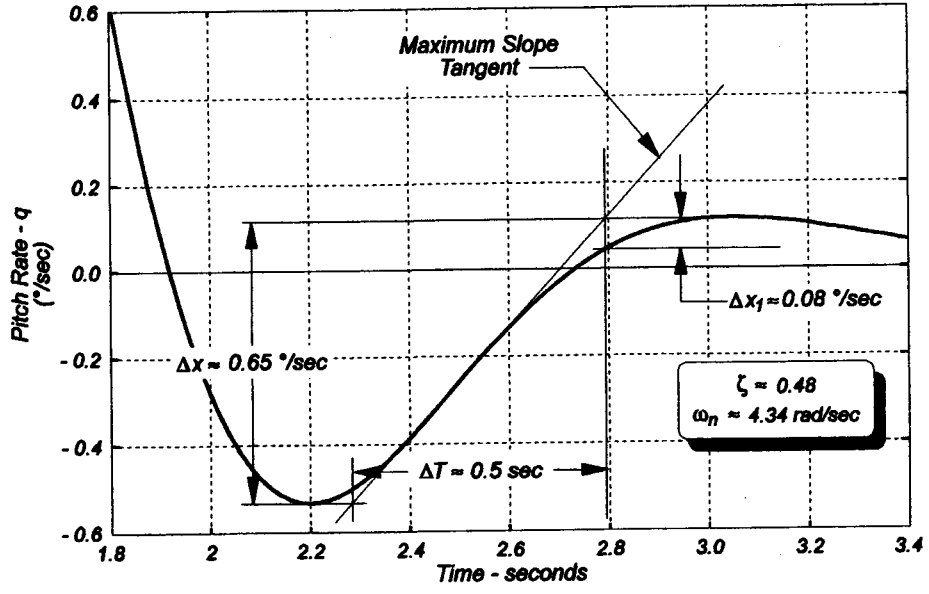

Similarly using the same ratio to obtain $\omega_n \Delta T \approx 2.17$ from Fig. 9.23,

$$\omega_n = \frac{\omega_n \Delta T}{\Delta T} \approx \frac{2.17}{0.50}$$

$\omega_n \approx 4.34$ rad / sec

The values obtained from these two graphical procedures are reasonable. Since the response data were generated mathematically, we know the actual values for and $_n$. These actual values are:

$\zeta = 0.493$ and $\omega_n = 4.27$ rad / sec

9.2.8 Calculation of Lateral-Directional Parameters from Response Data

This section illustrates how the techniques of the previous paragraphs can be applied to analysis of the lateral-directional response to a step aileron input to obtain estimates of all the roots of the quartic. The development follows closely Appendix VB from Chalk[8].

Naturally, we will continue to assume that linearity (and, therefore, superposition) holds and that the response represents the usual roll mode, spiral mode, and Dutch roll mode that are common to most rigid aircraft modes of motion. The complete roll rate response to the hypothesized step aileron input might appear as shown in Fig. 9.26.

From such a roll rate response, we will see that typical components which correlate to the eigenvalues of the lateral-directional quartic are of the form shown in Fig. 9.27. We are postulating a convergent roll mode, a divergent spiral mode and a moderately damped, medium frequency Dutch roll oscillation. It would be easy to synthesize the output response by simply adding up each of these contributions to the total response. Indeed, the time domain equation of such a total response illustrates this addition process that is common to linear systems:

$$p(t) = K_s e^{-\frac{t}{\tau_s}} + K_r e^{-\frac{t}{\tau_r}} + K_{Dr} e^{-\zeta_{Dr}\omega_{nDr}t} \cos\left(\omega_{nDr}\sqrt{1-\zeta_{Dr}^2} + \Psi_{phase}\right)$$

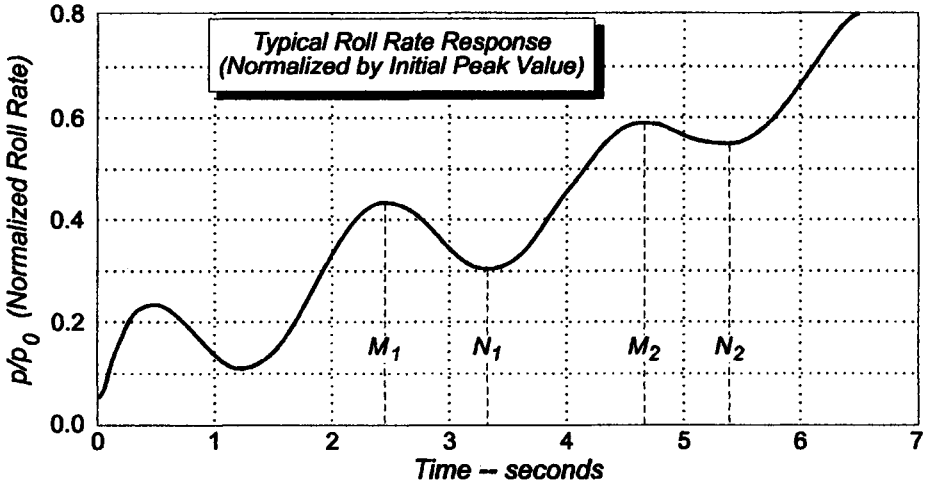

Fig. 9.26 Roll Rate Response to a Step Input

But our task is not to add up the components from a known analytical result; instead we seek to break down a measured response that already contains all the components and identify the individual parameters -- K_s, τ_s, K_r τ_r, K_{Dr}, ζ_{Dr}, and ω_{nDr}. Chalk presents both a graphical technique and an analog-matching approach, but we will restrict our discussion to the graphical method in this introductory text.

This technique produces good results only for a relatively conventional airplane with a Dutch roll damping ratio less than approximately 0.3 and when the spiral and roll modes are widely separated in frequency. This latter assumption allows us to expect that the roll mode will have little influence after the first few seconds. Typically, τ_r is about 1 second and such a first order mode will have reached approximately 95% of its final value within 3τ after the excitation is removed. Consequently, after about 3-4 seconds, we can anticipate that the residual oscillation is composed almost entirely of the spiral mode and the Dutch roll mode. Let us look at breaking out the spiral mode first from the time history data after we can reasonably expect these two modes of motion to dominate.

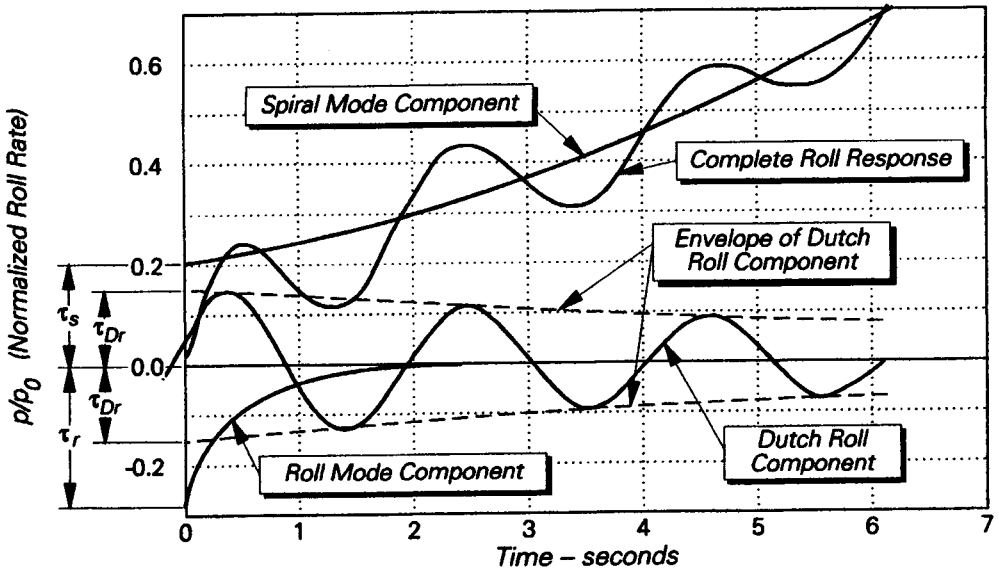

Fig. 9.27 Components of a Roll Rate Response to a Step Input

First, pick out the maximum and minimum points of the response from about 3 seconds onward (to avoid contamination from the roll mode) and plot them on semilog paper as sketched in Fig. 9.28. Rigorously, the points of tangency of the Dutch roll envelope to the total response should be plotted, but simply taking the peaks is well within any graphical accuracy you are likely to attain. However, if you decide to numerically implement this technique on a computer, keep this subtle point in mind. Local maxima and minima for times less than 3 times the roll mode time constant (τ_r) should be ignored in this envelope estimation. Clearly, we must have an oscillatory response measurement that lasts long enough so that these later peak roll rates are well-defined. Smooth curves are then drawn through the upper and lower peaks (maxima and minima, respectively) to define the envelope of the spiral mode and the Dutch roll mode components on the semilog working plot. The numerical average between the envelope boundaries defines the spiral mode component. This average should be a straight line on the semilog plot and K_s is the intersection of this straight line with the zero time axis. (K_s is also called the spiral mode residue.)

The slope of the average straight line defining the spiral mode on the semilog plot yields the time constant for this mode of motion through the following relationship:

$$\tau_s = \frac{\Delta t}{\ln \frac{x_2}{x_1}}$$

Of course, the time-to-double-amplitude (for a divergent spiral mode as has been sketched) or the time-to-half-amplitude (for a convergent spiral mode) can then be calculated directly using: t_2 or $t_{1/2} = 0.693\tau_s$

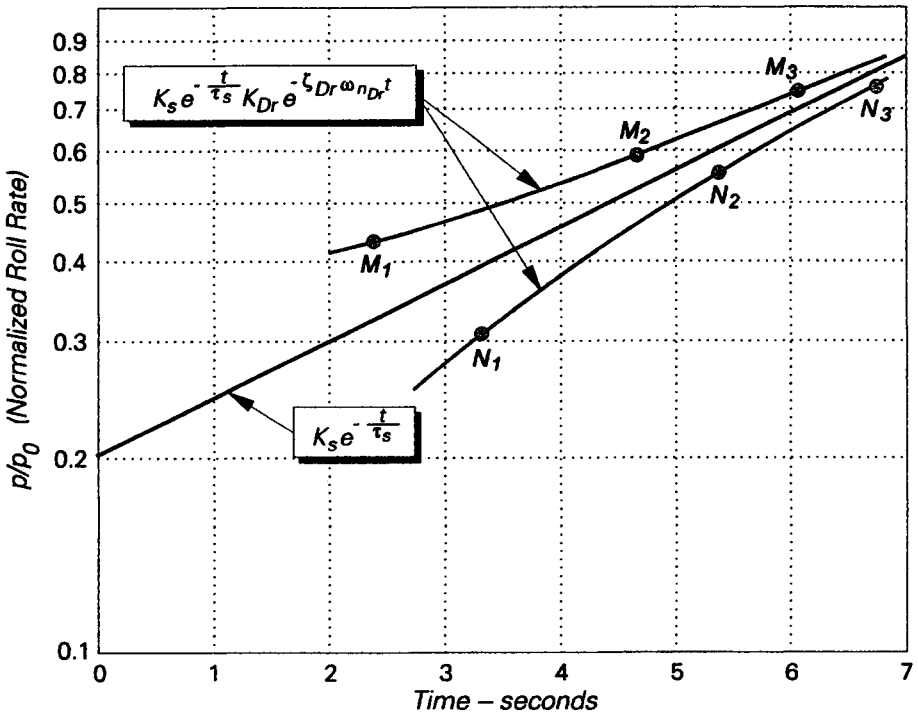

Fig. 9.28 Extracting the Spiral-Dutch Roll Mode Envelopes

The next step in the graphical procedure is to plot the spiral component on the linear time scales and subtract it directly from the overall response time history (Fig. 9.29). The resulting plot will contain both the roll and the Dutch roll mode components of the response. But the spiral mode will have been removed. The only points that must be plotted carefully are those in the first three seconds (so the roll mode can be extracted accurately) and the peaks of the Dutch roll oscillation at later times in the oscillation. Figure 9.29 (next page) illustrates this step and the complete curves are shown there for clarity, with illustrative points marked with triangles to show what you must do to actually obtain and accurate estimate of the modal components.

Now, we return to semilog paper and plot the peaks (the later ones, of course) from the combined roll mode-Dutch roll mode envelope (Fig. 9.29). This procedure is illustrated in Fig. 9.30. As this sketch shows, this plot usually results in two parallel straight lines, one for the local maxima and one for the local minima. Of course the slope of either of these lines should define ζ_{Dr}. If ζ_{Dr} has been previously estimated, this estimate should be checked against these measured slopes. Do not forget that, strictly speaking, the Dutch roll envelope does not touch the peaks. Rather the tangent points are just to the right of the peaks for the convergent oscillation. This angular displacement is approximately $\sin^{-1}\zeta$ (in degrees); the time equivalent of the angle comes from the period of the damped Dutch roll oscillation (T_{Dr}): $\frac{T_{Dr}\sin^{-1}\zeta_{Dr}}{360}$. For low damping ratios ($\zeta_{Dr} < 0.3$), this displacement is small and can be safely ignored.

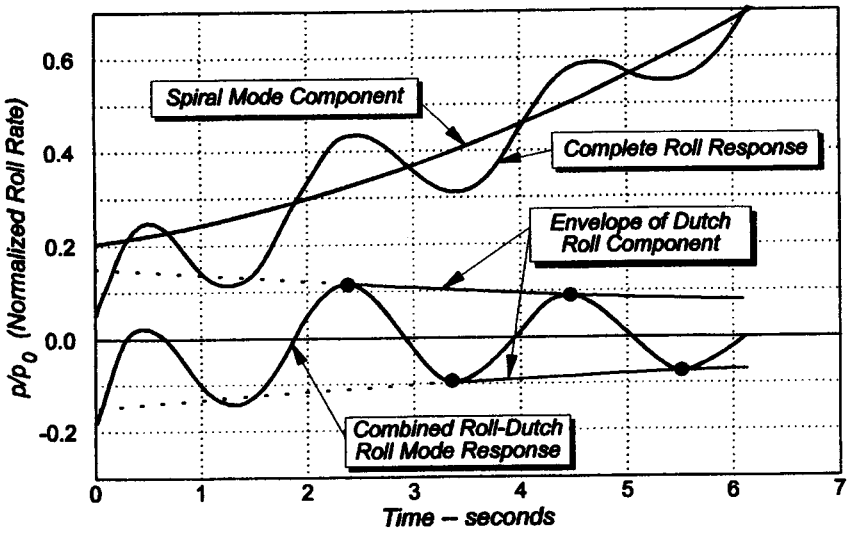

Fig. 9.29 Combined Roll Mode-Dutch Roll Mode Components

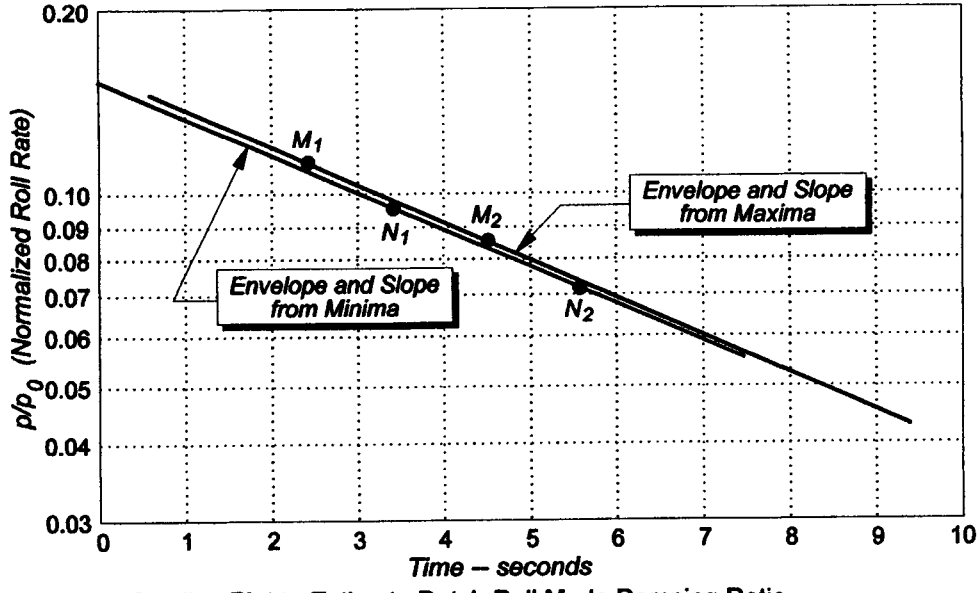

Fig. 9.30 Semilog Plot to Estimate Dutch Roll Mode Damping Ratio

Finally, the estimated Dutch roll envelope is transferred back to the combined roll-mode-Dutch roll mode time history (Fig. 9.29) to estimate the roll mode time constant. Often, it is useful to enlarge the first few seconds of the oscillation, as shown in Fig. 9.31.

The Dutch roll mode period and damping ratio are now known; they are used to reconstruct the initial part of the Dutch roll component (enlarged scale of Fig. 9.31). This reconstructed oscillation is subtracted graphically from the combined roll-Dutch roll mode component time history to yield the roll mode time history trace. This estimate for the roll mode component of the time history is also illustrated in Fig. 9.31. For the interested stu-

dent, an alternate method of determining the initial Dutch roll mode that utilizes polar plots is given by Chalk. In the interest of brevity, that alternative will not be covered.

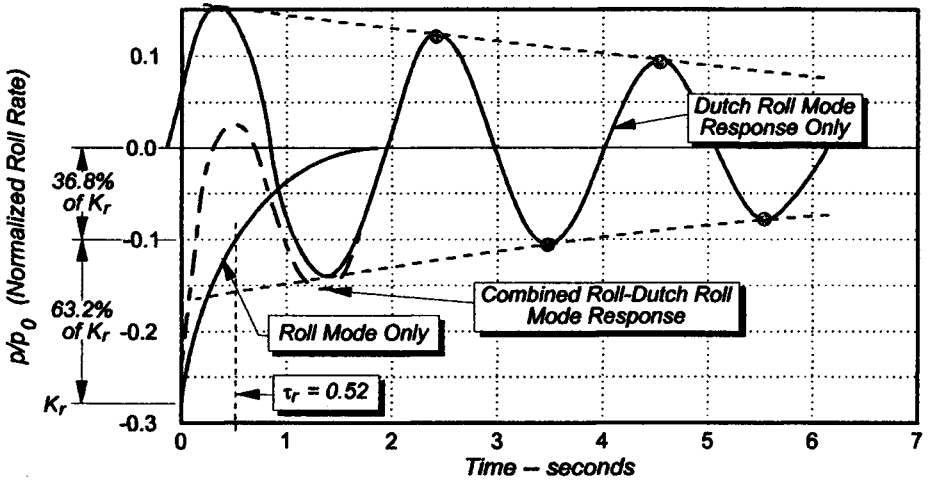

Fig. 9.31 Estimation of the Roll Mode Component

The roll mode time constant comes from Fig. 9.31. Calculating $0.368K_r$ and drawing a horizontal line at that value of normalized roll rate, the time where this horizontal line intersects the estimated roll rate time history is τ_r. We could also go back to the semilog plot and find K_r as the intersection of the straight line at $t = 0$ seconds, just as we did for the spiral mode. Another way to obtain τ_r is to simply calculate it from a time increment and the natural logarithm of the corresponding amplitude ratio: $\tau_r = \dfrac{t_{k+1} - t_k}{\ln(p_{k+1} / p_k)}$. Both alternative methods are illustrated in Fig.9.32.

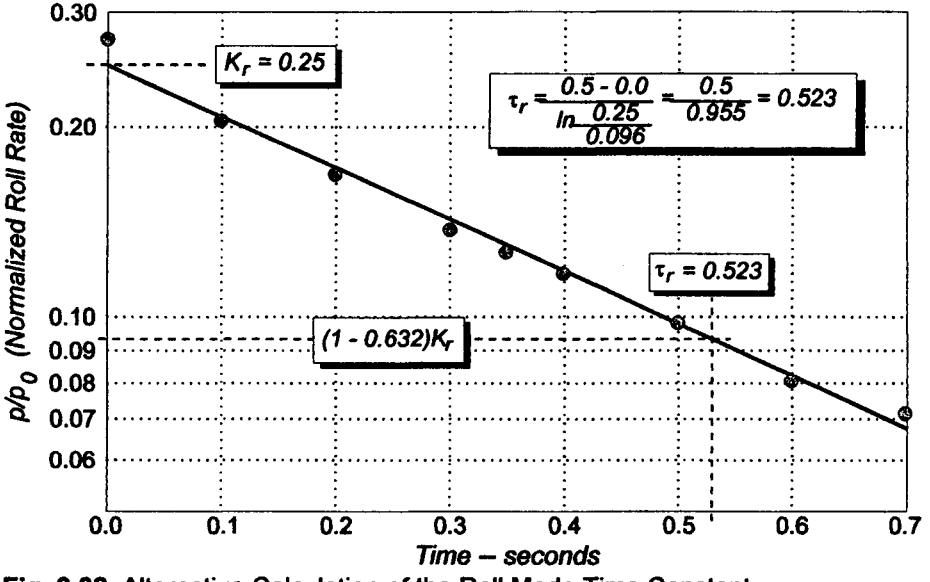

Fig. 9.32 Alternative Calculation of the Roll Mode Time Constant

9.3 SUMMARY

Dynamic flight tests are one of the most challenging types of tests you will encounter as a flight test engineer. They require a thorough understanding of stability and control principles, a moderate knowledge instrumentation that can record the necessary parameters automatically, insight into handling qualities and how pilot ratings were developed, knowledge of the types of standard inputs (pilot-induced or not) that produce responses adequate for analysis, and at least an introductory understanding of how to extract dynamic measures of merit from response data. This chapter has explained each of these fundamentals. The serious student of flight test dynamics should continue his study with more training in experimental instrumentation, sampling theory, and in parameter estimation. Each of these topics offers the flight test engineer more advanced tools. However, the goal of this chapter has been met in introducing the subject of dynamic measurements.

REFERENCES

1 Anderson, J. D., Jr., **Introduction to Flight** (3rd Edition), McGraw-Hill Book Company, New York, 1989.

2 "Fixed Wing Stability and Control: Theory and Flight Test Techniques," USNTPS-FTM-No. 103, Naval Air Test Center, Patuxent River, Maryland, Jan. 1975 (Revised Nov. 1981).

3 "Military Specification, Flying Qualities of Piloted Airplanes," MIL-F-8785C, Nov. 1980.

4 Etkin, B., **Dynamics of Flight - Stability and Control**, (2nd Edition), John Wiley & Sons, New York, 1982.

5 Roskam, J., **Airplane Flight Dynamics and Automatic Control**, Part 1, Roskam Aviation and Engineering Corporation, Lawrence, Kansas, 1979.

6 McRuer, D., Ashkenas, L., and Graham, D., **Aircraft Dynamics and Automatic Control**, Princeton University Press, Princeton, New Jersey, 1973.

7 Kuo, B. C., **Automatic Control Systems** (6th Edition), Prentice-Hall Inc., Englewood Cliffs, New Jersey, 1991.

8 Chalk, C. R., et al, "Background Information and User Guide for MIL-F-8785B (ASG), Military Specification - Flying Qualities of Piloted Airplanes," AFFDL-TR-60-72, Air Force Flight Dynamics Laboratory, Wright-Patterson AFB, Ohio, Aug. 1969.

9 "Stability and Control Flight Test Theory," Vol. I, Chapter 6, AFFTC-TIH-77-1 USAF Test Pilot School, Edwards AFB, California, Revised Feb. 1977.

10 Cooper, G. E. and Harper, R. P., Jr., "The Use of Pilot Rating in the Evaluation of Aircraft Handling Qualities," NASA TN-D5153, Apr. 1958.

11 Harper, R. P., Jr. and Cooper, G. E., "Handling Qualities and Pilot Evaluation," **Journal of Guidance, Control, and Dynamics**, Vol. 9, Sept.-Oct. 1986, pp. 515-529.

12 Blakelock, J. H., **Automatic Control of Aircraft and Missiles** (2nd Edition), John Wiley & Sons, Inc., New York, 1991.

13 Iliff, K. W, "Parameter Estimation for Flight Vehicles," **Journal of Guidance, Control, and Dynamics**, Vol. 12, Sept.-Oct. 1989, pp. 609-622.

14 Ljung, L., **System Identification: Theory for the User**, Prentice-Hall Inc., Englewood Cliffs, New Jersey, 1987.

15 Dolbin, B.H., "Study of Some Hand-Computing Techniques to Determine the Approximate Short Period Mode from Airplane Responses," FDM No. 371, Cornell Aeronautical Laboratory, Inc., Mar. 1966.

16 Neal, T. P., "Frequency and Damping from Time Histories: Maximum Slope Method," **Journal of Aircraft**, Vol. 4, Jan.-Feb. 1967, pp. 76-78.

17 Nelson, R. C., **Flight Stability and Control and Automatic Control**, McGraw-Hill Book Company, New York, 1989.

18 "Military Standard, Flying Qualities of Piloted Aircraft," MIL-STD-1797A, Jan. 1990.

Chapter 10

PRINCIPLES OF AEROELASTICITY

Aeroelasticity[1,2] is the study of the interaction between fluid forces, structural (elastic) forces, and inertial forces. The three-ring diagram shown in Figure 10.1 helps to underscore the interdisciplinary nature of aeroelasticity.

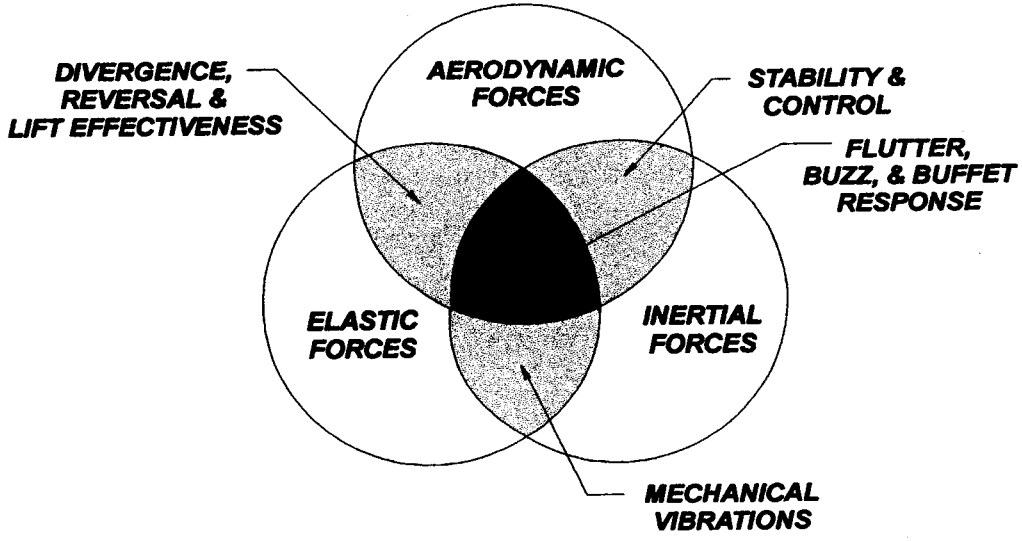

Fig. 10.1 Interdisciplinary Nature of Aeroelasticity

The combination of any two rings represents a discipline of aerospace engineering. The combination of elastic and inertial forces forms the study of mechanical vibrations. The combination of inertial and aerodynamic forces forms the study of rigid-body vehicle stability and control. The combination of aerodynamic and elastic forces forms the study of static aeroelasticity. The combination of all three rings forms the study of dynamic aeroelasticity. Other disciplines such as control, thermal, and damage (aging aircraft) issues may be considered as additional overlapping rings.

10.1 ANALYTICAL FOUNDATIONS

10.1.1 Aeroelastic Definitions

As in most specialties within aerospace engineering, aeroelasticity has its own jargon and special use language. To begin, we need to establish a common set of terminology for the phenomena unique to aeroelastic analysis.

10.1.1.1. Aeroelastic Divergence.

***Aeroelastic divergence** is a static aeroelastic instability leading to catastrophic failure of the structure, and occurs when the aerodynamic forces exceed the elastic restoring forces of the structural configuration.*

10.1.1.2. **Control Reversal**.

> ***Control reversal*** *is the loss of aerodynamic effectiveness for a control surface due to deformation of the primary structure to which the surface is attached.*

10.1.1.3 **Lift Effectiveness**.

> ***Lift Effectiveness*** *is the change in aerodynamic loads due to wing flexibility, which typically leads to a change in the load distribution and an increase in lift.*

Two characteristics of aeroelasticity are evident in the preceding definitions: (1) aeroelasticity is dependent upon the flexibility of the vehicle's structure, and (2) aeroelasticity involves a feedback between aerodynamic loads and structural deformations.

10.1.1.4 **Flutter**. Flutter is a dangerous structural dynamics phenomenon. From a flight test perspective it is definitely a hazardous type of flight envelope expansion.

> **Flutter** is a dynamic instability in which the structural modes that are affected by aerodynamic loads coalesce to form a single aeroelastic mode that rapidly grows with diverging oscillatory motion to structural failure.

Aerodynamic loads, especially those that are unsteady in character, are the source of excitation energy for this destructive type of structural dynamics. Two or more interacting modes of motion merge -- dependent upon flight conditions -- to form a single aeroelastic frequency and mode of motion that resembles a combination of the participating modes. From an energy perspective, energy is extracted from the aerodynamic flow field and is absorbed by the structure. For subcritical conditions, structural and aerodynamic damping dissipates this energy; for critical conditions, system damping is lost thereby leading to a growing oscillatory motion that results in catastrophic flutter.

10.1.2 Aeroelastic Equations of Motion

In general, the equations of motion for the aeroelastic system may be cast in a form similar to that of the forced mass-spring-damper system discussed in Chapter 9. Writing them in matrix form

$$\boldsymbol{M}\ddot{\boldsymbol{q}} + \boldsymbol{C}\dot{\boldsymbol{q}} + \boldsymbol{K}\boldsymbol{q} = \boldsymbol{F}_A \tag{10.1}$$

where $\boldsymbol{M}$, $\boldsymbol{C}$, and $\boldsymbol{K}$ are the matrices that represent the structural mass, damping, and stiffness, respectively, and $\boldsymbol{q}$ is the vector of generalized coordinates. In aeroelastic systems, $\boldsymbol{F}_A$ denotes the time-dependent, motion-dependent (that is, the "unsteady") aerodynamic loads,

$$\boldsymbol{F}_A = \boldsymbol{M}_A\ddot{\boldsymbol{q}} + \boldsymbol{C}_A\dot{\boldsymbol{q}} + \boldsymbol{K}_A\boldsymbol{q} + \boldsymbol{F} \tag{10.2}$$

where $\boldsymbol{M}_A$, $\boldsymbol{C}_A$, and $\boldsymbol{K}_A$ depict aerodynamic inertial, damping, and stiffness contributions which depend upon flowfield conditions (Mach number, altitude, and velocity) as well as the motion of the vehicle's structure, and $\boldsymbol{F}$ denotes the external loads such as those arising from gusts, turbulence, and buffeting. Equations 10.1 and 10.2 may be combined,

$$(M - M_A)\ddot{q} + (C - C_A)\dot{q} + (K - K_A)q = F \tag{10.3}$$

This expression may be solved in either the frequency domain or the time domain. For the frequency domain approach, harmonic motion is assumed so that $q = \beta e^{\lambda t}$; thus, substitution into eqns. 10.3 gives:

$$\left(\lambda^2 (M - M_A) + \lambda (C - C_A) + (K - K_A)\right)\beta = 0 \tag{10.4}$$

F is not considered in this homogeneous solution. Equations 10.4 are solved as eigenvalue problems in which the eigenvalues are complex numbers; hence, $\lambda = \delta + j\omega$, where δ represents the aeroelastic damping and ω represents the aeroelastic frequency. β is the aeroelastic mode shape associated with the complex eigenvalue. Thus, the response of the structure of the vehicle is $q = \beta e^{\delta t} e^{\pm j\omega t}$, where $e^{\delta t}$ represents a decaying or growing motion depending upon the sign and $e^{j\omega t}$ represents a constant amplitude oscillatory motion. We note that the possibility of negative damping comes from the presence of aerodynamic forces.

Three important trends must be monitored during flight tests:

(1) changes in frequency characteristics for changes in flight conditions,

(2) changes in damping characteristics, and

(3) changes in amplitude of response.

These changes are related to the motion described by $e^{\delta t}$ and $e^{j\omega t}$.

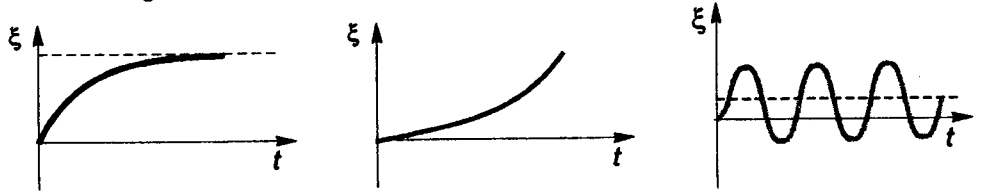

(a) Exponential Rise to Steady-State *(b) Exponential Divergence (Unbounded)* *(c) Undamped Sinusoid (Neutral Dynamic Stability)*

Fig. 10.2 Oscillatory Motion

The eigenvalues indicate damping characteristics dependent upon different dynamic pressures (or other flight conditions). In traditional mechanical vibration analysis the natural frequency is given by the imaginary part of the root. The real part, which represents the damping, was typically zero. However, the presence of unsteady, motion-dependent aerodynamic forces creates damping and, although naturally occurring structural damping will lead to a decaying motion, aerodynamic sources may lead to loss of damping.

The concept of complex aeroelastic modes may be illustrated by considering the classical bending-torsion aeroelastic response of a high aspect ratio wing. Experiments (or analysis) on wings show that all spanwise sections of the wing have bending and torsional components. The modes associated with bending and torsion have distinct frequencies and phase relationships. However, unsteady aerodynamic loads contribute to these frequencies and phase relationships; and, the knowledge of these phase relationships are valuable in flutter identification. At flutter, frequencies, mode shapes, and phasing coa-

lesce to form a single aeroelastic flutter mode. Hence, the determination of the complex eigensolution (frequencies and mode shapes) is of value.

It is important to note that the aerodynamic matrices in eqns. 10.4 depend upon the frequency of motion (as well as Mach number and dynamic pressure) and, consequently, the solutions of eqns. 10.4 are typically obtained with an iterative algorithm. Popular methods for finding the solution to the flutter equations include the *k*-method and the *p-k* method[3] in which velocity-damping (i.e., "*V-g*") diagrams and velocity-frequency diagrams[4] are constructed from the roots of the eigenvalue solutions ("*k*" is the reduced frequency to be discussed in the next section). In the k-method, the damping term is multiplied by $(1 + jg)$ in which a fictitious damping, g, is introduced which permits the solution to the complex eigenvalue problem. Essentially, damping is assumed to be proportional to stiffness but in phase with velocity. Consequently, frequency and damping is found for increasing velocity. As indicated in Figure 10.3, a *V-g* diagram displays the roots of the solution. The exact solution of the flutter conditions occurs when $g = 0$ (note: that the "*V-g*" terminology is an unfortunate choice since the same symbology is also used to describe aircraft load diagrams). In aeroelasticity, V is a velocity (in many cases, V is a nondimensional velocity referred to as the flutter speed index) and g represents the overall damping of the aeroelastic system.

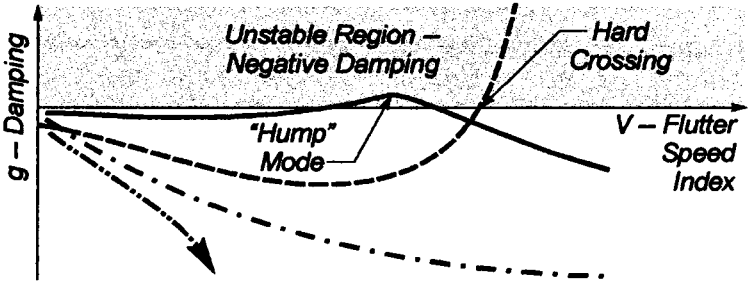

Fig. 10.3 Velocity-Damping Diagram

The roots of eqn. 10.4 are examined for stability characteristics. The number of roots is equal to the number of degrees of freedom in the system. For typical aeroelastic analyses, such as that for a wing structure or a complete aircraft, these degrees of freedom are associated with the structural mode shapes used in the analysis. These roots are traced for increasing values of velocity. The roots will naturally begin as those associated with a positively-damped system since the motion will decay with naturally occurring structural damping (consider the case of no aerodynamic effects). However, as velocity increases the path of one or more of these roots may advance into the negatively-damped regime. The crossing (sign change) represents the location of the neutral stability and indicates the flutter velocity. In certain cases, one might find that for higher velocities, a root will again become positively damped, indicating that the aeroelastic system is again stable. It is noted that the "Hump" mode illustrated in Fig. 10.3 may be eliminated with additional structural damping and, consequently, this instability may be suppressed. Regardless of structural damping, the hard crossing is present. The instability associated with the lowest velocity will always be of interest.

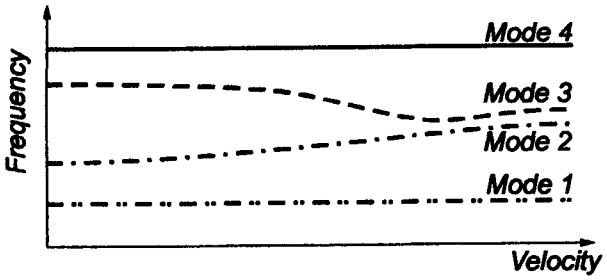

Fig. 10.4 Frequency-Velocity Diagram

In addition to examining the change in damping for increasing velocities, analysis of frequency behavior for changes in velocity as illustrated in Fig. 10.4 reveals the sensitivity of aeroelastic modal frequencies to flight conditions. The frequencies are the natural frequencies of the structure when the velocity is equal to zero. These frequencies change as the velocity increases since the aerodynamic loads couple the structural dynamics of the system. More importantly, these "aeroelastic" frequencies converge toward a common frequency as the velocity increases. The velocity at the point where any two (or more) frequencies coalesce is one indicator of the instability boundary for the aeroelastic system; however, damping must also be examined since the loss of system damping is the more significant measure. During flight tests both damping and frequency are monitored to identify their respective sensitivity to flight conditions -- zero damping and coalesced frequencies are of concern. In addition, changes in the amplitude of response for changes in flight conditions should be monitored.

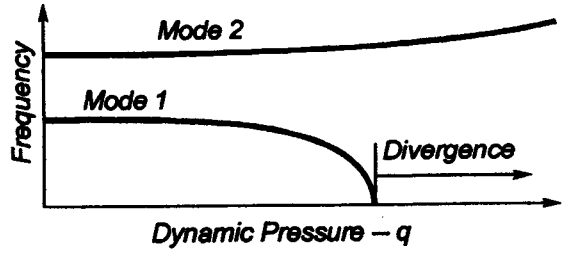

Fig. 10.5 Frequency-Velocity Diagram Indicating Divergence

A root associated with system damping may also vanish as it approaches zero and, simultaneously, a frequency of the system approaches zero. This zero frequency root represents aeroelastic divergence since a characteristic of divergence is that the frequency of the diverging mode approaches zero at the divergence speed. This characteristic provides an approach to identify potential aeroelastic divergence behavior in real time during flight tests. For example, the primary frequency of a beam with an aerodynamic load on the tip is sketched in Fig. 10.5. In actuality, this solution is representative of a slender beam-like structure such as a wind tunnel sting or aircraft sensor probe with an aerodynamically sensitive device attached to the tip. The aerodynamic loading is dependent upon the displacement and rotation of the tip, as well as the velocity of the flow; consequently, the deformation-dependent loads lead to aeroelastic divergence.

As an alternative approach to the frequency domain solution, time domain solutions (i.e., numerical integration) of the governing equations (eqns. 10.3) provide a simulation of the physical response. However, in such a time domain solution the task of modeling the aerodynamic loads may be more complicated. Although physical properties associated with the structure are fixed, the flowfield characteristics such as density, velocity, dynamic pressure, etc. (or, more appropriately, the nondimensional similarity parameters) are changed to examine various flight conditions.

The motion for three different values of dynamic pressure is shown in Figs. 10.6-10.8.

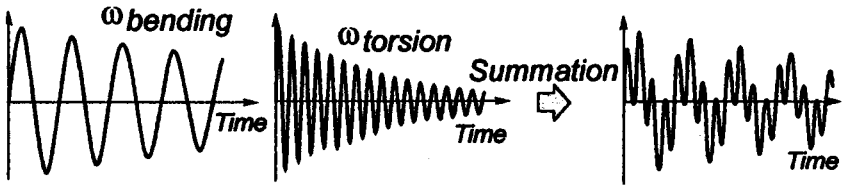

Fig. 10.6 Decaying Motion in the Time Domain

Figure 10.6 shows a decaying motion for a value of dynamic pressure below flutter conditions and illustrates that the response is, in reality, the superposition of multiple responses such as individual bending and torsion contributions.

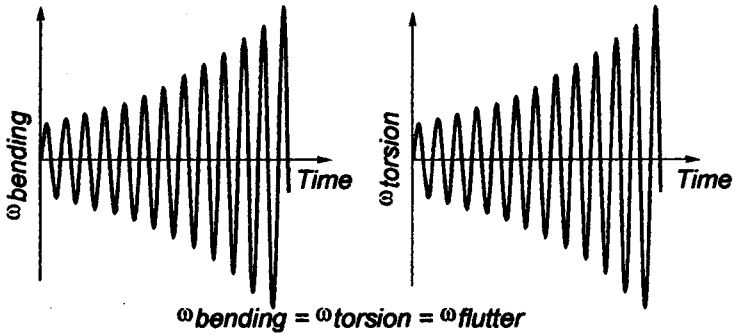

Fig. 10.7 Divergent Motion in the Time Domain

Figure 10.7 shows a growing motion for a dynamic pressure that exceeds the conditions for flutter and, as suggested by the figures, the modes of motion have coalesced to a common frequency.

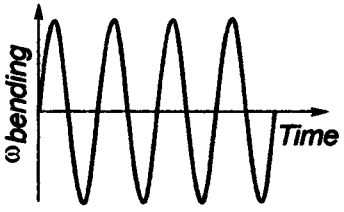

Fig. 10.8 Undamped Motion in the Time Domain

Figure 10.8 illustrates a motion with constant maximum amplitude; that is, it is neutrally damped (although the motion may appear similar, this response should not be confused with limit cycle oscillations found only in nonlinear systems). This case suggests the dynamic pressure (and/or Mach number) for the aeroelastic instability has been

reached. Lower values of dynamic pressure show damped motion. Higher values of dynamic pressure show growing motion. A difficulty associated with the time-domain approach is the identification of the precise point where the behavior is neutral.

10.1.3 Aeroelastic Similarity Parameters

It is both convenient and efficient to eliminate unnecessary free variables in analyses or experiments by identifying similarity parameters. For example, dimensional analysis (introduced in Chapter 4) reveals that only two nondimensional parameters – Mach number and Reynolds number – are necessary to characterize the flow and flowfield effects on lifting surfaces. These two parameters address fluid density, viscosity, velocity, speed of sound, temperature, physical dimensions, and related variables.

In a comparable fashion, dimensional analysis for the aeroelastic equations reveals additional nondimensional terms that must be considered. The **reduced frequency** is defined as

$$k \equiv \frac{c\omega}{2V_\infty} \tag{10.5}$$

where c is a reference length (typically the mean aerodynamic chord), ω is the frequency of vibration, and V_∞ is the freestream velocity. The reduced frequency is the ratio of the vibratory motion to the velocity of flow over the vehicle's surface, and represents a measure of how fast unsteady disturbances are moved downstream relative to the transverse (vibratory) motion.

The **mass ratio** is defined as

$$\mu = \frac{4m}{\rho \pi c^2 b} \tag{10.6}$$

where m is the mass of the vehicle, ρ is the density of the fluid, and b is the wing span. The mass ratio is a measure of the ratio of the vehicle's mass to the mass of the air that the vehicle displaces as it moves relative to the surrounding fluid.

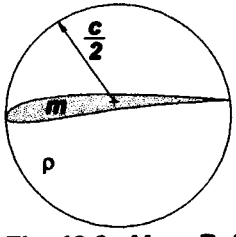

Fig. 10.9 Mass Ratio Geometry

An additional term, the **flutter speed index** (alluded to earlier) is defined as

$$\overline{V} = \frac{2V_\infty}{c\omega\sqrt{\mu}} \tag{10.7}$$

This parameter contains both the mass ratio and reduced frequency. As the analyst compares experimental and analytical results in aeroelastic investigations, not only the geometry but also the mass distribution and structural stiffness must be similar in order for the comparisons to be valid. Results are often expressed in terms of flutter speed index and mass ratio. If two systems have identical flutter speed indices and mass ratios, then the reduced frequency is identical, since eqn. 10.7 is an obvious combination of eqns. 10.5 and 10.6. Clearly, the equality of these parameters insures dynamic similarity between the two systems.

10.1.4 Static Aeroelastic Phenomena

Static aeroelastic phenomena involve the combination of aerodynamic loads and structural flexibility. Static aeroelastic phenomena include aeroelastic divergence, control surface reversal, and lift effectiveness. An example of static aeroelasticity is the effect of aerodynamic loads on the lift distribution of a wing. The aerodynamic loads cause the wing to deform (twist and bend) and, in turn, this new shape will result in new aerodynamic loads. Naturally, one should expect a balance of forces to occur about this new deformed shape. One also observes that, as a result of deformations, the load distribution is altered and the center of pressure shifts. As a consequence, control and stability characteristics are affected.

10.1.4.1. **Aeroelastic Divergence**. Of course, the possibility exists that the forces will not balance since the structural deformations may continue to grow as a consequence of feedback from the deformation-dependent aerodynamic loads. These loads may give rise to even greater deformations. Eventually the surface will fail if this type of feedback interaction continues.

> ***Aeroelastic divergence** is a static aeroelastic instability leading to catastrophic failure of the structure, and occurs when the aerodynamic forces exceed the elastic restoring forces of the structural configuration.*

Aeroelastic divergence occurs when the elastic restoring forces associated with the structural stiffness are exceeded by the aerodynamic forces. As stated, aerodynamic loads are not constant; rather, these loads are dependent upon the displacement of the structure. The equations that describe static aeroelasticity may be derived from eqn. 10.3

$$(\boldsymbol{K} - \boldsymbol{K_A})\boldsymbol{q} = \boldsymbol{0} \tag{10.7}$$

in which velocity and acceleration forces are not considered. $\boldsymbol{K_A}$ is the aerodynamic stiffness matrix, which is composed of aerodynamic derivatives and flow properties. The dynamic pressure, q_∞, may be isolated such that the expression may be rewritten as $q_\infty \underline{\boldsymbol{K}}_{\boldsymbol{A}}$ where $q_\infty \equiv \frac{\rho V_\infty^2}{2}$. Therefore, eqn. 10.7 may be written as

$$(\boldsymbol{K} - q_\infty \underline{\boldsymbol{K}}_{\boldsymbol{A}})\boldsymbol{q} = \boldsymbol{0} \tag{10.8}$$

Equation 10.8 is an eigenvalue problem in which q_∞ are the eigenvalues associated with aeroelastic divergence and $\boldsymbol{q}$ are the eigenvectors associated with the shape at di-

vergence. The term ($K - q_\infty \underline{K}_A$) represents the aeroelastic stiffness that approaches zero as q_∞ increases.

Altitude and compressibility effects may be considered. Since $V_\infty = M_\infty a_\infty$, the dynamic pressure may be written as $q_\infty \equiv \frac{\rho(M_\infty a_\infty)^2}{2} = q_\theta M_\infty^2$ where q_θ is a reference dynamic pressure associated with the speed of sound and density at a specific altitude. It is important to note that the aerodynamic properties in $\underline{K}_A$ depend upon Mach number.

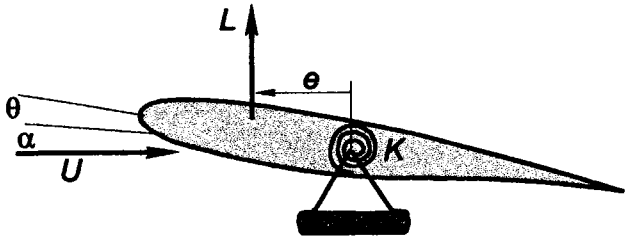

Fig. 10.10 Free-Body Diagram for Aeroelastic Divergence Example

Aeroelastic divergence is illustrated through the following example. In Fig. 10.10, a rigid wing section is mounted to an elastic support that permits one degree of freedom motion. The wing section has a center of gravity, which is not necessarily coincident with the spring support representative of the elastic axis. Aerodynamic loads act through the aerodynamic center. The equation of static equilibrium for the wing deflected from the balanced system appears as follow:

$$Le - K\theta = 0 \tag{10.9}$$

where K is the spring stiffness, θ is the rotation degree of freedom, L is the lift, and e is the distance between the elastic axis and the aerodynamic center (e is a measure of aerodynamic eccentricity). The weight of the wing is not at issue since θ is the displacement from the static equilibrium position. These parameters are all constant except for the lift.

Lift is a function of dynamic pressure, which depends upon the velocity and fluid density. Furthermore, lift is a function of the total angle of attack, $\alpha + \theta$, where α is the angle of attack at equilibrium. (Be careful; again, the symbology is confusing, since θ has been previously used -- in Chapter 6, especially -- to denote the Euler pitch attitude angle. Remember that in this context, θ is the perturbation from the static equilibrium position). Thus, lift is expressed as

$$L = q_\infty S C_{L_\alpha}(\alpha + \theta) \tag{10.10}$$

where S is the reference area, and C_{L_α} is the aerodynamic derivative defined by the slope of the lift curve. We define the aerodynamic derivative as the load per unit deflection or per unit rotation. Substituting eqn. 10.10 into equation 10.9,

$$(K - q_\infty S e C_{L_\alpha})\theta = q_\infty S e C_{L_\alpha}\alpha \tag{10.11}$$

which is a scalar form of the multiple degree-of-freedom system (eqn. 10.8) and solving eqn. 10.11 directly for θ leads to

$$\theta = \frac{q_\infty S e C_{L_\alpha} \alpha}{K - q_\infty S e C_{L_\alpha}} \tag{10.12}$$

The aerodynamic contribution in eqns. 10.11 and 10.12 appears with the structural stiffness. In fact, one observes that the aerodynamic contribution is a negative stiffness. As the dynamic pressure is increased, the term in the brackets approaches zero; consequently, θ approaches infinity. The terms in the denominator form the expression for the critical dynamic pressure at which aeroelastic divergence occurs. When the bracketed terms in the denominator approach zero, the result is therefore of special interest; thus, solving this term for q_∞ leads to

$$\boxed{q_{\infty,DIV} = \frac{K}{S e C_{L_\alpha}}} \tag{10.13}$$

One observes that the aerodynamic eccentricity, e, may be negative (i.e., the aerodynamic center is behind the elastic axis) which suggests a negative divergence pressure exists. Obviously, this is not physically possible which means that divergence is not possible. Thus, design considerations that minimize the effect of eccentricity will alleviate aeroelastic divergence.

Graphically this feature can be illustrated by superimposing and comparing the force-displacement behavior of the structure with the lift-displacement behavior. The structural and aerodynamic stiffness is the slope -- the differences in the stiffness represent the ***aeroelastic*** stiffness. The force-displacement curve is fixed for a given structure; however, the lift-displacement curve depends upon the dynamic pressure. At a critical dynamic pressure, $q_{\infty,\,DIV}$, the two curves coincide, indicating neutral static stability. In physical terms, at this (and higher) dynamic pressure no structural restoring capability exists. This instability is catastrophic, as deformations grow rapidly, and without oscillation, to structural failure.

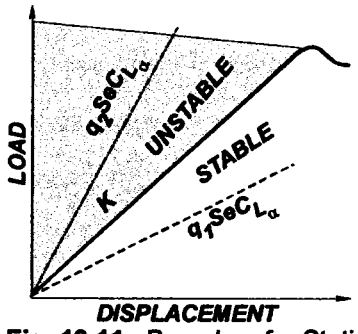

Fig. 10.11 Boundary for Static Aeroelastic Divergence

Although this illustration is quite simple, the concept is essentially the same for large degree of freedom systems as described by eqn. 10.8. In fact, it is noted that $q_{\infty,DIV}$ described by eqn. 10.13 is the eigenvalue of eqn. 10.11. Equation 10.13 may be expanded to illustrate altitude and compressibility effects. The dynamic pressure may be related to Mach number by

$$q_{\infty,DIV} = q_e (M_{\infty,\,DIV})^2 \tag{10.14}$$

Also, as previously stated, the aerodynamic derivatives are dependent upon flow conditions. The Prandtl-Glauert rule may be used to illustrate the effect of compressibility on the lift, thus

$$C_{L_\alpha} = \frac{C_{L_\alpha,0}}{\sqrt{1-M_\infty^2}} \tag{10.15}$$

where $C_{L_\alpha,0}$ represents the derivative for incompressible flow. Substituting eqns. 10.14 and 10.15 into eqn. 10.13 yields

$$q_e(M_{\infty,DIV})^2 = \frac{K\sqrt{1-M_{\infty,DIV}^2}}{SeC_{L_\alpha,0}} = q_{0,DIV}\sqrt{1-M_{\infty,DIV}^2} \tag{10.16}$$

where $q_{0,DIV}$ represents a reference divergence pressure for the incompressible assumption and q_e is a reference dynamic pressure associated with the speed of sound at a particular altitude. Equation 10.16 may be solved for the divergence Mach number ($M_{\infty,DIV}$) and compared to the reference conditions. We observe that divergence is improved with an increase in altitude and we note that compressibility effects must be included to provide the real boundary. We also note that, although not considered in this model, the aerodynamic center moves rearward for increases in Mach number; thus, the aerodynamic eccentricity, e, is affected.

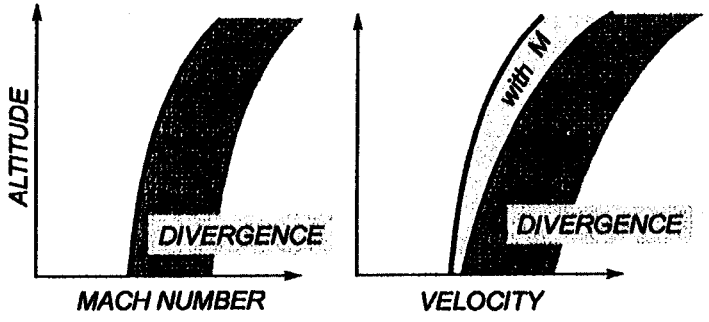

Fig. 10.12 Boundary for Static Aeroelastic Divergence (Mach Number Effects)

Divergence is a static aeroelastic phenomenon, one which is often confused with yield or ultimate load failures. However, we show through eqn. 10.13 and Fig. 10.11 that aeroelastic divergence is independent of the yield or ultimate loads; rather, divergence depends upon the stiffness of the structure and the aerodynamic derivatives.

We could extend our development to a wing, which is stiff in bending but comparably responsive in torsion. In this case, we simplify the structural model by discretizing the wing into separate spanwise sections and we introduce the concept of influence coefficients. Influence coefficients represent the inverse of the stiffness; these coefficients relate the deformation at a specific point due to loads at all sections. For torsional behavior, these coefficients describe the torsional rigidity. We would solve the matrix of this multiple degree-of-freedom system for the critical dynamic pressure that leads to divergence.

10.1.4.2. **Control Reversal**. Control surface reversal occurs due to the deformations of the structure. As the structure deforms, the ability of the control surface to produce a desired reaction approaches zero. The surface is said to lose effectiveness. Further deformations result in the reversal of control surface performance; that is, deflecting the surface produces the opposite effect from that which was intended.

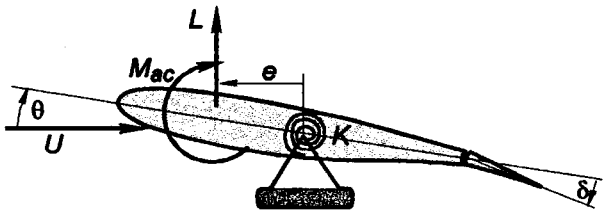

Fig. 10.13 Control Surface Reversal

Our single degree-of-freedom example is now extended to include control surface loads. An important premise for understanding control reversal is that the purpose of the control surface is to create a lift load that leads to a moment for maneuver. Thus, if the wing section represents the outboard portion of a wing, then the new lift leads to a rolling maneuver. On a vertical tail section the rudder is meant to produce a side force that causes a yawing moment. However, if no lift or side force is generated for any control input due to flexibility of the fixed structure, then no maneuvering moments are created.

Summing moments about the elastic axis of the wing-control surface model:

$$\sum M_{EA} = 0 \quad \Rightarrow \quad Le + M_{ac} = K\theta \quad \Rightarrow \quad \theta = \frac{Le + M_{ac}}{K} \tag{10.17}$$

in which the aerodynamic lift is

$$L = L_{wing} + L_{control} = qSC_{L_\alpha}\theta + qSC_{L_\delta}\delta \tag{10.18}$$

and the aerodynamic moment at the aerodynamic center is

$$M_{ac} = qScC_{m_\delta}\delta \tag{10.19}$$

where δ is the control input. Substituting eqns. 10.18 and 10.19 into eqn. 10.17 yields

$$\theta = \frac{Le + M_{ac}}{K} = \frac{\left(qSC_{L_\alpha}\theta + qSC_{L_\delta}\delta\right)e + qScC_{m_\delta}\delta}{K} \tag{10.20}$$

or, solving eqn. 10.20 explicitly for θ

$$\theta = \frac{qeSC_{L_\delta}\delta + qScC_{m_\delta}\delta}{K - qeSC_{L_\alpha}} \tag{10.21}$$

The creation of lift is of primary interest, thus eqn. 10.21 is substituted into eqn. 10.18

$$L = qS\left(C_{L_\alpha}\frac{qeSC_{L_\delta}\delta + qScC_{m_\delta}\delta}{K - qeSC_{L_\alpha}} + C_{L_\delta}\delta\right) = qS\left(\frac{KC_{L_\delta} + qScC_{m_\delta}C_{L_\alpha}}{K - qeSC_{L_\alpha}}\right)\delta \tag{10.22}$$

Control reversal occurs when no lift is created, regardless of the control input. From the numerator of eqn. 10.22, we obtain the dynamic pressure that leads to zero (or negative) values (note: by the NASA convention, $C_{m,\delta}$ is negative; see Chapter 6).

$$L \le 0 \quad \text{or} \quad \boxed{q_{rev} = \frac{K}{ScC_{m_\delta}} \frac{C_{L_\delta}}{C_{L_\alpha}}} \tag{10.23}$$

Also, divergence conditions appear through eqn. 10.22 as the denominator approaches zero for increasing dynamic pressure.

$$L \to \infty \quad \text{or} \quad \boxed{q_{div} = \frac{K}{eSC_{L_\alpha}}} \tag{10.24}$$

10.1.5 Dynamic Aeroelastic Phenomena

Dynamic aeroelastic phenomena include flutter, buzz, buffet, and dynamic response. With these phenomena, airframe motion, aerodynamic loads, and structural deformations are dependent upon one another. Flutter is an instability in which the structural response is excited by the presence of the aerodynamic loads as the structure extracts energy from the flow field. The interested reader is referred to the works of Theodorsen and Garrick[5], Bisplinghoff, et al.[1], and Fung[2], as well as the descriptions provided in references 6 and 7.

Types of flutter include: coupled bending-torsion flutter associated with high aspect ratio lifting surfaces, panel flutter associated with low aspect ratio lifting surfaces, control-surface flutter, flutter of plate and shell-like structures, propeller-whirl flutter, and stall flutter. All of these flutter instabilities, with the exception of stall flutter, are characterized by the coalescence of modes. Stall flutter occurs due to flow separation that occurs during cyclic motion. In this case, the transfer of energy from the flow to the wing does not rely on the coalescence of modes; rather, the wing is "forced" due to energy lost due to stall. Buffet is an instability that occurs due to flow separation or the wake produced from the structure. Buzz is an instability that occurs due to shock wave oscillations. In general, dynamic response of the aircraft due to gusts and atmospheric disturbances is important to characterize since, even in the absence of instabilities, it is necessary to understand how the dynamic response will affect load distributions and ride qualities.

Flutter is a dynamic instability in which the structural modes that are affected by aerodynamic loads coalesce to form a single aeroelastic mode that rapidly grows with diverging oscillatory motion to structural failure.

10.1.5.1. Bending-Torsion Flutter. Of these dynamic aeroelastic phenomena, the bending-torsion flutter mechanism provides the insight into the nature of these instabilities. As previously stated, flutter occurs when the structure extracts energy from the flow field. This structure may be the primary lifting surface, a control surface, the fuselage, or the entire vehicle. As the structure vibrates in a subcritical flow field, the aerodynamic forces damp the vibration of the structure; however, as the speed (or dynamic pressure) increases, a critical condition is reached in which the energy from the flow field

feeds the vibration of the structure. This critical point represents the onset of flutter. Flutter is destructive in nature; but, fortunately, flutter boundaries may be identified.

Flutter results from the interaction of inertial, structural, and aerodynamic forces and, typically, flutter is the result of coupled modes of motion. The pitch and plunge motion is representative of a wing with bending and torsional response. Although these equations of motion are straightforward, they apply to more representative aerospace structures. A minimum of two degrees of freedom is used since a wing limited only to bending motion will not flutter and a wing limited only to torsional motion will exhibit only stall flutter at high angles of attack. Although unlikely, it is possible for a single degree-of-freedom to flutter in torsion for very specific center-of-gravity and elastic-axis locations (see reference 1).

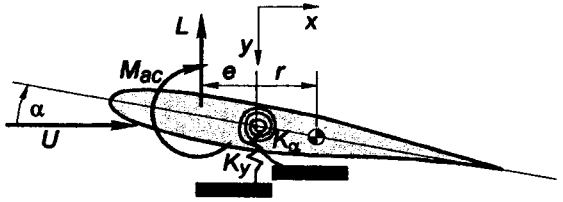

Fig. 10.14 Bending and Torsional Flutter

The wing in Fig. 10.14 is limited to motion in two degrees of freedom. It has a "plunging" motion, which is translational motion perpendicular to the flow, and a "pitching" motion, which is rotational motion about the elastic axis. The linearized equations of motion for the system are:

$$\begin{pmatrix} m & mr \\ mr & I \end{pmatrix}\begin{pmatrix} \ddot{y} \\ \ddot{\alpha} \end{pmatrix}+\begin{pmatrix} K_y & 0 \\ 0 & K_\alpha \end{pmatrix}\begin{pmatrix} y \\ \alpha \end{pmatrix}=\begin{pmatrix} -L \\ M \end{pmatrix} \tag{10.25}$$

where m is the mass of the wing, r is the distance between the center of mass and the elastic axis, I is the moment of inertia referenced to the elastic axis, K_y and K_α are spring constants associated with the plunge and pitch motion, respectively, L is the aerodynamic lift and M is the aerodynamic moment referenced to the elastic axis.

The form of this equation is identical to eqn. 10.1. Note that in this general form, the discussion of aeroelasticity is not limited to a system of two degrees of freedom. The mass and stiffness matrices may be representative for any aeroelastic system. Structural damping, C, may also be considered.

In real problems, these matrices may be very large. Analytically, the system is often represented through finite element methods to accurately model the structure and the associated modal characteristics. Experimentally, these matrices may be derived using measurements and employing modal methods. The modes and frequencies of such analyses are used in the solution process.

Although a wing may possess a very high number of vibration modes, only the lower modes are typically used since the flutter mechanism is driven by the fundamental modes. For example, the lowest ten to fifteen modes usually capture the primary behavior of the structure (the reader is referred to reference 7 for specific case studies). This number may increase as interaction with higher modes such as those that are associated with control surfaces becomes important. Typically, the nature of classical flutter employs the primary torsion mode with the first or second bending mode. Of importance now is to un-

derstand the content of these equations, the solution of these equations, and interpretation of results.

Examination of eqns. 10.25 in closer detail reveals that the equations are coupled through the mass matrix, as evidenced by the presence of off-diagonal terms in the matrix. We could have chosen a set of coordinates in which the system is coupled through the stiffness matrix, but the stability characteristics would be identical. The choice of coordinates is for convenience in the solution. This 'inertial' coupling occurs since the center of mass does not coincide with the elastic axis; the relative location of the center of mass plays an important role in aeroelastic design as mass-balancing inherently improves stability margins.

The aerodynamic loads, *L* and *M*, are unsteady, which means these loads are motion dependent. For example, Theodorsen[5] (also see Fung[2]) provided a very rigorous development of the unsteady potential flow equation that led to the classical solution for incompressible unsteady aerodynamic loads

$$L = \pi\rho b^2\left(\ddot{y} + V_\infty\dot{\alpha} - \frac{c}{2}a\ddot{\alpha}\right) + 2\pi\rho V_\infty\frac{c}{2}C\left(\dot{y} + V_\infty\alpha + \frac{c}{2}\left(\frac{1}{2}-a\right)\right)\dot{\alpha} \tag{10.26}$$

$$M = \pi\rho\frac{c^3}{8}\left(-a\ddot{y} + \left(\frac{1}{2}-a\right)V_\infty\dot{\alpha} + \left(\frac{1}{8}-a^2\right)\frac{c}{2}\ddot{\alpha}\right) + 2\pi\rho V_\infty\frac{c^2}{4}C\left(\frac{1}{2}+a\right)\left(\dot{y} + V_\infty\alpha + \frac{c}{2}\left(\frac{1}{2}-a\right)\dot{\alpha}\right) \tag{10.27}$$

where *C(k)* is Theodorsen's Function and is a complex function of the reduced frequency, k, and *a* is the nondimensional distance (in terms of c/2) from the elastic axis to the midchord and is a measure of aerodynamic eccentricity with respect to the elastic axis.

A quasi-steady aerodynamic model, appropriate for low frequency motion ($k < 0.1$), is found from eqns. 10.26 and 10.27 as

$$L = 2\pi\rho V_\infty\frac{c}{2}\left(\dot{y} + V_\infty\alpha + \frac{c}{2}\left(\frac{1}{2}-a\right)\dot{\alpha}\right) \tag{10.28}$$

$$M = 2\pi\rho V_\infty\frac{c^2}{2}\left(\frac{1}{2}+a\right)\left(\dot{y} + V_\infty\alpha + \frac{c}{2}\left(\frac{1}{2}-a\right)\dot{\alpha}\right) = \frac{c}{2}\left(\frac{1}{2}+a\right)L \tag{10.29}$$

However, a source of aerodynamic damping is present in either form.

Harmonic motion for *y* and α is assumed for the solution and, as a result, an eigenvalue problem is formulated as previously discussed. In the simplest form, all terms are grouped in a single matrix. The roots to the equation resulting from the expansion of the determinant of the matrix provide the stability properties. The solution is complex such that the roots contain damping and frequency information. Again, it is noted that the aerodynamic properties depend upon the velocity, which is also contained within the eigenvalue. The solution requires an iterative process (see Hassig[3]).

10.1.5.2 **Example: Quasi-Static Aeroelasticity**. Stability characteristics are obviously affected by the matrices found in the governing eqns. 10.25. The designer of the airplane has some control over inertial, elastic, or aerodynamic coupling. Typically, the only parameters modified are associated with the flowfield (that is, velocity, dynamic pres-

sure, and altitude) and solving these equations in the frequency domain permits one to examine damping and frequency characteristics.

To further understand the flutter mechanism, an illustration based upon the two degree-of-freedom system is presented in which the aerodynamic loads are modeled by the static terms in eqns. 10.28 and 10.29 . Thus, eqns. 10.25 become,

$$\begin{pmatrix} m & mr \\ mr & I \end{pmatrix}\begin{pmatrix} \ddot{y} \\ \ddot{\alpha} \end{pmatrix}+\begin{pmatrix} K_y & 0 \\ 0 & K_\alpha \end{pmatrix}\begin{pmatrix} y \\ \alpha \end{pmatrix}=\begin{pmatrix} -q_\infty S C_{L_\alpha}\alpha \\ q_\infty S C_{L_\alpha} e\alpha \end{pmatrix} \tag{10.30}$$

or, with rearrangement

$$\begin{pmatrix} m & mr \\ mr & I \end{pmatrix}\begin{pmatrix} \ddot{y} \\ \ddot{\alpha} \end{pmatrix}+\begin{pmatrix} K_y & q_\infty S C_{L_\alpha} \\ 0 & K_\alpha - q_\infty S C_{L_\alpha} e \end{pmatrix}\begin{pmatrix} y \\ \alpha \end{pmatrix}=\begin{pmatrix} 0 \\ 0 \end{pmatrix} \tag{10.31}$$

Harmonic motion is assumed such that $y = Ye^{i\omega t}$ and $\alpha = A\,e^{i\omega t}$

$$\left(-\omega^2\begin{pmatrix} m & mr \\ mr & I \end{pmatrix}+\begin{pmatrix} K_y & q_\infty S C_{L_\alpha} \\ 0 & K_\alpha - q_\infty S C_{L_\alpha} e \end{pmatrix}\right)\begin{pmatrix} Y \\ A \end{pmatrix}=\begin{pmatrix} 0 \\ 0 \end{pmatrix} \tag{10.32}$$

These equations are simplified by dividing through the mass and introducing similarity parameters previously defined,

$$\left(-\omega^2\begin{pmatrix} 1 & r \\ r & r_\alpha^2 \end{pmatrix}+\begin{pmatrix} \omega_y^2 & \dfrac{2C_{L_\alpha}V_\infty^2}{\mu\pi c} \\ 0 & \omega_\alpha^2 r_\alpha^2 - \dfrac{2C_{L_\alpha}V_\infty^2 e}{\mu\pi c} \end{pmatrix}\right)\begin{pmatrix} Y \\ A \end{pmatrix}=\begin{pmatrix} 0 \\ 0 \end{pmatrix} \tag{10.33}$$

where μ is the mass ratio, r_α is the radius of gyration, and ω_y and ω_α are the uncoupled natural frequencies of the system.

$$\left(-\omega^2\begin{pmatrix} 1 & r \\ r & r_\alpha^2 \end{pmatrix}+\begin{pmatrix} \omega_y^2 & \dfrac{2C_{L_\alpha}V_\infty^2}{\mu\pi c} \\ 0 & \omega_\alpha^2 r_\alpha^2 - \dfrac{2C_{L_\alpha}V_\infty^2 e}{\mu\pi c} \end{pmatrix}\right)\begin{pmatrix} Y \\ A \end{pmatrix}=\begin{pmatrix} 0 \\ 0 \end{pmatrix} \tag{10.34}$$

To put the equations into a more convenient nondimensional form, the first equation is divided by the reference length and the second equation is divided by the square of the reference length, and both equations are divided by ω^2. Thus,

$$\left(-\begin{pmatrix} 1 & \bar{r} \\ \bar{r} & \bar{r}_\alpha^2 \end{pmatrix}+\begin{pmatrix} \left(\dfrac{\omega_y}{\omega}\right)^2 & \dfrac{2C_{L_\alpha}V_\infty^2}{\mu\pi c^2\omega^2} \\ 0 & \left(\dfrac{\omega_\alpha}{\omega}\right)^2 \bar{r}_\alpha^2 - \dfrac{2C_{L_\alpha}V_\infty^2\bar{e}}{\mu\pi c^2\omega^2} \end{pmatrix}\right)\begin{pmatrix} \bar{Y} \\ A \end{pmatrix}=\begin{pmatrix} 0 \\ 0 \end{pmatrix} \tag{10.35}$$

where the overbar signifies a nondimensional length with respect to the reference length.

The flutter speed index is identified within the aerodynamic terms, thus, in final form,

$$\begin{bmatrix} -1+\left(\frac{\omega_y}{\omega}\right)^2 & -\bar{r}+\bar{V}^2 \\ -\bar{r} & -\bar{r}_\alpha^2+\left(\frac{\omega_\alpha}{\omega}\right)^2 \bar{r}_\alpha^2-\bar{V}^2\bar{e} \end{bmatrix} \begin{Bmatrix} \bar{Y} \\ A \end{Bmatrix} = \begin{Bmatrix} 0 \\ 0 \end{Bmatrix} \tag{10.36}$$

where the slope of the lift curve is assumed to be $C_{L_\alpha} = 2\pi$ (the value from theoretical aerodynamics). However, this "quasi-static" assumption is an extremely simplified and misleading "model" for the aerodynamic loads as it is important to note that aerodynamic terms such as C_{L_α} depend upon the eigenvalue, ω, in addition to the Mach number. In more representative formulations of eqns. 10.36, an iterative process is necessary because the flutter speed index also contains ω.

Several comments are made in reference to eqns. 10.36:

(1) Equations 10.36 are in the eigenvalue form for the aeroelastic system. The determinant of the matrix forms a quadratic equation for the roots, ω^2, which represent the aeroelastic frequencies as a function of the flutter speed index, $\bar{V}$.

(2) For the case of $\bar{V} = 0$, the roots of eqns. 10.36 provide the natural frequencies as a function of the mass imbalance, $\bar{r}$. The uncoupled natural frequencies are found for the case $\bar{r} = 0$.

(3) For the case of $\bar{V} \neq 0$, Fig. 10.15 illustrates the characteristic behavior of the aeroelastic frequencies for increasing velocities. The flutter region is found as the two roots coalesce to a common frequency.

Equations 10.36 may be solved as a standard quadratic

$$\omega_1^2, \omega_2^2 = \frac{-B \pm \sqrt{B^2-4AC}}{2A} = \frac{-B \pm \sqrt{D}}{2A} \tag{10.37}$$

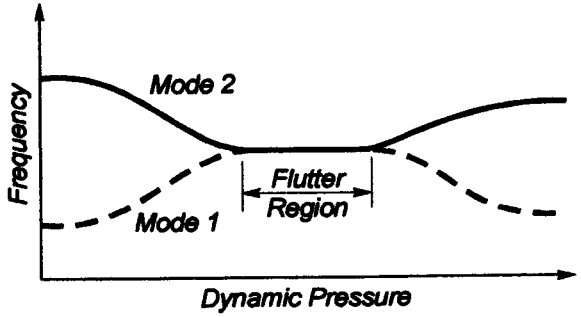

Fig. 10.15 Coupling of Flutter Modes

Solving the (flutter) determinant of eqns. 10.36, reveals that the roots become complex conjugates with the single real root providing the frequency at flutter. Thus, from eqn. 10.37, flutter occurs when $D = 0$. Also, aeroelastic divergence -- the "zero frequency" instablity -- is found by examining the case of $C = 0$ since terms A and B are motion dependent.

(4) Aerodynamic loads introduce coupling in the system through two mechanisms. Most obvious is the fact that the loads will not usually act through the elastic axis; thus, lift leads to a moment. The second source of coupling exists since the unsteady aerodynamic loads are dependent upon the displacements and velocities.
(5) The formulation illustrates the use of the similarity parameters.
(6) An extremely simplified formulation of the aerodynamics is used. In reality, the aerodynamics depend upon the Mach number and reduced frequency. Standard aeroelastic methodologies, such as the "k method" or "p-k method" require an iterative solution since the aerodynamic properties depend upon the reduced frequency. The aeroelastic frequency, ω, that is the eigenvalue also appears in the reduced frequency and flutter speed index.

10.1.6 Matched Point Analysis

V-g Diagrams (and other solution methods) represent the aeroelastic damping of the system for changes in flowfield conditions. The complexity of determining the aerodynamic loads often necessitates solutions at specific altitudes and Mach numbers. Thus, the critical velocity for aeroelastic instability is found for different altitudes (mass ratios) and different Mach numbers. Not immediately obvious here is an inherent paradox in the solution. That is, if one selects an altitude and Mach number to perform analysis, then the velocity is predetermined. Why ? In the atmosphere a speed of sound is associated with each altitude (and the temperature of the air at that altitude); and, together, the Mach number and speed of sound specify a velocity,

$$V_\infty = M_\infty a_\infty \tag{10.38}$$

Is this velocity the same as the velocity from analyses? No, typically, the velocities are quite different except for fortuitous circumstances. Therefore, we must extend the analysis to include the "matched point" solution.

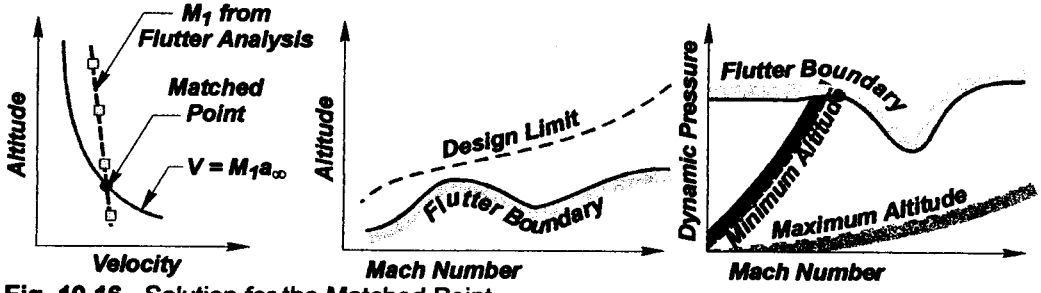

Fig. 10.16 Solution for the Matched Point

In this approach, as illustrated in the left-hand view of Fig. 10.16, the flutter velocity (obtained from the *V-g* diagram) is plotted for a series of altitudes at constant Mach number. The intersection of a curve through these results (the curve given by the velocity found from eqn. 10.38) leads to a "matched point" in which the altitude, velocity, and Mach number are consistent. This process is repeated over a range of Mach numbers to complete a set of data -- the Mach numbers, altitudes, and velocities -- for which flutter occurs and from which the flutter boundaries, as shown in the middle and right views of Fig. 10.16, are generated. It is noted that flutter is primarily a low altitude, transonic instability as suggested by these figures.

10.1.7 FAR Advisory Circulars: Parts 23 and 25.

As suggested in the Advisory Circulars[4,6], velocity-damping (V-g) and velocity-frequency (V-ω) diagrams are widely-accepted approaches used to examine the results of flutter analyses.

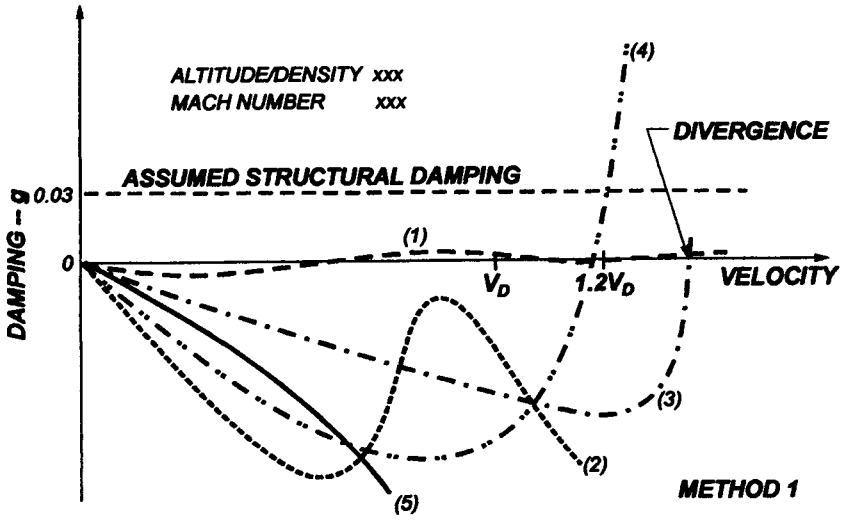

Fig. 10.17 V-g Diagram for Five-Mode Analysis (adapted from AC 25.629-1[4])

In Fig. 10.17, a velocity-damping diagram is sketched for an aircraft represented by 5 aeroelastic modes. The roots are found for increasing values of velocity and reduced frequency. Of particular interest is the root that leads to the negatively damped system (root 4 in the sketch). Structural damping affects the onset of flutter. In the absence of measured damping, a damping factor of 0.03 for structural damping is assumed (Method 1) as a conservative value. Method 2 uses actual damping. Either way, structural damping manifests itself as a vertical shift of the velocity axis in the V-g diagram -- a consequence of the solution methodology.

The presence of structural damping eliminates the apparent instability indicated by the soft flutter crossing ("hump mode") associated with root 1. Aeroelastic divergence is characterized by a root that abruptly terminates at zero damping -- a mode indicated by root 3 in Fig. 10.17.

It is noted that civilian aircraft require a 20% margin of safety for flutter clearance, whereas military aircraft require a 15% margin of safety for flutter clearance. Thus, in Fig. 10.17, V_D is the design velocity upon which a 20% margin as applied. The flutter crossing of root 4 represents $1.2V_D$. Other than the exact crossing from stable to unstable, the path of the roots should not be used to infer stability behavior as the solution strategy is only correct at zero damping (sinusoidal behavior was assumed). Also, since the velocity associate with the flutter crossing is associated with an altitude and Mach number, consideration must be given to the aforementioned "matched-point" analysis.

In Fig. 10.18 a velocity-frequency diagram illustrates an aircraft represented by 5 aeroelastic modes. The natural frequencies (such as those measured through a ground

vibration test) of the aircraft are represented at zero velocity, and the affect of aerodynamic loads on these frequencies is seen as a function of velocity. Although flutter can not be determined solely from this figure, aerodynamic-sensitive modes tend to coalesce as the flutter velocity is approached. Aeroelastic divergence is noted for the mode that approaches zero frequency. *Accelerometers mounted to the aircraft should be used to monitor frequencies during flutter tests.*

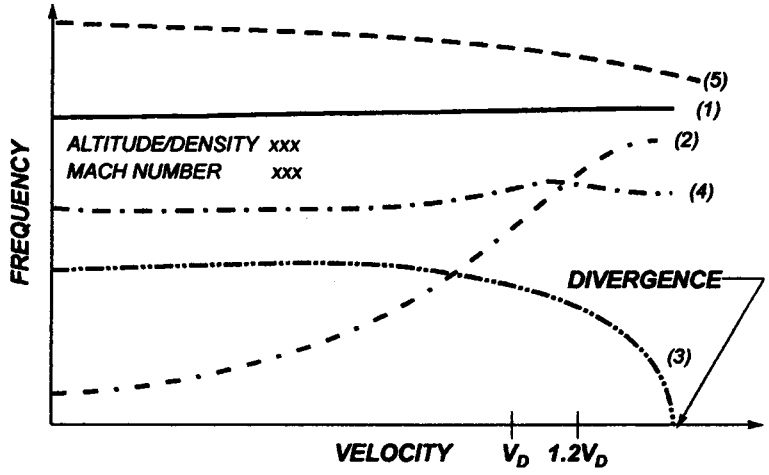

Fig. 10.18 Velocity-Frequency Diagram for Five-Mode Analysis (adapted from AC 25.629-1[4])

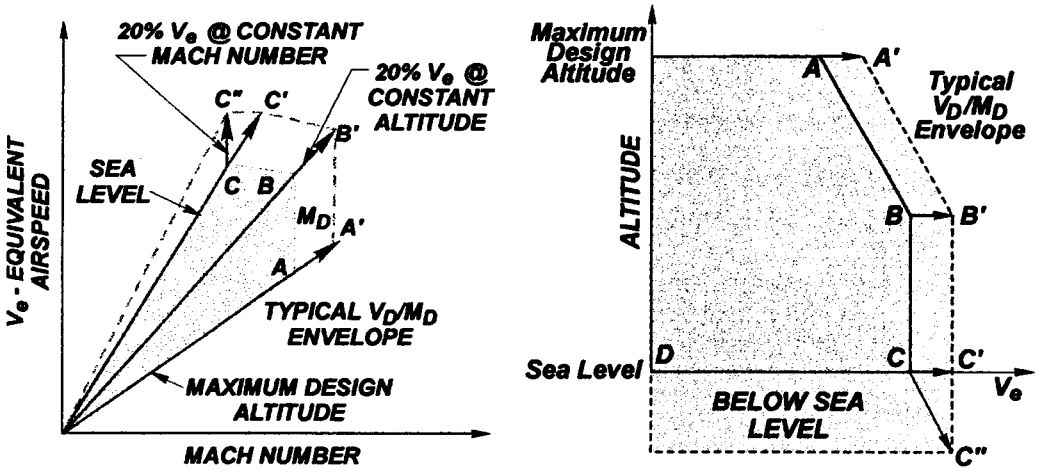

Fig. 10.19 Flutter Envelopes from *V-g* / Matched Point Solutions. (adapted from AC 25.629-1[4])

Flutter conditions -- velocities, densities, and Mach numbers -- are used to construct flutter clearance envelopes according to FAR standards. Figure 10.19 illustrates two standard envelopes. A 20% margin is required at constant altitude (A-A', B-B', C-C'), and a 20% margin is formed for constant Mach number at sea level. This latter case results in clearance below sea level and, although flight at this altitude is obviously not feasible, this

boundary is necessitated by the low-altitude, high dynamic pressure variables that most affect flutter.

10.1.8 Wind Tunnel Tests

Wind tunnel tests provide the intermediate information necessary to qualify design concepts prior to full scale testing. Earlier, the requirement to satisfy similarity parameters identified through dimensional analysis was addressed. These similarity parameters included the Mach number, reduced frequency, mass ratio, and the flutter speed index. If the similarity parameters are identical, then one may compare experimental and analytical results with a measured degree of confidence.

A major difference between wind tunnel test procedures and atmospheric flight test procedures is the controlled test environment. The temperature, Mach number, velocity, and density may be controlled in the wind tunnel. In atmospheric tests, nature dictates the dependency between the altitude (density) and air temperature (speed of sound). This dependency creates the need for the Matched Point solution to properly interpret the analytical results.

Since environmental control is possible in the wind tunnel test scenario, all but one of the test parameters may be held constant when identifying the flutter boundary. Typically, one of two methods is employed to determine a point on the flutter boundary. In the first method, the Mach number is maintained and the total pressure is increased in the wind tunnel (this is analogous to maintaining Mach number while decreasing altitude during flight tests). In the second method, the dynamic pressure is increased through the use of the fan speed to increase the flow velocity (this is analogous to maintaining constant altitude while increasing aircraft velocity during flight tests). Mach number and dynamic pressure both increase with this second method.

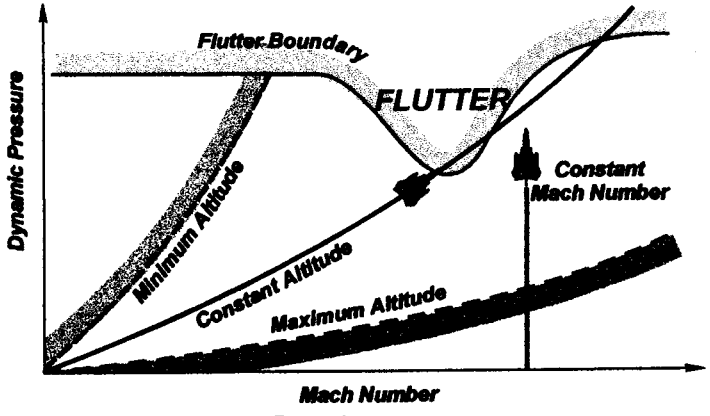

Fig. 10.20 The Flutter Boundary

The typical approach to establishing the flutter boundary – normally critical dynamic pressure versus Mach number – in the wind tunnel is illustrated in Fig. 10.20. The flutter boundary is shown with the classical "flutter bucket" at which the minimum dynamic pres-

sure (or "transonic dip") for flutter is typically found in the transonic regime. The subsonic and supersonic regimes routinely have nearly constant flutter dynamic pressures.

An initial test is planned to identify a flutter-free path throughout the Mach number range. This test is accomplished by increasing the speed of the flow to well beyond the anticipated transonic dip of the flutter bucket. As stated previously, this method increases both the dynamic pressure and the Mach number, and this method resembles the constant altitude flight test. (Note: Conducting a constant altitude flight test at the maximum flight altitude typically identifies this flutter-free path.) Next, the speed is decreased and the tunnel pressure (stagnation) is increased to provide a higher dynamic pressure for this same Mach number, and this method resembles a constant Mach dive maneuver. Then, the speed of the flow is increased until the instability is detected establishing a point on flutter boundary. This process is repeated several times to complete the description of the flutter bucket *on the subsonic side of the transonic dip.*

The flat regions of the flutter boundary – the subsonic and supersonic regime – are found by increasing pressure at constant Mach number. The region of the flutter boundary beyond the transonic dip is found by significantly decreasing the tunnel pressure (returning to the conditions associated with the original flutter-free path) and, then, increasing velocity to obtain higher Mach numbers. Beyond the transonic dip, the pressure increases for a constant Mach number.

> *We observe that, at points on the flutter boundary beyond the transonic dip,* **a decrease in velocity** *may cause onset of flutter. Therefore, in wind tunnel tests, instead of reducing fan speed, the total pressure is dropped to avoid triggering the instability by entering the transonic dip from supersonic conditions. In flight tests, this drop is analogous to an increase in altitude at constant Mach number.*

Although these methods establish points on the flutter boundary, it is not desirable to actually test on the instability boundary (i.e., "hit" a hard flutter point) due to the highly destructive nature of flutter. Therefore, subcritical response techniques are used in both wind tunnel and flight tests. As suggested by the name, these methods examine the dynamic response of the structure prior to the onset of the instability. This examination includes frequency, damping, and/or amplitude trends for increases in airspeed, and an extrapolation to actual flutter conditions. The structure or aircraft must be spared. These techniques will now be described in further detail.

10.1.9 Ground Vibration Tests

Ground vibration tests (GVTs) are used to identify natural frequencies and mode shapes of the aircraft structure. Kehoe[8] and Norton[9] provide a thorough discussion of a GVT program in support of flight tests. Also, albeit a general theory of mechanical vibrations is not presented herein, the interested reader is referred to Craig[10].

As previously presented, the equations of motion for the general mechanical system with mass, damping, and stiffness may be represented as

$$\boldsymbol{M}\ddot{\boldsymbol{x}} + \boldsymbol{C}\dot{\boldsymbol{x}} + \boldsymbol{K}\boldsymbol{x} = \boldsymbol{F} \tag{10.39}$$

where $\boldsymbol{M}$, $\boldsymbol{C}$, and $\boldsymbol{K}$ are parameters associated with the physical system, $\boldsymbol{F}$ is external forcing, and $\boldsymbol{x}$ is the structural response. If two of three components -- physical parameters, external forcing, or response -- are known, then the third component may be found.

In analyses, the physical parameters and external forcing are known, and the response is simulated. In GVTs, the response due to a known external forcing is measured, from which the physical parameters are derived.

As depicted in Fig. 10.21, in GVT strategies the accelerometer (or strain gage, if appropriately located) is used to measure response due to an input. Typically, this input is from a mechanical shaker or impact hammer. The response determines vibration characteristics -- namely, the natural frequency, natural mode shape, and structural damping.

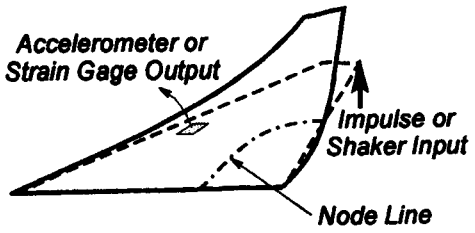

Fig. 10.21 Wing Mode Shape

The fundamental wing modes found with a modal survey are illustrated in Fig. 10.22.

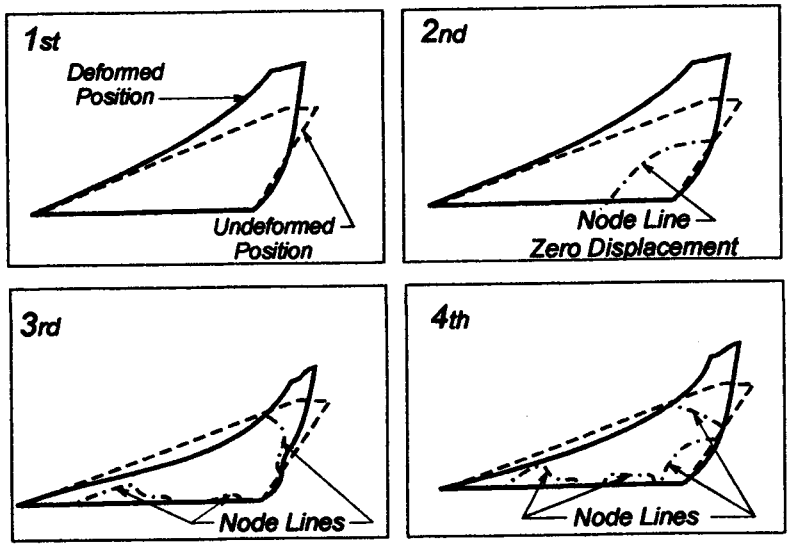

Fig. 10.22 Wing Modes

Several supporting comments are in order:

(1) A GVT may use a single accelerometer from which measurements are obtained at many locations on the structure, or the GVT may use an array of many accelerometers to provide simultaneous measurements. In either case, a family of mode shapes is found.

(2) The "reciprocity" principle suggests that the source of excitation may be placed at any location leading to equivalent modal characteristics. However, node lines (as illustrated in Fig. 10.22) are lines of zero displacement and should be avoided as modal excitation is difficult at these locations. The GVT should be conducted with

more than one input source to confirm identification of all modes. For example, the second mode of Fig 10.22 would be missed if the shaker were positioned along the node line.

(3) The GVT identifies modes that should be tracked during flight tests. The GVT will identify the optimal placement of accelerometers during flight tests. Often, a single accelerometer may be used during flight tests to track a mode identified during the GVT. Strain gages may be present from prior tests (airframe loads, etc) and may be used to measure vibratory response; however, the location may not be optimal and signal to noise ratios may be too low.

(4) The underlying theory associated with the GVT assumes linear behavior. Thus, sources of nonlinearities such as freeplay, sources of damping, and excess compliance in the structure must be identified and/or minimized. Linearity may be verified through static load-deflection tests. Preloading of the structure will eliminate freeplay. Partial deflation of tires and landing gear struts during the GVT will help distinguish rigid-body modes from flexible-body modes.

(5) Mode shapes exhibit the property of orthogonality (see reference 10). Mathematically speaking, measurements should behave as

$$\Phi^T M \Phi = I \quad \text{and} \quad \Phi^T K \Phi = \Lambda \tag{10.40}$$

where Φ is a transformation matrix whose columns are comprised of the normalized eigenvectors (mode shapes), I is the identity matrix, and Λ is a diagonal matrix consisting of the natural frequencies, ω^2. Orthogonality should be verified, with the existence and relative magnitude of the off-diagonal terms in the matrices resulting from the operation $\Phi^T M \Phi$ and $\Phi^T K \Phi$ providing a validation of the quality of measurements.

Again, the GVT measures the output response through an accelerometer (or strain gage) from an input normally provided by a shaker or impact hammer. A modal survey, conducted as part of the GVT, determines the modal characteristics of the primary modes for the different configurations. These measured modes are used to validate analysis or may be used to develop a model for predictions.

Of primary interest for flight test applications is the use of these measured modes to observe, in real-time, changes of vibration characteristics -- that is, monitor aerodynamically sensitive modes that may lead to aeroelastic instabilities.

10.2 FLIGHT TEST METHODS

At the stage when flight tests are required, aeroelastic analyses have identified the flutter boundary and wind tunnel tests have verified this boundary. In addition, math models of the structure have predicted the vibrational characteristics and measurements have verified the actual modal characteristics. Now, we extend our theory and ground-based test experience to flight tests. Several supporting references are suggested which include the efforts of Norton[9], Kehoe[11], and van Nunen and Piazzoli[12], as well as material addressing flutter test techniques provided in references[13,14].

Expansion of the flutter envelope is an iterative process from inception of a new configuration to flight testing of the full scale aircraft. As the process continues and updated

flutter calculations improve with new knowledge, a foundation is created for flight tests that confirm an understanding of aeroelastic frequency and damping characteristics.

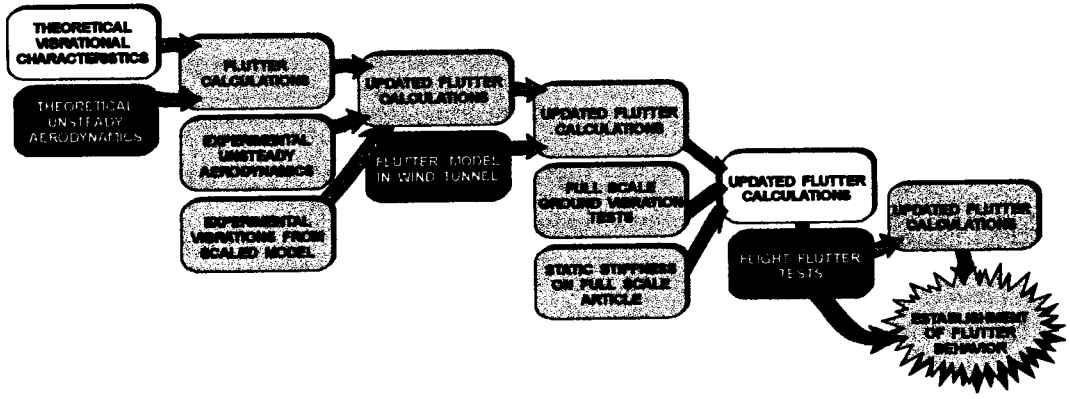

Fig. 10.23 Flutter Expansion Flow Diagram (Adapted from Norton[9])

10.2.1 Flutter Excitation In Flight

Structural vibrations must be excited at flight conditions to examine aeroelastic sensitivity and validate predictions. As illustrated in the Fig. 10.24, several approaches are available. Techniques include:

- *natural atmospheric turbulence*
- *mechanical excitation devices (mass eccentric devices)*
- *aerodynamic excitation devices (oscillating vanes)*
- *pre-programmed loads from flight control systems*
- *pyrotechnic devices ("bonkers")*
- *pilot-induced control surface pulses or "stick raps")*

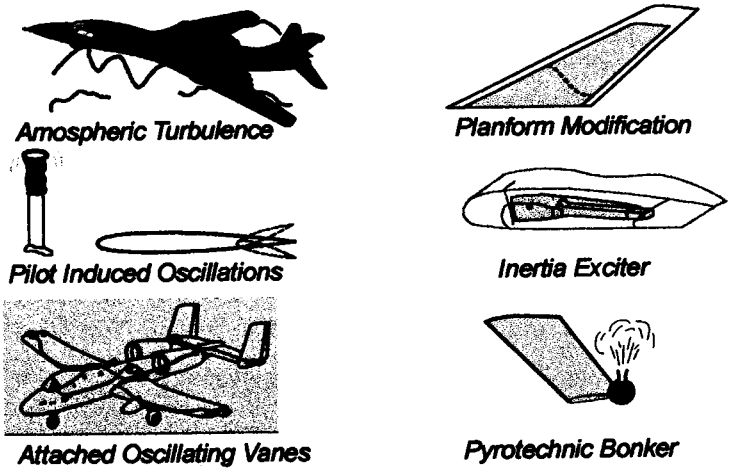

Fig. 10.24 Flutter Excitation Schemes

Input loads may take several forms, and include: sudden impulses intended to simulate a 'step' input (stick raps and bonkers), frequency sweep and dwell loads (shakers), and random loads (turbulence). The purpose of these loads is to excite the structure at a specific frequency, or range of frequencies, and observe the response characteristics -- in particular, damping and frequency characteristics -- for changes in flight conditions. The advantages and disadvantages of each form of possible excitation are discussed briefly in the following sections.

10.2.1.1 **Natural Atmospheric Turbulence.** (including wake and buffet induced vibrations): The advantages are obvious simplicity and low hardware or aircraft modification cost. Disadvantages include: (1) excitation parameters (frequencies swept, dwell times) are not controllable; (2) data reduction requires more sophistication due to low signal-to-noise ratios; (3) quality of data collection depends on atmospheric conditions; (4) all modes are excited simultaneously and closely spaced modes may require additional data collection; and (5) excitation levels will vary with altitude.

10.2.1.2 **Mechanical Devices**. Advantages include: (1) efficient use of test time; (2) precise control of frequency sweeps and dwell times; (3) short duration at test points; (4) similar excitation at all altitudes; (5) data reduction is more dependable; (6) signal-to-noise ratios are higher; and (7) specific modal frequencies can be targeted. The disadvantages of using such devices include: (1) systems may be bulky and adversely affect certain modes; (2) added complexity increases chances of test aborts; (3) external actuators may affect the aerodynamics (4) data storage requirements are increased; and (5) short duration at test points requires high quality signal processing and high data rates.

In lieu of additional flight test hardware, the presence of existing on-board flight control systems (FCS) in many aircraft configurations provides in-flight excitation. Pre-programmed inputs of sine-sweep, sine-dwell, and targeted frequencies are often used successfully with automatic flight control systems. Concerns with the use of FCS actuation include notch filters or other such limitations that prevent excitation at specific frequencies, or undesirable feedback between the pre-programmed inputs and vehicle response/performance.

10.2.1.3 **Pilot Induced Oscillations and Stick Raps**. Allowing the pilot to excite the structural dynamics is a classical flight test approach. Advantages are: (1) no alteration of mass or aerodynamics since no additional hardware is used; (2) pilot exercises some control of excitation; and (3) reasonable time spent at each test point. The disadvantages of manual excitation include: (1) input frequency is limited by human response time; (2) only the lower modal frequencies (up to about 5 Hz) may be adequately excited; (3) considerable test time may be required if pulses are required in both directions and about each of the axes.

10.2.2 Flutter Envelope Expansion

The flight envelope, including the required margin of safety, must be free of flutter. The test program must consider all store configurations, fuel management scenarios, and alternative vehicle configurations. As previously stated, flutter depends on flight conditions such as velocity, altitude, and Mach number; therefore, the test program must consider these parameters. Furthermore, an ordered priority must be used in exploring the effects of each parameter.

10.2.2.1 **Time Histories Versus Frequency Dependence**. Like wind tunnel tests, flight tests are initiated at the lowest dynamic pressures (Fig. 10.15). Hence, aircraft are normally tested at higher altitudes first since lower densities dictate both lower dynamic pressures and mass ratio effects. Higher speeds are evaluated by making shallow dives to achieve test speeds that cannot be attained in straight and level flight. However, higher speeds alone may not necessarily illuminate the flutter speed boundaries. The frequency of the input also affects the response of the modes of interest.

At a specific test point, output data are obtained and analyzed for frequency and damping characteristics. Measurements from devices such as accelerometers are often in the form of a response time history. Typically, 60 seconds of data are obtained at a specific test point. Given an adequate sampling rate and sufficient measurements, the data are transformed (normally by Fourier transforms) to the frequency domain. Figure 10.25 provides a simplified illustration of the frequency response derived from transformation of time domain measurements, and shows the amplitude of response as a function of frequency.

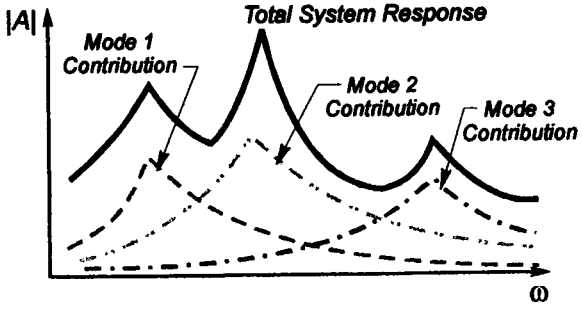

Fig. 10.25 Typical Frequency Response

Several prefatory comments are appropriate as one considers the frequency response behavior depicted in Fig. 10.25.

(1) The peaks associated with the system frequency response indicate the aeroelastic frequencies of the system, and these peaks may be observed to shift with changes in test conditions. For the zero velocity case, these peaks represent the natural vibration frequencies of the aircraft. As flutter is approached, two or more of these peaks will merge toward a common peak. As aeroelastic divergence is approached, one of these peaks will migrate toward zero frequency.

(2) Forced excitation from any external sources (such as vortex shedding, actuator movement, oscillating shocks, and other sources with an embedded frequency content) at an aeroelastic (natural) frequency will result in large amplitude response.

(3) As depicted in Fig 10.25, the response of the structure is the superposition of all modes. The magnitude of response is the additive affect of each mode -- for example, although the first mode (lowest frequency) dominates the response at that frequency, contributions from higher modes are present.

(4) During tests using mechanical excitation methods, a sinusoidal ("sine") sweep through a range of frequencies will identify aeroelastic frequencies indicated by peak amplitudes; the "sine dwell" at specific frequencies will permit examination of specific modes.

(5) The random input -- from turbulence or mechanical excitation -- will excite all modes and frequencies simultaneously. The aeroelastic frequencies will be identified by the peak response.
(6) Structural (no-flow) and aeroelastic damping can be identified through the sharpness of the frequency response. The "half-power" method, for example, is one technique used to derive damping from the frequency response spectrum.[10]
(7) Modal characteristics must be understood (almost always based on GVTs) prior to flight tests. The presence of rigid body motion and external vibratory sources will be observed in the frequency response, and these effects must be identified.

The accelerometer output time history is often used for test points far-removed from the flutter boundary. For example, frequency trends are tracked by counting cycles and damping trends are tracked by using the half-amplitude method[10] in which the number of cycles needed for the amplitude to halve is directly related to damping. Also, the "log-dec" method[10] (logarithmic-decrement) is often used to derive damping from the decay rate.

10.2.2.2 **Procedures Requiring Dives**. Dives may be required to achieve higher airspeeds and dynamic pressures for envelope clearance. An altitude band of approximately ±1000 feet near the targeted test altitude is usually acceptable to obtain data at an altitude (mass ratio) assumed constant. Obviously, descent rates associated with large dive angles give large altitude changes and may not allow completion of the sweep -- repeated dives may be necessary to complete a test point. Care must be taken in dive procedures to guarantee that airspeed increments are controlled.

The sweep rate available with mechanical excitation may be changed to complete the sweep within this altitude band. Often, the "burst and decay" method is used in which a targeted frequency is excited ("burst") for a few cycles, and the decay from this excitation measured. Frequency dwells may be conducted in a dive if a suitable forced excitation system is installed and averages of data may be needed if atmospheric excitation is used. Test points flown in a dive with control surface excitation done by the pilot are usually pulses applied about one axis at a time and several passes through the altitude band may be required for a statistically significant data sample.

10.2.3 Subcritical Response Techniques

Wind tunnel tests and flight tests are required to establish precise flutter boundaries for the vehicle or component. Yet, since flutter is destructive by nature, testing at, or even near, the boundary is highly undesirable. Therefore, subcritical response techniques are employed to predict the onset of instabilities by extrapolating damping and frequency trends. These techniques require the use of accelerometers and/or strain gages. These instruments are mounted on the critical components so measurements of the modal characteristics can be recorded and monitored in "real time".

Modal parameters of primary interest include the frequency, damping, and amplitude characteristics. Our development of aeroelastic theory in Section 10.1 shows that shifts in frequency and damping parameters identify the presence of aeroelastic instabilities. We must take advantage of these characteristics to predict where the instability exists based upon measured response at subcritical conditions. Several subcritical response techniques have been developed; one such method is referred to as the "Peak-hold" method as used by Cole[15]. The peak-hold method requires measurement of the maximum am-

plitude of the response of a contributing mode. This measurement must be made at stabilized flight conditions – constant dynamic pressure, altitude, and Mach number – and measurements are repeated for several flight conditions. Using the results of Cole to illustrate, responses measured at several dynamic pressures are illustrated in Fig. 10.26.

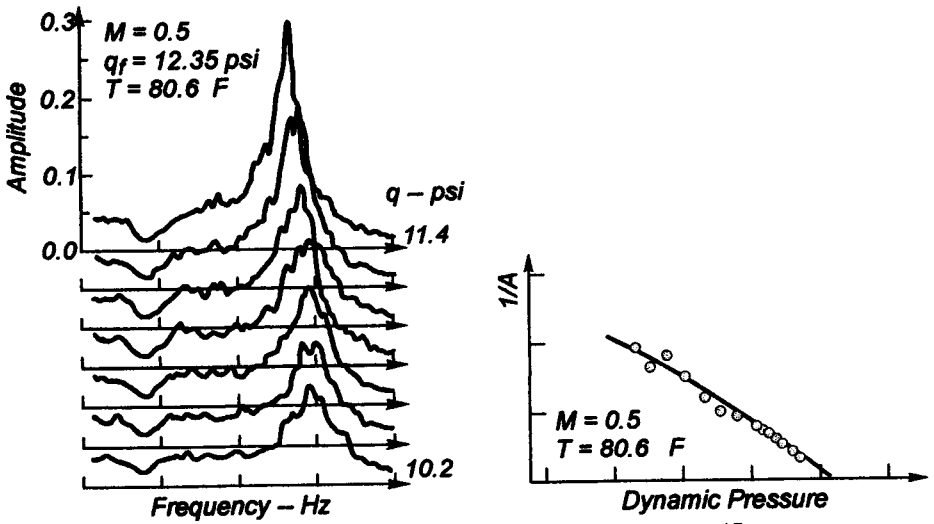

Fig. 10.26 Results of Peak-Hold Method (Adapted from Cole[15])

An inspection of the responses in Fig. 10.26 reveals a broad peak for the vibration of particular modes. This broad peak suggests well-damped modes. As the dynamic pressure is increased, the response appears as a narrow peak. The inverse of the maximum amplitude is plotted versus the dynamic pressure (right side of Fig. 10.26). As the dynamic pressure is increased towards the critical dynamic pressure, the inverse of the maximum amplitude approaches zero. This inverse is extrapolated to this zero value which corresponds to the flutter dynamic pressure. Changes in frequency as noted by the shift in the peak, and changes in damping as noted by the width of the peak, also provide indicators that may be used to predict the onset of the instability.

Example 10.1: X-29. The significant efforts of Kehoe and Rivera[16] and others (such as Freudinger[17]) are cited to provide a detailed discussion of flutter clearance flight test programs. As an illustration, certain results of the X-29 flutter clearance project are briefly discussed.

The ground vibration test (GVT) is used to identify frequencies and modes during flight tests. Table 10.1 describes the aircraft mode, modal frequency, and potential aeroelastic instability in which the mode may participate (according to analytical predictions). Several forms of instability are predicted for the X-29, and include: (1) flutter; (2) divergence – aggravated by the forward sweep design of the X-29; (3) aeroservoelastic instabilities – beyond the scope of this text, but an instability that involves an interaction of the flight control system with flexible vehicle modes; and (4) body-freedom flutter – an instability that is caused by the interaction of flexible modes with rigid body modes). In the following table, "D" indicates a potential Divergence instability, "F" indicates a potential Flutter instability, and "ASE" indicates a potential AeroServoElastic instability.

The GVT also identifies the optimal location of accelerometers to track modes. Although the GVT may have used hundreds of accelerometers to characterize a specific mode shape, the flight test will only require a few judiciously place accelerometers. Fig. 10.27 (next page) shows the relative placement of a few accelerometers on the X-29.

Table 10-1: Mode Type, Frequency, and Nature of Instability

MODE	FREQUENCY Hz	POTENTIAL MECHANISM FOR INSTABILITY
First Symmetric Wing Bending	8.6	D, ASE
First Antisymmetric Wing Bending	11.3	ASE
First Fuselage Vertical Bending	11.6	ASE
First Fuselage Lateral Bending	12.5	ASE
First Fin Bending	15.2	F
Canard Pitch	21.0	D, F
Second Fuselage Vertical Bending	24.3	ASE
Second Symmetric Wind Bending	26.3	ASE, F
Second Antisymmetric Wing Bending	26.8	ASE
Inboard Flap Rotation	31.3	F
Wing Torsion-Outboard Flap Torsion	35-37.0	F
Midflap Torsion	38.7	F
Canard Pitch-Bending	42.0	F
First Fin Bending	50.0	F
Inboard Flap Torsion	51.5	F

Adapted from Kehoe and Rivera[16]

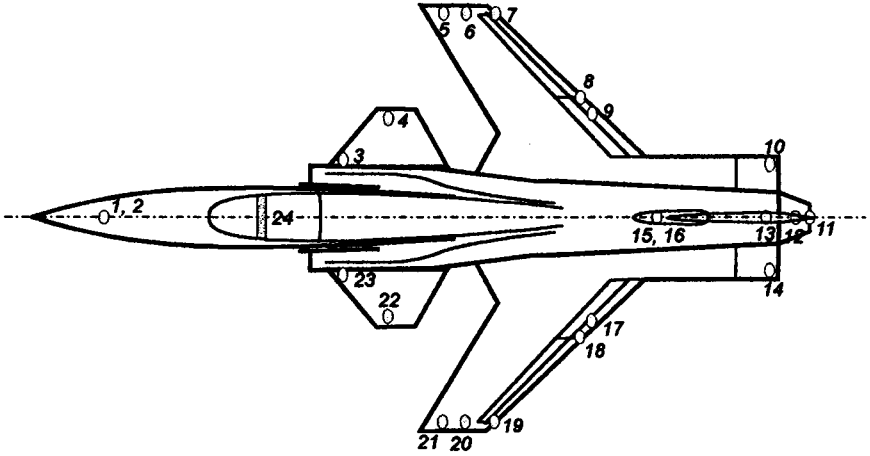

Fig. 10.27 Location of Accelerometers for the X-29 (Adapted from Kehoe and Rivera[16])

It is well worth noting that placement of a single accelerometer on the wing tip permits tracking of the bending mode. A second accelerometer on the other wing permits tracking of symmetric vs. antisymmetric bending modes. And, a second accelerometer mounted on each wing – with one placed near the leading edge and the other placed near the trailing edge – permits tracking of torsional modes.

Figure 10.28 (on the following page) superimposes predicted flutter boundaries onto the flight envelope – displayed in the standard format as described previously. Symmetric modes and antisymmetric modes are shown. A 20% margin of safety on the limit velocity (V_L) is used. Several modes are found to approach the required clearance envelope; most notably, a midflaperon flutter mechanism that penetrates deeply into the planned flight envelope. These predictions used an extremely conservative value of structural damping (0.02 - 0.03) that leads to conservative (low) predictions of flutter speed. However, tests are required to clear the flight envelope.

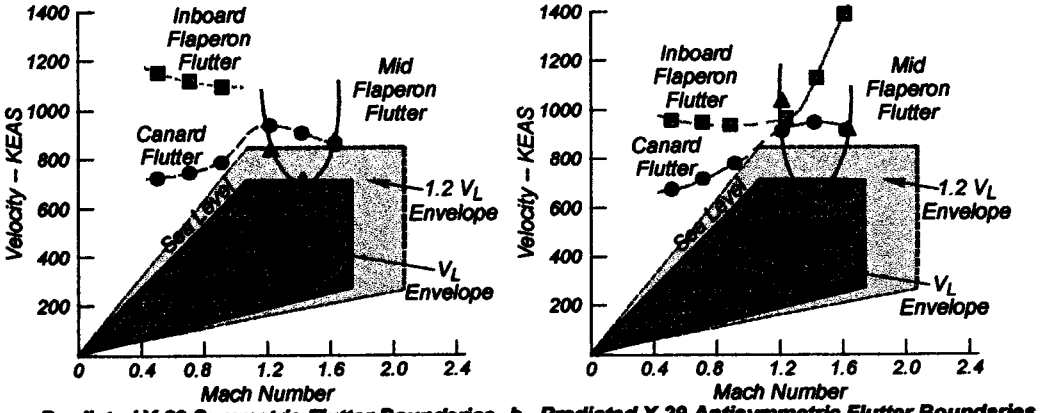

a. Predicted X-29 Symmetric Flutter Boundaries *b. Predicted X-29 Antisymmetric Flutter Boundaries*

Fig. 10.28 Predicted X-29 Flutter Boundaries (Adapted from Kehoe and Rivera[16])

Scale model (16% dynamically scaled model) wind tunnel tests were conducted to investigate the midflaperon flutter mechanism. As depicted in Fig. 10.29, several wind tunnel tests were conducted and, in particular, tests were conducted well within the regime of predicted flutter. No instabilities were experimentally measured -- differences with the analytical predictions of Fig. 10.28 are attributed to structural damping being greater than assumed. Structural damping delayed flutter onset.

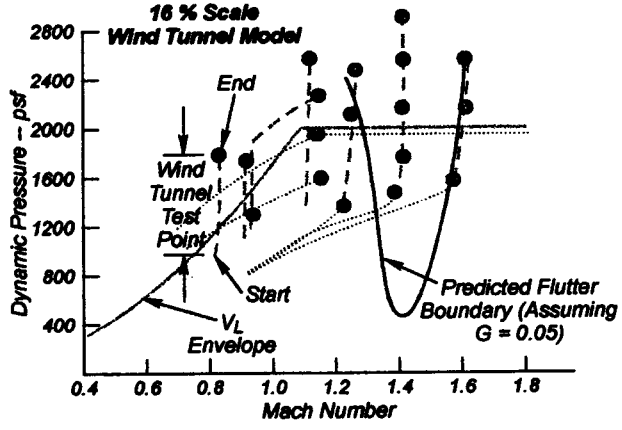

Fig. 10.29 X-29 Midflaperon Flutter Boundary Prediction (Adapted from Kehoe and Rivera[15])

Following extensive analysis, ground vibration tests, and wind tunnel investigations, a flight test program was initiated that uses a build-up approach. That is, flight tests were conducted in increments from lowest risk to highest risk, and proceeded from low speeds to high speeds beginning at highest altitudes and finishing at lowest altitudes. Thus, confidence was established prior to approaching potential flutter boundaries. Figure 10.30 shows the flutter test matrix flown. It is noted that no instabilities were found within the flight envelope, and it is noted that the maximum Mach number for the vehicle was established at M_∞=1.4 for reasons other than aeroelastic concerns.

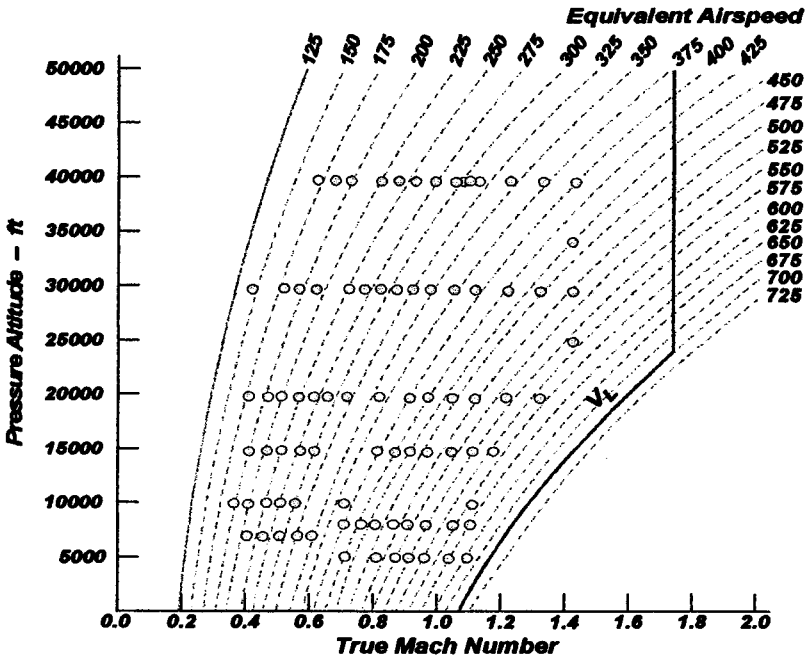

Fig. 10.30 X-29 Flutter Flight Test Matrix (Adapted from Kehoe and Rivera[15])

10.2.4 Rules of Thumb

In light of the previous discussion, it is appropriate to identify methods of raising the flutter velocity or possibly eliminating flutter altogether. All of these suppression approaches have one purpose: to break the coupling, whether it be aerodynamic, inertial (mass), or elastic. Furthermore, today's flight control systems may be used to suppress the onset of aeroelastic instabilities by affecting the phase relationships of the coupled system or create offsetting loads.

One commonly used approach is to mass balance the system. Mass balancing requires the addition or redistribution of mass so that the center of gravity is moved forward. Control surfaces and rotor blades often use ballast. An increase in mass lowers the natural frequency; mass positioned away from the center of mass lowers the natural frequency in torsion; and, an increase in structural stiffness raises the natural frequency.

The presence of flutter and divergence is influenced heavily by the character of the primary torsional mode. The vibration characteristics of the structure may be adjusted to eliminate or delay the onset of flutter. An increase in the spread between the participating modal frequencies will delay the onset of flutter. Typically, the primary torsional mode is higher than the primary bending mode; therefore, increasing the torsional stiffness or reducing the moment of inertia (redistribution of mass) is usually advantageous. The addition of structural damping also provides flutter alleviation. Other than the aeroelastic modes, "aerodynamic stiffening" is typical, as most system frequencies will rise slightly in the presence of increasing aerodynamic loads.

Wing sweep has a significant effect on certain aeroelastic instabilities. As suggested in Fig. 10.31, forward sweep adversely affects the divergence boundary and aft sweep

adversely affects control reversal. Relative to these other instabilities, flutter is affected little by sweep.

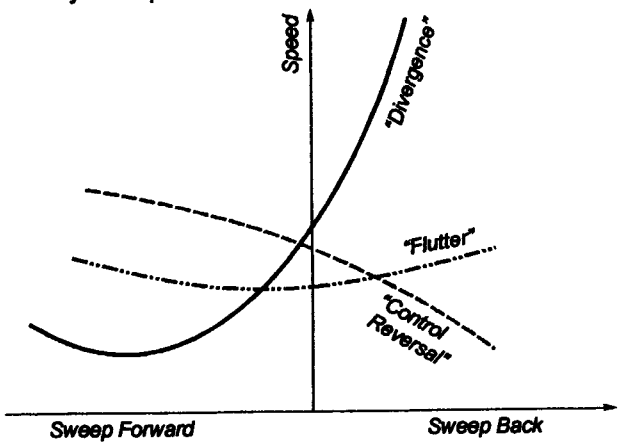

Fig. 10.31 Sweep Effects (Adapted from Bisplinghoff[1])

Angle of attack effects are minimal except for vortex-shedding phenomena. However, wind-up turns are often used at the completion of certain test points to demonstrate insensitivity to angle of attack (see reference 17). Control surface flutter modes are most sensitive to altitude (mass ratio) effects. Also, control surface "buzz" will be eliminated with reduced free-play of the control surface actuator.

The GVT must identify all modes of interest and flutter analysis demands the use of all participating modes. For example, a large transport could be modeled with the first 3 bending modes and first 2 torsional modes[7], since bending-torsion flutter is typical. However, higher-order modes are necessary for multi-control surface aircraft; for example, analysis of the F-18 High Angle-of-Attack Research Vehicle (HARV)[17] and X-29 Forward Sweep Wing (FSW) Research Aircraft[16] required in excess of 25 modes.

10.3 SUMMARY

"Some fear flutter because they do not understand it,
others fear flutter because they do" .... Theodore von Karman

In this chapter we have examined both static and dynamic aeroelastic instabilities such as divergence and flutter. The highly-destructive nature of these instabilities requires a judicious approach to identify boundaries and clear the flight envelope. Ground-based tests and studies that include ground vibration tests, wind tunnel tests, and flutter analyses are necessary to provide a strong foundation of understanding prior to flight tests. Flight tests at flutter or divergence conditions are not performed directly; rather, subcritical methods that include a continual examination of frequency, damping, and amplitude of response are used to identify instabilities via extrapolation approaches. A build-up approach in the flight test program that permits the lowest risk test points (low velocity, high altitude) to be conducted first is advised. The flight test team should be formed with an emphasis on appropriate experience and expertise, and one should proceed cautiously and "expect the unexpected".

REFERENCES

1 Bisplinghoff, R. L., Ashley, H., and Halfman, R. L., **Aeroelasticity**, Addison-Wesley, Massachusetts, 1955.

2 Fung, Y. C., **An Introduction to the Theory of Aeroelasticity**, John Wiley and Sons, New York, 1955.

3 Hassig, H. J., "An Approximate True Damping Solution of the Flutter Equation by Determinant Iteration", AIAA Journal of Aircraft, Vol. 3, No. 11, Nov. 1971, pp. 885-889.

4 ANM-110, "Flutter Substantiation of Transport Category Airplanes," Advisory Circular of U. S. Department of Transportation FAA, 1985.

5 Theodorsen, T. and Garrick, I. E., "Mechanism of Flutter – A Theoretical and Experimental Investigation of the Flutter Problem," NACA TR-685, 1940.

6 ACE-100, "Means of Compliance with Section 23.629, Flutter," Advisory Circular of U. S. Department of Transportation FAA, 1985.

7 "Introduction to Flutter of Winged Aircraft," von Karman Institute for Fluid Dynamics, Lecture Series 1992-01, von Karman Institute, 1992.

8 Kehoe, M. W., "Aircraft Ground Vibration Testing At The NASA Ames-Dryden Flight Research Facility," NASA TM-88272, NASA Ames Research Center, Dryden Flight Research Center, California, July 1987.

9 Norton, W. J., "Structures Flight Test Handbook," AFFTC-TIH-90-001, Air Force Flight Test Center, Edwards AFB, California, Nov. 1990.

10 Craig, R. R., Jr., **Structural Dynamics - An Introduction to Computer Methods**, John Wiley and Sons, New York, 1981.

11 Kehoe, M. W., "Aircraft Flight Flutter Testing at the NASA Ames-Dryden Flight Research Facility," NASA Technical Memorandum 100417, NASA Ames Research Center, Dryden Flight Research Facility, California, May 1988.

12 van Nunen, J. W. G. and Piazzoli, G., "Aeroelastic Flight Test Techniques and Instrumentation," AGARD Flight Test Instrumentation Series, AGARD-AG-160, Vol. 9, AGARD, London, England, Feb. 1979.

13 "Flutter Testing Techniques," NASA SP-415, NASA, 1976.

14 "Flutter Flight Testing Symposium," NASA SP-385, NASA, 1958 (reprint 1975).

15 Cole, S. R., "Exploratory Flutter Test in a Cryogenic Wind Tunnel," AIAA Paper No. 85-0736, Florida, American Institute of Aeronautics and Astronautics, 1985.

16 Kehoe, M. W. and Rivera, J. A. , "Flutter and Aeroservoelastic Clearance of the X-29A Forward-Swept Wing Airplane," NASA Technical Memorandum 100447, California: NASA Ames Research Center, Dryden Flight Research Facility, Sept. 1989.

17 Fruedinger, L. C., "Flutter Clearance of the F-18 High Angle-of-Attack Research Vehicle With Experimental Wingtip Instrumentation Pods," NASA Technical Memorandum 4148, NASA Ames Research Center, Dryden Flight Research Facility, California, 1989.

Chapter 11

POST-STALL GYRATIONS AND SPINS

So far in this introductory survey of flight test, the motions under discussion have been well-behaved small perturbations from some equilibrium condition. The angle of attack has been less than the stall angle of attack. Classically, this angle of attack is thought of as that angle where the C_L-α curve has a sharp break as shown in Fig. 11.1. If the trajectory proceeds on to higher angles of attack, the vehicle may go out of control and go through completely uncommanded maneuvers. This chapter briefly summarizes the theory for these kinds of post-stall motions and outlines some of the precautions that must be taken when tests are planned that deliberately place the vehicle in this hazardous flight regime outside of the normal operating envelope.

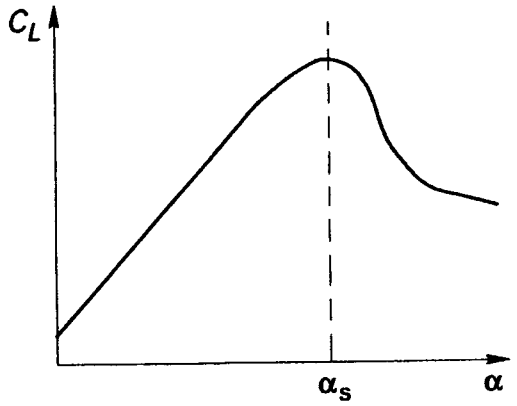

Fig. 11.1 Classical Aerodynamic Stall

The hazardous nature of post-stall flight tests underscores the importance of conducting them. During the 1970s post-stall accidents generated a considerable amount of research aimed at preventing loss of control. Through careful tailoring of the aerodynamic configuration and skillful use of automatic control systems, designers have been able to create highly spin-resistant airplanes. The payoff in this design emphasis became evident during the flight test programs of the current generation of operational fighters. The F-14, F-15, F-16, and F-18 all have remarkably good high angle of attack characteristics compared to their predecessors. The latter three airplanes all completed rigorous high angle of attack programs without the loss of a single airplane to an out-of-control incident: an unprecedented safety record in fighter development! But it is not enough to simply design departure- and spin-resistant airplanes. Maneuverability in the post-stall arena is important for a significant number of tactical situations[1]. At the time of this writing there are three major research projects in flight test[2,3,4] meant to help understand and exploit any tactical advantages that come from maneuvering at angles of attack well above the stall. The YF-22 and YF-23 Advanced Tactical Fighter prototypes have demonstrated significant capability in this part of the flight envelope. With this sort of thrust in design requirements (driven, of course, by perceived operational advantages) and the inherent hazards associated with high angle of attack testing, it is imperative that an introduction to flight test engineering include a discussion of post-stall testing.

11.1 THEORETICAL FOUNDATIONS

11.1.1 Post-Stall Definitions

The terminology used to discuss the post-stall flight regime is unique and an expanded vocabulary is a necessity. Our first step, then, is to understand what a stall, a departure, the incipient spin, a post-stall gyration (PSG), and a developed spin are and how they differ from one another. These definitions are the subject of this section.

11.1.1.1. **Stall**. No two source documents define stall in exactly the same way. The FAA Flight Training Handbook[5] defines this term about as simply as possible:

> *A **stall** occurs when the smooth airflow over the airplane's wing is disrupted and the lift degenerates rapidly.*

These words describe the classical stall as depicted in Fig. 11.1. On the other hand, military specifications define the stall in subtly different terms:

> *The angle of attack for maximum usable lift at a given flight condition is the **stall angle of attack**[6].*

The same document explains "maximum usable lift" by spelling out conditions other than reaching the peak of the C_L-α curve that may limit available lift. Possibilities include:

Uncontrollable pitch, roll, or yaw	Excessive sink rates
Intolerable buffet	Inability to perform altitude corrections

Stall occurs when a maximum usable angle of attack or airspeed is reached. It is not always an uncontrollable event in itself; rather, it merely describes a critical condition reached by the lift-generating surfaces of the vehicle. Exceeding this critical condition may cause drastic changes in the trajectory followed by the vehicle and in its response to control inputs. The airplane may become uncontrollable. Nonetheless, a stall does not inevitably lead to loss of control.

11.1.1.2 **Departure**. If a stall does not always produce uncontrolled flight, what event does mark the transition from controlled to uncontrolled flight? The military has coined the term "departure" for that event.

> ***Departure** is that event in the post-stall flight regime which precipitates a PSG, spin, or deep stall*[6].

Notice two things about this definition. First, departure occurs in the post-stall flight regime; that is, the stall always precedes or is at least coincident with the departure event. It can be inferred, then, that the angle of attack for maximum usable lift is always less than or equal to the departure angle of attack. Secondly, only one of three motions may result from a departure: the airplane either enters a PSG, a spin, or a deep stall. Implicit in this definition of departure is the idea that an immediate recovery cannot be made. For example, a general aviation airplane whose stall is defined in the classical sense illustrated

by Fig. 11.1, may recover immediately if the longitudinal control pressures are relaxed when the stall occurs. However, the same airplane might go out of control, or depart, if ailerons were deflected significantly at the time stall occurred. With pro-spin ailerons applied, the same docile general aviation airplane might readily spin. By the definition of the term, it would then have departed. This latter fact suggests that one must specify susceptibility or resistance to departure for given control positions, along with other configurational parameters.

The departure event is usually a large amplitude, uncommanded, and divergent motion. Such descriptive terms as nose slice or pitch-up are commonly used to portray departure. By uncommanded motions, it is meant that the pilot or controller did not intend the control movements to produce the actual motions which resulted. The airplane may not follow the pilot's commands for a number of perfectly valid aerodynamic reasons:

> High local α may render control surfaces ineffective.
>
> The pilot may be unable to position the control stick properly due to lateral or transverse accelerations at his cockpit position.

In either of these cases, the motion is uncommanded. A divergent motion is one which either continuously or periodically increases without bound. Some airplanes, like the T-33, periodically "buck" when forced past the stall; that is, the nose periodically rises and falls. However, there is no divergence unless full aft stick, ailerons, or some other pro-spin control is held. The T-38 will occasionally produce a non-divergent lateral oscillation near the stall angle of attack. Neither of these motions is usually counted as a departure, though their presence does warn of impending departure if the controls are further abused. In sum, a departure is a very difficult event to precisely describe, but there is little doubt in the pilot's mind when it has occurred!

11.1.1.3 **Post-Stall Gyration**. A post-stall gyration is an uncontrolled motion about one or more axes following departure[6]. It is also a difficult term to define concisely because it occurs in so many different forms. Frequently, the motions appear to be completely random about all three axes and no more descriptive adjective or noun can be applied than PSG. A snap roll or a tumble are motions that fit the definition of a PSG, and these more common (if less precise) words are sometimes used. The primary difficulty lies in distinguishing between a PSG and the incipient phase of a spin, especially an oscillatory spin. The chief distinguishing feature is that a PSG may involve angles of attack that are intermittently below the stall angle of attack, whereas the angle of attack must be greater than the stall angle of attack for a spin to exist.

11.1.1.4 **Spin**. Finally, a spin must be defined[6].

> ***A spin is a sustained yawing and rolling rotation at angles of attack above the stall angle of attack.***

Sometimes the spin is defined as a yawing rotation rather than a yawing and rolling rotation, but such a definition would only be valid for a perfectly flat spin with $\alpha = 90°$. Typically, the yaw rate about the z body axis is the dominating rotation. The pilot of an airplane will likely consider a sustained yaw rate one of the most important visual cues that

he is in a spin. In fact, if the spin is steep (that is, the angle of attack is relatively low, near α_s), pilots often have difficulty in recognizing the motion as a spin. Such a trajectory may be perceived as a roll rather than a spin. A steep inverted spin is another kind of spin that can be even more confusing and disorienting because the body axis roll and yaw rates are in opposite directions. Even in an inverted spin, the yaw rate dictates the direction of rotation and the control manipulations necessary to recover.

11.1.1.5 **Deep Stall**. The last out-of-control flight condition to be discussed is called the deep stall:

> *A **deep stall** is an out-of-control flight condition in which the airplane is in equilibrium at an angle of attack well above α_s while experiencing negligible rotational velocities.*

The deep stall is distinguished from a post-stall gyration by the lack of significant angular rates. Some maneuvers with graphic names like "falling leaf" are categorized as deep stalls, but so are others that have large amplitude angle of attack oscillations. In a deep stall, there is almost always a very high rate of descent. It is fairly common for the lateral and directional controls to be ineffective and sometimes even the longitudinal control loses its authority. The latter condition, of course, is to be avoided in any design. The motion during a deep stall may not be steady. Oscillations in angle of attack may be quite large in amplitude. These oscillations sometimes are helpful in that longitudinal control inputs of the appropriate frequency have been used to dynamically generate the moments necessary to recover from the deep stall.

11.1.2 Spin Modes

Three types of adjectives are used to describe the general characteristics of a given spin and they identify the spin mode. The sign of the angle of attack, for example, classifies a spin as either upright ($\alpha > 0$) or inverted ($\alpha < 0$). Average values of angle of attack also classify a spin as either flat or steep, meaning that flat spins occur at high α and steep spins occur with lower α. Finally, the peak amplitudes of the oscillations compared with the average value of rate of rotation spells out the oscillatory character of the spin mode. One descriptive modifier from each of these adjective groups may be used to characterize the spinning motion. Table 11.1 summarizes these modifiers.

Table 11.1 Spin Mode Modifiers

Group 1	Group 2	Group 2
Upright	Steep	Smooth
		Mildly Oscillatory
Inverted	Flat	Oscillatory
		Highly Oscillatory
		Violently Oscillatory

Mode identification terminology can be confusing. The most confusing facet of adjective identifier usage is associated with groups 2 and 3 in Table 11.1. The example[7] in Table 11.2 should help clarify usage of these modifiers.

Table 11.2 F-4E Spin Modes

Mode Description	Average AOA (°)	AOA Oscillations (°)	Yaw Rate (°/sec)	Roll Rate (°/sec)	Pitch Rate (°/sec)
Steep-Smooth	42	±5	40-50	50	15
Steep-Mildly Oscillatory	45-60	±10	45-60		
Steep-Oscillatory	50-60	±20	50-60 (with large oscillations)	Same as yaw rate	
Flat-Smooth	77-80	Negligible	80-90	25	7

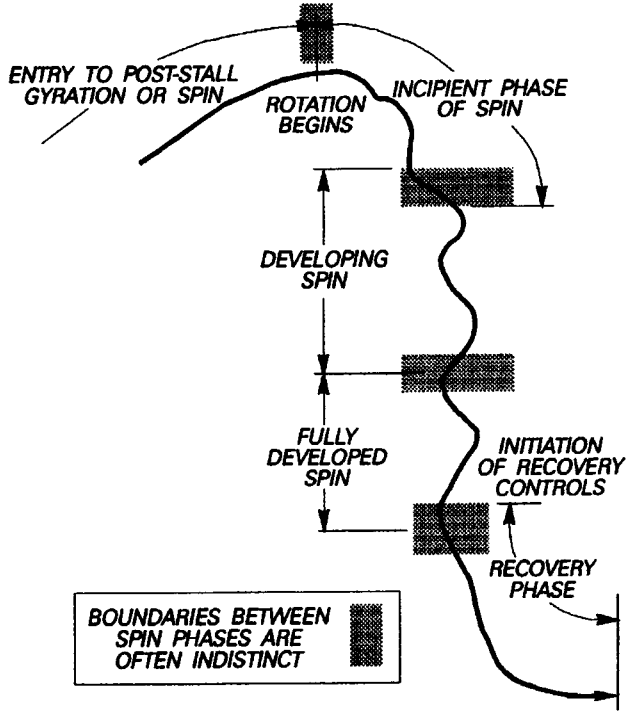

Fig. 11.2 Spin Phases

11.1.3 Spin Evolution

A fully developed spin is an equilibrium dynamic state. However, this state of equilibrium is not reached by every trajectory that progresses into this nonlinear post-stall flight region. Moreover, equilibrium for the strongly coupled, large amplitude governing equations is not necessarily a steady state solution in the classical linear sense; it is more often

a periodic solution (like a limit cycle). Such a complicated trajectory does not occur instantaneously; the transient motions are quite observable and are especially important to the flight test planner (as well as to the operational pilot!). We will discuss three stages or phases (Fig. 11.2) of spin evolution; but, keep in mind that not all spins will reach equilibrium. Thus, a given spin trajectory may pass through all or only one of the phases. It does not always progress through the complete evolution to the fully developed equilibrium state.

11.1.3.1 **Incipient Phase**. The incipient phase of a spin is the initial, transitory part of the motion during which it is impossible to identify the spin mode. The yawing and rolling rotation (usually perceived by the pilot as yaw rate) begins as the incipient phase begins. The cue to the pilot of an incipient is that of a sustained, though not necessarily steady, yawing rotation. Even during this incipient phase, the angle of attack is greater than the stalled angle of attack. This characteristic, stalled angle of attack in the spin is one of the distinctions between the incipient phase of the spin and any post-stall gyration that occurs after departure. The incipient phase of the spin ends when a recognizable mode can be identified. Sometimes, this mode is not recognizable in flight but must be identified by examining data traces. To summarize, the incipient phase of the spin is a transitory motion easily confused with a PSG, but distinct from either a PSG or the developed phase of a spin.

11.1.3.2 **Developing Phase**. The developing phase of a spin is that stage of the motion in which the spin mode can be ascertained. Oscillations may be present, but the mean periodic motion is discernible. The aerodynamic forces and moments may not be completely balanced by the corresponding linear and angular accelerations, but equilibrium conditions are being approached. Generally, it is evident when the developed phase is in progress, though the exact point at which it began may be unclear. Since the motion is approaching an equilibrium state, it is frequently advisable to initiate recovery before true equilibrium is achieved. For example, during the T-38 test program, warning lights were installed to signal a buildup of yaw rate. Recoveries were initiated when these lights came on at approximately 85°/sec. In the flat spin mode of this basic trainer, a peak yaw rate of 165°/sec was achieved, even when recovery controls were applied when the lights came on. The longitudinal acceleration at the pilot's station was approximately 3.5g and the spin could only be terminated by deployment of the spin chute[9]. The developing spin, while it may be more comfortable because it is usually less oscillatory than the incipient spin, can be deceptively dangerous. Careful preflight planning and continuous monitoring of the testing is absolutely essential when you plan to stay in a spin while it is developing.

11.1.3.3 **Fully Developed Phase**. A spin is fully developed when it reaches the final equilibrium state. In this stage of its evolution the motion is typically a repetitive periodic trajectory. Theoretically, all the states would be constants and all linear and angular accelerations would be zero on average over a complete period. Instantaneously, at least some of the state rates of change would be nonzero if the motion is oscillatory in any fashion. Practically, attaining this state may take a very long time. It may also be hard to recognize in the cockpit or from real-time telemetry data if the periodic motion is oscillatory. One very important type of fully developed spin is, however, quite recognizable. The flat spin, in which the angle of attack is theoretically 90°, is just such a case. The difficulty in recognizing a post-stall equilibrium condition is one of the main dangers inherent in

post-stall/spin flight tests. It is one of the main reasons this kind of testing must be considered hazardous and treated with special attention to detail throughout the test planning cycle and during the conduct of such tests. All systems, whether they are unique to the test effort or are simply production systems, must be capable of and allow the test pilot to safely recover from the worst case of dynamic equilibrium in a fully developed spin. Thus, the fully developed phase of the spin deserves considerable attention from the flight test engineer. Consequently, we will shortly develop six degree-of-freedom, fully coupled, nonlinear equations of motion for a rigid aircraft in this kind of trajectory. But before we proceed to these equations, we have to understand what kind of flight path to anticipate and the underlying aerodynamic forcing functions so we can make intelligent approximations.

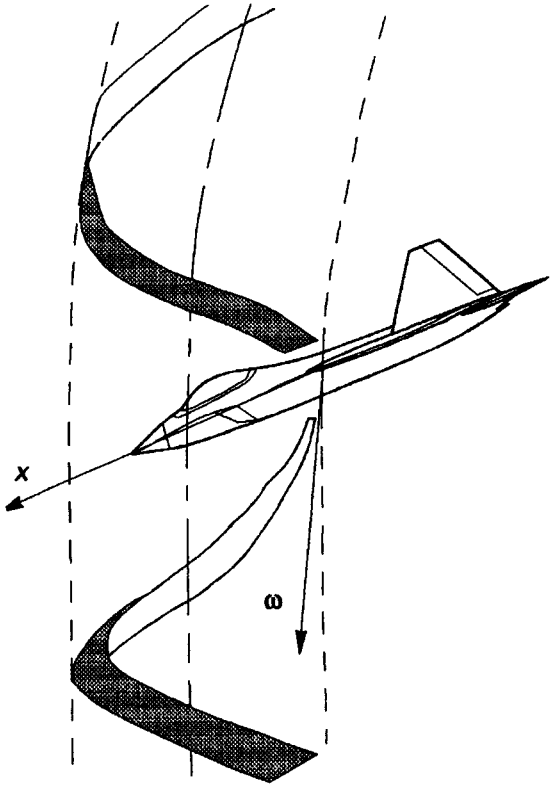

Fig. 11.3 Helical Flight Path in a Fully Developed Spin

11.1.4 Flight Path in a Spin

A spin is a coupled motion that requires all six equations of motion for satisfactory analysis. Extreme attitudes and large angular rates are often encountered in such motions. In the general case the airplane center of gravity describes a helical path while it rotates about an axis of rotation at the center of the helix. As sketched in Fig. 11.3, the helical path may be curved and the total angular velocity vector is continually changing in both magnitude and direction. In general the wings are not level and sideslip is not zero.

This general motion is very complex. However, if we make the following simplifying assumptions, some of the basic characteristics of spin trajectories can be clarified.

11.1.4.1 **Assumptions**. The following assumptions simplify the analysis while allowing us to keep the more important features of spin trajectories in focus. Assume:

a fully developed spin in which the helical axis is vertical (ω is constant)
no sideslip, which infers that the wings are horizontal
the side force is negligible compared to the lift and the drag

These assumptions mean that the angular velocity vector ω is approximately parallel to the helical flight path (and, consequently, to the relative wind).

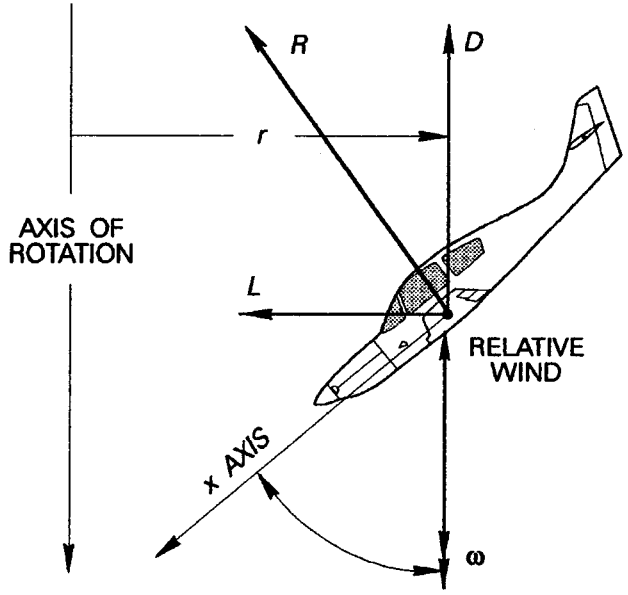

Fig. 11.4 Changes in Lift and Drag Coefficients at High Angles of Attack

11.1.4.2 **Balance of Forces**. Next, consider the balance of forces in a such a steady spin without sideslip as shown in Fig. 11.4. Because of assumption 3, the resultant aerodynamic force acts within the plane of symmetry and is approximately normal to the wing chord. Summing the vertical forces gives:

$$W = D = \frac{\rho V^2 S C_D}{2} \tag{11.1}$$

Similarly, the forces in the horizontal direction just balance the centripetal acceleration and

$$mr\omega^2 = L = \frac{\rho V^2 S C_L}{2} \tag{11.2}$$

The physical implications of these two seemingly trivial equations are extremely important. First, eqn. 11.1 says that, as α increases, C_D increases and, consequently, true airspeed decreases. Since the trajectory is vertical, true airspeed is approximately equal to rate of descent. In other words, as α increases, the airplane becomes more and more like

a rotating bluff body in the descent and the descent rate slows in a flat spin. Furthermore, for $\alpha > \alpha_s$, C_L decreases as α increases. With these facts in mind, the left side of equation 11.2 must decrease as α increases. It will be shown shortly that the rotation rate ω tends to increase with increasing α. In turn, then, the radius of the helix r must decrease rapidly as α increases. These observations suggest that in a fully developed, flat spin, ω and V are nearly coincident. The angular difference between the flight path and vertical is approximated by Babister[7] as: $tan\lambda = \frac{r\omega}{V}$. A typical variation of λ with angle of attack is about 5.5° at an α of 50° and about 1° at an α of 80°. Hence, it is justified to assume in fully developed spins that ω is nearly parallel to $V$and, for flat spins, the two vectors are essentially coincident.

These assumptions are valid only if the wings are horizontal and sideslip is zero. This complexity is beyond the scope of this introductory text; both Babister[8] and Kerr[9] provide insight into these topics for the interested reader. Remember, these comments are valid only for the fully developed spin. The underlying physical phenomena are clarified by considering this simplified case, and hopefully, these simplifications will give the student a better appreciation of the more complex components of this type of motion.

11.1.5 Aerodynamic Factors in a Spin

In the post-stall flight regime aerodynamic forces acting upon the vehicle are very different than those acting upon it during flight at low angle of attack. Aerodynamic derivatives, usually described as linearized approximations with first order partial derivatives, are highly dependent on both α and β and second order derivatives may be important. Often these derivatives change sign rapidly as flows separate and reattach and vortex lift patterns break down. Terms which are not particularly significant at low angle of attack may become very important. Stough[10] and his associates at Langley have concluded that, at least for straight-wing, wing-loaded airplanes (general aviation aircraft), the aerodynamic behavior of the wing is often the single most important factor in how the airplane itself enters and recovers from a post-stall maneuver. Though these conclusions cannot be blindly applied to all airplanes, they do suggest that looking that the wing's behavior is a good place to start our consideration of post-stall aerodynamics.

11.1.5.1 **Autorotative Couple of the Wing**. The wing is often the major contributor to the aerodynamic mechanism that initiates and sustains autorotation. If a wing is operating at a low α and a sudden local change in α occurs due to a rapid roll, there is a restoring moment developed because of the increase in lift generated by the higher α on the downgoing half of the wing and the decrease in lift on the half of the wing that is moving up (see the left side of Fig. 11.5, page 270, where ΔC_{L_1} and ΔC_{D_1} occur). On the other hand, when a wing operating at $\alpha > \alpha_s$ (see the right side of Fig. 11.5, where ΔC_{L_2} and ΔC_{D_2} occur) is rolling rapidly, the downgoing wing experiences a loss in lift and an increase in drag. This loss of lift creates an even larger rolling moment and the increase in drag produces a yawing moment in the direction of the roll. This latter situation is clearly unstable and self-perpetuating; it leads to an autorotation.

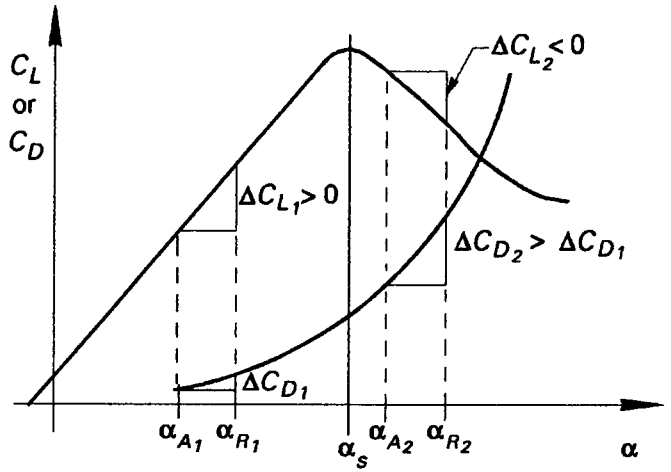

Fig. 11.5 Aerodynamic Mechanisms for Autorotative Moments

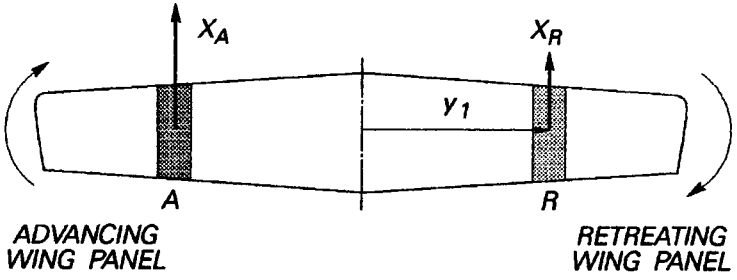

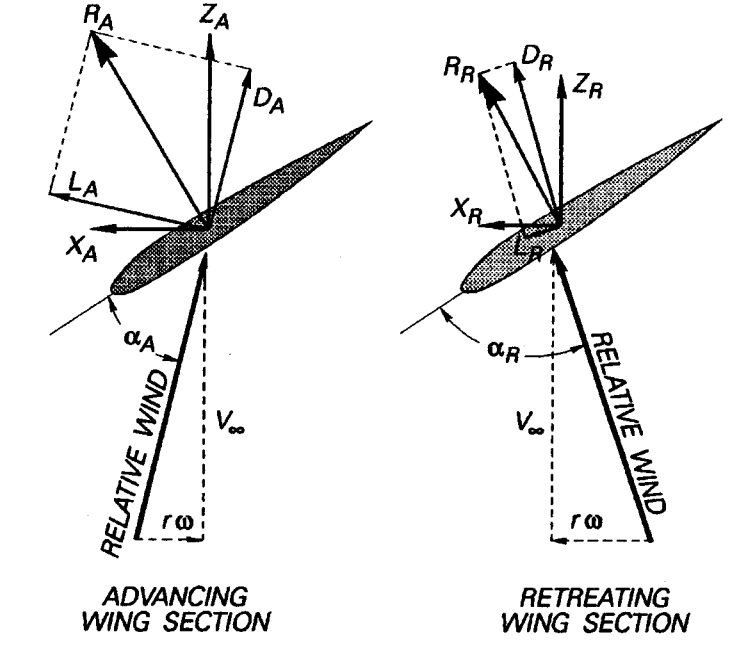

Fig. 11.6 Lift and Drag on Advancing and Retreating Wing Panels

A more complete understanding of the aerodynamic mechanism that is driven by the wing comes from Fig. 11.6 (page 270), where the orientation of the resultant forces is shown, as well as the components of the resultant forces resolved along the inertial *x* and *z* axes. The net difference in the ***X*** forces at corresponding sections in the advancing wing panel and in the retreating wing panel produces a couple $(X_A - X_R)2y_1$. This couple is shown at the top of this plan view of the wing. The yawing moment produced by the term $(X_A - X_R)2y_1$ is positive for a positive yaw rate. The rolling moment produced by the couple $(Z_A - Z_R)2y_1$ is also positive. Thus, the incremental moments generated as the angular velocity becomes significant lead to a moment contribution from the wing that propels the airplane into a spin. Of course, eventually the damping in yaw and damping in roll will become large enough to substantially oppose the autorotative motion, but it is quite clear that a fully developed spin can be sustained indefinitely. It is an equilibrium dynamic state.

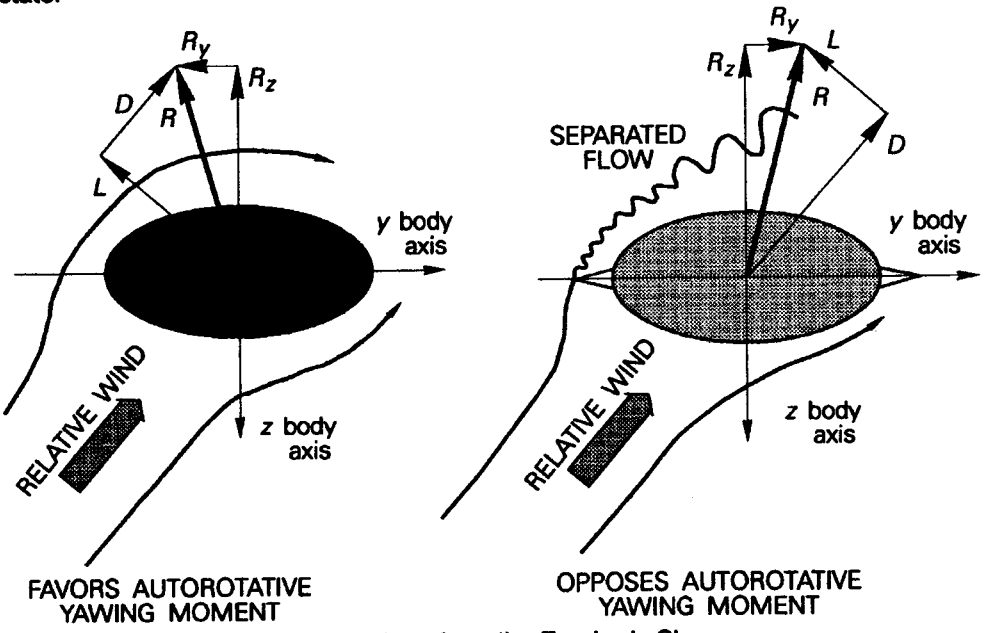

Fig. 11.7 Aerodynamic Contributions from the Forebody Shape

11.1.5.2 **Effect of Forebody Shape**. The fuselage, especially the nose, may also contribute significant aerodynamic moments with $\alpha > \alpha_s$. The pressure field around the nose depends strongly on its cross-sectional shape. Since the flow character is highly dynamic, often dominated by vortex shedding, prediction of the aerodynamic contribution of the forward fuselage components is rather difficult. Small geometric changes in this region can make dominating changes in rolling and yawing moment coefficient in the post-stall flight regime. One possible fuselage effect is illustrated in Fig. 11.7. In these sketches we are looking at a roughly elliptical cross-section for a fuselage nose as an observer facing forward in the airplane. Naturally, this shape acts like an airfoil, producing both aerodynamic forces perpendicular (like lift) and parallel (like drag) to the local flow direction. This local flow direction is strongly influenced by the rotational rate of the airplane. As shown on the left side of Fig. 11.7, if the aircraft is rolling and yawing to the left and the net aerodynamic force vector is to the left, the local effect is to reinforce the au-

torotative rolling and yawing moments. The right side of Fig. 11.7 shows the same cross-section modified with a strake. With this modification the nose produces an aerodynamic moment that opposes autorotation. The spin characteristics of the T-37 trainer were considerably improved by such a modification, incorporated during its flight tests.

11.1.5.3 **Effect of Damping Derivatives**. Aerodynamic damping derivatives are significantly affected at high angles of attack, especially roll damping (C_{l_p}). In fact, often both C_{l_p} and C_{n_p} become positive at or near α_s. These aerodynamic effects can be deduced by considering moments produced by the local lift and drag forces depicted in Figs. 11.4 and 11.6. Several authors consider this loss of damping to be one of the main aerodynamic factors resulting in autorotative behavior[8,11,11]. Obviously, a complete discussion of these aerodynamic coefficients and how they behave in the post-stall flight regime is beyond the scope of this introductory text. But, these references suggest additional reading for the interested student.

Now, we turn our attention to the other side of the equation: the inertia terms.

11.1.6 Effect of Mass Distribution

The moments of inertia are the most obvious and meaningful measures of mass distribution. The inertial forces and moments, which depend directly on the mass distribution, are particularly important in the post-stall motion of a vehicle because they are of the same order of magnitude as the aerodynamic forces and moments. This relative sizes of the inertial forces and moments and the aerodynamic forces and moments are features peculiar to flight at post-stall angles of attack.

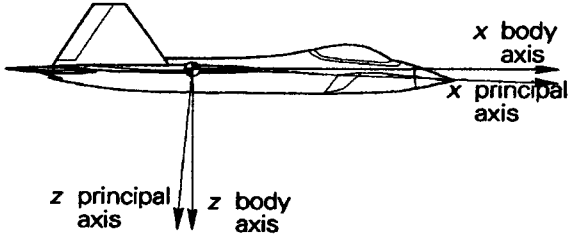

Fig. 11.8 Relationship Between Body and Principal Axes

11.1.6.1 **Principal Axes**. Orthogonal body axes for which all three products of inertia are zero are called the principal axes for the body. Principal axes can be found for any rigid body. If the vehicle has a plane of symmetry, as most aircraft and missiles do, it is fairly easy to choose a coordinate system that approximates the principal axes. The xz plane is simply chosen to lie in the plane of symmetry, thus guaranteeing that both $I_{xy} = I_{yz} = 0$. The direction of the x axis is usually chosen so it can be easily identified with configuration geometry. (Thus, the term **fuselage reference line (FRL)** is often seen in airplane layout drawings.) For brevity this reference set of body axes is usually called simply the body axes. (Strictly speaking, the principal axes and the stability axes used with linearized, small perturbation equations of motion are also body axes.) To simplify our later discussion and to make the large amplitude equations of motion easier to

understand, we will take the body axes and the principal axes to coincide. An illustration of the difference between these two body axes is shown in Fig. 11.8.

In the principal axis system, one of the moments of inertia is the maximum possible for the body. Choosing body axes that are close to principal axes means the product of inertia I_{xz} is quite small. A small value of I_{xz} reduces the cross coupling between the large amplitude moment equations that govern the symmetric (longitudinal) motion and the asymmetric (lateral-directional) motion. For the linearized small perturbation equations, this term had to be negligible in order to separate the longitudinal equations from the lateral-directional ones. That simplification gave us the luxury of solving two quartic characteristic equation sets rather than a higher order characteristic equation. Even though I_{xz} is typically small due to our choice of body axes, its coupling effects can rarely be ignored in post-stall maneuvers. We will specifically show in a later section that pitch rate can have a significant effect on ω, even if I_{xz} can be safely ignored.

11.1.6.2 **Relative Density**. The relative density parameter μ is a measure of the ratio of the airplane's density to the density of the air its volume displaces. It is a very useful nondimensional parameter that appears in the equations we need.

$$\mu = \frac{2m}{\rho S b} \tag{11.3}$$

11.1.6.3 **Center and Radius of Gyration**. Two other definitions are used in discussing mass distribution: center of gyration and radius of gyration. The center of gyration of a body with respect to an axis is that point at which the mass of the body could be concentrated and the resulting mass moment of inertia about the specified axis would be unchanged. Similarly, the radius of gyration k_i with respect to an axis is the distance from the center of gyration to that reference line. Recalling the basic definitions of the mass moments of inertia, we can write expressions for each of the three radii of gyration:

$$\begin{aligned} \int (y^2 + z^2)dm \equiv I_x &= k_x^2 m \\ \int (x^2 + z^2)dm \equiv I_y &= k_y^2 m \\ \int (x^2 + y^2)dm \equiv I_z &= k_z^2 m \end{aligned} \tag{11.4}$$

11.1.6.4 **Relative Magnitude of Airplane Moments of Inertia**. The relative sizes of moments of inertia for an airplane are a convenient means of classification (as suggested in Fig. 11.9). The moment of inertia about the z body axis is always the largest of these inertias; this fact is assured because airplanes have very little mass outside the xy plane. From a mass-distribution point of view, the vehicle is "flattened" into this plane. A wing-loaded airplane is defined as one that has more mass concentrated in the wings. The wings may be structurally heavy; fuel may be carried inside integral tanks in the wing; engines may be slung in nacelles from the wing; or stores may be loaded externally on pylons attached to the wings. Any one or all these factors cause more mass to be located in the wings. $I_z > I_x > I_y$ for wing-loaded airplanes. Figure 11.9a illustrates such an airplane. A neutrally loaded airplane is one in which the wing and the fuselage have

roughly equal mass, that is, $I_x = I_y$ (Fig. 11.9b). Finally, a fuselage-loaded airplane is one in which most of the mass is concentrated in the fuselage (Fig. 11.9c). Most modern fighter airplanes are fuselage-loaded, which helps to give them very distinctive spin characteristics. We can gain some insight into just what kinds of spin modes might develop for different mass distributions (or "loadings") by careful inspection of the equations of motion.

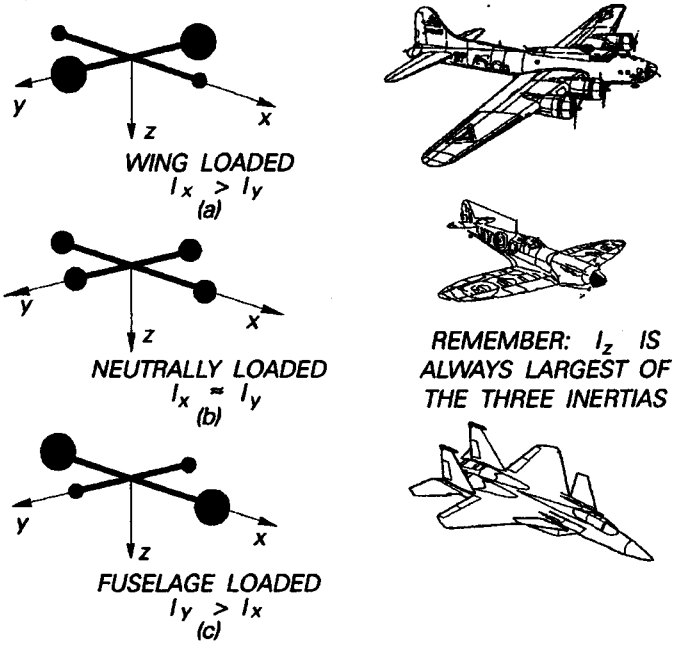

Fig. 11.9 Relative Magnitude of Aircraft Moments of Inertia

We have been referring to the large amplitude equations of motion freely and discussing terms within these equations; it is now time to examine these equations directly.

11.1.7 Simplification of the Post-Stall Equations of Motion

The equations of motions describing aircraft dynamics in the post-stall flight regime are more complicated than the linearized, small perturbation ones we have discussed and used in previous chapters. The post-stall equations differ in the following ways:

- all six rigid body degrees of freedom must be considered in any solution -- pitching motions do affect lateral-directional response and vice versa;
- the changes in states are often quite large -- small perturbations in angular positions, rates, and accelerations are simply not warranted; and
- the aerodynamic coefficients are not constants -- the stability derivatives are functions (and seldom analytic ones at that) of both angle of attack and sideslip angle at least.

11.1.7.1 **Simplifying Assumptions**. The basic simplification we will use is that only a fully developed spin with the wings horizontal will be considered. This motion state is an equilibrium condition, in which the aerodynamic forces and moments and the inertial forces

and moments are balanced. To further simplify the discussion, we will further require that all applied moments are aerodynamic ones; in fact, we will not allow even propulsive moments. This latter assumption will avoid a lengthy and confusing discussion of moments generated by gyroscopic couples due to rotating parts in the engines. Also, any coupling between the propulsion system and the controls can be ignored with this simplification. Summarizing these simplifications:

- Because the wings are horizontal, the angular velocity vector ω lies entirely within the xz plane. Its only components are P and R; Q is zero.
- Furthermore, the velocity vector and ω are parallel at all times.
- The velocity vector (and ω) is vertical for a fully developed spin, that is V = rate of descent.
- The angular velocity vector is constant, making $\dot{P} = \dot{Q} = \dot{R} = 0$ and the time per turn constant.
- The body axes are assumed to coincide with the principal axes, allowing us to take $I_{xz} = 0$.

The last assumption above simply allows us to ignore the terms containing the product of inertia I_{xz} in each of the moment equations.

The force balance takes on one of the two following forms. In an inertial frame of reference or a body frame of reference, the vector equations are:

$F = m\frac{dV}{dt}$ for the inertial frame or $F = m\left(\frac{dV}{dt} + \omega x V\right)$ for the rotating body axis frame of reference. Since we will only look at steady state conditions, $\frac{dV}{dt} = 0$ in either reference system. Also, ω and V are parallel (assumption 2), so $F = 0$ in body axis coordinates.

11.1.7.2 **Simplified Large Amplitude Moment Equations**. The summation of moments is by far the more important balance for equilibrium and it is usually only considered in the rotating frame of reference. In component form the moment equations are:

$$\begin{aligned}
\frac{dP}{dt}I_x + QR(I_z - I_y) - \left(\frac{dR}{dt} - QR\right)I_{xz} &= \mathcal{L} \\
\frac{dQ}{dt}I_y + PQ(I_x - I_z) - \left(R^2 - P^2\right)I_{xz} &= M \\
\frac{dR}{dt}I_z + PQ(I_y - I_x) - \left(\frac{dP}{dt} - PQ\right)I_{xz} &= N
\end{aligned} \qquad (11.5)$$

Applying our assumptions and solving for the angular accelerations:

$$\begin{aligned}
\frac{dP}{dt} &= \frac{\mathcal{L}}{I_x} + \frac{QR(I_y - I_z)}{I_x} \\
\frac{dQ}{dt} &= \frac{M}{I_y} + \frac{RP(I_z - I_x)}{I_y}
\end{aligned} \qquad (11.6)$$

$$\frac{dR}{dt} = \frac{N}{I_z} + \frac{PQ(I_x - I_y)}{I_z}$$

The first term on the right side of eqns. 11.6 represents the aerodynamic contribution to the angular acceleration and the second term describes the inertial contribution to the pertinent acceleration. Thus, simply rewriting these three moment equations in terms of the angular accelerations shows clearly that, for equilibrium to occur (that is, for a spin to become fully developed and all angular accelerations to vanish), an inertial term must balance an aerodynamic term in each equation. Notice that even with our simplifying assumptions we have not eliminated coupling between the equations of motion. These simplified equations also suggest that, to accurately calculate absolute angular accelerations, it is important to know the moments of inertia accurately. Obtaining them experimentally is a tedious job[12], one that flight test personnel are often tasked to complete.

Before we expand the aerodynamic terms, it is useful to point out a difference in the usual nondimensionalization of aerodynamic coefficients for use in the coupled equations that govern post-stall trajectories. These equations differ from the small perturbation equations that spawned our original nondimensionalization of stability derivatives. They cannot be separated into uncoupled longitudinal and lateral-directional subsets. Typically, data sets must be modified from our usual concept of stability derivatives for use in modeling post-stall dynamics. We have already seen how pitching moment coefficients (C_m) are based on wing semichord as a reference length, while both rolling and yawing moment coefficients (C_ℓ and C_n) are based on wing semispan. For the data to represent the same aerodynamic moments in the large amplitude equations of motion, a common reference length must be chosen. For this kind of analysis it is common practice to base pitching moment on wing span and designate it as C_{mb}. Numerically, the usual small-perturbation pitching moment coefficient is altered by $C_{mb} = C_m \frac{c}{b}$. The aerodynamic terms in eqns. 11.6 can be rearranged using the radius of gyration of eqns. 11.4.

$$\frac{\mathcal{L}}{I_x} = \frac{\rho V^2 SbC_\ell}{2k_x^2 m} = \frac{V^2 C_\ell}{2\mu k_x^2} \quad \text{and} \quad \frac{dP}{dt} = \frac{\mathcal{L}}{I_x} + \frac{QR(I_y - I_z)}{I_x}$$

$$\frac{M}{I_y} = \frac{\rho V^2 SbC_{mb}}{2k_y^2 m} = \frac{V^2 C_{mb}}{2\mu k_y^2} \quad \text{and} \quad \frac{dQ}{dt} = \frac{M}{I_y} + \frac{RP(I_z - I_x)}{I_y} \tag{11.7}$$

$$\frac{N}{I_z} = \frac{\rho V^2 SbC_n}{2k_z^2 m} = \frac{V^2 C_n}{2\mu k_z^2} \quad \text{and} \quad \frac{dR}{dt} = \frac{N}{I_z} + \frac{PQ(I_x - I_y)}{I_z}$$

Expressing the definitions of the aerodynamic moments in nondimensional terms,

$$\frac{dP}{dt} = \frac{\rho V^2 SbC_\ell}{2k_x^2 m} + \frac{QR(I_y - I_z)}{I_x}$$

$$\frac{dQ}{dt} = \frac{\rho V^2 SbC_{mb}}{2k_y^2 m} + \frac{RP(I_z - I_x)}{I_y} \tag{11.8}$$

$$\frac{dR}{dt} = \frac{\rho V^2 SbC_n}{2k_z^2 m} + \frac{QR(I_x - I_y)}{I_z}$$

11.1.8 Aerodynamic Conditions for Dynamic Equilibrium

Combining eqns. 11.8 with the first assumption, gives equilibrium conditions.

$$0 = C_{\not}$$

$$-\frac{\rho V^2 SbC_{mb}}{2k_y^2 m} = \frac{RP(I_z - I_x)}{I_y} \qquad (11.9)$$

$$0 = C_n$$

Remember that these equations are greatly simplified; they do not completely represent post-stall motion. But they allow us to introduce the idea that a fully developed spin is an equilibrium or "trim" condition, just like straight and level flight. With no external disturbances, the airplane will remain in this dynamic state until it impacts the ground. Now, let's look at each of the component moment equations above and understand their implications for a fully developed spin. We will start with the pitching moment equation, since it appears to have the most interesting form in eqns. 11.9.

11.1.8.1 **Pitching Moment Equation**. Consider eqn. 11.9b in conjunction with typical pitching moment curves for fighter type aircraft (Fig. 11.10). Also, from our original definition of a spin, α must be greater than α_s. For the typical highly maneuverable airplane, our simplified pitching moment equation implies that the term with C_{mb} in it must be of opposite sign to the inertial term on the right side of eqn. 11-9b. For an upright spin, this condition means that C_{mb} must be negative, since in an upright spin P and R are of the same sign (see Fig. 11.11 on the next page). Combining this observation with the fact that $I_z > I_x$ for any airplane, clinches the argument that $C_{mb} < 0$.

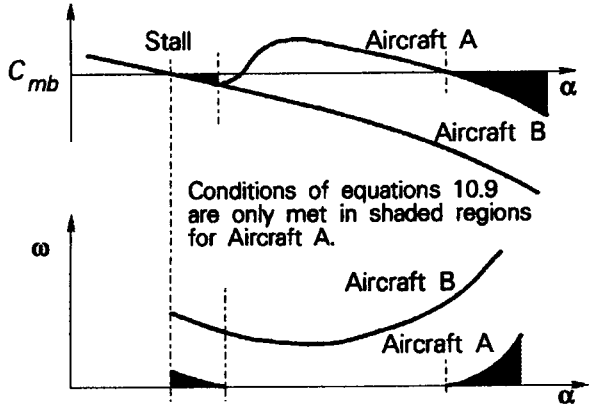

Fig. 11.10 Pitching Moment Coefficient in a Steady Spin

The slope of the C_{mb} - α curve must be negative for stability in any flight regime, even post-stall conditions. This slope must be negative for static longitudinal stability at either low or high angles of attack. Said another way, $\frac{dC_{mb}}{d\alpha} > 0$ represents a divergent

situation in which the pitch acceleration is not zero. Having such a nonzero angular acceleration about any axis (in our case about the *y* axis) violates the basic assumption of constant ω that we have used do define a fully developed, steady spin. Said another way, any disturbance in α produces a ΔC_{mb} that tends to restore disturbances α to its initial value only if $\frac{dC_{mb}}{d\alpha} < 0$.

Figure 11.10 recapitulates and summarizes the pitching moment constraints for a fully developed spin by directly comparing two different aircraft, each with quite different dynamic equilibrium possibilities. Aircraft B is clearly capable of sustaining a fully developed upright spin at any angle above α_s, insofar as the pitching moment equation is concerned. For this aircraft, C_{mb} and $\frac{dC_{mb}}{d\alpha}$ are always negative. However, airplane A can only meet the two constraints suggested above if α is in the shaded regions in the Fig. 11.10. Airplane A has two possible spin modes indicated in the sketch, while airplane B has only one. To be sure, the pitching moment is not the whole story; the rolling and yawing moment equilibrium equations must also be considered and we should give our attention to how they impact dynamical equilibrium. But first, an estimate of ω for each of the potential equilibrium conditions is useful and is easily obtained.

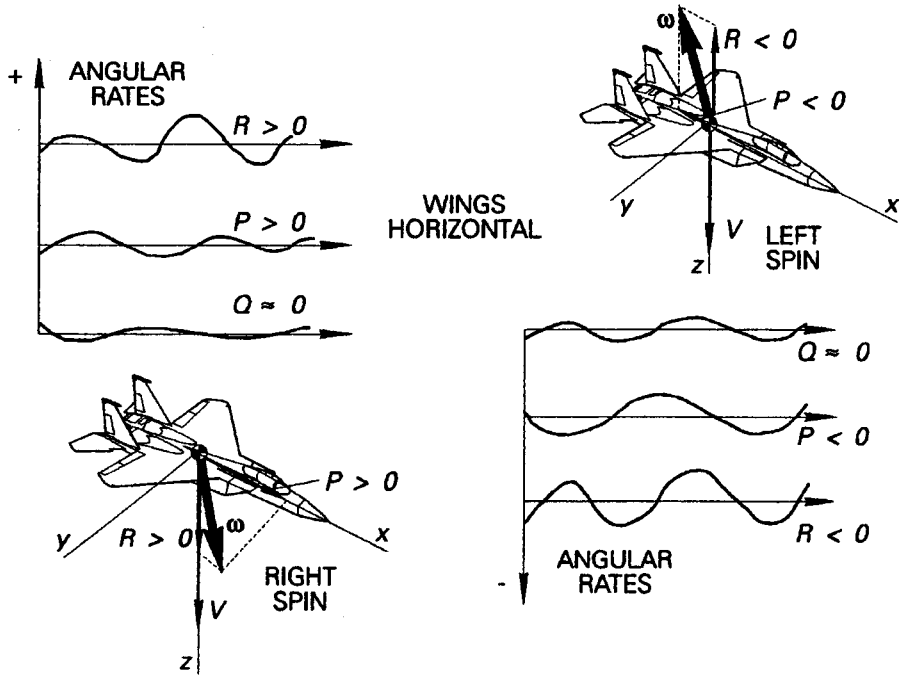

Fig. 11.11 Angular Velocity Components in a Typical Upright Spin

Figure 11.11 also emphasizes that $P = \omega\cos\alpha$ and $R = \omega\sin\alpha$ for our idealized, fully developed spin. Substituting these expressions into eqn. 11.6b gives

$$-\frac{M}{I_y} = \frac{(I_z - I_x)}{I_y} = \omega^2 \sin\alpha\cos\alpha \quad \text{or, solving for } \omega,$$

$$\omega = \sqrt{\frac{-2M}{(I_z - I_x)\sin 2\alpha}} \tag{11.10}$$

Equation 11.10 suggests that the minimum rotation rate occurs near an angle of attack of 45°, though the nonlinearities in C_{mb} at these flight conditions may be strong enough to change the angle of attack for minimum rotation rate noticeably. But eqn. 11.10 tells only part of the story; it does not spell out all the conditions for equilibrium that must be met for a fully developed spin to occur.

11.1.8.2 **Rolling and Yawing Moment Equations**. Equations 11.9 suggest other constraints that must be met for a fully developed spin to occur. Although we did not emphasize the point in the preceding paragraph, all the aerodynamic derivatives (even C_{mb}) are functions of α, β, and ω. Following Anglin and Scher[13], we have considered C_{mb} to be solely a function of α in spite of its dependence on other parameters. It is also convenient to take C_ℓ and C_n as functions of ω alone, even though there is little justification for these assumptions, other than that lateral-directional parameters are more directly linked to rotation rate, while the longitudinal parameters are usually more directly linked to angle of attack. These assumptions are useful to the understanding process, but C_{mb}, C_ℓ, and C_n are all affected by α, β, and ω. Next, consider the constraints imposed by the rolling and yawing moment equations.

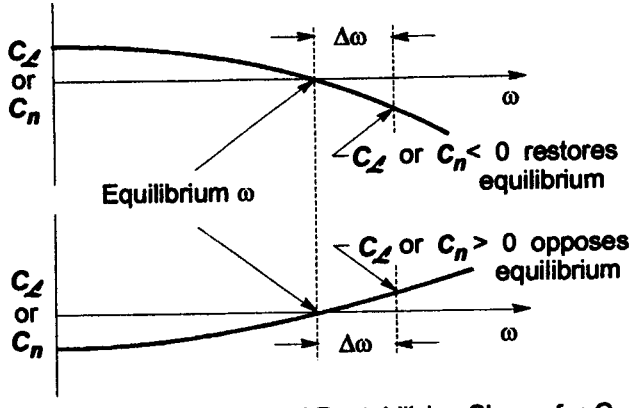

Fig. 11.12 Stabilizing and Destabilizing Slopes for C_ℓ and C_n

For a fully developed spin to occur the overall rolling moment and yawing moment coefficients, C_ℓ and C_n, must be zero and their rates of change with respect to ω must be negative. The first pair of these conditions is explicitly stated in eqns. 11.9. The second pair of conditions is a requirement for stability very much like the one that says C_{m_α} must be negative for static longitudinal stability to exist. Figure 11.12 illustrates this idea. If an increase in ω produces and increase in either or both rolling and yawing moment, then one or both of these total moments cannot remain in equilibrium for small changes in ω. That is, any change in rotation rate will cause the autorotative moments to diverge away from the nominally stable rotation rate. For a true equilibrium state to exist, any deviation from

this "trim" or equilibrium ω must cause an increment in both C_l and C_n that tends to restore rolling and yawing moment to its equilibrium (zero) state.

These aerodynamic constraints are rarely all met exactly for an actual airplane spin. In other words, a true fully developed spin is an idealization and does not often occur in practice. It is much more common to have oscillatory spins in which these conditions are almost met, but the true equilibrium is never quite reached. From an engineering perspective, while it is still useful to base our concepts on idealizations like the fully developed spin, it is even more important to be able to estimate actual spin behavior from computed and wind tunnel aerodynamic data. Even though we expect less than perfect fulfillment of the assumptions listed, these estimates are quite important to safe and efficient flight test planning. Consequently, the estimates are often in the purview of the flight test engineer. The following example shows how such estimates can be made.

11.1.8.3 **Estimation of Spin Equilibrium States**. Anglin and Scher[13] have described in some detail just how they estimated spin characteristics from both experimental and computational evidence for a model of the McDonnell F3H Demon, a carrier-based fighter of 1960s vintage. Although their original use of this empirical estimation process was intended to help them save computer time by establishing appropriate initial conditions for numerical modeling of high angle of attack trajectories, it serves as an excellent example of how to estimate post-stall behavior for flight test planning exercises. Later test planning refinements likely will be based first on the results of computer modeling of the trajectories and, when they become available, certainly on previous post-stall flight tests. The procedure is summarized below and the interested student is referred to the original document[13] by Anglin and Scher for fuller details and a numerical example.

To use this procedure for test planning, one must have some prediction of the variation of rolling and yawing moments as functions of ω or, more commonly the nondimensional form $\frac{\omega b}{2V}$. The rotary balance is one means of obtaining these data experimentally and that is how Anglin and Scher obtained their data. It should be emphasized that each of the aerodynamic derivative variations in this data base were obtained by steadily rotating a model about an axis parallel to the relative wind direction in the vertical wind tunnel. Therefore, no oscillation in the angular rates are part of these data. If there were aerodynamic hysteresis (and there usually is in high angle of attack aerodynamic coefficients), these data would not account for it. This limitation (and similar shortcomings) on the data should always be kept in mind when making estimations like these.

Partly because the rotary balance rolling moment data for the F3H model were not "well-behaved", Anglin and Scher ignored the rolling moment data and concentrated on the yawing moment. This simplification amounted to discarding two of the limitations listed previously. The procedure then includes the following steps:

- Examine the pitching moment curve and the yawing moment curve from the rotary balance tests to locate nondimensional rotation rate(s) $\frac{\omega b}{2V}$ for which $C_n = 0$ and for which $\frac{dC_n}{d\left(\frac{\omega b}{2V}\right)} < 0$. There may be more than one of these potential equilibrium points. This step is meant to identify rotational rates for which the aerodynamic

yawing moment is zero. To strictly apply the constraints of the previous section, we would have to repeat this process for rolling moment as well. Moreover, both conditions would have to be met simultaneously for a true developed spin mode to exist. Working with actual numerical data quickly convinces the practicing engineer that such idealized conditions do not exist often.

- Next, utilize the rotary balance pitching moment data and the rotational rate (or rates if more than one exists) selected from the previous step to find a point on the pitching moment curve where the inertial moment and the aerodynamic moment are identical. Notice that this second step in the estimation procedure assumes that pitching moments were measured in (or can be interpolated from) the rotary balance data set for the $\frac{\omega b}{2V}$ at which $C_n = 0$ (as described in the preceding paragraph). Equation 11.10, rearranged to show the equality between the inertial pitching moment and the aerodynamic pitching moment, forms the basis for this second step in the procedure.

$$C_{mb} = -\frac{(I_z - I_x)\omega^2 \sin 2\alpha}{\rho V^2 S b} \tag{11.11}$$

C_{mb} is a function of $\frac{\omega b}{2V}$ and must be chosen to correspond to the candidate equilibrium value of $\frac{\omega b}{2V}$ that came out of step one. To check for an aerodynamic moment equal to the inertial pitching moment coefficient calculated from eqn. 11.11, a plot of the measured aerodynamic pitching moment coefficients and the calculation from this equation can be made. Figure 11.13 illustrates such a plot. The intersection point represents a potential equilibrium point and, thus, a possible spin mode. Even though it is not illustrated on the sketch in Fig. 11.13, it is quite possible to have more than one intersection point and, consequently, more than one spin mode. The angles of attack for which a spin mode may exist are likely to occur in the vicinity of the angle of attack indicated by the point of intersection. Moreover, using this angle of attack and the value of C_{mb} indicated, ω for the estimated spin mode can be calculated. Then, individual roll and yaw rates can be estimated from this calculated ω and the estimated equilibrium angle of attack.

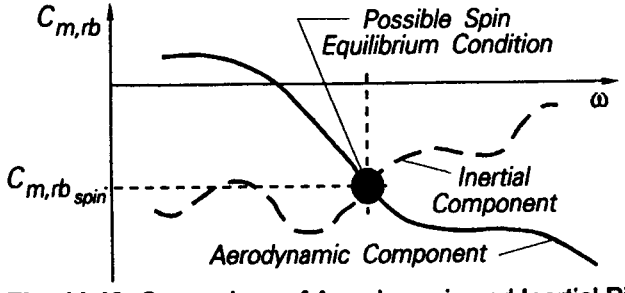

Fig. 11.13 Comparison of Aerodynamic and Inertial Pitching Moment Coefficients

A comparison of the estimates that resulted from this procedure and computer simulations for the F3H Demon is shown in Table 3 (on the following page). It is unfortunate

that flight test results from the spin tests of the actual airplane are not available for comparison to the computational and to the wind tunnel predictions.

Table 11.3. F3H Demon Computed Spin Modes Versus Estimated Spin Modes

Computed Modes			Estimated Modes		
α (°)	ω (rad/sec)	V (ft/sec)	α (°)	ω (rad/sec)	V (ft/sec)
36.0	1.88	294	38.2	1.90	285
37.0	2.18	372	45.1	1.83	327
	Oscillated out of spin		48.2	1.89	453
51.8	2.18	619	50.5	2.18	620
80.0	4.72	494	70.0	3.50	515
36.5	2.80	380	37.4	2.69	365

11.2 POST-STALL/SPIN TEST PREPARATION AND FLIGHT SAFETY

Post-stall/spin flight testing is one of the most hazardous forms of testing. By the very nature of the flight regime, the skill of the test pilot and the knowledge of the test engineer will be stretched to new boundaries by such tests. After all, the test airplane and its crew are deliberately put at risk in order to make the vehicle safer for normal operations. Consequently, flight test techniques are largely reduced to taking extraordinary preparation measures so that exposure to dangerous conditions is minimized. A large amount of data must be collected during fairly brief events; and, while the pilot's qualitative opinion is still valuable, he cannot adequately function as a sensor in such highly dynamic tests. He can be easily misled during such maneuvers. Test equipment and test procedures that are specifically designed to reduce the risk of catastrophic errors must be installed, verified, and used. As the title of this section differs from the "Test Method" of earlier chapters, so do the planning and conduct of post-stall/spin tests from the usual performance and stability and control tests.

11.2.1 Pre-Test Planning and Preparation

Planning for any flight test must start several months before the vehicle rolls off the assembly line. The planning must include decisions like:

- What are the objectives of the tests? What critical questions must be answered?
- What data are required to substantiate answers to the critical questions? How can these data best be collected? What hardware is essential and what instrumentation is available? What specialized instrumentation is required?
- What special training will be required by the crew? What criteria should be used in selecting the crew?
- What safety procedures are to be followed?
- How will the flight test support (chase aircraft, real-time test monitoring, video or camera coverage, communications links, and the like) be provided? Is radar coverage required? What air traffic control coordination is needed?

In answering such questions (and this list of questions is by no means exhaustive), the flight test team must be guided by two competing principles:

Test objectives are the prime drivers behind the test; they must be met.

Safety to the flight test crew, the test resources and to the public are important (sometimes overriding) constraints to meeting test objectives.

11.2.1.1 **Test Objectives**. Although setting clear test objectives is one of the first (both in importance and certainly in chronology) points that a flight test team must address, it is not always given the high priority is deserves. Engineers often think too much in terms of specific problems and quantified answers, without first being sure of what the purpose of their problem-solving is and determining if the problems they are solving are the ones that should be addressed. That approach to hazardous flight testing is courting disaster! For at least the last twenty years government test agencies have been required to produce a master plan for doing test and evaluation[14]. Most companies have done similar planning for flight test certifications for at least that long. There is no phase of testing where such an overview of test objectives is more important than in post-stall flight testing.

But most embryo flight test engineers ask: Are these objectives not the responsibility of the design team (or the system program office or the company project manager)? The answer is yes, but...! The manager ultimately responsible for the success of the design (whatever his title) is the decision-maker who sets objectives and their priorities. But you, as his flight test "experts" are his primary adviser on whether or not and how his critical questions can be answered by flight test. As that "expert," you will be called upon to help insure that all and only pertinent objectives are set, as well as being tasked to indicate how best to go about meeting them. To give professionally sound advice in this role means that you must understand the goals that should be set (you may even have to explain to the project manager why certain critical questions must be asked) and you must appreciate how and why the test objectives are prioritized. You must be both responsible and responsive. The governing principles in setting test objectives are:

Do all demonstrations that are essential to meet the requirements laid down by the customer and/or the certifying agency.

Accept only those objectives that contribute to meeting the requirements.

Research or exploratory objectives are relevant only when the program itself is structured for research purposes or experimental exploration in flight is the best (or only) way to credibly resolve an unknown. Quite clearly these two principles are paradoxical; they compete, sometimes even contradict! The compromises they imply must be settled **before** tests begin.

At about this stage you are probably ready for concrete examples -- enough of these abstract platitudes! (Abstract they are, platitudes they are -- but **guiding principles worth remembering** they also are!) So, let's look at some representative post-stall flight test objectives for a high performance fighter built for USAF service and for a single engine general aviation airplane.

The first step in writing such objectives is to scrutinize all applicable requirements that pertain to the post-stall flight regime. For the fighter, applicable requirements would include at the least the intent of MIL-F-8785C[15] (or MIL STD 1797A, which is not releasable for textbooks such as this one!) and MIL-S-83691 (USAF)[6] and the specific contractual paragraphs that modify or augment these high angle of attack specification documents. The following excerpts from the latter document spell out typical demonstration requirements that lead to "essential" test objectives. (In these excerpts specific numbered paragraph and table references, as well as most of the notes, are omitted for clarity.)

Table 11.4. Progressive Test Phases for Post-Stall Demonstration Maneuvers

Test Phases	Maneuver Requirements					
	Control Application	Smooth AOA Rate		Abrupt AOA Rate		Tactical
		One g	Accelerated	One g	Accelerated	
A Stalls	Pitch control applied to achieve the specified AOA rate, lateral/directional control inputs as normally required for the maneuver task. Recovery initiated after the pilot has a positive indication of: (a) A definite g-break, (b) a rapid angular divergence, or (c) the aft stick stop has been reached and AOA is not increasing.	Class: I, II, III, IV	Class: I, II, III, IV	Class: I, II, III, IV	Class: I, IV	Class: I, IV
B Stalls with Aggravated Control Inputs	Pitch control applied to achieve the specified AOA rate, lateral/directional controls as required for the maneuver task. When condition (a), (b), or (c) from above has been attained, controls briefly misapplied, intentionally or in response to unscheduled aircraft motions, before recovery attempt initiated.	Class: I, II, III, IV	Class: I, II, III, IV	Class: I, II, III, IV	Class: I, IV	Class: I, IV
C Stalls with Aggravated Control and Sustained Control Inputs	Pitch control applied to achieve the specified AOA rate, lateral/directional controls as required for the maneuver task. When condition (a), (b), or (c) has been attained, controls are misapplied, intentionally or in response to unscheduled aircraft motions and held for 3 seconds before recovery attempt is initiated.	Class: I, II, III, IV	Class: I, II, III, IV	Class: I, II, III, IV	Class: I, IV	Class: I, IV
D Spin Attempts*	Pitch control applied abruptly, lateral/ directional controls as required for the maneuver task. When condition (a), (b), or (c) has been attained, controls applied in the most critical positions to attain the expected spin modes of the aircraft and held for up to 15 seconds before recovery attempt is initiated, unless the pilot definitely recognizes a spin mode.			Class: I, IV	Class: I, IV	Class: I, IV

*This phase required only for training aircraft which may be intentionally spun and for Class I and IV aircraft in which sufficient departures or spins did not result in Test Phases A, B, or C to define characteristics.

Flight Test Demonstration. Each airplane type shall demonstrate, by flight test according to Table 11.4, the degree of compliance with the stall warning, loss-of-control warning (when required), resistance to loss of control, loss-of-control prevention, out-of-control recover, and spin recovery criteria as specified in MIL-F-

8785. The flight test investigation shall include an extensive evaluation of those maneuvers that may potentially result in AOA excursions to and beyond a permissible AOA flight limit, thereby subjecting the airplane to possible loss of control. Unless otherwise specified, the use of prolonged pro-spin controls to sustain a spinning condition shall not be required except for trainer-type aircraft to be cleared for intentional spins. However, reasonably delayed recovery attempts after a stall or departure, or exaggerated misapplication of controls following a stall or departure, to simulate possible incorrect pilot responses, shall be investigated under the least conservative circumstances to ascertain the degree of spin resistance/susceptibility for operational users. When spins do result as a natural consequence of testing through departures from controlled flight, a satisfactory spin recovery technique shall be demonstrated in accordance with MIL-F-8785. The results of these tests shall be used to establish the stall and service flight limit AOA's.

Stall/Spin Flight Test Variables. The contractor shall establish, with the approval of the procuring activity, which of the following parameters are variables to be tested for influence on stall and post-stall flight characteristics.

(a) Configuration
(b) Gross weight
(c) Center of gravity
(d) Stability and control augmentation system status
(e) External store loadings*
(f) Stall and departure speed, altitude, and attitude
(g) Thrust effects
(h) Gyroscopic effects

*The external store loadings should include as a minimum:

(1) No external stores
(2) Symmetric, fuselage-heavy [if significantly different from (1)]
(3) Symmetric, wing-heavy
(4) Asymmetric (maximum allowable asymmetry)

The military specification[6] that most succinctly spells out these demonstration requirements lays out a progressively more and more demanding series of test phases. The point in this progression where the airplane departs and/or spins determines whether or not the vehicle is departure-resistant or departure-susceptible and spin-resistant or spin-susceptible. Table 11.5 summarizes these demonstration requirements.

Table 11.5 Definitions of Departure and Spin Susceptibility and Resistance

Test Phase	Classification	
	Departures	Spins
A - Stalls	Extremely Susceptible	Extremely Susceptible
B - Stalls with Aggravated Control Inputs	Susceptible	Susceptible
C - Stalls with Aggravated and Sustained Control Inputs	Resistant	Resistant
D - Spin Attempts	Extremely Resistant	Extremely Resistant

Tables 11.4 and 11.5 are only a very small part of the whole of the military documents that govern how a post-stall test matrix must be put together for a military airplane. But they serve our purpose here which is to merely introduce the student to some of the requirements and point him to those documents that would completely govern a specific test. These documents and, most importantly the contractual specifications themselves, set the test objectives.

Similarly, for civilian certification the following paragraphs from FAR Part 23[16] drive post-stall flight test objectives for a general aviation airplane.

23.21 **Proof of Compliance**

(a) Each requirement of this subpart must be met at each appropriate combination of weight and center of gravity within the range of loading conditions for which certification is requested. This must be shown --

(1) By tests upon an airplane of the type for which certification is requested, or by calculations based on, and equal in accuracy to, the results of testing; and

(2) By systematic investigation of each probable combination of weight and center of gravity location, if compliance cannot be reasonably inferred from combinations investigated.

(b) The following general tolerances are allowed during flight testing. However, greater tolerances may be allowed in particular tests:

Item	*Tolerances*
Weight	+5%, - 10%
Critical items affected by weight	+5%, -1%
C. G.	±7% total travel

23.151 **Acrobatic maneuvers**

Each acrobatic and utility category airplane must be able to perform safely the acrobatic maneuvers for which certification is requested. Safe entry speeds for these maneuvers must be determined.

23.201 **Wings level stall**

(a) For an airplane with independently controlled roll and directional controls it must be possible to produce and to correct roll by unreversed use of the rolling control and to produce and to correct yaw by unreversed use of the directional control, up to the time the airplane pitches.

(b) For an airplane with interconnected lateral and directional controls (2 controls) and for an airplane with only one of these controls, it must be possible to produce and correct roll by unreversed use of the rolling control without producing excessive yaw, up to the time the airplane pitches.

(c) The wings level stall characteristics of the airplane must be demonstrated in flight as follows: The airplane speed must be reduced with elevator control until the speed is slightly above the stalling speed, then the elevator control must be pulled back so that the rate of speed reduction will not exceed one knot per second until a stall is produced, as shown by uncontrollable downward pitching motion of the air-

plane, or until the control reaches the stop. Normal use of the elevator control for recovery is allowed after the pitching motion has unmistakably developed.

(d) Except where made inapplicable by the special features of a particular type of airplane, the following apply to the measurement of loss of altitude during a stall:

(1) The loss of altitude encountered in the stall (power on or power off) is the change in altitude (as observed on the sensitive altimeter test installation) between the altitude at which the airplane pitches and the altitude at which horizontal flight is regained.

(2) If power or thrust is required during stall recovery the power or thrust used must be that which would be used under the normal operating procedures selected by the applicant for this maneuver. However, the power used to regain level flight may not be applied until flying control is regained.

(e) During the recovery part of the maneuver it must be possible to prevent more than 15 degrees of roll or yaw by the normal use of controls.

(f) Compliance with the requirements of this section must be shown under the following conditions:

(1) Wing flaps: Full up, full down, and intermediate, if appropriate.

(2) Landing Gear: Retracted and extended.

(3) Cowl Flaps: Appropriate to configuration.

(4) Power: Power or thrust off, and 75% percent maximum continuous power or thrust.

(5) Trim: $1.5V_{S_1}$ or at the minimum trim speed, whichever is higher.

(6) Propeller: Full increase rpm position for the power off condition.

23.203 **Turning flight and accelerated stalls**

Turning flight and accelerated stalls must be demonstrated in flight as follows:

(a) Establish and maintain a coordinated turn in a 30 degree bank. Reduce speed by steadily and progressively tightening the turn with the elevator until the airplane is stalled or until the elevator has reached its stop. The rate of speed reduction must be constant, and:

(1) For a turning flight stall, may not exceed one knot per second; and

(2) For an accelerated stall, be 3 to 5 knots per second with steadily increasing normal acceleration.

(b) When the stall has fully developed or the elevator has reached its stop, it must be possible to regain level flight without:

(1) Excessive loss of altitude

(2) Undue pitchup;

(3) Uncontrollable tendency to spin;

(4) Exceeding 60 degrees of roll in either direction from the established 30 degree bank; and

(5) For accelerated entry stalls, without exceeding the maximum permissible speed or the allowable limit load factor.

(c) Compliance with the requirements of this section must be shown with:

(1) Wing flaps: Retracted and fully extended for turning flight and accelerated entry stalls, and intermediate, if appropriate, for accelerated entry stalls;

(2) Landing Gear: Retracted and extended;

(3) Cowl Flaps: Appropriate to configuration;

(4) Power: 75% percent maximum continuous power;

(5) Trim: $1.5V_{S_1}$ or at the minimum trim speed, whichever is higher.

23.205 **Critical engine inoperative stalls**

(a) A multiengine airplane may not display any undue spinning tendency and must be safely recoverable without applying power to the inoperative engine when stalled. The operating engines may be throttled back during the recovery from stall.

(b) Compliance with paragraph (a) of the section must be shown with:

(1) Wing flaps: Retracted.

(2) Landing Gear: Retracted.

(3) Cowl Flaps: Appropriate to level flight critical engine inoperative.

(4) Power: Critical engine inoperative and the remaining engine(s) at 75 percent maximum continuous power or thrust or the power or thrust at which the use of maximum control travel just holds the wings laterally level in the approach to stall, whichever is lesser.

(5) Propeller: Normal inoperative position for the inoperative engine.

(6) Trim: Level flight, critical engine inoperative, except that for an airplane of 6,000 pounds or less maximum weight that has a stalling speed of 61 knots or less and cannot maintain level flight with the critical engine inoperative, the airplane must be trimmed for straight flight, critical engine inoperative at a speed not greater than $1.5V_{S_1}$.

23.207 **Stall warning**

(a) There must be a clear and distinctive stall warning, with the flaps and landing gear in any normal position, in straight and turning flight.

(b) The stall warning may be furnished either through the inherent aerodynamic qualities of the airplane or by a device that will give clearly distinguishable indications under expected conditions of flight. However, a visual stall warning device that requires the attention of the crew within the cockpit is not acceptable by itself.

(c) The stall warning must begin at a speed exceeding the stalling speed by a margin of not less than 5 knots, but not more than the greater of 10 knots or 15 percent of the stalling speed, and must continue until the stall occurs.

23.221 **Spinning**

(a) *Normal category.* A single-engine, normal category airplane must be able to recover from a one-turn spin or a 3-second spin, whichever takes longer, in not more than one additional turn, with the controls used in the manner normal used for recovery. In addition --

(1) For both the flaps-retracted and flaps-extended conditions, the applicable airspeed limit and positive limit maneuvering load factor may not be exceeded;

(2) There may be no excessive back pressure during the spin recovery; it must be impossible to obtain uncontrollable spins with any use of the controls.

(3) For the flaps-extended conditions, the flaps may be retracted during recovery.

(b) Utility category. A utility category airplane must meet the requirements of paragraph (a) of this section or the requirements of paragraph (c) of this section.

(c) Acrobatic category. An acrobatic category airplane must meet the following requirements:

(1) The airplane must recover from any point in a spin, in not more than one and one-half additional turns after normal recovery application of controls. Prior to normal recovery application of the controls, the spin test must proceed for six turns or 3 seconds, whichever takes longer, with flaps retracted, and one turn or 3 seconds, whichever takes longer, with flaps extended. However, beyond 3 seconds, the spin may be discontinued when spiral characteristics appear with flaps retracted.

(2) For both the flaps-retracted and flaps-extended conditions, the applicable airspeed limit and positive limit maneuvering load factor may not be exceeded. For the flaps-extended conditions, the flaps may be retracted during recovery, if a placard is installed prohibiting intentional spins with flaps extended.

(3) It must be impossible to obtain uncontrollable spins with any use of the controls.

(d) *Airplanes "characteristically incapable of spinning".* If it is desired to designate an airplane as "characteristically incapable of spinning", this characteristic must be shown with --

(1) A weight five percent more than the highest weight for which approval is requested;

(2) A center of gravity at least three percent aft of the rearmost position for which approval is requested;

(3) An available elevator up-travel four degrees in excess of that to which the elevator travel is to be limited for approval; and

(4) An available rudder travel seven degrees, in both directions, in excess of that to which the rudder travel is to be limited for approval.

These requirements documents are the foundation upon which the flight test planner builds the rest of his preparation. The first step in laying out an overall test plan is to set these objective down and be sure that all interested parties agree to them.

But not only must the test objectives be clearly stated, they must also be prioritized. Notice that in setting down objectives and relating them to requirements, no relative priorities were suggested. Before the test team can construct an efficient test matrix and do detailed test planning, the relative importance of each of the objectives must be established. This prioritization governs the order of testing as well as the allocation of test resources. Again, the flight test team and the design team must function as one entity in this

phase of test preparation. There must be agreement between these two groups, even though complete unanimity on the final decisions is not likely.

With the overall test objectives stated and prioritized, the flight test team can focus on how to acquire data best and other aspects (usually safety) of test preparation.

11.2.1.2 **Data Requirements**. In a sense the engineer reverts back to his profession in the next phase of preparation for post-stall testing. He leans on experience (both his and others) to decide what data are needed to answer the questions posed by the objectives. He should seek practical and efficient ways to generate and collect these data and lay out the manner of presenting data so that key questions will be clearly answered with quantitative engineering results wherever possible. He devises detailed test plans from which estimates of time, money, and people required to complete post-stall flight tests can be made. This phase of test preparation will necessarily be an iterative process. Available time and resources usually shrink during the course of a project; requirements that were overlooked in the goal-setting phase will often surface here. There are few general principles that apply to all classes of aircraft, but there are some guidelines to follow.

(1) Question all data requirements. "Acid test" questions include:

(a) Which objective do these data underpin?

(b) What is the relative priority of the objective pursued?

(c) Who will use the data or will the data be used?

(2) Is there a simpler, more cost-effective, or safer way to provide the essential data?

(a) Did or can component testing/ground simulation provide similar data?

(b) If so, how much flight data are needed to verify component tests?

(3) Will the proposed data matrix provide an adequate basis for management decisions later?

(a) Is the experimental sample size statistically relevant?

(b) Will test constraints likely bias or skew the results?

(4) Is there a more efficient way to acquire the data in flight?

(a) Could extended flight times (like air refueling might provide) allow coverage of more of the test matrix in each flight?

(b) Is real-time test monitoring adequate to show when repeated test points are necessary?

(c) How much redundancy in test support (radar coverage, chase aircraft, communications links, data paths, etc.) is needed?

As these questions are considered, the importance of efficient, reliable data acquisition will surface as a relevant issue.

11.2.1.3 **Instrumentation for Post-Stall Flight Tests**. The instrumentation suite for post-stall testing is usually more extensive and more specialized than is used for conventional stability and control testing. How does it differ? First, the ranges of the dynamic variables when the airplane is operating at high angle of attack are usually much greater. Angle of attack variations from the trim condition may be ±90° or more, instead of ±15°, as is typically expected while in the normal operating envelope. Angular rates may be doubled or tripled over those encountered at low angles of attack. Accelerations may be

about the same in magnitude, but the acceleration directions change much more rapidly during post-stall maneuvers. Table 6 shows typical differences between sensor ranges for post-stall flight testing and for conventional low angle of attack testing.

But what kinds of sensors are needed and how do the motions encountered in the post-stall flight regime affect experimental measurements and how must the data be handled? Conventional parameters like those shown in Table 6 are ordinarily what is recorded for post-stall tests; nothing out of the ordinary is on this list. But the list is not exhaustive either; there are other measurements that are sometimes needed. We also must keep track of all control surface positions, throttle position, and a number of discrete events like gear position, flap position, speed brake position, and the like. For the control positions, complete time histories sampled at moderately high frequencies are usually necessary. The sample rates for fast-acting surfaces should be an order of magnitude higher than the highest motion frequency of interest, even though the sampling theorem only requires that the sample rate be double the frequency of highest interest. Since control surface movements can be rather quick, especially when driven by the high rate actuators on modern high performance aircraft, the data rate for the control inputs is often the most important criterion in selecting instrumentation specifications for flight tests interested only in the rigid body motion states. Of course, for analyzing structural modes or other high frequency issues, other sensors may dictate the critical sample rate. In any case the bandwidth of the instrumentation sensors must be carefully tailored to the post-stall flight regime.

Table 11.6. Typical Sensors Needed for Stability and Control Data

Sensor	Low Angle of Attack	High Angle of Attack
	Typical Ranges	Typical Ranges
α	-5° to 15°	±90°
β	±5°	±30°
P	±70°/sec	±100°/sec
Q	±20°/sec	±50°/sec
R	±20°/sec	±100°/sec
ϕ	±30°	±90°
θ	±10°	±90°
ψ	±20°	±360°
n_x	±0.25g	±0.5g
n_y	±0.25g	±0.5g
n_z	±4g	±4g

11.2.1.4 **Test Team Training**. Typically, the test pilot is the only test team member singled out for special training during the preparation for post-stall training. This practice is a mistake! While the test pilot's background, training, and currency are the most meaningful and deserve considerable attention, the entire team needs to prepare for hazardous tests like these with deliberate focus. The underlying principle is:

When you deliberately explore the limits and boundaries of the flight envelope, ***anticipate every eventuality*** *you can.*

Even when you prepare as fully as time and resources allow, post-stall tests often reveal unexpected characteristics and behavior. But, pre-test preparation that includes both the pilot (or pilots) and the entire engineering support team will do much to eliminate surprises. First, how should the pilot be selected and trained?

There is no substitute for **recent experience** in post-stall testing, though the emphasis should be on overall experience, not just recency. The most valuable foundation is actual post-stall testing in a broad array of airplanes. If the vehicle to be tested were my personal design, a test pilot who had done at least one other post-stall test program would be my choice. If the size and nature of the project permit (or even require) more than one test pilot, give this experienced pilot the responsibility for training the other participants. In military programs, the senior pilot for the contractor typically will do most of the exploratory demonstrations. He should normally be tasked with the training and preparation of every pilot who flies a post-stall test flight.

What elements should this training and preparation include? One of the most valuable considerations in preparing to conduct high angle of attack testing is a formal training course similar to those given by the USAF or USN Test Pilot Schools, the Empire Test Pilots' School, or by the French Test Pilot School. Of course, not every company or entrepreneur will have access to such personnel, but this reservoir of talent has the best basic background of formal training for post-stall testing.

Once the project pilot is chosen, preparation has only begun. It is imperative that whatever his (or their) experience level is, there should also be recent experience in an aircraft quite similar to the type to be tested. If possible, this "in-flight simulation" should be flown into post-stall maneuvers of the most extreme type anticipated. If there is no aircraft available for actual post-stall practice, project pilots should seek out the most realistic simulator they can find, preferably one where large amplitude motions can be experienced. The time spent in such a device, especially if it has high fidelity both in motion and in cockpit layout to the test airplane, is an ideal place for rehearsing and modifying both "normal" data collection (if data collection during post-stall maneuvers is ever normal) and emergency procedures. Realistic, repetitious practice of test profiles will give the pilots confidence, recent experience, and efficient procedures for data collection and allow them to make the best use of flight test time.

These simulations should also include as much of the test team as will be involved in real-time monitoring and quick-look data reduction. The engineers/pilots who will act as test conductors and chase aircrew need to practice communication procedures and refine operational instructions. They should be just as familiar with safety rules (like minimum altitudes for recovery, altitudes for bailout, expected control sequences, and the like) as are the pilots who will fly the test vehicle. The flight test and systems engineers who will monitor key parameters (control surface positions, angular rates, engine performance, emergency recovery subsystems, ground tracking, and all essential support details) should also rehearse their roles as part of the team. The senior flight test engineer should insist that every team member participate in one or more dry runs -- including exposure to emergency situations -- if the entire team is to function efficiently. Every team member must understand and accept his or her responsibilities, know the procedures, and

appreciate the consequences if he/she fails to meet his obligations during a test flight. Above all, hazardous flight testing is an exercise in **group discipline**. The test conductor can best guard against a breakdown in discipline with realistic practice sessions, both before test flights actually begin and periodically during a program. This continuation training is particularly important if there are long breaks between test phases or a significant number of new personnel must be assimilated into the test team.

11.2.2 Safety Precautions and Special Equipment

Having discussed some of the general aspects of preparation for post-stall testing, we now turn to more specific ways to make such tests safer. We should have no illusions. Post-stall testing is not inherently safe; the test airplane and the crew will be deliberately put at risk in either marginally controllable or out-of-control portions of the flight envelope. As we have already emphasized, all flight testing should be planned to start with benign flight conditions and progress incrementally to more difficult or more dangerous ones. This principle is called the "build-up approach" and is designed to preclude unwittingly pushing past boundaries beyond which there is no recovery. However, post-stall testing involves flights where nonlinear dynamical relationships and the large number of variables that are involved make it impossible to perfectly determine in advance safe increments in test parameters. The only alternatives that can reduce risks are (1) reduce the likelihood of potential failures and (2) take extraordinary precautions to mitigate the consequences of events that are still likely to occur. This section provides practical guidance for the flight test engineer planning a high angle of attack test series. It involves both procedural and hardware suggestions; and, though it would be highly presumptuous (and patently false!) to claim that these suggestions are comprehensive, they are a very good starting point.

11.2.2.1 **Emergency Recovery Devices**. Whenever anyone lays out a serious post-stall flight test program, inevitably these questions arise:

> *Is an emergency recovery subsystem needed? If so, what type and what kind of design requirements must be spelled out?*

The first question should almost always be answered yes. Only airplanes with tightly limited flight envelopes or very unusual design characteristics can avoid encounters with post-stall flight. Even then, very few designers are willing to bet their reputations that no post-stall flight tests at all are necessary. Even "spin-proof" airplanes have been involved in post-stall accidents. However, how answering the second question is not so easy. It cannot be answered without consideration of the following additional question:

> *What is the intended use of the design (or modification of an existing design)?*

It makes no sense to do full-blown spin tests, for example, for a large commercial airliner. Thus, the "post-stall" program for such a vehicle is almost exclusively aimed at precluding stalls – a very limited "post-stall" (if indeed it can be called by that name) test series is in order. Most business aircraft with near centerline thrust should be treated in the same way. However, past experience has shown that even these kinds of airplanes can have post-stall catastrophes if the configuration is quite unusual or not well-known. For example, at least one early T-tail transport design[17] ran into such difficulties, as have

corporate jets[18] with similar design features. There is also reason to pay careful attention to post-stall certification for canard and three-surface configurations.

Is it responsible to ignore post-stall testing based on handbook limitations intended for the design?

Now this question is harder to answer and we are treading dangerously close to subjective opinion entirely. But, to offer a design to any segment of the flying public without having explored post-stall behavior is neither wise nor responsible. (It may also be legally indefensible in today's litigious judicial environment.) No matter what the contracting agency or certification authority requires, a professional design team owes that consideration to their customers. Please note that this professional obligation is related to vehicle characteristics and intended use, not certification requirements alone. The design process is simply not complete until predictions and engineering estimates have been validated to some margin slightly beyond the published flight envelope.

There are two types of devices usually considered for emergency recovery from spins; those which modify the ratio of aerodynamic and inertial forces and those which add additional control authority about one or more axes. Far and away the most commonly used emergency recovery scheme is some form of parachute which alters the pitching and yawing moments rather drastically. They have been used on almost every type of airplane from sailplanes to 30-ton fighters.

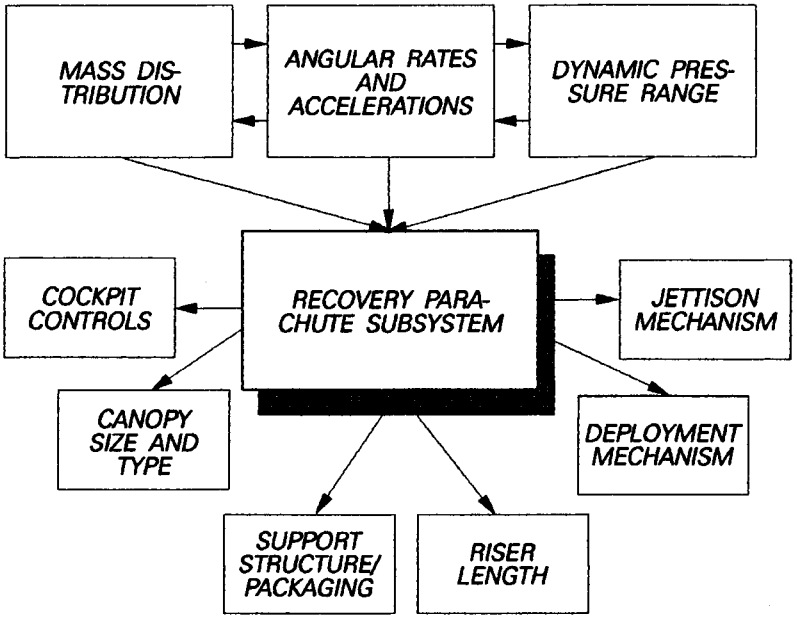

Fig. 11.14 Emergency Parachute Recovery Subsystem Design Parameters

Design and validation of a spin recovery parachute subsystem[19] is peculiar to each configuration and thus often becomes the responsibility of the project flight test engineer. the inertia distribution matrix, the likely equilibrium spin rotation rates, and an estimate of the dynamic pressure range over which the parachute must operate are key design pa-

rameters. Figure 11.14 suggests the compromises associated with designing such a subsystem and how each of these parameters are affected by one another.

Sizing of the canopy and its porosity are fundamental to the success or failure of this critical subsystem. Typically an off-the shelf canopy can be used and canopy characteristics are fairly completely documented[20]. Drag coefficients and opening shock load overshoots may be estimated empirically, but often ground tests are necessary to validate the assumptions. The numerical values for these parameters are strongly dependent on canopy porosity. The canopy material, its shape, and whether the canopy is solid, slotted, or vented in any way all affect the parachute drag coefficient and the opening shock loads drastically. These short duration loads are often considerably higher than the steady aerodynamic loads. Increasing the porosity and reefing the canopy so that it opens more slowly both tend to lower opening shock and thus reduce the severity of the impact loads on the risers and the attachment structure. A more porous canopy is also less likely to oscillate at the end of the risers after it is fully inflated. In fact oscillatory instability of the canopy can cause the airplane-parachute combination to be dynamically unstable after recovery from the out-of-control condition. Such dynamic behavior can be very uncomfortable (and quite unnerving!) to the pilot who is depending on this device to recover from this kind of situation. However, since a recovery parachute is typically jettisoned shortly after it performs its function, dynamic instability of the airplane-parachute combination is often of secondary importance.

The riser design and length also are quite important[19]. The risers should be long enough to guarantee that the canopy opens well away from the aircraft itself. The likely worst case rotation rates and attitude combinations should be studied, as well as probable low pressure, separated flow regions, so provisions can be made to forcibly propel the parachute canopy into relatively clear air before the opening sequence is allowed to begin. For this reason, canopy bags or reefing, along with drogues or ejectors are typically used to extract the parachute from its storage canister. Once the canopy opens successfully, riser length is another important factor affecting the oscillation frequency. Consideration should be given to keeping this frequency distinct from either the longitudinal short period or the lateral-directional Dutch roll frequencies of the rigid airplane.

Rocket thrusters have been used as an alternative to spin parachutes[21]. This emergency recovery subsystem is an example of adding extra control devices to guarantee recovery from out-of-control situations. Potential advantages for such devices include:

- They can be installed so as to produce controlled moments about each axis.
- Multiple units can provide redundancy (or capability to make multiple recoveries) if the weight penalty is not too severe. Obviously, this capability could also be provided by rocket motors that can be restarted. Rarely, however, would this level of complexity be justified.
- Such thrusters could also be used to drive the airplane into different spin modes (for research purposes), though such usage has never occurred to the author's knowledge.

Disadvantages to such devices include:

- Usually they involve additional complexity, both from a mechanical perspective and in terms of safe operation. Rocket thrusters almost always multiply safety

concerns because of the larger number of failures and the consequences of some of those failures that are possible.

- More often than not, the thrusters are pyrotechnic devices (or are susceptible to explosion at least). Again, safety issues are harder to resolve satisfactorily when multiple pyrotechnics must be carried for each flight.
- It is difficult to safely verify the adequacy of recovery thrusters for their intended purpose.

Of course, both rocket thrusters and a spin recovery parachute can be installed, but rarely are. One such exception[22] was the F-100F, a version of the Super Saber that was highly susceptible to a flat spin from which aerodynamic controls could not recover the airplane. Both a spin chute on the aft fuselage and rocket thrusters on the wing tips were installed for the post-stall testing. Unfortunately, when the test aircraft entered the expected flat spin mode, the recovery rockets did not stop the rotation and the parachute streamed and wrapped around the vertical tail. The test airplane was lost when both emergency recovery devices failed to perform their intended function.

Finally, the flight test team must pay careful attention to how emergency recovery devices are actuated, controlled, monitored, and terminated (jettisoned, in the case of parachutes). First, all controls for this system must be accessible to and easily identified by the pilot even under the most extreme conditions of aircraft loading and stress. The pilot must be able to activate and deactivate (or jettison) this emergency system even when cockpit g levels are high and oscillatory. (This fact may also suggest part of the reason why additional pilot restraints are often used for post-stall testing.) Moreover, there must be reliable and complete warning of any malfunction or other condition that affects pilot actions with regard to the emergency recovery subsystem. Indicator lights are one means for providing these warnings. Parachute/thruster arming, position of jettison mechanism, test limits (angular rates, minimum altitudes, and the like), flight control system status, and engine health are typical candidates for warning/caution displays during post-stall tests.

11.2.2.2 **Chase Aircraft**. In addition to a reliable emergency recovery subsystem, post-stall test teams often rely heavily on chase aircraft. Typically, these support aircraft are flown by backup pilots for the project and they often carry aerial photographers. The functions of this supporting aircraft and crew include:

- Visually checking the test aircraft for configuration; for loss of access covers, gear doors, etc.; and for obvious structural or system failures during a maneuver.
- Clearing the airspace for the test vehicle.
- Calling out critical events -- minimum altitudes, engine failure, and emergency procedures -- to the test aircrew.
- Advising the test pilot and the test conductor of any anomalies observed.

The chase pilot is a critical supporting player. His piloting task is very demanding and he needs to have powers of observation every bit as keen as those of the test pilot. He must be completely familiar with all planned mission profiles, overall test objectives, as well as detailed test restrictions. To meet all these responsibilities, project pilots who will fly such chase sorties should practice for them -- just as the rest of the test team should rehearse. For the test pilot and the supporting chase aircrew, this practice time is absolutely mandatory.

11.2.2.3 **Procedural Precautions**. The whole of section 11.2 is built around the premise of test team discipline. Any engineer or pilot who is charged with the overall responsibility for this class of flight testing must be a stickler for discipline. Insisting that comprehensive, written procedures are developed, followed, and modified constructively is a mark of professionalism. It is absolutely necessary for the successful post-stall test team leader to demand discipline. Here are some practical suggestions for setting up such procedures:

- Establish some form of independent review process to examine the planning and procedures. The scope of this review can vary from a single experienced consultant to a full-blown, structured "red-blue" team approach. The effort expended on this review will largely be dictated by the size and economy of the project, but it should **never** be omitted.
- Test procedures, especially for hazardous tests like post-stall tests, evolve from safety constraints wrapped around clearly stated test objectives. But safety is overriding.
- Be sure procedures are communicated. Keep them simple, straightforward, and to the point. Practice and repeat the good ones; revise the bad ones.

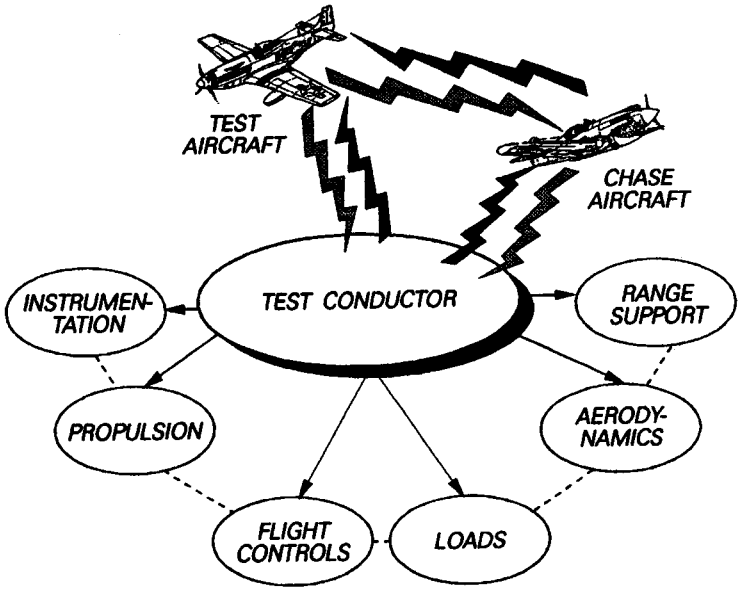

Fig. 11.15 Post-Stall Flight Test Team Communications Net

- Keep the command lines during a test crisp and clear. The test conductor is the maestro (he carries the responsibility); the test pilot is the soloist; and the chase pilot is the harmony. But everyone else on the test team plays an essential background instrument. If that musical metaphor sounds overdone -- nobody talks to the pilots on the radio except the test conductor, or at the test conductor's request. Supporting test engineers relay pertinent information to the test conductor, who decides what is essential to the conduct of the test. Flying a productive test sortie is always a demanding task; flying a productive post-stall mission can be downright hectic. It is the test conductor's job to see that mission objectives are not

destroyed by confusion and indecision. Figure 11.15 illustrates this decision-making net for a typical post-stall flight test.

- Guarantee that everyone on the test team knows the envelope limits and the reasons for them. The senior flight test engineer must take the lead in this training; everyone must be completely aware of each flight's objectives -- both primary and secondary -- and the steps planned to reach them.
- **Never** go beyond a test plan. This rule should be iron-clad; you simply must not "shoot-from-the-hip" in this environment. True, the detailed flight profiles should always plan more than can be accomplished; but the alternatives and the relative priorities are to be spelled out in the briefing on the ground **before** takeoff.

If these six guidelines are followed, deliberate, disciplined procedures will result and the whole test series will reflect that disciplined philosophy.

11.2.2.4 **Real-Time Monitoring of Post-Stall Tests**. The engineering process that we suggest needs to be so tightly disciplined must still react efficiently. Adequate information fed back to the test support engineers during post-stall maneuvers is essential to the process. Larger and adequately funded post-stall programs may have all relevant dynamic time histories telemetered back to the control room during a flight. These fortunate engineers may even have the computer power and software sophistication available to cross-plot and partially analyze these real-time data. They might, for example, superimpose dynamic states on α-β axes, rather than just time axes. Graphic images of the airplane's rotation and inertial attitude may be useful. Plots of predicted boundaries and actual motions could be overlaid. For such a rich data environment the possibilities for real-time monitoring are almost infinite. At the other extreme, where there may only be radio communications between the test pilot and the chase pilot, the real-time analysis and advice may be quite subjective. But that fact does not make it unimportant. Any outside observer's observations can be useful information (data) in this often confusing test environment. Recording a running commentary from both the test pilot and the chase pilot are wise and inexpensive "real-time" tools in post-stall tests. The point is: real-time information -- at any level between the extremes described in this paragraph -- is valuable and must not be ignored. Plan to collect it.

11.3 SUMMARY

In this concluding chapter we have introduced the student to what is in reality an advanced topic in flight test. Most of the principles that apply to post-stall testing also apply to other forms of hazardous test: flutter envelope expansion, weapon separation tests, low level avionics system (like terrain-following) evaluations, and similar activities. The major themes of careful planning, thorough preparation, and unyielding discipline carry over into these other forms of flight testing as well. Of course, the engineering tasks, measurement techniques, and support required will differ. But these basic principles will still be valid. In that sense, this chapter serves to draw attention to the three most themes of all kinds of flight testing, even as it serves to introduce advanced topics through a specific example. And those themes -- planning, preparation, and discipline -- pervade all.

REFERENCES

1 Herbst, W. B., "Future Fighter Technologies," **Journal of Aircraft**, Vol. 17, No. 8, Aug. 1980, pp. 561-566.

2 Gilbert, W. P. and Gatlin, D. H., "Review of NASA High-Alpha Technology Program," Paper at NASA High-Angle-of-Attack Technology Conference, NASA Langley Research Center, Oct. 30-Nov. 1, 1990.

3 Nix, J., "X-31 EFM: The Experiment Continues," Paper at NASA High-Angle-of-Attack Technology Conference, NASA Langley Research Center, Oct. 30-Nov. 1, 1990.

4 Trippensee, G. A. and Ishmael, S., "Overview of the X-29 High-Angle-of-Attack Program," Paper at NASA High-Angle-of-Attack Technology Conference, NASA Langley Research Center, Oct. 30-Nov. 1, 1990.

5 Flight Training Handbook, AC-61-21A, Federal Aviation Administration, 1980.

6 Military Specification, MIL-S-83691(USAF), "Stall/Post-Stall/Spin Flight Test Demonstration Requirements for Airplanes," Apr. 1972.

7 McElroy, C. E. and Sharp, P. S., "Stall/ Near Stall Investigation of the F-4E Aircraft," FTC-SD-70-20, Air Force Flight Test Center, Edwards Air Force Base, California, Oct. 1970.

8 Babister, A. W., **Aircraft Stability and Control**, Macmillan Company, New York: 1961.

9 Kerr, T. H., "General Principles of Spinning," **AGARD Flight Test Manual**, Volume II, Chapter 8, Pergamon Press, New York: 1962.

10 Chambers, J. R. and Stough, H. P., III, "Summary of NASA Stall/Spin Research for General Aviation Configurations," AIAA Paper 86-2597, Oct. 1986.

11 Stough, H. P., III, DiCarlo, D. J., and Steward, E. C., "Wing Modification for Increased Spin Resistance," SAE Paper 830720, Apr. 1983.

12 Turner, H. L., "Measurement of the Moments of Inertia of an Airplane by a Simplified Method," NACA TN 2201, Ames Aeronautical Laboratory, Moffett Field, California, Oct. 1950.

13 Anglin, E.L. and Scher, S. H., "Analytical Study Aircraft-Developed spins and Determination of Moments Required for Satisfactory Spin Recovery," NASA TN D-2181, Feb. 1964.

14 DOD 5000.3, "Test and Evaluation," Department of Defense, Dec. 1975.

15 Military Specification MIL-F-8785C, "Flying Qualities of Piloted Airplanes," Nov. 1980.

16 Federal Aviation Regulations, Part 23, Airworthiness Standards: Normal, Utility, Aerobatic and Commuter Category Airplanes, Federal Aviation Administration, June 1974 (Changes 1-26, as of Oct. 1989).

17 "British Aircraft Corp. Still Aims at Initial BAC 111 Delivery Dates," **Aviation Week and Space Technology**, Nov. 11, 1963, p.45.

18 "Prototype Canadair Challenger Lost," **Flight International**, Apr. 19, 1980, p. 1174.

19 Burk, S. M., "Review of Airplane Spin-Recovery Parachute Systems Technology," Paper at the AFFDL/ASD Stall/Post-Stall/Spin Symposium, Wright-Patterson AFB, Ohio, Dec. 1971.

20 Bixby, H. W., Ewing, E. G., and Knacke, T. W., "Recovery Systems Design Guide," AFFDL-TR-78-151, Air Force Flight Dynamics Laboratory, Wright-Patterson AFB, Ohio, Dec. 1978.

21 Knacke, T. W., "Recovery System Design Manual," NWC TP 6575, Naval Weapons Center, China Lake, California, Jul. 1985.

22 Farmer, G. H., "Flight Test Investigation to Determine the Effectiveness of a Rocket as an Emergency Spin Recovery Device," WADC Technical Report 53-396 (AD 76422), Wright Air Development Center, Ohio, Aug. 1958.

23 Wykes, J. H., "An Analytical Study of the Dynamics of Spinning Aircraft, Part III, Calculated and Flight Test Spin Characteristics of an F-100F with Strakes," WADC Technical Report 58-381 (AD 243600), Wright Air Development Center, Ohio, Feb. 1960.

LIST OF SYMBOLS

Symbol	Definition	Units
CHAPTER 1		
	None	
CHAPTER 2		
a	speed of sound	fps
a_0	standard day sea level speed of sound	fps
C	volume of instrument chamber	ft^3
C_L	lift coefficient	none
d	internal diameter of tubing or distance along the speed course line	ft
D	diameter of pitot-static tube	ft
g	gravitational acceleration	ft/sec^2
g_0	gravitational acceleration in ideal atmosphere	ft/sec^2
h	geopotential altitude	ft
h_a	absolute altitude	ft
h_c or h_{cal}	calibrated altitude	ft
$h_{cal_{altimeter}}$	calibrated altitude measured at the altimeter	ft
$h_{cal_{eyepiece}}$	calibrated altitude measured at the eyepiece	ft
$h_{cal_{ramp}}$	calibrated altitude measured on the parking ramp	ft
$h_{cal_{pacer}}$	calibrated altitude of the pacer aircraft	ft
h_{cal_t}	test day calibrated altitude	ft
h_g	geometric altitude	ft
h_i	geopotential altitude at the base of the *i*th layer or indicated altitude read from the altimeter	ft
$h_{i_{test}}$	indicated nominal altitude for the test point	ft
h_{ic}	instrument corrected altitude	ft
h_{ic_t}	test day instrument corrected altitude	ft
h_p	pressure altitude	ft
h_ρ	density altitude	ft
k_i	temperature lapse rate in the base of the *i*th layer	°R/ft
K	temperature recovery factor	none
L	length of tubing	ft
m	mass	slugs
M	Mach number	none
M_∞	freestream Mach number	none
n	load factor	none
p	pressure	psf
p_i	standard day pressure at the base of the ith layer	psf

LIST OF SYMBOLS (Continued)

Symbol	Definition	Units

CHAPTER 2 (continued)

p_s	sensed pressure	psf
p_T	total pressure	psf
p_0	standard day sea level pressure of the atmosphere	psf
p_∞	freestream static pressure	psf
p_{T_∞}	freestream total pressure	psf
q or $\overline{q}$	dynamic pressure	psf
q_{ic}	instrument corrected dynamic pressure	psf
q_{ic_t}	test day instrument corrected dynamic pressure	psf
q_c	sensed dynamic pressure	psf
R	universal gas constant	$ft^2/sec^2°R$
R_E	radius of the earth	ft
t_i	indicated temperature	°F
t_1	time at beginning of speed course run	sec
t_2	time at end of speed course run	sec
T	temperature	°R
T_i	temperature at the base of the ith layer or indicated temperature	°R
T_{ic}	instrument corrected temperature	°R
T_{std}	standard day temperature	°R
T_T	total temperature	°R
T_∞	freestream temperature	°R
$\mathcal{V}$	volume	ft^3
V or V_∞	true airspeed	knots or fps
V_{avg}	average true airspeed for speed course	knots or fps
V_{cal}	calibrated airspeed	knots or fps
$V_{cal_{pacer}}$	calibrated airspeed for the pacer aircraft	knots or fps
V_e	equivalent airspeed	knots or fps
V_i	indicated airspeed	knots or fps
$V_{i_{test}}$	indicated nominal airspeed for the test point	knots or fps
V_{ic}	instrument corrected airspeed	knots or fps
V_{ic_t}	test day instrument corrected airspeed	knots or fps
x	distance from eyepiece to plane of sighting grid	in
	or a variable	various
y	height of airplane as measured on the sighting grid	in
	or a variable	various
z	distance from eyepiece to plane of tower flyby line	ft
Δh	height above the plane of the eyepiece	ft
$\Delta h_{cal_{altimeter}}$	calibrated altitude error measured at the altimeter	ft

LIST OF SYMBOLS (Continued)

Symbol	Definition	Units

CHAPTER 2 (continued)

$\Delta h_{cal_{eyepiece}}$	calibrated altitude error measured at the eyepiece	ft
$\Delta h_{cal_{pacer}}$	calibrated altitude error for the pacer aircraft	ft
Δh_{ic}	altimeter instrument error correction	ft
$\Delta h_{ic_{pacer}}$	altimeter instrument error correction for the pacer aircraft	ft
Δh_{ic_t}	test day altimeter instrument error correction	ft
$\Delta h_{ic_{test}}$	altimeter instrument error correction for the nominal test point	ft
Δh_{pc}	altimeter static position error correction	ft
$\Delta h_{pc_{pacer}}$	altimeter static position error correction for the pacer aircraft	ft
Δh_{pc_t}	test day altimeter static position error correction	ft
Δp_p	static position error	psf
ΔT_{ic}	temperature instrument error correction	knots or fps
ΔV_c	compressibility correction	knots or fps
ΔV_{ic}	airspeed instrument error correction	knots or fps
$\Delta V_{ic_{pacer}}$	airspeed instrument error correction for the pacer aircraft	knots or fps
$\Delta V_{i_{test}}$	instrument corrected airspeed for the nominal test point	knots or fps
ΔV_{pc}	airspeed static position error correction	knots or fps
$\Delta V_{pc_{pacer}}$	airspeed static position error correction for the pacer aircraft	knots or fps
α	angle of attack	°
γ	ideal ratio of specific heats for air (1.4)	none
δ	pressure ratio	none
λ	lag constant	psf^2/sec
μ	viscosity	slugs/ft-sec
μ_0	standard day sea level viscosity	slugs/ft-sec
ρ	density of the atmosphere	$slugs/ft^3$
ρ_i	standard day density at the base of the ith layer	$slugs/ft^3$
ρ_{std}	standard day density	$slugs/ft^3$
$\rho_{tropopause}$	standard day density at the tropopause	$slugs/ft^3$
ρ_T	total density	$slugs/ft^3$
ρ_0	standard day sea level density of the atmosphere	$slugs/ft^3$
σ	density ratio	none
σ_{std}	standard day density ratio	none
$\sigma_{tropopause}$	standard day density ratio at the tropopause	none
θ	temperature ratio	none
θ_t	test day temperature ratio	none

LIST OF SYMBOLS (Continued)

Symbol	Definition	Units

CHAPTER 3 (only those symbols not previously introduced are listed)

AF	acceleration factor	none
b	span	ft
C_1	constant for induced drag expression	lbs
D	drag or	lbs
	engine characteristic length	ft
D_{std}	standard day drag	lbs
D_t	test day drag	lbs
E	total energy (kinetic plus potential)	ft-lbs
e	span efficiency factor	none
$\dot{h}$	time rate of change of pressure altitude	fps
k	ratio of specific heats	none
L	aerodynamic lift	lbs
M_{std}	standard day Mach number	none
M_t	test day Mach number	none
N	engine speed	rpm
n_{std}	standard day/weight load factor	none
n_t	test day/weight load factor	none
V_V	vertical component of true airspeed	knots, mph, or fps
P_s	specific excess power	fps
P_{s_t}	test day specific excess power	fps
R_c	radius of curvature	ft
R/C	rate of climb	fpm or fps
T_n	net thrust	lbs
$T_{n_{std}}$	standard day net thrust	lbs
T_{n_t}	test day net thrust	lbs
T_{∞_i}	indicated freestream temperature	°R
$T_{\infty_{ic}}$	instrument corrected freestream temperature	°R
$T_{\infty_{std}}$	standard day freestream temperature	°R
T_{∞_t}	test day freestream temperature	°R
THP_A	thrust horsepower available	hp
$THP_{A_{std}}$	standard day thrust horsepower available	hp
THP_{A_t}	test day thrust horsepower available	hp
THP_R	thrust horsepower required	hp
$THP_{R_{std}}$	standard day thrust horsepower required	hp
THP_{R_t}	test day thrust horsepower required	hp
V_H	horizontal component of true airspeed	knots, mph, or fps
V_{s_0}	power off stall speed, landing configuration	knots, mph, or fps
V_{s_1}	power off stall speed, clean configuration	knots, mph, or fps
V_V	vertical component of true airspeed	knots, mph, or fps

LIST OF SYMBOLS (Continued)

Symbol	Definition	Units

CHAPTER 3 (continued)

V_{W_i}	wind velocity at point *i*	knots, mph, or fps
V_{∞_t}	test day true airspeed	knots, mph, or fps
$\dot{V}_\infty$ or $\dot{V}$	time rate of change of true airspeed	fps/sec
W	weight	lbs
W_{avg}	average weight	lbs
W_{std}	standard (nominal) weight	lbs
W_t	test day weight	lbs
$h_{corrected}$	corrected (for weight change) indicated altitude	ft
h_e	energy height or specific energy height	ft
$\dot{h}_e$	time rate of change of energy height (= P_s)	fps/sec
w_f	fuel flow rate	lbs/hr
ΔD_i	increment of induced drag	lbs
Δh	increment of altitude	ft
Δh_a	increment of absolute altitude	ft
Δh_e	increment of energy height or specific energy height	ft
Δh_i	increment of indicated altitude	ft
$\Delta P_{s_{wt}}$	specific excess power weight correction (induced drag)	fps
Δp_∞	increment of freestream static pressure	psf
ΔT_n	increment of net thrust	lbs
Δt	increment of time	sec
ΔW	increment of weight	lbs
ΔV_∞	increment of true airspeed	knots, mph, or fps
$\Delta\gamma$	increment of flight-path angle	°
δ_t	test day pressure ratio	none
δ_{std}	standard day pressure ratio	none
γ	flight-path angle	°
Φ_T	angle between the thrust line and the fuselage reference line	°
ρ_t	test day density	slugs/ft^3

CHAPTER 4 (only those symbols not previously introduced are listed)

A or A_1	constant for first term in power equation	hp-ft-sec/lb
a	parameter for solving Buckingham Pi equations	none
B or B_1	constant for second term in power equation	hp-sec/lb-ft^3
	or number of blades for a propeller	none
BHP_r	brake horsepower required	hp
BHP_t	test day brake horsepower available	hp
BHP_{std}	standard day brake horsepower available	hp

LIST OF SYMBOLS (Continued)

Symbol	Definition	Units
CHAPTER 4	(continued)	
b	parameter for solving Buckingham Pi equations	none
C_D	drag coefficient	none
C_{D_i}	induced drag coefficient	none
C_{D_p}	parasite drag coefficient	none
C_{L_i}	propeller integrated design lift coefficient	none
C_m	aircraft pitching moment coefficient	none
C_P	power coefficient	none
C_Q	torque coefficient	none
C_{D_p}	parasite drag coefficient	none
c	propeller local chord	ft
	or parameter for solving Buckingham Pi equations	none
	or specific fuel consumption (SFC)	lbs/hr-hp
c_{ℓ_d}	blade section design lift coefficient	none
c_t	thrust specific fuel consumption (TSFC)	lbs/hr-lb
D	drag	lbs
	or propeller diameter	ft
E	endurance	hours
E_{max}	maximum endurance	hours
J	propeller advance ratio	none
$K_{n_{ic}}$	propeller torque meter scale factor	none
K_V	ratio of equivalent airspeed to equivalent airspeed for minimum power	none
L	fundamental unit for length	ft
MAP_t	test day manifold pressure	in Hg
MAP_{std}	standard day manifold pressure	in Hg
m	fundamental unit for mass (slugs = lb-sec^2/ft)	slugs
n	propeller rotational rate	revolutions/sec
	or number of fundamental variables	none
PIW	generalized power	none
p	number of fundamental units	none
Q	propeller torque	ft-lbs
Q_{ic}	instrument corrected propeller torque meter reading	ft-lbs
R	propeller radius	ft
R	range	nm
r	radius to a given airfoil section on a propeller	ft
r_h	propeller hub radius	ft
SR	solidity ratio	none
T_j	temperature in the jth engine component	°R

LIST OF SYMBOLS (Continued)

Symbol	Definition	Units
CHAPTER 4	(continued)	
T_t	test day temperature	°R
t	fundamental unit for time	sec
$V_{E_{max}}$	true airspeed for maximum endurance	knots, mph, or fps
$V_{e_{mp}}$	equivalent airspeed for minimum power	knots, mph, or fps
VIW	generalized true airspeed	none
W_E	aircraft weight at the end of a cruise segment	lbs
W_0	aircraft weight at the beginning of a cruise segment	lbs
$\dot{w}_a$	weight flow rate of air through an engine	lbs/sec
X	net thrust from the jet exhaust for a turboprop	lbs
η_b	burner efficiency	none
η_c	compressor efficiency	none
η_i	inlet efficiency	none
η_n	propeller efficiency	none
η_P	propeller efficiency	none
η_t	turbine efficiency	none
π_i	ith nondimensional grouping from Buckingham Pi theorem	none
CHAPTER 5	(only those symbols not previously introduced are listed)	
a	acceleration during takeoff or landing	ft/sec^2
$\bar{a}$	average acceleration during takeoff or landing	ft/sec^2
CFL	critical field length	ft
$C_{L_{max}}$	maximum lift coefficient	none
$C_{L_{tran}}$	lift coefficient during transition segment	none
BFL	balanced field length	ft
F	net accelerating force during takeoff roll	lbs
F_f	frictional force during takeoff roll	lbs
h_{tran}	vertical height at end of takeoff transition	ft
L_L	lift during landing	lbs
m	mass of the airplane of object studied	slugs
$\overline{P}_V$	average excess power during takeoff	hp
RA	runway available (actual runway length less allowance for lineup)	ft
R_c	radius of curvature for takeoff or landing trajectory	ft
s_a	horizontal distance to clear an obstacle of specified height (after liftoff for takeoff or before touchdown for landing)	ft
$s_{a_{se}}$	horizontal distance to clear an obstacle of specified height (during a single engine takeoff)	ft
s_{CL}	horizontal distance during acceleration to climb speed	ft
s_{DEC}	horizontal distance covered between engine failure and initiation of braking during an aborted takeoff	ft

LIST OF SYMBOLS (Continued)

Symbol	Definition	Units

CHAPTER 5 (continued)

s_{EF}	horizontal distance from brake release to engine failure	ft
s_{FA}	horizontal distance from obstacle clearance to landing flare	ft
s_G	horizontal distance from brake release to liftoff	ft
s_{G_L}	horizontal distance from touchdown to complete stop	ft
s_{G_2}	horizontal distance covered during takeoff rotation	ft
s_{LO}	horizontal distance from brake release to liftoff	ft
$s_{LO_{se}}$	horizontal distance from engine failure to liftoff	ft
s_{L_2}	horizontal distance covered during landing rotation	ft
s_{REF}	horizontal distance from brake release to attaining V_{REF}	ft
s_{STOP}	horizontal stopping distance after application of brakes	ft
s_{tran}	horizontal distance covered during takeoff (or landing) transition	ft
s_{CL}	horizontal distance during acceleration to climb speed	ft
T	thrust	lbs
T_L	thrust during landing	lbs
$\overline{T}_V$	average excess thrust during takeoff	lbs
t_r	time for rotation during takeoff or landing	sec
$\overline{V}$	true airspeed where average excess thrust occurs	fps
V_B	true airspeed at initiation of braking during an aborted takeoff	fps
V_{CEF} or V_1	critical engine failure speed	fps
V_{CL}	true airspeed during initial climb segment of takeoff	fps
V_{LO}	true airspeed at liftoff	fps
V_{LOF}	true airspeed at liftoff based on $1.2V_s$	fps
V_{REF}	refusal speed	fps
V_{mca}	air minimum control speed	fps
V_{mcg}	ground minimum control speed	fps
V_{SSE}	safe single engine speed	fps
V_s	stall speed	fps
V_{TD}	touchdown speed	fps
V_{TOS}	takeoff safety speed	fps
V_W	wind speed during takeoff or landing	fps
$V_{2_{min}}$	minimum takeoff speed for FAR Part 25	fps
W_L	weight of aircraft during landing	fps
ΔC_L	increment of lift coefficient	none
Δn	increment of load factor	none
Φ	slope of runway	°
μ	coefficient of friction	none
μ_b	coefficient of friction for braking during landing roll	none
θ_{CL}	change in pitch angle during takeoff transition	°

LIST OF SYMBOLS (Continued)

Symbol	Definition	Units
CHAPTER 6	(only those symbols not previously introduced are listed)	
A	constant coefficient in stick force equation	lbs
a	lever arm distance in gearing mechanism for control stick	ft
a_j	lift curve slope produced by deflection of the *j*th control surface	per ° or radian
a_e	lift curve slope produced by elevator deflection	per ° or radian
B	constant coefficient in stick force equation	lbs/psf
b	lever arm distance in gearing mechanism for control stick	ft
C_{h_e}	elevator hinge moment coefficient	none
C_{h_0}	hinge moment coefficient at zero lift and zero control surface deflection	none
$C_{h_{\alpha_j}}$	rate of change of hinge moment coefficient for the *j*th control surface with changes in local angle of attack	per ° or radian
$C_{h_{\delta_e}}$	rate of change of hinge moment coefficient with elevator deflection	per °
$C_{h_{\delta_j}}$	rate of change of hinge moment coefficient for the *j*th control surface with changes in surface deflection	per °
$C_{h_{\delta_{tab}}}$	rate of change of hinge moment coefficient for the *j*th control surface with changes in surface tab deflection	per °
C_L'	lift coefficient with the elevator free to float	none
C_{L_j}	trim lift coefficient produced by the *j*th control surface	none
$C_{L_{trim}}$	trim lift coefficient for the airplane	none
C_{L_α}	lift curve slope for the airplane	per radian
C_{L_α}'	lift curve slope for the airplane with elevator floating	per radian
$C_{L_{\alpha_j}}$	lift curve slope produced by the *j*th control surface	per radian
$C_{L_{\alpha_t}}$	lift curve slope for the horizontal tail	per radian
$C_{L_{\alpha_{wb}}}$	lift curve slope for the wing-body	per radian
$C_{L_{\delta_e}}$	change in lift coefficient with elevator deflection	per ° or radian
$C_{L_{\delta_j}}$	change in lift coefficient with deflection of the *j*th control surface	per ° or radian
C_{m_0}	zero lift pitching moment coefficient about cg	none
C_{m_0}'	zero lift pitching moment coefficient about cg with the elevator free to float	none
$C_{m_{0_{wb}}}$	zero lift pitching moment coefficient for the wing-body alone	none
C_{m_α}	change in pitching moment coefficient with change in α	per radian
C_{m_α}'	change in pitching moment coefficient with change in α with the elevator free to float	per radian
$C_{m_{\delta_e}}$	change in pitching moment coefficient with elevator deflection (elevator effectiveness)	per ° or radian
c	lever arm distance in gearing mechanism for control stick	ft

LIST OF SYMBOLS (Continued)

Symbol	Definition	Units
CHAPTER 6	(continued)	
$\bar{c}$	mean aerodynamic chord	ft or inches
c_e	elevator chord	ft
cg	center of gravity	acronym
d	lever arm distance in gearing mechanism for control stick	ft
e	lever arm distance in gearing mechanism for control stick	ft
F	free elevator factor	none
F_s	stick force	lbs
G	gearing ratio (or gain)	°/inch
H_e	elevator hinge moment	ft-lbs
i_t	horizontal tail incidence angle	° or radians
$\mathcal{L}$	net aerodynamic rolling moment about the x axis	ft-lbs
ℓ_s	control stick lever arm in gearing expression	ft
ℓ_t	distance from aircraft cg to horizontal tail aerodynamic center	ft
M	net aerodynamic pitching moment about the y axis	ft-lbs
N	net aerodynamic yawing moment about the z axis	ft-lbs
P or p	x component of angular velocity	°/sec or rad/sec
Q or q	y component of angular velocity	°/sec or rad/sec
$\bar{q}$	dynamic pressure	psf
R or r	z component of angular velocity	°/sec or rad/sec
S	wing planform area (reference area)	ft^2
SM	stick-fixed static margin	none
SM_{free}	stick-free static margin	none
S_e	elevator surface area	ft^2
S_t	horizontal tail planform area	ft^2
s	control stick travel	in
U	x component of linear velocity of the aircraft center of gravity	fps
V	y component of linear velocity of the aircraft center of gravity	fps
V_H	horizontal tail volume coefficient	none
V_H'	horizontal tail volume coefficient with elevator free to float	none
V_{H_n}	horizontal tail volume coefficient with the cg located at the neutral point	none
V_{H_n}'	horizontal tail volume coefficient with the cg located at the neutral point with the elevator free to float	none
$V_{V_{corrected}}$	vertical velocity corrected for engine thrust	none
W	z component of linear velocity of the aircraft center of gravity	fps
W_j	weight of the jth control surface	lbs
X	x component of the net aerodynamic force	lbs
Y	y component of the net aerodynamic force	lbs
Z	z component of the net aerodynamic force	lbs

Symbol	Definition	Units
CHAPTER 6	(continued)	
$x_{ac_{wb}}$	aerodynamic center of the wing-body	ft or inches
x_{cg}	location of the center of gravity along the *x* axis	ft or inches
x_j	location of the *j*th control surface cg relative to the hinge line	ft or inches
x_{np}	neutral point	ft or inches
x_{np}'	neutral point with the elevator free to float	ft or inches
$x_{inertial}$	inertial *x* axis	ft or inches
$y_{inertial}$	inertial *y* axis	ft or inches
$z_{inertial}$	inertial *z* axis	ft or inches
ΔC_L	change in lift coefficient	none
ΔC_m	change in pitching moment coefficient	none
α'	aircraft angle of attack with the elevator free to float	° or radians
α_{trim}	trim angle of attack	° or radians
α_{wb}	angle of attack of the wing-body	° or radians
α_j	local angle of attack at the *j*th control surface	° or radians
β	angle of sideslip	° or radians
δ_a	aileron deflection	°
$\delta_{a_{left}}$	left aileron deflection	°
$\delta_{a_{right}}$	right aileron deflection	°
δ_e	elevator deflection	°
$\delta_{e_{trim}}$	elevator angle to trim	°
δ_j	control surface deflection of the *j*th control surface	°
$\delta_{j_{free}}$	free floating angle of the *j*th control surface	°
δ_r	rudder deflection	°
δ_{tab}	control surface tab deflection	°
$\delta_{tab_{trim}}$	control surface tab deflection to trim	°
γ_{PA}	flight-path angle in the power approach flight condition	°
ε	downwash angle	°
ε_0	downwash angle when wing-body lift is zero	°
Φ	Euler roll angle	°
$\dot{\Phi}$	Euler roll rate	°/sec
Θ	Euler pitch angle	°
$\dot{\Theta}$	Euler pitch rate	°/sec
ω	angular velocity	°/sec or rad/sec
Ψ	Euler yaw angle	°
$\dot{\Psi}$	Euler yaw rate	°/sec

LIST OF SYMBOLS (Continued)

Symbol	Definition	Units

CHAPTER 7 (only those symbols not previously introduced are listed)

b_e	span of the elevator	ft
C_{m_q}	pitch damping derivative	none
$C_{m_{q_t}}$	tail contribution to pitch damping derivative	none
C_N	normal force coefficient	none
K	correction coefficient accounting for wing-body contributions to the pitch damping derivative	none
L_{trim}	aircraft lift in the trim or wings-level equilibrium state	lbs
MM	stick-fixed maneuver margin	none
n_z	normal acceleration of the aircraft cg	none
n_0	load factor in equilibrium (trimmed) flight	none
q_0	body axis pitch rate in equilibrium (trimmed) flight	°/sec
$\overline{q}_t$	dynamic pressure at the horizontal tail	psf
x_{mp}	maneuver point	ft or inches
x_{mp}'	maneuver point with the elevator free to float	ft or inches
ΔC_{h_e}	change in elevator hinge moment coefficient	none
ΔF_s	change in stick force	lbs
Δq	change in pitch rate	rad/sec
$\Delta\alpha$	change in aircraft angle of attack	°
$\Delta\alpha_t$	change in angle of attack at the horizontal tail	°
$\Delta\alpha_w$	change in angle of attack at the wing	°
$\Delta\delta_e$	change in elevator deflection	°
α_{pu}	aircraft angle of attack during a wings-level pull-up	°
μ	relative mass parameter	none
θ	change in local angle of attack at the horizontal tail during a wings-level pull-up	°
τ	ratio of elevator lift effectiveness to stabilizer lift effectiveness	none
Ω	aircraft inertial turn rate	°/sec

CHAPTER 8 (only those symbols not previously introduced are listed)

a_r	side force curve slope produced by rudder deflection	per radian
$C_{h_{\alpha_F}}$	change in hinge moment due to change in local angle of attack	none
$C_{h_{\delta_r}}$	change in hinge moment due to rudder deflection	per °
$C_{L_{\alpha_a}}$	lift curve slope with ailerons deflected	per ° or radian
$C_{\mathcal{L}}$	rolling moment coefficient	none
$C_{\mathcal{L}_\beta}$	dihedral effect	none
$C_{\mathcal{L}_p}$	roll damping derivative	none
$C_{\mathcal{L}_r}$	rolling moment change due to yaw rate	none
$C_{\mathcal{L}_{\delta_a}}$	aileron control effectiveness	per °
$C_{\mathcal{L}_{\delta_r}}$	change in rolling moment coefficient due to rudder deflection	per °

LIST OF SYMBOLS (Continued)

Symbol	Definition	Units
CHAPTER 8	(continued)	
C_n	yawing moment coefficient	none
C_{n_p}	change in yawing moment coefficient due to roll rate	none
C_{n_r}	yaw damping derivative	none
C_{n_β}	directional (or weathercock) stability	none
$C_{n_{\beta fixed}}$	directional (or weathercock) stability with the rudder fixed	none
$C_{n_{\delta_a}}$	adverse yaw	per °
$C_{n_{\delta_r}}$	rudder control effectiveness	per °
C_Y	side force coefficient	none
C_{Y_F}	vertical tail contribution to side force coefficient	none
C_{Y_F}'	vertical tail contribution to side force coefficient (rudder free)	none
C_{Y_β}	change side force coefficient due to sideslip	none
$C_{Y_{\delta_a}}$	side force coefficient due to aileron deflection	per °
$C_{Y_{\delta_r}}$	side force coefficient due to rudder deflection	per °
$C_{Y_{\alpha_F}}$	side force coefficient due to local angle of attack change	per °
F_a	aileron force	lbs
ℓ	distance from aircraft centerline to tip parachute force line	ft
ℓ_V	distance from aircraft cg to vertical tail aerodynamic center	ft
P	indirect measurement of tip parachute force	lbs
S_a	aileron surface area	ft^2
T	tip parachute force	lbs
V_A	design maneuver speed	fps or mph or knots
V_F	local true airspeed at the vertical tail (fin)	fps
V_{FE}	maximum flap extended speed	fps or mph or knots
V_{LE}	maximum landing gear extened speed	fps or mph or knots
$V_{FC/MC}$	maximum speed for stability characteristics	fps or mph or knots
Y_F	side force contribution of the vertical tail (fin)	lbs
y	distance from aircraft centerline to wing center of pressure	ft
z_V	distance from aircraft x body axis to vertical tail center of pressure	ft
ΔC_n	increment of yawing moment coefficient	none
ΔC_{n_β}	increment of directional (or weathercock) stability	none
ΔN	increment of yawing moment	ft-lbs
ΔY_r	increment of side force due to rudder deflection	lbs
$\Delta\delta_a$	change in aileron deflection	°
$\Delta\delta_r$	change in rudder deflection	°
α_F	angle of attack of the vertical tail	°
$\delta_{r_{free}}$	rudder angle free to float	°
σ	sidewash angle	°

LIST OF SYMBOLS (Continued)

Symbol	Definition	Units
CHAPTER 9	(only those symbols not previously introduced are listed)	
A	state matrix	various
B	control matrix	various
A_i	state matrix (not normalized)	various
B_i	control matrix (not normalized)	various
C_i	normalizing matrix (inverse is used to normalize A_i and B_i)	various
a_i	general coefficients for second order differential equation	various
C_{L0}	trim lift coefficient	none
C_{X_u}	nondimensional stability derivative	none
C_{X_α}	nondimensional stability derivative	none
$C_{X_{\delta e}}$	nondimensional control derivative	none
C_{Z_u}	nondimensional stability derivative	none
C_{Z_α}	nondimensional stability derivative	none
$C_{Z_{\dot\alpha}}$	nondimensional stability derivative	none
$C_{Z_{\delta e}}$	nondimensional control derivative	none
C_{m_u}	nondimensional stability derivative	none
C_{m_α}	nondimensional stability derivative	none
$C_{m_{\dot\alpha}}$	nondimensional stability derivative	none
$C_{m_{\delta e}}$	nondimensional control derivative	none
c	damping coefficient	lbs/fps
D	derivative operator with respect to $\hat{t}$	none
I_x	mass moment of inertia about x stability axis	slug-ft^2
I_{xz}	mass product of inertia about x and z stability axes	slug-ft^2
I_y	mass moment of inertia about y stability axis	slug-ft^2
I_z	mass moment of inertia about z stability axis	slug-ft^2
i_A	nondimensional mass moment of inertia about x stability axis	none
i_B	nondimensional mass moment of inertia about y stability axis	none
i_C	nondimensional mass moment of inertia about z stability axis	none
i_E	nondimensional product of inertia about x and z stability axes	none
K_{Dr}	Dutch roll mode residue	various
K_r	roll mode residue	various
K_s	spiral mode residue	various
k	spring constant	lbs/in
$\mathcal{L}_p$	dimensional stability derivative	per sec
$\mathcal{L}_r$	dimensional stability derivative	per sec
$\mathcal{L}_v$	dimensional stability derivative	per ft-sec
$\mathcal{L}_{\dot v}$	dimensional stability derivative	per ft
$\mathcal{L}_\beta$	dimensional stability derivative	per rad-sec^2
$\mathcal{L}_{\delta_a}$	dimensional control derivative	per rad-sec^2

LIST OF SYMBOLS (Continued)

Symbol	Definition	Units
CHAPTER 9	(continued)	
$\mathcal{L}_{\delta_r}$	dimensional control derivative	per rad-sec^2
ℓ	characteristic length	ft
M_i	local maxima in response variable oscillation	various
M_q	dimensional stability derivative	per sec
M_u	dimensional stability derivative	per ft-sec
M_w	dimensional stability derivative	per ft-sec
$M_{\dot{w}}$	dimensional stability derivative	per ft
M_{δ_e}	dimensional control derivative	per rad-sec^2
M_i	local minima in response variable oscillation	various
N_p	dimensional stability derivative	per sec
N_r	dimensional stability derivative	per sec
N_v	dimensional stability derivative	per ft-sec
$N_{\dot{v}}$	dimensional stability derivative	per ft
N_β	dimensional stability derivative	per rad-sec^2
N_{δ_a}	dimensional control derivative	per rad-sec^2
N_{δ_r}	dimensional control derivative	per rad-sec^2
N_x^y	transfer function matrix (input y, output x)	none
P_0	angular velocity about the x stability axis in trim condition	rad/sec
p	perturbation in angular velocity about the x stability axis	rad/sec
p_0	initial peak value of roll rate response	°/sec or rad/sec
$\hat{p}$	nondimensional angular velocity about the x stability axis	rad/sec
$\dot{p}$	angular acceleration about the x stability axis	rad/sec^2
Q_0	angular velocity about the y stability axis in trim condition	rad/sec
q	perturbation in angular velocity about the y stability axis	rad/sec
$\hat{q}$	perturbation in angular velocity about the y stability axis	rad/sec
R_0	angular velocity about the x stability axis in trim condition	rad/sec
r	perturbation in angular velocity about the x stability axis	rad/sec
$\hat{r}$	perturbation in angular velocity about the x stability axis	rad/sec
s	Laplace operator	none
T	period of an oscillation	sec
t	time	sec
t^*	normalizing unit of time	sec
t_i	sample time points	sec
t_p	time-to-peak-amplitude	sec
t_r	rise time	sec
t_s	settling time	sec
t_2	time-to-double-amplitude	sec
$t_{1/2}$	time-to-half-amplitude	sec

LIST OF SYMBOLS (Continued)

Symbol	Definition	Units
CHAPTER 9 (continued)		
$\hat{t}$	nondimensional time	none (airsecs)
U_0	x axis velocity component of aircraft cg at trim conditions	fps
u	linearized perturbation in x axis velocity of aircraft cg	fps
$\boldsymbol{u}$	control vector	various
v	linearized perturbation in y axis velocity of aircraft cg	fps
W_0	z axis velocity component of aircraft cg at trim conditions	fps
w	linearized perturbation in z axis velocity of aircraft cg	fps
X_q	dimensional stability derivative	ft per rad-sec
X_u	dimensional stability derivative	per sec
X_w	dimensional stability derivative	per sec
$X_{\dot{w}}$	dimensional stability derivative	ft per rad-sec
X_{δ_e}	dimensional control derivative	ft per rad-sec^2
$\boldsymbol{x}$	state vector	various
Y_p	dimensional stability derivative	per rad
Y_r	dimensional stability derivative	per rad
Y_v	dimensional stability derivative	per sec
$Y_{\dot{v}}$	dimensional stability derivative	none
Y_β	dimensional stability derivative	ft per rad-sec^2
Y_{δ_a}	dimensional control derivative	per rad-sec
Y_{δ_r}	dimensional control derivative	per rad-sec
Z_q	dimensional stability derivative	ft per rad-sec
Z_u	dimensional stability derivative	per sec
Z_w	dimensional stability derivative	per sec
$Z_{\dot{w}}$	dimensional stability derivative	ft per rad-sec
Z_{δ_e}	dimensional control derivative	ft per rad-sec^2
Δx_i	increment in response variables	various
Δt_i	increment in time	sec
α	perturbation in angle of attack	°
β	perturbation in sideslip angle	°
Δ	characteristic matrix	various
δ_{a_0}	aileron deflection at the trim condition	°
δ_{e_0}	elevator deflection at the trim condition	°
δ_{r_0}	rudder deflection at the trim condition	°
ϕ	perturbation in bank angle or roll angle	°
λ	eigenvalue	various
λ_s	spiral mode eigenvalue	various
Θ_0	inertial pitch angle at trim conditions	°
θ	perturbation in inertial pitch angle	°

LIST OF SYMBOLS (Continued)

Symbol	Definition	Units
CHAPTER 9	(continued)	
τ	time constant	sec
τ_{Dr}	Dutch roll mode time constant	sec
τ_r	roll mode time constant	sec
τ_s	spiral mode time constant	sec
ω_d	damped frequency	rad/sec
ω_n	undamped natural frequency	rad/sec
$\omega_{n_{Dr}}$	Dutch roll undamped natural frequency	rad/sec
$\omega_{n_{sp}}$	short period undamped natural frequency	rad/sec
ω_{n_p}	phugoid undamped natural frequency	rad/sec
ψ	perturbation in heading angle	°
ψ_{phase}	phase angle	° or rad
ζ	damping ratio	none
ζ_{Dr}	Dutch roll damping ratio	none
ζ_{sp}	short period damping ratio	none
ζ_p	phugoid damping ratio	none
CHAPTER 10	(only those symbols not previously introduced are listed)	
a	distance (fraction of semichord) from midchord to elastic axis	none
a_∞	freestream speed of sound	fps
c	chord, reference length	ft
$C(k)$	Theodorsen's Function	none
C	damping matrix	lb-sec/ft, ft-lb-sec
C_A	aerodynamic damping matrix	lb-sec/ft, ft-lb-sec
C_{L_δ}	change in lift per control surface deflection	per ° or radian
C_{M_δ}	change in moment per control surface deflection	per ° or radian
$C_{L_\alpha,0}$	slope of lift curve for incompressible flow	per ° or radian
e	distance from elastic axis to aerodynamic center	ft
F	external force vector	lbs, ft-lb
F_A	motion dependent aerodynamic force vector	lbs, ft-lb
g, G	damping	none
I	mass moment of inertia	slugs-ft^2
I	identity matrix	none
k	reduced frequency	none
K	spring constant	lbs/ft, ft-lbs/rad
K	stiffness matrix	lb/ft, ft-lb/rad
K_A	aerodynamic stiffness matrix	lb/ft, ft-lb/rad

LIST OF SYMBOLS (Continued)

Symbol	Definition	Units

CHAPTER 10 (Continued)

$\underline{K_A}$	aerodynamic stiffness matrix with q_∞ removed	ft, ft^3/rad
M	aerodynamic moment	ft-lbs
M_∞	Mach number	none
$\boldsymbol{M}$	mass matrix	slugs, slugs-ft^2
q	generalized coordinate vector	various
q_a	reference dynamic pressure for a_∞ at altitude	psf
r	distance from elastic axis to center of mass	ft
r_α	radius of gyration	ft
$\overline{V}$	Flutter speed index	none
V_D	design speed	fps
V_L	limit speed	fps
y	plunge motion	ft
α	pitch deflection, or angle of attack	radians
β	eigenvector	various
δ	damping ratio, or control surface deflection	none, radians
Φ	matrix of eigenvectors	various
Λ	matrix of eigenvalues	psf, (rad/sec)^2
μ	mass ratio	none
θ	elastic twist	radians
ω	frequency	rad/sec
ω_h	natural frequency in plunge - uncoupled	rad/sec
ω_α	natural frequency in pitch - uncoupled	rad/sec

CHAPTER 11 (only those symbols not previously introduced are listed)

C_{mb}	pitching moment coefficient based on wing span	none
$C_{m,rb}$	pitching moment coefficient from rotary balance data	none
$C_{m,rb_{spin}}$	potential equilibrium pitching moment coefficient from rotary balance data	none
D_A	drag force due to advancing wing panel	lbs
D_R	drag force due to retreating wing panel	lbs
$\boldsymbol{F}$	force vector	lbs
I_{xy}	mass product of inertia about x and y stability axes	slug-ft^2
I_{yz}	mass product of inertia about y and z stability axes	slug-ft^2
k_x	radius of gyration about x stability axis	ft
k_y	radius of gyration about y stability axis	ft
k_z	radius of gyration about z stability axis	ft
L_A	lift force due to advancing wing panel	lbs
L_R	lift force due to retreating wing panel	lbs

LIST OF SYMBOLS (Continued)

Symbol	Definition	Units
CHAPTER 11	(continued)	
R	resultant aerodynamic force	lbs
R_A	advancing wing panel contribution to resultant aerodynamic force	lbs
R_R	retreating wing panel contribution to resultant aerodynamic force	lbs
R_y	y component of resultant aerodynamic force	lbs
R_z	z component of resultant aerodynamic force	lbs
r	helix radius in a fully developed spin	ft
V	velocity vector for the aircraft cg	fps
X_A	aerodynamic force in x direction on advancing wing panel	lbs
X_R	aerodynamic force in x direction on retreating wing panel	lbs
Z_A	aerodynamic force in z direction on advancing wing panel	lbs
Z_R	aerodynamic force in z direction on retreating wing panel	lbs
ΔC_{D_1}	increment in drag coefficient between advancing and retreating wing at low angle of attack	none
ΔC_{D_2}	increment in drag coefficient between advancing and retreating wing at high angle of attack	none
ΔC_{L_1}	increment in lift coefficient between advancing and retreating wing at low angle of attack	none
ΔC_{L_2}	increment in lift coefficient between advancing and retreating wing at high angle of attack	none
α_A	local angle of attack of an advancing wing section	°
α_R	local angle of attack of a retreating wing section	°
α_{A_1}	angle of attack of the advancing wing at low angle of attack	°
α_{A_2}	angle of attack of the advancing wing at high angle of attack	°
α_{R_1}	angle of attack of the retreating wing at low angle of attack	°
α_{R_2}	angle of attack of the retreating wing at high angle of attack	°
α_s	stall angle of attack	°
λ	helix angle in a spin	°
μ	relative density parameter	none